Handbook of Transition Metal Polymerization Catalysts

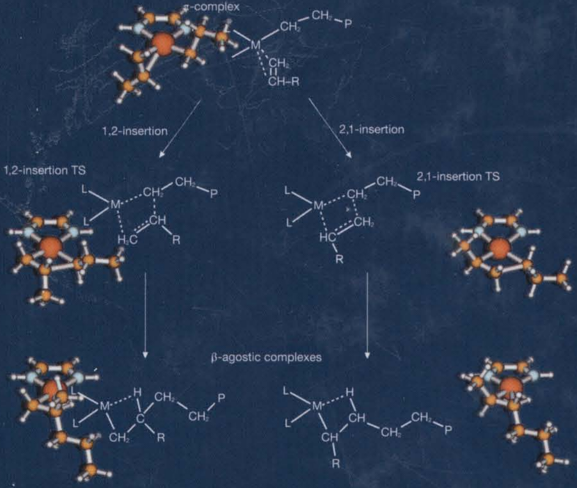

Edited by

RAY HOFF

ROBERT T. MATHERS

WILEY

HANDBOOK OF TRANSITION METAL POLYMERIZATION CATALYSTS

HANDBOOK OF TRANSITION METAL POLYMERIZATION CATALYSTS

Edited by

Ray Hoff
Chemplex Company (Retired)
Adjunct Faculty, Roosevelt University
Schaumburg, IL

Robert T. Mathers
Chemistry Department
Pennsylvania State University
New Kensington, PA

WILEY

A JOHN WILEY & SONS, INC., PUBLICATION

Copyright © 2010 by John Wiley & Sons, Inc. All rights reserved.

Published by John Wiley & Sons, Inc., Hoboken, New Jersey
Published simultaneously in Canada

No part of this publication may be reproduced, stored in a retrieval system, or transmitted in any form or by any means, electronic, mechanical, photocopying, recording, scanning, or otherwise, except as permitted under Section 107 or 108 of the 1976 United States Copyright Act, without either the prior written permission of the Publisher, or authorization through payment of the appropriate per-copy fee to the Copyright Clearance Center, Inc., 222 Rosewood Drive, Danvers, MA 01923, 978-750-8400, fax 978-750-4470, or on the web at www.copyright.com . Requests to the Publisher for permission should be addressed to the Permissions Department, John Wiley & Sons, Inc., 111 River Street, Hoboken, NJ 07030, 201-748-6011, fax 201-748-6008, or online at http://www.wiley.com/go/permission.

Limit of Liability/Disclaimer of Warranty: While the publisher and author have used their best efforts in preparing this book, they make no representations or warranties with respect to the accuracy or completeness of the contents of this book and specifically disclaim any implied warranties of merchantability or fitness for a particular purpose. No warranty may be created or extended by sales representatives or written sales materials. The advice and strategies contained herein may not be suitable for your situation. You should consult with a professional where appropriate. Neither the publisher nor author shall be liable for any loss of profit or any other commercial damages, including but not limited to special, incidental, consequential, or other damages.

For general information on our other products and services or for technical support, please contact our Customer Care Department within the United States at 877-762-2974, outside the United States at 317-572-3993 or fax 317-572-4002.

Wiley also publishes its books in a variety of electronic formats. Some content that appears in print may not be available in electronic formats. For more information about Wiley products, visit our web site at www.wiley.com.

Library of Congress Cataloging-in-Publication Data:

Hoff, Raymond E.
Handbook of transition metal polymerization catalysts / Ray Hoff, Robert T. Mathers.
p. cm.
Includes index.
ISBN 978-0-470-13798-7 (cloth)
1. Polymerization. 2. Transition metal catalysts. 3. Metathesis (Chemistry)
I. Mathers, Robert T. II. Title.
QD281. P6H57 2009
668.9′2–dc22

2009005621

Printed in the United States of America

10 9 8 7 6 5 4 3 2 1

CONTENTS

Introduction vii

About the Authors xiii

1 **Commercially Available Metal Alkyls and Their Use in Polyolefin Catalysts** 1
Dennis B. Malpass

2 **Porous Silica in Transition Metal Polymerization Catalysts** 29
Thomas J. Pullukat and Robert E. Patterson

3 **Computational Modeling of Polymerization Catalysts** 53
Monika Srebro and Artur Michalak

4 **Scale-Up of Catalyst Recipes to Commercial Production** 103
C. P. Cheng

5 **Commercialization of Olefin Polymerization Catalysts: Model for Success** 113
C. E. Capshew

6 **Supported Magnesium/Titanium-Based Ziegler Catalysts for Production of Polyethylene** 131
Thomas E. Nowlin, Robert I. Mink, and Yury V. Kissin

7 **Stereospecific α-Olefin Polymerization with Heterogeneous Catalysts** 157
John Severn and Robert L. Jones, Jr.

8 **$MgCl_2$-Supported $TiCl_4$ Catalysts for Production of Morphology-Controlled Polyethylene** 231
Long Wu and Sieghard E. Wanke

9 **Product Morphology in Olefin Polymerization with Polymer Supported Metallocene Catalysts** 261
Long Wu and Sieghard E. Wanke

10 Review of Phillips Chromium Catalyst for Ethylene Polymerization **291**
Max P. McDaniel

11 Silica-Supported Silyl Chromate–Based Ethylene Polymerization Catalysts **447**
Kevin Cann

12 Ethylene Polymerization and α-Olefin Oligomerization Using Catalysts Derived from Phosphoranes and Ni(II) and Ni(0) Precursors **459**
Scott Collins

13 Late Transition Metal–Catalyzed Co- and Terpolymerization of α-Olefins with Carbon Monoxide–Polyketones: Synthesis and Modification **467**
Timo M. J. Anselment, Manuela Zintl, Maria Leute, Rüdiger Nowack and Bernhard Rieger

14 Copper Catalysts for Olefin Polymerization **497**
Anna Maria Raspolli Galletti

15 Ring-Opening Metathesis Polymerizations and Acyclic Diene Metathesis Polymerizations with Homogeneous Ruthenium and Molybdenum Catalysts and Initiators **513**
Robert T. Mathers

16 Cobalt Ziegler–Natta Catalysts for Synthesis of Poly-*cis*-1,4-Butadiene **537**
Ray Hoff

Appendix A Pyrophoricity of Metal Alkyls **551**
Dennis B. Malpass

Appendix B Rheological Terms for Polymerization Catalyst Chemists **563**
Gregory W. Kamykowski

Index **567**

GENERAL INTRODUCTION

Polymer synthesis employs two main reaction types: step growth and chain growth. Chain growth polymerizations account for a large portion of commodity plastics and synthetic elastomers. The polymerization mechanisms involve all of the highly reactive intermediates of organic chemistry: free radicals, carbonium ions, carbanions, and coordinatively unsaturated metal species.[1] The action of these reactive intermediates on appropriate monomers fits the classical definition of catalysts. They repeatedly promote the same reaction of monomer addition, taking part in each step of monomer molecule addition, and they do this by lowering the activation energy of the incorporation step.

This book was started with the intention that it be a comprehensive handbook for a particular group of polymerization catalysts. The criterion for a catalyst to be in the group was that, in each case, the catalyst exerts some distinctive control on the nature of the polymers formed. Traditional free-radical initiators were excluded because with these the polymer properties depend more strongly on the monomer-derived radicals at chain ends than on the chemical structure of the initiating compounds, whether they are peroxides or hydroperoxides, azo compounds, or redox initiators.[1]

This book includes recent advances and historically important catalysts. Additionally, selective chapters will serve as an informative guide to methods and reagents that are widely used in the field.

Transition metal catalysts for olefin polymerization, often called coordination catalysts, fit the criterion for inclusion in this book. They involve coordinatively unsaturated reactive intermediates. The site of growth for the polymer chains is a metal–carbon bond into which new monomer molecules are successively inserted. Because the metal atom is exactly at the monomer insertion point, the identity of the metal and its ligands greatly influence polymer properties compared to normal free-radical initiators. In 1973, W. L. Carrick[2] described how different metal atoms, such as vanadium, titanium, zirconium, and hafnium, influenced reactivity ratios for olefin copolymerizations. In contrast, the composition of copolymers in traditional free-radical polymerization depends on the *Q–e* electronic numbers[1] of the monomers.

It is certain that many other catalysts as defined above should also be in this book. Certain compounds involved in metal-mediated free-radical polymerization and ring-opening polymerization agents may meet the criterion. For example, in the first case there are the compounds involved in catalytic chain transfer polymerization which feature a weak cobalt–carbon bond. For the second case, ring–opening polymerizations of cyclic esters with appropriate metal alkoxides are proposed to proceed by monomer coordination and addition at a metal-to-oxygen bond with distinctive results dependent on not only the metal identity but also the structure of the metal compound as well.[3] Unfortunately these subjects are also excluded.

Some readers may be familiar with the myriad of catalysts for petroleum refining and the technology of their use in industry. They are a vast part of the world's catalysis enterprise. But there is an important difference in the use of petroleum-refining catalysts and the modern polymerization catalysts of industry that may be relevant to newer polymerization catalysts. In the petroleum industry hydrotreating, hydrocracking, reforming, and isomerization catalysts are all retained in some type of bed while reactant streams pass through and reaction mixtures exit. When these catalysts become inefficient with age, they are for the most part regenerated. Regeneration may even be carried out continuously. On the other hand, as of the year 2008, no well-known polymerization catalyst is regenerated. In many polymerization processes the solid polymer products are isolated with intermingled catalyst residues. This is true for various polyolefin processes, solution, slurry, and gas-phase polymerization. Extraction of the residues is a costly step on a commercial scale.

Ziegler–Natta catalysts for polyethylene and polypropylene are one of the main varieties of coordination catalysts. In their early years, some treatment to remove catalyst residues was necessary for acceptable commercial products. However, with the highly reactive catalysts now used for the manufacture of polyolefins, the products are suitable for most end uses without removal of the residues, and in each case the cost of the catalyst is only a small fraction of the total cost of manufacturing. This book deals with polymerization catalysts that afford commercially acceptable high yields of polymer with respect to catalyst mass (catalyst productivity).

This book also deals with catalysts that currently have modest or low productivity under the best known conditions. There is interest in these catalysts because they have a real potential for the synthesis of polymer products of much greater value. A hypothetical example is a polymer made with a palladium catalyst that is far superior to anything known for fabricating an artificial heart valve. The value of such an application could bear the cost of palladium recovery and modest productivity. Probably with such a catalyst, the best strategy for recovering palladium might be to retain it on a monolithic support as in automobile catalytic converters or on pellets in a manner similar to petroleum-refining catalysts. This necessitates that the polymer be kept in solution following chain transfer while the catalyst remains bonded to the support.

It is notable that the chromium catalysts discovered by Hogan and Banks[4] have been improved by diligent research, and, in fact, the Phillips chromium catalysts are now superactive with commercial productivites of a million pounds of polyethylene per pound of chromium common. However, they had low productivity in the beginning, and in the 1958 patent[4] Hogan and

Banks reported using the catalysts in captive beds and proposed regeneration. If it turns out that ruthenium or palladium polymerization catalysts are commercialized by means of retaining the catalyst on a fixed or semifixed bed, credit should be given to chemists of the last century who already had the idea.

Most polymerization catalyst chemists are familiar with the propagation step in olefin polymerization by coordination catalysts. The series of proposed propagation mechanisms started with the Cossee hypothesis in 1964. Then, the Green–Rooney mechanism in 1978 was followed in 1983 by a modification involving agostic interaction proposed by Maurice Brookhart and Malcolm L. H. Green.[5] The latter modification has been of great use in explaining the highly branched ethylene polymers formed by nickel and palladium catalysts.[6]

These mechanisms presume the existence of a metal-to-alkyl group bond into which the monomers are successively inserted. They do not explain how this first metal–alkyl bond, if needed, is formed. The main concern of Cossee was the original Ziegler–Natta catalysts which comprise the reaction mixtures formed by transition metal compounds and certain reactive metal alkyl and hydride compounds. In one of Karl Ziegler's early patents filed in 1958 the transition metals of the compounds in claim 1 are those of "Groups IVB, VB, VIB, including thorium and uranium, metals of group VIII of the periodic system and manganese."[7] It was hypothesized that among the products in the reaction mixtures there were compounds with a transition metal–alkyl or transition metal–hydride bond with the alkyl or hydride coming from the second reagent.[2] In modern terms the transition metal compound is called the catalyst, and the second reagent is the cocatalyst. There are three related facts: (1) With the thermally activated chromium-on-silica catalysts invented by Paul Hogan and Robert L. Banks of Phillips Petroleum Company no cocatalyst of any kind is needed to obtain great reactivity. (2) Although many metallocene compounds used as polymerization catalysts have metal–alkyl bonds by prior synthesis, cocatalysts such as MAO (methylaluminoxane) or discrete Lewis acidic activators that both give rise to a positively charged metal alkyl partnered with a weakly coordinating anion are nonetheless needed for high polymerization activity under convenient conditions.[8] (3) In ROMP (ring-opening metathesis polymerization) suitable metal compounds sometimes require cocatalysts for activity[9] but also there metal carbene complexes that do not.[10] For more about these three facts please refer to appropriate chapters in this book (A Review of the Phillips Chromium Catalyst for Ethylene Polymerization, Product Morphology in Olefin Polymerization with Polymer-Supported Metallocene Morphology, and Ring-Opening Metathesis Polymerizations (ROMP) and Acyclic Diene Metathesis (ADMET) with Homogeneous Ruthenium and Molybdenum Catalysts).

The first chapter deals with metal alkyls and other compounds that function as cocatalysts with a large number of catalysts. The second chapter examines the varieties of porous silica that are either necessary or valuable in certain catalyst formulations. The following chapter on computer modeling explains a useful tool for catalyst chemists. Not all of the catalysts in this book have been, or ever will be, manufactured on the scale needed for the production of commodity polyolefin plastics. However, there are chapters on catalyst scale-up and commercialization which are introductions to these necessary activities. These two chapters contain information that will probably be helpful to all polymerization catalyst chemists.

In the Ziegler patent cited above, copper was not claimed as a catalyst component although all of the other 3*d* transition metals were. This book has a chapter Copper Catalysts for Olefin Polymerization. Since Ziegler's time the preferred numbering of the groups in the periodic table has changed. Dr. Galletti has copper in group 11 but Karl Ziegler would have written group IB.

As stated above, one of the most important attributes of catalysts used in the manufacture of major synthetic plastics and elastomers is high productivity. The catalyst systems, however, in concert with monomer concentrations and reaction temperatures, also control polymer properties. Catalyst systems are key to tailoring (1) molecular weight (MW) and molecular weight distribution (MWD), (2) comonomer incorporation and molecular shape, (3) stereoregularity (including at least isotacticity, syndiotacticity, and cis, trans, and 1,2-additions for dienes), and for polymers made in slurry- and gas-phase processes (4) polymer particle morphology. The first three of these are consequences of the chemical nature of the active sites within the catalyst system, but the fourth depends as well on the geometric arrangement of the active sites within catalyst particles or a support.

Well-regulated particle morphology permits higher space–time yields in polymerization plants, increases the bulk density, eliminates fines and minimizes dust explosions, and, perhaps most important, helps prevent reactor fouling. In an extreme ideal case excellent particle shape may allow elimination of the common pelletizing step. Information on morphology control may be found in these chapters: Porous Silicas for Transition Metal Polymerization Catalysts, Supported Magnesium/Titanium–Based Ziegler Catalysts for the Production of Polyethylene, Stereospecific Polymerization with "Traditional" Ziegler–Natta Catalysts, $MgCl_2$-Supported Ti Catalysts for the Production of Morphology-Controlled Polyethylene, and Product Morphology in Olefin Polymerization with Polymer-Supported Metallocene Catalysts.

With solution polymerization processes particle morphology does not apply, but the catalyst system remains the major tool to tune polymer properties. Finding a catalyst for a new polymer type and then designing and modifying it to secure the optimum properties and synthesis condition is demanding. We hope this book and what others may do with it will help.

The authors who have contributed to this book have great knowledge and impressive credentials. Brief biographies for each of them follow immediately after the references for this introduction.

REFERENCES

1. Stevens, M. P., *Polymer Chemistry: An Introduction*, 3rd ed. Oxford University Press, New York, 1999, Chapter 6.
2. Carrick, W. L., *Adv. Polym. Sci.*, **1973**, 12, 65–86.
3. O'Keefe, B. J., Breyfogle, L. E, Hillmyer, M. A., and Tolman, W. B., *J. Am. Chem. Soc.*, **2002**, 124, 4384–4393.
4. Hogan, J. P., and Banks, R. L., Phillips Petroleum Company, U.S. Patent No. 2,825,721, 1958.
5. (a) Grubbs, R. H., and Coates, G. W., *Acc. Chem. Res.*, **1996**, 29, 85–93; (b) Cossee, P., *J. Catal.*, **1964**, 3, 80–88; (c) Ivin, K. J., Rooney, J. J., Stewart, C. D., Green, M. L. H., and Mahtab, R., *J. Chem. Soc. Chem. Commun.* **1978**, 604–606; (d) Henrici-Olive, G., and Olive, S., *Angew. Chem. Int. Ed.*, **1967**, 6, 790–798; (e) Brookhart, M., Green, M. L. H., and Parkin, G., *PNAS*, **2007**, 104, 17, 6908–6914.
6. Leatherman, M. D., Svejda, S. A., Johnson, L. K., and Brookhart, M., *J. Am. Chem. Soc.*, **2003**, 125, 3068–3081.
7. Ziegler, K., Breil, H., Martin, H., and Holzkamp, E., Karl Ziegler, U.S. Patent No. 3,113,115, 1963.
8. Vatamanu, M., Boden, B. N., and Baird, M. C., *Macromolecules*, **2005**, 38, 9944–9949.
9. (a) Nomura, K., Sagara, A., and Imanishi, Y., *Macromolecules*, **2002**, 35, 1583–1590; (b) Nakayama, Y., Tanimoto, M., and Shiono, T., *Macromol. Rapid Commun.*, **2007**, 28, 646–650; (c) Hiya, K., Nakayama, Y., and Yasuda, H., *Macromolecules*, **2003**, 36, 7916–7922.
10. Grubbs, R. H., Schwab, P., and Nguyen, S., California Institute of Technology, U.S. Patent No. 7,288,666, 2007.

ABOUT THE AUTHORS

Dennis B. Malpass Dennis Malpass was born and raised in Biloxi, Mississippi. He studied chemistry at Tulane University in New Orleans, Louisiana, and received a B.S. in 1966. He then attended graduate school at the University of Tennessee in Knoxville, Tennessee, and studied main-group organometallic chemistry under Professor Jerome F. Eastham. He received his Ph.D. in 1970 and began his career with Texas Alkyls (now Akzo Nobel). His industrial career spanned 33 years working on synthesis, characterization, and application of metal alkyls, especially aluminum alkyls in Ziegler–Natta polymerization of olefins.

His work included development of viable commercial processes for trimethylaluminum, a crucial raw material for many single-site catalyst systems. He was also codiscoverer of *n*-butylethylmagnesium (BEM) in 1978, still employed today to produce catalysts in the manufacture of many millions of tons of polyethylene worldwide.

He has more than 70 patents and publications. He retired in 2003 and now lives in Magnolia, Texas.

Robert E. Patterson Dr. Robert E. Patterson is director of R&D operations for PQ Corporation of Valley Forge, Pennsylvania, a leading producer of silicates, zeolites, glass beads, and silica gels. He joined PQ in 1978 after receiving his B.S. and Ph.D. degrees in chemistry from Rensselaer Polytechnic Institute, where his doctoral thesis was on foams and antifoams. This experience later proved useful at PQ, where Dr. Patterson led the company's research program on precipitated silica defoamers.

After a-3½ year hiatus as corporate planning manager, Patterson returned full time to R&D in 1991 and in 1999 assumed technical responsibility for all silica products, incl uding adsorbents for beer stabilization and edible oil purification, as well as supports for chromium catalysts in the production of high-density polyethylene. His responsibilities were later expanded to focus on market development of higher value new end uses for silica products. More recently he was made site manager for PQ's corporate research laboratory and pilot plant as well as manager of the facility's analytical and information services departments.

Dr. Patterson is the author of over 35 technical publications, including papers, posters, and patents. He has contributed chapters to four books and is the author of the article on silica in the *Kirk Othmer Encyclopedia of Chemical Technology*. He was previously chairman at the Specialty Silica Summit 2007 and a co-chairman at the Ralph K. Iler Memorial Symposium on the Colloid Chemistry of Silica.

Thomas J. Pullukat After receiving his Ph.D. from Purdue University, West Lafayette, Indiana, Thomas J. Pullukat joined Chemplex Company (Rolling Meadows, Illinois) in 1967. His initial assignment was in catalyst research. At Chemplex, he developed new silica-supported chromium catalysts (Phillips type) for the economical particle form (PF) process. The first direct synthesis of polyethylene milk bottle grade in the PF process was commercialized in 1971. Several other silica–chromium catalysts for the production of polyethylene for use in cereal package liners, 55-gallon drums, geomembrane, and construction barricades were commercialized. A silica-based Ziegler–Natta catalyst for the gas-phase fluidized-bed polyethylene process also was developed. Another silica-based polypropylene catalyst resulted from research on catalysts for the BASF gas-phase process. Over the years, Chemplex merged with Northern Petro and then with USI. The new company was named Quantum. During the mergers, he held several positions: manager, catalysis/polymer physics/analytical and senior research manager, catalyst research/scale-up.

In 1991, Dr. Pullukat left Quantum (now Equistar) to join PQ Corporation (Valley Forge, Pennsylvania). At PQ, he directed the development of technology for the production of silica-based catalysts. Several high-pore-volume chromium catalysts have been commercialized. A silica-based Ziegler–Natta catalyst and silica supports for single-site catalysts have been developed. In 2000 he became responsible for global marketing and technical service of silica catalyst products.

At present he is the president of SILCAT Consultants, a technology and marketing company involved in developing solutions to improve the economics of polyethylene production. He is the author of 45 U.S. patents and over 15 scientific publications. He also has chaired several scientific conferences and is an invited speaker in catalysis symposiums.

Artur Michalak Dr. Artur Michalak (born in 1968) graduated from Jagiellonian University (Kraków, Poland). He received his Ph.D. in theoretical chemistry in the Department of Theoretical Chemistry, Faculty of Chemistry, Jagiellonian University, and then held a postdoctoral fellowship at the University of Calgary, joining the research group of Professor Tom Ziegler. In 2004 he received his D.Sc. degree (habilitation). He is employed as associate professor in the Faculty of Chemistry, Jagiellonian University. He is currently a vice-dean of the Faculty of Chemistry. His main research subjects include chemical bond theory, theoretical description of organometallic systems, and modeling of catalytic processes, in particular polymerization and copolymerization of α-olefins catalyzed by transition metal complexes. He authored over 50 articles in international scientific journals.

the author of the article on silica in the *Kirk Othmer Encyclopedia of Chemical Technology*. He was previously chairman at the Specialty Silica Summit 2007 and a co-chairman at the Ralph K. Iler Memorial Symposium on the Colloid Chemistry of Silica.

Thomas J. Pullukat After receiving his Ph.D. from Purdue University, West Lafayette, Indiana, Thomas J. Pullukat joined Chemplex Company (Rolling Meadows, Illinois) in 1967. His initial assignment was in catalyst research. At Chemplex, he developed new silica-supported chromium catalysts (Phillips type) for the economical particle form (PF) process. The first direct synthesis of polyethylene milk bottle grade in the PF process was commercialized in 1971. Several other silica–chromium catalysts for the production of polyethylene for use in cereal package liners, 55-gallon drums, geomembrane, and construction barricades were commercialized. A silica-based Ziegler–Natta catalyst for the gas-phase fluidized-bed polyethylene process also was developed. Another silica-based polypropylene catalyst resulted from research on catalysts for the BASF gas-phase process. Over the years, Chemplex merged with Northern Petro and then with USI. The new company was named Quantum. During the mergers, he held several positions: manager, catalysis/polymer physics/analytical and senior research manager, catalyst research/scale-up.

In 1991, Dr. Pullukat left Quantum (now Equistar) to join PQ Corporation (Valley Forge, Pennsylvania). At PQ, he directed the development of technology for the production of silica-based catalysts. Several high-pore-volume chromium catalysts have been commercialized. A silica-based Ziegler–Natta catalyst and silica supports for single-site catalysts have been developed. In 2000 he became responsible for global marketing and technical service of silica catalyst products.

At present he is the president of SILCAT Consultants, a technology and marketing company involved in developing solutions to improve the economics of polyethylene production. He is the author of 45 U.S. patents and over 15 scientific publications. He also has chaired several scientific conferences and is an invited speaker in catalysis symposiums.

Artur Michalak Dr. Artur Michalak (born in 1968) graduated from Jagiellonian University (Kraków, Poland). He received his Ph.D. in theoretical chemistry in the Department of Theoretical Chemistry, Faculty of Chemistry, Jagiellonian University, and then held a postdoctoral fellowship at the University of Calgary, joining the research group of Professor Tom Ziegler. In 2004 he received his D.Sc. degree (habilitation). He is employed as associate professor in the Faculty of Chemistry, Jagiellonian University. He is currently a vice-dean of the Faculty of Chemistry. His main research subjects include chemical bond theory, theoretical description of organometallic systems, and modeling of catalytic processes, in particular polymerization and copolymerization of α-olefins catalyzed by transition metal complexes. He authored over 50 articles in international scientific journals.

Monika Srebro Monika Srebro was born in Tarnow, Poland, in 1982. In 2006, she received her M.Sc. in Chemistry and has started her Ph.D. studies under the supervision of Dr. Artur Michalak in the Department of Theoretical Chemistry at the Jagiellonian University in Cracow. In 2007, she obtained her B.Eng. in Materials Engineering from the University of Science and Technology in Cracow. Her main research topic is molecular modeling of polymerization of α-olefins and their copolymerization with polar monomers catalyzed by transition-metal-based complexes.

C. P. Cheng Dr. Chung Ping (C. P.) Cheng received his B.S. in Chemical Engineering at the University of Wisconsin-Madison and his M.Ch.E. and Ph.D. from the University of Delaware. After graduation, he joined Akzo-Nobel (then Stauffer Chemical) and began his long career in Ziegler–Natta catalysts. While at Akzo-Nobel, he worked on development of the manufacturing processes for first- and third-generation Ziegler–Natta catalysts. In 1988, Dr. Cheng joined Quantum Chemical (now part of Lyondell-Basell) as section leader in catalyst scale-up working on the development of various polypropylene and polyethylene catalysts. In 1991, he moved to Catalyst Resources Inc. (CRI, then part of Phillips Petroleum, and after several changes of ownership, now part of BASF) and worked for 16 years on the development of polyolefin catalysts and the application of these catalysts in polymerization processes. He is part of the team that successfully commercialized the Lynx polypropylene catalyst to all polymerization process platforms. Since 2007, he has been with Süd-Chemie as the chief technology officer of the Polyolefin Catalyst Division, working out of Shanghai, China. Dr. Cheng has several patents and many publications in the polyolefin area and is a frequent speaker at international polyolefin conferences.

C. E. Capshew Dr. Charles Capshew majored in chemistry and mathematics at today's SWOSU (Weatherford, Okhahoma). For the next five years he was a U.S. Air Force pilot and was deployed three times to Vietnam and Southeast Asia flying reconnaissance and bombing missions. After earning a Ph.D. in Organic Chemistry at the University of Texas at Austin under Dr. Rowland Pettit, he joined the Phillips Petroleum Company (and Chevron Phillips Chemical Company in 2000) and spent 27 years in polyolefins, retiring in 2004. His career span R&D, product development, marketing, manufacturing, and quality management. His career required frequent worldwide travel. He is credited with 13 U.S. patents and seven other publications. In 1994 his industrial accomplishments were recognized by his alma mater where he was honored as a distinguished graduate. Since his formal retirement from Phillips and Chevron Phillips, Dr. Capshew has been serving as an independent contracting consultant in polyolefins to Chevron Phillips. His volunteer efforts have included work with the Society of Plastics Engineers, the American Chemical Society, and civic organizations, and he has spent many hours supporting various school athletic teams and "retired" after being a quarterback club president. He and his wife, Loni, have been married 38 years and have three children and three grandchildren.

Thomas E. Nowlin Thomas Nowlin received a B.S. in Chemistry from the University of Iowa in 1967, Ph.D. in Chemistry from Michigan State University 1971, and M.B.A. degree from Rutgers University in 1982. He was commisioned a second lieutenant in the USAR Chemical Corps in February 1971 and served two years active duty at Edgewood Arsenal from 1971 to 1973. He retired as a LTC from the USAR Chemical Corps in 1989 with 20 years of service. Dr. Nowlin was a research Chemist for Union Carbide Corporation from 1973 to 1979 in Bound Brook, New Jersey, and worked for Mobil Chemical Company, Edison, New Jersey, as a research chemist from 1980 to 2000. He investigated olefin polymerization catalysts from 1977 to 2000 and received over 50 U.S. patents for Mobil Oil Corporation, mostly in the area of Ziegler and metallocene catalysts for ethylene polymerization. He has published 20 papers in chemical journals from 1971 to 2000.

Robert I. Mink Robert I. Mink received his Ph.D. from the University of Illinois at Urbana and then held a postdoctoral fellowship at Cornell University. He has worked for Akzo Nobel and Mobil Chemical Company. His area of research has focused on the synthesis of ethylene and propylene polymerization catalysts. He holds over 40 U.S. patents in the area of polymerization catalysts and has co-authored publications related to polymerization catalysts and the chemical mechanisms in olefin polymerization reactions.

Yury V. Kissin Yury Kissin (born in 1937) received his degree in polymer chemistry in 1965 at the Institute of Chemical Physics in Moscow investigating α-olefin polymerization reactions with heterogeneous Ziegler–Natta catalysts. Since 1960 until 1977 he worked at the Institute of Chemical Physics studying kinetics of polymerization reactions of ethylene, propylene, and higher α-olefins and the structure of polyolefins and catalysts by infrared. He immigrated to the United States in 1979 and worked as a research associate first at Gulf Research and Development Company in Pittsburgh, Pennsylvanie (1980–1985), and then at Edison Research Center of Mobil Chemical Company, New Jersey (1985–2000). His main research subjects were synthesis of Ziegler–Natta catalysts, kinetics of polymerization and oligomerization reactions, and spectroscopic studies of polymerization catalysts. Since 2000 he is a visiting scientist at the Department of Chemistry of Rutgers University, New Jersey, where he studies kinetics of olefin polymerization reactions with Ziegler–Natta and late-period transition metal catalysts. He authored 3 books (*Isospecific Polymerization of Olefins*, Springer, 1985; *Polymers and Copolymers of Higher α-Olefins, Hanser*, 1997; *Alkene Polymerization Reactions with Transition Metal Catalysts*, Elsevier, 2008), 20 articles in chemical/polymer encyclopedias, approximately 200 scientific articles, and over 40 patents in the fields of synthesis of Ziegler–Natta and metallocene catalysts.

John Severn John Severn completed his Ph.D. in Organometallic Chemistry at the University of Sussex under the supervision of Professor M. F. Lappert in 1998. In 1999 he joined the group of Professor R. van Santen at Eindhoven University of Technology as a postdoc, working on the immobilization of α-olefin polymerization catalysts and the use of silsesquioxanes as homogeneous models. Then he joined the Dutch Polymer Institute in 2001, working with Dr. John Chadwick on the immobilization of single-site α-olefin polymerization catalyst, before joining Avantium Technologies B.V. in 2004, developing high-throughput experimentation (HTE) techniques for polyolefin catalysis. Since 2005 he has been with Borealis Polymer Oy, Finland, initially as a researcher and is currently task leader for single-site catalysis and HTE implementation within Borealis.

Robert L. Jones, Jr. Robert L. Jones started his studies at the University of Houston, completing graduate programs in both biology (M.Sc. 1979) and chemistry (M.Sc. 1990). In 1985 he joined the research team of Dr. John A. Ewen at Fina (LaPorte, Texas), where he synthesized ligand and metallocene complexes and performed polymerizations with commercial and experimental polyolefin catalysts. In 1990 he joined Himont (Lake Charles, Louisiana) as the plant polymer chemist specializing in ultrahigh molecular weight polyethylene (UHMWPE). In 1992 he moved into Himont R&D, working in the field of long-range catalyst research in Ferrara, Italy, at the Giulio Natta R&D Center, then Montell Polyolefins North American R&D Center in Elkton Maryland, and with Basell Polyolefines in Germany (Ludwigshafen and Frankfurt/Höchst). In 2005 he completed his doctorate at the Technical Universität Kaiserslautern under the direction of Professor H. Sitzmann. In 2007 he joined The Polymer Technology Group in Berkeley, California, where he is currently a staff scientist, designing and synthesizing polymers for biomedical application.

Sieghard E. Wanke Sieghard Wanke obtained his B.Sc. and M.Sc. in Chemical Engineering from the University of Alberta and a Ph.D. in Chemical Engineering from the University of California, Davis. He worked for Celanese, Canada and Celanese Research in New Jersey for two years in the area of heterogeneous catalysis. In 1970, he joined the Department of Chemical Engineering, now the Department of Chemical and Materials Engineering, at the University of Alberta as an assistant professor and he has been a professor since 1978; he served as the department chair for 14 years. His research areas are heterogeneous catalysis and reaction engineering with emphasis on supported metal catalysts and catalytic olefin polymerization.

Long Wu Long Wu graduated from Tianjin University with a B.Eng. in Polymer Science and Engineering in 1986. From 1986 to 1993, he conducted research on Ziegler–Natta catalysts and olefin polymerization at the Shanghai Research Institute of Chemical Industry. In 1999, he received a Ph.D. in Chemical Engineering from the University of Alberta, under the supervision of Drs.

David T. Lynch and Sieghard E. Wanke. He then remained in Dr. Wanke's group as a research associate. The main focus of his research at the University of Alberta has been on catalysis and reactor engineering, with a particular emphasis on morphology-controlled olefin polymerization.

Max P. McDaniel Dr. Max P. McDaniel received a Ph.D. in Physical Chemistry in 1973 from Northwestern University where he studied the porosity and redox capacity of chromia, followed by a year in Lyon, France, as a CNRS Chercheur Associé de Catalyse. McDaniel joined Phillips Petroleum Company in 1975 to work on Cr/silica catalysts under J. Paul Hogan, discoverer in 1951 of the Phillips polymerization catalyst and founder of the high-density polyethylene (HDPE) industry. McDaniel held various technical and leadership positions at Phillips (now Chevron-Phillips), always involved in its polyethylene catalyst, resin development, and licensing programs. An inventor of much of the Phillips catalyst technology, McDaniel has authored some 100 scientific publications and lectures and holds over 250 U.S. patents.

Kevin Cann Kevin Cann received his Ph.D. from the University of Texas at Austin. He joined Union Carbide Corporation in 1979 working in the polyolefin catalyst area. Since the merger with The Dow Chemical Company (2001), he has worked for Univation Technologies, which continues to license Unipol™ gas-phase polyethylene technology worldwide. His research areas have included development of Ziegler–Natta, chromium, and single-site catalysts for production of linear low-density polyethylene, high-density polyethylene, ethylene propylene diene monomer rubber (EPDM), and polybutadiene polymers in the fluid bed gas-phase process. He has over 35 U.S. patents and more than 30 publications and papers.

Scott Collins Professor Scott Collins was born and educated in Calgary, Alberta, Canada. He received his B.Sc. degree in 1979 and his Ph.D. in 1983, both from the University of Calgary, working with Thomas G. Back in the area of synthetic, organoselenium chemistry. He had a postdoctoral stay with Satoru Masamune at M.I.T., working on the synthesis of doubly bonded group 14 (Si, Ge, and Sn) compounds and bicyclic, tetrasilanes for a period of about 1½ years. He joined the Chemistry Department at the University of Waterloo in 1985, where he initiated a research program in asymmetric and polymerization catalysis using chiral, ansa-metallocene complexes. He was the first scientist in Canada to study metallocene-catalyzed olefin polymerization and cyclic olefin polymerization using metallocene catalysts, and his group also discovered group transfer polymerization of acrylates and methacrylates using zirconocene initiators. He held the Nova/Natural Sciences and Engineering Research Council Industrial Research Chair for a period of five years while at the University of Waterloo and was involved in the development of new, single-site group 4 catalysts for ethylene polymerization, novel anchoring technology for single-site catalysts, and the study of new cocatalysts and scavengers for single-site catalyst activation. He joined the faculty in the Department of

Polymer Science at The University of Akron in 2000 where he initiated work in Ni-catalyzed ethylene polymerization and cationic polymerization of isobutene using chelating diboranes, including the first aqueous suspension polymerization of isobutene. He will be leaving Akron to join the Instituto Universitario de Investigación de Catálisis Homogénea (IUCH) affiliated with the Universidäd de Zaragoza, España, in 2009.

Bernhard Rieger Bernhard Rieger obtained his Ph.D. in Chemistry at the Ludwig-Maximilians-Universität, Munich, in 1988. After a postdoctoral research at the University of Massachusetts at Amherst, Department of Polymer Science and Engineering, from 1988 till 1989, he joined the BASF Company from 1989 until 1991 for research about metallocene polymerizations. After his habilitation from 1991 until 1995 at the Eberhard-Karls-University in Tübingen, he was a professor at the University of Ulm from 1995 on as well as head of the Department of Materials and Catalysis until 2006. Since then he has been head of the WACKER Chair of Macromolecular Science at the Technische Universität, München. His main research interests are homogeneous polymerization catalysis, where numerous publications concern the alkene/CO copolymerization as well as silicon-containing polymers and self-assembled functional surface structures.

Timo M. J. Anselment Timo Anselment was born in Berlin in 1981, studied chemistry at the Technische Universität München, and obtained his Diploma Grade at the Chair of Macromolecular Chemistry of Professor Oskar Nuyken under the supervision of Dr. Rainer Jordan in 2006. He joined the staff of Professor Bernhard Rieger in 2007 at the WACKER Chair of Macromolecular Chemistry and is working on his Ph.D. thesis about phosphine–sulfonate complexes for alkene/CO copolymerizations.

Manuela Zintl Manuela Zintl majored in chemistry at the University of Ulm graduating in June 2003. She did her graduate work with Dr. Bernhard Rieger at Ulm. Since February 2008 she has been Scientific Content Manager with InfoChem GmbH, Munich, Germany. InfoChem is a software company specializing in chemical structure and reaction information.

Rüdiger Nowack Rüdiger Nowack attended the University of Ulm from 1998 to 2003 earning his diploma in June 2003. His dissertation for his Ph.D (2008) is titled "Neutral Nickel and Palladium Complexes as Catalysts in Copolymerizations of Polar and Non-Polar Monomers" and he also was a student of Professor Bernhard Rieger. Since October 2007 he has been Technical Sales Manager/Product Development with Zelu Chemid GmbH, a producer of polyurethane products in Murr, Germany.

Maria Leute Maria Leute graduated from the University of Ulm in 2003 with a chemistry major and "Mit Auszeichnung" (excellent) grade. Her Ph.D.

is also from the University of Ulm where she worked under Dr. Bernhard Rieger. (Thesis title: "Macromolecules with Phosphorus Functionalities"). She now has the position of R&D Manager with Wacker Chemie AG in Munich, Germany.

Anna Maria Raspolli Galletti Anna Maria Raspolli Galletti graduated from the University of Pisa, Italy, in Industrial Chemistry. She obtained her Ph.D. in Chemical Sciences in 1986. Since 2000 she has been an associate professor of industrial chemistry at the University of Pisa. Her main research topic is applied catalysis, in particular polymerization and oligomerization catalysis, catalytic copolymerization of olefins with polar monomers, synthesis of nanostructured catalysts and their industrial application, and catalytic conversion of renewable products in fine chemicals. At the present time her interest is also devoted to the use of microwaves irradiation for catalyst synthesis and for catalytic reactions. She has scientific collaborations with many Italian and European universities and industries. She co-authored more than 100 papers in peer review journals, 16 patents, and 3 books and made more than 100 symposium presentations.

Robert T. Mathers Robert Mathers received his Ph.D. in Polymer Science from The University of Akron in 2002 under the direction of Professor Roderic P. Quirk. After two years of postdoctoral research at Cornell with Professor Geoffrey W. Coates in the Department of Chemistry and Chemical Biology, he joined Pennsylvania State University. Since 2004, he has been an assistant professor of chemistry at the New Kensington campus. His research interests focus on integrating renewable resources and catalysis for polymer synthesis.

Ray Hoff Ray Hoff graduated from Beloit College in Wisconsin with a B.S. in Chemistry in 1956, and immediately began research work on phenol-formaldehyde resins at the Westinghouse Research Center in Churchill Borough, Pennsylvania. In 1964 he obtained a Ph.D. in Organic Chemistry from the University of Utah and began work at the B.F. Goodrich Research Center in Brecksville, Ohio. He was primarily involved with synthetic rubber projects using cobalt Ziegler–Natta catalysts and aklylithium anionic initiators. From 1967 to 1993 he was engaged in ethylene polymerization catalyst work with Chemplex Company and its successors. The main catalyst types were Phillips thermally-activated chromium catalysts and magnesium-modified Ziegler catalysts. Since 1993 he has worked as a consultant and chemistry teacher, most recently as adjunct faculty with Roosevelt University, Schaumburg, Illinois.

He is an inventor for 29 United States patents and author of 11 journal articles.

Gregory W. Kamykowski Dr. Kamykowski received a BS in Chemistry from Loyola University, Chicago and a PhD in Physical Chemistry from the University of Wisconsin, where he studied under Professor John D. Ferry. He has had a number of industrial positions, including Chemplex Company in Rolling Meadows, Illinois, L. J. Broutman & Associates in Chicago, and Morton International in Woodstock, Illinois.

Currently he is a Senior Application Scientist for rheology for TA Instruments with an office in Schaumburg, Illinois. He has lectured on rheology in many locations including Roosevelt University in Schaumburg.

Dr. Kamykowski is a member of the Society of Rheology, the Society of Plastics Engineers, and American Society for Testing and Materials.

1 Commercially Available Metal Alkyls and Their Use in Polyolefin Catalysts

DENNIS B. MALPASS
Akzo Nobel Polymer Chemicals (retired), Magnolia, Texas 77354

1.1 INTRODUCTION

Organometallics are defined as compounds that contain a *direct* carbon–metal bond. Such compounds may be regarded as the interface between organic and inorganic chemistry. There are two basic types of organometallics: metallocenes and metal alkyls. Metallocenes contain a carbon–metal *pi* (π) bond and most often involve transition metals from groups 3–11 of the periodic table and aromatic ligands such as cyclopentadienyl ("Cp") or indenyl.[1,2] Metal alkyls are defined as organometallic compounds containing a carbon-to-metal *sigma* (σ) bond.

Metal alkyls are essential to the performance of industrial Ziegler–Natta (ZN) catalysts and most single-site catalysts (SSCs that do not require cocatalysts were recently reported[3] but are not yet in industrial use). This chapter will stress practical aspects of metal alkyls, particularly those used with transition metal polyolefin catalysts. We will answer questions such as:

- What are the distinguishing properties of metal alkyls?
- Which are the commercially important metal alkyls?
- How do metal alkyls function in polyolefin catalyst systems?
- What are the impurities in commercial metal alkyls and how do these impurities influence catalyst performance?
- What selection criteria are used for metal alkyls in polyolefin catalyst systems?

Handbook of Transition Metal Polymerization Catalysts Edited by Ray Hoff and Robert T. Mathers
Copyright © 2010 John Wiley & Sons, Inc.

Key synthetic chemistries will be mentioned but are not discussed in depth. Detailed reviews of production, properties, and applications of metal alkyls are available elsewhere.[4–12]

In manufacture of polyolefins, the most important metal alkyls are those of aluminum and magnesium. Other organometallics are employed in production of polyolefins but in much smaller quantities. These include organometallic compounds containing boron and zinc and a range of metallocenes. First-generation supported chromium catalysts ("Phillips catalysts") do not require metal alkyls.[13] However, performance of some chromium catalysts developed in the 1970s–1980s is improved by metal alkyls.[13,14] Metallocenes will not be discussed in detail in this chapter but will be addressed in the context of SSCs in subsequent chapters.

Note that the definition of organometallics excludes compositions such as metal alkoxides, metal carboxylates, and chelated metal complexes involving nitrogen and phosphorus, since there is an intervening heteroatom between the carbon and the metal. Hence, many nonmetallocene SSCs based on late transition metals[15,16] are not technically organometallic compounds, though active centers are believed to contain direct metal–carbon σ bonds.

1.2 METAL ALKYLS IN ZIEGLER–NATTA CATALYSTS

Aluminum alkyls and magnesium alkyls fulfill several roles in ZN polymerization catalyst systems. The two most important are as raw materials for catalyst synthesis and as cocatalysts (sometimes called "activators") for the transition metal catalyst. These key functions are illustrated in simplified equations below.

- *Metal alkyls in catalyst synthesis:* Reduction of the transition metal "precatalyst," exemplified below with titanium tetrachloride and ethylaluminum sesquichloride (EASC):

$$2TiCl_4 + 2(C_2H_5)_3Al_2Cl_3 \rightarrow 2TiCl_3\downarrow + 4C_2H_5AlCl_2 + C_2H_4 + C_2H_6 \quad (1.1)$$

  Production of a support, as shown in Eq. 1.2 with a dialkylmagnesium compound and anhydrous HCl:

$$R_2Mg + 2HCl \rightarrow MgCl_2\downarrow + 2RH\uparrow \quad (1.2)$$

- *Metal alkyls as cocatalysts:* Alkylation of the reduced transition metal compound to produce active centers for polymerization, illustrated below with triethylaluminum (TEAL) and $TiCl_3$:

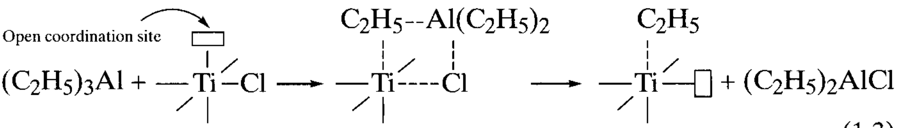

(1.3)

Aluminum alkyls also serve the purpose of scavenging catalyst poisons (water, O_2, etc.). Poisons enter as parts-per-million (ppm) contaminants in materials commonly used in polyolefin processes such as monomer, comonomer, solvents, and chain transfer agents. Reaction of the aluminum alkyl with contaminants generates alkylaluminum derivatives that are not as damaging to catalyst performance. For example, water reacts with TEAL to produce small amounts of ethylaluminoxane:

$$2(C_2H_5)_3Al + H_2O \rightarrow (C_2H_5)_2Al{-}O{-}Al(C_2H_5)_2 + 2C_2H_6\uparrow \qquad (1.4)$$

Typically, aluminum alkyls are used in large excess in ZN catalyst systems. Aluminum–titanium ratios of 20–40 are common in industrial polyethylene processes. Hence, there is ample TEAL to fulfill the roles discussed above. Aluminum alkyls also are involved in chain transfer, but this is a minor function. (Hydrogen is used most often for chain transfer/termination reactions with modern ZN catalysts.)

Aluminum alkyls are preferred as cocatalysts because other metal alkyls are either too expensive or perform poorly. When tried as cocatalysts, magnesium alkyls may completely deactivate ZN catalysts. The reason for this is unknown, but it may stem from overreduction of the transition metal or blockage of active centers caused by strong coordination of magnesium alkyl. Use of zinc alkyls often lowers catalyst activity and reduces polymer molecular weight by acting as a chain transfer agent.

The vast majority of modern ZN catalysts employ aluminum alkyls as cocatalysts, while magnesium alkyls are used solely as raw materials for the production of catalysts.

1.3 ALUMINUM ALKYLS

The term "aluminum alkyl" is meant to include any compound that contains an alkylaluminum grouping and encompasses R_3Al, R_2AlCl, $R_3Al_2Cl_3$ (the so-called sesquichlorides), $RAlCl_2$, R_2AlOR', and R_2AlH. Among commercially available aluminum alkyls, R is typically a C_1–C_4 alkyl. Methylaluminoxanes are also aluminum alkyls and have become important in recent years as cocatalysts for SSCs. However, methylaluminoxanes exhibit significantly different properties than conventional aluminum alkyls and will be discussed separately (see Section 1.5).

Aluminum alkyls have been produced commercially since 1959 using technology originally licensed by Nobel laureate Karl Ziegler.[9] Aluminum alkyls are pyrophoric and violently reactive with water.[4,6,12] Considering these properties, it is remarkable that millions of pounds of aluminum alkyls are produced each year and have been supplied to the polyolefin industry worldwide for half a century with relatively few safety incidents.

Principal aluminum alkyls available in the merchant market (and their common acronyms) are provided in Table 1.1. Typical properties of commercially available aluminum alkyls are summarized below:

- Most ignite spontaneously when exposed to air and are explosively reactive with water. (Please see the appendix for a discussion of pyrophoricity of metal alkyls.)
- Aluminum alkyls are typically clear, colorless liquids at ambient temperature and are miscible in all proportions with aliphatic hydrocarbons (HCs). Large quantities of aluminum alkyls are supplied as solutions in HCs, because solutions are *perceived* to be safer.
- R_3Al compounds (R = ethyl or higher) contain small amounts of R_2AlH. Hydride content is expressed as AlH_3 by tacit convention among major suppliers and typically ranges from about 0.02% (wt) in TEAL to about 0.5% in triisobutylaluminum (TIBAL).

R_3Al compounds also commonly contain small amounts of other trialkylaluminum compounds (R'_3Al). This is usually a consequence of the purity of starting materials or of side reactions during manufacture, such as addition of an ethylaluminum moiety in TEAL across ethylene to produce an *n*-butylaluminum group (Figure 1.1).

R'_3Al contents are low, often <0.5% (by wt). An exception is TEAL where *n*-butylaluminum content (from the reaction above, expressed as tri-*n*-butylaluminum) is typically ~5%.

In the vast majority of ZN catalyst systems, hydride content and the presence of small amounts of other trialkylaluminum compounds (R'_3Al) are not damaging to performance. However, for certain polypropylene (PP) catalysts that employ alkoxysilanes as external donors, hydride can cause a reduction in isotactic content and lowered catalyst activity.[51] Additional tests with TEAL containing up to 16% R'_3Al with a modern supported PP catalyst showed no loss of isotacticity and no loss of activity.[51]

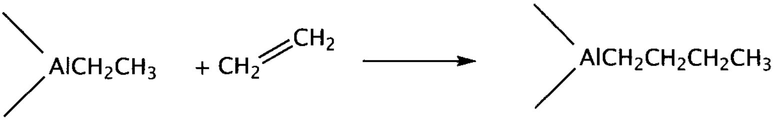

Figure 1.1 Insertion of ethylene into an ethyl group–aluminum bond to form butylaluminum.

TABLE 1.1 Principal Commercially Available Aluminum Alkyls

Product	Acronym	Formula	CAS Number	Theoretical wt % Al
Trimethylaluminum	TMAL	$(CH_3)_3Al$	75-24-1	37.4
Dimethylaluminum chloride	DMAC	$(CH_3)_2AlCl$	118-58-3	29.2
Methylaluminum sesquichloride	MASC	$(CH_3)_3Al_2Cl_3$	12542-85-7	26.3
Triethylaluminum	TEAL	$(C_2H_5)_3Al$	97-93-8	23.6
Diethylaluminum chloride	DEAC	$(C_2H_5)_2AlCl$	96-10-6	22.4
Diethylaluminum iodide	DEAI	$(C_2H_5)_2AlI$	2040-00-8	12.7
Ethylaluminum sesquichloride	EASC	$(C_2H_5)_3Al_2Cl_3$	12075-68-2	21.8
Ethylaluminum dichloride	EADC	$C_2H_5AlCl_2$	563-43-9	21.3
Isobutylaluminum dichloride	MONIBAC[a]	$i\text{-}C_4H_9AlCl_2$	1888-87-5	17.4
Tri-*n*-butylaluminum	TNBAL	$(C_4H_9)_3Al$	1116-70-7	13.6
Triisobutylaluminum	TIBAL	$(i\text{-}C_4H_9)_3Al$	100-99-2	13.6
Diisobutylaluminum hydride	DIBAL-H	$(i\text{-}C_4H_9)_2AlH$	1191-15-7	19.0
Tri-*n*-hexylaluminum	TNHAL	$(C_6H_{13})_3Al$	1116-73-0	9.6
Tri-*n*-octylaluminum	TNOAL	$(C_8H_{17})_3Al$	1070-00-4	7.4
Di-*n*-octylaluminum iodide	DNOAI	$(C_8H_{17})_2AlI$	7585-14-0	7.1
"isoprenylaluminum"	IPRA	Not available	70024-64-5	Not available
Diethylaluminum ethoxide	DEAL-E	$(C_2H_5)_2AlOC_2H_5$	1586-92-1	20.7
Ethylpropoxyaluminum chloride	EPAC	$(C_2H_5)(C_3H_7O)AlCl$		17.9
Diisobutylaluminum butylated oxytoluene	DIBAL-BOT	$(i\text{-}C_4H_9)_2AlO[C_6H_2(CH_3)(t\text{-}C_4H_9)_2]$	56252-56-3	7.5

Note: IPRA: Also called ISOPRENYL. Complex composition produced by reaction of isoprene (2-methyl-1,3-butadiene) with TIBAL or DIBAL-H. DIBAL-BOT: Also called diisobutylaluminum 2,6-di-*t*-butyl-4-methylphenoxide; produced by equimolar reaction of TIBAL with BHT.

[a] MONIBAC: Acronym from "monoisobutylaluminum dichloride."

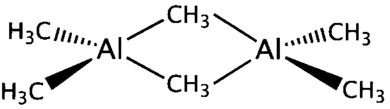

Figure 1.2 Trimethylaluminum dimer.

Aluminum alkyls also contain ppm amounts of aluminoxanes and alkoxides resulting from reaction with water (see Eq. 1.4 and oxygen, respectively. Water and oxygen enter as contaminants (typically <5 ppm) in process materials, for example, nitrogen, ethylene, and hydrogen. Aluminoxanes and alkoxides are usually undetectable (below 500 ppm) and, at these levels, cause no problems in polyolefin catalyst systems.

Total assays are not routinely conducted on commercially available aluminum alkyls. Since impurities mentioned above are also organometallics, total organometallic content of commercially available metal alkyls will typically exceed 99%. The balance is mostly process oils (a purified white mineral oil is used as lubricant and in agitator seals) and small amounts of solvents (mostly C_6–C_8 aliphatic HC) used to wash reactors and process lines.

- Aluminum alkyls are highly reactive with many of the common organic solvents. Indeed, reaction with halogenated hydrocarbons (CCl_4, $CHCl_3$, etc.) may be explosive after a quiescent period.[17] Organic compounds with acidic protons, such as alcohols and carboxylic acids, may be violently reactive with aluminum alkyls. Carbonyl compounds, such as ketones, aldehydes, and esters, react with aluminum alkyls. Ethers and tertiary amines form exothermic coordination complexes.
- R_3Al are reactive with CO_2.[18] In fact, reaction of trimethylaluminum (TMAL) with CO_2 has been used to produce methylaluminoxane cocatalysts for SSCs[19–21] (see Section 1.5.3). The R_3Al/CO_2 reaction is easily controlled and has been used to passivate aluminum alkyl waste streams.[22] However, R_3Al are unreactive with CO. Aluminum alkyls containing halogen or oxygen (DEAC, DEAL-E, etc.) are not reactive with CO_2.
- Lower molecular weight aluminum alkyls (C_1, C_2, and isoC_4) are distillable under vacuum. However, higher homologs (n-C_4 to n-C_8) are not distillable in industrial process equipment and are purified by filtration.
- Most trialkylaluminum compounds are associated as dimers, except when steric bulk of alkyl groups (*t*-butyl, isobutyl, etc.) prevents association. For example, TMAL associates via three center–two electron bonding[24] (also called "electron-deficient" bonding[25]) as depicted in Figure 1.2.
- At low temperature, proton nuclear magnetic resonance (NMR) spectra of TMAL show separate signals for terminal and bridging methyls. However, at room temperature, rapid alkyl exchange occurs and methyls are indistinguishable by NMR.

- Halogenated and oxygenated aluminum alkyls are even more strongly associated, most often as dimers. Heteroatom-containing ligands assume bridging positions. This may be exemplified by DEAL-E, which is dimeric with dative bonds between oxygen and an adjacent aluminum (Figure 1.3).
- In general, aluminum alkyls are stable indefinitely if stored properly (under dry inert gas and away from heat). Storage stability of aluminum alkyls may be illustrated anecdotally. At the aluminum alkyl manufacturing site formerly known as Texas Alkyls (now Akzo Nobel), a small carbon steel cylinder of DEAC was returned after having been stored unopened for 10 years in a customer's laboratory. The product was sampled and analyzed. The DEAC was still clear (free of particulates), though it had a faint amber tint after 10 years. Within analytical variance, aluminum and chloride contents and the hydrolysis gas composition were essentially unchanged.
- Aluminum alkyls demonstrate moderate to excellent thermal stability, depending on ligands. Thermal stability is especially important for aluminum alkyls used in solution processes for polyethylene since these often operate at >190 °C. Table 1.2 provides thermal stability data on selected aluminum alkyls. Lower R_3Al's decompose slowly at elevated temperatures, but thermal stability diminishes as chain length or branching increases. While quality may be lowered, violent decomposition does not occur. *An exception is TMAL, which undergoes potentially hazardous self-accelerating decomposition above* 120 °C*. Decomposition of TMAL is highly exothermic and is accompanied by generation of large amounts of methane.*[23] *If confined, an explosion could result.* Thermal decomposition of aluminum alkyls typically occurs by β-hydride elimination, exemplified in Figure 1.4 with TIBAL. Aluminum alkyls that contain ligands with halogen or oxygen are more stable thermally than the analogous R_3Al compounds. While TEAL begins to decompose at ~120°C, DEAC is stable up to 174 °C and DEAL-E up to 192 °C.

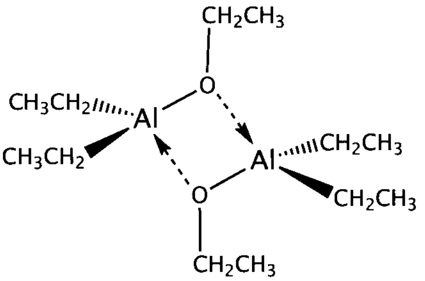

Figure 1.3 Dimer structure of diethylaluminum ethoxide.

TABLE 1.2 Thermal Decomposition Data of Selected Aluminum Alkyl Compounds

Product	Decomposition Temperature (°C)[a]	% Decomposed (3 h at 180 °C)
Triethylaluminum	120	64
Tri-*n*-butylaluminum	100	87
Triisobutylaluminum	50	92
Tri-*n*-octylaluminum	60	90
Diethylaluminum chloride	174	2
Diisobutylaluminum chloride	165	4
Diethylaluminum ethoxide	192	0

[a] Estimated temperature at which decomposition is first observed in inert atmosphere.

Source: Data from G. Sakharovskaya, N. Korneev, N. Smirnov, and N. Popov, *J. Gen. Chem. USSR*, 44, 560 (1974).

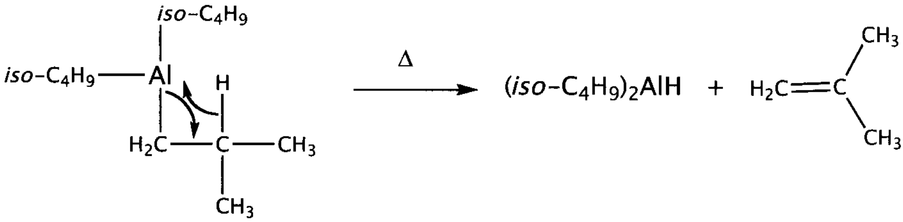

Figure 1.4 Decomposition of triisobutylaluminum.

1.4 PRICING AND SELECTION CRITERIA FOR ALUMINUM ALKYLS

In the early history of ZN catalysts, chlorinated aluminum alkyls such as DEAC and EASC were the most important and functioned as both reducing agents and cocatalysts. They were readily available and relatively inexpensive and performed well with first-generation ZN catalysts. However, as supported ZN catalysts began to emerge in the 1970s, TEAL supplanted EASC and DEAC because TEAL performed better. TEAL remains today the largest volume aluminum alkyl. Many millions of pounds are sold each year to the global polyolefin industry.

As usual, cost is a primary consideration in selecting an aluminum alkyl. Commercial prices for aluminum alkyls are currently between about \$5 and \$10 per pound but can be higher for "specialty" products such as TMAL, DEAI, and isoprenylaluminum (IPRA). The latter products require either multistep processes and/or expensive raw materials, for example, elemental iodine. Detailed current pricing for aluminum alkyls may be obtained from major commercial suppliers listed below:

- Akzo Nobel (formerly Texas Alkyls)
- Albemarle (formerly Ethyl Corp.)
- Chemtura (formerly Crompton, Witco, and Schering)

Though DEAC and EASC remain less costly than TEAL, they are not typically used with supported catalysts because they perform poorly. For example, they may cause lower catalyst activity or reduced stereoregularity in polypropylene. They also leave chloride-containing residues in the polymer that can corrode equipment or degrade the polymer.

TIBAL is a commercially available R_3Al that performs comparably to TEAL with many ZN catalysts and is slightly lower in price (per pound) than TEAL. So, why is TIBAL not the number one selling aluminum alkyl? The reason is that, if other factors are equal, polyolefin manufacturers buy on the basis of *contained* aluminum. Since TEAL contains about 70% more aluminum than TIBAL on a molar basis, TIBAL actually costs *more* than TEAL based on aluminum content. This can be illustrated as follows: Assume that a world-scale LLDPE manufacturing facility uses 200,000 pounds per year of TEAL as cocatalyst and that TIBAL and TEAL perform equally (at the same Al/Ti) in the process. Assume further that the price of each is $10/pound. This amounts to an annual TEAL cost of $\$2.00 \times 10^6$. The amount of contained aluminum in 200,000 pounds of TEAL (typical Al content of 23.2%) is 46,400 pounds. However, the amount of TIBAL (typical Al content of 13.6%) needed to obtain 46,400 pounds of aluminum is about 341,000 pounds or an annual cost of $\$3.41 \times 10^6$. Hence in this illustration, the annual cost advantage of TEAL relative to TIBAL amounts to $\$1.4 \times 10^6$.

As mentioned above, selection of cocatalyst is often dictated by cost. In some cases, however, advantages of an alternative cocatalyst transcend the cost factor. This could be because the alternative cocatalyst provides better process performance (higher catalyst activity, improved kinetic profile, etc.) or enhanced polymer properties. For example, use of TMAL as cocatalyst in place of TEAL in a gas-phase linear low-density polyethylene (LLDPE) process provides product with lower extractables and improved film tear strength.[26] Use of IPRA as cocatalyst can result in ultrahigh molecular weight polyethylene (PE) with broader molecular weight distribution (MWD).[27,28] (IPRA is a complex composition[29] produced by reaction of TIBAL or DIBAL-H with 2-methyl-1,3-butadiene, also known as isoprene.) Enhanced properties can translate into superior polymer performance and such resins command higher prices, thereby overcoming the increased cost of cocatalyst.

1.5 METHYLALUMINOXANES

1.5.1 Conventional Methylaluminoxane

Conventional methylaluminoxane is produced by partial hydrolysis of TMAL in toluene. Reaction must be closely controlled. Unfortunately, explosions and serious injuries have been reported during preparations of methylaluminoxane. Water must be introduced at low temperature and in forms that moderate the potentially violent reaction. Water has been introduced as hydrated salts, ice shavings, or atomized spray. Even with these precautions, explosive reactions have occurred. In most cases, polyolefin producers leave synthesis of methylaluminoxane to aluminum alkyl manufacturers to obviate handling the highly pyrophoric TMAL and attempting to control its reaction with water. A simplified overall reaction is given as

$$x(CH_3)_3Al + xH_2O \rightarrow \sim(CH_3AlO)_x\sim + 2xCH_4\uparrow \qquad (1.5)$$

Yields are low (usually <60%). The toluene-soluble product is called methylaluminoxane (MAO) or, less commonly, polymethylaluminoxane (PMAO). MAO has been offered commercially since the late 1980s. Recently, improved commercial processes with much higher yields have been developed.[61]

Though MAO was reported to be an excellent cocatalyst for metallocene SSC by Kaminsky, Sinn, and co-workers[52] in the late 1970s and has been the subject of intense study since then, its precise composition remains poorly understood. Typical properties of commercially available MAO are summarized below:

- As isolated from toluene solution, neat MAO is an amorphous, friable white solid containing 43–44% Al (theory 46.5%). It is virtually insoluble in aliphatic hydrocarbons but has excellent solubility in aromatic hydrocarbons. MAO is supplied commercially as a toluene solution containing ~13% Al, which corresponds to ~28% concentration of MAO. Like most commercially available aluminum alkyls, it is pyrophoric and explosively reactive with water.
- Differential scanning and accelerating rate calorimetry (DSC, ARC) studies have shown MAO to be thermally stable at least up to about 220 °C.[23] MAO decomposes exothermically without melting above ~220 °C.
- Commercially available MAO contains residual TMAL (15–30%), called "free TMAL" or "active aluminum." Both reductions and increases in SSC activity have been said to occur because of free TMAL.[30–32]
- Gas chromatographic (GC) analysis of hydrolysis gas from MAO typically shows >99% methane. The balance is mostly ethane.
- Proton NMR analysis suggests that the CH_3/Al in MAO is about 1.4.[33] Measurement of the volume of methane generated upon hydrolysis will always show higher CH_3/Al (typically 1.6–1.8) because of free TMAL.
- MAO is not distillable. However, if MAO is subjected to vacuum distillation conditions, some of the so-called free TMAL will distill.[19,33]
- Storage stability of MAO solutions is poor.[19–21,33] Freshly prepared MAO solutions form gels within a few days when stored at ambient temperatures (>20 °C). Lower storage temperatures (0–5 °C) delay gel formation.

Consequently, MAO manufacturers store and transport molecular weights (MAO) solutions in refrigerated containers.

- Published data on MAO isolated from toluene have shown a wide range of molecular weights (MWs) (300–3000 amu, primarily using cryoscopic methods). Possible reasons for the irreproducibility were proposed by Beard et al., who showed that cryoscopic MW measurements of commercially available MAO are influenced by several variables, such as process oils, residual solvent (toluene), and TMAL content.[33] Beard reported "corrected" cryoscopic MWs of about 850, suggesting x in Eq. 1.5 to be about 15.

Perhaps the most important drawback of MAO is its cost (see Section 1.5.5), which is substantially higher than conventional aluminum alkyls (10–20 times). Despite its high cost and untoward features, MAO remains the most widely used cocatalyst for SSC.

1.5.2 Modified Methylaluminoxanes

Modified methylaluminoxanes (MMAOs) have been offered commercially since the early 1990s. MMAO[34] is a generic term encompassing all products wherein some of the methyl groups are replaced by other alkyl groups, usually isobutyl or *n*-octyl. All MMAOs contain >65% methyl groups and, as such, remain predominantly MAO.

Most MMAOs are prepared by reaction with water, as previously shown for MAO. However, the process for MMAOs permits the more controllable reaction of R_3Al with water *before* the TMAL/water reaction is attempted.[34] It is suggested that a coordination complex forms between TMAL and preformed alkylaluminoxane, resulting in a more moderate reaction of TMAL with water. This sequence of reactions is depicted as

$$2R'_3Al + H_2O \rightarrow R'_2AlOAlR'_2 + 2R'H \tag{1.6a}$$

$$(CH_3)_3Al + R'_2AlOAlR'_2 \rightarrow (CH_3)_3Al{\leftarrow}O{-}(AlR'_2)_2 \tag{1.6b}$$

$$(CH_3)_3Al{\leftarrow}O{-}(AlR'_2)_2 + H_2O \rightarrow \sim\!(RAlO)\!\sim + RH \tag{1.6c}$$

where R is 65–95% methyl and the balance R′.

There are several versions of MMAOs (differentiated by a suffix, e.g., MMAO-3A), each with different composition and properties (See Table 1.3.). One (MMAO-7) is produced by a nonhydrolytic method (described below). Another (MMAO-12) contains ~95% methyl groups and is the MMAO that most closely approximates MAO.

Relative to conventional MAO, MMAOs exhibit much improved storage stability and some are highly soluble in aliphatic hydrocarbons. (Manufacturers of PE prefer to avoid toluene because of toxicity concerns, especially if

TABLE 1.3 Commercially Available Alkylaluminoxane Compounds

Product	Acronym	Approximate Formula	wt % Al[a]	Comment
Methylaluminoxane	MAO	$-((CH_3)AlO)_x-$	46.5	Also called PMAO, available only in toluene solution
Polymethylaluminoxane improved performance	PMAO-IP	$-((CH_3)AlO)_x-$	46.5	Product by nonhydrolytic process, available only in toluene solution
Modified methylaluminoxane, type 3A	MMAO-3A	$-((CH_3)_{0.7}(i\text{-}C_4H_9)_{0.3})AlO)_x-$	38.2	Available in heptane
Modified methylaluminoxane type 7	MMAO-7	$-((CH_3)_{0.86}(n\text{-}C_8H_{17})_{0.14})AlO)_x-$	37.6	Produced via nonhydrolytic process, available in Isopar E™
Modified methylaluminoxane, type 12	MMAO-12	$-((CH_3)_{0.95}(n\text{-}C_8H_{17})_{0.05})AlO)_x-$	42.9	Available only in toluene
Isobutylaluminoxane, type 65	IBAO-65	$-((i\text{-}C_4H_9)AlO)_x-$	27.0	Available only in hydrocarbon solution, O/Al ~0.65
Bis(diisobutylaluminum)oxide	DIBAL-O	$(i\text{-}C_4H_9)_2AlOAl(i\text{-}C_4H_9)_2$	18.1	Available only in hydrocarbon solution, O/Al ~0.50

Notes: (1) Chemical Abstracts Service registry numbers, reading down: 120144-90-3, 206451-90-3, 146905-79-5, 206451-54-9, 206-54-9, 220326-29-4, 998-00-5. (2) Isopar E™ is a trade name of Exxon Mobil Corporation for an aromatics-free hydrocarbon liquid mixture, boiling range 114–140 °C. (3) DIBAL-O is also known as tetraisobutydilaluminoxane (TIBAO).

resins are destined for food contact.) Most importantly, because yields are higher, MMAO formulations are less costly than MAO. However, since MMAOs contain other types of alkylaluminoxanes, they do not duplicate performance of standard MAO in many SSC systems. Consequently, MMAOs should be considered niche cocatalysts for SSCs.

1.5.3 Nonhydrolytic Methylaluminoxanes

A nonhydrolytic method has been reported[19–21] for production of MAOs suitable as cocatalysts for SSCs. This alternative synthesis avoids altogether the hazardous reaction of TMAL with water and affords essentially quantitative recovery of aluminum values. Because the product provides higher activity in a standard ethylene polymerization test using *rac*-ethylenebis(indenyl)zirconium dichloride, it was dubbed PMAO-IP (from polymethylaluminoxane-improved performance).

Though many precursors may be used, the simplest method involves reaction of CO_2 with TMAL to form an intermediate. Subsequent pyrolysis produces PMAO-IP. The detailed chemistry is complex and involves evolution of methane and other hydrocarbons, including products resulting from Friedel–Crafts reactions with toluene. A simplified equation is

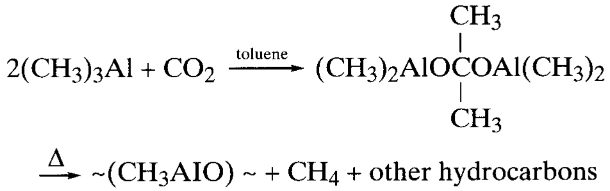

$$2(CH_3)_3Al + CO_2 \xrightarrow{\text{toluene}} (CH_3)_2AlO\overset{CH_3}{\underset{CH_3}{C}}OAl(CH_3)_2 \qquad (1.7)$$

$$\xrightarrow{\Delta} \sim(CH_3AlO)\sim + CH_4 + \text{other hydrocarbons}$$

Reactant proportions are chosen such that the O/Al in PMAO-IP is ~0.8,[20] as it is in conventional MAO.[33] PMAO-IP contains much lower free TMAL than hydrolytic MAO, which may explain the higher activity with selected SSCs. It appears to be especially effective in solution processes for polyethylene. However, performance of PMAO-IP does not extend across the entire range of SSCs and it cannot be considered a "drop-in" replacement for conventional MAO.

1.5.4 Other Alkylaluminoxanes

Other alkylaluminoxanes are also available, more easily produced and less costly than MAO. Ethylaluminoxane (EAO; see Eq. 1.4) and isobutylaluminoxane (IBAO) have been used industrially since 1970 in catalyst systems for polymerization and copolymerization of epichlorohydrin to produce elastomers.[35] However, EAO and IBAO perform poorly as cocatalysts for SSCs. Preparation and properties of alkylaluminoxanes have been extensively reviewed.[32,36,37]

Alkylaluminoxanes have been shown to exist as highly associated oligomeric, cage, or cluster structures.[38,39] Barron et al., prepared *t*-butylaluminoxane (TBAO) by equimolar direct hydrolysis of tri-*t*-butylaluminum at −78 °C followed by thermolysis. TBAO was found to be primarily hexameric and nonameric, though some higher aggregates were also observed. Barron and co-workers proposed a nonameric cluster structure for MAO wherein aluminum is exclusively tetracoordinate.[40] IBAO, a commercially available alkylaluminoxane isomeric with TBAO, has been shown to have a cryoscopic MW of approximately 950,[41] in agreement with nonameric association.

1.5.5 Why Are MAOs So Costly?

All commercially available MAOs employ TMAL as the starting material. Because TMAL must be manufactured by less efficient processes,[23] it is much more expensive than other R_3Al compounds. This, coupled with low yields of MAO from typical processes for hydrolysis of TMAL, translates to very high costs for MAOs. Additionally, MAOs must be used in huge excess in many SSC systems, further increasing the cost. (Ratios of Al to transition metal >100 are common.) Even though nonhydrolytic MAO and the various MMAOs are obtained in higher yields than MAO, they are also derived from TMAL and remain very expensive relative to conventional aluminum alkyls. Commercially available alkylaluminoxanes are listed in Table 1.3.

1.5.6 Pricing and Selection Criteria of MAOs

Unlike conventional aluminum alkyls, MAOs are supplied only in solution. When MAO became widely available in the early 1990s, pricing methods for solutions of MAO were not consistent. Suppliers used different pricing based upon $/wt of contained Al, $/wt of the calculated amount of contained MAO, or $/wt of solution. Calculations below demonstrate a method of converting prices to a common basis so that direct comparisons may be made.

Assume that three suppliers provide the following pricing for 5000 pounds of a toluene solution of MAO containing 13.3% Al (the typical concentration of commercially available MAO):

Supplier X: $150/lb of contained Al
Supplier Y: $100/lb of contained MAO
Supplier Z: $35/lb of MAO solution

Pricing by supplier X uses the amount of aluminum supplied to the customer as determined by an accurate analytical method. Hence, the cost of MAO from supplier X would be

$$5000\,\text{lb} \times 0.133 \times \$150/\text{lb of contained Al} = \$99{,}750$$

Supplier Y would calculate that the solution containing 13.3% Al corresponds to a 28.6% solution of MAO using the theoretical amount of aluminum in "pure" MAO (46.5%). The cost of MAO from supplier Y would then be calculated as

$$5000\,\text{lb} \times (0.133/0.465) \times \$100/\text{lb of contained MAO} = \$143{,}011$$

The cost of MAO from supplier Z is calculated straightforwardly using the total weight of solution:

$$5000\,\text{lb} \times \$35/\text{lb of MAO solution} = \$175{,}000$$

Ultimately, performance of the MAO in the specific customer application is the most important criteria for selection. A low price is of little value if performance is poor. Since polyolefin manufacturers use different SSCs and processes, each must select the MAO that provides acceptable performance at the most attractive price. This is usually determined through laboratory and pilot plant evaluations.

1.6 MAGNESIUM ALKYLS

1.6.1 Properties of Magnesium Alkyls

Impetus for using magnesium alkyls in ZN catalyst synthesis was provided by the discovery that magnesium salts, especially $MgCl_2$,[42] are excellent supports for ZN catalysts. Magnesium alkyls encompass both Grignard reagents (organomagnesium halides, RMgX) and dialkylmagnesium compounds (R_2Mg). The two are linked by the so-called Schlenk equilibrium:

$$2RMgX \rightleftarrows R_2Mg + MgX_2 \tag{1.8}$$

Grignard reagents are produced by reaction of an alkyl halide with magnesium metal in an ether, usually diethyl ether or tetrahydrofuran. Detailed discussions of the Schlenk equilibrium and preparation and properties of Grignard reagents and R_2Mg compounds are beyond the scope of this text, but excellent reviews are available.[43,44] A survey of processes for commercially available dialkylmagnesium compounds is also available.[46]

Dialkylmagnesium compounds have been shown to be highly associated in linear structures wherein magnesium atoms are tetracoordinate as depicted in Figure 1.5.

The α-carbon atom in each R bridges adjacent magnesium atoms *via* three center–two electron bonding,[24] mentioned previously in the discussion of TMAL association. Because n is very large for simple R_2Mg ($R = CH_3$ to

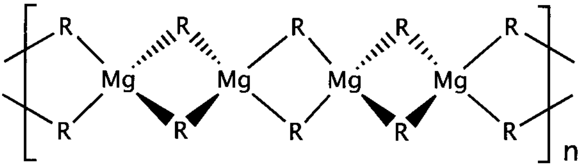

Figure 1.5 Dialkylmagnesium oligomer structure.

n-C_4H_9), such compounds are essentially polymeric. Hence, high molecular weight (rather than ionic character) accounts for the poor HC solubility of R_2Mg.

Since excessive amounts of ethers lower activity of polymerization catalysts, Grignard reagents were not preferred for industrial ZN catalyst preparations that began to emerge in the 1970s. However, most of the R_2Mg known in the early 1970s were insoluble in HC and were poorly suited to industrial production.

In the mid-1970s, an interim product was developed. It took advantage of the HC solubility of complexes of R_2Mg compounds. Addition of R_3Al to the reaction product of *n*-butyl chloride with magnesium in heptane affords an ether-free, HC-soluble complex of di-*n*-butylmagnesium (DNBM).[45] Such reactions are exemplified in Eq. 1.9 with TEAL:

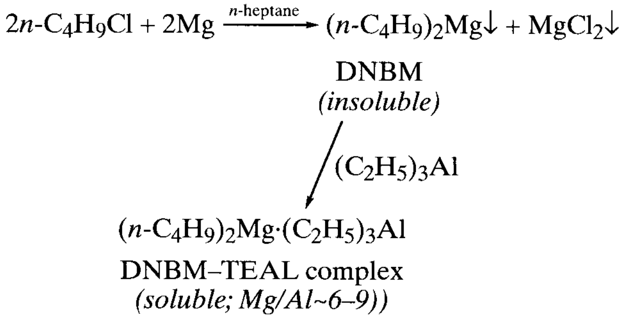

$$\begin{array}{c} 2n\text{-}C_4H_9Cl + 2Mg \xrightarrow{n\text{-heptane}} (n\text{-}C_4H_9)_2Mg\downarrow + MgCl_2\downarrow \\ \text{DNBM} \\ \textit{(insoluble)} \\ \swarrow (C_2H_5)_3Al \\ (n\text{-}C_4H_9)_2Mg\cdot(C_2H_5)_3Al \\ \text{DNBM–TEAL complex} \\ \textit{(soluble; Mg/Al}\sim\textit{6–9))} \end{array} \tag{1.9}$$

Though the complex is shown as if it were discrete, rapid alkyl exchange occurs and alkyls are "scrambled" in the DNBM–TEAL complex.

Discovery of several HC-soluble "unsymmetrical" dialkylmagnesium compounds (RMgR') allowed more facile processes[46] and products that contained much lower amounts of R_3Al. Currently, the following RMgR' are offered commercially:

- *n*-butyl(ethyl)magnesium (BEM),
- *n*-butyl(*n*-octyl)magnesium (BOM or BOMAG®), and
- *n*-butyl(*sec*-butyl)magnesium (also called dibutylmagnesium, or DBM).

RMgR' are supplied only as HC solutions, usually 10–20% in *n*-heptane. (They cannot be supplied as the neat products because of the difficulties of handling infusible solids that are pyrophoric.)

BEM and BOM are manufactured by similar processes (reaction of alkyl chlorides with magnesium powder in HC). However, DBM must be produced by a different process. Although production of DBM begins with reaction of *n*-butyl chloride/Mg as in Eq. 1.9, *sec*-butyllithium is used to introduce the *sec*-butyl groups needed to render the composition HC soluble (Because *sec*-butyl chloride does not react with magnesium in the absence of donor solvents, *sec*-butyllithium must be used to introduce *sec*-butyl groups; see reference 46 for details on process chemistry.)

Though the nomenclature of RMgR' might suggest near-equal amounts of R and R', that is true only for BEM. Yield of HC-soluble BEM is maximized when the ratio of *n*-butyl to ethyl is ~1.0.[47] However, the ratio of *n*-butyl to *n*-octyl in BOM is 2.5–3.0 and the *n*-butyl to *sec*-butyl ratio in DBM is typically 1.3–1.5. The reason for this is economic. For BOM and DBM, the cost of *n*-butyl chloride is significantly lower than *n*-octyl chloride and *sec*-butyllithium, respectively.

BEM and BOM are inherently HC soluble, but the solutions are very viscous. Consequently, a viscosity-reducing agent must be added. A small quantity of TEAL (1–2 mol %, relative to Mg) is most commonly used for this purpose. TEAL forms nascent coordination complexes with the RMgR', thereby lowering the molecular weight of the magnesium alkyl and solution viscosity is reduced by two orders of magnitude. (The amount of TEAL required for viscosity reduction of BEM or BOM is much smaller than that required for solubilization of DNBM depicted in Eq. 1.9.)

DBM solutions are free flowing and do not require viscosity reducers. DBM differs from BEM and BOM in another way. At low temperatures (below ~5 °C), a white precipitate may form in DBM solutions. To prevent this, a small quantity of *n*-octyl chloride was introduced (beginning in the mid-1980s) with *n*-butyl chloride. This generates *n*-octylmagnesium groupings that function as "antifreeze" in commercially available DBM. The overall proportions of *n*-butyl to *sec*-butyl to *n*-octyl in DBM are approximately 55:41:4.

As isolated from solution, BEM is an amorphous white solid that slowly decomposes without melting above about 140 °C. The molecular weight of BEM has been determined (cryoscopically in cyclohexane) to be about 2700 amu. As mentioned above, BEM solutions are highly viscous. Even at relatively low concentrations (~15% by weight), solution viscosities are $>10^3$ mPa·s in the absence of a viscosity-reducing agent.

Magnesium alkyls are stable indefinitely if stored properly (under dry inert gas and away from heat). BEM is thermally stable up to about 140 °C. However, DBM undergoes extensive decomposition at elevated temperatures. This occurs because *sec*-butyl groups in DBM readily undergo β-hydride elimination to produce butene-1 and MgH_2 as in

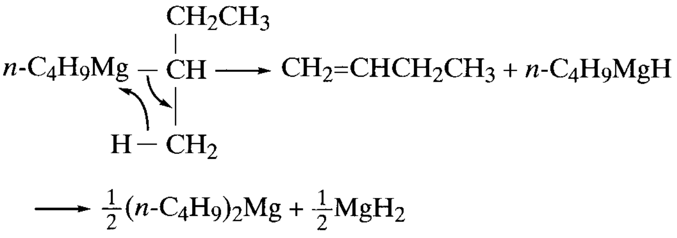

$$n\text{-}C_4H_9Mg\overset{\displaystyle CH_2CH_3}{-CH}\cdots\underset{}{H-CH_2} \longrightarrow CH_2{=}CHCH_2CH_3 + n\text{-}C_4H_9MgH \longrightarrow \tfrac{1}{2}(n\text{-}C_4H_9)_2Mg + \tfrac{1}{2}MgH_2 \qquad (1.10)$$

Also, butene-2 may be formed by β-hydride elimination from the methylene of the *sec*-butyl group. In both cases, the intermediate alkylmagnesium hydride is unstable and decomposes further to R_2Mg and magnesium hydride. The overall effect of subjecting DBM solutions to high temperatures is loss of soluble magnesium and appearance of a precipitate.

1.6.2 Modified BEM Compositions

Modified versions of BEM are produced by reaction of small amounts of 2,6-di-*t*-butyl-4-methylphenol, also known as butylated hydroxytoluene (BHT), with standard BEM, as in

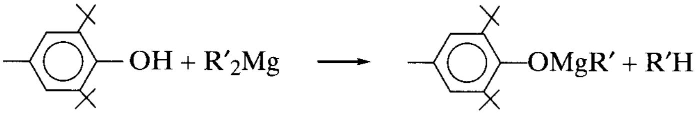

(1.11)

BHT is added in approximately 0.5 and 1.0% amounts (molar, relative to Mg). These formulations, known as BEM-2436 and BEM-4436, respectively, are used to produce catalysts primarily for production of LLDPE. Because BHT is added in such small quantities, BEM-2436 and BEM-4436 are compositionally very close to standard BEM. Specifically, BEM-2436 and BEM-4436 contain 99.0 and 98.0 wt % BEM, respectively, and the balance is the product of Eq. 1.11. BHT is regenerated by hydrolysis when the resin is exposed to moist air. Because BHT functions as an antioxidant for polyolefins, BHT residues cause no problem for the polymer.

Though BHT was added initially as a viscosity-reducing agent,[48] its viscosity-lowering effect is slight compared to that of TEAL. However, small quantities of BHT improved the performance of BEM in selected catalyst systems and BEM-2436 and BEM-4436 became commercial products.

Another derivative of BEM that has been offered commercially is the product known as *n*-butyl(ethyl)magnesium *n*-butoxide (BEM-B), produced by the reaction of one equivalent of *n*-butyl alcohol with BEM:

$$R'_2Mg + n\text{-}C_4H_9OH \rightarrow (n\text{-}C_4H_9O)MgR' + R'H\uparrow \qquad (1.12)$$

where R′ is ~50% ethyl and ~50% *n*-butyl.

Unlike BEM-2436 and BEM-4436, BEM-B is compositionally very distinct from standard BEM. Because *n*-butyl alcohol is typically used in slight excess (~3%), there is no remaining "free BEM" after reaction. While HC solutions of standard BEM are viscous, BEM-B solutions are mobile and do not require viscosity reducers.

The ethyl group in BEM may be slightly more reactive than the *n*-butyl. In the reaction to produce BEM-B illustrated in Eq. 1.12, the ethyl/*n*-butyl proportion in the BEM starting material is typically about 49/51. In the resultant BEM-B, the proportion of ethyl/*n*-butyl is ~47/53. Some of this apparent disparity may be due to the difficulty of removing by-product *n*-butane (relative to ethane) from the solution of BEM-B, thereby inflating the amount of *n*-butane observed in the GC analysis of the hydrolysis gas.

1.6.3 Pricing and Selection Criteria for RMgR'

Commercially available dialkylmagnesium compounds used in the production of polyolefin catalysts are listed in Table 1.4. BEM (including BEM-2436 and BEM-4436) is the most important and hundreds of metric tons are supplied annually, primarily to producers of LLDPE worldwide.

Since there are only minor differences in reactivity of alkyl groups in RMgR′, selection hinges largely on cost. However, as in the discussion of TEAL and TIBAL pricing (see Section 1.4), it is important to consider the cost of *contained* magnesium rather than the cost per pound of RMgR′.

TABLE 1.4 Commercially Available Magnesium Alkyl Compounds

Product	Formula	wt % Mg[a]	CAS No.[b]
Di-*n*-butylmagnesium[c]	$(n\text{-}C_4H_9)_2Mg$	17.8	1191-47-5
n-Butyl(ethyl)magnesium[d]	$n\text{-}C_4H_9MgC_2H_5$	22.0	62202-86-2
n-Butyl(ethyl)magnesium *n*-butoxide[e]	$n\text{-}C_4H_9(C_2H_5)Mg_2(O\text{-}n\text{-}C_4H_9)_2$	17.3	
n-Butyl(*n*-octyl)magnesium[f]	$(n\text{-}C_4H_9)_{1.5}Mg(n\text{-}C_8H_{17})_{0.5}$	14.8	94279-45-5
n-Butyl(*sec*-butyl)magnesium[g]	$n\text{-}C_4H_9Mg\text{-}sec\text{-}C_4H_9$	17.9	39881-32-8

[a] Theoretical.

[b] Chemical Abstracts Service registry no.

[c] DNBM, available only as a complex with triethylaluminum, Mg/Al in the complex from 6 to 9.

[d] BEM, also available as modified versions called BEM-2436 and BEM 4436, obtained by adding 0.5 and 1.0mol % BHT (2,6-di-*t*-butyl-4-methylphenol) to the standard.

[e] BEM-B, considered a commercial in 2003, now a developmental product.

[f] BOM. The *n*-butyl-to-octyl ratio is typically 2.5–3.0, theoretical Mg percent calculated for *n*-butyl/*n*-octyl ratio = 3.

[g] DBM. The *n*-butyl/*sec*-butyl ratio is typically 1.3–1.5.

For illustration, assume that separate customers use 100,000 pounds per year of the three major RMgR' products with the following prices:

- Customer A uses BEM at $25/lb supplied as a solution typically containing 3.31% Mg.
- Customer B uses BOM at $20/lb supplied as a solution typically containing 2.93% Mg.
- Customer C uses DBM at $30/lb supplied as a solution typically containing 2.64% Mg.

Using the theoretical amount of magnesium (see Table 1.4) in each product, the annual cost of each RMgR' may be calculated as follows:

- Customer A's annual cost for BEM = $25/lb × 100,000 lb × (0.0331/0.220) = ~$376,000.
- Customer B's annual cost for BOM = $20/lb × 100,000 lb × (0.0293/0.146) = ~$401,000.
- Customer C's annual cost for DBM = $30/lb × 100,000 lb × (0.0264/0.176) = ~$450,000.

Even though the BEM price is intermediate on the basis of $/lb of RMgR', its total cost is lowest because it contains higher magnesium content than BOM and DBM. Using the prices above but converting from dollars per pound of RMgR' to dollars per pound of contained magnesium, the adjusted prices are:

- BEM: $114/lb of magnesium.
- BOM: $137/lb of magnesium.
- DBM: $170/lb of magnesium.

1.7 ORGANOBORON COMPOUNDS

Though produced in substantially smaller quantities than aluminum and magnesium alkyls, two types of organoboron compounds are used in industrial polyolefin catalyst systems. Both are σ-bonded organometallics. Triethylborane (TEB) and arylboranes (including the closely related arylborates) are the most important, though used in different ways. TEB is used in third-generation silica-supported chromium ("Phillips") catalysts.[13] Arylboranes and arylborates are used as cocatalysts for SSC. Principal commercially available organoboron compounds are listed in Table 1.5, though not all are used in polyolefin catalyst systems.

Like TEAL, TEB is a clear, colorless liquid that ignites upon contact with air. Unlike TEAL, TEB is monomeric and unreactive with water. TEB burns

TABLE 1.5 Commercially Available Organoboron Compounds

Name	Formula	Formula Weight	CAS No.[a]	Boiling Point (°C at mm Hg)	Stability	Remark
Triethylborane	$(C_2H_5)_3B$	97.99	97-94-9	95 at 760	Excellent	Used in third-generation Phillips catalysts
Tri-*n*-butylborane	$(n\text{-}C_4H_9)_3B$	182.15	122-56-5	170 at 222	Excellent	Not used in polyolefin technologies
Diethylborane methoxide	$(C_2H_5)_2OCH_3$	99.96	7397-46-8	88-89 at 760	Excellent	Not used in polyolefin technologies
Diethylborane isopropoxide	$(C_2H_5)_2OCH(CH_3)_2$	128.02	74953-03-0	115-117 at 760	Excellent	Not used in polyolefin technologies
Tris(pentafluorophenyl)borane	$(C_6F_5)_3B$	512.0	1109-15-5		Good	Melting point 126–131 °C cocatalyst for SSC[b]
Lithium tetrakis(pentafluorophenyl) borate	$Li^+ (C_6F_5)_4B^-$	685.9			Poor	Used as cocatalyst for SSC
Trityl tetrakis(pentafluorophenyl) borate	$Ph_3C^+(C_6F_5)_4B^-$	922.1			Poor	Used as cocatalyst for SSC
N,N-Dimethylanilinium tetrakis(pentafluorophenyl) borate	$PhNH(CH_3)_2^+(C_6F_5)_4B^-$	801.1	118612-00-3		Poor	Used as cocatalyst for SSC

[a] Chemical Abstracts Services registry numbers.

[b] SSC = single site catalysts.

with a green flame. Though TEB decomposes slowly (to R_2BH and RBH_2 and ethylene) above ~100 °C, DSC tests have shown that TEB does not undergo *hazardous* exothermic decomposition at least up to ~200 °C. When stored properly (under nitrogen and away from heat), TEB is indefinitely storage stable.

TEB may be manufactured by reaction of TEAL with borate esters or by direct hydroboration of ethylene.[49] TEB has been commercially available since the 1960s but only became important as an adjuvant for Phillips catalysts in the mid-1980s.[13] TEB broadens molecular weight distribution by increasing the low-molecular-weight fractions of polyethylene. This suggests that TEB somehow facilitates chain transfer for supported chromium catalysts.

Arylboranes are conveniently prepared by reaction of the corresponding Grignard reagent with BF_3/etherate as shown in Figure 1.6 for tris (pentafluorophenyl)borane ("FAB"). FAB may be used to produce "ate complexes"[50] that are even stronger Lewis acids. FAB and ate complexes have been offered commercially since the mid-1990s and are used as cocatalysts for SSC in place of (or in combination with) methylaluminoxanes. Though a variety of fluorinated boranes and borates have been synthesized and used as cocatalysts for SSC,[51b] the most widely available (beyond FAB) are the products of Eqs 1.13–1.15:

Lithium tetrakis(pentafluorophenyl)borate (LTB):

$$(C_6F_5)_3B + C_6F_5Li \rightarrow Li^+(C_6F_5)_4B^- \tag{1.13}$$

Trityl tetrakis(pentafluorophenyl)borate (TTB):

$$Li^+(C_6F_5)_4B^- + Ph_3CCl \rightarrow Ph_3C^+(C_6F_5)_4B^- + LiCl \tag{1.14}$$

N,N-Dimethylanilium tetrakis(pentafluorophenyl)borate (NTB):

$$Li^+(C_6F_5)_4B^- + PhNH(CH_3)_2^+Cl^- \rightarrow PhNH(CH_3)_2^+(C_6F_5)4B^- + LiCl \tag{1.15}$$

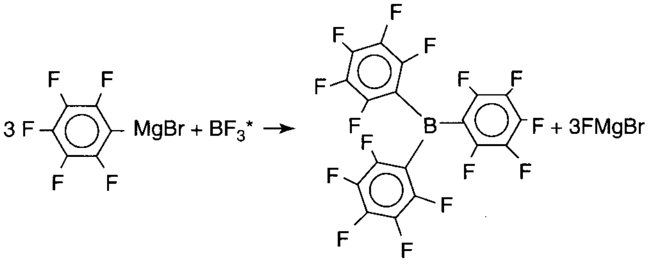

*Added as BF_3-etherate

Figure 1.6 Synthesis of tris(pentafluorophenyl)borane (FAB).

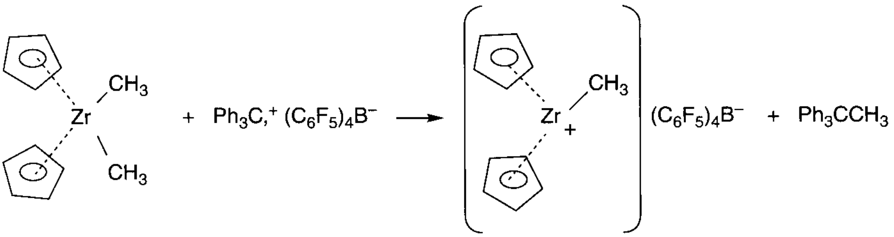

Figure 1.7 Activation of metallocene by tritylterakis(pentafluorophenyl)borate (TTB).

Arylboranes are typically white crystalline solids, essentially insoluble in aliphatic HC and sparingly soluble in aromatic solvents. They are virtually unreactive with air and water. The borates from Eqs 1.13–1.15 exhibit poor thermal stability and are not storage stable.[52]

FAB, LTB, TTB, and NTB are strongly Lewis acidic and are capable of abstracting a ligand from metallocenes to generate cations (thought to be active centers for polymerization by SSC) as illustrated in Figure 1.7 with TTB and dimethylzirconocene. Further, the anionic counterions are weakly coordinated to the cationic SSC. (Weak coordination by the anion is thought to be essential for the cationic SSC to polymerize olefins.) The main advantage of arylboranes and borates is that they can be used in stoichiometric amounts, unlike aluminoxanes, which must be used in huge excess.

1.8 ORGANOZINC COMPOUNDS

Organozinc compounds were used widely in organic synthesis until displaced early in the twentieth century by the more versatile, more reactive Grignard reagent.[53] Diethylzinc (DEZ) is the only organozinc compound with a significant role in polyolefins. DEZ [Chemical Abstract Service (CAS) registry number 557-20-0] is among the earliest organometallic compounds synthesized. Sir Edward Frankland, an English chemist and pioneer in organometallic chemistry, synthesized DEZ from zinc metal and ethyl iodide in the mid-nineteenth century.[54–56]

DEZ is a monomeric, linear molecule which exists as a clear colorless liquid at ambient T. DEZ is distillable (boiling point ~117 °C) and highly soluble in HC. It is pyrophoric and reacts vigorously with water, though reaction is not as difficult to control as R_3Al reactions with water. DEZ is unreactive with CO_2.

Purity of commercially available DEZ is quite high. GC analysis of hydrolysis gas typically shows 99.8% ethane and observed zinc content is 52.7% (theory 52.9%).

Though stable when stored under an inert atmosphere at ambient temperature, DEZ is not stable at high temperatures. *Caution! DEZ decomposes violently above 120* °C. DEZ is also light sensitive, apparently undergoing homolytic scission of the C–Zn bond, ultimately leading to zinc metal, which causes turbidity. Since commercially available DEZ is supplied and stored only in steel containers, light sensitivity is usually not a concern. DEZ has been produced commercially since the 1960s. It has been used as a chain transfer agent (CTA) in Ziegler–Natta catalyst systems in the past.[57,58] Today, chain transfer in ZN catalyst systems is achieved chiefly by hydrogenolysis. However, significant quantities of DEZ are still employed in the polyolefin industry.

DEZ is used as a scavenger of poisons from process equipment for production of PE by supported chromium (Phillips) catalysts. Chromium catalysts are notorious for the difficulty of initiating polymerization after a "turn-around." When process equipment is taken out of service for maintenance, the interior of reactors may be exposed to ambient air. This introduces oxygen and water, severe poisons for chromium catalysts. Even after inert gas (nitrogen) is reintroduced after maintenance activities are completed, trace amounts of poisons remain in the equipment and on interior surfaces. Exposure of process equipment to DEZ removes these poisons. When reactors are started up again, polymerization initiates more readily.

A unique industrial application of DEZ was recently disclosed.[59,60] DEZ is being used in production of Dow's INFUSE® block copolymers of ethylene and octene-1. A mixed SSC system involving hafnium and zirconium is used. The mechanism is called "chain shuttling." It is believed to occur by transfer of polymeric chains between transition metals through the intermediacy of DEZ. This is consistent with the propensity of DEZ to function as a chain transfer agent.

ABBREVIATIONS

ARC	Accelerating rate calorimetry
BEM	*n*-Butylethylmagnesium
BEM-2436	BEM to which has been added 0.5 mol % BHT
BEM-4436	BEM to which has been added 1.0 mol % BHT
BEM-B	*n*-Butylethylmagnesium *n*-butoxide
BHT	Butylated hydroxy toluene (also called 2,6-di-*t*-butyl-4-methylphenol)
BOM	*n*-butyl-*n*-octylmagnesium
BOMAG	*n*-butyl-*n*-octylmagnesium
CAS	Chemical Abstract Services
Cp	Cyclopentadienyl (C_5H_5) group; often a ligand in metallocenes or SSCs
DBM	Dibutylmagnesium
DEAC	Diethylaluminum chloride
DEAL-E	Diethylaluminum ethoxide
DEB-M	Diethylboron methoxide
DEB-IP	Diethylboron isopropoxide
DEZ	Diethylzinc

DIBAL-H	Diisobutylaluminum hydride
DNBM	Di-*n*-butylmagnesium
DSC	Differential scanning calorimetry
EAO	Ethylaluminoxane
EASC	Ethylaluminum sesquichloride; $Et_3Al_2Cl_3$
FAB	Tris(pentafluorophenyl)borane
GC	Gas chromatographic
HC	Hydrocarbon
IBAO	Isobutylaluminoxane
IPRA	Isoprenylaluminum; reaction product of TIBAL or DIBAL-H with isoprene
ISOPRENYL	See IPRA
LLDPE	Linear low-density polyethylene
LTB	Lithium tetrakis(pentafluorophenyl)borate
MAO	Methylaluminoxane
MMAO	Generic term used for modified methylaluminoxanes; various types designated by suffix
MW	Molecular weight
MWD	Molecular weight distribution
NMR	Nuclear magnetic resonance
NPL	Nonpyrophoric limit
NTB	*N*,*N*-Dimethylanilium tetrakis(pentafluorophenyl)borate
PE	Polyethylene
PMAO	Polymethylaluminoxane
PMAO-IP	Polymethylaluminoxane, improved performance
PP	Polypropylene
SSC	Single site catalyst
TBAO	*t*-Butylaluminoxane
TEAL	Triethylaluminum
TEB	Triethylborane
THF	Tetrahydrofuran
TIBAL	Triisobutylaluminum
TMAL	Trimethylaluminum
TTB	Trityl tetrakis(pentafluorophenyl)borate
ZN	Ziegler–Natta catalysts

REFERENCES

1. Crabtree, R. H., *The Organometallic Chemistry of the Transition Metals*, 3rd ed., Wiley-Interscience, New York, 2001, p. 130.
2. Collman, J. P., Hegebus, L. S., Norton, J. R., and Finke, R. G., *Principles and Applications of Organotransition Metal Chemistry*, 2nd ed., University Science Books, Mill Valley, CA, 1987, p. 166.
3. Goodall, B. L., Allen, N. T., Conner, D. M., Kirk, T. C., McIntosh, L. H., and Shen, H., *Novel Catalysts for the Controlled Copolymerization of Olefins and Acrylates*

to Linear, High Molecular Weight Copolymers, presented at the International Conference on Polyolefins, Society of Plastics Engineers, Houston, TX, February 25–28, 2007.

4. Zietz, J. R., *Ullmann's Encyclopedia of Industrial Chemistry*, 5th ed., Vol. A1, VCH Verlagschellshaft, Weinheim, 1985, p. 543.
5. Bickelhaupt, F. and Akkerman, O., *Ullmann's Encyclopedia of Industrial Chemistry*, 5th ed., Vol. A15, VCH Verlagschellshaft, Weinheim, 1985, p. 626.
6. Malpass, D. B., Fannin, L. W., and Ligi, J. J., *Kirk-Othmer Encyclopedia of Chemical Technology*, Vol. 16, Wiley, New York, 1981, 3rd ed., p. 559.
7. Hartley, F. R., and Patai, S., *The Chemistry of the Metal Carbon Bond*, Wiley, New York, Vol. 1: *The Structure, Preparation, Thermochemistry and Characterization of Organometallic Compounds*, 1983; Vol. 2: *The Nature and Cleavage of Metal-Carbon Bonds*, 1984; Vol. 3: *Carbon-Carbon Bond Formation Using Organometallic Compounds*, 1985; Vol. 4: *The Use of Organometallic Compounds in Organic Synthesis*, 1987.
8. Eisch, J. J., in *Comprehensive Organometallic Chemistry II: A Review of the Literature 1982–1994*, Vol. 1, Abel, E. W., Stone, F. G. A., and Wilkinson, G., Eds., Pergamon, New York, 1995, p. 431; Eisch, J. J., in *Comprehensive Organometallic Chemistry: The Synthesis, Reactions, and Structures of Organometallic Compounds*, Vol. 1, Wilkinson, G., Stone, F. G. A., and Abel, E. W., Eds., Pergamon, New York, 1982, p. 555.
9. Ziegler, K., in *Organometallic Chemistry*, ACS Monograph 147, H. Zeiss, Ed., Reinhold, New York, 1960, p. 194.
10. Lindsell, W. E., in *Comprehensive Organometallic Chemistry: The Synthesis, Reactions, and Structures of Organometallic Compounds*; Vol. 1, Wilkinson, G., Stone, F. G. A., and Abel, E. W., Eds., Pergamon, New York, 1982, p. 155.
11. Lindsell, W. E., in *Comprehensive Organometallic Chemistry II: A Review of the Literature 1982–1994*, Vol. 1, Abel, E. W., Stone, F. G. A., and Wilkinson, G., Eds., Pergamon, New York, 1995, p. 57.
12. Zietz, J. R., Robinson, G. C., and Lindsay, K. L., in *Comprehensive Organometallic Chemistry: The Synthesis, Reactions, and Structures of Organometallic Compounds*, Vol. 1, Wilkinson, G., Stone, F. G. A., and Abel, E. W., Eds., Pergamon, New York, 1982, p. 368.
13. Beaulieu, B., McDaniel, M., and DesLauriers, P., *Polyethylene Catalyst Development*, paper presented at the International Conference on Polyolefins, Society of Plastics Engineers, Houston, TX, February 27, 2005.
14. Karol, F. J., *Encyclopedia of Polymer Science and Technology*, Suppl. Vol. 1, 1976, p. 120.
15. Ittel, S. D., Johnson, L. K., and Brookhart, M., *Chem. Rev.*, **2000**, 100, 1169.
16. Britovsek, G. J. P., Gibson, V. C., Kimberly, B. S., Maddox, P. J., McTavish, S. J., Solan, G. A., White, A. J. P., and Williams, D. J., *Chem. Commun.*, **1998**, 848.
17. Though a few combinations of halogenated hydrocarbons with aluminum alkyls are stable, others may decompose violently. In some cases, blends give the initial appearance of compatibility but may decompose explosively after an induction period. Extreme caution is urged. See Thomas, W. H., *Ind. Eng. Chem. Prod. Res. Dev.*, **1982**, 21, 120.

18. Ziegler, K., *Organometallic Chemistry*, ACS Monograph 147, H. Zeiss, Ed. Reinhold, New York, 1960, p. 240. Reactivity of R_3Al compounds with CO_2 has been known for many decades but it was not until the 1990s that methylaluminoxanes from TMAL/CO_2 reaction were shown to have utility as cocatalysts for SSC. See also references 19–21.
19. Smith, G. M., Rogers, J. S., and Malpass, D. B., in *Proceedings of the 5th International Congress on Metallocene Polymers*, Düsseldorf, Germany, organized by Schotland Business Research, Skilman, NJ, March 31–April 1, 1998.
20. Smith, G. M., Rogers, J. S., and Malpass, D. B., in *Proceedings of MetCon '98*, organized by The Catalyst Group, Spring House, PA, June 10–11, 1998.
21. Smith, G. M., Palmaka, S. W., Rogers, J. S., and Malpass, D. B. (Akzo Nobel), U.S. Patent No. 5,381,109, 1998.
22. Piotrowski, A. M., and Ligi, J. J., Texas Alkyls, U.S. Patent No. 4,875,941, 1989.
23. Malpass, D. B., *Methylaluminum Compounds*, paper presented at Polyolefins 2001—The International Conference on Polyolefins, South Texas Section of SPE, Houston, TX, February 27, 2001.
24. Collman, J. P., Hegebus, L. S., Norton, J. R., and Finke, R. G., *Principles and Applications of Organotransition Metal Chemistry*, University Science Books, Sausalito, CA, 1987, p. 100.
25. Ziegler, K., *Organometallic Chemistry*, ACS Monograph 147, H. Zeiss, Ed., Reinhold, New York, 1960, p. 207.
26. Allen, L. M., Hagerty, R. O., and Mohring, R. O., Mobil Oil Corp., U.S. Patent No. 4,732,882, 1988.
27. Ehlers, J., and Walter, J., Hoechst, U.S. Patent No. 5,587,440, 1996.
28. Malpass, D. B., Exxon Research and Engineering Co., U.S. Patent No. 4,593,010, 1986.
29. Ligi, J. J., and Malpass, D. B., *Encyclopedia of Chemical Processing and Design*, Vol. 3, Marcel Dekker, New York, 1977, p. 32.
30. Tritto, I., Mealares, C., Sacchi, M. C., and Locatelli, P., *Macromol. Chem. Phys.*, **1997**, 198, 3963.
31. Reddy, S. S., Radhakrishnan, K., and Sivaram, S., *Polym. Bull.*, **1996**, 36, 165.
32. Chen, E. Y.-X., and Marks, T. J., *Chem. Rev.*, **2000**, 100, 1391.
33. Beard, W. R., Blevins, D. R., Imhoff, D. W., Kneale, B., and Simeral, L. S., paper presented at the International Polyolefin Conference, The Institute of Materials, London, November 1997; see also Imhoff, D. W., Simeral, L. S., Sangokoya, S. A., and Peel, J. H., *Organometallics*, **1998**, 17, 1941.
34. Crapo, C. C., and Malpass, D. B., Texas Alkyls, U.S. Patent No. 5,041,584, 1991.
35. Vandenberg, E. J., *Chemtech*, **1983**, 13, 474.
36. Pasynkiewicz, S., *Polyhedron* **1990**, 9, 429.
37. Reddy, S. S., and Sivaram, S., *Prog. Polym. Sci.*, **1995**, 20, 309.
38. Mason, M. R., Smith, J. M., Bott, S. G., and Barron, A. R., *J. Am. Chem. Soc.* **1993**, 115, 4971.
39. Harlan, C. J., Bott, S. G., and Barron, A. R., *J. Am. Chem. Soc.* **1995**, 117, 6465.
40. Barron, A. R., *Organometallics*, **1995**, 14, 3581.
41. Malpass, D. B., *Properties of Aluminoxanes from Akzo Nobel*, Akzo Nobel Polymer Chemicals product pamphlet MA 03.324.01, January 2003.

42. Chien, J. C. W., *Advances in Polyolefins: The World's Most Widely Used Polymers*, Plenum, New York, 1987, p. 256.
43. Lindsell, W. E., in *Comprehensive Organometallic Chemistry: The Synthesis, Reactions, and Structures of Organometallic Compounds*, Vol. 1, Wilkinson, G., Stone, F. G. A., and Abel, E. W., Eds., Pergamon, New York, 1982, p. 155.
44. Lindsell, W. E., in *Comprehensive Organometallic Chemistry II: A Review of the Literature 1982–1994*, Vol. 1, Abel, E. W., Stone, F. G. A., and Wilkinson, G., Eds., Pergamon, New York, 1995, p. 57.
45. Malpass, D. B., and Fannin, L. W., *J. Organomet. Chem.*, **1975**, 93, 1.
46. Malpass, D. B., Fannin, L. W., and Ligi, J. J., *Kirk-Othmer Encyclopedia of Chemical Technology*, Vol. 16, 3rd ed., Wiley, New York, 1981, p. 559.
47. Fannin, L. W., and Malpass, D. B., Texas Alkyls, U.S. Patent No. 4, 127,507, 1978.
48. Malpass, D. B., and Webb, D. W., Texas Alkyls, U.S. Patent No. 4,547,477, 1985.
49. Malpass, D. B., Fannin, L. W., and Ligi, J. J., *Kirk-Othmer Encyclopedia of Chemical Technology*, Vol. 16, 3rd ed., Wiley, New York, 1981, p. 563.
50. An ate complex is a combination of a Lewis acid with a base to give a negative ion in which the central atom has a higher than normal valence; see Smith, M. B., and March, J., *March's Advanced Organic Chemistry*, 5th ed., Wiley, New York, 2001, p. 339.

51a. Band, E., and Taylor, D., *The Effect of Hydride in Triethylaluminum on Propylene Polymerizations*, paper presented at the Akzo Nobel Metal Alkyls Symposium 1996, Scheveningen, The Netherlands, May 1996.

51b. Chen, E. Y.-X., and Marks, T. J., *Chem. Rev.*, **2000**, 100, 1395; see also Brintzinger, H. H., Fischer, D., Muelhaupt, R., Rieger, B., and Waymouth, R. M., *Angew. Chem., Int. Ed. Engl.*, **1995**, 34, 1143.

52. Sinn, H., and Kaminsky, W., *Adv. Organomet. Chem.*, **1980**, 18, 99; Sinn, H., Kaminsky, W., Vollmer, H. J., and Woldt, R., *Angew. Chem. Int. Ed. Engl.*, **1980**, 19, 390.
53. Coates, G. E., Green, M. L. H., and Wade, K., *Organometallic Compounds*, Vo. 1, 3rd ed., Methuen & Co, London, 1967, p. 121.
54. Frankland, E., *Q. J. Chem. Soc.*, **1861**, 13, 177.
55. Frankland, E., and Dobbin, L., *J. Chem. Soc., Trans.*, **1878**, 33, 545.
56. Frankland, E., *Q. J. Chem. Soc.*, **1850**, 2, 297.
57. Vandenberg, E. J., and Repka, B. C., in *High Polymers*, Vol. 29, Schildknecht, C. E., and Skeist, I., Eds., Wiley, New York, 1977, p. 370.
58. Krentsel, B. A., Kissin, Y. V., Kleiner, V. I., and Stotskaya, L. L., *Polymers and Copolymers of Higher a-Olefins*, Hanser/Gardner Publications, Cincinnati, DH, 1997, p. 46.
59. Swogger, K., *Polyolefin Technology: Recent Past and Future*, paper presented at the International Conference on Polyolefins, Society of Plastics Engineers, Houston, TX, February 25–28, 2007.
60. Martin, S., *Teaching Old Polymers New Tricks Using Catalysis*, paper presented at the International Conference on Polyolefins, Society of Plastics Engineers, Houston, TX, February 24–27, 2008.
61. Roberg, J. K., and Burt, E. A., Albermarle Corp., U.S. Patent No. 5,663,394, 1997.

2 Porous Silica in Transition Metal Polymerization Catalysts

THOMAS J. PULLUKAT
SILCAT Consultants, Lake Mary, Florida 32746
ROBERT E. PATTERSON
PQ Corporation, Conshohocken, Pennsylvania 19428

2.1 INTRODUCTION

Transition metal catalysts for the polymerization of olefins are vital to the plastics industry. There are three types of polyolefin catalysts in commercial use: chrome-on-silica (Phillips) catalysts, titanium halide/aluminum alkyl (Ziegler–Natta) catalysts, and organometallic (metallocene) catalysts. The first example of a silica-supported catalyst is the chrome–silica type discovered by J. Paul Hogan and Robert Banks in the early 1950s. Great strides have been made in developing this catalyst over the years. The current catalyst technology is very versatile and is used in producing high-density polyethylene (HDPE) for large and small blow molding, film, pipe, sheet, and wire/cable coating applications. The surface chemistry and physical properties of the silica play a key role in influencing catalyst performance. The original Ziegler–Natta catalysts were based on magnesium or aluminum supports, but in the early 1980s silica-supported Ziegler–Natta catalysts were commercialized for the production of polyethylene (PE) and isotactic polypropylene. Here also the surface chemistry and physical properties of silica play an important role in determining catalyst performance and polymer properties. Silica is the preferred support for organometallic catalysts, but at present there are limited data to illustrate the effect of silica support on catalyst performance in these systems.

Handbook of Transition Metal Polymerization Catalysts Edited by Ray Hoff and Robert T. Mathers
Copyright © 2010 John Wiley & Sons, Inc.

2.1.1 History of Polyethylene Catalysts

The first commercial polyethylene was produced by Imperial Chemical Industries in the 1930s using a free-radical polymerization process that required extreme pressures of 50–300 MPa at temperatures of 100–300 °C with careful control over the oxygen content of the ethylene feedstock (since oxygen acts as a free-radical initiator).[1] Polyethylene made by free-radical polymerization is the low-density type (LDPE).

In the early 1950s, Hogan and Banks of Phillips Petroleum[2] discovered chrome oxide–silica catalysts, which produce HDPE in processes that are efficient at pressures of only about 4 MPa. The first commercial plant was built in 1955. Today these materials are commonly called Phillips catalysts, and since the time of their commercialization silica gel has played a vital role in the production of polyethylene. In Phillips catalysts the silica is not merely a support; it is essential for activity and strongly influences other process and polymer characteristics.

In 1953, Karl Ziegler discovered another practical approach to produce polyethylene at relatively low pressures, utilizing the combination of a transition metal halide with an aluminum trialkyl cocatalyst.[3,4] Titanium, rather than chromium, became the preferred transition metal. The first commercial plant was built in 1956. Today these materials are commonly called Ziegler catalysts, and they are equal in importance to the Phillips catalysts but produce HDPE with different characteristics and thus are useful in different applications. In particular, Ziegler catalysts produce HDPE having a narrower molecular weight distribution than HDPE produced from Phillips catalysts. Ziegler and Natta received the Nobel Prize in 1963 for production of vinyl polymers using solid-state stereoregulating catalysts.

For Ziegler catalysts, a support is not required for activity but is essential for efficient polymerization—in terms of polymer morphology control and reactor fouling prevention—in both slurry and gas-phase processes. Both magnesium dichloride and silica gel have been widely used as supports for Ziegler–Natta catalysts.[5]

As early as 1967, organometallic catalysts began to emerge from research laboratories.[6] These transition metal catalysts employ silyl chromates (e.g., triphenylsilyl chromate) and metallocenes (e.g., cyclopentadienyl zirconium dichloride) along with a methyl aluminoxane (MAO) cocatalyst.[7] MAO provides a much higher boost in activity than conventional aluminum alkyl cocatalysts owing to its higher acidity. Today these materials are commonly called single-site catalysts, and they produce HDPE with a narrower molecular weight distribution than Phillips or even Ziegler catalysts.

2.1.2 Consumption

Polyethylene is the most widely used plastic in the world, accounting for 39% of the most common thermoplastics and 62% of polyolefins. Total consumption in 2004 was about 61 million metric tons, of which 27 million metric tons was HDPE—the most widely used form of polyethylene.[8]

Worldwide polyolefin capacity in 2006 was about 103 million metric tons, of which about 35 million metric tons was HDPE. The projected increase in polyolefin capacity from 2006–2012 is about 36 million metric tons.[9] The total value of the polyolefin catalyst market in 2006 is about $800 million, of which 48% is polypropylene, 36% HDPE, and 16% linear LDPE (LLDPE).

Silica-based chrome catalysts are used for roughly half of all HDPE production, with Ziegler catalysts accounting for nearly the other half. More than half of these Ziegler catalysts are supported on silica. Metallocenes accounted for the production of only about 2.7 million metric tons of polyolefins in 2006; most of this was LLDPE, with only ~4% HDPE. The growth rate of metallocene-catalyzed polyolefins is, however, quite high: from 2006–2012 the projected average annual growth rate (AAGR) is 12.5%.[9]

2.2 PRODUCTION OF SILICA GEL CATALYSTS

2.2.1 Production of Hydrogel Precursor

Silica gels are an amorphous form of SiO_2[10,11] and are the most widely used supports for polyolefin catalysts. They have relatively high surface areas and pore volumes per unit mass. They also have chemically reactive groups on the surface (silanols), most of which are within the pore structure. Their particle sizes and shapes can be controlled to optimize catalyst performance. Processes to make silica gels useful in catalysts are well known.[12,13] The chemical and physical properties of silica gels greatly affect the performance of polymerization catalysts as well as the properties of polyethylenes produced.

One process[14] for making silica-supported catalysts is shown in Figure 2.1. The first step is the formation of a silica hydrosol, which soon sets into a solid

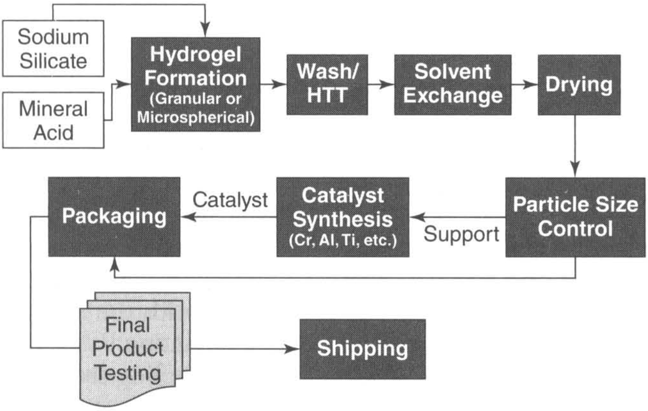

Figure 2.1 Silica-supported catalyst manufacturing process.

silica hydrogel typically having a water content of 75–85%. Commercial processes are in use to produce both granular and microspherical gels. Granular gels are produced under acid-set conditions where gel times are on the order of minutes. Microspherical gels are produced under alkaline-set conditions where gel times are less than 1 s, facilitating the rapid formation of solid spheres from droplets shot out of a nozzle. Microspherical gels are typically set from hydrosols containing a higher water content (which avoids nozzle clogging in the short gel times), and as a result they have the potential to produce catalysts with higher final pore volumes. The shape (granular vs. spherical), size of the final catalyst particles, and active metal distribution in the silica particle are important because catalyst particles are replicated by the growing polymer. The particle strength is important as well because it influences fines generation during handling and the way the particles fragment during polymerization.[15]

After the hydrogel is fully formed, it is subjected to a washing and hydrothermal treatment (HTT) stage in which the gel is washed free of impurities, particularly sodium (which influences thermal stability), and surface area is adjusted to the desired value by heating to a specified temperature, time, and alkaline pH. The final catalyst properties of surface area (SA), maximum potential pore volume (PV), and pore size distribution are largely determined during these stages. Average pore diameter (PD) is a function of SA and PV and cannot be controlled independently. The principles by which these porosimetry properties are controlled have been discussed in detail by Iler and Barby.[11,16]

2.2.2 Production of Dried Catalyst Support

The next two steps of organic solvent exchange and drying are carefully carried out to preserve as much as possible the PV of the gel by reducing the surface tension of pore liquid during drying. Water has a much higher surface tension than virtually all organic solvents. Replacing water with a miscible solvent having lower surface tension results in less shrinkage force applied to the pore walls as the liquid–vapor meniscus moves down the capillary during the drying process. The resultant material is commonly called silica aerogel. The effect of the composition of the pore liquid on the final PV is illustrated in Figure 2.2 for a typical high-PV microspherical silica support. Even small amounts of residual water lead to substantial loss of PV.

Besides solvent washing, other methods of preserving PV upon drying are well known. For example, supercritical drying is recognized as a method of producing silica catalyst supports[17]; it is effective because it eliminates the liquid–vapor meniscus entirely. Similarly, freeze drying is recognized as a method of producing silica supports because it avoids the liquid–vapor interface by removing the pore liquid through sublimation.[12,18,19] Spray drying is utilized to produce medium PV products when drying from water because shrinkage is limited by high drying rate.[20]

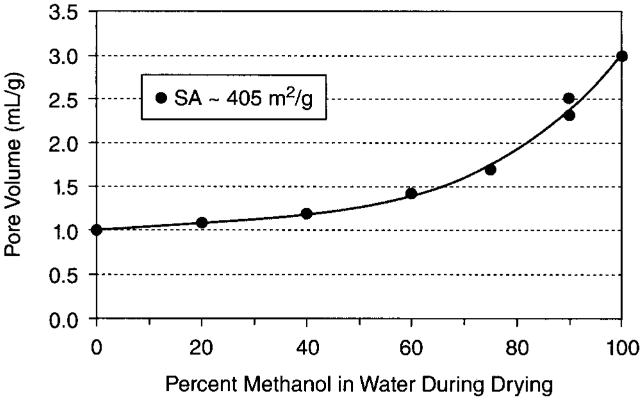

Figure 2.2 Effect of solvent on PV of silica after drying.

TABLE 2.1 Typical Polyolefin Catalyst-Grade Silicas

	Microspherical Grades				Granular Grades			
Property	Grace 955	PQ ES70	PQ MS-3040	PQ MS-3050	PQ EP10	PQ CS-2133	PQ CS-2040	PQ CS-2050
SA (m^2/g)	270	275.6	400	500	290	360	425	550
PV (mL/g)	1.65	1.6	3.0	3.0	1.6	2.4	2.5	2.6
PD (Å)	244	233	300	240	220	270	240	195
Particle size (μm)	40	40	90	90	90	90	90	90

The final step in the production of a silica catalyst support is particle size control. Granular (nonspherical) supports may undergo a milling process to achieve the desired particle size, whereas spherical supports generally avoid milling to preserve their morphology. Removal of fines and oversize particles may be accomplished by various classification techniques, such as screening.

2.2.3 Production of Finished Catalyst

The dry silica aerogel is the raw material for catalyst synthesis procedures. Some typical commercial catalyst-grade silicas and their properties are listed in Table 2.1. Both spherical and granular particle shapes are commercially available (Figure 2.3). As will be seen, SA, PV, and PD strongly affect catalyst performance. After the step of particle size control, the support is impregnated with chromium, and in some cases other metals such as titanium, aluminum, or boron, to form the finished polyolefin catalysts. Before use the catalyst must be activated by heating at high temperatures in air to oxidize Cr(III) to Cr(VI); during polymerization Cr(VI) is reduced by ethylene to Cr(II), which is believed to be the predominant active species.[21]

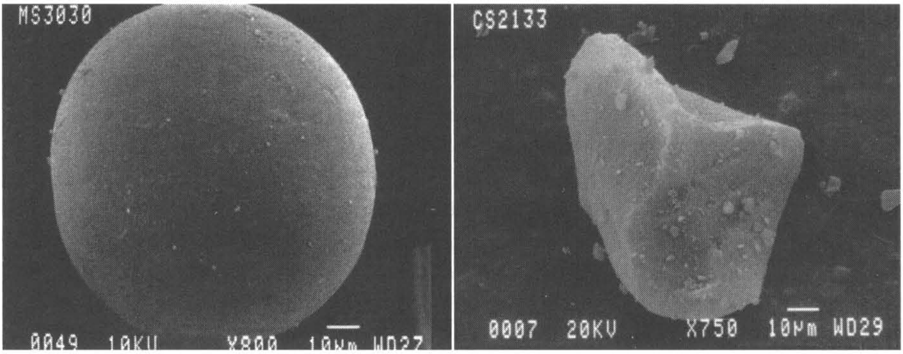

Figure 2.3 Typical microspherical (left) and granular silica catalyst supports.

2.3 INFLUENCE OF SILICA GEL PROPERTIES AND POLYMERIZATION CONDITIONS ON CATALYST PERFORMANCE

2.3.1 Experimental Conditions Utilized in These Studies

Bench Polymerization Unless otherwise noted, the following conditions were utilized. Catalyst samples were activated in dry air at the desired temperature in a quartz tube under fluidized conditions. The air was removed by nitrogen flow after activation and the activated catalyst was transferred to a storage vessel under high-purity nitrogen. Slurry polymerization runs were carried out in either a 1- or a 2-L reactor. The reactors were first filled with the desired amount of isobutane, brought up to the desired temperature, and saturated with ethylene at a fixed ethylene partial pressure. This ethylene partial pressure was maintained during the course of polymerization. Then the activated catalyst sample (about 0.05–0.1 g) was charged into the reactor, followed by the injection of 1-hexene in case of copolymerization. The slurry was stirred at 700 rpm during the reaction. When the targeted productivity (about 2500 g PE/g Cat) was reached, the ethylene flow was stopped, the reactor was purged with nitrogen, and the vessel was slowly depressurized to allow evaporation of isobutane. The reactor was then opened to recover the polymer.

Catalyst and Polymer Characterization Density of the polymer was measured on a D-H100 Toyo Seiki densimeter. Die swell was determined on an LCR 7001 Dynisco capillary rheometer using a capillary die of L/D = 1 and entrance angle of 120°. Environmental stress crack resistance (ESCR) was determined by the notched constant tension load (NCTL) test based on American Society for Testing and Materials (ASTM) D5397. A dumbbell-shaped notched specimen was immersed in a surfactant solution (10% Igepal CO-630) at 50 °C and subjected to a constant stress (800 psi). The apparatus used was from BT Tech, model AA-S-AA-000. Multipoint surface area was determined by the Brunauer, Emmett, and Teller (BET) method. Pore volume was determined by the Barrett, Joyner, and Halenda (BJH) method on degassed samples by nitrogen adsorption/desorption utilizing a Quantachrome Autosorb-6 instrument. Melt index (MI) and high load melt index (HLMI) were determined according to method ASTM D1238 at 190 °C using weights of either 2.16 kg (MI) or 21.6 kg (HLMI).

2.3.2 Chrome–Silica Catalysts

Chromium–silica catalysts, as a general rule, are best used to make high-density polyethylene (0.935–0.965 g/cm^3) of broad molecular weight distribution. These molecular properties are suitable for blow-molding, pipe, thermoforming, and film applications. Although the polymer properties can be controlled to a certain extent by varying polymerization conditions—such as polymerization temperature, ethylene concentration, and use of cocatalyst and hydrogen—the most critical parameter in controlling polymer properties is the catalyst itself. Both the physical and chemical properties of the catalyst have pronounced influence on the properties of the polymers produced. Broadly speaking, chrome–silica catalysts for HDPE production can be categorized as medium- (~1.6 mL/g) or high-pore-volume (>2.1 mL/g) products, with the latter commanding significantly higher performance advantages than the medium-pore-volume catalysts.

Effect of Pore Size It has long been recognized that the pore size of the catalyst affects the molecular weight and thus the MI of the polymer produced.[22,23] It is generally true that the larger the average pore size of the catalyst, the higher the melt index of the polymer produced, and thus the lower the average molecular weight. This is illustrated in Figure 2.4 for catalysts containing 1.0% chromium and supported on two different types of silica gel products made from different processes. These catalysts have pore volumes ranging from 2.29

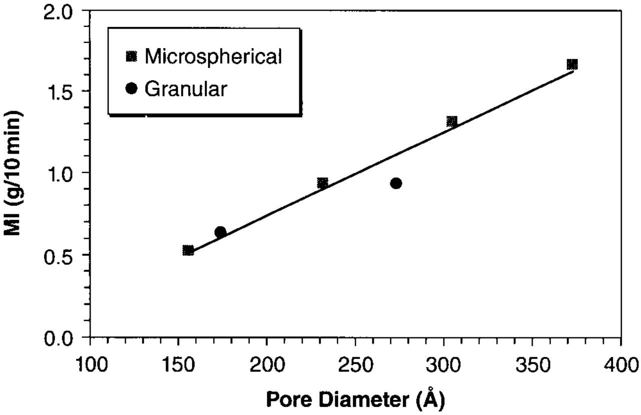

Figure 2.4 Effect of average PD on polymer MI. All catalysts contained 1.0 wt % Cr and were activated at 870 °C. Homopolymerization of ethylene was conducted at 105 °C using 10 mole % ethylene in isobutane.

to 3.00 mL/g, surface areas from 307 to 668 m^2/g, and average pore diameter from 156 to 373 Å. Despite differences in PV and SA, the MI of polymers clearly correlates with the average pore diameter of the catalyst.

Yet there is no satisfactory explanation for this correlation. The amorphous structure of silica gel makes an understanding of its surface chemistry much more difficult, and for this reason an understanding of the interaction between chromium and the silica surface and of the structure of the active sites is similarly challenging. One hypothesis by McDaniel et al. suggests long-chain branching (LCB) as a possible explanation.[21,24] McDaniel et al. studied a set of samples created with different pore sizes by varying pore volume while maintaining surface area constant. They postulated that LCB became more likely in small pores since the active sites were closer together; thus the vinyl group terminating one chain might more easily become incorporated into another chain growing from a neighboring site to form a long-chain branch. The authors themselves admitted later that this explanation was unsatisfactory.[24] The study reported here also confirms that the LCB hypothesis is unsatisfactory. In our study, the pore size of the four microspherical catalyst was changed by varying SA while maintaining PV nearly constant—the opposite of the case for the samples studied by McDaniel et al. At higher surface area, and consequently smaller pore diameter, the active sites must be farther apart owing to the lower chromium surface density, which reduces the probability of forming long-chain branches.

Effect of Surface Area The SA of the catalyst can greatly affect catalyst activity, as illustrated in Figure 2.5 for three catalysts of roughly similar PV. Catalyst activity increases linearly with increasing SA. At the same chromium loading (1.0 wt %), the surface chromium density is lower for catalyst with higher SA. It has long been established that the lower the surface chromium density, the higher the catalyst activity per chromium site.[25] However, it should

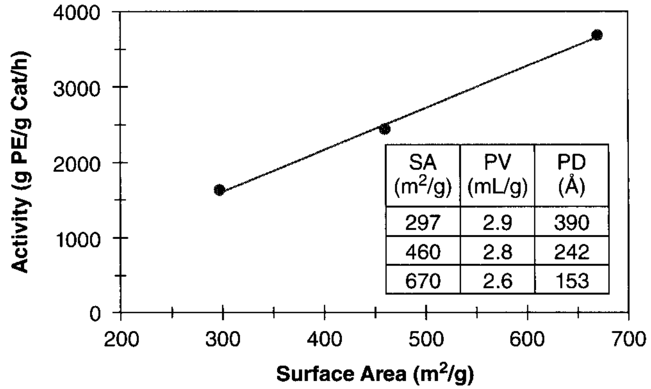

SA (m^2/g)	PV (mL/g)	PD (Å)
297	2.9	390
460	2.8	242
670	2.6	153

Figure 2.5 Effect of SA on catalyst activity. All catalysts contained 1.0% Cr, were prepared from PQ microspherical silica supports having the properties shown, and were activated at 650 °C. Ethylene polymerization was conducted at 98 °C.

be pointed out that increasing SA of the catalyst at constant PV decreases its average PD, and as we have already seen, this will cause the polymer produced to have lower MI.

The SA of the catalyst also affects two very important resin properties: ESCR and die swell. The higher the catalyst SA, the higher the ESCR (Figure 2.6) but the higher the die swell as well (Figure 2.7). In both of these figures, all catalysts contained 1.0% Cr and were activated at 650°C; all HDPE polymer samples had similar HLMI (8 g/10 min) and density (0.950 g/mL).

At the same chromium loading, the average distance between two nearest-neighbor active sites increases with increasing catalyst SA. This reduces the probability of short polyethylene molecules, with the vinyl end group formed at a neighboring active site being incorporated into a growing chain at an active site nearby, and thus reduces the formation of LCB. Thus catalysts with higher SA lead to polymers with better ESCR (owing to lower LCB) but also higher die swell.

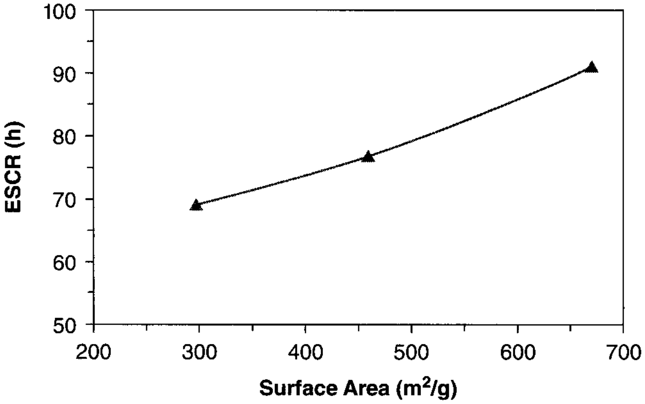

Figure 2.6 Effect of catalyst SA on ESCR.

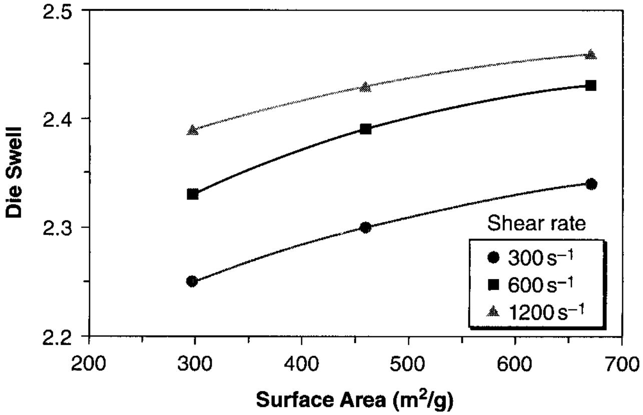

Figure 2.7 Effect of catalyst SA on die swell.

Effect of Pore Volume At equal SA, increasing the PV also increases ESCR. This is illustrated in Figure 2.8 for two pairs of catalysts, each pair having roughly the same SA but widely different PVs. The reason for this is not known at this time.

Effect of Chromium Loading In addition to its physical properties, the chemical properties of the catalyst also have a pronounced effect on polymer properties. For chrome–silica catalysts, chief among these chemical properties is the concentration of chromium itself. Chromium loading on silica catalysts affects both activity and polymer molecular weight (as indicated by viscosity changes). McDaniel et al. report a table of several polymer properties for polyethylene samples made from a series of silica–titania catalysts with varying Cr content.[26] In Figures 2.9 and 2.10 we have plotted some of those data.

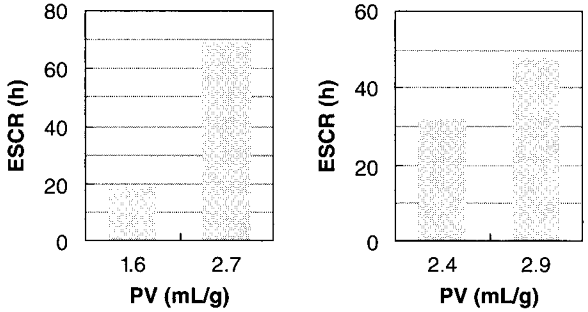

Figure 2.8 Effect of PV on ESCR at constant surface area. For the chart at left, both catalysts had surface areas of about 290 m²/g and Cr content of 1.0%; activation was at 550 °C, and both resultant HDPE polymers had HLMI of 8 g/10 min and density of 0.953 g/mL. For the chart at right, both catalysts had surface areas of about 500 m²/g, Cr content of 1.0%, and Ti content of 2.4%; activation was at 650 °C, and both resultant HDPE polymers had MI of 0.3 g/10 min and density of 0.953 g/mL.

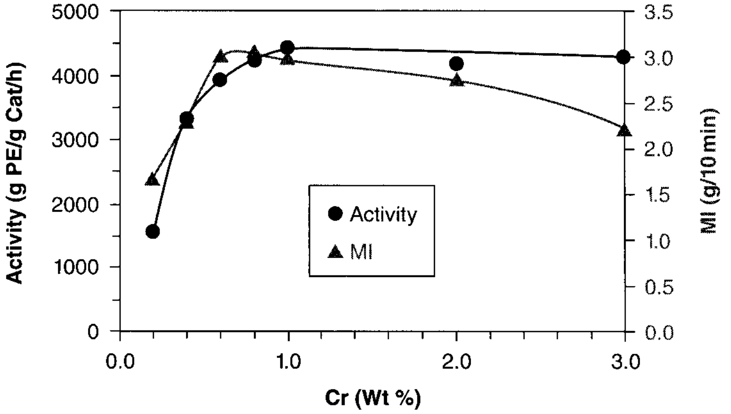

Figure 2.9 Effect of Cr loading on activity and MI.

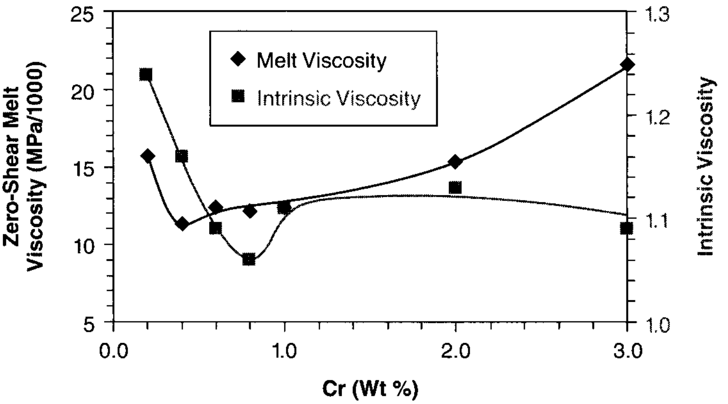

Figure 2.10 Effect of Cr loading on viscosity.

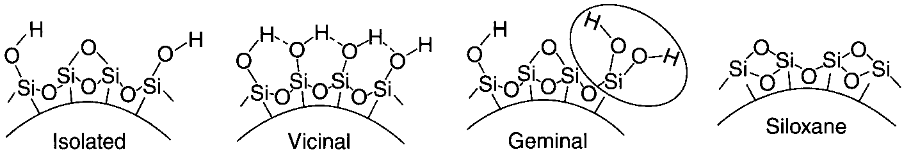

Figure 2.11 Silica surface groups.

As Cr content increases, both activity and MI increase rapidly to a maximum. Similarly, as Cr content increases, both melt viscosity and intrinsic viscosity decrease rapidly to a minimum. Upon closer inspection it is apparent that differences in these curves can be related to whether the measurement is made on molten or dissolved polymer. Activity and intrinsic viscosity (both measured in solution) peak at about the same Cr content and then both level off, whereas MI and zero-shear melt viscosity (both measured on molten polymer) peak at lower Cr content and do not level off. The authors interpreted these data in terms of increased entanglement in the melt versus solution, an indication that long-chain branching increases with Cr loading.

Effect of Activation Temperature The surface of silica gel consists of mixture of silanol (Si–OH) and siloxane (Si–O–Si) groups, with the proportion of siloxane groups increasing as the silica is heated to higher and higher temperatures. The silanol groups are further subdivided into three types: isolated silanols, in which the hydroxyls are too far apart to interact; vicinal silanols, in which the hydroxyls on two neighboring silicon atoms are close enough to hydrogen bond with one another; and geminal silanols, in which a single surface silicon atom has two hydroxyl groups attached. These groups are illustrated in Figure 2.11.

Upon heating, these silanol groups condense to form siloxane groups, splitting off water. However, the three different types of silanol groups undergo

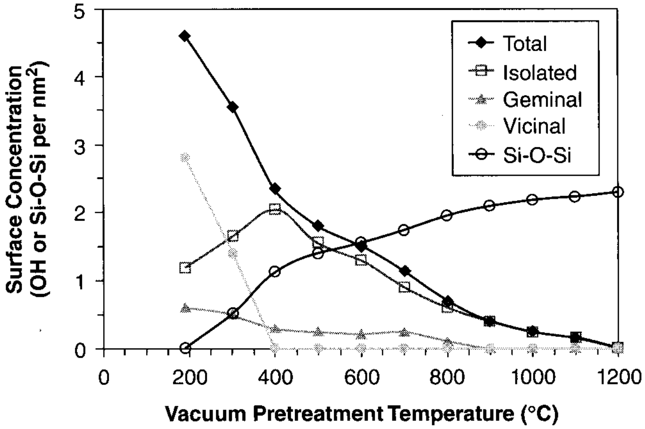

Figure 2.12 Surface hydroxyl density as function of temperature to which silica was heated in vacuum.

condensation in different temperature ranges; the hydrogen-bonded types condense at substantially lower temperatures than the isolated silanols. Thus, when a silica gel is heated at relatively low temperatures the surface density of isolated silanols actually increases while the density of vicinal and geminal silanols decreases. These principles are illustrated in Figure 2.12, in which we plot data published by Zhuravlev.[27]

An appreciation of these principles of silica surface chemistry is necessary to understand the impact of varying activation conditions on catalyst performance and polymer properties. Changing the activation temperature will change the silanol population.

In general, increasing the activation temperature increases the activity of chrome–silica catalysts for HDPE, but the effects can be complex depending upon the exact composition of the catalyst and its mode of preparation. For example, consider the effect of activation temperature on activity for the two different catalysts shown in Figure 2.13. Activity was much more sensitive to activation temperature for catalyst A than for catalyst B.

The effect of activation temperature on MI is shown in Figure 2.14 and on environmental stress crack resistance in Figure 2.15. Within the range studied, as activation temperature is increased, MI goes up—an indication of decreasing average polymer molecular weight. However, at the same time ESCR goes down.

This is in agreement with the observations reported by McDaniel et al., who also found that MI potential increased as the activation temperature of the catalyst increased. This is attributed to the reduction of hydroxyl density, which affects the proximity of hydroxyl groups to active sites in small versus large pores. However, at the onset of catalyst sintering, the MI potential decreased drastically.[24,28,29]

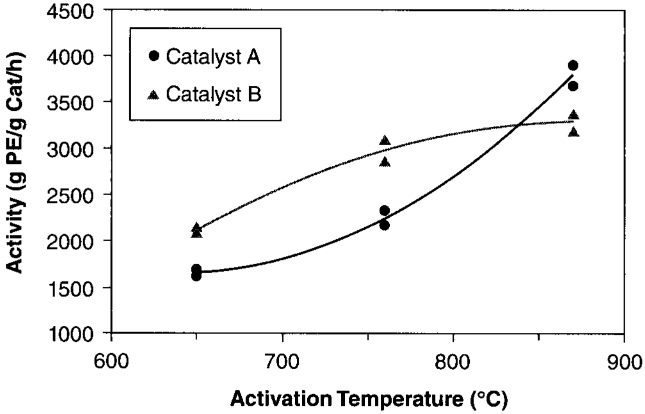

Figure 2.13 Effect of activation temperature on activity of two different chrome–silica catalysts used to produce HDPE. Catalyst A had a PV of 1.6 mL/g, SA of 279 m^2/g, and Na_2O content of 550 ppm; catalyst B had a PV of 2.0 mL/g, SA of 295 m^2/g, and Na_2O content of 90 ppm. Both had Cr contents of ~1.0%.

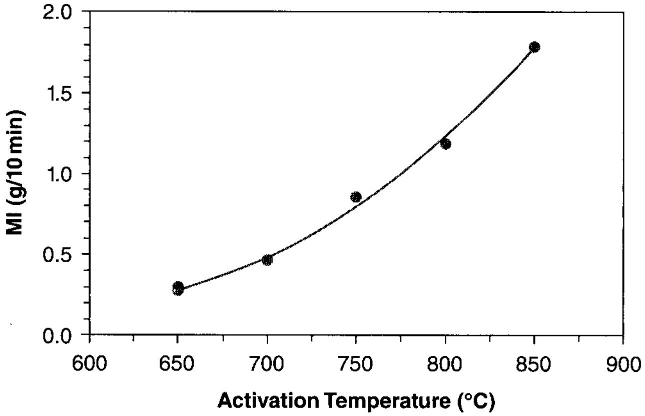

Figure 2.14 Effect of activation temperature on MI of HDPE produced from silica catalyst containing 1.0% Cr and 2.3% Ti. Homopolymerization was conducted at 105 °C.

In summary, all of these effects of activation temperature are probably related to dehydroxylation of the silica surface. Silanols are believed to inhibit the active center, and silanol condensation no doubt introduces strain into the surface. Silanols appear to stabilize growing polymer chains, favoring chain growth over chain termination.[21]

Effect of Impurities It has long been known that chrome–silica catalysts are particularly sensitive to catalyst poisons such as water, oxygen, carbon monoxide, sulfur compounds, and halogens.[30] Thus, ethylene and other raw

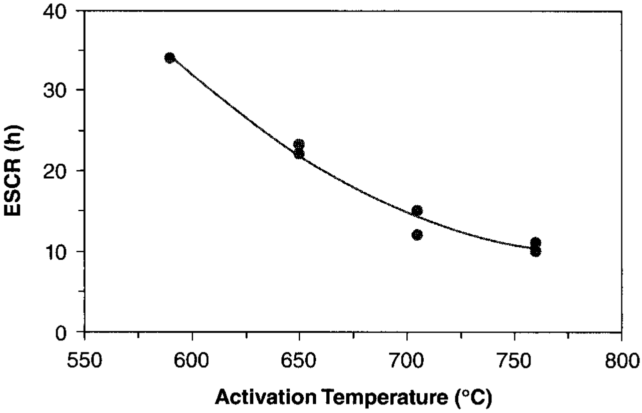

Figure 2.15 Effect of activation temperature on ESCR of HDPE produced from chrome–silica catalyst. Since ESCR is also a function of MI and density, the experimental model was designed to generate data that would allow a comparison of all polymers at a density of ~0.953 g/mL and an MI of ~0.3 g/10 min.

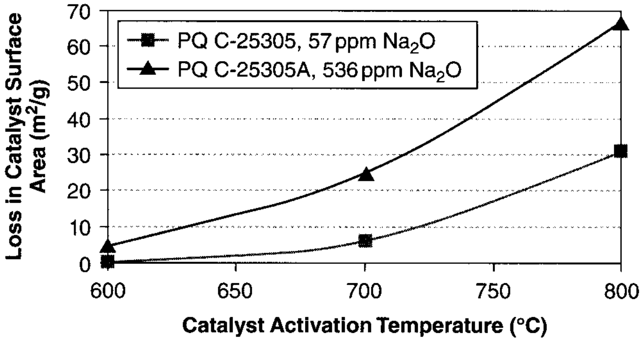

Figure 2.16 Loss of SA upon activation at different temperatures for two catalysts differing only in sodium content.

materials (e.g., isobutane in the case of typical slurry processes) must be carefully purified before use.

Of special interest is the effect of sodium as in impurity in the catalyst itself. As indicated in Patterson (see Ref. 10, Section 2.1) silica gel catalyst supports are typically derived from sodium silicate. As such, they will contain some residual level of a sodium salt (e.g., sodium sulfate if the acid used to produce the gel is sulfuric acid) depending upon the efficiency of the washing process. Sodium is not a poison per se, but at higher levels it affects the ability of the catalyst to maintain surface area upon activation and at lower levels it influences polymer properties.

Figure 2.16 shows the effect of sodium content in the final catalyst on SA loss during activation at different temperatures. Both catalysts had the following properties prior to activation: SA ~ 500 m^2/g, PV ~ 2.3 mL/g, [Cr] ~ 1.0%, and [Ti] ~ 2.5%. However, catalyst C-25305A contained 10 times the level of Na_2O as catalyst C-25305. At an activation temperature of only 600 °C, the loss of SA is nearly the same for both catalysts. But at higher activation temperatures the loss of SA becomes progressively higher for C-25305A owing to its higher sodium content.

Figure 2.17 shows the effect of sodium content on PV loss during activation at different temperatures for the same two catalysts. A similar trend is observed.

Residual sodium in the catalyst affects ethylene polymerization characteristics and polymer properties as well. Figure 2.18 shows the effect on MI, HLMI, and comonomer (1-hexene) incorporation of sodium added to a Cr/Ti

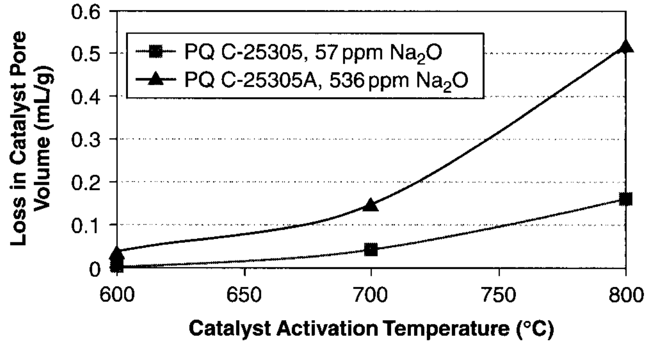

Figure 2.17 Loss of PV upon activation at different temperatures for two catalysts differing only in sodium content.

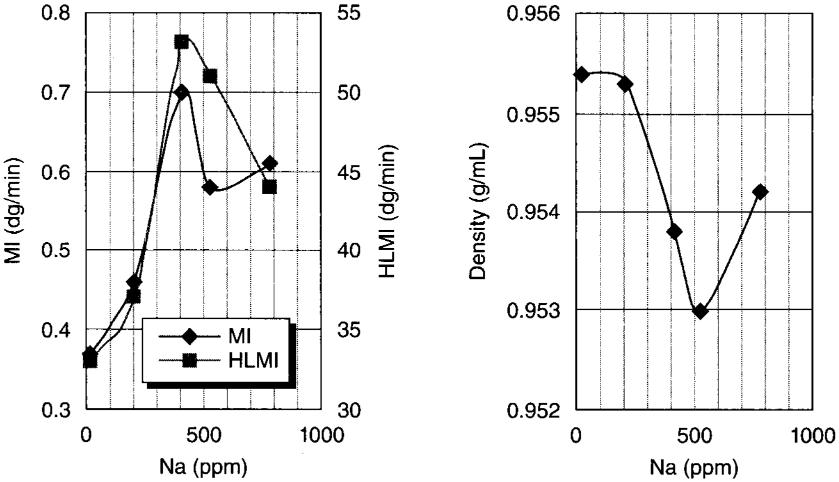

Figure 2.18 Effect of added sodium on MI (left) and comonomer incorporation (right). The starting catalyst was PQ C-25307, which typically has the following properties: SA ~ 500 m^2/g, PV ~ 2.3 mL/g, [Cr] ~ 1.0%, and [Ti] ~ 3.5%.

catalyst. In all cases the measured properties go through an inflection point at ~400–500 ppm Na for this catalyst.

Other workers have made similar observations. Sodium increases MI (up to a point), decreases the sintering onset temperature (above which SA loss becomes rapid), and narrows the molecular weight distribution (as evidenced by lower polydispersity, or M_w/M_n, at the same HLMI).[24]

Effect of Modification by Titanium The incorporation into chrome–silica catalysts of other metals such as titanium can have a pronounced effect on catalyst performance. In general, there are two primary approaches by which another metal may be added. The metal may be incorporated during the formation of the silica gel, often referred to as *cogelation*. For example, silica–titania cogels can be produced by adding sodium silicate to an acid containing a titanium compound; reacting a chromium compound with the resultant dry cogel produces an olefin polymerization catalyst.[31] Alternatively, the metal may be incorporated by a coating process, often referred to as *surface impregnation*. For example, an olefin polymerization catalyst may be prepared by heat curing an alkyl titanium ester to a fluidized bed of a dry chrome–silica catalyst.[32]

An important development made in the 1970s led to resins of modified molecular weight distributions and crystal morphology. This development, the introduction of a small amount of titanium into the catalyst, led to the world's first high-speed blow-molding resin for gallon milk bottles produced by direct synthesis.[32] An important feature of titanium-modified catalysts is a change in polymerization kinetics relative to the unmodified chrome–silica catalyst. The titanium–chromium silica catalysts begin polymerization from their first contact with ethylene. In contrast, polymerization with unmodified chromium catalysts is characterized by an induction period that frequently lasts 5–15 min. In continuous polymerization, which involves steady addition of catalyst and removal of product, titanium-modified catalysts provide greater productivity. The shorter the residence time, the greater this advantage. Another important effect of titanium modification is an increase in MI (Figure 2.19). As Ti is added to a chrome–silica catalyst substrate, MI rises rapidly at first and then more slowly.

In chromium–silica catalysts, hexavalent chromium is stabilized on silica in the form of silyl chromates, as schematically illustrated in Figure 2.20. In the case of activated titanium-modified chrome catalysts, the chromates are bound to the silica surface through titanium.[33] In titanium-modified chrome catalysts, titanium most likely changes the electron density of the active chromium species. The less electronegative Ti atoms lead to an increase in electron density at the Cr atoms, which may cause reduction of Cr(VI) to be more rapid (accounting for the observed elimination of induction time), and also cause destabilization of the chromium–carbon bond, facilitating polymer chain termination (thus affecting polymer molecular weight and accounting for the observed influence on MI). Referring again to Figure 2.20, each Cr requires

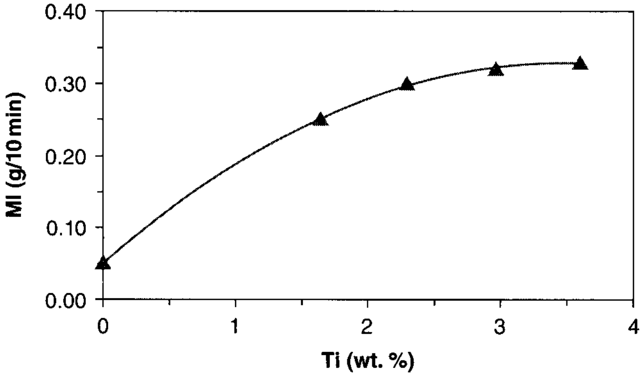

Figure 2.19 Effect of Ti loading on MI. The starting catalyst was PQ C-25300, which typically has the following properties: SA ~ 500 m^2/g, PV ~ 2.3 mL/g, and [Cr] ~ 1.0%. All catalysts were activated at 650 °C and ethylene polymerizations were conducted at 105 °C.

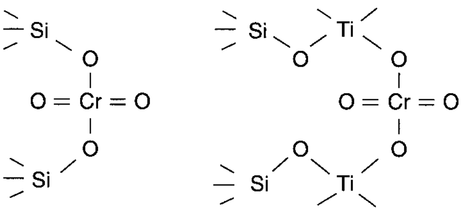

Figure 2.20 Active species on surface of chrome–silica catalyst (left) and titanium-modified chrome–silica catalyst (right).

TABLE 2.2 Effect of Increasing Ti Loading at Constant Cr Loading on Polydispersity of Resultant HDPE

Ti/Cr Molar Ratio	Polydispersity Index
0.0	6.6
1.8	7.7
2.3	9.7
3.2	10.6
4.6	10.1

two titanium atoms for the chromate formation (corresponding to a Ti/Cr weight ratio of 2.2), which may explain why, at 1.0% chromium concentration, the MI increase is greatest from 0 to 2.2% titanium and then levels off from 2.2 to 3.7% titanium, as shown in Figure 2.19.

As shown in Table 2.2, titanium modification broadens the molecular weight distribution of the polymer produced.[34] Again the effect is greatest as the molar ratio of Ti/Cr rises from 0 to about 2.3 and levels off at higher ratios. One potential disadvantage of titanium-modified catalysts is that, in the experience of some end users, they have been found to produce HDPE that exhibits an odor or taste, making such resins problematic for use in food contact applications. This is probably a result of the broader molecular weight distribution, leading to the inclusion of low-molecular-weight polyethylene species.

In general, titanium-modified catalysts have higher activity and produce polymers with better ESCR but also higher die swell. Taking all of these characteristics into account, titanium-modified chrome–silica catalysts are particularly suitable for the production of HDPE used in blow molding of large parts with high ESCR, for film having high strength and low MVTR (moisture vapor transmission rate), and for pipe.

Effect of Modification by Aluminum Another important development is the modification of chrome–silica catalysts with aluminum, which produces results similar in many ways to modification by titanium.[35] For example, compare Figure 2.21, which shows the effect of aluminum loading on MI, with Figure 2.19, which shows the same effect for titanium. Under the conditions of these tests the trends are quite similar, although the curve levels off more rapidly in the case of aluminum modification.

Like titanium-modified chrome–silica catalysts, activity increases with Al loading (Figure 2.22). Aluminum modification also reduces induction time, broadens molecular weight distribution, and increases ESCR and die swell. These characteristics make aluminum-modified chrome–silica catalysts particularly suitable for the production of HDPE used in general-purpose blow molding, pipe, large containers, and film.

Summary of Influence of Catalyst Type The general attributes of the main commercial varieties of chrome–silica catalysts are summarized in Table 2.3.

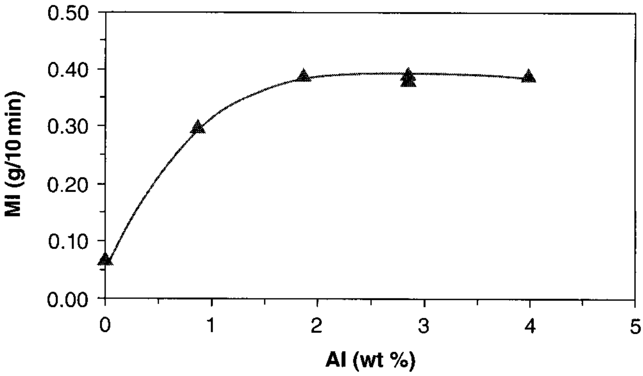

Figure 2.21 Effect of Al loading on MI. The starting catalyst was PQ C-24300, which typically has the following properties: SA ~ 400 m²/g, PV ~ 2.3 mL/g, and [Cr] ~ 1.0%. All catalysts were activated at 650 °C and ethylene copolymerizations (with 1-hexene) were conducted at 101 °C.

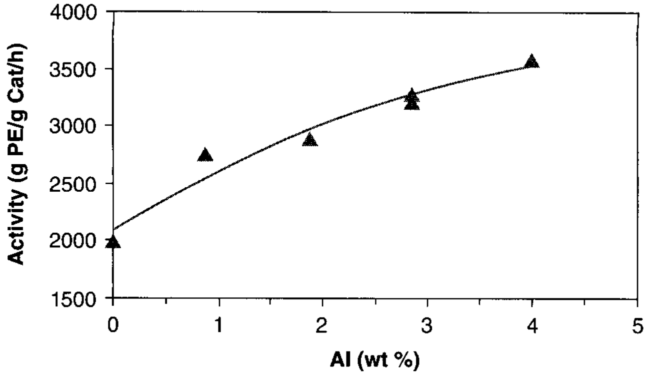

Figure 2.22 Effect of Al loading on activity. The starting catalyst and conditions were the same as in Figure 2.21.

TABLE 2.3 Influence of Catalyst Type on Polymerization Characteristics and HDPE Resin Properties

		HPV		
Property	MPV, Cr/Silica	Cr/Silica	Cr/Ti/Silica	Cr/Al/Silica
Activity	Standard	Higher	Highest	Higher
Induction period	Standard	Shorter	None	None
Melt index	Low	Medium	Higher	High
Molecular weight distribution	Broad	Broad	Broadest	Broader
ESCR	Standard	Better	Best	Better
Die swell	Standard	Standard	Highest	Higher
Film strength	Standard	Better	Best	Better
Odor/taste	Acceptable	Acceptable	Problematic	Acceptable

Note: HPV = high pore volume; MPV = medium pore volume.

2.3.3 Ziegler–Natta Catalysts

The original Ziegler–Natta catalysts had very poor activity, so in an effort to obtain higher transition metal reactivity, some researchers investigated depositing the transition metal compounds on various high-SA supports. By 1965, inventors from Cabot Corporation had patents disclosing the use of a pyrogenic silica support (Cab-O-Sil) having a particle size smaller than 1 µm.[36] However, this approach was not successful at the time. The simple combination of titanium tetrachloride on silica yielded low-reactivity catalysts; furthermore, Cab-O-Sil would have led to a polymer particle size too small for slurry and gas-phase processes.

Subsequently a patent by Stevens and George[37] disclosed the combination, or reaction product, of a magnesium compound with a porous silica material followed by reaction with titanium tetrachloride. The resulting catalyst component exhibited enhanced reactivity as well as the excellent handling and polymer particle control characteristic of the Phillips chromium catalysts. However, the catalyst preparation procedure they taught was cumbersome, involving multiple solvent washing and intermediate drying steps. Several other patents for magnesium–titanium–silica catalysts with cumbersome procedures appeared before a simplified synthesis was made known.[38] United States patent 4,263,171 of April 1981 was the first of several patents by scientists at Chemplex Company that taught silica–magnesium–titanium catalyst synthesis by a one-vessel process that eliminated all solvent washing and intermediate drying steps. By modifying the silica surface chemically, it was possible to alter the molecular weight distribution.[39–41] This fact indicates that the silica is more than an inert carrier. The reactivity of the simplified catalyst remained high enough to eliminate catalyst removal steps.

Both magnesium chloride and silica are being used as supports for Ziegler–Natta catalysts, and both afford the particle morphology control essential in gas-phase and slurry polymerization processes. However, consideration of the factors involved in polymerization processes allows the identification of five ways in which silica has advantages over magnesium chloride: (1) The absence of chlorine in silica obviously decreases the chloride content of the catalyst. This results in less chloride residue in the polymer products and consequently less color, odor, and corrosiveness. (2) The magnesium chloride–supported catalysts frequently exhibit very high rates of polymerization in the first 5 min followed by a decline, whereas silica-supported catalysts exhibit rates that are more uniform over time. (3) Silica catalysts have excellent flow properties, and their performance in catalyst feeders is often more consistent than magnesium chloride–supported catalysts. (4) Silica-supported catalysts can be used with Al/Ti molar ratios as low as 5 when trialkylaluminum compounds are the cocatalyst. Lower cocatalyst addition leads to polymer with lower odor and taste, which is important in food packaging applications. (5) Finally, there is virtually no waste generated in the preparation of silica catalysts since all of the materials added are retained on the silica.[42]

Effect of Silica Surface Chemistry and Pore Size As previously explained in the section on the effect of activation temperature, silica surfaces contain highly reactive hydroxyl groups that fall broadly into two categories: isolated and hydrogen bonded. These two categories of hydroxyl groups behave differently toward dehydroxylation and reaction with organic reagents. When heated, hydrogen-bonded hydroxyls are eliminated at temperatures below about 500 °C, whereas isolated hydroxyls are eliminated at higher temperatures. When reacted with hexamethyldisilazane, the isolated hydroxyls are preferentially converted to trimethylsilyloxy groups, whereas hydrogen-bonded hydroxyls do not react readily.[43]

In the case of silica-based Ziegler–Natta catalysts, it is possible to utilize these principles to control the molecular weight distribution of the polymers

TABLE 2.4 Effect of Silica Treatment on Ziegler–Natta Catalyst Performance

Silica Treatment	Activity (g PE/g Cat/h)	MI (dg/min)	ER
Calcined at 600 °C	717	0.2	4.3
HMDS	3650	1.0	1.0

Note: Polymerization conditions: isobutane slurry, 100 °C, 30 psi H_2, 100 psi C_2H_4, triisobutyl aluminum cocatalyst at Al/Ti = 20 (molar ratio).

they produce by tailoring the surface chemistry of the silica support. A comparison will suffice to demonstrate the effect (Table 2.4). The silica-based catalysts involved are those in which silica is treated with an organomagnesium compound and titanium tetrachloride. In one case the silica is calcined at 600 °C for 5 h before catalyst preparation. In the other case the same grade of silica is first treated with hexamethyldisilazane (HMDS). When polymer samples from the two catalysts are compared, the HMDS-treated catalyst has higher activity and produces polyethylene of higher MI and narrower molecular weight distribution (as determined by ER, the high-molecular-weight polydispersity as defined by Shroff and Mavridis[44]).

A comparative study of Ziegler–Natta catalysts supported on medium- and high-PV silica gels showed higher activity for the catalyst on high-PV silica gel because it was possible to increase the loading of the active components on that support.[45] Another study of Ziegler–Natta silica gel catalysts showed that silica gels modified with alumina and zinc showed higher activity. This was attributed to the increased acidity of the support.[46]

2.3.4 Organometallic Catalysts

At present there is very little published information on the effect of silica gel properties on organometallic catalysts. A recent review article (in Chinese), while emphasizing the importance of silica gel properties on the performance of metallocene catalysts supported on silica gel treated with methyl aluminoxane, acknowledges the lack of fundamental studies and systematic understanding.[47]

Pullukat, Shinomoto, and Gillings showed that metallocene catalysts gave higher activity when supported on high- rather than medium-PV silica gel as a result of the higher metal loading possible only with the high-PV support.[48] In addition, two recent U.S. patents are of interest. Kellum and Maeger disclose that silyl chromate catalysts made on high-SA supports with high PV (3 mL/g) produce HDPE with stress crack resistance properties comparable to or better than those exhibited by bimodal HDPE.[49] Šindelář et al. disclose that silyl chromate catalysts promoted with magnesium alkyls produce HDPE with exceptional properties suitable for pipe.[50]

2.4 CONCLUSIONS

In the production of HDPE, the final polymer properties are determined by the combination of catalyst properties, catalyst activation conditions, and polymerization conditions. We have demonstrated that the physical and chemical properties of silica gel supports play a crucial role in controlling the performance of polyolefin catalysts and the properties of the polyethylene produced from them. Chrome catalysts having the combination of high surface area and high pore volume are of particular commercial value, and their relatively higher cost is justified by the unique advantages they provide, including higher catalyst melt index potential, increased catalyst activity, and improved resin ESCR.

When silica is used as the support for Ziegler–Natta catalysts, the surface chemistry of silica gel greatly influences polyethylene molecular weight distribution. The surface chemistry in turn is influenced by silanol distribution, which can be altered by pretreatment with selective reactants such as hexamethyldisilazane.

The influence of silica properties on the performance of silica-supported organometallic or single-site catalysts is an area of intensive industrial research. Since this field is in its infancy compared to chrome–silica and Ziegler–Natta catalysts, less information has been published in the open literature.

REFERENCES

1. Facett, E. W., Gibson, R. O., Perrin, M. W., Patton, J. G., and Williams, E. G., Imperial Chemical Industries, British Patent No. 471,590, 1937.
2. Hogan, J. P., and Banks, R. L., Phillips Petroleum Company, U.S. Patent No. 2,825,721, 1958.
3. Ziegler, K., Holzkamp, E., Breil, H., and Martin, H., *Angew. Chem.*, **1955**, 67, 541.
4. Ziegler, K., Breil, H., Holzkamp, E., and Martin, H., U.S. Patent No. 3,257,332, 1966.
5. Kashiwa, N., Tokuzumi, T., and Fujimura, H., Mitsui Petrochemicals Industries, U.S. Patent No. 3,642,746, 1972.
6. Carrick, W. L., Karapinka, G. L., and Turbett, R. J., Union Carbide, U.S. Patent No. 3,324,095, 1967.
7. Sinn, H., and Kaminsky, W., *Adv. Organomet. Chem.*, **1980**, 18, 99.
8. Benham, E., and McDaniel, M., HDPE, in *Kirk-Othmer Encyclopedia of Chemical Technology*, Vol. 20, 5th ed., Wiley-Interscience, Hoboken, NJ, 2006, pp. 149–179.
9. Arjunan, P., Swamy, J. N., and Singh, B. B., Polyolefin catalyst markets, paper presented at Flexpo, 2007 Conference, Bangkok, Thailand, October 17–19, 2007.
10. Patterson, R. E., Silica—Introduction, in *Kirk-Othmer Encyclopedia of Chemical Technology*, Vol. 21, 4th ed., Wiley-Interscience, New York, 1977, pp. 977–1005. [Errata: in bibliography on p. 1005, references 96 and 97 should cite reference 95, not 93.]

11. Iler, R. K., *The Chemistry of Silica-Solubility, Polymerization, Colloid and Surface Chemistry, and Biochemistry*, Wiley-Interscience, New York, 1979.
12. Aboutboul, H. A., Krekeler, J. H., and Kirch, W., National Petro Chemicals, U.S. Patent No. 3,652,214, 1972.
13. Krekeler, J. H., Aboutboul, H. A., and Kirch, W., National Petro Chemicals, U.S. Patent No. 3,652,216, 1972.
14. Pullukat, T., and Hu, Y., *Current Achievements in Heterogeneous Olefin Polymerization Catalysts*, Sankeisha Co., Nagoya, Japan, 2004, p. 57.
15. Ray, W. H., in *Future Technology for Polyolefin and Olefin Polymerization Catalysis*, Terano, M., and Shiono, T., Eds., Technology and Education Publishers, Tokyo, Japan, 2002, p. 19.
16. Barby, D., Surface properties of silicas, in *Characterization of Powder Surfaces*, Parfitt, G. D., and Sing, K. S. W., Eds., Academic, New York, 1976, pp. 353–425.
17. Dunn, B. C., Cole, P., Covington, D., Webster, M. C., Pugmire, R. J., Ernst, R. D., Eyring, E. M., Shah, N., and Huffman, G. P., *Appl. Catal. A*, **2005**, 278, 233–238.
18. Xiao, X., and Butler, J. R., Fina Technology, U.S. Patent application 2004235657, 2004.
19. Xiao, X., and Butler, J. R., Fina Technology, U.S. Patent application 20060183955, 2006.
20. Patterson, R. E., *High Pore Volume Silica Supports for Chromium Catalysts in the Production of High-Density Polyethylene*, Specialty Silica Summit 2007, Atlanta, GA, April 23–25, 2007.
21. McDaniel, M. P., in *Advances in Catalysis*, Vol. 33, Eley, D. D., Pines, H., and Weiss, P. B., Eds., Academic, Orlando, FL, 1985, pp. 47–98.
22. Hogan, J. P., and Kitchen, A. G., Phillips Petroleum, U.S. Patent No. 3,225,023, 1965.
23. McDaniel, M. P., *J. Polym. Sci. Polym. Chem.*, **1983**, 21, 1217.
24. McDaniel, M. P., Witt, D. R., and Benham, E. A., *J. Catal.*, **1998**, 176, 344–351.
25. Hogan, J. P., *Appl. Ind. Catal.*, **1983**, 1, 149.
26. McDaniel, M. P., Rohlfing, D. C., and Benham, E. A., *Polym. Reaction Eng.*, **2003**, 11, 101–132.
27. Zhuravlev, L. T., *Colloids Surf. A Physicochem. Eng. Aspect*, **2000**, 173, 1–38.
28. McDaniel, M. P., and Welch, M. B., *J. Catal.*, **1983**, 82, 98–109.
29. McDaniel, M. P., Welch, M. B., and Dreiling, M. J., *J. Catal.*, **1983**, 82, 118–126.
30. J. P. Hogan, Olefin copolymerization with supported metal oxide catalysts, in *Copolymerization*, Ham, G. E., and Alfrey, T., Eds., Interscience, New York, 1964, pp. 89–113.
31. Dietz, R. E., Phillips Petroleum, U.S. Patent No. 3,887,494, 1975.
32. Pullukat, T. J., and Shida, M., Chemplex Co., U.S. Patent No. 3,780,011, 1973.
33. Pullukat, T. J., Hoff, R. E., and Shida, M., *J. Polym. Sci. Polym. Chem. Ed.*, **1980**, 18, 2857–2866.
34. Shida, M., and Cancio, L. V., *Polym. Eng. Sci.*, **1971**, 11, 124–128.
35. Katzen, S. J., and Rekers, L. J., National Petro Chemicals, U.S. Patent No. 4,252,926, 1981.

36. Orzechowski, A., and MacKenzie, J. C., Cabot Corp., U.S. Patent No. 3,166,542, 1965.
37. Stevens, J., and George, M., Solvay & Cie, U.S. Patent No. 3,787,384, 1974.
38. Shida, M., Pullukat, T. J., and Hoff, R. E., Chemplex Co., U.S. Patent No. 4,263,171, 1981.
39. Pullukat, T. J., and Hoff, R. E., Chemplex Co., U.S. Patent No. 4,374,753, 1983; Hoff, R. E., Chemplex Co., U.S. Patent No. 4,402,861, 1983; Pullukat, T. J., and Hoff, R. E., Chemplex Co., U.S. Patent No. 4,478,988, 1984.
40. Pullukat, T. J., and Hoff, R. E., Chemplex Co., U.S. Patent No. 4,530,912, 1985; Pullukat, T. J., and Hoff, R. E., Chemplex Co., U.S. Patent No. 4,530,913, 1985; Pullukat, T. J., and Hoff, R. E., Norchem, U.S. Patent No. 4,578,440, 1986.
41. Lynch, M. W., and Pullukat, T. J., Chemplex Co., U.S. Patent No. 4,510,299, 1985.
42. Pullukat, T. J., and Hoff, R. E., *Catal. Rev. Sci. Eng.*, **1999**, 41, 389–428.
43. Blitz, J. P., *Colloids Surf.*, **1992**, 63, 11–19.
44. Shroff, R., and Mavridis, H., *J. Appl. Polym. Sci.*, **1995**, 57, 1605–1626.
45. Luo, H., Tang, R., and Gao, K., *J. Catal.*, **2002**, 210, 328–339.
46. Muñoz-Escalona, A., Martín, A., and Hidalgo, J., *Eur. Polym. J.*, **1981**, 17, 367–372.
47. Yaming, W., and Chuanfeng, L., Progress of metallocene catalysts supported on silica gel, in *Xiandai Suliao Jiagong Yingyong [Modern Plastics Process. Appl.]*, **2004**, 16, 43–46.
48. Pullukat, T. J., Shinomoto, R., and Gillings, C., *Plast. Rubber Compos. Process. Appl.*, **1998**, 27, 8–11.
49. Kellum, G. E., and Maeger, P. L., Chevron Chemical Co., U.S. Patent No. 6,673,736, 2004.
50. Šindelář, P., Havránek, M., Salajka, Z., Pešta, P., Št pánková, K., and Jansa, L., Chemopetrol A.S., U.S. Patent No. 6,569,966, 2003.

3 Computational Modeling of Polymerization Catalysts

MONIKA SREBRO and ARTUR MICHALAK
Department of Theoretical Chemistry, Jagiellonian University,
30-060 Cracow, Poland

3.1 INTRODUCTION

Molecular modeling at different levels of approximation is widely used as a practical tool in almost all areas of chemistry at the present time. As a result of a rapid increase in computational power of modern computers in recent years, quantum-chemical ab initio methods are not limited to small, model systems any longer. Computational methods based on quantum chemistry can nowadays be applied for relatively large molecules, and thus they are commonly used in the modeling of complex chemical processes. In particular, in the area of catalysis, quantum-chemical molecular modeling can be utilized to examine the elementary reaction steps of the catalytic cycle at the molecular level. This can provide the deep fundamental understanding of how the catalyst operates that is ultimately required for rational catalyst engineering and further technological innovations.

Among various ab initio methods of quantum chemistry, density functional theory (DFT) has become especially popular as a reasonable compromise between computational cost and the level of accuracy. DFT methods are currently widely applied in modeling of various chemical reactions, in particular those involving transition metal complexes.

The main purpose of this chapter is to review recent computational studies in the area of α-olefin polymerization catalyzed by transition metal complexes. Some aspects of theoretical studies of the polymerization and copolymerization processes have been recently reviewed.[1–3]

In the first part, basic ideas of computational modeling will be briefly summarized. This part is not intended to be a detailed and systematic theoretical introduction to modern computational methods of quantum chemistry. It will

---

Handbook of Transition Metal Polymerization Catalysts Edited by Ray Hoff and Robert T. Mathers
Copyright © 2010 John Wiley & Sons, Inc.

be rather focused on the topics that are especially important in mechanistic studies of chemical processes, with some emphasis on their practical aspects. A systematic introduction to molecular modeling and computational methods of quantum chemistry can be found in many excellent textbooks[4–6] and review articles.[7]

The second part of the chapter, which is the main part, presents a comprehensive review of the results of theoretical studies on the polymerization catalysts as well as on the main mechanistic steps in the process.

3.2 COMPUTATIONAL MODELING OF CHEMICAL REACTIONS

3.2.1 Potential Energy Surface

A starting point in a theoretical description of molecular systems is the Schrödinger equation, which provides a wave function of the system. Unfortunately, exact solutions of the Schrödinger equation exist only for model systems and one-electron atoms. For many-electron systems only approximate wave functions can be obtained. For a molecular system, the total wave function depends of the electronic and nuclear coordinates. The basic approximation that is applied in typical quantum-chemical calculations is the Born–Oppenheimer approximation.[8] By separating the electronic and nuclear motion, it introduces the concept of the potential energy surface (PES), a hypersurface upon which nuclei move. Thus, within the Born–Oppenheimer approximation, an electronic wave function depending parametrically on the nuclear coordinates must be determined. A single point on the PES corresponds to a single molecular geometry. Knowledge of electronic energy for different molecular geometries allows one to solve the nuclear equations of motions, with a potential given by the PES. However, in the most commonly used *static* approach, the quantum-chemical calculations are restricted to determination of the electronic wave function, electronic energy, and other properties, only for a few characteristic points on the PES (a few molecular geometries), without further consideration of nuclear dynamics.

A schematic representation of a PES is shown in Figure 3.1. Minima on the PES correspond to stable molecular geometries (reactants and products of chemical reactions). Transition structures/transition states (TSs) of chemical reactions correspond to first-order saddle points. Thus, the energy difference between the minima corresponding to reactants and products allows a discussion of the thermochemistry of a reaction. Similarly, the equilibria between alternative isomers of reactants/products can be discussed on the basis of the respective energy differences. Correspondingly, information on the reaction kinetics can be extracted from the energy differences between the transition structures and the reactants, corresponding to activation energy.

The typical quantum-chemical calculations performed to model the elementary steps of a chemical process thus involve (i) determination of the minima on the PES which are important for the reaction in question

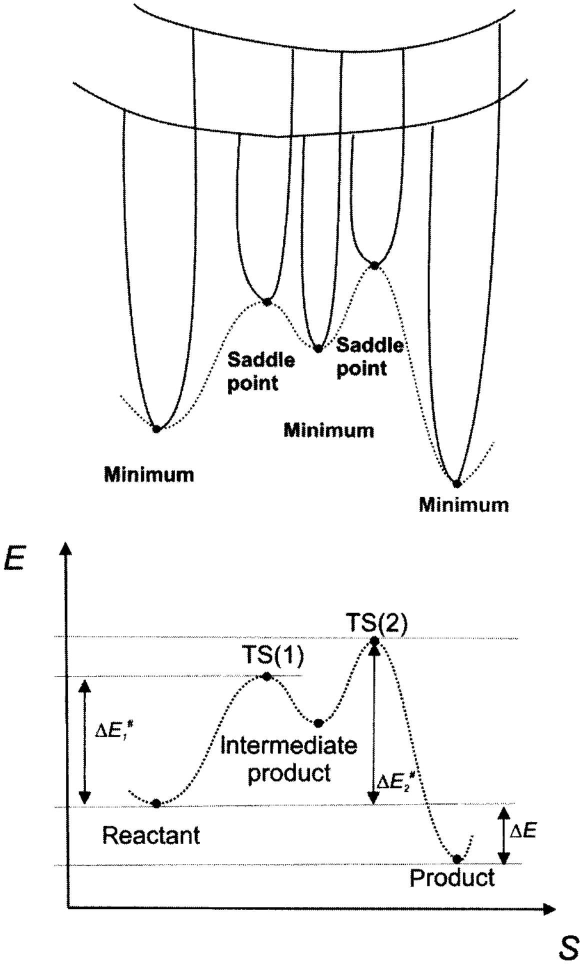

Figure 3.1 Schematic representation of potential energy surface (top) and corresponding reaction profile (bottom).

(geometry optimization of the reactants and products) and (ii) determination of the TS structure on the PES (TS optimization). An example of the reaction profile for a sequence of elementary reactions corresponding to propagation of a polymer chain in the ethylene polymerization process catalyzed by the Ni–diimine catalyst is shown in Figure 3.2. In this example, the calculations involved optimization of the geometry of isolated ethylene (a), isolated β-agostic complex with *n*-propyl alkyl (b), ethylene π-complex (c), γ-agostic complex with *n*-pentyl alkyl—an immediate insertion product (e), β-agostic complex with *n*-pentyl alkyl—a final insertion product (g), as well as optimization of transition structures for ethylene insertion (d: $TS^{(c \rightarrow d)}$) and for isomerization between γ- and β-agostic complexes (f: $TS^{(d \rightarrow e)}$).

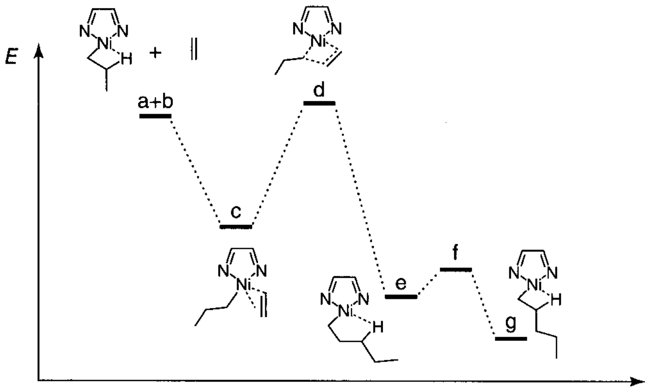

Figure 3.2 Example energy profile for chain propagation pathway for ethylene polymerization catalyzed by model Ni–diimine catalyst.

Knowledge of the wave function (or electron density in DFT) for minima and saddle points on the PES allows the calculation of other physical quantities which are used as the electronic structure descriptors, reactivity indices, spectroscopic parameters, and so on.

3.2.2 Wave-Function-Based Methods and Density Functional Theory

The "traditional" quantum-chemical approach within Born–Oppenheimer approximation is based on the electronic Schrödinger equation, $\hat{H}\Psi = E_{\mathrm{el}}\Psi$, that gives the electronic energy E_{el} and the wave function Ψ; here $\hat{H}$ stands for the electronic energy operator (Hamiltonian). Since the general form of the wave function is not known for many-electron systems, numerous computational methods developed in previous decades assume a different approximate form of the wave function. Thus, those traditional approaches can be characterized in a simplified way as looking for the approximate wave function with the exact Hamiltonian. The most important starting point for more advanced methods of this group is the Hartree–Fock (HF) method with an approximation for the wave function given in a form of a single Slater determinant built of one-electron molecular orbitals.

The HF method neglects the correlation energy, often important in the case of chemical reactions, especially those involving transition metal complexes. The electron correlation methods assume the wave function as a combination of many Slater determinants. The most important groups of such post-HF approaches are variants of configuration–interaction (CI) methods, complete active-space–self-consistent field (CAS-SCF), multiconfigurational SCF (MC-SCF), Møller–Plesset perturbation theory (MP: MP2, MP4), or coupled-cluster (CC) approaches. A detailed discussion of those methods is beyond the scope of this chapter. It should only be emphasized that the HF method scales formally as N^4 with the number of the basis functions N (i.e., with the size of the system). The post-HF methods scale as N^5 (e.g., configuration interaction singles (CIS), second-order Møller–Plesset (MP2), recovering ~94% of the correlation energy), N^6 (e.g., CISD, recovering 94.5% of the correlation energy), N^7 (e.g., fourth-order Møller–Plesset (MP4), recovering 99.5% of the correlation energy) up to N^{10} (e.g., coupled-cluster with single, double, triple, and quadruple excitations (CCSDTQ), recovering 99.9% of the correlation energy). Such a scaling makes these methods nonpractical for large molecular systems.

Density functional theory represents an alternative approach based on different philosophy. It has been proved by Hohenberg and Kohn[9] that knowledge of the electron density, $\rho(\mathbf{r})$, is formally sufficient to determine the ground-state electronic energy (and any physical quantity). The Kohn–Sham[10] method is a practical prescription to determine the exact density for a given energy functional. The exact form of the energy functional of the density, however, is not known. The unknown part of the functional is called the exchange correlation (XC) functional, as it describes nonclassical exchange and correlation terms. Thus, DFT approaches can be characterized in a simplified way as looking for the exact density with the approximate energy functional.

The simplest approximate form of the XC functional, depending on the density only, is the local density approximation (LDA),[10] which gives the accuracy sufficient only for very qualitative considerations. Improved XC functionals are based on the density and the density gradients; the group of "gradient" functionals includes popular functionals defined by Becke and Perdew (BP),[11–13] Lee, Yang, and Parr (LYP),[14] Perdew and Wang (PW86, PW91),[15–17] and Perdew, Burke, and Emzerhof (PBE, RPBE).[18–20] Another group of popular XC functionals are so-called hybrid functionals; the exchange part of those functionals is a combination of the gradient-based exchange term and the exact exchange from HF theory. The most popular functional of this group is the Burke three-parameter Lee–Yang–Parr (B3LYP) functional.[21]

The general accuracy of the gradient and hybrid functionals is roughly similar. The choice of the XC functional for a given problem and given class of compounds should be based on literature teaching (if it exists) or on a comparison of calculated values with experiment. In the case of polymerization processes with transition metal catalysts both gradient and hybrid functionals have been commonly used. Their performance depends on the type of complexes comprising the catalysts. For example, an excellent performance of the gradient functionals has been demonstrated for the late transition metal complexes. On the other hand, the gradient functionals are known to fail for the high-spin complexes, for which the hybrid functionals seem to be more appropriate.

It should be emphasized that DFT methods account for the correlation energy, though in an approximate way. The overall accuracy of DFT is comparable to the MP2 method. However, typical DFT methods scale as N^3 (or N^4 in the case of hybrid functionals). Thus, they often represent a good compromise between computational cost and accuracy.

3.2.3 Basis Sets in Molecular Calculations

In both wave-function-based quantum chemistry and DFT a choice of basis sets is one of the factors of crucial importance for accuracy of the calculations. In the wave-function-based quantum chemistry the one-electron molecular orbitals, used in construction of the total wave function, are expressed as a linear combination of the basis set functions. In the Kohn–Sham (KS) DFT auxiliary one-electron KS orbitals are similarly expanded in the basis set. Most often the basis set is constructed from the "atomic orbitals," that is, the Slater-type or Gaussian-type functions centered in atomic positions.

A few schemes to classify and describe the basis sets are commonly used. This topic goes definitely beyond the scope of this chapter. One of the factors of importance is the number of the basis function used. With this respect, the basis sets are often described as *single zeta* (SZ), *double zeta* (DZ), *triple zeta* (TZ), and so on. Minimum basis sets (SZ) for an atom consist of such number of the functions that corresponds to the number of its occupied atomic orbitals; for example, for oxygen atom the SZ basis set consists of five functions: one $1s$, one $2s$, and three $2p$ atomic orbitals. In DZ basis sets, each occupied atomic orbital is described by two functions with two different exponents and in TZ by three functions with three exponents. Thus, TZ basis set for an oxygen atom consists of 15 functions, for instance. In *double-zeta valence* (DZV) and *triple-zeta valence* (TZV) basis sets, a doubled or tripled number of functions is used for valence shell only.

In addition, *polarization functions* are often used to allow for spatial flexibility of the orbital; these functions correspond to higher angular momentum, for example, *d*-type functions for oxygen. For the systems with loosely bound electrons (e.g., in anions), additional *diffuse basis functions* should be used. They are characterized by a small value of exponent and thus extend very far from the nuclei.

There is no general rule concerning the basis set choice. In routine DFT calculations the basis sets of TZP (*triple-zeta polarization*) quality are recommended for transition metals and of DZP quality for the main-group elements. In combination with advanced post-HF methods for electron correlation the extended basis sets should be used to achieve a required level of accuracy. Nevertheless, for a particular problem/property and for specific systems, a basis set convergence should be checked; here a literature search can be helpful.

It is important to point out that for systems containing heavier atoms the *all-electron* calculations are not practical since the computational cost grows quickly with the number of electrons in the system. Therefore, it is common to tackle explicitly only the valence electrons and to represent the influence of core orbitals by various pseudopotentials/effective core potentials (model potentials)[22,23] or the frozen-core approximation.[24] In the pseudopotential/effective core potential approach the orbitals for the core electrons are replaced by a potential (dependent on the nucleus–electron distance) that is parametrized to reproduce the atomic valence orbitals obtained as a result of the all-electron calculations. In the frozen-core approximation the orbital representation is used for both core and valence electrons. However, the orbitals for the core electrons are frozen; that is, they are represented by a fixed expansion in a basis set. Thus, only the valence orbitals are optimized in the calculations; their orthogonality to the frozen-core orbitals must be preserved in the calculations. Use of pseudopotential or frozen-core approaches allows one to perform quantum-chemical calculations practically for the whole periodic table of elements; for heavier elements the reduction in the computational cost is substantial. In principle, both approaches lead to the reasonable accuracy for the energy differences. Use of the pseudopotential approaches is limited, however, in the case of properties that explicitly depend on the core electron density or core orbitals [e.g., nuclear magnetic resonance (NMR), x-ray photoelectron spectroscopy (XPS) parameters].

3.2.4 Relativistic Effects

For the systems involving heavy elements, relativistic corrections should be included due to the fact that the velocity of the core electrons becomes comparable to the speed of light. The relativistic term in the total energy is significant even for lighter atoms, but it practically disappears in the energy differences. For the third-row elements and higher, the relativistic correction can substantially affect the energy differences.

3.2.5 Geometry Optimization and Transition State Optimization

Geometry optimization is done in an iterative process: For the initial geometry the wave function/electron density is optimized, forces acting on nuclei are computed, the nuclei are moved according to forces, and the process is repeated until convergence is achieved; that is, the assumed convergence criteria are fulfilled. Geometry optimization can usually be performed in a routine way. In the popular programs for quantum-chemical calculations many effective algorithms for geometry optimization are implemented and can be used in an automatic way. One should have in mind, however, that the convergence of the geometry optimization can be affected by a quality of initial geometry; the closer the starting point is to the real minimum, the sooner it is going to be reached. For the systems with multiple minima on the PES (i.e., most of the interesting cases) there is no guarantee that the global minimum is going to be reached; most often, the optimization started from the point close to the local minimum will be finished in this minimum. Therefore, for the complex systems one should check existence of alternative isomers and conformers.

Another practical issue is a choice of the coordinates in which the geometry optimization is performed. The optimization in internal coordinates is usually converged faster than in the Cartesian coordinates.

Transition state optimization is more complicated due to the fact that the transition structure corresponds to the saddle point on the PES. TS optimization started from geometry distant from the TS usually fails. Thus, finding the initial structure for optimization of the TS requires extra calculations. A common way to find such approximate TS geometry is to perform a set of constrained optimizations for different values of *reaction coordinate*, that is, a geometric parameter that describes the transition between reactants and products, for example, the distance between the atoms forming the bond. The geometry corresponding to the highest energy/zero gradient along the profile can be used as the starting point for the optimization of TS. An example concerning insertion of ethylene with the Ni-anilinotropone catalyst is shown in Figure 3.3.

The TS geometry should be validated by computations of vibrational frequencies. The first-order saddle point is characterized by exactly one imaginary frequency (one negative eigenvalue of the Hessian matrix). Also, the located TS should be checked to make sure that it corresponds to the transition between the assumed reactants and products and not to the transition

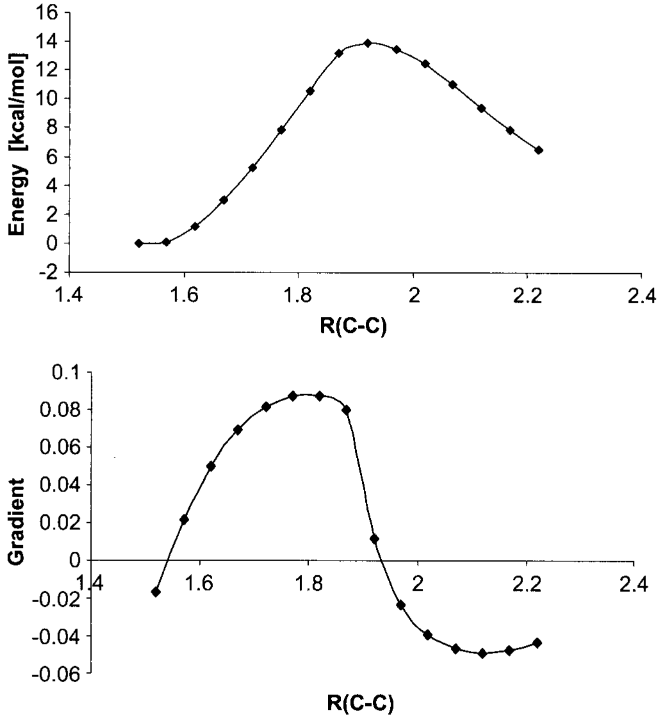

Figure 3.3 Example profiles for energy and energy gradient for ethylene insertion pathway determined from DFT calculations for model Ni–anilinotropone catalyst; a distance between the ethylene and alkyl carbon atoms was used as a reaction coordinate.

between other minima on the PES. This can be done by determination of the reaction paths on the PES from TS to the reactant and products. One of the most commonly used reaction paths is described by the *intrinsic reaction coordinate*,[25] often implemented in quantum-chemical programs.

3.2.6 Thermodynamics

The thermodynamic functions can be easily computed based on the statistical mechanics. The standard expressions for the translational, rotational, and vibrational contributions are used in the programs for quantum-chemical calculations. It should be noted that the thermodynamic functions are usually computed automatically when vibrational analysis is performed, since the cost of such calculations is negligible, compared to the cost of vibrational analysis. It should be pointed out that the computed frequencies are very sensitive for the accuracy of the geometry optimization. In principle, prior to frequency calculations, the molecular geometry should be optimized at the same level of theory, with the tight optimization criteria.

3.3 MODELING CATALYST PROPERTIES AND POLYMERIZATION PROCESSES

In this part of the chapter we will review the results of theoretical studies on the polymerization catalysts performed by many research groups with use of different theoretical methods. Let us start with some general comments on the polymerization mechanism.

The most widely accepted mechanism of the ethylene polymerization process catalyzed by organometallic complexes is based on the original Cossee–Arlman idea.[26–30] In a general case, the major mechanistic steps in the process include (Figure 3.4): (i) activation of a precatalyst by a cocatalyst or via a dissociation reaction, resulting in formation of the catalytic active species; (ii) chain initiation, involving complexation of an olefin into a vacant coordination site at the metal center, with formation of an olefin π-complex and subsequent insertion of the coordinated monomer into the metal–alkyl bond; (iii) chain propagation, involving an uptake of free monomer and its insertion into a metal–polymer chain bond—a sequence of consecutive chain propagation

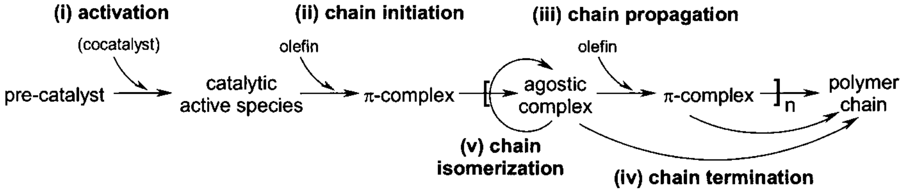

Figure 3.4 Basic steps in polymerization mechanism.

steps leads to a growth of the polymer chain; (iv) chain termination that concludes a polymerization cycle; and (v) chain isomerization leading to formation of branched structures of the growing macromolecule.

Mechanistic details of the polymerization process presented above were fairly well established based on the extensive and thorough studies carried out by experimentalists and theoreticians. The main goal of this account is to give a comprehensive review of theoretical research on the elementary reactions of the polymerization processes catalyzed by the metallocene and postmetallocene transition metal complexes. Since a great number of computational results have been published so far in this area, it is not possible to summarize all of them. We shall focus on the theoretical results considering the catalyst properties and those that give a general mechanistic insight into the progress of particular steps of the polymerization, that is, catalyst activation, chain initiation, propagation, termination, and isomerization. Where applicable, the early and late transition metal catalysts will be discussed separately. The last section will be devoted to the copolymerization of ethylene with polar monomers catalyzed by late transition metal complexes.

3.3.1 Computational Studies on Catalyst Properties

Since the "metallocene revolution"[31–33] period, both academic and industrial research laboratories have been carrying research focus on the development of new organometallic complexes serving as single-site polymerization catalysts. The studies have included almost all transition metals, some lanthanides as well as a few main-group elements, combined with a great variety of ligands.[34–37] Although ligands bound to the metal center are not directly involved in the catalytic process, their presence seems to be crucial for controlling the steric and electronic nature of the catalyst active site. They also prevent formation of the secondary active sites, eventually giving rise to high-molecular-weight polymers. In that way they affect both the catalyst performance and the properties of the polymer produced. Thus, understanding the interaction between ancillary ligands and the metal center can certainly contribute to a rational design of new efficient catalysts for the olefin polymerization.

The electronic influence of ligands on the catalytic activity of the metal center can be characterized on the basis of their σ-donor/π-acceptor properties. The energy of the highest molecular orbital and the chemical hardness/softness quantities, related to the highest–lowest molecular orbital (HOMO–LUMO) gap, are the simplest but quite informative computational indices that reflect donor properties of the ancillary ligands. Better donor ligands have higher value of HOMO energy and are more soft or polarizable. In consequence, they can more efficiently bind to an electron acceptor center, that is, the metal center.

The DFT study on the electronic properties of cyclopentadienyl derivatives and their heteroaromatic analogues in zirconium-based complexes has been recently performed by Nagy et al.[38] This study was focused on a relationship between electronic properties of the ligands and the catalyst activity. As it was shown, the donor ability of ligands can be directly correlated with the relative stability of the cationic active species. Namely, softer ligands with an extended π-electron system have the strongest stabilizing effect. The ligand properties also have a direct influence on the reactivity of the active species toward ethylene, comonomer, or chain transfer agents. The chemical softness of the coordinated ligand was found to be correlated with LUMO energy of the zirconocenium cation. Namely, an increase in the ligand chemical softness results in an increase in the LUMO energy. Furthermore, a reasonably good correlation between the experimental reactivity of the metal center and the LUMO energy of the zirconocenium cation leads to a conclusion that the LUMO energy can be used as a simple reactivity index for rough prediction of the catalyst activity. Thus, the results show that the soft ancillary ligands give rise to high reactivity of the metal center toward olefin insertion.

Recently, the calculated energies of HOMO and LUMO as well as the local softness, defined by Yang and Parr,[39] have been used as reactivity descriptors in the three-dimentional quantitative structure–activity relationship (3D-QSAR) analysis of the metallocene-based catalysts activity.[40,41] The QSAR methodology, commonly used in medicinal chemistry, is based on a statistical, quantitative correlation of chemical activities of a compound with its physicochemical properties as well as with descriptors that encode some features of its geometric and electronic structure. The results provide useful correlations between experimental activity and the steric factors (shape of molecule), energy of LUMO, and local softness. This study further confirmed that the donor/acceptor character of ancillary ligands has a significant effect on the catalytic activity of the complex.

Finally, in the context of presented results, it must be emphasized that there still exits a necessity for theoretical research focused on the understanding of the ancillary ligand–metal center interaction. Here, the use of the theoretical methods directly addressing the "classical" Dewar–Chatt–Duncanson model of donation/back-bonding in transition metal systems[42,43] seems to be justified. One such technique, based on analysis of the natural orbitals for chemical valence (NOCV),[44,45] allows for a direct separation of the contributions to the deformation (differential) density $\Delta\rho$ from the ligand → metal and metal → ligand electron charge transfer processes. NOCV can be a valuable tool in studies of the polymerization catalysts[44,45] as they provide a quantitative measure of the donation and back-bonding charge transfer. A systematic analysis of the donation/back-bonding trends can lead to better understanding of the structure–activity relationship as far as the influence of both the metal and the ancillary ligand is concerned.

3.3.2 Activation Process and Counteranion Effects

The majority of polymerization processes carried out by single-site transition-metal-based catalysts requires, in a first step, generation of coordinatively unsaturated cationic active species. In general, in this *activation* process, a precatalyst, $(L)_2M(CH_3)_2$, reacts with a cocatalyst, A, which abstracts one of the alkyl groups to produce an activated catalyst—an electrophilic species with cationic character, $[(L)_2M(CH_3)]^+$. The cocatalysts are generally Lewis acids, such as tris(pentafluorophenyl)borane ($B(C_6F_5)_3$) or methylaluminoxane (MAO). MAO is the cocatalyst that is most often used in both academic research and industrial applications.

The abstraction of a precatalyst alkyl group results as well in the generation of the anionic form of a cocatalyst, $[(CH_3)A]^-$. Therefore, activation of the dimethyl precatalyst, $(L)_2M(CH_3)_2$, by a Lewis acid, A, leads in fact to the formation of a contact ion pair, in which the anionic counterion is bound to the metal center by a methyl bridge, $[(L)_2M(CH_3)]^+[(\mu\text{-}CH_3)A]^-$.

Early Transition Metal Catalysts A great number of theoretical research work[46–65] suggests that the counterion may in some cases play a significant role in the polymerization process, primarily by controlling ion pair formation and dissociation equilibria that directly affect the olefin complexation to the metal center. Accordingly, in this section we will focus attention on the ion formation and ion separation processes, especially in the context of the binding competition between olefin, solvent, and counteranion.

Theoretical studies on ion pair formation and ion pair separation processes were carried out at different levels of quantum-chemical calculations for a variety of cationic polymerization catalysts and their anionic counterions.[51,53,55,57,59,62]

The DFT study on activation by $B(C_6F_5)_3$ cocatalyst and subsequent ion pair formation for a series of mono(cyclopentadienyl), constrained-geometry, and bis(cyclopentadienyl) titanium and zirconium precatalysts was performed by Chan et al.[53] The authors considered three possible ion pair formation processes, resulting in (i) a $\mu\text{-}CH_3$ (or μ-F) contact ion pair, (ii) an olefin-separated ion pair with a monomer (ethylene) placed between the cation and the anion, and (iii) a solvent-separated ion pair with a solvent (toluene) molecule located between the cation and the anion (Figure 3.5).

The contact ion pair formation energy was calculated as the energy difference between the neutral precursors and the contact ion pair. Thus, it includes the methide abstraction energy. In the case of separated ion pairs, their energies of formation were obtained with respect to the free ethylene/toluene molecule and the contact ion pair, thus corresponding directly to the ethylene and toluene complexation energy. The solvent (toluene) effects were incorporated into the DFT calculation with the use of the conductor-like screening model (COSMO). To analyze an influence of ancillary ligands on the stability of the contact ion pair, changes in Hirshfeld atomic charges due to the ion pair formation were used as a rough estimate of the electron-donating ability of ligands attached to a metal center.

The results showed that the enthalpy of methide abstraction to form a contact ion pair is exothermic for all investigated systems, ranging from −19.1

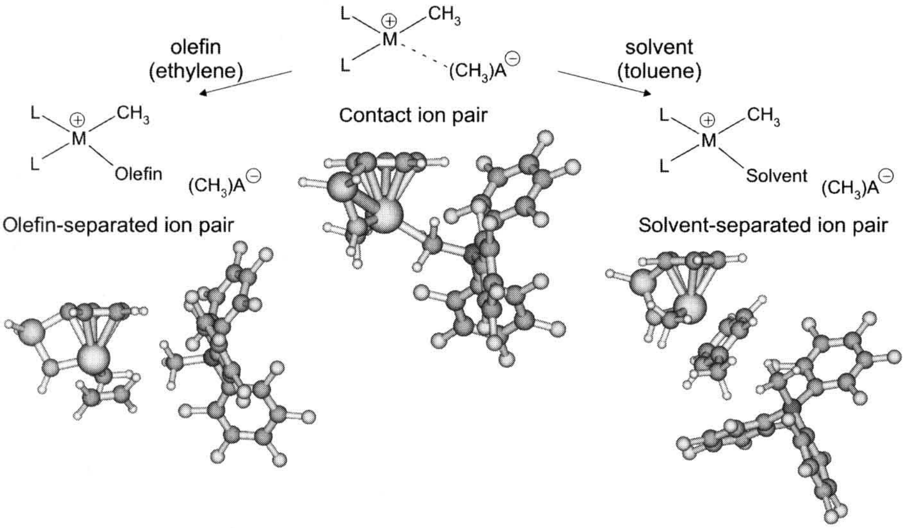

Figure 3.5 Contact, olefin-separated, and solvent-separated ion pairs from $H_2SiCp(NH)Ti(CH_3)_2$ precursor used here as an example (geometry from ref. 53).

to −12.9 kcal/mol, for $Cp_2Zr(CH_3)_2$ and $CpTi(CH_3)_3$, respectively. It depends on both the metal center and the electron-donating ability of the ligands. Namely, the lower enthalpy was always obtained for the zirconium analogue of the considered precatalysts. For example, values of −15.5 and −19.1 kcal/mol were obtained for $Cp_2Ti(CH_3)_2$ and $Cp_2Zr(CH_3)_2$, respectively. Concerning the ligand effect, it was found that an increase in the electron donation from ancillary ligands results in more negative values for enthalpy. For example, for the zirconium system with bis-cyclopentadienyl derivatives, the following order was obtained: Cp (−19.1) < 1,2-$(CH_3)_2$Cp (−23.8) < $(CH_3)_5$Cp (−27.5 kcal/mol). It was also found that solvation has rather negligible effect on the energy of ion pair formation.

Investigation of the reactions of the contact ion pair with an olefin (ethylene) and a solvent (toluene) (Figure 3.5) showed that the insertion of the ethylene into the contact ion pair to form the olefin-separated ion pair is an endothermic process for all studied systems, while such an insertion of toluene, resulting in the formation of the solvent-separated ion pair, is either exothermic [for both mono(cyclopentadienyl) systems and the Zr-based constrained-geometry catalyst] or endothermic [for Ti-based constrained-geometry catalyst and both of the bis(cyclopentadienyl) catalysts]. The latter result, together with the least endothermic ethylene complexation energy of 6.1 and 8.2 kcal/mol for bis(cyclopentadienyl) titanium and zirconium precatalysts, respectively, led the authors to the conclusion that these systems should have the highest activity.

Recently, the systematic study of the interaction between a series of cationic polymerization catalysts and the anionic counterions in terms of ion pair formation and ion pair separation energies has been performed by Xu et al.[59] The list of considered catalysts and counterions includes $(1,2\text{-}(CH_3)_2Cp)_2Zr(CH_3)^+$, $(NPR_3)_2Ti(CH_3)^+$, $(Cp)(NCR_2)Ti(CH_3)^+$, $(CpSiR_2NR')Ti(CH_3)^+$, $(Cp)(OSiR_3)Ti(CH_3)^+$, $(Cp)(NPR_3)Ti(CH_3)^+$, and $B(C_6F_5)_4^-$, $(CH_3)B(C_6F_5)_3^-$, as well as two structural models for MAO: $Al(CH_3)_3\text{–}MAO(CH_3)^-$ and $MAO(CH_3)^-$. The example structures of ion pairs studied in this work are presented in Figure 3.6. The enthalpies of ion pair formation processes were calculated with respect to neutral precursors and the contact ion pair, while the enthalpies of ion pair separation were determined with respect to the contact ion pair and the coordinatively unsaturated cation and counteranion. The solvent (cyclohexane) effects were modeled by means of the COSMO method.

As previously, the enthalpy of ion pair formation was found to be exothermic for all considered catalytic systems and dependent on both the electron-donating properties of the ancillary ligands and the type of counterion. Nevertheless, among the titanium-based systems, the ion pair formation energy follows in general the same trend for the three anions $(CH_3)B(C_6H_5)_3^-$, $Al(CH_3)_3\text{–}MAO(CH_3)^-$, and $MAO(CH_3)^-$. Namely, $(NP(CH_3)_3)_2Ti(CH_3)^+ <$

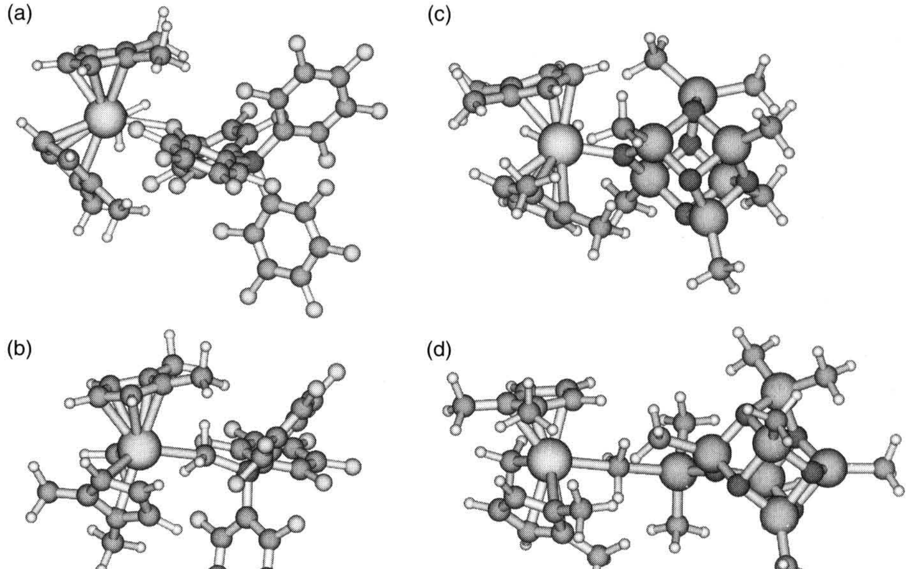

Figure 3.6 Structures of ion pairs formed by $(1,2\text{-}(CH_3)_2Cp)_2Zr(CH_3)^+$ with series of counterions: (*a*) $B(C_6F_5)_4^-$, (*b*) $(CH_3)B(C_6F_5)_3^-$, (*c*) $MAO(CH_3)^-$, and (*d*) $Al(CH_3)_3\text{–}MAO(CH_3)^-$ (geometry from ref. 59).

$(Cp)(NP(CH_3)_3)Ti(CH_3)^+ < (Cp)(NC(CH_3)_2)Ti(CH_3)^+ < (CpSi(CH_3)_2N(CH_3))Ti(CH_3)^+ \leq (Cp)(OSi(CH_3)_3)Ti(CH_3)^+$. For example, the corresponding enthalpies for $Al(CH_3)_3$–$MAO(CH_3)^-$ are $-15.3 < -13.6 < -12.0 < -5.5 < -1.5$ kcal/mol.

Furthermore, the dissociation of a contact ion pair to produce the coordinatively unsaturated cation was found to be highly endothermic and strongly dependent on the catalytic (cation/anion) system; for example, the ion pair dissociation enthalpies vary between the values of 55.7 kcal/mol obtained for $(1,2\text{-}(CH_3)_2Cp)_2Zr(CH_3)^+/B(C_6H_5)_4^-$ and 129.8 kcal/mol calculated for $(CpSi(CH_3)_2N(CH_3))Ti(CH_3)^+/MAO(CH_3)^-$. As it was demonstrated, for the same catalyst but with different anions, the ion separation energy increases in the order $B(C_6H_5)_4^- < (CH_3)B(C_6H_5)_3^- < Al(CH_3)_3$–$MAO(CH_3)^- < MAO(CH_3)^-$. Thus, for $B(C_6H_5)_4^-$ the weakest interaction with the cations was found. For the $(NP(CH_3)_3)_2Ti(CH_3)^+$ cation, the trend is reflected by following values of the ion pair separation enthalpy: $58.7 < 73.1 < 82.5 < 102.1$ kcal/mol. This system in most cases also exhibits the lowest separation energy among different catalysts interacting with the same counterion, even lower than that obtained for $(1,2\text{-}(CH_3)_2Cp)_2Zr(CH_3)^+$ used as a reference system. For the other systems, the separation energies are higher by about 10–20 kcal/mol. Finally, it is worth mentioning that no general relationship between ion pair formation and ion pair separation energies emerged from the studies.

Due to the high endothermicity of the ion pair dissociation process, it seems to be unlikely that such separated species will be present with an appreciable concentration in the reaction mixture. Although the solvation influences the exothermicity of the contact ion pair formation only slightly, it has been revealed that it significantly diminishes the endothermicity of the ion pair separation (even by 30–50 kcal/mol). It was also shown that such an effect increases with increasing solvent polarity (dielectric constant).[51,66] In the context of these results, the formation of the solvent-separated ion pair for some of the catalytic systems seems to be very likely. Thus, a presence of the solvent-separated ion pair can be of great importance since it can facilitate polymerization by providing higher accessibility of the cationic metal center to the incoming olefin or by a possible replacement of a solvent molecule by olefin in the first step in the polymerization process.

Finally, we would like to mention the comprehensive work of Zurek et al.,[62] presenting the results of the theoretical investigation concerning the structure and function of MAO, the most commonly used counterion. Due to the fact that MAO does not have a well-defined molecular structure, it is hard to characterize its dormant and active species present in olefin polymerization. The most likely structures of such species, that is, $(AlO(CH_3))_n$ cages, have been proposed by the authors on the basis of the their relative energies and a comparison of calculated and experimental ^{1}H- and ^{13}C-NMR chemical shifts. Such structures were further successfully used to investigate the mechanism of the polymerization process catalyzed by the metallocenes.

Late Transition Metal Catalysts Although the mechanism of catalytic activation seems now to be quite well understood, the complexity of the interaction between cocatalyst/counterion and catalytic active species results in an increasing interest in developing neutral late-transition-metal-based systems that do not require a cocatalyst and in consequence eliminates the ion-pairing problems. This class of olefin polymerization catalysts includes anilinotropone-based[67] and salicylaldimidato-based[68] nickel(II) complexes, for which the generation of the active site proceeds via the phosphine dissociation reaction.

As was shown on the basis of the combined DFT and molecular mechanics calculations, in the case of the Ni–salicylaldiminato complexes, the phosphine dissociation energy can be controlled by the size of the R group in the 3-position of the salicylaldiminato ring. Namely, the bulky substituent decreases the dissociation energy (27.3 vs. 20.9 kcal/mol for R = H and R = anthracenyl).[69] Furthermore, for the anilinotropone catalyst, the phosphine dissociation was found to be less endothermic than for the corresponding salicylaldiminato system (22.0 vs. 29.2 kcal/mol from DFT study).[70] This supports the experimental hypothesis[63] that the generation of the active site should be much easier in the case of the former catalyst.

3.3.3 Chain Initiation

As shown in Figure 3.4, generation of the catalytic active species during the activation process is followed by chain initiation. It proceeds via the complexation of the incoming olefin to the electron-deficient metal center to form a π-complex and the olefin insertion into the metal–carbon bond. As a result, a new vacant coordination site becomes available for the next olefin to coordinate and propagate the polymer chain in the chain propagation step of the catalytic cycle. Due to some similarities in both chain initiation and propagation, we shall discuss here only π-complexation. An overall view of insertion reactions will be given in detail in the next section.

Due to the fact that the coordination of the incoming olefin by the metal center to form a π-complex is required for all steps of the polymerization cycle, the olefin complexation energies are reported in almost every article presenting the results of theoretical modeling of the transition-metal-catalyzed polymerization processes. Therefore, in this chapter we will focus only on the most informative examples.

Early Transition Metal Catalysts A systematic DFT study on the complexation of ethylene to a number of transition-metal-based model catalysts was carried out by Margl et al.[71] A considered series of d^0 $\{L\}MC_2H_5^{n+}$ ($n = 0, 1, 2$) complexes included (i) Sc(III), Y(III), La(III), Ti(IV), Zr(IV), Hf(IV), Ce(IV), Th(IV), and V(V) as a representative sample of d^0 metal centers, M; (ii) $NH(CH)_2NH^{2-}$, $N(BH_2)(CH)_2(BH_2)N^{2-}$, $O(CH)_3O^-$, Cp_2^{2-}, $NHSi(H_2)C_5H_4^{2-}$, $[(O)(O(CH)_3O)]^{3-}$, $(NH_2)_2^{2-}$, $(OH_2)_2^{2-}$, $(CH_2)_2^{2-}$, and $NH(CH_2)_2NH^{2-}$ as examples of ligands, L. The ethyl group, C_2H_5, was used as a model for the growing polymer chain to allow for considering the β-agostic complex, which is commonly accepted to be the direct precursor of olefin insertion (a resting state of the metallocene catalyst). Accordingly, two modes of olefin coordination were studied, namely "frontsite" (FS) and "backside" (BS), in which ethylene is syn and anti to the β-agostic bond, respectively (Figure 3.7). The relative preference of these two binding modes seems to be crucial for the catalyst performance, since the latter results directly in the insertion reaction of the olefin between the metal–polymer chain bond and the former leads to either the insertion or the termination of the chain due to a transfer of the polymer β-hydrogen to the approaching monomer (β-hydrogen transfer, BHT).

The total energy gain for the process of π-complexation of ethylene, C_2H_4, to form the π-complex, $\{L\}M(C_2H_5)(C_2H_4)^{n+}$ ($n = 0, 1, 2$), that is, $\{L\}M(C_2H_5)^{n+} + C_2H_4 \rightarrow \{L\}M(C_2H_5)(C_2H_4)^{n+}$, was calculated with respect to free ethylene and the energetically most favorable isomer of the precursor $\{L\}M(C_2H_5)^{n+}$. The bond energies were further decomposed according to the Ziegler–Rauk energy-partitioning scheme that allows for separation of the electrostatic, Pauli repulsion, and orbital interaction as well as the geometry distortion and the relativistic contribution to the binding energy.

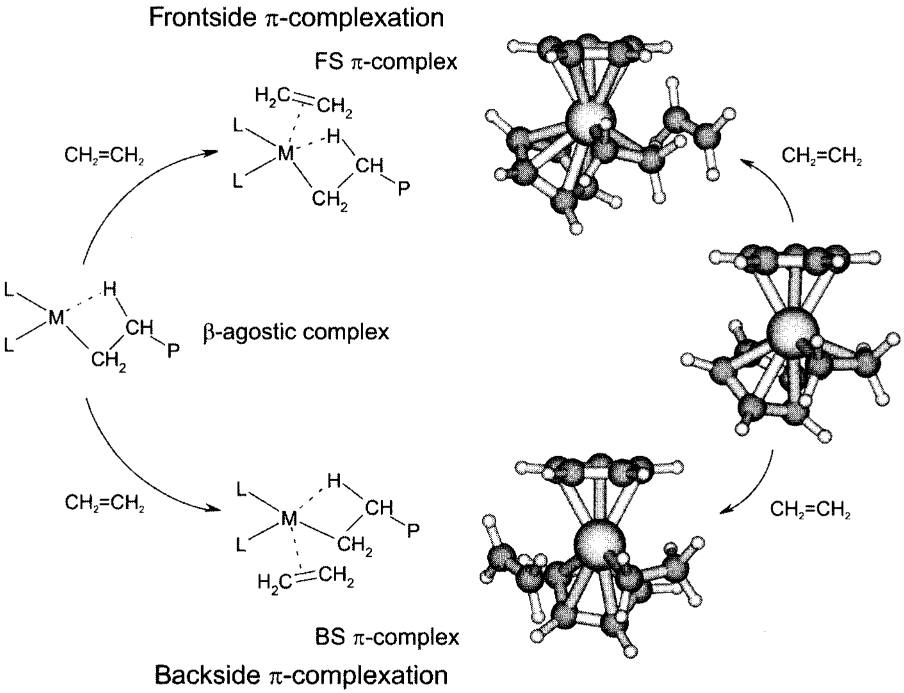

Figure 3.7 Frontside vs. backside complexation process for $\{Cp_2\}Ti(C_2H_5)^+$ used here as an example (geometry from ref. 71).

The results of geometry optimization show that the π-complexes demonstrate a slight preference of the olefin orientation with respect to the rest of the catalyst with the rotational barriers for torsion around the metal–olefin bond lower than 3.6 kcal/mol. The π-complexation energies calculated for all investigated compounds are generally exothermic, ranging from –54.3 (–49.5) to 0 (–1.2) kcal/mol for $\{NH(CH)_2NH\}Nb(C_2H_5)$ and $\{Cp_2\}Sc(C_2H_5)$ in the FS (BS) coordination mode, respectively. The complexation energies were found to be strongly dependent on both a metal center and ancillary ligands. Of importance are factors such as (i) the total charge on the metal fragment, (ii) the "accessibility" of the metal center, and (iii) the conformation of the precursor determined by the metal as well as ligands framework.

The results demonstrate that among studied systems more exothermic values of olefin uptake energy are obtained for doubly charged species, that is, $\{O(CH)_3O\}Zr(C_2H_5)^{2+}$ and $\{O(CH)_3O\}Ti(C_2H_5)^{2+}$: –39.4 and –38.5 kcal/mol, respectively. For single charged and neutral species, the exothermicity of the π-complex formation generally decreases. Namely, the calculated π-complexation energies range from –27 to –3 and from –14 to 0 kcal/mol for single charged cations and neutral complexes, respectively. The Ziegler–Rauk energy decomposition analysis demonstrated that it is the electrostatic term that is responsible for such a strong effect of the total charge. The only exception is the $\{NH(CH)_2NH\}Nb(C_2H_5)$ complex, for which the orbital interaction term seems to be the most important due to metal → ethylene back donation. Consequently, this system reveals the most exothermic olefin uptake energy among all considered catalysts, –54.3 (–49.5 kcal/mol) in the FS (BS) coordination mode.

As was shown, the π-complex formation energy depends also on the accessibility of the metal center, measured by the surface area of the metal open for the ethylene coordination. Such a surface area can be determined on the basis of atomic radii, derived from an electrostatic solvation model, which define the size of a sphere surrounding each atom of the molecule. Discarding those parts of the sphere that lie within another atomic sphere, the surface area associated with a given atom can be measured. The obtained relationship between the ethylene complexation energy and the accessible surface of the metal points out two areas of almost linear change in the olefin binding energy with the increase in the accessibility of the metal center. Namely, (i) an increase in the olefin binding energy between 0 and 30 bohr^2 (observed for Ti-, V-, Zr-, Hf-based complexes), which can be rationalized in the context of revealing the binding sites for the incoming olefin due to a decrease in steric constriction, and (ii) a decrease in the olefin binding energy beyond 50 bohr^2 (observed for Lu-, Th-, Ce-based complexes) corresponding to decay of the electrostatic stabilization energy stemming from significant distance between the ethylene and the metal center as well as an increase in the metal *d*-orbital energies due to their higher diffusiveness. The results discussed above led the authors to the conclusion that, with the use of such simple empirical rules based on the accessible surface area on the metal fragments, the π-complex formation energy can be predicted within an error of ±5 kcal/mol.

Finally, correspondence between the preference of the FS versus the BS π-complex and the favored conformation of precursor compounds was also revealed. Namely, it was shown that BS complexation is preferred over FS complexation only in the cases when the precursor compound is stable in a trigonal conformation and/or the energy difference between trigonal and tetrahedral conformations is small. Basically, a tendency to form a trigonal arrangement of ligands decreases with an increase in the metal atomic number (i.e., moving down the triad and from group III to group IV) and a decrease of electron donation and with a decrease in the "size" of the ancillary ligands. As a consequence, BS olefin uptake is favored over FS olefin uptake for light metals and for group III metals, such as the scandium, as well as for bulky and good π-donor ligands such as the amido ligand [BS vs. FS: −11.2 vs. −9.1, −9.8 vs. −11.0, −5.5 vs. −8.6 kcal/mol for $\{(NH_2)_2\}Sc(C_2H_5)$, $\{(CH_3)_2\}Sc(C_2H_5)$, and $\{(NH_2)_2\}La(C_2H_5)$, respectively].

The nature of the metal was found to be reflected not only by preference of the FS-versus-BS coordination mode but also in the average olefin complexation energy. Namely, exothermicity of the ethylene coordination is in general higher for second- than for first-row transition metals and the lowest for the third row. This fact can be rationalized by an increase in the metal *d*-acceptor orbital energy, going from Sc (Ti) to La (Hf) leading to a decrease in the stabilizing effect in the orbital interaction term. This effect can be further enhanced by the fact that the electrostatic interaction diminishes down the triads due to the increase of the metal size.

To summarize, since the formation of the ethylene π-complex is crucial for the next steps of the polymerization process, the complexation energy can be used as a rough estimate of precursor activity. The obtained results led authors to a conclusion that, among studied complexes, scandocene, $\{Cp_2\}Sc^+$, and titanocene, $\{Cp_2\}Ti^{2+}$, systems have a negligible polymerization activity due to very small complexation energies. Furthermore, competition between insertion and β-termination mechanisms can be controlled by both the metal center and the ancillary ligands since they have a direct influence on the BS-versus-FS complexation preference.

Late Transition Metal Catalysts At the end of this section, we would also like to discuss briefly one of the main differences between early- and late-transition-metal-based ethylene polymerization catalysts, that is, the resting state of the catalyst. Olefin polymerizations with early transition metal complexes reveal a greater than first-order dependence on olefin concentration,[72] which implies that the resting state of the catalyst does not have an olefin coordinated. Thus, the alkyl complex with agostic interaction (i.e., generally β-agostic complex) is the resting state in the case of the early transition metals. On the contrary, in the case of late transition metals, due to their zero-order dependence on olefin concentration,[35,73] an olefin π-complex was identified as the catalyst resting state.

This fact was directly confirmed by results of the quantum-mechanical calculations, revealing that for the latter systems the energy of the ethylene coordination to the metal center is higher in comparison to early d^0 transition metal complexes. For example, the complexation energies from DFT/B3LYP calculations[98] obtained for diimine systems, $(HN(CH)_2NH)M(R)^+$ for M = Ni, Pd, and Pt and R = CH_3 (C_3H_7) are −27.9 (−11.6), −31.7 (−18.0) and −43.6 kcal/mol, respectively. The corresponding values for Ti- and Zr-chelating alkoxides, $(C_6H_4O)(C_6H_4O)M(CH_3)^+$, are −26.8 and −24.9 kcal/mol, respectively.

An increase in the exothermicity of the π-complexation observed for late transition metal complexes can be explained in terms of the classical Dewar–Chatt–Duncanson model of donation/back-donation contributions to the metal–ligand bonding. Since the Ti(IV) and Zr(IV) catalysts have d^0 metal center, for such systems only the olefin → metal donation contributes to bonding. Late transition metals, such as Ni and Pd, participate in both donation and back donation and thus can form stronger olefin π-complexes.

Based on the available results of the calculations at the DFT/BP level, which was found to give the best agreement with experimental data, one can notice that various generic (model) postmetallocene catalysts reveal rather similar values of ethylene complexation energies: −19.4 for $(HN(CH)_2NH)Ni(C_3H_7)^+$,[75] −18.8 for $(HN(CH)_2NH)Pd(C_3H_7)^+$,[46] −18.2 and −17.1 for $(HN(CH)(C_6H_4)O)Ni(C_3H_7)$ with alkyl trans to N and O, respectively,[69] −20.6 and −21.5 for $(HN(C_7H_5)O)Ni(C_3H_7)$ with alkyl trans to N and O, respectively,[70] and −18.3 kcal/mol for $(SiH_3N(CH)NSiH_3)Ni(C_3H_7)$.[76] As it was shown, in most of these cases the ethylene uptake reaction leads to the destruction of the β-agostic bond of the alkyl group (Figure 3.8*a*). Furthermore the olefin was found to bind to the metal center most strongly in the perpendicular arrangement with respect to the plane of the catalyst. The few exceptions include Fe– and Co–bis(iminopyridine)[77–79] as well as Ni–diimine catalysts.[75,80] For such systems the β-agostic interaction was found to be preserved but sightly weakened due to bonding of the ethylene molecule in the axial position, above the plane of the catalyst (Figure 3.8*b*).

Consequently, in such a case, introduction of the steric bulk into the catalyst structure can drastically reduce the calculated ethylene uptake energy, leading in some cases even to the destruction of the β-agostic alkyl bond. The following values of the ethylene complexation energy were obtained: −19.4 (−27.9) versus −14.7 (−20.4) for the model system, $(HN(CH)_2NH)Ni(C_3H_7)^+$ (DFT/BP[75]), and for the real catalyst, $((2,6\text{-}C_6H_3i\text{Pr}_2)N(C(CH_3))_2N(2,6\text{-}C_6H_3i\text{Pr}_2))Ni(C_3H_7)^+$ (DFT/BP[80]) (results in parentheses taken from DFT/B3LYP[82]), used here as an example. For the Pd–diimine system, due to less pronounced steric congestion, such an effect is almost negligible: −18.8 (−31.7) versus −19.1 (−29.8) kcal/mol for the generic and real catalyst (DFT/BP[46,81]) (results in parentheses taken from DFT/B3LYP[82]).

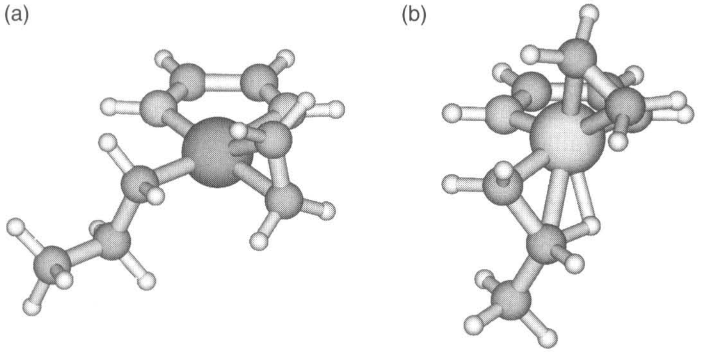

Figure 3.8 π-Complexes formed in late-transition-metal-based systems; as an example the generic diimine catalysts are used: (*a*) $(HN(CH)_2NH)Pd(C_3H_7)(C_2H_4)^+$ with β-agostic bond broken, and (*b*) $(HN(CH)_2NH)Ni(C_3H_7)(C_2H_4)^+$, for which β-agostic interaction was found to be preserved in the π-complex (geometry from refs. 75 and 81, respectively).

For the model Pd–diimine system, $(HN(CH)_2NH)Pd(C_3H_7)^+$, it was also shown that the propene coordination energy is larger than that of ethene, –20.9 versus –18.8 kcal/mol,[46] due to enhanced propene → Pd charge transfer. Nevertheless, in the case of the real catalyst with bulky aryl groups on the diimine ligands, this electronic factor is overridden by steric factors, that is, an increase in steric repulsion between the methyl group of propene and an aryl substituents, absent in the ethylene case. This results in higher preference of ethylene π-complexation compared to α-olefins, such as propene: –19.1 versus –16.8 kcal/mol for $((2,6\text{-}C_6H_3iPr_2)N(CAn)_2N(2,6\text{-}C_6H_3iPr_2))Pd(C_3H_7)^+$ with ethylene and propene, respectively.[81] The conclusions for the real catalyst are consistent with experimental data.

3.3.4 Chain Propagation

As was mentioned in the previous section, coordination of the incoming olefin to the metal center to form a π-complex is the first step of the chain initiation process. Such a π-complexation assists in the migratory insertion of the olefinic monomer into the metal–alkyl bond via a transition state in which the metal ion, the α-carbon atom of the alkyl, and the two carbon atoms of the monomer participate in the bond formation/bond-breaking process. As a result, a new carbon–carbon bond is formed and a polymer chain is elongated by a two-carbon unit. It is generally accepted that the direct product of the insertion is a higher, γ- or δ-, agostic intermediate, which can easily rearrange into the more stable β-agostic final product by a simple rotation of the alkyl chain characterized by a small activation barrier. Finally, a new vacant coordination site becomes available for the next olefin to coordinate, insert, and consequently propagate the polymer chain. Such a chain propagation process repeated many times leads to formation of a macromolecule. Due to its undeniable importance, this elementary reaction remains the basic object of the thorough theoretical research carried out at the different levels of quantum-chemical calculations. Nevertheless, we shall refer here to only a few of the great variety of available data.

The insertion barrier is calculated as the energy difference between the insertion transition state and the most stable conformation of the π-complex. It is generally assumed that the insertion barrier does not change much as the polymer chain becomes longer. Substantial differences can be observed only in two opposite cases, namely, when the monomer inserts into the bond between a metal and an alkyl, which is represented by either (i) a very short (methyl group) or (ii) a very long polymer chain.

In the case of late transition metals, the barrier for the first insertion was found to be always lower in comparison to the subsequent insertion: 11.1 versus 17.5 kcal/mol for $(HN(CH)_2NH)Ni$-based systems (DFT/BP[75]), 18.8 versus 18.9 kcal/mol for $(SiH_3N(CH)NSiH_3)Ni$-based complexes (DFT/BP[76]), 9.9 versus 10.5 kcal/mol for $(HN(CH)_2NH)Ni$-based systems, and 16.3 versus 17.5 kcal/mol for $(HN(CH)_2NH)Pd$-based systems (DFT/B3LYP[83,84]). As is clearly seen, in general, the difference between the first and second insertion barrier is rather subtle due to the fact that for such systems the insertion transition state does not show agostic stabilization. The differences can be simply rationalized by the increase in the steric repulsion between the alkyl chain and the catalyst after the change of the methyl to the propyl group.

As far as the early-transition-metal-based systems are concerned, the first insertion differs more strongly from the subsequent one than in the case of the late metal catalysts. It is a result of the fact that the methyl group does not provide agostic interaction in the resting catalyst state, that is, β-agostic species accepted to be a direct precursor of the olefin insertion and thus in the ethylene π-complex. As a consequence, the significant structural difference between the π-complex and the transition state is observed for the first insertion, which is considered to be responsible for its higher activation barrier, compared to subsequent insertions.[85]

Consequently, as a model for the growing polymer chain in modeling the chain propagation reaction, either the ethyl or propyl group is used, since they ensure appropriate physical accuracy without increases in computational effort. However, owing to the fact that the ethyl group was shown to be an insufficient model of the growing chain for some elementary reactions, for example, β-hydrogen elimination,[86] the propyl group seems to be the optimal choice for modeling polymerization processes.

Early Transition Metal Catalysts Let us start the discussion about the insertion mechanism and energetics from early-transition-metal-based systems. For these compounds, the existence of the two stable conformations of the π-complex, namely FS and BS, in which the ethylene is located respectively syn and anti to the β-agostic bond, leads to the two possible FS and BS insertion

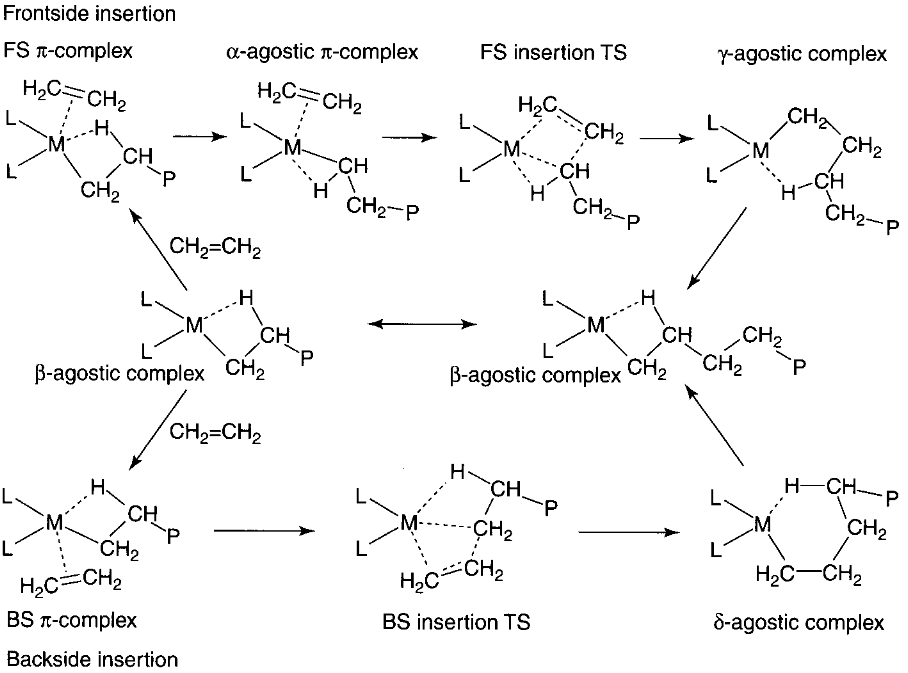

Figure 3.9 Frontside (top) vs. backside (bottom) insertion mechanism.

paths (Figure 3.9). In both cases, the agostic interaction was found to be vital throughout the insertion reaction by providing stabilization of the carbon network during the bond-breaking and bond formation process.

When the olefin attack starts from the FS π-complex (FS mechanism presented in the top panel of Figure 3.9), the growing chain has to primarily rearrange its β-agostic conformation via a rotation around the bond between the metal and α-carbon atom of the alkyl to reach an α-agostic structure.[87,88,92] Consequently, the transition state is predominantly stabilized by an α-agostic bond and the direct product of the insertion is a γ-agostic intermediate. Due to a substantial barrier of such a polymer reorientation, it was assumed to be one of the main rate-limiting steps in the entire polymerization catalysis.

When the olefin attack starts from a BS π-complex (BS mechanism shown in the bottom panel of Figure 3.9), the insertion can undergo directly without any rotation of the polymer chain through the transition state with the strong β-agostic interaction. Unlike the FS insertion, of which the direct product is the γ-agostic species, the BS insertion results at first in a δ-agostic complex.

Among a great number of theoretical data concerning the FS and BS insertion processes for the early-transition-metal-based catalysts,[85,87–100] we would like to focus attention to the comprehensive review given by Margl et al.[96] This systematic DFT/BP investigation of the chain propagation by ethylene insertion into the metal–ethyl bond for a number of $\{L\}M(C_2H_5)^{n+}$ fragments,

$n = 0, 1, 2$, is a continuation of the study on the ethylene polymerization processes catalyzed by d^0 transition metals. More details about the system studied were provided in Section 3.3.3.

The results show that ethylene insertion barriers for the FS (BS) insertion pathway, calculated with respect to the FS (BS) π-complex, are rather low, ranging from 0 to 15.3 kcal/mol for d^0 complexes, and depend on both the metal and ligand frameworks. Generally small insertion barriers observed for such systems, and in some cases even no barrier, can be rationalized by electronic factors. Namely, the crucial factor seems to be the absence of an olefin–polymer chain antibonding interaction due to the lack of the metal *d* electrons, which could occupy emerging carbon–carbon antibonding molecular orbitals in the transition state. The confirmation of this point is provided by non-d^0 systems with Ti(III) and Nb(III) metal centers. The electron transfer into the olefin π* orbital leads to the occupation of the C–C antibonding interaction in the insertion transition state and thus to the creation of an electronic barrier for the insertion process. The barriers of 22.0 and 46.8 kcal/mol were found for $\{(NH_2)_2\}Ti(C_2H_5)(C_2H_4)$ and $\{HN(CH)_2NH\}Nb(C_2H_5)(C_2H_4)$, respectively.

Nevertheless, the authors concluded that not all transition-metal-based complexes with nonzero *d*-electron metal centers will reveal such a substantial insertion barrier. The donation of *d* electrons into ancillary ligand orbitals, the inappropriate symmetry of the metal *d* orbitals, as well as their low energy compared to the olefin–polymer antibonding interaction guarantee a low barrier for ethylene insertion. Due the latter, many of the late-transition-metal-based complexes were found to be efficient catalysts that do not exhibit significantly higher olefin insertion barriers compared to metallocenes.

For no bulky ancillary ligands such as L = NH_2, OH, and CH_3, the FS insertion barrier was found to increase as one moves from group III to IV metals and down the triad, with more pronounced effect observed for group IV cations. Namely, the following order was determined: Sc (2.6) < Y (5.5) < La (6.9) and Ti (4.3) < Zr (7.6) < Hf (12.9 kcal/mol using the amido ligands, L = NH_2, as an example). This trend originates from the ability of the precursor $\{L\}M(C_2H_5)^{n=0,+1}$ to adopt the trigonal planar conformation, decreasing from Sc to La and from Ti to Hf. The similar planar metal–ligand arrangement is also acquired in the insertion transition state. Thus, the stronger inclination of the precursor complex to form such a framework is, the smaller the deformation of catalyst geometry required to attain the transition state, the lower the barrier of the FS insertion. In the case of the BS insertion processes, the corresponding barrier heights depend little on the identity of the metal center, since they do not require such a deformation of the metal–ligand framework. Namely, the following values of the BS insertion barrier were obtained: 4.8, 5.0, 4.1, 4.8, and 5.7 kcal/mol for the $\{(NH_2)_2\}M(C_2H_5)(C_2H_4)^{n=0,+}$ complexes with M = Sc, Y, La, Ti, and Zr, respectively.

For such sterically minimal ligands, due to a facile alkyl rotation, it was also found that the FS and BS insertion pathways proceed via the identical or nearly identical transition states in terms of geometry and/or total energy.

Thus, in such cases, the relative heights of the FS and BS insertion barriers depend mainly on the relative energies of the FS and BS π-complexes. The lower BS insertion barrier derived from the lower stabilization of the BS π-complex corresponds to the higher FS insertion barrier stemming from the higher stabilization of the FS π-complex and vice versa: 1.0 (−19.8) versus 5.5 (−24.4) and 4.8 (−11.2) versus 2.6 (−9.1) kcal/mol for, respectively, $\{(CH_3\}_2\}Ti(C_2H_5)(C_2H_4)^+$ and $\{(NH_2\}_2\}Sc(C_2H_5)(C_2H_4)$ used here as an example, the values in parentheses corresponding to the ethylene complexation energies given by Margl et al.[71]

Alongside the nature of the metal center and ancillary ligands, one more factor that can influence the insertion barriers is the steric bulk of the ligands attached to the metal ion. Much lower insertion barriers obtained for the $\{Cp_2\}Hf$-based complex, 4.0–6.5 kcal/mol, compared to those calculated for relatively small Hf systems with L = NH_2, OH, and CH_3, 12.5–17.0 kcal/mol, led to the conclusion that even complexes with metal centers, which intrinsically reveal high barriers for the ethylene insertion into the metal–alkyl bond, can be made workable catalysts by introduction of steric congestion into their structure. Steric bulk forces the alkyl chain into planar arrangement, resulting in a decrease of the insertion barrier. Furthermore, by restricting torsional freedom of the polymer chain, the steric bulk provides separation of the FS and BS insertion pathways, which is important for stereoregular polymerization.

Late Transition Metal Catalysts In the case of the late-transition-metal-based systems, for which the ethylene uptake reaction leads to the destruction of the β-agostic bond of the alkyl chain, there is no necessity to consider two, FS and BS insertion pathways. Due to the perpendicular orientation of the olefin with respect to the catalyst plane, the insertion process is accompanied by the rotation of the monomer and/or polymer chain into the molecular plane to facilitate the formation of the new carbon–carbon bond. As a result a γ-agostic intermediate is formed. In such cases, the following values of the ethylene insertion barrier were found from calculation at the DFT/BP level: 18.8 for $(HN(CH)_2NH)Pd(C_3H_7)(C_2H_4)^+$,[47] 15.3 and 25.0 for $(HN(CH)(C_6H_4)O)Ni(C_3H_7)(C_2H_4)$ with alkyl trans to N and O, respectively,[69] 17.7 and 27.2 for $(HN(C_7H_5)O)Ni(C_3H_7)(C_2H_4)$ with alkyl trans to N and O, respectively,[68] and 18.9 kcal/mol for $(SiH_3N(CH)NSiH_3)Ni(C_3H_7)(C_2H_4)$;[76] the generic catalysts were used here as an example.

For catalysts which reveal β-agostic interaction in the π-complex, the insertion can proceed in at least two different fashions. In the case of Ni–diimine systems such a process was found to undergo either (i) directly by shrinking the distance between ethylene and the α-carbon atom of the polymer chain or (ii) by first shifting the ethylene into the molecular plane by displacing the β-agostic bond and subsequently shrinking the ethylene–alkyl distance.[75,80] As was shown based on the results of DFT/BP calculations, the former reveals a slightly higher value of activation barrier: 17.5 versus 16.8 kcal/mol.

For the Fe- and Co-bis(imine)pyridine catalysts in turn one can consider simply FS and BS insertion pathways, by analogy to early-transition-metal-based systems.[77–79]

Nevertheless, in all situations presented above, in both the presence and absence of the β-agostic interaction in the π-complex, the olefin insertion transition state was found to look quantitatively similar. Namely, the monomer and α-carbon atom of the growing polymer chain are situated in equatorial positions around the metal center. Furthermore, no noticeable agostic stabilization, typical for early-transition-metal-based systems, was found.

On the other hand, similar to metallocene-based Ziegler–Natta catalysts, the decrease in the insertion barrier can be achieved by the introduction of bulky substituents on the ancillary ligands attached to the metal center, namely 16.8 (9.9) versus 13.2 (3.8) kcal/mol for the model system, $(HN(CH)_2NH)Ni(C_3H_7)(C_2H_4)^+$ (DFT/BP[75]), and for the real catalyst, $((2,6\text{-}C_6H_3\textit{i}Pr_2)N(C(CH_3))_2N(2,6\text{-}C_6H_3\textit{i}Pr_2))Ni(C_3H_7)(C_2H_4)^+$ (DFT/BP[80]) (results in parentheses taken from DFT/B3LYP[82]), used here as an example. As was mentioned above, the insertion transition state for postmetallocenes adopts an in-plane conformation with the monomer and α-carbon atom of the alkyl located in the equatorial positions around the metal center, which are not affected by the bulky substituents of the ancillary ligands. Thus, such a reduction cannot stem from a change in the relative energies of the transition states, but it was found to be mainly a result of the steric destabilization of the corresponding π-complexes: −19.4 versus −14.7 for $(HN(CH)_2NH)Ni(C_3H_7)^+$ (DFT/BP[75]) and $((2,6\text{-}C_6H_3\textit{i}Pr_2)N(C(CH_3))_2N(2,6\text{-}C_6H_3\textit{i}Pr_2))Ni(C_3H_7)^+$ (DFT/BP[80]). In the case of the Pd–diimine systems, due to longer Pd–N bonds, the steric congestion around the metal center is less pronounced, which results in the preservation of the ethylene complexation energy, −18.8 versus −19.1 kcal/mol for generic, and real catalysts, and thus in the preservation of the insertion barrier height, 18.8 versus 18.9 kcal/mol (DFT/BP[46,81]).

Finally, we would like to discuss briefly the chain propagation process for the higher than ethylene α-olefins using as an example the propylene insertion reaction for the Pd–diimine catalyst studied by Michalak et al.[46,81] Similar research for Ni(II)- and Pd(II)-salicylaldiminato systems was carried out by Liu et al.[101]

In the case of substituted olefins, such as propylene, two possible olefin insertion pathways must be considered, that is, 1,2- and 2,1-insertion (Figure 3.10). The former, corresponding to the insertion of unsubstituted olefin, that is, ethylene, occurs when the secondary (substituted) olefin carbon atom forms a bond with the α-carbon atom of the growing polymer chain, leading finally to a β-agostic complex with a primary (unsubstituted) carbon atom of the olefin attached to the metal center (left panel of Figure 3.10). In the latter, a product of the insertion is the β-agostic complex with a secondary (substituted) olefin carbon linked to the metal center, which is a result of the formation of the bond between the primary (unsubstituted) carbon atom of the olefin and the α-carbon atom of the alkyl (right panel of Figure 3.10).

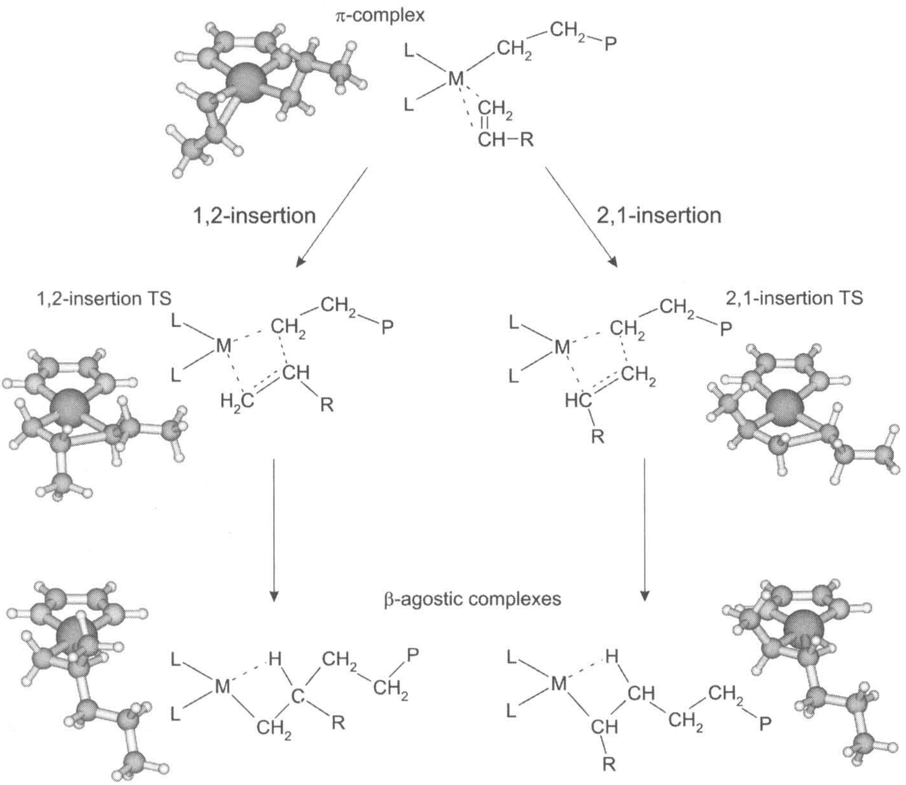

Figure 3.10 1,2- (left) vs. 2,1-insertion (right) process for the propene polymerization catalyzed by generic Pd–diimine system used here as an example (geometry taken from ref. 46).

The calculated values of the 1,2- and 2,1-insertion barriers, that is, 22.7 versus 20.7 for the generic (model) catalyst, $(HN(CH)_2NH)Pd(C_3H_7)(C_2H_3CH_3)^+$, show that the 2,1-insertion pathway is preferred. This fact can be rationalized by means of the lower distortion energy of propene in the 2,1-insertion transition state leading to its higher stabilization and thus decrease in the insertion barrier height. Similarly, the lower distortion energy of the ethylene in comparison to that of the propene in the 2,1-insertion transition state results in the more favorable insertion of the ethylene (18.8 kcal/mol).

In the case of a real catalyst with bulky substituents on the diimine ligand, $((2,6\text{-}C_6H_3iPr_2)N(C(An))_2N(2,6\text{-}C_6H_3iPr_2))Pd(C_3H_7)(C_2H_3CH_3)^+$, the calculated propylene 1,2- and 2,1-insertion barriers were found to be lower compared to these obtained for the model system, namely, 17.5 and 16.9 versus 22.7 and 20.7 kcal/mol, respectively. Since the presence of bulky substituents has practically no influence on the transition state energy, the decrease in the 1,2-insertion barrier stems mainly from the destabilization of the corresponding π-complex (from −20.9 for generic to −16.8 kcal/mol for real catalysts).

Therefore, due to the fact that the steric congestion does not affect the olefin complexation energy of the ethylene and thus preserves its insertion barrier (18.9 kcal/mol), the real catalyst reveals more favorable propylene insertion barriers in comparison to the ethylene case. As far as the 2,1-insertion process is concerned, the steric effect of the aryl substituents is much more significant owing to a steric repulsion between the propene methyl and an aryl group on the ancillary ligand in the transition state. Consequently, the decrease in the 2,1-insertion barrier is also observed. In summary, the higher drop in the 1,2- compared to the 2,1-insertion barrier of the propene leads to the decrease in relative preference of the latter over the former and thus to the leveling of their relative probabilities.

3.3.5 Chain Termination

In light of the previous sections, it can be concluded that the catalytic activity of the transition-metal-based complex in the polymerization processes is affected by all steps of the catalytic cycle, that is, activation, complexation, and insertion. Nevertheless, the successful formation of the catalytic species and olefin π-complex together with low insertion barriers does not guarantee successful formation of the polymer chain. This is due to the fact that there is always competition between chain propagation and termination.

Chain termination plays a critical role in determining one of the fundamental properties of polymers, that is, molecular weight. A few possible chain termination reactions can theoretically take place, namely, (i) bimolecular, direct BHT from the growing macromolecule to the coordinated olefin, for which a starting structure is an FS π-complex with the monomer located syn to the β-agostic bond, suggested for the first time by Stehling et al.;[102] (ii) unimolecular β-hydrogen elimination (BHE) from the growing macromolecule to the metal center, for which a starting structure is a β-agostic alkyl complex (when a methyl group is transferred to the metal, the reaction is called β-methyl elimination); (a great number of theoretical results concerning BHE and BHT have been published so far for various catalytic systems; to the most representative belong refs. 69, 74, 75, 77–87, 91, 94, 95, 97, 98, 100, 103, and 104); (iii) the reaction of molecular hydrogen with the catalytic active species (hydrogenolysis process), the most used in industrial production, in which the chain growth is regulated by injection of H_2 into the reactor (some theoretical investigations into this issue were carried out by Musaev et al.[83,84,104] and Petitjean et al.[105]); (iv) other reactions, including these, which lead to a deactivation of the catalyst, such as oligomerization or dimerization of catalyst, monomer C–H σ-bond metathesis with a hydrogen transfer from a coordinated olefin to the α-C of the polymer chain [theoretically studied by Woo et al. for Ti(IV)-constrained geometry catalyst[86]], chain transfer to counteranion or counteranion group transfer to the metal center, modeled by Wondimagegn et al.[61] for C_6F_5 group transfer from $[MeB(C_6F_5)_3]^-$ to a series of titanium- and zirconium-based catalytic systems.

Due to the fact that the greatest number of theoretical research is focused on BHT and/or BHE termination processes as well as their mutual preferences, here we will limit our discussion to only these two mechanisms.

Early Transition Metal Catalysts Let us first present the results of the systematic DFT study on the termination reactions for a series of transition-metal-based complexes carried out by Margl et al.[74] This work comprises a third part of a project, which was aimed at giving a comprehensive and unified description of d^0-metal-catalyzed olefin polymerization processes, with reference to all their main elementary reactions, that is, π-complexation (see Section 3.3.3), propagation (see Section 3.3.4), and termination. The authors considered two fundamental chain termination reactions, namely BHT and BHE, for an impressive set of catalysts of the general composition $\{L\}MR^{n+}$ ($n = 0, 1, 2$) with R = C_2H_5 for BHT pathway and R = C_3H_7 for BHE pathway, due to the fact that an ethyl group was found to overestimate the activation barrier as well as the thermodynamic barrier for the elimination process (for more details of studied systems see Section 3.3.3).

The mechanism of the β-hydrogen transfer termination process is schematically presented in the top panel of Figure 3.11. As was mentioned above, the starting structure for such a reaction is the β-agostic FS olefin π-complex. The

β-Hydrogen transfer (BHT)

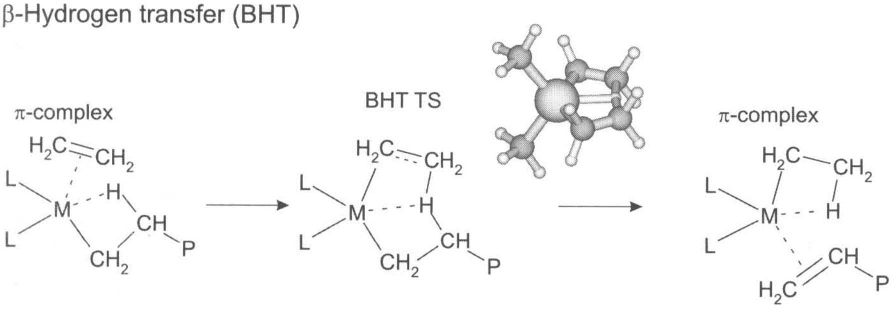

β-Hydrogen elimination (BHE)

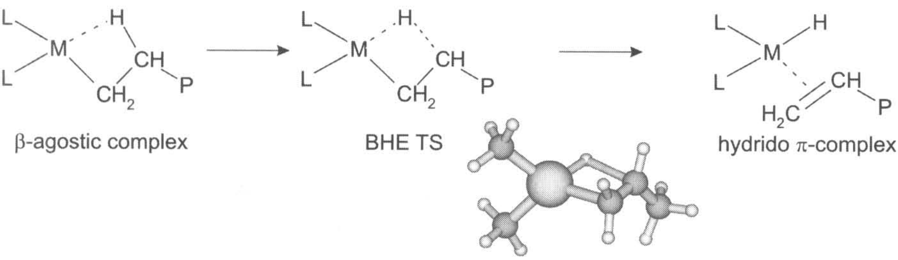

Figure 3.11 β-Hydrogen transfer (top) vs. β-hydrogen elimination (bottom) mechanism with transition states illustrated by $\{(CH_3)_2\}TiR^+$ systems (geometry taken from ref. 74).

BHT process was found to proceed via a pseudomirror symmetric transition state with the transferred hydrogen atom located at approximately equal distance from the β-carbon of the ethyl chain and the syn carbon of the ethylene monomer.

The results show that the BHT barriers, calculated relative to the π-complex, $\{L\}M(C_2H_5)(C_2H_4)^{n+}$ ($n = 0, 1, 2$), change from 3.3 to 21.3 kcal/mol for $\{(CH_3)_2\}Ti(C_2H_5)(C_2H_4)^+$ and $\{(O)(O(CH)_2O)\}V(C_2H_5)(C_2H_4)^+$, respectively. Based on the analysis of various complexes, some systematic trends concerning the metal influence can be drawn.

First, for both considered d^0 metal groups, III and IV, BHT exhibits comparable values of activation barrier, with slightly higher results obtained for group III due to their lower ability to stabilize olefinic ligands in comparison with the cationic group IV center (8.6–12.7 versus 3.3–9.6 kcal/mol for groups III and IV, respectively). Furthermore, for representatives of group V, $\{(O)(O(CH)_2O)\}V(C_2H_5)(C_2H_4)^+$, as well as the non-$d^0$ group IV, $\{(NH_2)_2\}Ti(C_2H_5)(C_2H_4)$ and for heterogeneous Ti(III) the following values of BHT barrier were obtained, respectively: 21.3, 18.4, and 19.6 kcal/mol. Thus, the significant increase in the BHT barrier was revealed compared to the d^0 systems.

Second, the BHT activation barrier increases slowly moving down the triads, from lighter to heavier metals, for both considered d^0 metal groups III and IV: 10.0 (7.2) versus 11.0 (8.4) versus 12.2 (9.6) for $\{(NH_2)_2\}M(C_2H_5)(C_2H_4)^{n=0,+}$ for M = Sc (Ti), Y (Zr), La (Hf). This trend can be attributed to the change in the metal–carbon (M–C) and metal–hydride (M–H) bond strengths.

Finally, steric congestion around the metal center results in a substantial increase in the BHT barrier height. This is because less space is available for the formation of the BHT transition state. Since the BHT transition state demands a great amount of free coordination space on the metal center to be able to bind two olefin ligands together with hydride, the systems built of small ions with bulky ligands, such as $\{Cp_2\}Sc(C_2H_5)(C_2H_4)$, $\{Cp_2\}Ti(C_2H_5)(C_2H_4)^+$, and $\{(O)(O(CH)_2O)\}V(C_2H_5)(C_2H_4)^+$, reveal higher BHT barrier: 13.9, 8.4, and 21.3 kcal/mol, respectively. Thus, it seems possible to enforce a high BHT barrier by the introduction of bulky ligands in the catalyst, which will guarantee imposing steric constraints on its active site.

In the case of the BHE mechanism of the termination process presented in the bottom panel of Figure 3.11, the starting structure is the β-agostic alkyl complex. This reaction was found to proceed through a transition state with a substantially elongated bond between the β-carbon and β-hydrogen. As a result, an olefin hydrido product is formed. The BHE barriers calculated with respect to the most stable conformation of the precursor (β-agostic alkyl complex, $\{L\}M(C_3H_7)^{n+}$ with $n = 0, 1, 2$), range from 9.8 to 33.7 kcal/mol for $\{DPZ\}Zr(C_3H_7)(C_2H_4)^+$ and $\{Cp_2\}Ti(C_3H_7)(C_2H_4)^+$, respectively, whereas the reaction energies (the total energy of the BHE product relative to $\{L\}M(C_3H_7)^{n+}$ with $n = 0, 1, 2$) were found to be roughly 2–5 kcal/mol lower. The only exceptions are sterically open Hf-based complexes, such as $\{(NH_2)_2\}HfC_3H_7(C_2H_4)^+$,

$\{(OH)_2\}HfC_3H_7(C_2H_4)^+$, and $\{(CH_3)_2\}HfC_3H_7(C_2H_4)^+$, which tend to form both kinetically (high BHE barriers) and thermodynamically (low BHE reaction energies, by ~12 kcal/mol in comparison to the BHE barriers) preferred elimination products.

Although a different alkyl group was used in this case as a model for the growing polymer chain (a propyl instead of an ethyl group), a comparison between BHE and BHT barriers obtained for studied systems shows that the latter is lower. Consequently, it led to the conclusion that BHE proceeds slower than β-hydrogen transfer on the condition that the starting structures of both these elementary reactions are present in equal concentration. Thus, the BHT termination process seems to be the more effective chain termination mechanism under the experimental conditions of high monomer partial pressure. The importance of the BHE termination process increases only in the limit of low monomer concentrations or if the formation of a π-complex is disfavored due to steric constraints, for example.

Despite the fact that there is no clear trend of the BHE barrier with a variation of the metal or the ligands, the results provide some practical hints concerning the possible adjustment of the BHE barrier by modification of the metal/ligands that may be useful in a rational catalyst design. A first- or second-row metal should be used if one desires a lower BHE barrier and a third-row metal to enforce a higher one (compare values: 18.6 versus 17.0 versus 26.5 kcal/mol for $\{(CH_3)_2\}M(C_3H_7)(C_2H_4)^+$ with M = Ti, Zr, Hf used here as an example). The increase in the BHE barrier height observed for the heaviest metals in triads can be rationalized by weak olefin and/or weak hydride binding.

In the case of a ligand framework, its influence on the BHE barrier height was also found to be significant. However, a relation between the ligand structure/properties and the BHE barrier is rather complex and somewhat dependent on the metal center used. Namely, for larger (smaller) metal ions the increase in the steric bulk leads to a decrease (increase) in BHE barrier (compare values 10.3 versus 33.7 kcal/mol for $\{Cp_2\}MC_3H_7(C_2H_4)^+$ with M = Zr and Ti used here as an example). The opposite effect observed for a small metal center stems from the lowering of π-complexation stabilization energy of the transition state due to the steric congestion.

It should be pointed out that the complete mechanism of the termination process, in addition to the hydride transfer to the monomer (BHT) or the metal (BHE), includes dissociation of the resulting vinyl-terminated macromolecule. It can proceed either by a first-order mechanism, the dissociation of the π-complex, leaving behind the β-agostic alkyl complex, or by a second-order mechanism, associative displacement, whereby an incoming monomer replaces the terminated chain. The latter seems to be more favorable since the energy loss due to dissociation of the π-complex is compensated for by the energy gain stemming from formation of a new π-complex. Nevertheless, the authors took into account only the first-order mechanism of the terminated chain ejection, which is the exact reverse of the ethylene uptake reaction discussed thoroughly in the first part of a series of papers given by Margl et al.[71] (for more details see Section 3.3.3). The energetics of the ejection process showed that the metal hydride, a product of the BHE reaction, binds an olefin stronger than the metal alkyl complex, a product of the BHT reaction, owing to smaller steric congestion (0–27 kcal/mol vs. >33 kcal/mol for the ejection of an olefin after BHT and BHE, respectively). It led to the conclusion that when BHE elementary reactions take place it is more likely to end in chain isomerization than in chain ejection and thus termination. The above confirms the dominance of the BHT over the BHE chain termination mechanism under steric constraints around the metal center and/or sufficient monomer concentration

Finally, a comparison between FS insertion (see Section 3.3.4) and BHT termination processes, originating from the same structure, the β-agostic FS olefin π-complex, provided valuable conclusions for designing an efficient catalyst. Namely, the catalysts with group III metals exhibit a high intrinsic aptitude toward chain propagation due to good separation (4–8 kcal/mol) between FS insertion and BHT barriers. In the group IV metals, such a separation is much smaller and reverses its sign, in favor of propagation, when one moves from Ti to Hf. Thus, to design a workable catalyst based on this group of metals, it is necessary to find an appropriate ligand framework, which will minimize the insertion barrier. In this context, the introduction of steric congestion by means of bulky ancillary ligands was found to be important due to the fact that it ensures both a decrease in the insertion barrier and a simultaneous increase in the BHT termination barrier.

Late Transition Metal Catalysts The preference of BHT over the BHE chain termination mechanism was also confirmed for late-transition-metal-based polymerization catalysts. For those systems (i) no stable minimum exists for the olefin hydrido product and (ii) an olefin is strongly bound in the hydrido complex; thus, highly endothermic dissociation of the terminated chain can prevent BHE, even if it is favored by a lower barrier compared to BHT. The former was revealed, for example, for Ni–diimine systems.[75,80] In that case the geometry optimization starting from a tentative olefin hydrido complex always led to the β-agostic alkyl complex. The latter was found for salicylaldiminato nickel(II) catalysts.[69] For the $(2,6\text{-}C_6H_3i\text{Pr}_2N(CH)(3\text{-}C_6H_3NO_2)O)Ni(C_3H_7)$ complex the following values of BHE product dissociation reaction, BHE and BHT barriers, were obtained: 38.0, 12.5 and 29.9 kcal/mol.

Furthermore, in postmetallocenes, the BHT to the incoming monomer was found to proceed via a weak five-coordinated bis(olefin) hydrido π-complex, in which the transferred hydrogen is shared roughly equally between two olefinic ligands placed in the axial position, over and below the coordination plane formed by the aromatic ring of the catalyst. As was also shown, for generic (model) systems, the corresponding termination barriers are generally lower than those obtained for the insertion process: 9.7 versus 16.8 kcal/mol for $(HN(CH)_2NH)Ni(C_3H_7)^+$.[75]

Introduction of aryl substituents on ancillary ligands leads to a destabilization of the axial coordination sites needed, as mentioned above, for the olefin approach and, as a consequence, a substantial increase in the BHT barrier can be observed;[69,80,82,104] compare the values 9.7 versus 18.6 kcal/mol for the model system, $(HN(CH)_2NH)Ni(C_3H_7)^+$,[75] and for the real catalyst, $((2,6\text{-}C_6H_3i\text{Pr}_2)N(C(CH_3))_2N(2,6\text{-}C_6H_3i\text{Pr}_2))Ni(C_3H_7)^+$.[80] The above supports the previous finding that for early-transition-metal-based complexes there is a possibility of control of the BHT activation barrier by the size of the ligand framework around the metal center. Due to the fact that such steric congestion leads also to the simultaneous decrease in the insertion barrier, this factor remains the most important for the increase of the catalytic activity.

3.3.6 Chain Isomerization and Branching

As a result of the simple chain propagation, proceeding via consecutive repetitions of ethylene complexation and insertion, linear macromolecules are formed. The growing need to create polymers with new properties leads, however, to increased interest in the controlled production of highly branched macromolecules with a specific microstructure.

In traditional approaches branching is introduced in the polyethylene structure in either homopolymerizations of monomers with complex structure or copolymerizations of the ethylene with short-chain α-olefin comonomers, such as 1-hexene.[106] The late-transition-metal-based catalysts, such as Ni– and Pd–diimine as well as Ni–anilinotropone complexes, were found to lead to highly branched products. Branches in these polyolefins are formed as a result of relatively fast alkyl chain isomerization reactions. Furthermore, the microstructure of obtained polymers was found to be affected by a number of factors, such as temperature, pressure, and the metal and steric bulk of the ancillary ligands.

According to the generally accepted mechanism, schematically presented in Figure 3.12, the chain isomerization process proceeds via (i) unimolecular β-hydrogen elimination from the growing chain of the polymer to a metal center to form a hydride olefin π-complex, (ii) subsequent 180° rotation of the

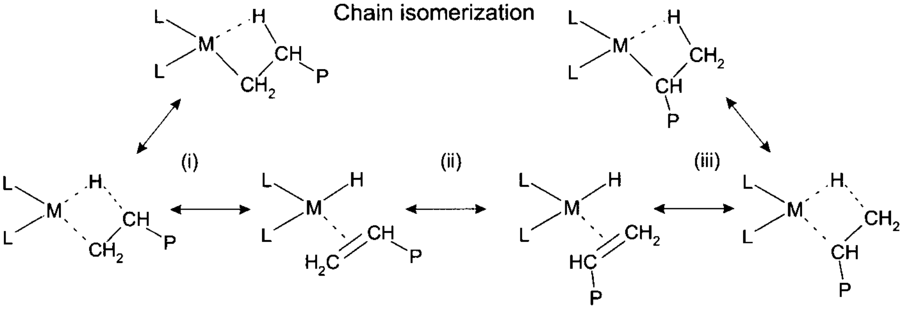

Figure 3.12 Chain isomerization mechanism.

vinyl-terminated polymer chain around its coordination axis, and finally (iii) its reinsertion into the metal-hydride bond resulting in a more stable, compared to the initial, β-agostic complex with a secondary (of higher order depending on the starting alkyl structure) carbon atom (a branching point) attached to the metal center. Such a process repeated many times leads to *chain walking*, that is, the migration of the metal center down the polymer chain and consequently formation of longer chain branches. Due to the fact that the first step of this mechanism is common for both chain isomerization and termination, the progress of the former is dependent on the strength of binding an olefin in the hydrido complex. Highly endothermic dissociation (ejection of the vinyl-terminated chain) prevents BHE termination and facilitates the isomerization reaction.

Early Transition Metal Catalysts Use of the early-transition-metal-based complexes as catalysts for the ethylene polymerization processes leads in general to formation of linear polymeric products. Consequently, in such cases, there seems to be no need to include the chain isomerization step in the theoretical modeling of the catalytic polymerization cycle. Few available studies on this issue concern such systems as zirconocenes, $(Cp)_2ZrR^+$ and $((CH_3)_5\text{–}Cp)_2ZrR^+$ with R = C_2H_5, C_3H_7, C_4H_9,[85,107] as well as the Ti(IV)-constrained geometry catalyst, $(CpSiH_2NH)TiR^+$ with R = C_2H_5, C_3H_7,[86] used here as an example.

The results confirm that the energetically most easily accessible pathway of the alkyl chain isomerization process is that of the classical reaction sequence, that is, β-hydrogen elimination, olefin rotation, and reinsertion. Both alternative mechanisms, (i) the "direct" reaction mode with the β-hydrogen atom migrating from the β- to the α-carbon atom of the alkyl chain[107] and (ii) the alkyl σ-bond metathesis process involving the transfer of a hydrogen atom from an ejected free polymer chain to the α-carbon atom attached to the metal ion,[86] have higher activation barriers. Namely, for the alternative-versus-classical chain isomerization route the respective barriers are 31.1 versus 17.9 for $(Cp)_2Zr(C_2H_5)^+$ (or 11.7 for the isomerization of a primary to a secondary $(Cp)_2Zr(C_3H_7)^+$, propyl → isopropyl)[107] and 18.4 versus 16.0 kcal/mol for $(CpSiH_2NH)TiR^+$ with R = C_2H_5 and C_3H_7.[86] However, due to the fact that the internal barrier is substantially higher for the isomerization (calculated relative to the β-agostic alkyl complex energies) than for the insertion step (calculated with respect to the ethylene π-complex), 12.0 (10.0) versus 8.8 (4.3) and 16.0 versus 3.1 kcal/mol for (Cp)Zr- ((Cp*)Zr-)[85] and Ti-based complexes,[86,88] respectively, such a process is of less importance as far as the metallocenes are concerned.

Late Transition Metal Catalysts In the case of the late transition metal catalysts, the chain isomerization reactions are often more probable than for those based on the early metals, sometimes giving rise to hyperbranched polymers.[35] Consequently, the alkyl chain isomerization process should be included in modeling the polymerization reaction.[46,70,75,76,80–84,108,110–112]

The generally lower internal barriers of the isomerization compared to the corresponding insertion barriers obtained on the basis of the quantum-chemical calculations proved that, indeed, for such systems chain isomerization can successfully compete with chain propagation leading to the formation of the branched polymers. The following values of the internal barriers for the isomerization of a primary (*n*-propyl, *n*-butyl) to a secondary alkyl (*iso*-propyl, *sec*-butyl) versus the insertion process (given in parentheses) were obtained: 12.8 (16.8) and 15.3 (13.2) for the model, $(HN(CH)_2NH)Ni(C_3H_7)^+$, and the real, $((2,6\text{-}C_6H_3iPr_2)N(C(CH_3))_2N(2,6\text{-}C_6H_3iPr_2))Ni(C_3H_7)^+$, Ni–diimine catalysts (DFT/BP[75,80]), 8.8 (27.2) and 2.7 (17.7) for $(HN(C_7H_5)O)Ni(C_3H_7)(C_2H_4)$ with alkyl trans to O and N (DFT/BP[70]), and 4.1–5.2 (18.9 kcal/mol) for $(SiH_3N(CH)NSiH_3)Ni(C_3H_7)$ (DFT/BP[76]). The increase in the isomerization barrier revealed by the real Ni–diimine system in comparison with its generic analogue can be simply rationalized by an increase in steric congestion, influencing the barrier for olefin rotation. This is consistent with the substantially lower isomerization barrier observed for the model Pd–diimine catalyst (5.8 kcal/mol),[46] compared to its Ni analogue (12.8 kcal/mol), since in the Pd catalyst the metal–nitrogen bonds are elongated, which decreases the steric repulsion and makes the branching more prominent.

A very comprehensive study on the branching in the olefin polymerization catalyzed by late-transition-metal-based catalysts was carried out by Michalak et al.[46,81,108,110] Here, we briefly present only the results concerning the propylene polymerization catalyzed by generic and real Pd–diimine systems.[46,75]

The complexity of polymer chain growth in such a process is schematically presented in Figure 3.13. As was mentioned above (see Section 3.3.4) for substituted olefin, two possible, namely, 1,2- and 2,1-, insertion pathways must be considered. The former leads to a β-agostic product with primary carbon atom of the propylene attached to the metal center. In the latter, a β-agostic complex with a secondary olefin carbon linked to the palladium is formed. In both cases, one methyl branch is introduced into the growing polymer chain.

Nevertheless, before olefin uptake, both products of the possible insertions can isomerize and thus the number of branches can differ from that expected from regular, subsequent 1,2- and 2,1-insertion reactions. The β-agostic complex formed as a result of the 1,2-insertion (2,1-insertion) may rearrange to the complex with the tertiary (primary) carbon atom connected to the metal center. Consequently, the isomerization reaction leads to either (i) the introduction of an additional methyl branch when it proceeds after the 1,2-insertion or (ii) the removal of a methyl branch and straightening of the chain when it follows after the 2,1-insertion.

The structures present in chain isomerization reactions studied in the propylene polymerization catalyzed by generic Pd–diimine systems according to the isomerization mechanism (Figure 3.12) are shown in Figure 3.14. The results of the research performed reveal that the activation energies for isomerization of the 1,2- (top panel of Figure 3.14) and 2,1-insertion products

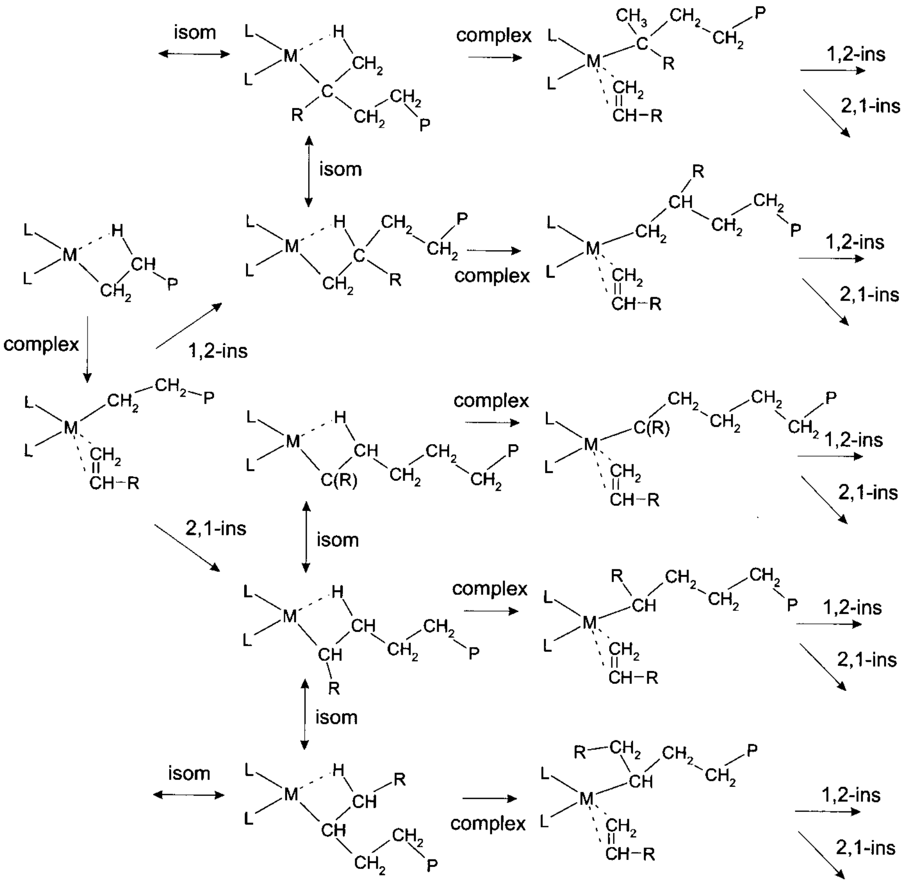

Figure 3.13 Chain growth and isomerization reactions in substituted olefin polymerization processes.

(bottom panel of Figure 3.14) are lower than the insertion barriers, namely for a generic Pd–diimine catalyst: 4.6 versus 22.7 and 5.8 versus 20.7 kcal/mol.

Furthermore, while the isomerization occurring after the 1,2-insertion leads to the more stable β-agostic product with tertiary carbon atom connected to the metal center (for the model system by 3.4 kcal/mol with respect to the corresponding β-agostic insertion product), the rearrangement reaction following the 2,1-insertion results in the less stable complex with primary carbon atom linked to the palladium (by 1.6 kcal/mol), of which stability decreases additionally for the real catalyst with large aryl substituents on the diimine ligand. The latter is therefore not a thermodynamically favorable process. The steric congestion, however, leads also to the higher stabilization and thus preference of the olefin π-complex with a linear chain. That is, even though the chain-straightening reaction results in the formation of the less stable alkyl isomer, afterward the more stable catalyst resting state can be produced.

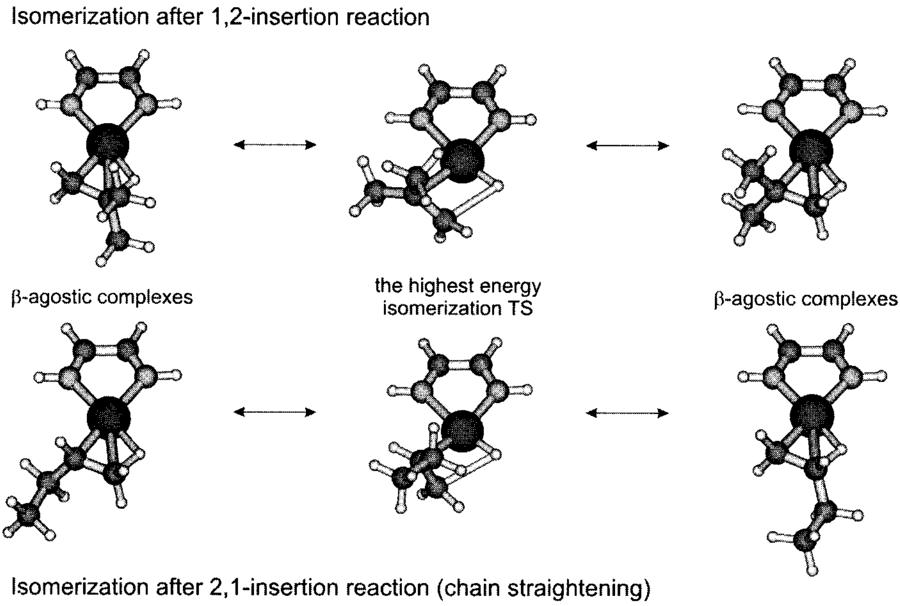
Isomerization after 1,2-insertion reaction
β-agostic complexes
the highest energy isomerization TS
β-agostic complexes
Isomerization after 2,1-insertion reaction (chain straightening)

Figure 3.14 Isomerization reactions in propylene polymerization catalyzed by generic Pd–diimine system (geometry from ref. 46).

Thorough studies on the mechanism and energetics of both possible insertion modes (see Section 3.3.4) as well as isomerization processes enabled the authors to conclude that the experimentally observed lower degree of polyolefin branching than resulted from regular, subsequent 1,2- and 2,1-insertion reactions cannot be easily explained only by means of the ratio of 1,2- to 2,1-insertion, which for real catalyst is nearly equal to unity. The two other important factors, controlling the polyolefin branching, namely the relative stability of isomer alkyl complexes as well as the relative stability of isomer olefin complexes, were revealed. Nevertheless, on the basis of quantum-chemical results, it is not possible to directly explain and predict the topology of the resulting polymer without the aid of statistical methods. Also, other factors, such as reaction conditions (temperature and olefin pressure), must be taken into account. As was shown, it can be successfully realized by the use of the stochastic approach.[70,108,110]

3.3.7 Copolymerization of Ethylene and α-Olefins with Polar Monomers

Finally, we would like to briefly discuss the process of copolymerization of ethylene and higher olefins with monomers containing donor atoms. Since the incorporation of even small amounts of polar monomers dramatically modifies the polymer properties in comparison to regular polyolefins, the controlled copolymerization of α-olefins with monomers bearing a polar functional group remained and still remains in the interest of both academic and industrial researchers. Presently, an overwhelming number of available polar copolymers are produced in radical polymerization processes under high-temperature and high-pressure conditions. The "metallocene revolution" in the olefin polymerization field has however led to growing interest in the development of a new class of efficient copolymerization catalysts based on organometallic complexes. Here, use of the late transition metals as catalytic active centers is especially promising, due to their lower oxophilicity and higher functional group tolerance compared to their early analogues. The development of such single-site copolymerization catalysts would not only create new, less expensive routes to commercially available copolymers but also, providing random progress of incorporation polar groups into polymer chain, it could enable the synthesis of new materials, potentially possessing new, interesting properties.

Basically, the copolymerization of α-olefins with polar monomers, for example, carbon oxide or nitrogen-/oxygen-containing olefins, such as vinyl amines, ethers, esters, ketones, nitriles, proceeds via the same reaction mechanism as that of traditional α-olefin Ziegler–Natta homopolymerization. Therefore, the same elementary reactions must be taken into account in the theoretical modeling of the catalytic cycle, namely π-complexation, 1,2- and 2,1-insertion, isomerization, and termination. Nevertheless, the presence of the donor atoms provided by polar monomers forces some specificity of these particular steps of the catalytic cycle with the formation of the σ-complexes and chelates being of most importance. The details concerning the mechanism and energetics of the particular elementary reactions in the copolymerization of ethylene with polar monomers for various late-transition-metal-based systems can be found in a number of works published so far.[63,113–129] Here, we give only a general view of such a process with a particular emphasis on its intrinsic features.

According to the standard Cossee–Arlman mechanism for α-olefin polymerization, the monomer insertion into the metal–polymer chain bond follows the complexation of the olefin by its double C=C bond, resulting in the formation of the π-complex. The polar vinyl monomer may be however bound to the metal center either by its double C=C bond or its functional group to form, respectively, the π- or σ-complex (Figure 3.15*a*). Thus, as insertion of the polar monomer in a random copolymerization mechanism may start from the π-complex only, the result of a too stable σ-complex formation is poisoning of the catalyst. Consequently, the competition between these two possible binding modes is one of the main factors determining the catalyst activity. Some systematic research on the preference of the binding mode for oxygen- and nitrogen-containing vinyl monomers was carried out by Michalak and Ziegler[117] and Deubel and Ziegler.[120] Similarly, in the case of the CO monomer, two binding modes must be considered, namely with a carbon or oxygen atom bound to the metal center, among which the former facilitates the insertion and the latter poisons the catalyst.

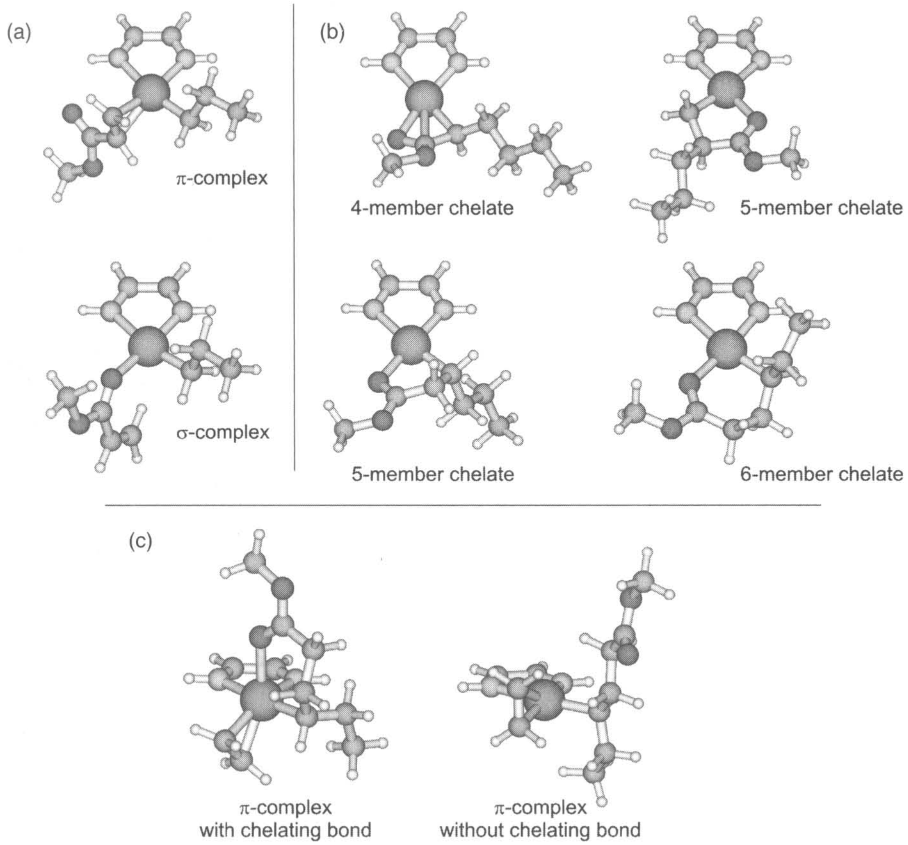

Figure 3.15 Crucial structures present in ethylene–methyl acrylate copolymerization catalyzed by generic Pd–diimine catalyst: (*a*) methyl acrylate π– and σ-complexes, (*b*) 4-, 5-, and 6-member chelates, and (*c*) ethylene π-complexes with (most stable) and without (of higher energy) chelating bond (geometry from ref. 118).

Analysis of the polar comonomer binding mode can therefore be used as a screening test enabling selection of the best prospective catalytic candidates for the copolymerization. Namely, the complexes with a relatively strong preference toward σ-complex formation can be excluded from further studies. Nevertheless, the polar monomer π-complexation does not imply the successful copolymerization process. It can be clearly demonstrated using as an example vinylamine comonomer, $C_2H_3NH_2$, and generic Pd–diimine catalyst, $(HN(CH)_2NH)Pd(C_2H_5)^+$.[120,121] The results of the DFT/BP calculations showed that vinylamine bound to the palladium center in the diimine complex reveals a higher preference toward the π- than the σ-coordination mode with the following values of complexation energy: −30.2 versus −23.9 kcal/mol for the π- and σ-complex, respectively. However, due to the fact that the activation barrier for the vinylamine insertion is much higher than for ethylene insertion

(28.0 vs. 20.9 kcal/mol), the copolymerization of these monomers seems to be rather difficult.

The insertion of a polar monomer into the metal–polymer chain bond results in the formation of chelates (Figure 3.15*b*), which were found to be more stable than typical products of the nonpolar olefin insertion, that is, the agostic complexes, namely, –20.0 versus –4.7 kcal/mol, relative to the acrylate π-complex, for the six-member chelate and β-agostic product of the 2,1-acrylate insertion into the Pd–alkyl bond catalyzed by the Pd–diimine system used here as an example.[118] In such a case, a six-member chelate was shown to be the catalyst resting state by both experimental[130] and theoretical[118,122] research.

Due to the high stability of such chelating complexes, the chain propagation of the copolymerization process, including as previously the π-complexation and subsequent insertion steps, must proceed via the chelate-opening reaction by the monomer. Accordingly, the barrier for opening the six-member chelate, as the most stable of all possible chelates, may be considered the crucial parameter characterized by the copolymerization process.

As was shown for the Pd catalyst, the chelating metal–oxygen bond may not be broken at the monomer uptake stage, and consequently such a bond may be still be present in the most stable geometries of the π-complexes. Two possible chelate-opening mechanisms can therefore be considered, namely (i) one-step, in which the insertion reaction starts from the preferred complexes with an unbroken chelating bond (Figure 3.15*c*) and leads finally to the destruction of such a bond, and (ii) two-step, in which first the chelating bond is broken at the π-complex stage (Figure 3.15*c*), and then the olefin is inserted, starting from higher energy isomeric systems without a metal–oxygen bond. Due to the high activation barrier obtained for the former (30.7 kcal/mol for the six-membered chelate), such a two-step mechanism seems to be preferred for the Pd catalyst (18.0–21.0 kcal/mol).[118]

3.4 CONCLUDING REMARKS

Molecular modeling is nowadays commonly used in mechanistic studies of the catalytic processes, including the olefin polymerization catalyzed by the transition-metal-based complexes. Both force-field-based molecular mechanics and various ab initio quantum-chemical methods have been successfully applied in this field. In this chapter we have reviewed recent quantum-chemical studies on the coordination polymerization catalysts/processes, with the main focus on DFT results. As has been demonstrated, the computational investigations have contributed to the understanding of practically all aspects of the process. One of the main advantages of theoretical modeling is a separation of all the mechanistic steps, including the elementary reactions that are difficult or inaccessible for experimental techniques. A strength of the computational studies also lies in the fact that the simplified model complexes that are often not active as catalysts in reality can be directly compared with the real, working systems, thus providing conclusions that cannot be obtained by experimental techniques. On the other hand, theoretical computations are always restricted to a model, built a priori from the limited set of elementary reactions and species considered, while in reality some other species can be present, some other reactions can proceed, increasing or decreasing the catalyst activity. Theoretical and experimental studies often provide complementary conclusions that combined together give the overall picture of the process. Therefore, a rational design of new efficient catalysts should be based on interdisciplinary research involving both experimental and theoretical techniques.

ACKNOWLEDGMENT

This work was supported by research grant N N204 227534 (2275-B-H03-2008-34) from the Ministry of Science and Higher Education in Poland.

REFERENCES

1. Angermund, K., Fink, G., Jensen, V. R., and Kleinschmidt, R., Toward quantitative prediction of stereospecificity of metallocene-based catalysts for α-olefin polymerization, *Chem. Rev.*, **2000**, 100, 1457–1470.
2. Rappé, A. K., Skiff, W. M., and Casewit, C. J., Modeling metal-catalyzed olefin polymerization, *Chem. Rev.*, **2000**, 100, 1435–1456.
3. Michalak, A., and Ziegler, T., Late transition metals as homo- and co-polymerization catalysts, *Top. Organomet. Chem.*, **2005**, 12, 145–186.
4. Leach, A. R., *Molecular Modeling: Principles and Applications*, 2nd ed., Prentice-Hall, Englewood Cliffs, NJ, 2001.
5. Jensen, F., *Introduction to Computational Chemistry*, 2nd ed., Wiley, New York, 2006.
6. Piela, L., *Ideas of Quantum Chemistry*, Elsevier, New York, 2006.
7. Ziegler, T., and Autschbach, J., Theoretical methods of potential use for studies of inorganic reaction mechanisms, *Chem. Rev.*, **2005**, 105, 2695–2722.
8. Born, M., and Oppenheimer, J. R., Zur quantentheorie der moleküle, *Ann. Phys.*, **1927**, 84, 457–484.
9. Hohenberg, P., and Kohn, W., Inhomogeneous electron gas, *Phys. Rev. B*, **1964**, 136, 864–871.
10. Kohn, W., and Sham, L. J., Self-consistent equations including exchange and correlation effects, *Phys. Rev. A.*, **1965**, 140, 1133–1138.
11. Perdew, J. P., Density-functional approximation for the correlation energy of the inhomogeneous electron gas, *Phys. Rev. B*, **1986a**, 33, 8822–8824.
12. Perdew, J. P., Erratum: Density-functional approximation for the correlation energy of the inhomogeneous electron gas, *Phys. Rev. B*, **1986b**, 34, 7406.
13. Becke, A. D., Density-functional exchange-energy approximation with correct asymptotic behavior, *Phys. Rev. A.*, **1988**, 38, 3098–3100.

14. Lee, C., Yang, W., and Parr, R. G., Development of the Colle-Salvetti correlation-energy formula into a functional of the electron density, *Phys. Rev. B*, **1988**, 37, 785–789.
15. Perdew, J. P., and Wang. Y., Accurate and simple density functional for the electronic exchange energy: Generalized gradient approximation, *Phys. Rev. B*, **1986**, 33, 8800–8802.
16. Perdew, J. P., and Wang, Y., Erratum: Accurate and simple density functional for the electronic exchange energy: Generalized gradient approximation, *Phys. Rev. B*, **1989**, 40, 3399.
17. Perdew, J. P., and Wang. Y., Accurate and simple analytic representation of the electron-gas correlation energy, *Phys. Rev. B*, **1992**, 45, 13244–13249.
18. Perdew, J. P., Burke, K., and Emzerhof, M., Generalized gradient approximation made simple, *Phys. Rev. Lett.*, **1996**, 77, 3865–3868.
19. Perdew, J. P., Burke, K., and Emzerhof, M., Generalized gradient approximation made simple, *Phys. Rev. Lett.*, **1997**, 78, 1396. [*Phys. Rev. Lett.*, 77, 3865 (1996)].
20. Hammer, B., Hansen, L. B., and Nørskov, J. K., Improved adsorption energetics within density-functional theory using revised Perdew-Burke-Emzerhof functionals, *Phys. Rev. B*, **1999**, 59, 7413–7421.
21. Stephens, P. J., Devlin, F. J., Chabalowski, C. F., and Frisch, M. J., Ab initio calculation of vibrational absorption and circular dichroism spectra using density functional force fields, *J. Phys. Chem.*, **1994**, 98, 11623–11627.
22. Frenking, G., Antes, I., Bohme, M., Dapprich, S., Ehlers, A. W., Jonas, V., Nauhaus, A., Otto, M., Stegmann, R., Veldkamp, A., and Vyboishchikov, S. F., Pseudopotential calculations of transition metal compounds: scope and limitations, *Rev. Comp. Chem.*, **1996**, 8, 63–143.
23. Cundari, T. R., Benson, M. T., Lutz, M. L., and Sommerer, S. O., Effective core potential approaches to the chemistry of the heavier elements, *Rev. Comp. Chem.*, **1996**, 8, 145–202.
24. te Velde, G., Bickelhaupt, F. M., Baerends, E. J., Fonseca Guerra, C., van Gisbergen, S. J. A., Snijders, J. G., and Ziegler, T., Chemistry with ADF, *J. Comp. Chem.*, **2001**, 22, 931–967.
25. Fukui, K., The path of chemical reactions—the IRC approach, *Acc. Chem. Res.*, **1981**, 14, 363–368.
26. Cossee, P., On the reaction mechanism of the ethylene polymerization with heterogeneous Ziegler-Natta catalysts, *Tetrahedron Lett.*, **1960**, 38, 12–16.
27. Cossee, P., Ziegler-Natta catalysis I. Mechanism of polymerization of α-olefins with Ziegler-Natta catalysts, *J. Catal.*, **1964**, 3, 80–88.
28. Arlman, E. J., Ziegler-Natta catalysis, II. Surface structure of layer-lattice transition metal chlorides, *J. Catal.*, **1964**, 3, 89–98.
29. Arlman, E. J., Ziegler-Natta catalysis, IV. The stereospecificity in the polymerization of olefins and conjugated dienes in relation to the crystal structure of $TiCl_3$ (α,β), *J. Catal.*, **1966**, 5, 178–189.
30. Arlman, E. J., and Cossee, P., Ziegler-Natta catalysis III. Stereospecific polymerization of propene with the catalyst system $TiCl_3$—$AlEt_3$, *J. Catal.*, **1964**, 3, 99–104.

31. Natta, G., Pino, P., Mazzanti, G., and Giannini, U., A crystallizable organometallic complex containing titanium and aluminum, *J. Am. Chem. Soc.*, **1957**, 79, 2975–2976.
32. Breslow, D. S., and Newburg, N. R., Bis-(cyclopentadienyl)-titanium dichloride—alkylaluminium complexes as catalysts for the polymerization of ethylene, *J. Am. Chem. Soc.*, **1957**, 79, 5072–5073.
33. Sinn, H., and Kaminsky, W., Ziegler-Natta catalysis, *Adv. Organomet. Chem.*, **1980**, 18, 99–149.
34. Alt, H. G., and Koppl A., Effect of the nature of metallocene complexes of group IV metals on their performance in catalytic ethylene and propylene polymerization, *Chem. Rev.*, **2000**, 100, 1205–1222.
35. Ittel, S. D., Johnson, L. K., and Brookhart, M., Late-metal catalysts for ethylene homo- and copolymerization, *Chem. Rev.*, **2000**, 100, 1169–1204.
36. Gibson, V. C., and Spitzmesser, S. K., Advances in non-metallocene olefin polymerization catalysis, *Chem. Rev.*, **2003**, 103, 283–315.
37. Nomura, K., Liu, J., Padmanabhan, S., and Kitiyanan, B., Nonbridged half-metallocenes containing anionic ancillary donor ligands: New promising candidates as catalysts for precise olefin polymerization, *J. Mol. Catal. A*, **2007**, 267, 1–29.
38. Nagy, S. M., Mack, M. P., and Hlatky, G. G., Modeling and catalytic performance of group 4 metal complexes with anionic heteroatomic ligands, in Patil, A. O., and Hlatky, G. G., Eds., *Beyond Metallocenes. Next-Generation Polymerization Catalysts*, ACS Symposium Series 857, American Chemical Society, Washington, DC, 2003, pp. 76–85.
39. Yang, W., and Parr, R. G., Hardness, softness, and the Fukui function in the electronic theory of metals and catalysis, *Proc. Natl. Acad. Sci. USA*, **1985**, 82, 6723–6726.
40. Cruz, V. L., Ramos, J., Muñoz-Escalona, A., Lafuente, P., Peña, B., and Martinez-Salazar, J., 3D-QSAR analysis of metallocene-based catalysts used in ethylene polymerization, *Polymer*, **2004**, 45, 2061–2072.
41. Cruz, V. L., Ramos, J., Martinez, S., Muñoz-Escalona, A., and Martinez-Salazar, J., Structure-activity relationship study of the metallocene catalyst activity in ethylene polymerization, *Organometallics*, **2005**, 24, 5095–5102.
42. Dewar, M. J. S., A review of the pi-complex theory, *Bull. Soc. Chim. Fr.*, **1951**, 18: C71–79.
43. Chatt, J., and Duncanson, L. A., Olefin co-ordination compounds. Part III. Infrared spectra and structure: Attempted preparation of acetylene complexes, *J. Chem. Soc.*, **1953**, 3, 2939–2947.
44. Mitoraj, M., and Michalak, A., Natural orbitals for chemical valence as descriptors of chemical bonding in transition metal complexes, *J. Mol. Model.*, **2007**, 13, 347–355.
45. Michalak, A., Mitoraj, M., and Ziegler, T., Bond orbitals from chemical valence theory, *J. Phys. Chem. A*, **2008**, 112, 1933–1939.
46. Michalak, A., and Ziegler, T., Palladium-catalyzed polymerization of propene: DFT model studies, *Organometallics*, **1999**, 18, 3998–4004.

47. Fusco, R., Longo, L., Masi, F., and Garbassi, F., Ethylene polymerization with homogeneous Ziegler-Natta catalysts: Theoretical study on the role of ion pairs in the polymerization mechanism, *Macromol. Rapid Commun.*, **1997a**, 18, 433–441.
48. Fusco, R., Longo, L., Masi, F., and Garbassi, F., Olefin polymerization with homogeneous Ziegler-Natta catalysts: A DFT quantum-mechanical study of the reactions of Cp_2MtCH_3Cl complexes (Mt = Ti, Zr) with $Al(CH_3)_3$ and MAO, *Macromolecules*, **1997b**, 30, 7673–7685.
49. Fusco, R., Longo, L., Proto, A., Masi, F., and Garbassi, F., Ethylene polymerization catalyzed by metallocene/methylaluminoxane systems: Quantum-mechanical study on the role of olefin separated ion pairs (OSIP) in the polymerization mechanism, *Macromol. Rapid Commun.*, **1998**, 19, 257–262.
50. Lanza, G., Fragalà, I. L., and Marks, T. J., Highly electrophilic olefin polymerization catalysts. Counteranion and solvent effects on constrained geometry catalyst ion pair structure and reactivity, *J. Am. Chem. Soc.*, **1998**, 120, 8257–8258.
51. Lanza, G., Fragalà, I. L., and Marks, T. J., Ligand substituent, anion, and solvation effects on ion pair structure, thermodynamic stability, and structural mobility in "constrained geometry" olefin polymerization catalyst: An ab initio quantum chemical investigation, *J. Am. Chem. Soc.*, **2000**, 122, 12764–12777.
52. Lanza, G., Fragalà, I. L., and Marks, T. J., Energetic, structural, and dynamic aspects of ethylene polymerization mediated by homogeneous single-site "constrained geometry catalysts" in the presence of cocatalyst and solvation: An investigation at the ab initio quantum chemical level, *Organometallics*, **2002**, 21, 5594–5612.
53. Chan, M. S. W., Vanka, K., Pye, C. C., and Ziegler, T., Density functional study on activation and ion-pair formation in group IV metallocene and related olefin polymerization catalysts, *Organometallics*, **1999**, 18, 4624–4636.
54. Klesing, A., and Bettonville, S., The effect of substituents on dimer formation and cation-anion interaction in silicon bridged bisindenyl zirconocene propylene polymerization catalysts, *Phys. Chem. Chem. Phys.*, **1999**, 1, 2372–2377.
55. Lanza, G., and Fragalà IL. Theoretical modeling of "constrained geometry catalysts" beyond the naked cation approach, *Top. Catal.*, **1999**, 7, 45–60.
56. Chan, M. S. W., and Ziegler, T., A combined density functional and molecular dynamics study on ethylene insertion into the $Cp_2ZrEt\text{-}MeB(C_6F_5)_3$ ion-pair, *Organometallics*, **2000**, 18, 5182–5189.
57. Vanka, K., Chan, M. S., Pye, C. C., and Ziegler, T., A density functional study of ion-pair formation and dissociation in the reaction between boron- and aluminium-based Lewis acids with $(1,2\text{-}Me_2Cp)_2ZrMe_2$, *Organometallics*, **2000**, 19, 1841–1849.
58. Nifant'ev, I. E., Ustynyuk, L. Y., and Laikov, D. N., DFT study of ethylene polymerization by zirconocene-boron catalytic systems. Effects of counterion on the kinetics and mechanism of the process, *Organometallics*, **2001**, 20, 5375–5393.
59. Xu, Z. T., Vanka, K., Firman, T., Michalak, A., Zurek, E., Zhu, C. B., and Ziegler, T., Theoretical study of the interactions between cations and anions in group IV transition-metal catalysts for single-site homogeneous olefin polymerization, *Organometallics*, **2002**, 21, 2444–2453.

60. Xu, Z. T., Vanka, K., and Ziegler, T., Influence of the counterion $MeB(C_6F_5)^-$ and solvent effects on ethylene polymerization catalyzed by $[(CpSiMe_2NR)TiMe]^+$: A combined density functional theory and molecular mechanism study, *Organometallics*, **2004**, 23, 104–116.
61. Wondimagegn, T., Xu, Z., Vanka, K., and Ziegler, T., C_6F_5-group transfer from $[MeB(C_6F_5)_3]^-$ to the metal center of L_2MMe^+ (M = Ti, Zr) as a deactivation pathway in olefin polymerization catalysis: A combined density functional theory and molecular mechanics investigation, *Organometallics*, **2004**, 23, 3847–3852.
62. Zurek, E., and Ziegler, T., Theoretical studies of the structure and function of MAO (methylaluminoxane). *Prog. Polym. Sci.*, **2004**, 29, 107–148.
63. Yang, S.-Y., Szabo, M. J., Michalak, A., Weiss, T., Piers, W. E., Jordan, R. F., and Ziegler, T., The exploration of neutral azoligand-based Grubbs type palladium(II) complex as potential catalyst for the copolymerization of ethylene with acrylonitrile: A theoretical study based on density functional theory, *Organometallics*, **2005b**, 24, 1242–1251.
64. Silanes, I., Mercero, J. M., and Ugalde, J. M., Comparison of, Ti, Zr, and Hf as cations for metallocene-catalyzed olefin polymerization, *Organometallics*, **2006**, 25, 4483–4490.
65. Yang, S.-Y., and Ziegler, T., Combined Car-Parrinello QM/MM dynamic study on the propagation and termination steps of ethylene polymerization catalyzed by $[Cp_2ZrR(\mu\text{-}Me)B(C_6F_5)_3]$ (R = Me, Pr), *Organometallics*, **2006**, 25, 887–900.
66. Yang, S.-H., Huh, J., and Jo, W.-H., Effect of solvent polarity on the initiation and the propagation of ethylene polymerization with constrained geometry catalyst/MAO catalytic system: A density functional study with the conductor-like screening model, *Macromolecules*, **2005a**, 38, 1402–1409.
67. Hicks, F. A., and Brookhart, M., A highly active anilinotropone-based neutral nickel(II) catalyst for ethylene polymerization, *Organometallics*, **2001**, 20, 3217–3219.
68. Wang, C., Friedrich, S., Younkin, T. R., Li, R. T., Grubbs, R. H., Bansleben, D. A., and Day, M. W., Neutral nickel(II)-based catalysts for ethylene polymerization, *Organometallics*, **1998**, 17, 3149–3151.
69. Chan, M. S. W., Deng, L., and Ziegler, T., Density functional study of neutral salicylaldiminato nickel(II) complexes as olefin polymerization catalysts, *Organometallics*, **2000**, 19, 2741–2750.
70. Michalak, A., and Ziegler, T., Polymerization of ethylene catalyzed by a nickel(+2) anilinotropone-based catalysts: DFT and stochastic studies on the elementary reactions and the mechanism of polyethylene branching, *Organometallics*, **2003c**, 22, 2069–2079.
71. Margl, P., Deng, L., and Ziegler, T., A unified view of ethylene polymerization by d^0 and d^0f^n transition metals. 1. Precursor compounds and olefin uptake energetics, *Organometallics*, **1998a**, 17, 933–946.
72. Yu, Z., and Chien, J. C., Molecular mechanics study of zirconocenium catalyzed isospecific polymerization of propylene, *J. Polym. Sci. A*, **1995**, 33, 125–135.
73. Johnson, L. K., Killian, C. M., and Brookhart, M., New Pd(II)- and Ni(II)-based catalysts for polymerization of ethylene and α-olefins, *J. Am. Chem. Soc.*, **1995**, 117, 6414–6415.

74. Margl, P., Deng, L., and Ziegler, T., A unified view of ethylene polymerization by d^0 and d^0f^n transition metals. 3. Termination of the growing polymer chain, *J. Am. Chem. Soc.*, **1999a**, 121, 154–162.
75. Deng, L., Margl, P., and Ziegler, T., A density functional study of nickel(II) diimine catalyzed polymerization of ethylene, *J. Am. Chem. Soc.*, **1997a**, 119, 1094–1100.
76. Collins, S., and Ziegler T., Theoretical modeling of ethylene insertion by nickel iminophosphonamide and amidinate complexes, *Organometallics*, **2007**, 26, 6612–6623.
77. Deng, L., Margl, P., and Ziegler, T. Mechanistic aspects of ethylene polymerization by iron(II)-bisimine pyridine catalysts: A combined density functional theory and molecular mechanics study, *J. Am. Chem. Soc.*, **1999**, 121, 6479–6487.
78. Margl, P., Deng, L., and Ziegler, T., Cobalt(II) imino pirydine assisted ethylene polymerization: A quantum-mechanical/molecular-mechanical density functional theory investigation, *Organometallics*, **1999b**, 18, 5701–5708.
79. Khoroshun, D. V., Musaev, D. G., Vreven, T., and Morokuma, K., Theoretical study on bis(imino)pyridyl-Fe(II) olefin poly- and oligomerization catalysts. Dominance of different spin states in propagation and β-hydride transfer pathways, *Organometallics*, **2001**, 20, 2007–2026.
80. Deng, L., Woo, T. K., Cavallo, L., Margl, P. M., and Ziegler, T., The role of bulky substituents in Brookhart-type Ni(II) diimine catalyzed olefin polymerization: A combined density functional theory and molecular mechanics study, *J. Am. Chem. Soc.*, **1997b**, 119, 6177–6186.
81. Michalak, A., and Ziegler, T., DFT studies on substituent effects in palladium-catalyzed olefin polymerization, *Organometallics*, **2000**, 19, 1850–1858.
82. Froese, R. D. J., Musaev, D. G., and Morokuma, K., Theoretical study of substituent effects in the diimine-M(II) catalyzed ethylene polymerization reaction using IMOMM method, *J. Am. Chem. Soc.*, **1998**, 120, 1581–1587.
83. Musaev, D. G., Froese, R. D. J., Svensson, M., and Morokuma, K., A density functional study of the mechanism of the diimine-nickel-catalyzed ethylene polymerization reaction, *J. Am. Chem. Soc.*, **1997a**, 119, 367–374.
84. Musaev, D. G., Svensson, M., Morokuma, K., Strömberg, S., Zetterberg, K., and Siegbahn, P., E. M., Density functional study of the mechanism of the palladium(II)-catalyzed ethylene polymerization reaction, *Organometallics*, **1997b**, 16, 1933–1945.
85. Thorshaug, K., Støvneng, J. A., Rytter, E., and Ystenes, M., Termination, isomerization, and propagation reactions during ethene polymerization catalyzed by $Cp_2Zr\text{-}R^+$ and $Cp^*{}_2Zr\text{-}R^+$. An experimental and theoretical investigation, *Macromolecules*, **1998**, 31, 7149–7165.
86. Woo, T. K., Margl, P. M., Ziegler, T., and Blöch, P. E., Static and ab initio molecular dynamics study of the titanium(IV)-constrained geometry catalyst $(CpSiH_2NH)Ti\text{-}R^+$. 2. Chain termination and long chain branching, *Organometallics*, **1997**, 16, 3454–3468.
87. Lohrenz, J. C. W., Woo, T. K., Fan, L., and Ziegler, T., A density functional study on the insertion mechanism and chain termination in Kaminsky-type catalysts; comparison of frontside and backside attack, *J. Organomet. Chem.*, **1995a**, 497, 91–104.

88. Woo, T. K., Margl, P. M., Lohrenz, J. C. W., Blöch, P. E., and Ziegler, T., Combined static and dynamic density functional study of the Ti(IV) constrained geometry catalyst $(CpSiH_2NH)Ti\text{-}R^+$. 1. Resting states and chain propagation, *J. Am. Chem. Soc.*, **1996**, 118, 13021–13030.

89. Meier, R. J., van Doremaele, G. H. J., Iarlori, S., and Buda, F., Ab initio molecular dynamics study of metallocene-catalyzed ethylene polymerization, *J. Am. Chem. Soc.*, **1994**, 116, 7274–7281.

90. Weiss, H., Ehrig, M., and Ahlrichs, R., Ethylene insertion in the homogenous Ziegler-Natta catalysis: An ab intio investigation on a correlated level, *J. Am. Chem. Soc.*, **1994**, 116, 4919–4928.

91. Woo, T. K., Fan, L., and Ziegler, T., A density functional study of chain growing and chain terminating steps in olefin polymerization by metallocene and constrained geometry catalysts, *Organometallics*, **1994**, 13, 2252–2261.

92. Fan, L., Harrison, D., Woo, T. K., and Ziegler, T., A density functional study of ethylene insertion into the M-CH_3 bond of the constrained geometry catalysts $[(SiH_2\text{-}C_5H_4\text{-}NH)MCH_3]^+$ (M = Ti, Zr, Hf) and $(SiH_2\text{-}C_5H_4\text{-}NH)TiCH_3$, *Organometallics*, **1995**, 14, 2018–2026.

93. Lohrenz, J. C. W., Woo, T. K., and Ziegler, T., A density functional study on the origin of the propagation barrier in the homogeneous ethylene polymerization with Kaminsky-type catalysts, *J. Am. Chem. Soc.*, **1995b**, 117, 12793–12800.

94. Yoshida, T., Koga, N., and Morokuma, K., Ab initio theoretical study on ethylene polymerization with homogeneous silylene-bridged group 4 metallocene catalysts. Ethylene insertion and β-elimination, *Organometallics*, **1995**, 14, 746–758.

95. Margl, P., Lohrenz, J. C. W., Ziegler, T., and Blöch, P. E., A dynamical density functional study on the reaction of ethylene with $Cp_2Zr(C_2H_5)^+$, *J. Am. Chem. Soc.*, **1996**, 118, 4434–4441.

96. Margl, P., Deng, L., and Ziegler, T., A unified view of ethylene polymerization by d^0 and d^0f^n transition metals. Part 2. Chain propagation, *J. Am. Chem. Soc.*, **1998b**, 120, 5517–5525.

97. Deng, L., Ziegler, T., Woo, T. K., Margl, P., and Fan, L., Computer design of living olefin polymerization catalysts: A combined density functional theory and molecular mechanics study, *Organometallics*, **1998**, 17, 3240–3253.

98. Musaev, D. G., and Morokuma, K., Theoretical studies of the mechanism of ethylene polymerization reaction catalyzed by diimine-M(II) (M = Ni, Pd and Pt) and Ti- and Zr-chelating alkoxides, *Top. Catal.*, **1999**, 7, 107–123.

99. Petitjean, L., Pattou, D., and Ruiz-López, M. F., Theoretical study of the mechanisms of ethylene polymerization with metallocene-type catalysts, *J. Phys. Chem. B*, **1999**, 103, 27–35.

100. Talarico, G., Blok, A. N. J., Woo, T. K., and Cavallo L. Comparison of ab initio and DFT methods for studying chain propagation and chain termination processes with group 4 polymerization catalysts. 1. The ansa-bis(cyclopentadienyl) zirconium catalyst, *Organometallics*, **2002**, 21, 4939–4949.

101. Liu, Y., Zhang, M., Drew, M. G. B., Yang, Z.-D., and Liu, Y. A. DFT study of propylene polymerization using neutral salicylaldiminato *nickel(II)* and *palladium(II)* as catalysts, *J. Mol. Struc. THEOCHEM*, **2005**, 726, 277–283.

102. Stehling, U., Diebold, J., Kirsten, R., Röll, W., Brintzinger, H. H., Jüngling, S., Mülhaupt, R., and Langhauser, F., ansa-Zirconocene polymerization catalysts

with anelated ring ligands—effects on catalytic activity and polymer chain length, *Organometallics*, **1994**, 13, 964–970.

103. Cavallo, L., and Guerra, G., A density functional and molecular mechanics study of β-hydrogen transfer in homogeneous Ziegler-Natta catalysis, *Macromolecules*, **1996**, 29, 2729–2737.
104. Musaev, D. G., Froese, R. D. J., and Morokuma, K., Molecular orbital and IMOMM studies of the chain transfer mechanisms of the diimine-M(II)-catalyzed (M = Ni, Pd) ethylene polymerization reaction, *Organometallics*, **1998**, 17, 1850–1860.
105. Petitjean, L., Pattou, D., and Ruiz-López, M. F., Theoretical study of hydrogenolysis termination processes in ethylene polymerization, *Tetrahedron*, **2001**, 57, 2769–2774.
106. Sunder, A., Heinemann, J., and Frey, H., Controlling the growth of polymer trees: Concepts and perspectives for hyperbranched polymers, *Chem. Eur. J.*, **2000**, 6, 2499–2506.
107. Prosenc, M.-H., and Brintzinger, H.-H., Zirconium-alkyl isomerizations in zirconocene-catalyzed olefin polymerization: A density functional study, *Organometallics*, **1997**, 16, 3889–3894.
108. Michalak, A., and Ziegler, T., Stochastic simulations of polymer growth and isomerization in the polymerization of propylene catalyzed by Pd–based diimine catalysts, *J. Am. Chem. Soc.*, **2002**, 124, 7519–7528.
109. Michalak, A., and Ziegler, T., A comparison of Ni- and Pd–diimine complexes as catalysts for ethylene/methyl acrylate copolymerization. A static and dynamic density functional theory study, *Organometallics*, **2003a**, 22, 2660–2669.
110. Michalak, A., and Ziegler, T., Exploring the scope of possible microstructures accessible from polymerization of ethylene by late transition metal single-site catalysts. A theoretical study, *Macromolecules*, **2003b**, 36, 928–933.
111. Michalak, A., and Ziegler, T., Modeling ethylene and propylene homopolymerization by late-transition-metal catalysts: A combined quantum mechanical and stochastic approach, *Kinet. Catal.*, **2006**, 47, 310–325.
112. Woo, T. K., and Ziegler, T., The influence of electronic and steric factors on chain branching in ethylene polymerization by Brookhart-type Ni(II) diimine catalysts: A combined density functional theory and molecular mechanics study, *J. Organomet. Chem.*, **1999**, 591, 204–213.
113. Koga, M., and Morokuma, K., Mechanism of carbonyl insertion reaction of Pd and Pt complexes. An ab initio MO study, *J. Am. Chem. Soc.*, **1986**, 108, 6136–6144.
114. Margl, P., and Ziegler, T., A nonlocal density functional study of the Pd(II)-assisted copolymerization of ethylene and, CO., *J. Am. Chem. Soc.*, **1996a**, 118, 7337–7344.
115. Margl, P., and Ziegler, T., Palladium(II)-assisted copolymerization of ethylene and CO: Influence of the chain end on the regularity of the polymer, *Organometallics*, **1996b**, 15, 5519–5523.
116. Svensson, M., Matsubara, T., and Morokuma, K., Theoretical study of Pd(II)- and Ni(II)-catalyzed alternating copolymerization of carbon monoxide with ethylene, *Organometallics*, **1996**, 15, 5568–5576.

117. Michalak, A., and Ziegler, T., DFT studies on the copolymerization of α-olefins with polar monomers: Comonomer binding by nickel- and palladium-based catalysts with Brookhart and Grubbs ligands, *Organometallics*, **2001a**, 20, 1521–1532.

118. Michalak, A., and Ziegler, T., DFT studies on the copolymerization of α-olefins with polar monomers: Ethylene-methyl acrylate copolymerization catalyzed by a Pd–based diimine catalyst, *J. Am. Chem. Soc.*, **2001b**, 123, 12266–12278.

119. von Schenck, H., Strömberg, S., Zetterberg, K., Ludwig, M., Åkermark, B., and Svensson, M., Insertion aptitudes and insertion regiochemistry of various alkenes coordinated to cationic (σ-R)(diimine)palladium(II) (R = —CH_3, —C_6H_5). A theoretical study, *Organometallics*, **2001**, 20, 2813–2819.

120. Deubel, D. V., and Ziegler, T., DFT study of olefin versus nitrogen bonding in the coordination of nitrogen-containing polar monomers to diimine and salicylaldiminato nickel(II) and palladium(II) complexes. Implications for copolymerization of olefins with nitrogen-containing polar monomers, *Organometallics*, **2002a**, 21, 1603–1611.

121. Deubel, D. V., and Ziegler, T., Challenge of the copolymerization of olefins with N-containing polar monomers. Systematic screening of nickel(II) and palladium(II) catalysts with Brookhart and Grubbs ligands. 2. Chain-propagation barriers, intrinsic regioselectivity, and Curtin-Hammet reactivity, *Organometallics*, **2002b**, 21, 4432–4441.

122. Philipp, D. M., Muller, R. P., Goddard III, WA., Storer, J., McAdon, M., and Mullins, M., Computational insights on the challenges for polymerizing polar monomers, *J. Am. Chem. Soc.*, **2002**, 124, 10198–10210.

123. Szabo, M. J., Galea, N. M., Michalak, A., Yang, S.-Y., Groux, L. F., Piers, W. E., and Ziegler, T., Copolymerization of ethylene with polar monomers by anionic substitution. Theoretical study based on acrylonitrile and the Brookhart diimine catalyst, *Organometallics*, **2005a**, 24, 2147–2156.

124. Szabo, M. J., Galea, N. M., Michalak, A., Yang, S.-Y., Groux, L. F., Piers, W. E., and Ziegler, T., Copolymerization of ethylene with polar monomers: Chain propagation and side reactions. A DFT study using zwitterionic Ni(II) and Pd(II) catalysts, *J. Am. Chem. Soc.*, **2005b**, 127, 14692–14703.

125. Szabo, M. J., Jordan, R. F., Michalak, A., Piers, W. E., Weiss, T., Yang, S.-Y., and Ziegler, T., Polar copolymerization by a palladium-diimine-based catalyst. Influence of the catalyst charge and polar substituent on catalyst poisoning and polymerization activity. A density functional theory study, *Organometallics*, **2004**, 23, 5565–5572.

126. Haras, A., Anderson, G. D. W., Michalak, A., Rieger, B., and Ziegler, T., Computational insight into catalytic control of poly(ethylene-methyl acrylate) topology, *Organometallics*, **2006a**, 25, 4491–4497.

127. Haras, A., Michalak, A., Rieger, B., and Ziegler, T., Theoretical analysis of factors controlling the nonalternating CO/C_2H_4 copolymerization, *J. Am. Chem. Soc.*, **2005**, 127, 8765–8774.

128. Haras, A., Michalak, A., Rieger, B., and Ziegler, T., Comparative study on catalytic systems for the alternating and nonalternating CO/ethylene copolymerization, *Organometallics*, **2006b**, 25, 946–953.

129. Mitoraj, M., and Michalak, A., DFT studies on isomerization reactions in the copolymerization of ethylene and methyl acrylate catalyzed by Ni–diimine and Pd–diimine complexes. *J. Mol. Model.*, **2005**, 11, 341–350.
130. Mecking, S., Johnson, L. K., Wang, L., and Brookhart, M., Mechanistic studies of the palladium-catalyzed copolymerization of ethylene and α-olefins with methyl acrylate, *J. Am. Chem. Soc.*, **1998**, 118, 888–899.

4 Scale-Up of Catalyst Recipes to Commercial Production

C. P. CHENG
Shanghai Süd-Chemie Catalysts Co., Jinshan, Shanghai, 201512

4.1 INTRODUCTION

Early-generation Ziegler–Natta (ZN) catalysts were relatively simple to prepare, involving reducing titanium tetrachloride with aluminum chloride, or an aluminum alkyl (Chapter 8). Since catalyst preparation was relatively simple and there were no other commercial sources, many early polymerization plants often incorporated catalyst manufacturing facilities. With the increasing complexities of each new generation of ZN catalyst, scale-up and manufacturing of these catalysts became more specialized operations. This is particularly true for polypropylene catalyst where the preparation is much more complicated and involves the use of large amounts of solvents and excess titanium chloride, which have to be recovered and recycled to make the process economically feasible. Even in simpler polyethylene catalyst recipes, the economics of scale favor the manufacture of catalysts by specialized catalyst manufacturers with a dedicated facility rather than an attachment to a polymerization plant. With the increasing demand for catalysts, nowadays catalysts are manufactured by a few specialized companies. Output of a world-scale catalyst plant is typically on the order of 100–200 MT/year, compared to the 10–15 MT/yr of catalyst that is used even in the largest polymerization plant. As of 2007, the estimated demand for fourth-generation polypropylene catalyst alone reached about 1500 MT/yr. Demands for polyethylene catalysts are easily many times this amount as polyethylene catalysts typically have much lower activity.

While a chemist developing a new catalyst recipe in the laboratory may prepare something on the order of 5–25 g of catalyst at a time, a commercial catalyst plant requires the production of at least 350 kg/day (100 MT/300 days/

Handbook of Transition Metal Polymerization Catalysts Edited by Ray Hoff and Robert T. Mathers
Copyright © 2010 John Wiley & Sons, Inc.

year), this is roughly a scale-up factor of about 20,000. Scaling up a laboratory recipe to commercial production is obviously no easy task, even with intermediate pilot plant steps. In addition to duplicating the laboratory catalyst recipe, many other factors have to be considered in order for the catalyst receipt to be commercially viable. A laboratory chemist may not worry about how much solvent is used to wash the catalyst or how long it takes to wash the catalyst. In a commercial production facility, these factors have the potential to make or break the project if not properly addressed. In this chapter, the approaches to optimizing the recipe and scale-up issues will be discussed.

4.2 FUNDAMENTALS OF PROCESS SCALE-UP

4.2.1 Dimensional Analysis

In a classical chemical engineering treatise, the hydrodynamcis of a system can be described by a set of mathematical equations called the equations of change.[1] These are complex differential equations that are not easy to solve for real-world problems. By carefully selecting the right parameters, the behavior of systems of similar configuration but different sizes can be analyzed using dimensional analysis without actually solving these equations. In most catalyst preparation steps, the hydrodynamics are often complex and not well understood, and the principle of dimensional analysis can be applied in scaling up.

The equations of change for a system are

$$(\nabla^* \cdot \mathrm{v}^*) = 0 \quad \text{(continuity)}$$

$$\frac{D\mathrm{v}^*}{Dt^*} = \left(\frac{1}{\mathrm{Re}}\right)(\nabla^{*2}\mathrm{v}^*) - \nabla^* p^* + \frac{1}{\mathrm{Fr}}\mathbf{g}/g \quad \text{(motion)}$$

$$\frac{DT^*}{Dt^*} = \left(\frac{1}{\mathrm{Re}\,\mathrm{Pr}}\right)(\nabla^{*2}T^*) + \frac{\mathrm{Br}}{\mathrm{Re}\,\mathrm{Pr}}\varphi_\mathrm{v}^* \quad \text{(energy)}$$

where v^* = dimensionless velocity
P^* = dimensionless pressure
t^* = dimensionless time

and the Re (Reynolds), Fr (Froude), Pr (Prandtl), and Br (Brinkmann) numbers are dimensionless groups describing the system. For detail treatments of these equations, refer to reference 1 (pp. 338–339).

It is not necessary to understand all the mathematics behind these equations, but it is important to understand the implications of the various terms in the equation when considering scale-up. The main principle for scale-up is to maintaining dynamic similarity for the laboratory system and the commercial system. This can be achieved by carefully choosing the parameters in both systems such that they have the same dimensionless terms.

As an example, consider the Reynolds number of a system, which is one of the most important parameter in flow analysis:

$$\mathrm{Re} = \frac{DV\rho}{\mu}$$

where D = characteristic length
V = characteristic velocity
ρ = density of fluid
μ = viscosity of fluid

If the Reynolds numbers are the same in both systems, both are described by the same set of dimensionless equations. If the boundary conditions are the same the two systems are mathematically identical or hydrodynamically equivalent. It is also desirable to maintain dimensional similarity between the laboratory system and the pilot- and/or commercial-scale system. This can be achieved by maintaining essentially the same geometry, for example, length-to-diameter ratio of reactors, shape of agitator impeller, and whether baffles are used.

In practice, maintaining the same Reynolds number may not be so easy. For example, if the same fluid is used (ρ and μ the same),

$$D_1V_1 = D_2V_2 \quad \text{or} \quad \frac{D_1}{D_2} = \frac{V_2}{V_1}$$

If the diameter ratio between the laboratory and commercial reactors is 100 (as scaling up from a 500-mL laboratory reactor to an 8-m^3 commercial reactor), a 100-fold difference in stirring speed is required to maintain the same Reynolds number. The typical speed for a commercial reactor is on the order of 60–100 rpm, and this means that the laboratory reactor would need an agitation speed of 6000–10,000 rpm, which often is quite difficult to do. In situations like this, other factors which influence the process step have to be considered and applied to compensate for the differences.

4.2.2 Reaction Kinetics, Heat and Mass Transfer

Catalyst preparation reactions, like all chemical reactions, are controlled by kinetics, heat and mass transfer. In a small laboratory-scale preparation, heat or mass transfer is often not an issue, and the reaction is most likely kinetic controlled. Kinetics control means the temperature of the reaction is the most important parameter. In a large-scale operation, heat and mass transfer limitations often come into play, resulting in a much more complex system. Take the simple case of heating up a reactor from ambient temperature to 150 °C. In the laboratory, this may take 15 min, but in a production reactor, this may take 2 h. The reaction taking place during this period must be taken into consideration when scaling up. Likewise, the turnover rate in a laboratory reactor could be orders of magnitude higher than a commercial-scale reactor. The localized concentration gradient or temperature gradient may exist in a large-scale reactor and not be present in laboratory reactors. It is important to determine in which regime the reaction is taking place for a successful scale-up.

4.3 CONSIDERATIONS IN SCALING UP LABORATORY RECIPE

Scaling up a laboratory recipe to commercial production involves making not only the desired catalyst but also the entire production process economically and environmentally feasible. The chemist's job is not done yet even after coming up with an optimized catalyst recipe. For commercial catalyst production to be viable, reactant and solvent recovery and waste treatment must be considered to complete the scale-up process.

The simplest way to scale up a recipe is to duplicate the set-up in the laboratory but make the equipment much larger. For simple catalyst recipes such as the early-generation ZN catalyst, this method worked well. Many early plants are designed such that they mimic laboratory equipment with simple continuous stirred tank reactors (CSTRs), decantation instead of filtration, and sometimes even glass equipment. With the increased complexities of modern catalyst recipes, this method is either not physically practical or not economically feasible. As the previous discussion indicated, even if we maintain dimensional similarity between systems, it is often not possible to maintain dynamic similarity.

Different approaches to scale-up are required when a completely new catalyst plant will be built or when the recipe is to be scaled up to existing equipment. When a new recipe is to be scaled up to a new catalyst plant, there is more freedom for the chemist or engineer to design and specify the process steps and equipment. On the other hand, if a recipe is to be scaled up to an existing plant, such as in the case when a modified recipe is being introduced, laboratory work should best be performed in a laboratory set-up that closely mimics the existing production plant.

Most laboratory chemists would use a round bottle glass flask to do the catalyst preparation. This is inexpensive and readily available. It works fine for simple impregnation or activation reactions and for initial recipe screening. For more complex catalyst preparation methods such as precipitation, the round-bottom flask is not a good platform for scale-up. Magnetic stirrers should be avoided as they do not scale up well, and they often cause breakup of the catalyst particles.

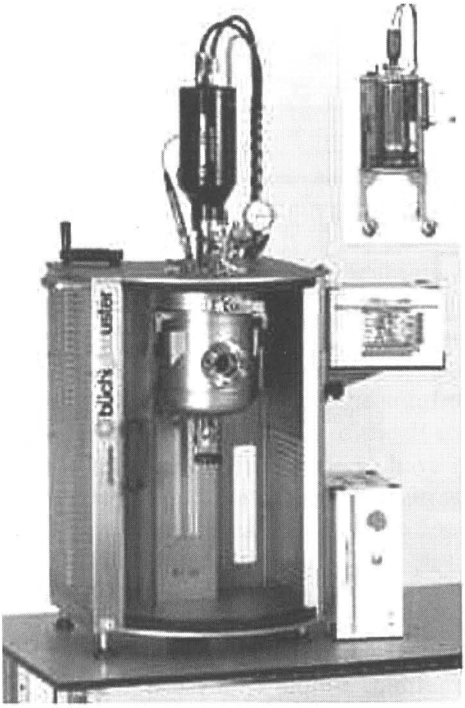

Figure 4.1 Büchi reactor.

A more advanced set-up would use a reactor that is designed to mimic a production-type CSTR. One example of such a set-up is the Büchi reactor shown in Figure 4.1. This is a jacketed reactor with interchangeable and variable-speed stirrers that can closely mimic the operation of a CSTR used in commercial-scale production. In such a system, dimensional and, to a large extent, dynamic similarity can be maintained between the laboratory and production systems.

In addition to scaling up the main reaction step, many other unit operations such as filtration, drying, and distillation have to be considered, and each step presents its own challenges.

4.4 MODERN POLYMERIZATION CATALYST PRODUCTION FACILITY

To understand the scale-up needs, it is useful to look at a modern polymerization catalyst production facility (Figure 4.2). Almost all modern polymerization catalysts are produced in batch processes, which typically contain the following process operations: raw materials purification, catalyst support formation, catalyst activation, drying and blending, solvent and reactant recovery and recycle, waste treatment, and off-gas treatment.

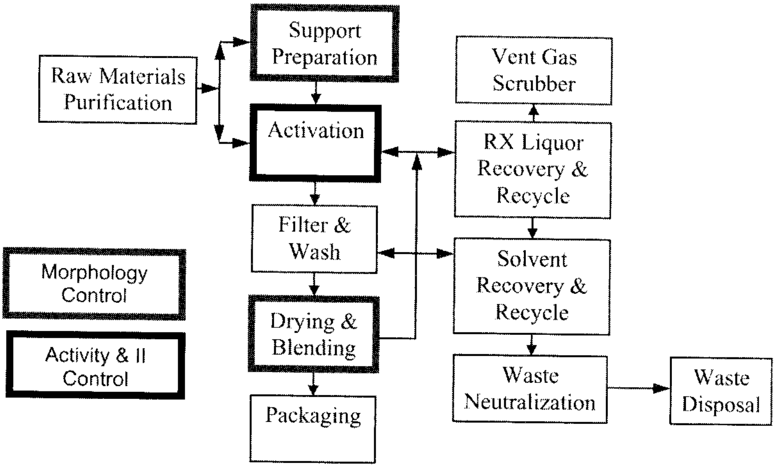

Figure 4.2 Schematic of modern polymerization catalyst production facility (from ref. 2).

Not all catalyst preparations require all these steps. For examples, in a silica support catalyst, the silica support is usually supplied by producers who specialize in preparing silica, which in itself is a complicated process deserving its own discussion. Sometimes simple catalyst systems can be prepared by the traditional incipient wetness impregnation method, thereby eliminating the reaction liquor and solvent recovery steps.

1. *Raw Materials Purification* It is well known that ZN catalyst preparation requires the highest purity raw materials. Even contaminants at the parts-per-billion (ppb) level can have a detrimental effect on catalyst performance. This is especially true for the hydrocarbon solvent that is used to wash the catalyst. Fortunately, the technology for purifying hydrocarbon solvents using molecular sieve adsorbents is well established and can be easily obtained from the adsorbent vendors.[3] Titanium tetrachloride can be obtained from producers in very pure form and there is no need for further purification, but care must be taken in its handling and storage to prevent contaminant such as iron (from storage tank) getting into the system. Other liquid raw materials can usually be purified using molecular sieves, so sometimes a simple purge with purified nitrogen is sufficient to strip off any oxygen or moisture that may be in the material.

2. *Catalyst Support Formation* Catalyst particle morphology is one of the most crucial aspects of catalyst performance, and this is often the most difficult step to scale up. A good summary of the various methods for forming catalyst support can be found in Chapter 8, and each of these methods has its own unique characteristics. A good understanding of the chemistry and the physical phenomena behind the preparation method is essential to successful scale-up.

In a typical fourth-generation ZN polypropylene catalyst such as the Mitsui catalyst,[4] support preparation is often done by precipitation. This is basically a crystallization and growth process. These processes have been well studied in classical chemical texts and journals.[5] The precipitation process must be precisely controlled to achieve the desired catalyst morphology. Controlling the temperature and rate of precipitation is most critical in this step. Scaling up can be difficult because of the hydrodynamic differences between the laboratory and commercial systems. However, it is still possible to choose equipment and parameters that will give predictable scale-up. Equipment such as the Büchi reactor described above is an invaluable tool because of the dimensional similarity to a commercial reactor.

Other support preparation methods[6–9] involve dissolving magnesium chloride in alcohol, then spray drying or quenching the solution to form spherical particles. This type of operation is much more difficult to scale up than precipitation reactions, since it is almost impossible to have hydrodynamic similarity between the laboratory and commercial systems. A trial-and-error approach has to be used in many cases. It is best to use a DOE (design of experiments) method[10] to screen the important variables, then narrow in on the ones that give the desired results.

3. *Catalyst Activation* Most often catalyst activation involves the reaction of titanium tetrachloride and other reactants (such as an aluminum alkyl) with the catalyst support. This step may be the most important and is the heart of the process, but the reaction mechanism is relatively well understood. Scale-up involves mostly the application of known chemical engineering principles to achieve the desired mass and heat transfer results. It is still not straightforward as many of the parameters in the laboratory cannot be duplicated on a large scale due to equipment or other physical limitations. The important points to consider are the heat and mass transfer limitations in the commercial-scale reactor and how to overcome these limitations. This may require adjustment to the laboratory recipe in terms of the addition method and addition rate of the reactants and the reaction temperature profile.

4. *Filter and Wash* Most catalyst systems are prepared in a slurry. The catalyst must be separated from the solvent and then washed free of any excess reactants such as $TiCl_4$ or alkyls. Efficient removal of the excess reactants is most important for quality and economics. The choice of filtration equipment is extremely important in the scale-up process. This step is often difficult to scale up as filtration time is very much dependent on batch size, but filtration time has strong influences on catalyst performance.

The simplest and most familiar to a laboratory chemist is decantation. This method works well if the catalyst particles are large and settle quickly. When scaled up to commercial scale, this method requires the least amount of capital investment (as basically just a pipe is required). The disadvantage of this type of operation is that a large amount of liquid is left with the catalyst, and it is typically not possible to get more than 30–40% solids. Thus the washing efficiency is very low and many washes are required to achieve the desired washing effect. Scaling up this type of filtration is straightforward. The main considerations are the amount of time that the slurry is allowed to settle and how many washes are required to reduce the excess reactant to the desired level. The settling time may affect the catalyst quality, especially in the mother liquor stage as the reaction is still going on and must be taken into consideration.

Many more efficient filtration methods are available on a commercial scale and each has its own pros and cons. A very good overview of the different types of process equipment available can be found on the Internet.[11] Scaling up (or in many cases scaling down) this equipment presents it own set of challenges. It is often difficult, if not impossible, for a chemist to mimic the filtration conditions of these industrial filters. While the equipment vendor may have smaller scale equipment available for testing, the air-sensitive nature of ZN catalyst makes this difficult, as very few equipment vendors are ready to test catalyst slurry containing titanium tetrachloride. The experience of the scale-up engineer and the equipment vendor would be very important for successful scale-up. Among the various filtration equipment available, the Nutsche-type filter is most often used for catalyst preparation. The Nutsche filter can be simulated in the laboratory by a fritted filter, facilitating the scale-up process.

5. *Drying and Blending* Blending is desirable to average batch-to-batch variations that are inherent to all batch processes. In this step, care must be taking not to damage the particle morphology produced in previous steps. This is also the place where classification of particles to further improve catalyst performance can take place. Again applying known chemical engineering principles and the choice of process equipment are key. Equipment vendors can provide valuable help.

6. *Solvent and Reactant Recovery and Recycle* This is the most important part of the scale-up process that a catalyst development chemist often overlooks. This part of the process is most important for the economic viability of the catalyst plant. An efficient recovery and recycle process will not only reduce raw material cost but also and most importantly will reduce waste disposal cost and environmental impact. The job of the chemist and engineer is to come up with a good scheme that can reuse most (if not all) of the reactant and by-product streams that are generated in the catalyst preparation. If the stream cannot be reused in catalyst preparation, often an alternate off-site outlet can be found to reuse the material. When reusing raw materials such as titanium tetrachloride and other wash solvents, it is important to determine the effect of trace impurities on catalyst quality. This will influence the design specifications for the solvent recovery system.

Distillation is the most often used technique in solvent recovery, and the distillation columns must be carefully designed to achieve the maximum efficiency. Physical and equilibrium properties data for designing distillation columns for the chemicals used in catalyst preparation (e.g., titanium chloride with aromatic hydrocarbons) are often not available in the open literature. It is important to spend the time and effort to obtain reliable physical properties data for use in the design. Once the data are available, modern design software such as the Aspen system can easily take the data and generate good column design.

7. *Waste Treatment* Most ZN catalyst recipes generate significant quantities of waste even with recovery and reuse. Often these are reactive wastes formed from reactions with titanium tetrachloride and usually come out of the bottom of the distillation column. With increasing restrictions on environmental regulations, these wastes have to be properly deactivated and neutralized before disposal.

The most common method for disposing titanium chloride containing waste is to react it with a base such as sodium or calcium hydroxide. In this process, hydrogen chloride is generated and has to be captured and treated. The organic phase must be separated from the inorganic phase and disposed of separately. The technology for this is well known, but due to the aggressive corrosive nature of hydrogen chloride and resulting hydrochloric acid, the choice of materials of construction must be carefully considered or else it would become a maintenance nightmare. This part can add significantly to the capital cost of building a catalyst plant as exotic materials may be required to withstand the corrosive waste.

8. *Off-Gas Treatment* Off-gas includes the nitrogen used to blanket all the equipment and any other vapor that may be generated during the catalyst production reactions. These streams often contain both titanium tetrachloride and organic vapor from the solvents. The common method is to vent the titanium tetrachloride containing stream to a caustic or water scrubber, and the organic vapors are vented to a flare or an activated carbon adsorber. Again the technology is well established but adds capital investment, and because of the aggressive, corrosive nature of HCl, this is often a high-maintenance area of the plant.

4.5 OTHER SCALE-UP CONSIDERATIONS

Most of the reactants used in ZN catalyst preparation are inherently dangerous. The air-sensitive nature of titanium tetrachloride and the pyrophoric nature of aluminum alkyls require special safety precautions in their handling. Other organic solvents such as hexane, toluene, and chlorobenzene can pose a chronic health hazard as well. The chemist responsible for developing a catalyst recipe should always keep the safety hazards in mind and avoid using the more hazardous chemical as much as possible. When scaling up any recipe, it is important to do a thorough safety review on the handling of the chemicals and the safety and suitability of the equipment.

Another often-forgotten aspect of scale-up is good recordkeeping. Carefully kept notes and observations during laboratory and pilot stages would be extremely useful in tackling production problems. This and other good advice on scale-up can be found in references 12 and 13.

REFERENCES

1. Bird, R. B., Stewart, W. E., and Lightfoot, E. N., *Transport Phenomena*, 2nd ed, Wiley, New York, 2007.
2. Cheng, C. P., *Recent Developments in Ziegler-Natta Polypropylene Catalyst*, paper presented at FlexPO 99, New Orleans, 1999.
3. www.Zeochem.com
4. Kioka, M., and Kashiwa, N., Mitsui Petrochemical Industries, U.S. Patent No. 4,952,649, 1990.
5. Genck, W., *Chem. Eng. Prog.*, **2008**, 104, 22–34.
6. Collina, G., Alessandrini, G., Evangelisti, D., and Aldrovandi, E., Basell Poliolefine Italia, World Patent application WO2006063973, 2006.
7. Invernizzi, R., and Ligorati, F., Enichimica Secondaria, U.S. Patent No. 4,506,027, 1985.
8. Iiskolan, E., and Koskinen, J., Neste Oy, U.S. Patent No. 4,829,034, 1989.
9. Karbasi, A. K., Leinonen, T., and Sormunen, P., Borealis Technology Oy, European Patent application 0,627,449 A1, 1994.
10. Box, G. E. P., Hunter, J. S., and Hunter, W. G., *Statistics for Experimenters: Design, Innovation, and Discovery*, 2nd ed., Wiley-Interscience, Hoboken, NJ, 2005.
11. Halberthal, J., Engineering aspects in solid-liquid separation, available: www.solidliquid-separation.com/pressurefilters/nutsche/nutsche.htm.
12. McConville, F. X., *Chem. Eng. Prog.*, **2007**, 103, 18–19.
13. McConville, F. X., *The Pilot Plant Handbook: A Unique Handbook for the Chemical Process Industry*, FXM Engineering and Design, Worcester, MA, 2002.

5 Commercialization of Olefin Polymerization Catalysts: Model for Success

C. E. CAPSHEW
Chevron-Phillips Chemical Company, Consultant (retired), Owasso, Oklahoma 74055

5.1 INTRODUCTION TO POLYPROPYLENE AND POLYETHYLENE

5.1.1 Scope of Chapter

After leaving graduate school in 1977, I was offered a position in the catalyst development group of Phillips Petroleum Company in Bartlesville, Oklahoma, working with Dr. Henry Hsieh on the development of new titanium-based catalysts. An ethylene polymerization catalyst was discovered that comprised a proprietary composition of magnesium and titanium. It has now run several decades in the Phillips loop reactor process.[1] An experienced team of chemists and engineers helped commercialize the catalyst and its resulting polymers. Little did I know that this was just the first of several commercialization experiences, including a five-year tour in a Phillips affiliate, Catalyst Resources (today a unit of BASF), to introduce several new catalysts and upgrade several polypropylene plants around the world.

During a career of 27 years with Phillips Petroleum and later Chevron Phillips Chemical Company, my experience with commercializing high-density polyethylene and polypropylene inventions broadened. This chapter will focus on experiences related to high-density polyethylene and polypropylene industries. Nevertheless, the lessons learned and the proposed operational model should have applicability to other olefin polymerization applications, and hopefully the reader will be able to select and apply those elements of the model as appropriate.

Handbook of Transition Metal Polymerization Catalysts Edited by Ray Hoff and Robert T. Mathers
Copyright © 2010 John Wiley & Sons, Inc.

For many years, tertiary references were lacking in the polyolefin industry —a characteristic of a young and changing industry. Fortunately, in recent years some such references, including this handbook, are beginning to appear. Consequently, it is not my intent to revisit content already reviewed in the literature, although I may make references to them. For example, Edward P. Moore, Jr. edited an excellent book on polypropylene in 1996, and this book contains an excellent review of the historical development of the polypropylene catalysts up through 1996.[2]

5.1.2 Make-or-Buy Decision for Catalyst

A number of olefin polymerization companies have developed and maintained strong technical organizations throughout the history of the polyolefin industry. These organizations typically focus on polymer or material development and often also employ catalyst development units. Alongside these product development units typically are process development units.

Decades of technical advancements have resulted today in very efficient polymer processing units in polyethylene and polypropylene. By and large, these units are based on very efficient catalysts, typically far advanced from those in operation 50 years ago.

Furthermore, markets have become fairly well defined for the various polymers and continue to grow at historically strong rates in both advanced and developing markets. The olefin polymerization industry continues to make remarkable advances in market applications spurred on by continuing developments in fundamental technology.

Spurring on these technical achievements in new and broader market applications were and are the catalyst development units maintained within the respective producers. Anyone around the industry very long will soon come to realize the catalyst determines much of the market leverage of the resulting polymers—and determines the efficiency of the process that produces the polymers. In other words "it's all about the catalyst"—or "the catalyst determines the polymer."

Historically, industry participants have designed only a few technical strategies to develop and advance catalyst technology. Some have invested great resources to become leading licensors of technology while others have employed strategies stressing more incremental advances. Still others have chosen to rely more heavily on the leading technical licensors and have employed more of a maintenance strategy for their catalyst development units. For example, after some 50+ years of commercial development, a leading high-density polyethylene licensor is Chevron Phillips Chemical Company while leading licensors of polypropylene technology include Basell and Dow Chemical (the owner of the former Union Carbide operation).

Despite the diverse nature of the historical participants in the polyolefin industry, those who maintain catalyst development units typically share a common dilemma. This dilemma is the classic "make-or-buy" decision for the next improved catalyst or next generation of catalyst. That is, who will produce the commercial supply of the next catalyst? If the polymer company has a promising laboratory invention, will the polymer company manufacture its own catalyst or will the polymer company contract supply from a custom catalyst manufacturer. Or is there a merchant market catalyst already available which the polymer company can purchase?

In approaching and solving this dilemma, there are four critical questions to address:

1. What is the potential patent position for your own invention—will it encroach upon another patent and chance litigation and possible royalty fees?
2. What are the developmental costs to take this invention from the laboratory to full-scale commercialization and does the polymer company have the internal expertise and resources for this development?
3. Are there merchant market catalysts available and what are their relative costs to your own costs?
4. What is the polymer marketing strategy of the company and can it be met with merchant market catalysts?

These questions are discussed in the following sections for the make-or-buy decision.

5.2 MAKE-OR-BUY DECISION FOR CATALYST: MAKE

The Patent Question There is little point in going forth with the commercialization of a laboratory invention if the intellectual position is questionable. This question must be addressed early in the invention with appropriate patent studies and filings to assess the potential patent's strength. And even with the granting of a U.S. patent, there is still the possibility of litigation from a competitive patent holder. Considering that the greatest fraction of the commercialization investment is postlaboratory, assessing potential patent strength is key in minimizing the risk of lost investment due to unsuccessful patent litigation—or at best the addition of a royalty fee onto the polymer's cost of production.

Internal Scale-Up and Commercialization or Contract Custom Manufacturer The scale-up of a laboratory invention is no trivial matter. For example, taking a laboratory invention to commercial scale typically scales from possibly grams through a pilot stage of possibly a few pounds to the commercial scale where scores or hundreds of pounds are produced in a batch. Typically the largest step in this scaling is between the laboratory scale and the pilot scale. Often more scale-up challenges are encountered at this stage rather than at the full commercial stage. Usually this pilot stage is the smallest stage where actual industrial sized equipment is used—for example, vessels, stirring blades, addition pumps, and so forth. Often the full commercial scale is simply an increase in size of this smaller scale equipment.

Investment in the pilot scale can be costly, depending on the expertise already in the polymer company. Moreover, the operating culture of this stage is more like that of a specialty or fine chemical operation than that of a polymer company. So not only is there an investment cost hurdle in getting through this stage, but also there may be a significant operating cultural challenge to overcome. With respect to investment, a laboratory may already be equipped with small equipment but a pilot facility involving pipes, pumps, steel vessels, and so on—as well as associated support equipment for large volumes of solvents and handling of wastes—may need to be created from scratch. Furthermore, often the first scale-up experiments may miss the mark, and totally new or at least redesigned equipment may be required. Easily a scale-up investment could hit seven figures for a first-generation commercial facility—for those without such facilities already on the ground.

More often than not polymer companies will not have such internal catalyst scale-up facilities in place because of the large operating expenses required to maintain and operate the facilities. Although they may be funding the development of improved or new catalysts, often there will not be in-house specialty chemical facilities to take these catalysts to commercial scale.

Although a few polymer companies maintain the catalyst scale-up capability in-house—either because of internal specialty chemical operations or a desire to be totally self-sufficient—it is more typical that the polymer company will not have such facilities readily available and will examine the feasibility for external scale-up and commercialization. It is strongly advisable, even for those self-sufficient companies, to examine this alternative route—the economic feasibility of contracting scale-up and production through an outside custom manufacturing house. Thus we come to the make-or-buy decision for even those polymer companies with self-sufficiency in catalyst production.

Therefore, with invention in-hand and assuming an adequate patent position, there should be an internal first-order estimate for cost of scaling up in-house (if possible) and final manufacturing cost for an in-house first-generation catalyst plant. After adequate nondisclosure agreements are in place, a reputable custom manufacturing company should be asked for its estimates for the same costs. Do not be surprised if the custom manufacturing company makes a strongly competitive offer. The best of companies will have much of the equipment already in place and may well have expertise in-house for the scale-up of the various chemical and physical reactions.

Are There Merchant Market Catalysts Available and What Are Their Costs Relative to Your Own Costs? For the alternative case, the polymer company should know well what catalysts are available on the merchant market. Excellent marketing intelligence will preclude the polymer company from trying to invent and commercialize a catalyst that might already be commercially available. A review of these catalysts may well conclude that any work by the polymer company cannot be justified economically, and a suitable merchant market catalyst can be purchased without any or limited investment by the polymer company.

What Is the Polymer Marketing Strategy of the Company and Can It Be Met with Merchant Market Catalysts? The marketing strategy of a polymer company really determines the feasibility of producing the company's polymers with merchant market catalysts. For example, if the marketing strategy is to produce "generic" polyethylenes or polypropylenes, there is typically little need for massive investments in catalyst development. The company's resources could be put to better use in market application support as well as incremental process optimization. On the other hand, if the marketing strategy of the company is to have the blow-molding benchmark in polyethylene or say the industry benchmark in polypropylene BOPP film, then there is justification for internal catalyst development.

Merchant market catalysts should be carefully evaluated because it must be remembered that they do not all perform equally. A sophisticated understanding of the capabilities of merchant market catalysts will lead to a realization that market differentiation is possible with such catalysts. On the other hand, they do offer the support for simple generic marketing efforts.

5.3 MAKE-OR-BUY DECISION: MAKE MODEL

If the decision is to make and commercialize the catalyst internally, there are a number of factors to work through—the same as any manufacturer of catalyst. First sizing must be understood. That is, how many pounds of catalyst will be required per year? This sets the size of the equipment and contributes significantly to the overhead cost to be borne by the catalyst. And this is especially a difficult question if the catalyst is supporting a new market application. For example, if marketing suggests the company will sell 400 million lb of polymer annually in five years and if the catalyst activity is 20,000 lb polymer/lb catalyst, then a plant needs to produce some 20,000 lb of catalyst annually. The next premise needs to set the annual operating hours for the catalyst plant. These two premises (and the detailed chemistry of the catalyst preparation) largely set the size of the equipment for the plant. If marketing thinks its estimate could be low, then design may call for easy expansion of the plant. Not much can be said if marketing overestimates the design—the company will be stuck with an oversized catalyst plant and one very expensive catalyst. A much easier proposition is if the catalyst is replacing another catalyst in existing market applications. There is much less risk in this case for marketing to miss its estimate either up or down.

When commercializing an internal invention, one of the greatest temptations is to hold on to the invention at a developmental stage and continue to work on the next improvement. Years can easily go by while the next generation is being promised. For example, in polypropylene first-generation catalysts operated for more than a decade before the significantly improved second-generation appeared. Likewise over similar time spans have come third and fourth and now fifth generations. Imagine if the industry had waited for the "ultimate" polypropylene catalyst. Likewise, there needs to be some wisdom exercised in when to push an internal invention into the commercial plant. More likely than not an improvement will be coming down the "pipeline" in a couple of years. This wisdom reflects a balance of possibly a new polymer market share and possibly some increased catalyst cost. Nevertheless, if the new catalyst can stand economically and technically on its feet, more likely than not, it should be pushed forward. The incremental improvement will be something to look forward to as possibly a cost improvement project. The bottom line is if the catalyst can be produced over and over again with the same specifications, if the polymer coming out of the plant reflects such precision of quality, if the catalyst is economical, and if the polymer plant runs without incident, most likely this "first generation" is ready to be launched.

However, there is one reservation about launching any new catalyst. In some applications there are long and extensive approval processes for market acceptance. An easy example is found in high-density polyethylene pipe resins. Working new resins through various industry and customer approval steps can take years. In such applications, bringing on new catalysts is time consuming and expensive.

Nevertheless, in this never-ending conflict about the timing when to go forward, there needs to be a good understanding of the first-generation catalyst's constraints, the key steps or hurdles in going to the next generation, and possibly the time requirements for such continued development. With these factors in mind reasonably sound decisions can be made about carrying forward a new catalyst.

In the internal commercialization of a catalyst, safety will be weaved throughout the process and will always be on the agenda. The preparation of catalyst on a large scale most likely involves many hazardous materials; consequently, process safety management will be a prerequisite. Throughout the design of the pilot facility as well as any commercial facility, the elements of process safety management must be adhered to. Hand in hand with safety will be compliance with environmental regulations, including possible environmental impact, handling of possibly hazardous wastes, the requirement for any new chemical to be on the Toxic Substances Control Act (TSCA) inventory, and the requirement for a premanufacturing notice (or at least a temporary research-and-development (R&D) exemption). Just as in safety management, polymer companies deciding to produce their own catalysts internally will have internal experts to guide the catalyst scientists through these requirements.

Parenthetically, it will be the norm for many scientists commercializing for the first time to give little attention to the waste streams and the handling of hazardous chemicals in a large-scale environment. What is very simple in a laboratory or dry box can be full of challenges in either a pilot plant or commercial plant. However, locating a catalyst plant in an existing chemical plant can simplify the design and minimize the cost of the catalyst plant. Several years ago an operator was asked where did his waste streams go from his catalyst plant. He pointed to the adjacent and large petrochemical complex and said "over there somewhere." Although at first glance this might be considered a comical response, indeed it is much simpler to tie waste streams and feedstreams into an existing complex than to build a grass-roots, self-contained catalyst plant responsible for its own hydrocarbon feedstock and waste management.

The application of cross-functional teams can expedite and simplify the scale-up and commercialization process and is the key to rapid and successful commercialization of a new catalyst. Typically the laboratory scientist will be working with gram-scale equipment while commercial operations will be working with multiple-pound pipes and pumps and vessels. It is critical to introduce the engineering staff early to the catalyst's synthesis and special requirements for the synthesis. This is the very best way to transfer technology and is not dependent on formal reports but on the ability for people to communicate accurately with one another.

For example, "catalyst teams" or CATPAKs were found to be extremely successful in taking something from a laboratory curiosity to commercial scale. CATPAKs may be called by other names, but they are composed of representatives of the stakeholders in the process. For example, the inventor or inventors will have the essential chemical knowledge for the various steps. Members of engineering—especially process and mechanical disciplines—will start to design the large-scale unit. Also, operational members from the plant are involved and provide first-hand experience. Other disciplines include safety, environmental, transportation, and marketing. Management must also be a key part of the team and must provide the vision and support for the team to be successful. A typical CATPAK team might be composed of a dozen or so active members.

Key to the success of these teams are frequent and regular meetings of the stakeholders where project schedule and current problems are reviewed and updated. In some cases, these meetings may be weekly. Likewise, there is no substitute for the inventor(s) being in the manufacturing facility, especially during early production runs where unexpected problems may arise.

One of the most successful examples of a CATPAK team involved representatives from two different companies (the inventing company and the catalyst manufacturer). The time the laboratory invention was presented to the CATPAK to the time there was a successful and complicated operational pilot plant was on the order of a year. And several very difficult scale-up problems were encountered and efficiently solved by the CATPAK. (It should be noted this "pilot unit" supplied sufficient catalyst for on-going commercial plant operations for several years.)

During these interactions with engineering, R&D, and the plant, several fundamental steps must be completed and as soon as possible. The distinct operational steps for the catalyst manufacture must be clearly identified. It is not unusual for a laboratory synthesis to gloss over one or more steps. Furthermore, what might take minutes in a laboratory preparation might take hours in a large facility. For example, in one commercialized catalyst involving seemingly three simple steps and only a few hours in the laboratory scaling to an industrial-scale reactor—on the order of 100 gallons—took the better part of 24 h and many more steps.

In the reviews of the operational steps, complete information must be developed at each step—temperatures, times of additions or mixings, addition rates, and so forth. Questions are especially encouraged at this step after the inventor goes through his or her laboratory sequence—there is no question too simple or obvious not to be asked at this stage.

Also, the leader of the team needs to keep in mind cost control throughout these processes. More likely than not the inventor will want a narrowly prescribed way to execute a step, and in some cases the execution of such requirements could be costly when a simpler alternative might be available. The inventor needs to maintain an open mind at this stage and not become too defensive as the engineers seek a more cost-effective way of accomplishing his or her desired task. Likewise, the engineer needs to be sensitive to the inventor's ownership of catalyst and understand he or she may feel threatened by questions. Inventors have been heard decrying how engineering is "trying to destroy" the catalyst!

The team also needs to be thinking ahead on how the catalyst will be packaged and shipped to the polymer plant. What will be the shipping classification of the catalyst? Will the catalyst go as a dry powder or as a slurry? This latter question has huge import to the design of the catalyst plant as well as what is required in the polymer plant. Typically, polymer plants are already running on a catalyst and have already in place some sort of feeding system. Management of polymer plants will be very reluctant to make additional investment to feed the new catalyst via a system they do not have already installed.

Also, the kind of shipping vessel must be carefully thought about. For example, will the shipping vessel be returnable or will the shipping vessel be a one-way container—a container which the polymer plant must properly dispose of.

Again referring back to the polymer plant and its existing feeding and material handling system, thought must be given to how the catalyst shipping vessel will be managed and handled in the polymer plant. Will there be special storage temperature requirements? Will there be special safe storage requirements? Again, polymer plant management will want to change little if anything in their system to handle the new catalyst. In other words, typically the new catalyst, no matter how grand or promising, must fit into the plant's existing feeding and material-handling system—if at all possible.

In summary, it is critical for the CATPAK team to address each of these items from the start of the catalyst preparation all the way through the catalyst consumption in the polymer plant. A checklist is recommended early on where a listing of these items can be monitored and managed. The checklist should be "living" because, most likely, new and more detailed concerns will be added as the project progresses. It is really embarrassing and possibly costly to come to the conclusion of a very successful catalyst development project only to have not considered some key and seemingly mundane items such as "material handling" in the polymer plant.

5.4 MAKE-OR-BUY DECISION: BUY MODEL

If the polymer company decides to purchase the catalyst for its plant(s) on the merchant market, there is a clearly defined path the company should follow in deciding what catalyst to purchase. This model assumes the polymer company has access to some sort of polymer pilot plant where potential catalysts can be tested and compared. However, the model also treats the case where the polymer company does not have such access.

In polypropylene, especially, there are a number of potential sources of catalyst supply without process licenses. Some of the better known include Basell, BASF, Mitsui, Toho, Davison (ex-U.S.), and Sud-Chemie. High-density polyethylene catalyst merchant market sources include Ineos, Davison, BASF, Japan Polyolefins, and Mitsui. Any of the merchant market catalyst sources will be glad to review their offerings in an introductory meeting where a nondisclosure agreement is not required. As a first step, it is recommended that each possible source of catalyst is reviewed prior to engaging in a nondisclosure agreement. Typically, the catalyst company will review the catalysts available and provide limited laboratory and maybe even pilot plant performance data. Nevertheless, enough information should be gleaned from the meeting to estimate the usefulness of the catalyst for your own application. Indeed, much of the information in this first meeting may well have already been presented in one or more trade conferences around the world.

Although the technical details may be limited, it is very appropriate at this early contact to get an estimate for the cost of the catalyst. Most likely any quote will be list price and often the catalyst supplier will prefer to talk in terms of cost of polymer produced rather than cost of catalyst. Nevertheless, the polymer company needs to know some catalyst price at this early stage.

After this first meeting, if the merchant catalyst is still a candidate, a suitable nondisclosure agreement is appropriate. Much more detailed information can be expected under a nondisclosure agreement. However, in some cases, especially with technical leaders, a nondisclosure agreement may not be wanted for fear of intellectual contamination, and such a company may opt for a nonanalysis agreement where the polymer company is allowed to test the catalyst in its own facilities, but it agrees not to analyze the catalyst.

Assuming a nondisclosure agreement is executed, the polymer company can improve the effectiveness of the first meeting (and improve efficiency of the overall process) if a list of questions is forwarded to the catalyst company. Table 5.1 contains examples of such questions.

TABLE 5.1 Questions for Catalyst Company

I. Outline for catalyst supplier discussions under nondisclosure

A. Description of catalyst system
   a. General description
   b. Degree of technical support from supplier
   c. Historical relationship with supplier

B. Catalyst performance
   a. Productivity
   b. Activity kinetics
   c. Expected variance
   d. MFR capability (hydrogen response)
   e. Expected polymer size distribution (fines)

C. Catalyst performance specifications

D. Catalyst supply commercial terms
   a. Contract length
   b. Cost

E. Catalyst packaging system
   a. Shipping packaging
   b. Required handling in plant

F. Catalyst need for pretreatment
   a. Conditions of pretreatment
   b. Specifications

G. Catalyst chemicals
   a. Availability
   b. Cost

H. Cocatalyst
   a. Supplier
   b. Cost

I. Plant considerations
   a. Donor system
   b. Catalyst handling system
   c. Cocatalyst system
   d. Rx operating temperature
   e. Reactor solids
   f. Visbreaking capability (polypropylene)

J. Polymer performance
   a. Mechanical properties
   b. Thermal properties
   c. Physical properties
   d. Odor/color
   e. Processability
   f. Compatibility with current market

TABLE 5.1 ***(Continued)***

II. Detailed questions for catalyst supplier under nondisclosure

A. Review the major products to be produced with the merchant catalyst company.

B. How would the catalyst supplier suggest the polymer producer have confidence that the catalyst can produce the desired product mix? Options include:
  a. Samples of catalyst products produced in a comparable process?
    1. Limitations on availability
    2. Timing constraints
  b. Availability of mechanical/physical properties for select grades?
    1. Specify the polymer requirements. For example, in polypropylene this might be xylene solubles. How is the catalyst controlled to achieve these objectives?
    2. Do the catalyst's polymers have any special additive requirements?
    3. Are samples of end-use products available—for example, film?
    4. Does the catalyst company have access to a polymer pilot plant where special polymers can be made? (This would be appropriate only if the polymer company does not have a pilot plant or does not wish to apply its pilot plant to this task.)
    5. Is there a possibility for third-party evaluations for applications like injection molding, film, fiber, and so on? If this is possible, what is the cost? What is their testing capability?
    6. What is the expected polymer morphology?
      i. The polymer company may need powder samples for material transport studies. Would small quantities of these be available?
    7. Polymer performance criteria
      i. Mechanical properties
      ii. Thermal properties
      iii. Physical properties
      iv. Odor/color
      v. Processability
      vi. Morphology and plant operability
      vii. Compatibility with current market

C. What technical support is available?
  a. What are the recommended donor ratios for different products (e.g., polypropylene)?
  b. Identity, source, cost of donors or other catalyst chemicals
  c. What is the licensing cost of these chemicals—if any?
  d. What support is available for design—assuming modifications are required in the polymer plant to host the merchant catalyst?

TABLE 5.1 ***(Continued)***

D. Catalyst
  a. What is required in the way of pretreatment of the catalyst (e.g., polypropylene or some polyethylene catalysts)?
    1. What technical support is available for the design and operation of any required pretreatment system (assuming the polymer's plant requires modification to host the merchant catalyst)?
      i. What are the pretreatment conditions?
      ii. What is the recommended prepolymer level, levels of donor, and TEAL and what is the temperature of prepolymerization and storage (e.g., specifically for polypropylene)? In polyethylene there may be some special activations.
      iii. What is the acceptable level of solids in the pretreatment reactor and holding vessels?
  b. What information is available concerning catalyst feeding?
  c. What are the catalyst activity kinetics?
  d. What is the catalyst MFR (or MI) capability?
  e. What is the catalyst productivity?
    1. What poisons affect catalyst productivity? What is the quantitative effect?
    2. Does the delivery method (how the catalyst is delivered to the polymerization reactor) affect productivity?
  f. What is the catalyst shipping packaging?
  g. What are the catalyst handling procedures?
  h. What sort of handling system is required?
  i. What are the catalyst specifications?
  j. What is the catalyst's visbreaking capability (polypropylene)?

E. Cocatalyst
  a. Who do you recommend as a cocatalyst supplier?
  b. What are recommended charge levels of cocatalyst?

F. Technical support
  a. What information is available to gauge operability in the polymer company's process?
  b. What is the maximum reactor temperature for both homopolymers and random copolymers?
  c. What is the required hydrogen concentration for all proposed resin types?
  d. What information is available with respect to conversion per pass?
  e. Describe technical support that is available on plant startup and after startup.

G. Commercial considerations
  a. Are there any marketing exclusions for the polymer made with the catalyst?
  b. Where will the catalyst be produced? What sort of inventory would the catalyst company recommend for the polymer plant?
  c. For planning purposes, what costs does the catalyst company envision for the catalyst system?

The questions in Table 5.1 are exhaustive and are heavily weighted toward polypropylene and high-density polyethylene catalysts. In many cases, several of these questions may be nonapplicable to individual polymer companies, but they can serve as a guide or checklist to develop questions that are more fitting to the individual case. As written, they can serve as a checklist for the key items to be reviewed with the merchant catalyst company.

In some cases, catalyst companies may be part of a larger polymer operation which may also offer licenses for either or both catalyst and process information. In such cases, the catalyst company may be reluctant to share such process information. This possibility calls for the polymer company scanning the market for all possible sources of catalyst and not limit conversations to the so-called leading purveyors of technology. For, historically, some catalyst companies are quite knowledgeable about both catalyst and polymer process information. This means the polymer company will have significantly less risk in applying this respective merchant catalyst in its own plant. However, there are "stand-alone" merchant catalyst companies that can offer little more than typical laboratory catalyst performance data and expect the customer to generate all other information in either their own pilot plant or their commercial facility.

Therefore, in these proprietary meetings, the polymer company needs to characterize key parameters for catalyst evaluation and process performance. Polymer samples made with the merchant catalyst need to be evaluated and compared with commercial polymers made with the existing catalyst. Again, these polymer samples can be produced either internally in a pilot plant or in special commercial plant test runs or they can be supplied by the merchant catalyst company. Sufficient polymer is required to enable comparison of key performance features between the products made with the existing catalyst and those made with the merchant catalyst. Polymer qualification must include this comparison to suitable benchmarks as well as suitable performance in the polymer customers' fabrication facility. Key customers must be identified before the evaluation starts, and key parameters must be identified and agreed to between the polymer company and the polymer customer.

5.5 OLEFIN POLYMERIZATION CATALYST CHANGE MODEL

Table 5.2 summarizes a model for replacing one catalyst with another. Successful application of the model depends on key factors being identified in making a catalyst change and understanding of the potential impact of such a change on the polymer company's customers. The model depends on the successful comparison of mechanical, physical, and inherent properties of the current commercial polymers and those envisioned by the new catalyst. The model is also exhaustive, assuming a significant catalyst change and potentially significant polymer property changes. Very possibly a more incremental change would necessarily involve fewer steps and a shorter project schedule.

TABLE 5.2 Model for Replacing One Catalyst with Another Catalyst

Step	0–6 Months	6–12 Months	12–18 Months	18–24 Months
Document current knowledge				
Identify key resins/customers	X			
Review key resins/customers	X			
Review key resin formulations	X			
Iteration 1				
Pilot plant production				
Initial production (1000 lb?)	X			
Acquire commercial lots	X			
Acquire competitive resins	X			
Resin characterization				
Determine key properties	X	X		
Mechanical, physical, inherent				
"Reengineer" competitive resins	X	X		
Reformulate as necessary		X		
Processing studies				
Injection molding		X		
Fiber as appropriate		X		
laboratory fiber studies		X		
Monofilament/multifilament		X		
Blow molding, extrusion		X		
Iteration 2				
Make adjustments as suggested in first iteration.		X		
Pilot plant run 2				
Evaluation of resins		X		
Sample key resins to key customers		X		
Customer feedback		X		
Iteration 3 if necessary			X	
Commercial plant conversion				
Engineering conversions if necessary		X	X	
Plant trial 1 of key resins			X	
Sample key customers			X	
Customer feedback			X	
Sample other customers				X
Plant conversion				X

The first step in a catalyst changeout is the identification of key resins and key customers. For example, key resins might include those with long-term approval processes or which are major components to the product mix. Typically key resins and key customers will match up one to one. That is, customers of key resins will automatically be identified as "key." Transparency is required with these customers, and there must be accurate knowledge of their position

TABLE 5.3 Typical Properties Examined in Polyolefins

Test Description	Units	Test Description	Units
Melt flow rate	g/10min	Heat deflection temperature, edgewise	°C
Capillary rheology	Poise	Heat deflection temperature, flatwise	°C
Density	g/mL	Hunter color (L,a,b,YI)	value
Rockwell hardness		Haze, total	%
Heat deflection temperature	°C	Light transmission	%
Vicat softening temperature	°C	Clarity	%
Tensile modulus, yield, break, elongation	psi	Gloss	%
Flexural modulus	psi	Tenacity, monofilament	g/denier
Notched izod	ft lbf/in.	Tenacity, multifilament	g/denier
Unnotched izod	ft lbf/in.	Ash	wt %
Dynatup, falling dart impact	in. lb	Corrosion value	
Gardner impact strength	in. lb	Hf scan	
MTS high-rate impact (multiaxial)	in. lb	GPC (M_w, M_n)	
		DSC (T_c, T_m)	

and requirements for any polymer changes. During the catalyst changeout process, close attention must be given to the satisfaction of these key customers. Some polymer producers, on the other hand, have made wholesale catalyst and polymer product line changeouts without a word to the customers. However, customer satisfaction and the security of the customer account could well be in jeopardy after such an event. Even in those cases where there will be incremental changes customers will appreciate being told of the coming change and will certainly appreciate the polymer company's rationale for its position that the change will be inconsequential.

If the polymer producer has a pilot plant available, early runs of the new catalyst will focus on verifying catalyst performance. After these early characterization runs, though, a significant run should be planned where key resins are produced. The size of the run will be a function of the number of key resins, the amounts needed for testing, and the size of the pilot plant. The resins from this run are then examined for mechanical, physical, and inherent properties—examples of which are listed in Table 5.3. The data from these experimental polymers should be compared with those data currently produced commercially and significant differences should be recorded. The effects, if any, should be assessed for these differences on the polymer customers. Polymer formulations should be examined for adequacy with the new catalyst. Where possible, key fabrication studies should be executed in key fabrication processes such as injection molding, blow molding, and sheet and film extrusion.

In the best of cases, the study may be concluded at this stage. In some cases, though, second or even third iterations may be required to modify polymer and/or formulations to match existing customer requirements. Once customer requirements are met, a larger pilot-scale run should be completed for samples for key customers.

Frankly, pilot plants are usually too small to produce production samples for customers. However, pilot-scale samples may be sufficient for customers' own laboratory examinations. The pilot limitation means actual customer production line testing may require commercial polymer plant runs before key customers totally accept a possible catalyst change and implied polymer change.

In many catalyst changes, the commercial plant will be capable of a plant test run with little engineering or operational change. This is certainly the best of cases and simplifies the scheduling of such a test. In such cases, the key resin or resins are produced in minimal runs and lots are shipped to customers with clearly defined markings so the customer will know for sure the lot or lots are "experimental." During these test runs, polymer company technical service support should be present to monitor the test and to compare its observations with those of the fabricator. This can head off possible confusion and misunderstanding if the polymer producer has its own eyes and hands on-site during the test. Unfortunately, events do occur that seemingly always wait for a test run before appearing! Often observations during a test run will be unrelated to the "experimental" polymer, and the resolution of these uncertainties must be prioritized for immediate review and conclusion.

Typically a single production run will suffice for most qualifications, but occasionally the fabricator will feed back data that are unexpected and possibly observable only in the commercial equipment. In such cases, and if the polymer producer concurs, some minor changes may be required at the commercial polymer plant whereupon a second test run will be planned. Nevertheless, once acceptance has been gained at key customers, conversion at the commercial plant can go forward.

This discussed model can take from as little as six months to two years or more to execute, depending on the difficulties encountered, resource priority, and possibility of long lead times for certain more sophisticated approvals. The average catalyst changeout could take 12–18 months, easily.

The discussion of the catalyst changeout model to this point has assumed pilot plant access or capability. In those cases where there is no such access, the model is still applicable although slightly modified. Where there is no pilot plant capability, the polymer company needs to glean as much information a possible from the merchant catalyst supplier via questions like those in Table 5.1. After a careful assessment of key customers and key resins and possible changes from the introduction of a different catalyst, the polymer company is faced with running a plant test to generate polymer first for its own internal evaluation and second for release as test lots to key customers. Depending on the complexity of the polymer company's product line and the success of the first test, there may be need for a second test before going commercial with the new catalyst.

REFERENCES

1. Capshew, C. E., Phillips Petroleum Co., U.S. Patent No. 4,363,746, 1980; Capshew, C. E., Short, J. N., Welch, M. B., and Dietz, R. E., Phillips Petroleum Co., U.S. Patent No. 4,325,837, 1980; Welch, M. B., Dietz, R. E., and Capshew, C. E., Phillips Petroleum Co., U.S. Patent No. 4,326,988, 1980; Capshew, C. E., Phillips Petroleum Co., U.S. Patent No. 4,384,087, 1981; Welch, M. B., Dietz, R. E., and Capshew, C. E., Phillips Petroleum Co., U.S. Patent No. 4,410,671, 1982.
2. Moore, E. P., Ed., *Polypropylene Handbook: Polymerization, Characterization, Properties, Processing, Applications*, Hanser, New York, 1996.

6 Supported Magnesium/Titanium-Based Ziegler Catalysts for Production of Polyethylene

THOMAS E. NOWLIN, ROBERT I. MINK, and YURY V. KISSIN
Mobil Chemical Company, Edison, New Jersey 08818

6.1 INTRODUCTION

Ziegler's original discovery in the early 1950s showed that the interaction of organometallic compounds such as triethylaluminum (TEAL) with titanium chloride compounds such as $TiCl_4$ or $TiCl_3$ produced an inorganic species that polymerized ethylene at relatively low pressures to a high-molecular-weight polymer. Not only was a new low-pressure process for the polymerization of ethylene disclosed, but a new type of linear polyethylene (PE), designated as high-density polyethylene (HDPE), had emerged.

The versatility of what are now known as Ziegler–Natta catalysts was extensively summarized in several books.[1–4] These books provided a broad discussion of Ziegler–Natta catalysts with a detailed discussion of all significant developments of the catalysts since the 1950s. These early catalysts are designated as first-generation Ziegler–Natta catalysts.

In this chapter Ziegler–Natta catalysts refer to catalysts that are capable of polymerizing and copolymerizing α-olefins, while Ziegler catalysts only refer to those catalysts used in ethylene homopolymerization and ethylene/α-olefin copolymerization reactions.

Significant improvements in the activity of Ziegler–Natta catalysts occurred in the early 1970s when it was found that the preparation of catalyst precursors containing a magnesium compound such as magnesium chloride or magnesium alkoxide in conjunction with either $TiCl_4$ or $TiCl_3$, as well as the usual trialkylaluminum cocatalysts, improved catalyst efficiency by at least one or

---

Handbook of Transition Metal Polymerization Catalysts Edited by Ray Hoff and Robert T. Mathers
Copyright © 2010 John Wiley & Sons, Inc.

two orders of magnitude.[5–13] Catalyst efficiencies of 100–1000 kg polymer/g titanium were reported. These magnesium/titanium-based catalysts are designated as second-generation Ziegler–Natta catalysts. Because of the very high activity of these second-generation catalysts, the residual catalysts do not need to be removed from the polymers and, consequently, catalyst removal steps were no longer necessary as a part of the manufacturing process. These developments provided the necessary technology to introduce a new type of polyethylene, referred to as linear low-density polyethylene (LLDPE) resins, which are also manufactured utilizing low-pressure processes. LLDPE resins are copolymers of ethylene and an α-olefin (1-butene, 1-hexene, or 1-octene) which contain a sufficient amount of an α-olefin to reduce the PE crystallinity and to provide polymers with densities of 0.91–0.94 g/mL. These second-generation catalysts are also used to manufacture HDPE resins (density range of 0.94–0.97 g/mL) with a relatively narrow molecular weight distribution.

6.2 PARTICLE FORM TECHNOLOGY

The term *particle form technology* refers to the process of forming granular PE particles that replicate the shape of the original catalyst particles. Hogan and Banks at Phillips Petroleum Company initially developed particle form technology in the mid-1950s for chromium-based catalysts. Hogan and Banks prepared chromium-based catalysts that were supported on silica by reacting a chromium compound with a porous silica at elevated temperatures. A strong chemical interaction between the chromium compound and the silica surface resulted.[14] The silica utilized for the chromium-based catalyst is an amorphous material of high porosity. Such silicas have an average particle size of 20–90 μm, a pore volume of ~1.5 mL/g, and a surface area of ~300 m^2/g. During the polymerization process, one silica-supported catalyst particle generates one polymer particle in which the original silica particle has been sufficiently fragmented to form residual catalyst particles less than 0.1 μm in size. This fragmentation eliminates a visible catalyst residue in the finished PE. These small fragments of catalyst particles are encapsulated into the granular polymer particle. Because of the high activity of the Phillips catalyst, catalyst removal steps are not required as part of the PE manufacturing process.

Second-generation Ziegler–Natta catalysts of high activity also employ particle form technology. Therefore, the particle size, the particle size distribution, and the porosity of supported second-generation Ziegler–Natta catalysts needed to be controlled over a certain range. Such requirements improve the reliability of these catalysts in both the slurry- and gas-phase polymerization processes. For example, very small catalyst particles produce very small polymer particles which may cause reactor fouling, while polymerization on very large catalyst particles generates a high level of heat that can melt polymer particles and thus foul the polymerization process.

Therefore, suitable supports for second-generation Ziegler–Natta catalyst systems must meet similar requirements in order to perform satisfactorily.

The particle size of the finished catalyst precursor should range from about 1 to 250 μm (a preferred range of 10–100 μm). Spherical catalyst precursor particles are preferred but not necessary. Catalyst particles should provide granular polymer particles of 500–5000 μm in diameter. Polymer particles of this size are optimal for the operation of the slurry- and gas-phase polymerization processes.

It is important that the supported catalyst particle possess sufficient porosity so that the active titanium species are uniformly distributed throughout the entire volume of the support. This is necessary so that the catalyst particles fragment uniformly during the polymerization process and produce catalyst residue particles less than 0.1 μm in size. Insufficient support fragmentation can produce visible inorganic gels in the finished polymer products and must be avoided. Catalysts with a surface area of 10–300 m^2/g have sufficient porosity so that the original catalyst particle will fragment in an acceptable manner.

6.3 SUPPORTS FOR HIGHLY ACTIVE ZIEGLER–NATTA CATALYSTS

The physical characteristics of the polymers produced with highly active Ti-based catalysts replicate those of the catalyst precursors and, in turn, the characteristics of the catalyst precursors are determined by the properties of the supports. Because the polymer morphology is highly influenced by the support, much research has been devoted to the synthesis of the desired supports. The important characteristics of the latter include particle size, particle size distribution, and particle shape (spherical or irregular). The supports can be generated simultaneously with the formation of catalyst precursors such as in precipitation reactions or, alternatively, the supports are prepared separately and then the appropriate reagents are added to them to produce the catalyst precursors. Temperatures, addition rates, holding times, and stirring rates all affect the nature of the support during its preparation. As mentioned previously, the combination of magnesium compounds with titanium chloride compounds results in catalysts of much higher activity compared to the catalysts containing only titanium chloride compounds. Therefore, magnesium compounds are usually used as supports. Thus, the magnesium compounds serve the dual role of a support and an activity enhancer. Examples of magnesium compounds (R = alkyl; X = halide) that have been used as either supports or precursors to form the supports include (1) magnesium chloride, $MgCl_2$ (anhydrous, hydrated, alcohol adducts); (2) magnesium alkoxides, $Mg(OR)_2$; (3) magnesium alkyls, MgR_2; (4) mixtures of magnesium and aluminum alkyls, MgR_2/AlR_3; and (5) Grignard reagents, RMgX. Typically, alkyls and alkoxides of magnesium will react with the titanium chloride compound during the preparation of the catalyst precursor to form an activated magnesium chloride support.

The majority of Ti-based catalysts used for the polymerization of propylene employ a magnesium compound as the support. Although Ti-based catalysts for the polymerization of ethylene can also employ a magnesium compound as a support, many of them are prepared based on silica as a support. In some cases the magnesium compound and titanium compound are reacted together and the resulting catalyst precursor is deposited inside the pores of the silica. The silica in this case is best considered as a carrier of the Mg/Ti inorganic species because the silica is not required to produce high-activity catalysts. The silica acts as a template to control the particle size and particle size distribution of the catalyst and the granular PE prepared from the catalyst. In other cases the magnesium compound and titanium compound are added to the silica, sequentially, in which case strong chemical bonds between the metal species and the silica surface are formed. In this regard, such catalysts are similar to the Phillips chromium-based catalyst, in that strong bonds between the chromium species and the silica surface are formed.

6.4 PREPARATIVE METHODS FOR CATALYST PRECURSOR

A wide variety of methods have been used to prepare catalyst precursors for the polymerization of ethylene. Some of these methods are discussed below. Most of the preparations employ a titanium chloride compound as the source of Ti, but mixtures of a titanium chloride compound and a titanium alkoxide compound have also been used.

6.4.1 Physical Impregnation of a Soluble Mg/Ti Precursor into Silica Pores

The dissolution of a magnesium compound and a titanium compound in a suitable solvent, usually an electron donor solvent such as tetrahydrofuran (THF), can lead to the formation of a new species (catalyst precursor) that provides a highly active Ziegler system when activated. Removing the solvent at elevated temperatures in the presence of a support material such as silica will precipitate the precursor into the pores of the silica. In this method it is necessary that the precursor remain dissolved until the amount of remaining solution is equal to or less than the pore volume of the porous silica support. If this is achieved, then the particle size distribution of the silica material is the same before and after the precursor has been impregnated. If compounds precipitate outside of the silica pores, then the precursor material will contain very small particles and these small particles will produce small polymer particles (polymer fines) during the polymerization process. Such polymer particles may foul the polymerization process. This is particularly important in the gas-phase polymerization process.

6.4.2 Chemical Impregnation onto the Silica Surface

The addition of a magnesium alkyl that is soluble in a noncoordinating solvent such as heptane to a slurry of silica in a noncoordinating solvent results in the fixation of a magnesium moiety onto the silica surface. This silica/magnesium intermediate may then be reacted with $TiCl_4$ or reacted sequentially with an electron donor and $TiCl_4$ to produce a Ziegler catalyst precursor impregnated onto the silica surface. Catalyst activities for these systems may be quite high. However, in this method care must be taken not to add more metal alkyl that can be fixed onto the silica surface, unless the excess metal alkyl in the supernatant layer is removed via filtration or decantation. Otherwise, upon addition of $TiCl_4$ not only will the silica/magnesium intermediate react with the $TiCl_4$, but so will the excess magnesium alkyl in the supernatant layer, leading to the precipitation of a solid. In this case the catalyst precursor would actually be a mixture of this precipitated solid and the treated silica.

6.4.3 Precipitated Precursors via Reduction of Titanium Halide with a Magnesium Alkyl

Typically, $TiCl_4$ is reduced with a magnesium alkyl in the presence or absence of an electron donor to form an activated $MgCl_2$ support containing a Ti species. Also, the reducing agent could be a Grignard reagent in an electron donor solvent such as THF. These reduction reactions lead to precipitated catalyst precursors. Temperatures, addition rates, holding times, and stirring rates are used to control the particle size and particle size distribution of the catalyst precursor.

6.4.4 Reaction of Magnesium Component with $TiCl_4$

A magnesium component such as $MgCl_2$, $MgCl_2 \cdot n(ROH)$, or $Mg(OR)_2$ is reacted with $TiCl_4$ or $TiCl_4/Ti(OR)_4$ mixtures to yield a catalyst precursor. Optionally, an electron donor such as an ester or ether is reacted with the magnesium component before the addition of the $TiCl_4$. Preparation of the magnesium component may be quite elaborate in order to form the desired characteristics of the catalyst precursor.

6.4.5 Spray-Drying Techniques

Reagents are dissolved into solution or melted at an elevated temperature and then sprayed through specially designed nozzles to form liquid droplets that are dried rapidly to create solid particles. Particle size and particle size distribution are controlled by the spray-drying conditions.

6.4.6 Ball-Milling Techniques

Solids such as magnesium chloride are mechanically agitated with metal spheres (usually stainless steel balls) contained in a closed metal container. The magnesium solid may be ball milled in the presence of an electron donor (ester). Usually the ball-milled solid is reacted with $TiCl_4$ to form the catalyst precursor.

6.5 EXAMPLES OF ZIEGLER CATALYST PRECURSORS

This section provides specific examples of the various catalyst precursor preparative methods outlined above in order to illustrate each technique.

The interaction of titanium tetrachloride complexes and magnesium chloride complexes at various Mg/Ti molar ratios in THF produced crystalline $MgCl_2/TiCl_4/THF$ complexes, which were highly active ethylene polymerization catalysts when combined with an aluminum alkyl. The structure of one of the complexes was determined by X-ray crystallography.

Thus, $TiCl_4(THF)_2$ in THF was added to $MgCl_2(THF)_{1.5}$ in THF at a Mg/Ti molar ratio of 1.3 to give a solid component, which when combined with triisobutylaluminum produced an ethylene polymerization catalyst with an activity of 4.8 kg PE/g cat. The molecular weight distribution of the resin was relatively narrow, a M_w/M_n value of 2.9.[5]

Saturated solutions of $MgCl_2(THF)_2$ and $TiCl_4(THF)_2$ in THF at a Mg/Ti molar ratio of 2 were mixed and yellow crystals were isolated.[15] Stoichiometry was shown to be $Mg_2TiCl_8(THF)_7$ formed via the reaction

$$TiCl_4(THF)_2 + 2\,MgCl_2(THF)_2 + THF\,(\text{solvent}) \rightarrow Mg_2TiCl_8(THF)_7$$

This complex contains the ionic species $[Mg_2Cl_3(THF)_6]^+$ $[TiCl_5(THF)]^-$ as shown by an X-ray crystal structure determination (Figure 6.1).

In this structure there is a di-octahedral magnesium cation in which the two Mg^{2+} atoms are bridged by three Cl atoms. The oxygen atoms of three THF molecules are coordinated to each Mg^{2+} atom. The Ti atom in the anion is pseudo-octahedrally coordinated with five Ti–Cl bonds and a Ti–O bond.

A catalyst precursor consisting of a $MgCl_2/TiCl_4/THF$ complex physically impregnated into the pores of silica was prepared and used to produce

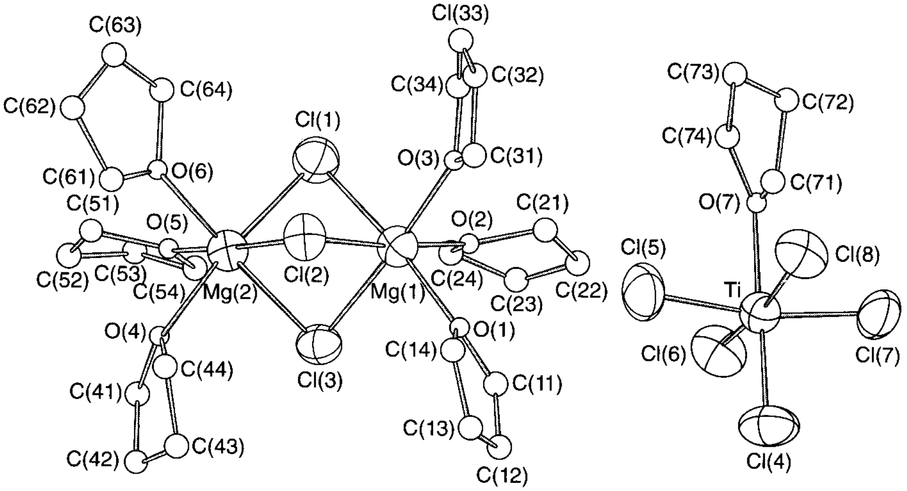

Figure 6.1 Crystal structure of $Mg_2TiCl_8(THF)_7$.

ethylene/1-butene copolymers.[8] A mixture of anhydrous $MgCl_2$ and $TiCl_4$ (Mg/Ti molar ratio of 3) in THF was heated to completely dissolve the material. Porous silica that had been calcined at 800 °C and treated with 4–8 wt % TEAL was added to the Mg/Ti solution. Removal of the liquid phase under nitrogen flow left a free-flowing powder having the same particle size as that of the silica. The catalyst precursor was partially activated by treating the catalyst precursor with an AlR_3 (triethylaluminum, triisobutylaluminum, tri-*n*-hexylaluminum, or tri-*n*-octylaluminum) solution and then the liquid phase was removed under nitrogen to yield a free-flowing powder, an impregnated partially activated catalyst precursor. This catalyst system was evaluated in a fluidized-bed gas-phase reactor for the production of ethylene/1-butene copolymers. The role of the silica was to (1) provide a finished catalyst precursor that was easily conveyed as a solid into the gas-phase reactor and (2) control the particle size and the particle size distribution of granular PE particles with a high poured bulk density and excellent material-handling characteristics that are necessary to maintain high production rates in a commercial process.

In a patent issued to Montedison complexes based on ethyl acetate were prepared.[6] A solution of anhydrous $MgCl_2$ in ethyl acetate and a solution of $TiCl_3$ (hydrogen reduced) in ethyl acetate were mixed and heated to 60 °C for 4 h. The ethyl acetate was removed by evaporation to isolate a light green powder. Analysis of the powder indicated a composition of $Mg_3Ti_2Cl_{12}$(ethyl acetate)$_7$. The activity of this catalyst system was ~200 kg PE/g Ti over 4 h residence time. Partial pressures of ethylene and hydrogen were 132 and 59 psi, respectively. Using $TiCl_4$ in place of $TiCl_3$ resulted in a pure crystalline complex with the composition $MgTiCl_6$(ethyl acetate)$_2$.

Adding $Mg(OC_2H_5)_2$ to $TiCl_4$ and heating at temperatures >100 °C, followed by filtration and washing steps, resulted in the formation of a solid powder containing 7 wt % Ti.[9] A redistribution reaction was proposed as shown below:

$$Mg(OC_2H_5)_2 + TiCl_4 \rightarrow MgCl_2 + Ti(OC_2H_5)_2Cl_2$$

Specific reaction conditions determined the extent of reaction that had taken place. The particle size distribution of this powder is shown in Figure 6.2 and was determined to be 7–30 μm with a median of 18.5 μm. The surface area of the powder was 60 m^2/g, which indicated that the powder had a high porosity with a pore volume of 1.16 cm^3/g.

Polymerization results for this catalyst showed that the high activity of this catalyst was due to an exceptionally high number of active sites (~70% of the titanium atoms) which was at least a factor of 10 higher than the early Ziegler catalysts. The particle size distribution of the polymer was identical to that of the catalyst precursor with the median value of the polymer shifting to much higher values depending on the polymerization time. These data, illustrated in Figure 6.2, suggested that every catalyst particle formed one polymer particle. Bohm's data by electron microscopy also showed that the original

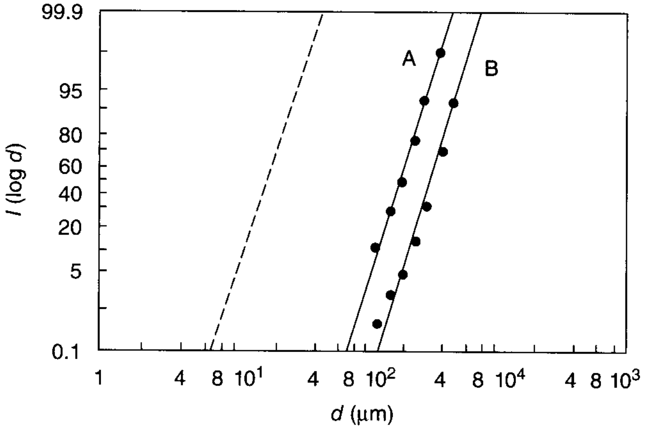

Figure 6.2 Comparison of particle size distribution of catalyst (---) and granular polyethylene for two polymerization times shown as lines *A* and *B*.

catalyst particles were completely disintegrated during the polymerization process as no catalyst residues were detected. Hence, catalyst residue must be smaller than ~50 Å.

Haward showed that the reaction of Grignard reagents such as butylmagnesium chloride in diethyl ether or didodecyl magnesium in iso-octane with $TiCl_4$ generated highly active catalysts in which the titanium center had been reduced to Ti(II) and Ti(III) by the magnesium compound.[12] Haward prepared a variety of catalysts by slowly adding $TiCl_4$ to a solution of the magnesium compound at 0–60 °C. Two important conclusions from this investigation were (1) catalyst systems prepared by reducing $TiCl_4$ with organomagnesium compounds are much more active (factor of 3–10) than catalysts prepared by reducing $TiCl_4$ with aluminum alkyls and (2) organomagnesium compounds reduced the titanium center to up to 41% Ti (II) and the catalyst systems still maintained a very high activity.

A spherical support of $MgCl_2 \cdot 3C_2H_5OH$ was prepared by combining anhydrous $MgCl_2$, anhydrous ethanol, vaseline oil, and silicone oil and then heating the mixture at high stirring speeds to 120 °C until the $MgCl_2$ was completely dissolved.[16,17] Eventually the mixture was discharged into a vessel containing anhydrous heptane and cooled. After filtering the mixture and drying the solid, the spherical support was then subjected to a thermal treatment until a partial dealcoholation was obtained. A residual ethanol content of ~35 wt% was obtained, corresponding to an ethanol–Mg molar ratio of 1.1 : 1. This spherical support was treated with an electron donor (ethyl benzoate or succinates) and $TiCl_4$. This procedure produced a catalyst precursor with spherical particles. The morphology of the polymer particles using this catalyst precursor was also spherical.[18]

Catalysts based on ethylmagnesium chloride in THF and $TiCl_4$ were prepared in the presence and absence of silica.[13] The silica was dried at 200 °C.

The silica (pore volume ~1.6 cm^3/g; surface area ~300 m^2/g; D_{50} particle size ~45 µm) was used as a template to control the particle size distribution of the catalyst precursor. Each catalyst was evaluated in ethylene/1-hexene copolymerization reactions at 80 °C in the presence of the cocatalyst TEAL at various 1-hexene/ethylene ratios. The ethylene reactivity ratio r_1 was determined for each catalyst from the simplified copolymerization equation[19]:

$$\frac{m_e}{m_h} = \frac{r_1 M_e}{M_h}$$

where m_e = mole fraction of ethylene in copolymer
m_h = mole fraction of 1-hexene in copolymer
M_e = molarity of ethylene in slurry solvent
M_h = molarity of 1-hexene in slurry solvent

and $r_1 = k_{ee}/k_{eh}$

where k_{ee} = rate ethylene adds to an ethylene-bound polymer chain
k_{eh} = rate 1-hexene adds to an ethylene-bound polymer chain

The catalyst prepared on silica exhibited very high reactivity with 1-hexene as indicated by an r_1 value of 26 whereas the catalyst prepared without silica exhibited an r_1 value of 125. Hence, the silica-supported catalyst reacts approximately five times better with 1-hexene than the catalyst prepared without the silica.

In addition, the copolymer produced from each of these catalysts was fractioned into five different fractions using hexane, heptane, and octane and the comonomer content was determined for each fraction. The results are shown in Table 6.1.

TABLE 6.1 Fractionation of Ethylene/1-Hexene Copolymers

	Unfractionated Polymer	Octane Insoluble	Octane Soluble	Heptane Soluble	Hexane Soluble	Cold Hexane Soluble
		Catalyst without Silica				
Content	100	21.2	60.8	14.0	2.9	1.1
C_H, mol %[a]	3.0	2.2	2.5	7.1	9.7	17.7
r_1	125 (average)	180	160	53	38	19
		Catalyst on Silica				
Content	100	71.5	12.2	4.6	4.0	7.6
C_H, mol %[a]	3.6	1.2	5.4	9.1	9.6	~25
r_1	26 (average)	90	19	11	10	4

[a] 1-Hexene content in copolymer, mol %.

TABLE 6.2 Fixation of Mg from DBM onto Silica Surface

Silica Calcination Temperature (°C)	Hydroxyl Content (mmol OH/g silica)	DBM Fixed (mmol Mg/g silica)
800	0.45	1.22
600	0.72	1.74
300	1.39	2.21

These data explain the relatively heterogeneous branching distribution of ethylene/1-olefin copolymers prepared with Ti/Mg Ziegler catalysts. For example, the catalyst prepared without silica contained at least five active sites that exhibited a range of r_1 values from ~19 to ~180, which varies by a factor of 9. The octane-insoluble fraction was produced by an active center that reacted very poorly with 1-hexene ($r_1 = 180$) while the cold hexane-soluble copolymer fraction was produced by an active center that reacted relatively well with 1-hexene, as indicated by an r_1 value of 19. The catalyst prepared on silica exhibited active sites with a range of r_1 values from 4 to 90, a factor of about 25.

Highly active Ziegler catalysts may also be prepared on silica via the interaction of magnesium alkyls with porous silica that has been calcined at 300–800 °C.[7] Metal alkyls react with the surface hydroxyl groups (Si–OH) to yield the corresponding alkane and a silica/metal intermediate. For example, dibutylmagnesium (DBM) reacts with silica to liberate butane and to form an intermediate in which a Mg moiety is chemically attached to the silica. The amount of DBM that can react with the silica depends upon the silica calcination temperature, as shown in Table 6.2.

As expected, the higher the silica calcination temperature the lower is the surface hydroxyl concentration and the lower is the Mg concentration on the silica surface. But the data indicate that the amount of DBM that can react with silica greatly exceeds the surface hydroxyl concentration. Hence, additional sites on the silica surface must be available to a DBM molecule besides the surface hydroxyl sites. Most likely the DBM molecule coordinates to the silica surface through an electron pair of an oxygen atom of a siloxane linkage (Si–O–Si). Further evidence for a second site comes from the fact that DBM will also fix to a silica in which the hydroxyl groups have been completely converted to trimethylsilyl groups as shown below:

$$\text{Si–OH} + \text{Me}_3\text{SiNMe}_2 \rightarrow \text{Si–O–SiMe}_3 + \text{Me}_2\text{NH}$$

Thus, silica calcined at 600 °C and then reacted with Me_3SiNMe_2 exhibited no residual hydroxyl groups as indicated by its infrared (IR) spectrum. However, when this silylated silica was reacted with DBM, the silylated silica had a Mg concentration of 0.85 mmol/g of silylated silica, demonstrating the presence of a second site of attack for the DBM molecule.

The interaction of the silica/magnesium intermediate with $TiCl_4$ provides a catalyst precursor. If the silica/magnesium intermediate is first treated with an electron donor (ketone, ester, acid chloride) and then reacted with $TiCl_4$, then this catalyst precursor when activated produces a highly active catalyst.[20]

Ball milling is a technique in which solid crystalline materials are physically degraded over a prolonged period (5–300 h) by rotating or vibrating a closed container of stainless steel balls with a solid material such as $MgCl_2$. The crystalline defects produced by the ball milling of the solid material are exhibited by significant changes in the X-ray diffraction pattern of the solid material. Galli published a detailed paper on the mechanical grinding of anhydrous $MgCl_2$ and liquid $TiCl_4$.[21]

Figure 6.3 shows the X-ray diffraction pattern after 20 h of milling $MgCl_2$ in the presence of $TiCl_4$. The lattice disorder of the milled solid is apparent from the shape of the X-ray pattern and is due to the disorder in the packing of the chloride anions. Ball-milling time is important in determining the amount of crystalline disorder obtained in the solid. Catalyst activity increases rapidly with ball-milling time up to about 20 h (160 kg PE/g Ti) and reaches a maximum activity after about 80 h (250 kg PE/g Ti). Additional milling up to 200 h has little effect on catalyst activity. Crystallite size also decreases with ball-milling time from ~100 Å after 20 h to ~50 Å after 80–200 h.

Molten $MgCl_2 \cdot 6H_2O$ was spray dried into spherical particles that were sieved to isolate the fraction of particles between 53 and 105 μm.[22] This fraction was then reacted with an excess of $TiCl_4$ under refluxing conditions, filtered, and the solid was washed several times with dry heptane to provide a supported catalyst precursor with a surface area of 33.7 m^2/g and a mean radius of the pores of 59 Å. This catalyst was evaluated in an ethylene homopolymerization reaction at 85 °C and exhibited an activity of ~50,000 g PE/g Ti/h/100 psi ethylene at a H_2/ethylene molar ratio of 1.4.

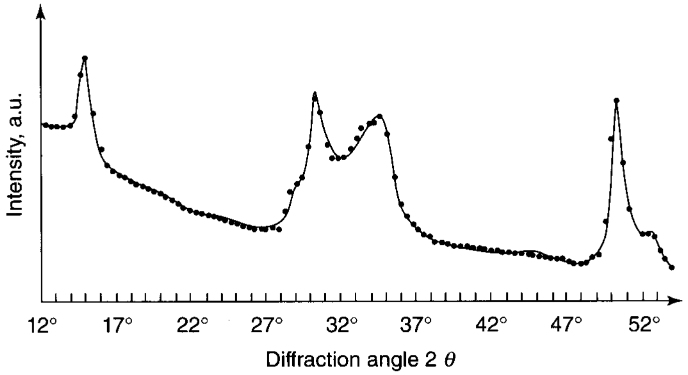

Figure 6.3 X-ray diffraction pattern of $MgCl_2$ (+$TiCl_4$) 20 h activated (solid line) fitted by proposed structural model.

6.6 KINETIC MECHANISM

6.6.1 Introduction

The standard kinetic scheme for ethylene/α-olefin copolymerization reactions usually includes several chain initiation reactions, chain propagation reactions, and chain termination reactions as shown below. In this scheme C* represents an active center and *m* is the number of ethylene and/or comonomer units in a polymer chain:

Chain propagation reactions:

$$\text{C*–E–Polymer} + \text{E} \rightarrow \text{C*–E–E–Polymer}$$

$$\text{C*–E–Polymer} + \text{M} \rightarrow \text{C*–M–E–Polymer}$$

$$\text{C*–M–Polymer} + \text{E} \rightarrow \text{C*–E–M–Polymer}$$

$$\text{C*–M–Polymer} + \text{M} \rightarrow \text{C*–M–M–Polymer}$$

Chain transfer reactions:

- Chain transfer reactions with hydrogen:

$$\text{C*–E–Polymer} + \text{H}_2 \rightarrow \text{C*–H} + \text{Polymer}$$

$$\text{C*–M–Polymer} + \text{H}_2 \rightarrow \text{C*–H} + \text{Polymer}$$

- Chain transfer reaction with ethylene:

$$\text{C*–E–Polymer} + \text{E} \rightarrow \text{C*–E} + \text{Polymer}$$

Chain initiation reactions:

- Chain initiation reaction after chain transfer to ethylene (E):

$$\text{C*–E}\,(m=1) + \text{E} \rightarrow \text{C*–E–E}\,(m=2)$$

- Chain initiation reaction with ethylene after chain transfer to hydrogen (H):

$$\text{C*–H} + \text{E} \rightarrow \text{C*–E}\,(m=1)$$

- Chain initiation reaction after chain transfer to α-olefin (M):

$$\text{C*–M}\,(m=1) + \text{E} \rightarrow \text{C*–E–M}\,(m=2)$$

- Chain initiation reaction with α-olefin after chain transfer to hydrogen:

$$C^*\text{–}H + M \rightarrow C^*\text{–}M \; (m = 1)$$

However, ethylene polymerization reactions in the presence of supported Ti-based Ziegler catalysts often exhibit behavior that is unusual compared to the polymerization reactions of α-olefins such as propylene, 1-butene, and so on. This behavior cannot be explained by the above-shown standard kinetic scheme.

Examples of unusual behavior found with ethylene polymerization reactions involving a supported Ti-based Ziegler catalyst include the following:

1. Ethylene is the most reactive olefin as found from the values of its reactivity ratios in copolymerization reactions.[2,3,23] Although ethylene is much more reactive than propylene (3–5 times) and hexene (>50 times), direct comparisons of polymer yields and activities show that ethylene never obtains the level of reactivity expected from its relative reactivity in copolymerization reactions.
2. Ethylene copolymerization reactions always proceed at substantively higher rates than ethylene homopolymerization reactions. Since ethylene is the most reactive olefin, addition of an α-olefin such as 1-hexene would be expected to decrease the polymerization reaction, not increase it.[24–30]
3. The reaction order n with respect to the partial pressure of ethylene (P_E) or to the concentration of ethylene in solution (C_E) in the rate of an ethylene homopolymerization reaction (R_{pol}) greatly exceeds first order[27,31,32]:

   $$R_{pol} = k \cdot (P_E)^n \quad \text{or} \quad R_{pol} = k \cdot (C_E)^n$$

   For example, ethylene homopolymerization reactions were carried out in slurry at different ethylene concentrations. Plotting the total yield as a function of ethylene concentration gave n as high as 1.7–2.0. Also, by varying the P_E in gas-phase reactions and plotting the relative rate versus pressure, a reaction order of 1.8 was determined.
4. Addition of hydrogen significantly decreases the ethylene polymerization rate, in contrast to the hydrogen effect observed in propylene polymerization reactions.[27]

Any proposed kinetic mechanism should be able to explain the above peculiarities.

6.6.2 Multicenter Sites

A new approach to understanding the ethylene polymerization kinetics and polymerization mechanism for supported Ti-based Ziegler catalysts is based on examining the molecular weight distribution data of the polymers produced with these catalysts.[33–36] These catalysts contain several types of active centers that produce different types of polymer molecules at different rates. Each active center has its own propagation rate and decay rate, produces polymer molecules of different molecular weights, and has different incorporation rates of comonomer into the polymer chains. Thus, each center produces a group of polymer molecules with a narrow molecular weight distribution of M_w/M_n of 2.0, according to the Flory theory. The fraction of the polymer molecules produced by a single type of active center is called a Flory component. These active centers are identified by the numerals I–V in the order of increasing molecular weights of the Flory components they produce.

The resolution of gel permeation chromatography (GPC) curves of ethylene polymers into Flory components is demonstrated in Figure 6.4. Typically,

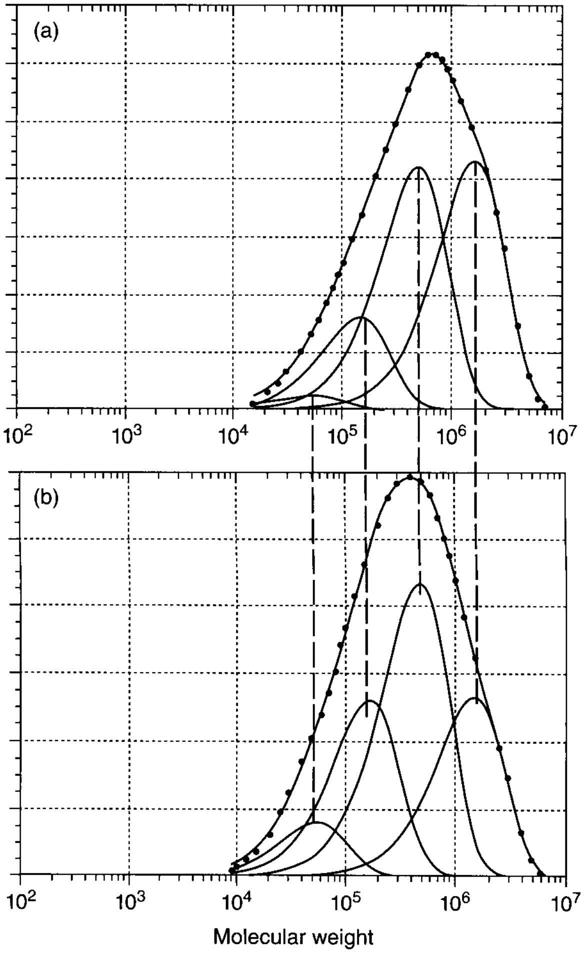

Figure 6.4 GPC curves of two ethylene homopolymers produced at different C_E [(*a*) 0.86 M, (*b*) 0.25 M, reaction time 240 min] and their resolution into Flory components.

four Flory components are present in the homopolymers and five Flory components are present in ethylene copoylmers.[33,34] Homopolymerization and copolymerization reactions in the absence and presence of hydrogen were carried out and the GPC curves of the polymers were resolved into Flory components. The properties of the Flory components of the polymers that were prepared under different polymerization conditions changed significantly, which led to a better understanding of the mechanism and kinetics of the polymerization catalysis.

The yields of Flory components produced by each center were determined from the product of the total polymer yield and the fraction of a Flory component. By plotting yields of Flory components as a function of C_E, the reaction order n for each center was obtained. Reaction orders in ethylene homopolymerization reactions for centers III, IV, and V were 1.7, 1.8, and 2.2, respectively.[33,34]

Hydrogen is used as a chain transfer agent in polymerization reactions with supported Ti-based Ziegler catalysts to control the molecular weight of the polymer. Homopolymerization reactions were carried out at 80 °C at the same ethylene partial pressure in the absence and presence of hydrogen. The reaction rate versus time is shown in Figure 6.5. The kinetic profile for both runs are very similar, which indicates that hydrogen does not greatly affect the activation and deactivation rates of the reaction centers. However, it is obvious from the kinetic profile that hydrogen suppresses the catalyst's activity.[3,33,34]

In Table 6.3 a comparison of the molecular weights and the fractions of the Flory components for two homopolymerization experiments at 80 °C in the absence and presence of hydrogen is shown. As expected, hydrogen significantly reduces the molecular weights of all the Flory components but does not significantly affect the contributions of the Flory components to the overall molecular weight distribution.[33,34]

Ethylene/1-hexene copolymerization reactions were compared to an ethylene homopolymerization reaction under similar conditions in the absence of hydrogen.[34] The kinetic profiles are shown in Figure 6.6. The kinetic profiles show that the initial rates of the copolymerization reactions are much higher but over time the effective rates in both types of reactions become similar.

Shown in Table 6.4 is a comparison of Flory components for an ethylene homopolymerization reaction and ethylene/1-hexene compolymerization reactions carried out at 85 °C in the absence of hydrogen.[33,34] The molecular weights of the components for the reactions are essentially the same, especially for the polymer chains produced by centers III, IV, and V. In contrast, 1-hexene strongly affects the relative fractions of the Flory components. The contributions of centers IV and V decrease, while the contributions of centers I, II, and III increase. These findings indicate that centers I, II, and III are strongly activated by 1-hexene, whereas centers IV and V are not. The former three centers decay much more rapidly than centers IV and V in the presence of 1-hexene. As a consequence, after ~3 h centers IV and V are producing most of the polymer chains.

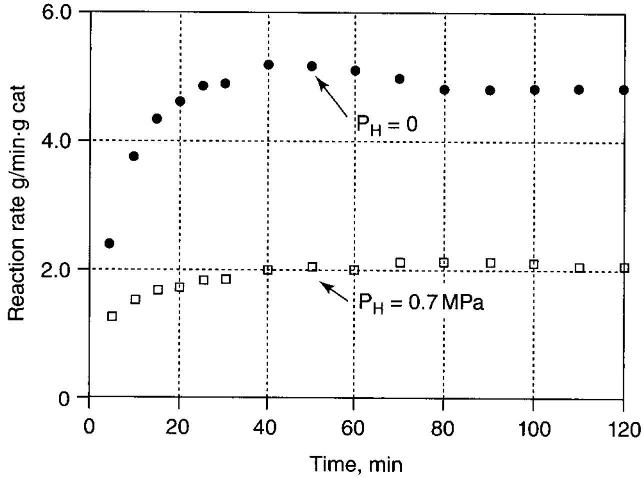

Figure 6.5 Hydrogen effect on kinetics of ethylene homopolymerization at 80 °C, $C_E = 0.26\,\text{M}$.

TABLE 6.3 Hydrogen Effect on Molecular Weights and Contents of Flory Components in Ethylene Homopolymerization Reactions: 1-h Experiments at 80 °C

P_H (MPa)	P_E (MPa)	Center	M_w	Fraction (%)
0	0.38	I	10,700	3.2
		II	47,500	10.6
		III	146,600	27.0
		IV	462,800	38.0
		V	1,577,000	21.1
0.69	0.38	I	1,550	2.6
		II	6,200	9.2
		III	18,500	24.9
		IV	50,300	45.2
		V	145,800	18.0

The overall kinetic curve of a polymerization reaction is the sum of the kinetic curves of each center. By carrying out copolymerization reactions under the same conditions at different residence times and analyzing the polymers by GPC, the fraction of each Flory component was determined as a function of time. This can be related to the reaction rate for each center. The kinetics of an ethylene/1-hexene copolymerization reaction in the absence of hydrogen is shown in Figure 6.7, where the calculated rates for each center and the overall reaction rate are plotted.[33,34] The graph shows that centers I, II, and III decay much more rapidly than centers IV and V and, therefore, the contributions of Flory components I, II, and III decrease over time. Because the former centers incorporate 1-hexene into copolymer chains much better, the 1-hexene content in the copolymers decreases with time, since centers I,

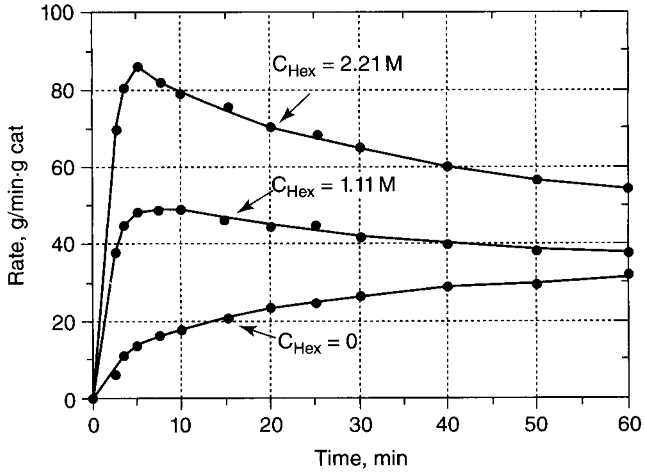

Figure 6.6 Comparison of ethylene homopolymerization and copolymerization kinetics at 85 °C: $C_E = 0.55$ M in all experiments. Copolymer compositions in these experiments (top to bottom) are 1.7, 0.6, and 0 mol % of 1-hexene.

TABLE 6.4 1-Hexene Effect on Flory Component Parameters in Absence of Hydrogen

C_{hex} (M)	[1-Hex][a] (mol %)	Center[b]	M_w	Fraction (%)
0	0	II	93,900	4.8
		III	145,100	15.2
		IV	451,600	45.2
		V	1,554,300	34.8
1.12	0.4	I	13,500	2.5
		II	45,500	9.0
		III	133,000	22.2
		IV	412,100	35.2
		V	1,344,800	31.1
2.24	0.9	I	13,100	4.0
		II	46,600	13.2
		III	141,100	25.2
		IV	436,800	33.6
		V	1,385,100	24.0

Note: Reactions at 85 °C, $P_E = 0.69–0.76$ MPa ($C_E = 0.53–0.56$ M), 4 h.

[a] 1-Hexene content in copolymer, mol %.

[b] Center I fraction negligible in absence of 1-hexene.

II, and III are strongly activated in the presence of 1-hexene, while centers IV and V are not. It is possible to estimate the copolymer composition of the Flory component that was produced by each center from the average copolymer composition and the relative contributions of each Flory component (shown in Table 6.5).[33,34]

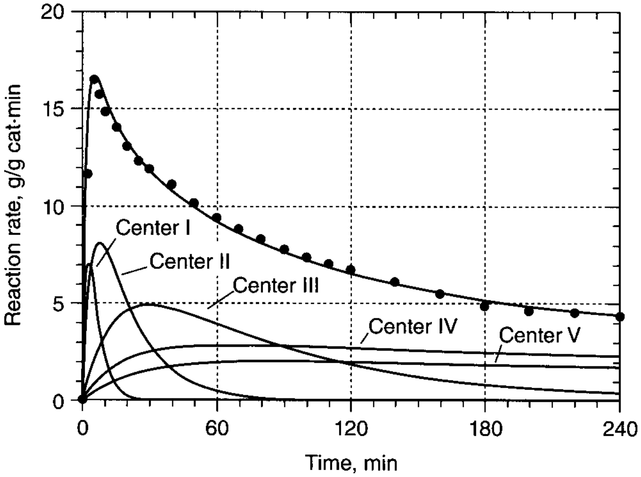

Figure 6.7 Kinetics of ethylene/1-hexene copolymerization reaction at 85 °C in absence of hydrogen. Points: experimental data, lines: calculated rates for each center.

TABLE 6.5 1-Hexene Content in Copolymer Generated by Each Center

1-Hexene Content (mol %)	Center
8.5–10	I
4.5–5.3	II
~0.6	III
~0.3	IV
~0.2	V

These data indicate that the different centers have different abilities to copolymerize ethylene and α-olefins and that this order declines in the sequence center I > center II > center III > center IV ≈ center V.

The kinetic description of ethylene/1-hexene copolymerization reactions in the presence of hydrogen is different from that of the corresponding homopolymerization reactions.[33,34] By performing a series of reactions for different periods of time and evaluating the polymers by GPC, the kinetic profiles of the centers and overall reaction were produced, similar to Figure 6.7. The average 1-hexene content decreased as the residence time of the copolymerization reaction increased. The data are summarized in Table 6.6.

A comparison of the reaction kinetics for copolymerization reactions in the absence and presence of hydrogen is shown in Figure 6.8.[33,34] Again, overall productivity decreased in the presence of hydrogen. Table 6.7 compares the yields of copolymer produced by each center in a 1-h-residence-time experiment under similar conditions. The results show that (1) for the most part the reactivities of centers I, II, and III in copolymerization reactions

TABLE 6.6 1-Hexene Content in Copolymer versus Residence Time

Time (min)	Normalized Yield (%)	1-Hexene in Copolymer (mol %)
5	6.0	3.4
15	17.2	2.6
60	47.8	2.2
120	69.2	2.1
240	100	2.0

TABLE 6.7 Hydrogen Effect on Reactivities of Active Centers and Copolymer Properties

$C_H{}^a$ (mol/L)	0	0.0204	0.0400
1-Hexene mol % in copolymer	0.6	1.2	1.3
Center I yield (g/g cat)	58.1	79.5	40.6
Center II yield (g/g cat)	249.7	264.6	249.9
Center III yield (g/g cat)	714.4	868.3	767.7
Sum of centers I–III yield (g/g cat)	1022	1212	1058
Center IV yield (g/g cat)	1213.9	639.8	459.3
Center V yield (g/g cat)	667.9	133.1	105.5
Sum of centers IV + V yield (g/g cat)	1882	873	565

[a] C_H is the hydrogen concentration in solution, mol/L; 1-h copolymerization at 85 °C, C_E = 0.51–0.55 M, C_{Hex} = 1.12 M.

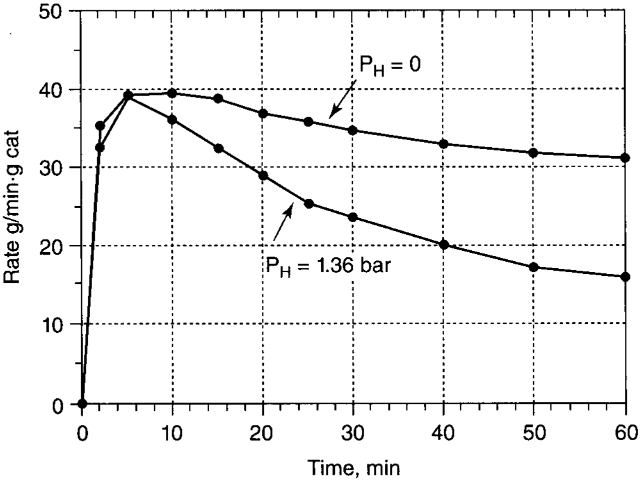

Figure 6.8 Hydrogen effect on kinetics of ethylene/1-hexene copolymerization at 85 °C, C_E = 0.55 M.

are not affected by hydrogen, in contrast to homopolymerizations; (2) similar to homopolymerization reactions, the reactivities of centers IV and V in copolymerization reactions are significantly reduced in the presence of hydrogen; and (3) consequently, the 1-hexene content in the copolymers produced under similar reaction conditions increases as the hydrogen concentration increases.[33,34]

6.6.3 Kinetic Interpretation of Ethylene Polymerization Reactions

The multicenter site analysis revealed that some of the active centers behave differently in the presence of an α-olefin such as 1-hexene. For example:

1. The reaction order n for each center with respect to C_E in ethylene homopolymerization reactions was significantly greater than first order.
2. In ethylene/α-olefin copolymerization reactions, those centers that incorporate an α-olefin into the polymer chain poorly (centers IV and V) retain this high reaction order ($n > 1$), while the reaction order changes to first order for those centers that incorporate an α-olefin into the polymer chain well (centers I, II, and III).
3. In homopolymerization reactions hydrogen suppresses the activity of all the centers whereas in ethylene/α-olefin copolymerization reactions hydrogen does not suppress the activity of those centers that incorporate an α-olefin into the polymer chain well (centers I, II, and III) but still does suppress the activity of centers IV and V.
4. The introduction of an α-olefin into a polymerization reaction increases the activity of those centers that incorporate an α-olefin into the polymer chain well (centers I, II, and III) but does not affect centers IV and V.

These observations are specific to ethylene polymerization reactions. Other α-olefin polymerization reactions do not exhibit this type of behavior. In some cases opposite behavior is observed. For example, propylene polymerization activity with the same catalysts increases in the presence of hydrogen but decreases when higher α-olefins are introduced into the reaction medium.

Kissin et al. have proposed a kinetic scheme that accounts for the peculiar kinetic features of ethylene polymerization reactions. The scheme is shown in Figure 6.9. The key assumption in the scheme is that the Ti–CH_2CH_3 species is unique in that it is unusually stable. This stability may arise from an unusually strong β-agostic interaction between the hydrogen atom of the methyl group and the Ti atom. Other Ti–alkyl species proposed in the scheme do not possess this stability. In this scheme formation of the Ti–CH_2CH_3 species occurs as a result of an ethylene insertion reaction into the Ti–H bond or after a chain transfer reaction with ethylene.

By postulating that the Ti–CH_2CH_3 species is in equilibrium with the β-agostic Ti complex and that the equilibrium strongly favors the β-agostic Ti

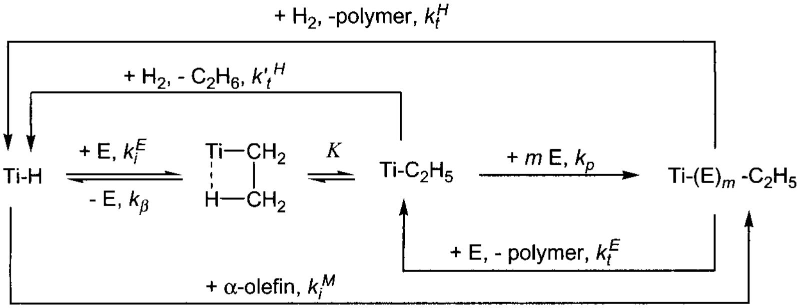

Figure 6.9 Proposed kinetic mechanism of ethylene polymerization reactions.

complex, as shown in the equation below, the unusual kinetic effects associated with ethylene polymerization reactions can be explained:

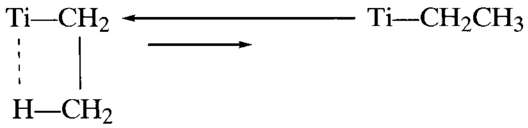

$$\begin{array}{l} \mathrm{Ti{-}CH_2} \\ \vdots \quad | \\ \mathrm{H{-}CH_2} \end{array} \overset{\xleftarrow{\qquad\qquad}}{\longrightarrow} \mathrm{Ti{-}CH_2CH_3} \tag{6.1}$$

The H atom interaction with the Ti atom in the β-agostic Ti complex makes the coordination sphere at the Ti atom saturated and, therefore, prevents its interaction with an ethylene molecule, whereas the Ti atom in the Ti–CH$_2$CH$_3$ species has a vacant site and reaction with ethylene is possible (chain growth reaction). Assuming that the reaction of the Ti–H bond with ethylene immediately produces the β-agostic Ti complex, the concentration of the active Ti–CH$_2$CH$_3$ species is low, which can account for the high reaction order with respect to the ethylene concentration.

A stabilized Ti–CH$_2$CH$_3$ species such as the β-agostic Ti complex is capable of undergoing hydrogenation with the formation of ethane and the generation of the Ti–H species (Figure 6.9). This explains why significant levels of ethane are observed in ethylene polymerization reactions with many Ti-based catalysts.

The decrease in catalyst activity in the presence of hydrogen can also be explained based on the kinetic scheme in Figure 6.9. Hydrogen reacts with the Ti–(E)$_m$–C$_2$H$_5$ species to yield polymer molecules and the Ti–H species. The Ti–H species immediately reacts with ethylene to form the inert β-agostic Ti complex. Increasing the hydrogen concentration translates into a higher fraction of the Ti–H species and, subsequently, to a higher fraction of the inert Ti agostic complex. The formation of this β-agostic Ti complex also explains the low catalyst activities in ethylene homopolymerization reactions.

When an α-olefin is present in a polymerization reaction, it inserts into the T–H bond to form a Ti–alkyl species. In the case of 1-hexene the species would be Ti–C$_6$H$_{13}$, which could also be viewed as Ti–(C$_2$H$_4$)$_3$–H, a short polymer chain. This reaction explains the activating effect of an α-olefin in ethylene copolymerization reactions. By inserting an α-olefin into the Ti–H species, the formation of the inert β-agostic Ti complex is bypassed. Those centers that are strongly activated by an α-olefin (centers I, II, and III) have high rate constants for the reaction between the Ti–H species and an α-olefin molecule. On the other hand, centers IV and V, which incorporate an α-olefin into a polymer chain poorly, will have low rate constants of this reaction.

The scheme also predicts that the β-agostic Ti complex can undergo β-hydride elimination to produce ethylene and the Ti–H species. If D_2 is used instead of H_2 as the chain transfer agent, the scheme predicts that deuterated ethylene molecules should form.[19,23] These deuterated ethylene molecules copolymerize with the protioethylene molecules to form protio/deuterioethylene copolymers. Similar to the hydrogen studies, ethylene homopolymerization reactions carried out in the presence of D_2 reduced catalyst activity and the GPC analysis of the polymers confirmed that D_2 significantly reduced the molecular weight of each Flory component. Gas chromatography/mass spectrometry (GC/MS) and IR analysis of the gas phase after completion of these ethylene homopolymerization reactions showed that the major components were ethylene and ethane and that both contained deuterium atoms. The ethylene contained C_2H_3D (~2.2%) and $C_2H_2D_2$ (~1.1%, products $CH_2{=}CD_2$, *cis-* and *trans*-CHD=CHD). The content of deuterium in the ethane was much higher. Analysis showed little ethane-d_0 and mostly ethane-d_1 (38.1%), ethane-d_2 (31.5), and ethane-d_3 (11.3%). The standard ethylene polymerization scheme would have predicted only ethane-d_2, namely 1,2-dideuterated ethane, as shown below:

$$\mathrm{Ti{-}D} + \mathrm{C_2H_4} \rightarrow \mathrm{Ti{-}CH_2CH_2D} \xrightarrow{D_2} \mathrm{Ti{-}D} + \mathrm{DCH_2CH_2D} \qquad (6.2)$$

The large yield of deuterated ethanes and the presence of deuterium in the ethylene molecules cannot be easily explained by the standard polymerization scheme, but it is explained by the existence of a stabilized β-agostic Ti complex.

IR spectra and ^{13}C-NMR spectra of the polymers confirm the presence of deuterium in the polymer chains. Ethylene units –CHD–CHD– and –CH_2–CD_2– were identified in the polyethylene chains. In contrast, when an ethylene homopolymerization reaction was carried out with a metallocene catalyst in the presence of D_2, most of the polymer molecules contained two D atoms, one at each chain end, (DCH_2–CH_2–(CH_2–CH_2)$_X$–CH_2–CH_2D). Also, the reaction products showed no evidence of the formation of deuterated ethylene. These results agree with the predictions of the standard polymerization scheme.

The results for the deuterium experiments can be explained by the scheme in Figure 6.9 when some additions are incorporated into the scheme (Figure 6.10).[33,37] Insertion of ethylene into the Ti–D bond affords the β-agostic Ti complex. Rapid exchange between the β-agostically coordinated C–H and C–D bonds in the CH_2D group can lead to ethylene-d_1. Exchange of the

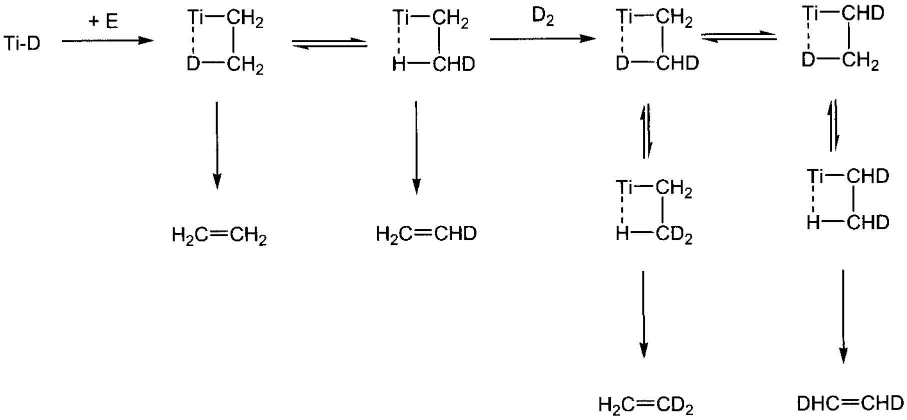

Figure 6.10 Formation mechanism of deuterated ethylenes.

hydrogen atom in the Ti–H species with D_2, followed by rapid scrambling of all the hydrogen and deuterium atoms, can produce complexes which undergo β-hydride elimination to afford the observed ethylene-d_2 products. These deuterated ethylene molecules should have a similar reactivity as CH_2=CH_2 and, therefore, will be converted into deuterated ethylene units in the polyethylene chains.

This mechanism also predicts that the insertion of an α-olefin into the Ti–H bond to form a Ti–alkyl species (chain initiation) should occur much more frequently than the insertion of ethylene into the Ti–H bond.[33,38] As a consequence, the fraction of the copolymer chains containing an α-olefin unit as the first unit in the chain should be significantly higher than the fraction of polymer chains containing ethylene as the first unit. GC analysis of the liquid phase after the completion of the ethylene copolymerization reactions and ^{13}C-NMR analysis of the copolymers supported the conclusion of a relatively higher probability of an α-olefin insertion into the Ti–H bond compared to that of ethylene. The data also revealed that the reactivity of ethylene insertion into a Ti–H bond is nearly an order of magnitude lower than the reactivity of ethylene insertion into a Ti–C bond. Chain initiation reactions with ethylene (leading to the Ti–CH_2CH_3 species) are relatively slow because of the predominant formation of the inert β-agostic Ti complex, whereas with an α-olefin chain initiation proceeds rapidly since the formation of the β-agostic Ti complex is bypassed.

6.6.4 Nonproductive Consumption of α-Olefins in Ethylene Copolymerization Reactions

Nonproductive use of α-olefins in ethylene/α-olefin copolymerization reactions involves those processes that do not lead to the formation of ethylene copolymers. Any evaluation of the different polymerization processes and catalysts for the manufacture of LLDPE resins must require a detailed understanding of the nonproductive consumption of comonomers used in the copolymerization process.

Typical nonproductive consumption of 1-hexene in such reactions includes:

1. Isomerization of 1-hexene into 2-hexene (cis and trans isomers):

   $$CH_2{=}CH{-}CH_2{-}CH_2{-}CH_2{-}CH_3 \rightarrow CH_3{-}CH{=}CH{-}CH_2{-}CH_2{-}CH_3$$

   2-Hexenes cannot copolymerize with ethylene and remain in the polymerization reactor.
2. Hydrogenation of 1-hexene:

$$CH_2{=}CH{-}CH_2{-}CH_2{-}CH_2{-}CH_3 + H_2 \rightarrow CH_3{-}CH_2{-}CH_2{-}CH_2{-}CH_2{-}CH_3$$

3. 1-Hexene participation in the formation of oligomers.

Typically, the most abundant oligomers are ethylene/1-hexene codimers such as C_8 products. 1-Hexene oligomers can be also generated via the cationic mechanism catalyzed by acidic components in the catalysts.

REFERENCES

1. Boor, Jr., J., *Ziegler-Natta Catalysts and Polymerizations*, Academic Press, New York, 1979.
2. Kissin, Y. V., *Isospecific Olefin Polymerization with Heterogeneous Ziegler-Natta Catalyst*, Springer, New York, 1985.
3. Krentsel, B. A., Kissin, Y. V., Kleiner, V. I., and Stotskaya, L. L., *Polymers and Copolymers of Higher Alpha-Olefins*, Hanser Publishers, Munich, 1997.
4. Ser van der Ven, *Polypropylene and Other Polyolefins*, Elsevier Publisher, Amsterdam, 1990.
5. Yamaguchi, K., Kanoh, N., Tanaka, T., Enokido, N., Murakami, A., and Yoshida, S., Mitsubishi Chemical Industries, U.S. Patent No. 3,989,881, 1976.
6. Giannini. U., Albizzati, E., Parodi, S., and Pirinoli, F., Montedison, U.S. Patent No. 4,124,532, 1978.
7. Nowlin, T. E., Mink, R. I., Lo, F. Y., and Kumar, T., *J. Polym. Sci. Pt. A Polym. Chem.*, **1991**, 29, 1167.
8. Goeke, G. L., Wagner, B. E., and Karol, F. J., Union Carbide, U.S. Patent No. 4,302,565, 1981.
9. Bohm, L. L., *Polymer*, **1978**, 19, 562.
10. Petkov, L., Kyrtcheva, R., Radenkov, P., and Dobreva, D., *Polymer*, **1978**, 19, 567.
11. Boucher, D. G., Parsons, I. W., and Haward, R. N., *Makromol.*, **1974**, 175, 3461.
12. Haward, R. N., Roper, A. N., and Fletcher, K. L., *Polymer*, **1973**, 14, 365.

13. Nowlin, T. E., Kissin, Y. V., and Wagner, K. P., *J. Polym. Sci. Pt. A Polym. Chem.*, **1988**, 26, 755.
14. Hogan, J. P., and Sailors, H. R., *J. Macromol. Sci. Chem. Pt. A*, **1981**, 15, 1377.
15. Sobota, P., Utko, J., and Lis, T., *J. Chem. Soc. Dalton Trans.*, **1984**, 2077.
16. Ferrais, M., Rosati, F., Parodi, S., Giannetti, E., Motroni, G., and Albizzati, E., Montedison, U.S. Patent No. 4,399,054, 1983.
17. Sacchetti, M., Cuffiani, I., and Pennini, G., Montell Technology, U.S. Patent No. 5,578,541, 1996.
18. Morini, G., Balbontin, G., Gulevich, Y. V., Kelder, R. T., Duijghuisen, H. P., Klusener, P. A., and Korndorffer, F. M., Montell Technology, WO 0063261, 2000.
19. Ham, G. E., *High Polymers, Copolymerization*, Vol. XVIII, Interscience, New York, 1964, p. 119.
20. Mink, R. I., and Nowlin, T. E., Mobil Oil, U.S. Patent No. 5,260,245, 1993.
21. Galli, P., Barbe, P., Guidetti, G., Zannetti, R., Martorana, A., Marigo, A., Bergozza, M., and Fichera, A., *Eur. Polym. J.*, **1983**, 19, 19.
22. Galli, P., Di Drusco, G., and De Bartolo, S., Montecatini Edison, U.S. Patent No. 3,953,414, 1976.
23. Kissin, Y. V., in *Transition Metal Catalyzed Polymerizations: Alkenes and Dienes*, Quirk, R. P., Ed., Harwood Academic, New York, 1983, p. 597, Part B.
24. Munoz-Escalona, A., Garcia, H., and Albornoz, A., *J. Appl. Polym. Sci.*, **1987**, 34, 977.
25. Spitz, R., Duranel, P., Masson, P., Darricades-Llauro, M. F., and Guyot, A., in *Transition Metal Catalyzed Polmerizations*, Quick, R. P., Ed., Cambridge University Press, New York, 1988, p. 719.
26. Calabro, D. C., and Lo, F. Y., in *Transition Metal Catalyzed Polmerizations*, Quick, R. P., Ed., Cambridge University Press, New York, 1988, p. 729.
27. Kissin, Y. V., *J. Mol. Catal.*, **1989**, 46, 220.
28. Tait, P. J. T., Downs, G. W., and Akinbami, A. A., in *Transition Metal Catalyzed Polmerizations*, Quick, R. P., Ed., Cambridge University Press, New York, 1988, p. 834.
29. Wang, J. G., Zhang, W. B., and Huand, B. T. *Makromol. Chem. Macromol. Symp.*, **1992**, 63, 245.
30. Tait, P. J. T., in *Transition Metals and Organometallics as Catalysts for Olefins Polymerization*, Kaminsky, W., and Sinn, H., Eds., Springer, Berlin, 1988, p. 309.
31. Han-Adebkum, G. C., and Ray, W. H., *J. Appl. Polym. Sci.*, **1997**, 65, 1037.
32. Kryzhanovskii, A. V., Gapon, I. I., and Ivanchev, S. S., *Kinet. Catal.*, **1990**, 31, 90.
33. Kissin, Y. V., Mink, R. I., and Nowlin, T. E., *Topics Catal.*, **1999**, 7, 69.
34. Kissin, Y. V., Mink, R. I., and Nowlin, T. E., *J. Polym. Sci. Pt. A Polym. Chem.*, **1999**, 37, 4255.
35. Kissin, Y. V., *Makromol. Chem. Macromol. Symp.*, **1993**, 66, 83.
36. Kissin, Y. V., *Makromol. Chem. Macromol. Symp.*, **1995**, 89, 113.
37. Kissin, Y. V., and Brandolini, A. J., *J. Polym. Sci. Pt. A Polym. Chem.*, **1999**, 37, 4273.
38. Kissin, Y. V., Mink, R. I., Nowlin, T. E., and Brandolini, A. J., *J. Polym. Sci. Pt. A Polym. Chem.*, **1999**, 37, 4281.

7 Stereospecific α-Olefin Polymerization with Heterogeneous Catalysts

JOHN SEVERN
Borealis Polymers Oy, Porvoo, Fl-06101 Finland

ROBERT L. JONES, Jr.
Polymer Technology Group, Berkeley, California 94710

7.1 INTRODUCTION

Over the last 60 years the ability to reduce olefin refinery gases or liquids to metastable plastics in a controlled manner has created the colossal polyolefin materials business. In 2008 an estimated 120 million tonnes of polyolefins will be produced.[1] If one considers that the world population was estimated at 6.7 billion people in March 2008,[2] then each person consumed ~18 kg of polyolefin this year. While this is a considerable per-capita consumption, it should be noted that polyolefins afford major environmental benefits in such areas as infrastructure (piping and energy transmission), allowing the safe and consistent supply of water and energy (electricity and gas etc) and the removal of sewage; advanced packaging: light and reliable packaging that increases the shelf-life of perishable goods and thus decreases petroleum fuel consumption for shipment because of less weight and less spoilage; automotive applications: and replacing metal with light material producing lighter automobiles and again further contributing to reduced transport emissions. Finally, polyolefins themselves are in effect a source of energy.[3]

This immense business has been brought about by catalysts and processes which control how macromolecules are assembled. By sequentially linking α-olefins, the chain length, skew, and branching present handles which tune properties. When the monomer is substituted (i.e., an α-olefin), additional opportunities including tacticity (control over regio-error-type linkages) and

---

Handbook of Transition Metal Polymerization Catalysts Edited by Ray Hoff and Robert T. Mathers
Copyright © 2010 John Wiley & Sons, Inc.

comonomer composition distribution become available. In addition, process developments have allowed the production of advanced materials such as heterophasic alloys. Control over chain length (molecular weight), the population distribution of the chain lengths (molecular weight distribution), and chemical (or comonomer) composition distribution (CCD) in and between the chains result in the ability of the chains to form crystallizable, ordered segments. The size and distribution of the crystallites and the ratio of soft amorphous space interspersed between the hard crystallizable segments result in material properties such as melting point, modulus (stiffness), and toughness (resistance to fracture when stressed).

The ability to control the above factors through the use of catalyst coordination polymerization can be seen throughout the previous and subsequent chapters. This chapter concentrates on the ability to control the polymer properties with heterogeneous stereospecific catalysts, focusing on polypropylene (PP) catalysts in particular.

7.1.1 Brief Introduction to Stereospecific Polymerization

Before discussing heterogeneous stereospecific catalysts it worth taking note of the types of polymers produced by such catalysts and how the catalysts build such structures.[4,5]

Polymers A regio- and stereospecific polymer has an organized relationship between sequential monomers. The α-olefin monomer insertion, orientation (the monomer has a "head" and a "tail"), and stereochemical configuration with respect to the other units in the chain backbone are keys to defining the properties of the final resin. Regularity with respect to monomer orientation is termed the *regiospecificity* of the polymerization. Regularity of the alkyl side-chain placement relative to the other alkyl side chains along the chain backbone is termed the *stereospecificity* of the polymerization. In polypropylene the relative orientation of each methyl group relative to the methyl groups on neighboring monomers, because each methyl group takes up space and constrains backbone bending, has a considerable effect on its ability to form crystals. There are four stereospecific microstructure sequences in polypropylene (Figure 7.1). In isotactic, all of the methyl groups have the same configuration with respect to the polymer backbone. In syndiotactic, the methyl groups have an alternating configuration. Atactic has a random configuration, while hemi-isotactic polypropylene consists of alternating methyl groups with the same configuration with respect to the polymer backbone and alternating methyl groups with a random configuration. Polypropylene polymers are based on long, short, or multiblock sequences of these four basic types. Misinsertion, whether it be as a stereo- or regioerror, can occur in the insertion of the monomer.

In addition to regio- and stereospecificity, important additional parameters of the polypropylene chain which influence polymer properties include the

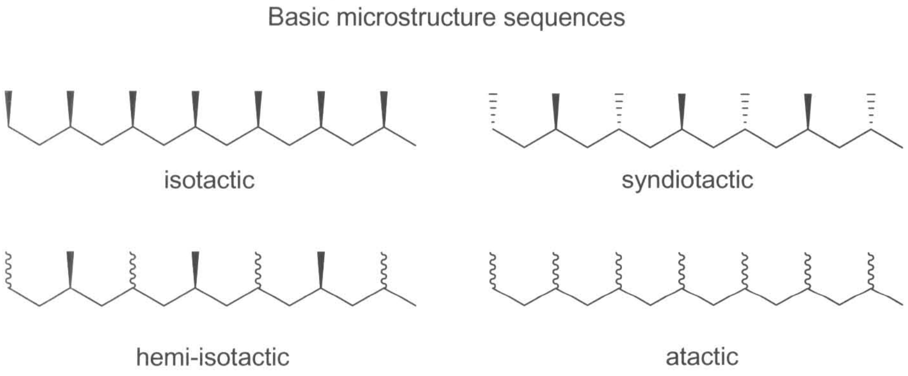

Figure 7.1 Basic microstructure sequences in polypropylene.

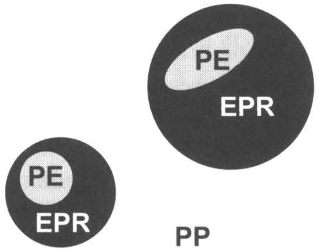

Figure 7.2 Simplified representation of heterophasic impact copolymer.

molecular weight, polydispersity, and composition and comonomer distribution in blends and copolymers. Polypropylene copolymers are most commonly based on ethylene or 1-butene. Copolymers and blends greatly expand the property range of polypropylenes. The incorporation of a comonomer molecule has a similar effect to stereo- or regiodefects in that it affects the ability of the polymer chains to form crystals. The comonomer is introduced into the chain "randomly" (polypropylene–random copolymers; PP-RACO); however, inter- and intrachain composition distribution can arise depending on the catalyst and process. In general, the goal is to achieve a homogeneous distribution of the comonomer molecules.

"Impact copolymers" (polypropylene–ethylene propylene; PP-EPR) synthesized directly in a multistage process are better described as heterophasic copolymers, with a composition that varies over a wide range of applications. Typical formulations would be 60–90% homopolymer (or PP-RACO) and 10–40% ethylene–propylene copolymer rubber (EPR) with ethylene concentration of 30–60%. The rubber component has a lower glass-transition temperature (T_g) and lower crystallinity and typically exists as a separate phase. Polyethylene is commonly present as a third phase (Figure 7.2).

Catalyst The commonly accepted mechanism for catalysis α-olefin chain propagation is based on the migratory insertion mechanism of Cossee–Arlman

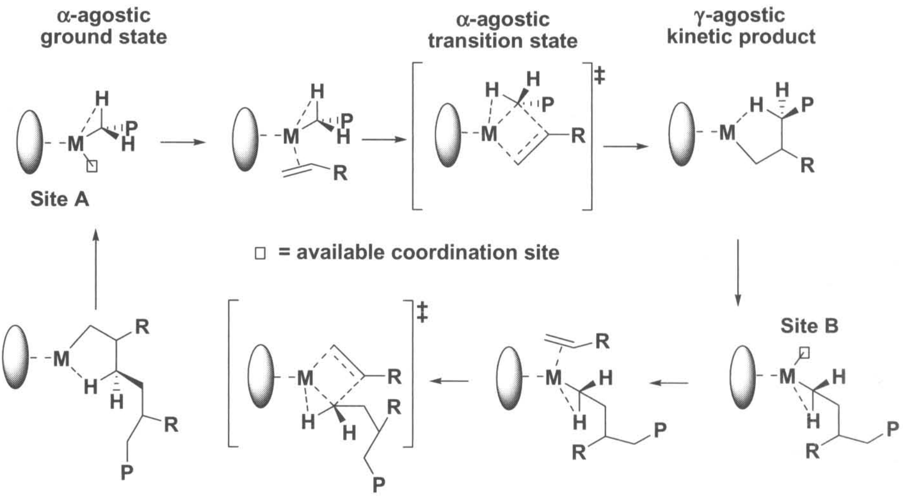
α-agostic ground state
α-agostic transition state
γ-agostic kinetic product
Site A
Site B
□ = available coordination site
M
H
P
R
‡

Figure 7.3 Schematic representation of migratory insertion.

and further refinements (Figure 7.3).[6–8] The mechanism is basically a two-step process in which the olefin first coordinates to an available coordination site at the metal center. In a limitless number of random orientations, a monomer arrives at the metal center. Expanding and contracting orbitals overlap, converge, and combine, dancing toward the lowest energy conformation between the metal and the monomer molecule. When this metal–olefin coordination is created in the presence of nonbonding interactions, there are limits in the degrees of freedom which can produce a carbon–carbon bond. In general, the monomer is coordinated at the metal center and is directed into a low-energy conformation based on nonbonded interactions. It is inserted via cis opening of the double bond leading to chain migration. A regular alternation of insertions at the two coordination sites is expected under a kinetic quench regime; at the other limit, a Curtin–Hammett regime can be observed in case of fast (relative to insertion) relocation of the growing polymer between the two metal coordination sites (e.g., under conditions of monomer starvation). In addition, the mechanism indicates that an olefin has to be face on to the metal with the double bond oriented in a parallel fashion to the metal alkyl bond.

The regiospecificity of a catalyst is dictated by nonequivalences in the two possible modes of coordination and insertion "head–tail" (1,2, or primary, insertion) or "tail–head" (2,1, or secondary, insertion), arising from the electronic and steric nature of the active metal center. The stereospecificity for any α-olefin polymerization catalyst [Ziegler–Natta (ZN) or single site] is governed by the catalyst's ability to discriminate between the two faces of the prochiral α-olefin molecule for a given mode of insertion (2,1 or 1,2). The steric control of the active site may be dictated by the chirality of the active catalyst site (enantiomorphic site control) or by the configuration (*R*, *S*) of the sterogenic carbon atom of the last inserted monomer unit (chain-end control). These are the essential types of stereocontrol mechanisms operating in propylene polymerization with various stereospecific catalysts.

There are three elements of chirality present in the intermediates and transition states can be rationalized as follows. A prochiral α-olefin molecule can coordinate via its two-faces at the active metal center. This gives rise to two non-superimposable re and si disastereoisomeric intermediate complexes (Figure 7.4). Taking into account the generally agreed-upon migratory insertion mechanism, an isotactic polymer is generated by a long series of insertions of either all re or si, while a syndiotactic polymer is generated by alternating sequences of re and si. Therefore enantiomorphic site control is the ability of a catalyst to impart information into the growing polymer chain based on low-energy orientations of incoming monomer directed by nonbonding interactions with the architectural arrangement of the ligand/steric environment surrounding the metal center and, finally, the configuration of the stereogenic tertiary carbon in the growing chain and in particular of the last inserted monomer unit.

Within all the above frameworks the site control of a polymerization catalyst is intimately linked to the energy differences between the disastereoisomeric situations that originate from the combination of two or more of the above elements of chirality. The structure of the catalyst defines the structure of the polymer. As previously pointed out, the polymer macromolecule is a result of the physical conditions of the polymerization and chemical interaction at the reactive center in the reaction dynamic (kinetic regime). Although

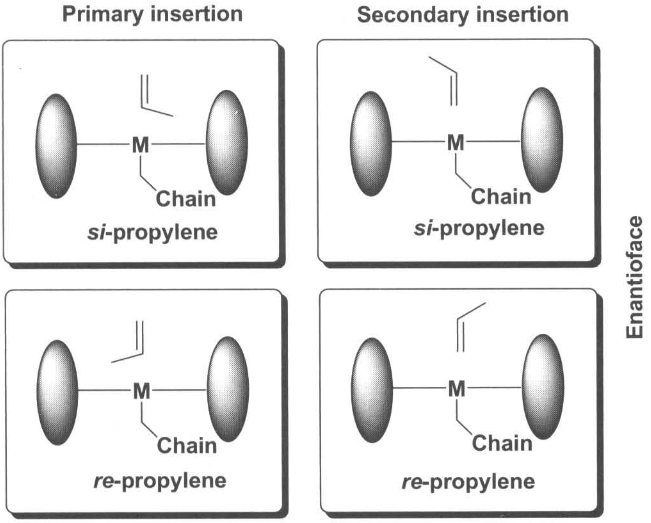

Figure 7.4 Non-superimposable re and si disastereoisomeric intermediate complexes.

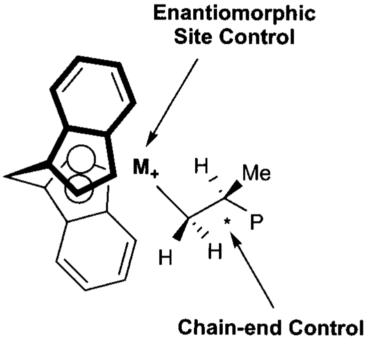

Figure 7.5 Chain structure control sites in metallocene catalyst.

played out on many levels, the effectiveness of the controlling structure is a major contributor to the final product properties: Chain molecular structure is a first principle (Figure 7.5).

Like most things in life, stereospecific polymerization is far from perfect, with misinsertions along a polymer chain occurring in various degrees depending on the catalyst and polymerization conditions. Such misinsertions are based on site errors and chain-end errors (Figure 7.6), which are described in greater detail in the reviews of Resconi et al.[9] and Busico and Cipullo.[10] The type and frequency of these errors affect the length of the crystallizable stereo regular sequences and hence has a considerable effect on the final polymer resin.

Polymerization conditions can also affect the stereospecificity of the polymer. At low monomer concentrations the chain can migrate from one coordination site to the other (re → si or vice versa) as the energy barrier for this transition is low and temperature dependent. Chain migration followed by insertion also leads to errors in the stereoregularity of the polymer chains. Polymer synthesis conditions such as low temperature and higher pressures can increase polymer tacticitity. Low monomer concentration leads to increased chain migration and greater stereoirregular insertions.[9,10]

The distribution of a (substituted) monomer within a macromolecule is best measured by nuclear magnetic resonance (NMR). The distribution of regularity in the molecule, that is, the relationship that creates asymmetries in the relationship one methylene unit has with the next, give rise to measurable magnetic differences.[10]

7.1.2 Why a Heterogeneous Catalyst

Commercial production of stereospecific polyolefins utilizes one or a combination of three main process types: solution phase, gas phase, and slurry/bulk phase. The processes can be further characterized into particle-forming (bulk- and gas-phase) and solution processes. Each process is suitable to produce particular resins with certain performance advantages.

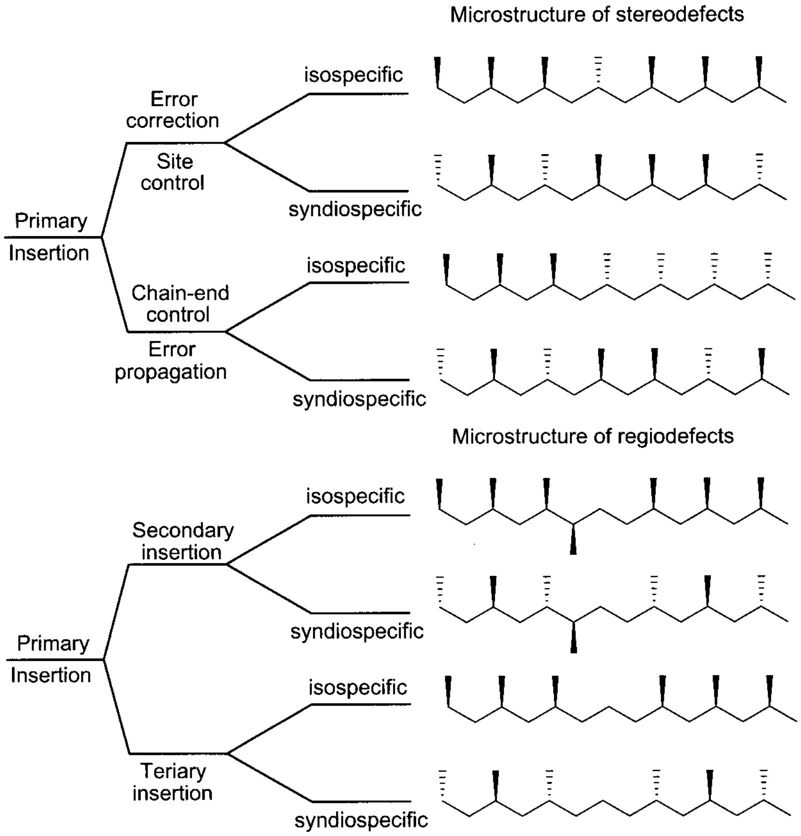

Figure 7.6 Stereo- and regiodefects in polypropylene.

Solution processes operate best for polymer resins having a low softening point and/or high solubility. In these processes the polymer is kept in solution (remains soluble) during the reaction process. This process is typically used for all stereospecific polymers derived from 1-butene or higher α-olefins. In these cases heterogeneous catalysts are often employed but not required.[11] Examples of such systems are the heterogeneous α-olefin polymerization catalysts that are prepared by anchoring a homoleptic early transition metal hydrocarbyl complex onto inorganic oxide supports. A number of studies on alkyl, alkylidene, or hydride complexes resulting from the reaction of homoleptic alkyl–zirconium (neopentyl, neopthyl, benzyl, and methylsilyl) with silica or alumina have been reported to produce highly active polymerization systems in the absence of a cocatalyst,[12–16] invariably producing elastomeric PP resins with broad molecular weight distributions which indicate multiple active sites. It should be noted, however, that $Zr(CH_2Ph)_4$, in combination with methylaluminoxane (MAO)[17] and $B(C_6F_5)_3$,[18] has been reported to produce polymer resins with narrow molecular weight distributions (MWDs).

In the manufacture of polypropylene, modern bulk- (liquid monomer) and gas-phase processes have largely replaced the earlier slurry processes in which polymerization was carried out in a hydrocarbon diluent. This is a result of the need to drive toward optimization and cost reduction while at the same time aiming for quality improvement ("quality up-cost down"). Such developments, allied with advancements in catalyst technology, have allowed the removal of as much "steel" (columns, evaporators, pumps, etc.) as possible from a process, reducing investment and operational costs. An example of this is the increased efficiency in terms of feedstock utilization of the polypropylene process. In 1964 polypropylene processes recovered 84% of the propylene employed as polypropylene, with the rest lost to atactic polypropylene (aPP) formation, ashing, and flaring, while today's process efficiencies are in excess of 99.7%.[3]

The polymerization process is an important factor in defining the requirements of a catalyst. Each proprietary process has its own limits in terms of monomer and comonomer concentrations, temperature, temperature control (ΔT), and residence time distribution. These factors place requirements on the catalyst in terms of its kinetic profile. The kinetic profile of the catalyst has a strong effect on the polymer target capability and can be tailored to a certain extent by all the components in the final catalyst (support, precatalyst, cocatalyst, and synthetic strategy).

The reader is reminded that heterogeneous catalysts are predominantly used to produce commercially viable products. Such processes are extremely large scale (150–500 kton/year) and operate continuously. They rely on solid heterogeneous catalyst particles that form discrete polymer particles to provide good reactor operability. In all commercial particle-forming polyolefin processes the catalyst remains in the finished polymer product unless extracted, which is a costly process. Therefore it is the catalyst productivity, that is, how much polymer is produced by how much solid catalyst (including complex, cocatalyst, and carrier), that is crucially important and not the activity of the metal alone. Typically, catalyst productivities above 10 kg PP/g catalyst are required for a commercially viable operation.

The above considerations place certain restrictions on what type of catalysis can be achieved in a commercially relevant particle-forming process. For example, heterogeneous "pseudoliving" polymerization is difficult to imagine in present commercial-scale processes. First, commercial processes are continuous, and most possess rather broad residence time distributions which would result it a broadening of the MWD of the polymer produced by a living polymerization. Second, requirements in terms of productivity would place restrictions on the molecular weight capability of the target resin, which would be directly related to the mean residence time and distribution.

As close to continuous operation as is possible is crucial for commercial processes, with modern world-scale plants able to produce in excess of 1000 tonnes of PP per day. Coupling this to the present market price for PP makes it is easy to understand what just one days loss in production could cost. One of the main factors to affect process operability is reactor fouling. Reactor fouling typically occurs when active species leach from the surface of the heterogeneous catalyst and start to polymerize homogeneously. Overheating of a catalyst/polymer particle through heat transfer problems or poor control of the processes can result in the formation of polymer deposits on the surfaces of a reactor, its internal parts such as gas distribution plates, heat exchangers, impeller blades and thermocouples, and additional process hardware such as recycling lines and compressors. These polymer deposits build up over a period of time, contributing to a decrease in the ability to control the process (heat transfer, catalyst efficiency, product throughput, and split control in cascaded processes) and hence the ability to produce the desired polymer resin to specification. This can spiral out of control to a point where the reactor needs to be shut down, cleaned, and restarted. Fouling is also detrimental to all parts of a polymerization process, including the reactor and its associated hardware (pumps, motor and gearboxes, etc.), which may need to be maintained or changed. The cleaning, maintenance, and restart process can take several days and is extremely costly and time consuming.

Recent process technology developments have been driven by product versatility and innovation and have allowed the production of value-added polypropylene-based products able to compete in nontraditional polyolefin markets. The most widely adopted manufacturing processes for polypropylene are Lyondell/Basell's Spheripol process, Dow's UNIPOL II, ABB Lummus's NOVOLEN, and INEOS's INNOVENE PP, with the former process in particular being most prevalent.

Lyondell/Basell has developed several process technologies over the years. In the Spheripol process, production involves a prepolymerization step at relatively low temperature followed by polymerization in a cascade of two loop reactors using liquid propylene; random copolymers are produced by introducing small quantities of ethylene into the feed. Two loop reactors are employed to improve the residence time distribution of the growing polymer particle and is needed to ensure that a significant amount of the catalyst has formed polymer under the first conditions before entering the next phase. This next phase consists of one or two gas-phase reactors for ethylene/propylene copolymerization, making it possible to produce heterophasic copolymers containing up to 40% of E/P rubber within the homopolymer matrix.[19] The development of the Spheripol process was based on ZN catalysts having spherical particle morphology. Further catalyst and process developments, including the manufacture and use of catalysts having varying degrees of porosity, led to the Lyondell/Basell Catalloy process (to be discussed in more detail later). This is a sophisticated modular technology based on three mutually independent gas-phase reactors in series. Random PP copolymers containing up to 15% comonomer can be obtained as well as heterophasic alloys containing high proportions of multimonomer copolymers. The feasibility of producing reactor-grade polymer blends containing up to 65% rubber phase arises from the use of a controlled porosity catalyst and the ability to control the porosity of the growing polymer particle during the early stages of polymerization.

Lyondell/Basell's most recent development in polypropylene process technology has been the introduction of the Spherizone process. The technology is based primarily on a gas-phase multizone circulating reactor, with the additional option of adding further multizone reactors or GPRs (gas-phase reactors).[20] In the multizone reactor, the growing polymer granule is continuously circulated between two polymerization zones: upward, by fast fluidization, in the "riser" leg, and downward, by means of gravity in a packed bed, in the "downer" leg. The monomer composition and the hydrogen concentration in the two legs can be different, and multiple short passes of the growing particle between the two zones leads to intimate and effective mixing of very different polymers.

INEOS INNOVENE PP technology was originally developed by Amoco. It is based on one or more horizontal stirred-bed GPRs in which liquid propylene is sprayed onto the polymer bed, vaporizing and efficiently removing the heat of the reactor. Homopolymers or random copolymers are produced in the first reactor, while the second reactor in series is utilized for impact copolymer manufacturing. The unique horizontal agitated bed and single injection point for the catalyst, typically at the opposite end of the the reactor to the product removal, result in a narrow residence time distribution, approaching plug flow behavior. This allows for rapid and efficient transitions between product grades and is also claimed to result in copolymers with excellent balance between stiffness and impact strength. Japan Polypropylene (formerly Chisso) has also developed a horizontal stirred-bed gas-phase process.

The Dow UNIPOL PP process has its roots in Union Carbide Corporation gas-phase technology and closely parallels the corresponding UNIPOL polyethylene process (Univation). The process is built around two cascaded vertical GPRs in which a cycled gas stream provides the fluidization of the growing polymer bed. The process operates in the condensed mode with heat removal being enhanced by the introduction of liquid propylene and propane feeds. The fluidized-bed reactor has extensive back mixing and a short residence time, which is claimed to shorten transition times. However, while the residence time is short, the residence time distribution may be not be ideal in terms of achieving impact copolymers with good copolymer flow and rubber efficiency.

ABB LUMMUS's NOVOLEN PP technology is based on the acquistion of Targor NOVOLEN PP technology from BASF in 2000. The technology is based on two vertical stirred-bed GPRs. The unique feature of this process is that it can be operated in two different modes (cascade or parallel). If the reactors are operated in a cascaded manner, the first reactor produces a homopolymer while the second produces impact copolymers. However, if the homopolymer or random copolymers are required, the process can be switched

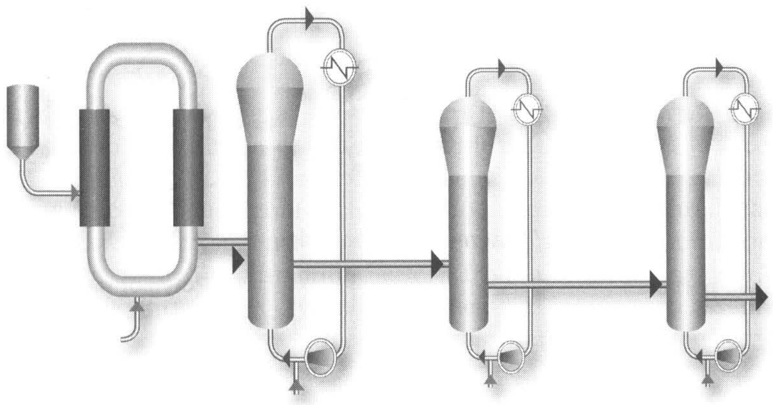

Figure 7.7 Schematic representation of Borstar PP® process.

to operate in parallel rather than in cascade. This allows for higher throughput and gives the significant advantage that no reactor is ever idle during normal operation.

Finally, one of the most robust and flexible industrial processes for the manufacture of value-added polypropylene is Borealis Borstar PP technology (Figure 7.7). The process is capable of operating under supercritical conditions, where the T_c and P_c values for propylene are 91.4 °C and 45.5 bars, respectively. As a result, Borealis catalysts are developed to yield peak activity while retaining exceptional stereoregularity in this region.[21]

7.1.3 Particle Growth

Heterogeneous polypropylene catalysts typically operate in particle-forming processes, such as slurry-, bulk-, or gas-phase polymerization technologies. Controlling the polymer particle growth and its morphology is crucially important in the commercial operation of these processes, gas phase in particular. As the growing polymer particle tends to replicate the initial catalyst morphology, the ability to control the later one is fundamental (Figure 7.8). The study of particle growth is an extensive and complex field, which due to constraints will not be discussed in great detail, but the reader is reminded of the fundamental importance of the subject and is directed to the reviews of Bartke[22] and McKenna and Soares.[23]

The characteristics of particle growth during the course of polymerization take into account such aspects as mass and heat transfer. Ineffective monomer mass transfer can limit the catalyst productivity, while ineffective removal of

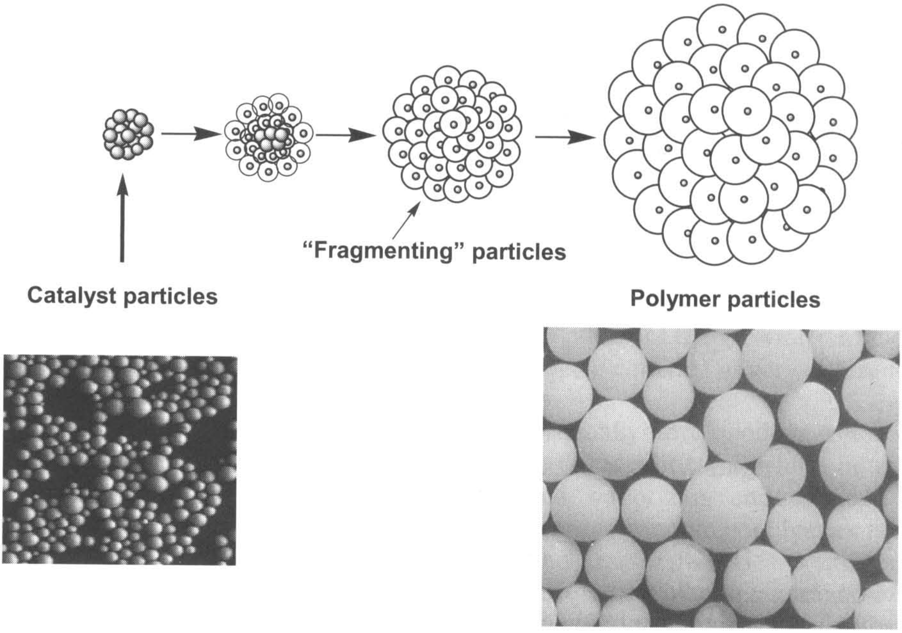

Figure 7.8 Schematic representation of model for polymer particle growth.

heat of polymerization from the growing particle in the early stages of polymerization can cause the formation of hot spots, which may in turn lead to catalyst decay. It is important that the mechanical strength of the catalyst particle is high enough to prevent disintegration leading to fines formation but low enough to allow controlled progressive expansion during polymerization. As polymerization proceeds, the initial catalyst support becomes fragmented and dispersed within the growing polymer matrix (Figure 7.8). The morphology of the starting support is replicated in the final polymer so that a spherical support in the size range 10–100 μm will give spherical polymer morphology with particle size generally in the range 100–3000 μm, dependent on the catalyst productivity. Extensive fragmentation and uniform particle growth are key features in the replication process and are dependent on a high surface area, a homogeneous distribution of catalytically active centers throughout the particle, and free access of the monomer to the innermost zones of the particle.

In the absence of prepolymerization, larger exotherms and mechanical stress occurring on the individual catalyst particles in the early stages of polymerization can cause serious operability problems. This is why processes such Lyondell/Basell's Spheripol include a prepolymerization step which yields a prepolymer particle with the capacity to mechanically withstand or reduce the reaction peak, which occurs on entering the main reactor.

7.2 TRADITIONAL ZIEGLER–NATTA CATALYST SYSTEMS

7.2.1 The Birth

In the early 1950s Giulio Natta and co-workers at the Milan Polytechnic began work on the polymerization of propylene with the then recently discovered catalysts of Ziegler.[24] In 1954 Paolo Chini, one of Natta's co-workers, fractionated the reaction product from such a reaction. He obtained three fractions, one of which was a crystalline, high-melting, white powder. Paolo Corradini subsequently obtained a diffraction pattern from a stretched sample of the white powder confirming its crystallinity, which was interpreted assuming all the asymmetric carbon atoms of the main chain were in the same steric configuration. At the end of the year, Natta presented the principal results at the Accademia dei Lincei in Rome and published a short communication on the unexpected stereoregularity, coining the term "isotactic chains" in the process.[25,26] The demonstration of stereoregular polymerization of an α-olefin led to a rapid growth in new polymers and industrial applications as the potential of ZN catalysts were realized. As a result, Giulio Natta, in recognition of his seminal contribution to the field of stereoregular polymerization, was jointly awarded the 1963 Nobel Prize for Chemistry along with Karl Ziegler.

Historical Development of Ziegler–Natta PP Catalysts The history of industrial ZN polypropylene catalysts is generally described in terms of evolutionary generations, corresponding to the chronological order of their development.[27] They range from titanium trichloride catalysts, employed in the manufacturing processes of the late 1950s and the 1960s, to the high-activity magnesium chloride–based catalysts, which have helped fuel the growth and development of this versatile polymer. Advances in process technology have gone hand in hand with the development of polypropylene catalysts, developing from a slurry-based process to the current state-of-the-art, cascade processes which combine bulk- or gas-phase technology allowing the production of complex copolymers with multiphase structures which have expanded the application range for PP. Further, the impact of catalyst and process development on the commercial success is illustrated by the rate of growth over the last 20 years which has seen the production of polypropylene grow from approximately 10,000 Kt per annum in the late 1990s to close to 45,000 Kt per annum for 2007 (Figure 7.9).[1]

7.2.2 $TiCl_3$ Catalysts (First and Second Generation)

The $TiCl_3$ catalysts used in early industrial PP processes were typically prepared by the reduction of $TiCl_4$ with an aluminum alkyl or aluminum metal, generating a solid $TiCl_3$ precipitate. The $TiCl_3$ exists in four crystalline modifications, α-, β-, δ-, and γ-forms. The β-modification has a linear chainlike structure, while the α-, δ-, and γ-forms possess a layer structure.[28,29] Typically,

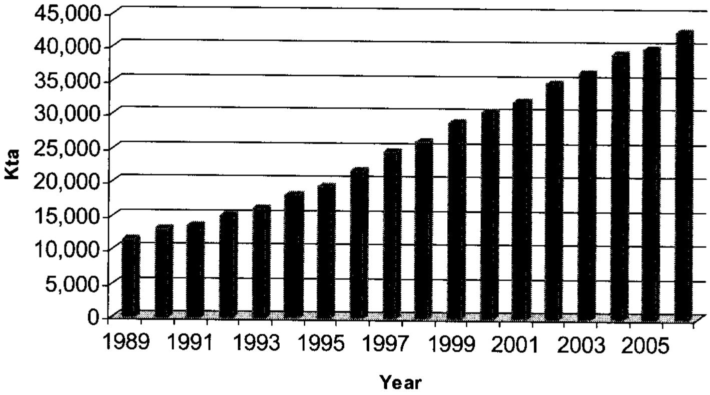

Figure 7.9 Global polypropylene production capacity (nameplate).

the reaction of $TiCl_4$ and $AlEt_3$ (at low Al/Ti ratios) at low temperatures in hydrocarbon solution resulted in the controlled precipitation of catalysts having spheroidal particle morphology, yielding the β-$TiCl_3$ form with cocrystallized $AlCl_3$. This precusor can be converted to the more stereoselective γ-form by heating to 160–200 °C.[30] The catalysts were typically activated by $AlEt_2Cl$ to afford poorly productive systems (~1 kg PP/g Cat) which in many cases yielded polypropylene resins that required extractive removal of atactic polymer and removal of catalyst residues (deashing).

An improved (second-generation) $TiCl_3$ catalyst developed by Solvay appeared in the 1970s.[31] The catalyst preparation procedure involved the chemical treatment of a $TiCl_3/AlCl_3$ /$AlEtCl_2$ precatalyst, previously produced by reaction of $TiCl_4$ with $AlEt_2Cl$. The catalytic activity could be greatly improved by extraction of the cocrystallized aluminum with diisoamyl ether giving a "pure" β-$TiCl_3$. Subsequent treatment with $TiCl_4$ catalyzed the phase transformation from the β- to the γ-form of $TiCl_3$ at a relatively mild temperature (<100 °C).[32] Lowering the temperature also prevented the growth of the catalyst particles. The success of the second-generation catalysts was due to the "new" morphology of the catalyst particles, resulting in smaller catalyst particles. In addition, the extraction of $AlCl_3$ with ether resulted in porous particles with a weakly bonded matrix. The innovation increased the activity and stereoselectivity and resulted in polymerization productivities in the range 5–20 kg/g catalyst in bulk propylene and produced polymers where the removal of the atactic fraction is spared.[33] It has been reported that for $TiCl_3$–$AlEt_3$ catalyst systems, the effect of temperature on the stereoregularity of the isotactic polymer fraction decreases in the range of –25–30 °C and then increases in the range of 30–120 °C.[34] On the other hand, with $TiCl_3$–$AlEt_2Cl$-based catalysts the stereoregularity typically decreases with increasing polymerization temperatures of 50–90 °C.[35] Despite the above, second-generation systems with donor technology are still in use today, although they have been overshadowed by the advent of the third- and later generation magnesium chloride–supported catalysts.

7.2.3 Third Generation

"Activated" $MgCl_2$ The prehistory of the third generation began in 1960, when Shell patented a catalyst for propylene polymerization that employed $TiCl_4$ supported on $MgCl_2$. The decisive step was achieved, however, in the late 1960s when Montecatini and Mitsui independently developed "activated" $MgCl_2$ as a support for $TiCl_4$ followed by the incorporation into the catalyst system of electron donors giving higher catalyst stereospecificity.[36–39] Initially, activated $MgCl_2$ was prepared by ball milling a mixture of magnesium chloride and ethyl benzoate, which leads to the formation of very small (≤3-nm-thick) primary crystallites of $MgCl_2$.[40] X-ray diffraction studies indicated that an activated δ-form of $MgCl_2$ possesses a rotational disorder in the stacking of the Cl–Mg–Cl triple layers.[41,42] The layers are disorderly stacked along c according to a hexagonal or cubic sequence or rotated by ±60° from each other.[43] Furthermore, high-resolution transmission electron microscopy (TEM) has shown that the crystal structure of $MgCl_2$ is severely distorted by ball milling, altering the structure from crystalline to amorphouslike.[44]

The combination of small crystalline size and large rotational disorder appears to lead to high catalyst activity.[45] Giannini[30] has indicated that, on preferential lateral cleavage surfaces, the magnesium atoms are coordinated with four or five chlorine atoms, as opposed to six chlorine atoms in the bulk of the crystal (001). These lateral cuts correspond to the (110) and (100) faces of $MgCl_2$, illustrated in Figure 7.10. However, more recently the (104) face has been implicated in the work of Busico et al.,[46] Terano et al.,[43] and Boero et al.[47] The (104) cut, as cleaved from bulk, possesses only magnesium atoms coordinated with five chlorine atoms and is very flat compared to the previous cuts. From a coordination point of view it is very similar to a reconstructed (100) face. Busico et al. trace the disagreement to the fact that Giannini[30] considered single structural layers of $MgCl_2$, that is, (pseudo-) bidimensional objects for which the index along the c axis is nominal and inmaterial and reports further that in full $MgCl_2$ crystals, relative to the (104) surface, the authentic (100) surface has a much higher coordinative unsaturation.

Location of Titanium Corradini and co-workers proposed that preferential titanium chloride coordination would occur on the later cuts, discussed above. In addition, the authors proposed that bridged, dinuclear Ti_2Cl_8 species coordinate to the (100) cut of $MgCl_2$ and give rise to the formation of chiral, isospecific active species, via close analogy to the isospecific site in $TiCl_3$-based systems (A, Figure 7.11).[48] This finding has recently been supported by Lee and Jo via DFT investigation.[49] The higher acidity of the (110) cut would lead to the preferential coordination of the donor, while the (100) cut is occupied

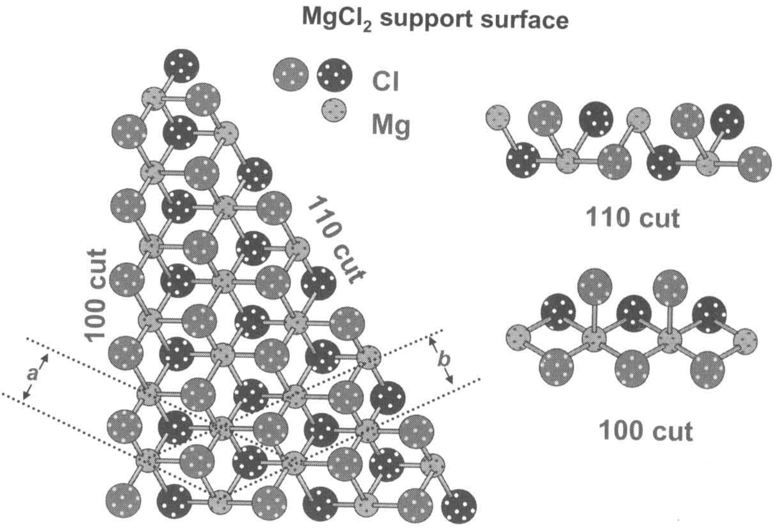

Figure 7.10 Crystal faces of magnesium dichloride.

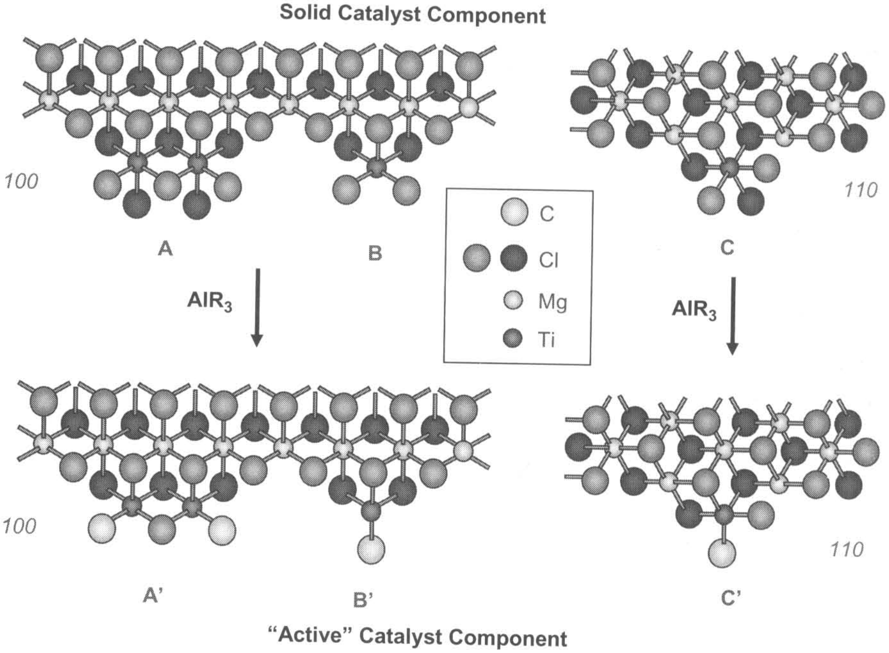

Figure 7.11 Proposed epitactic coordination of $TiCl_4$ on a $MgCl_2$ surface.

by Ti_2Cl_8 dimers. Computational investigations have suggested an extremely weak interaction between $TiCl_4$ and the (100) cut of $MgCl_2$ and that $TiCl_4$ desorption is very likely to occur.[43,50,51] However, recent spectroscopic studies using Fourier transform (FT)–Raman fortified with computational work have provided evidence for strong adsorption of $TiCl_4$ on the (110) lateral cut of $MgCl_2$, yielding a monomeric species with an octahedrally coordinated titanium center, which can be a precursor for active and stereospecific sites.[52,53] In addition, the monomeric complex was not removed by washing with solvent, whereas dimeric species (Ti_2Cl_8) on the (100) cut were found to be easily removable. The monomeric species was therefore concluded to be the active-site precursor in $MgCl_2$-supported catalysts.[52,53]

Internal/External Donors Third-generation catalysts commonly comprise $MgCl_2$, $TiCl_4$, and an "internal" electron donor which are combined with an aluminum alkyl cocatalyst such as $AlEt_3$ and an "external" electron donor added to the polymerization. The internal donor in third-generation catalysts is typically ethyl benzoate, which is used in combination with a second aromatic ester, such as methyl *p*-toluate or ethyl *p*-ethoxybenzoate (PEEB), as an external donor. An external donor is required due to the fact that a large proportion of the internal donor is lost as a result of reaction involving the cocatalyst such as alkylation and/or complexation reactions. The external donor replaces, to a large extent, the internal donor in the solid catalyst, maintaining high catalyst stereospecificity. It has been demonstrated that the most active and stereospecific catalyst systems are those which allow the highest incorporation of external donor,[54] with the effectiveness of a catalyst system depending more on the combination of donors than on the individual internal or external donor. The $MgCl_2$-supported systems possessing a portion of highly isospecific active sites in the absence of donors have been reported by Terano et al. via coordination of the cocatalyst $AlEt_2X$ (X = Et or Cl) in the vicinity of the active titanium center.[55]

The dominant active species in the third-generation catalyst is believed to be trivalent Ti(III) species, similar to first- and second-generation catalysts. Although active tetravalent Ti(IV) and divalent Ti(II) species may be present, however, the majority of reports indicate that Ti(II) is inactive in propylene polymerization.[56] It has been claimed that the $MgCl_2$ support and donors stabilize the titanium center toward "over"-reduction to Ti(II) species on contact with the alkyl aluminum cocatalyst, resulting in higher and more stable catalyst activity.[57] However, Kashiwa et al. discovered that contact of a third-generation catalyst with excess $AlEt_3$ at elevated contact temperature and time leads to a system which was extensively overreduced [Ti(III)–Ti(II) = 1:4]. The resultant system was inactive in propylene polymerization.[58] The majority of subsequent reports on the third-generation catalyst point to a range in the distribution of Ti(IV), Ti(III), and Ti(II) in the final catalyst depending on the contact time, temperature, or alkyl aluminum cocatalyst employed.[59–61]

7.2.4 Fourth Generation

The discovery and development of the fourth-generation phthalate/alkoxysilane-based catalyst systems was based on the consideration that bidentate phthalate donors (Figure 7.12) should be able to form strong chelating complexes with tetracoordinate Mg atoms on the (110) face of $MgCl_2$ or binuclear complexes with two pentacoordinate Mg atoms on the (100) face. As was the case for the third-generation catalysts, the function of the external donor is to replace the internal donor lost by alkylation and complexation reactions with the Al alkyl cocatalyst.[62] An additional feature was the development of spherical catalysts with controlled particle size and porosity, afforded via chemical rather than mechanical activation of magnesium chloride. All these features have contributed to the colossal commercial success of this type of catalyst, and at present this is the most widely used catalyst system in polypropylene production (Figure 7.9).

Catalyst Morphology Several different approaches have been followed for the preparation of catalysts having controlled particle size and morphology. Three main types of reactions have been employed: controlled preparation of a support material formed by complexation of $MgCl_2$ with an alcohol, which is subsequently titanated; the controlled precipitation of the reaction products of a magnesium alkyl or alkoxide with a chlorinating agent or $TiCl_4$; and finally the impregnation of a silica carrier with the catalyst reagents. The latter is the least frequently employed method for the production of ZN PP catalysts; however, it is a common technique in Ziegler polyethylene (PE) catalysts. Typically, a silica support is treated with a magnesium alkyl complex followed by chlorination (HCl) and addition of $MgCl_2$ and ethanol to form a support material that is converted into the final catalyst via titanation and external donor addition. Representative examples can be found in the work of Novolen/BASF.[63]

The archetypal example of controlled precipitation can be found in the work of Kashiwa and co-workers at Mitsui.[64] In this disclosure $MgCl_2$ is contacted with three equivalents of 2-ethyl hexanol in decane forming a uniform solution. Phthalic anhydride is subsequently added prior to mixing the homogeneous solution with $TiCl_4$. The mixture is allowed to react and precipitate in the presence of an internal donor (diisobutyl phthalate). The titanation step is then repeated on the solid component prior to washing. A further successful example of the precipitation method is the BRICI/Sinopec N-catalyst family.

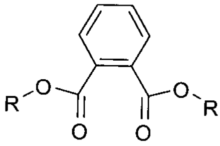

Figure 7.12 Phthalate donor.

In this concept anhydrous $MgCl_2$ is dissolved in a mixture consisting of an organic epoxide (epichlorohydrin) and tributyl phosphate in toluene to obtain a homogeneous solution. The solution is contacted with phthalic anhydride and treated with an excess of $TiCl_4$. The resultant solid support particles of microspherical form are obtained after heating. The solid catalyst is subsequently treated with the internal donor (diisobutyl phthalate) before isolating the solid, which is further contacted with $TiCl_4$ prior to extensive washing.[65] Additional examples of controlled precipitation can be seen in the work of Shell,[66] Amoco,[67] and Toho Titanium.[68]

Processes for the preparation of spherical $MgCl_2{\cdot}n$EtOH supports are based on spray drying or controlled precipitation techniques. In the latter, exemplified by the work of Basell and its previous incarnations and which forms the backbone of the Avant ZN range, molten emulsions of $MgCl_2{\cdot}n$EtOH ($n \approx 2$–3) adduct complex in paraffin oil are rapidly cooled to produce spherical particles with a relatively narrow particle size distribution. Similar carrier material is employed in the Sinopec/BRICI DQ catalyst.[69] Spray-dried supports are formed by contacting $MgCl_2$ with ethanol. The adduct is subsequently melted and injected into a cooled solvent or gas where it crystallizes as spherical particles of $MgCl_2{\cdot}n$EtOH ($n \approx 3$).[70–73]

The $MgCl_2{\cdot}n$EtOH ($n = 2$–3) complexes are generally crystalline and consist of a large number of covalent $[MgCl_2]n$ polymeric chains which basically yield the "activated" δ-form of $MgCl_2$ following extraction of ethanol to form the final catalyst. Relatively recently, Sozzani et al. characterized a number of adducts asserting that $n = 2.8, 1.5$ represents defined and stable $MgCl_2{\cdot}n$EtOH adducts.[74] Auriemma and De Rosa have shown that the high degree of nanoporosity of the derived catalysts may be due to intermediate formation of three-dimensional structures of "amorphous" or highly disordered crystalline $MgCl_2$ polynuclear chainlike species in equilibrium with the "activated" δ-form of $MgCl_2$. The authors postulate that the high degree of "nanoporosity" leads to an increase in the contour length of the lateral faces of $MgCl_2$, which is available for epitactic coordination of titanium and donor species. Further observations point to the fact that control over the $MgCl_2$/EtOH stiochiometry may play a key role in their formation.[75] Experimental observations have indicated that $MgCl_2{\cdot}n$EtOH support material in which $n = 3$ is desirable for preparing highly productive and stereoselective catalysts for the homopolymerization of propylene. Reduced alcohol contents in the support material either via initial stiochiometry or controlled dealcoholation yield systems with reduced activities and stereoselectivities in homopolymerization but yield catalysts suitable for ethylene–propylene copolymerization.[76] Catalysts derived from support material in which the ethanol contents are lower than 1.5 form the basis of the Basell so-called reactor granule technology which when utilized in their proprietary process technology (Catalloy) leads to the formation of heterophasic polyolefin alloys with particularly high rubber contents.[77–79]

Spherical $MgCl_2{\cdot}n$EtOH support materials formed via emulsion or spray-drying techniques are converted into the final catalyst via titanation steps. The reaction with excess $TiCl_4$ is undertaken in the presence of the dialkyl phthalate internal donor.[27] Temperatures of at least 80 °C and at least two $TiCl_4$ treatment steps are normally used in order to obtain high-performance catalysts in which the titanium is mainly present as $TiCl_4$ rather than the $TiCl_3OEt$ generated in the initial reaction with the support. Enhancements in the extraction of superfluous $TiCl_3OR$ from the final catalyst have been reported by Garorff and co-workers at Borealis.[80] The group utilized the addition of dioctyl phthalate as an internal donor "precursor" which undergoes a transesterification reaction to form the final internal donor with the by-product aiding in the extraction of the $TiCl_3OR$. Figure 7.13 illustrates the final morphology of such catalysts.

Catalysts obtained via these routes generally have a Brunauer–Emmett–Teller (BET) surface area of around 300 m^2/g and pore volumes in the range 0.3–0.6 cm^3/g.[27] In the past the general belief was that low surface area and compact catalyst particles are connected to low activity due to mass transfer limitations. However, the recent development by Leinonen and co-workers at Borealis has shown that a dense low-surface-area catalyst (~2 m^2/g) prepared via solidification from emulsion can possess high activities.[81]

Borealis emulsion–based catalyst preparation technology is performed in the absence of an external support. Instead of impregnating a carrier with a solution of the catalyst components, a two-phase liquid/liquid system is formed in which one phase contains a solution of the catalyst components.[82] The two-phase system itself can be formed either "in situ" by chemical reaction or

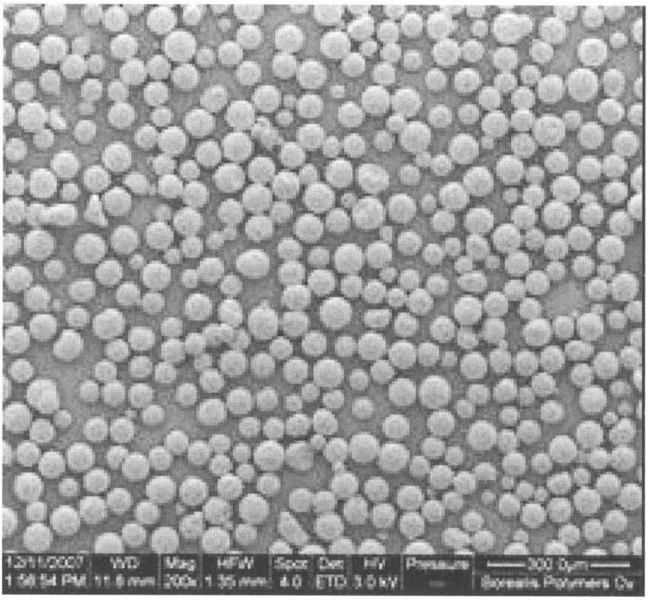

Figure 7.13 SEM micrograph of $MgCl_2$-supported catalyst. (Reproduced with permission from Borealis Polymers Oy.)

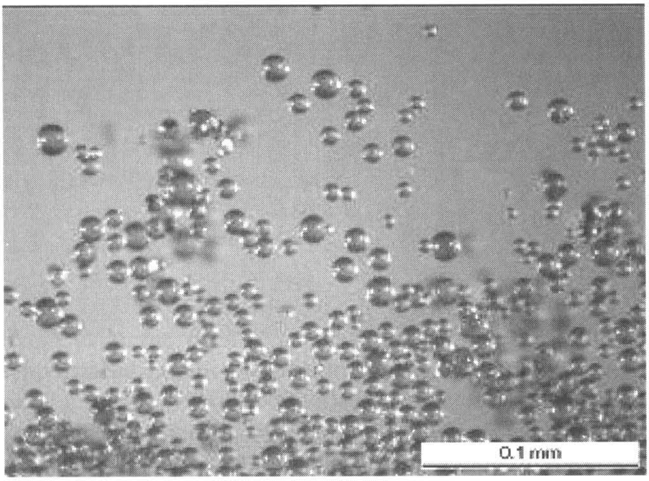

Figure 7.14 Optical image of emulsion-derived Ziegler–Natta catalyst. (Reproduced with permission from ref. 82; © 2007, Elsevier.)

simply by addition of an inert and immiscible solvent to the catalyst phase. In the second step this liquid/liquid system is then used to make an emulsion in which the solution of the catalyst components forms the dispersed phase. Finally, the catalyst components of the dispersed phase are solidified and homogeneously distributed in the form of dense transparent spherical particles of narrow particle size distribution (Figure 7.14). This technology has the added advantage of reducing the amount of $TiCl_4$ required for titanation. Powder X-ray diffraction (XRD) measurements indicated the presence of δ-$MgCl_2$ nanoribbons in the catalyst structure scanning electron microscopy (SEM) micrograms have revealed spherical surface species about 40–60 nm in diameter and chainlike structure within the catalyst particles, with the chains extending from the center of the particle to the surface (Figure 7.15). Evidently, activation and internal/external donor exchange are not adversely affected by this structure and the monomer does not encounter diffusion problems at the start of the polymerization. Such catalysts undergo rapid and complete fragmentation with controlled particle growth during polymerization, yielding compact polymer particles with high bulk densities (Figure 7.16).[83] In addition, the compact nature of the particles does not restrict the ability to produce heterophasic polymers.

The emulsion-based ZN PP catalyst has an inherent ability to insert the ethylene molecules evenly between the propylene molecules due to the homogeneous nature and distribution of its active sites. The good randomness with these catalyst reduces the problem with sticky ethylene-rich short chains, giving about 5 °C lower melting point (when compared with a standard reference catalyst having the same internal donor producing a random PP with similar ethylene concentration). Furthermore, good randomness leads to

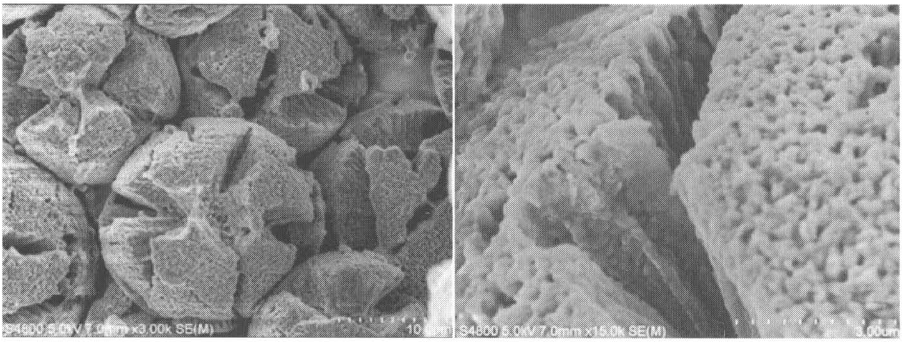
S4800 5.0kV 7.0mm x3.00k SE(M)
10.0µm
S4800 5.0kV 7.0mm x15.0k SE(M)
3.00µm

Figure 7.15 SEM microgram images of emulsion-derived Ziegler–Natta catalyst. (Reproduced with permission from ref. 82; © 2007, Elsevier.)

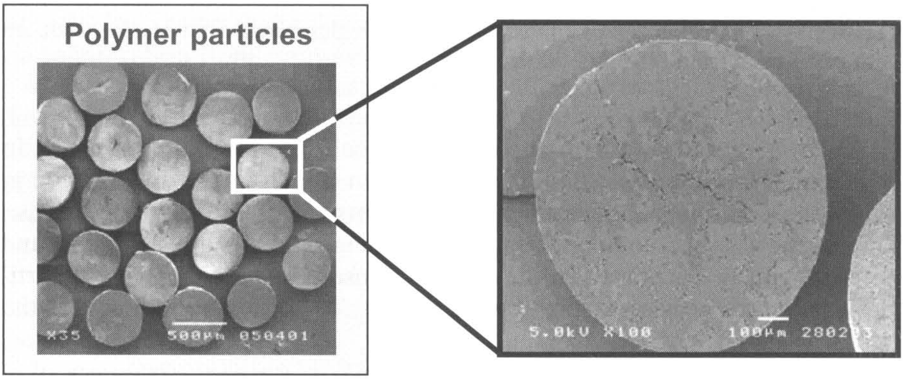

Figure 7.16 SEM images of polymer particles resulting from emulsion-based Ziegler–Natta catalyst.

resins with excellent optical properties, such as transparency. The amount of oligomers, <C15, in the final product is also significantly lower when using this catalyst compared to conventional ZN PP catalyst above. This results in additional advantages in the end product with regard to organoleptic properties, migration, blooming, and fuming.[84]

Chang et al. have detected a similar inner structure for a PP catalyst prepared by a precipitation method similar to the BRICI/Sinopec catalyst described above.[85] The authors report a "sea urchin"–type crystallinte structure for the catalyst particles: Particles are tightly filled with long rods of $MgCl_2$ crystallites and the planes of the Cl–Mg–Cl crystal layers are directed perpendicular to the lengths of the rods. SEM microgram images of the morphology of the catalyst particles suggest agglomerates of several spherical primary particles in which long rods of $MgCl_2$ crystallites emanate from a central (nucleation) point.[85]

Alkoxysilane External Donors The most effective alkoxysilane external donors for high catalyst stereospecificity are short-chain (Me or Et) alkoxysilanes containing relatively bulky groups alpha to the silicon atom.[84–94] The relationships between the structure of the silane compounds and their polymerization behavior have been discussed in detail by Härkönen and Seppala.[89–94] It has been recognized that silanes containing hydrocarbon substituents with the appropriate size and oxygen atoms with the appropriate electron density are required to produce highly isotactic polypropylenes.

The external donor not only decreases "less-tactics" formation but can also increase the degree of steric control at isospecific sites.[95] Sacchi et al. investigated the effect of silane donors on the highly sensitive first stereoregular insertion of propylene into a Ti–Et bond formed using the phthalate-based catalyst previously activated with ^{13}C-enriched $AlEt_3$.[96] The mole fractions of erythro (isotactic) placement in the isotactic polymer fraction were 0.67 with no external donor, 0.82 with $MeSi(OEt)_3$, and 0.92 with $PhSi(OEt)_3$. It was therefore concluded that the alkoxysilane external donor was present in the environment of at least part of the isospecific centers.

Typically, an industrial silane donor contains at least one secondary or tertiary carbon linked directly to the silicon atom. This bulky hydrocarbyl group is believed to protect the silane against removal from the catalyst surface via complexation with aluminum alkyl.[97] Examples of such donors can be seen in Figure 7.17, with cyclohexyl(methyl)dimethoxysilane ("C" donor) and dicyclopentyldimethoxysilane ("D" donor) being the most commonly employed.[97] When comparing the polymerization performance of cyclohexyl(methyl)dimethoxysilane and dicyclopentyldimethoxysilane the latter gives particularly high stereospecificity[98] and broader molecular weight distribution.[99]

The desired MWD of a polypropylene depends on the end-use application of the polymer. A narrow MWD and relatively low molecular weight are advantageous in fiber-spinning applications. In contrast, extrusion of pipes and thick sheets requires high melt strength and therefore relatively high molecular weight and broad molecular weight distribution. A broad molecular weight

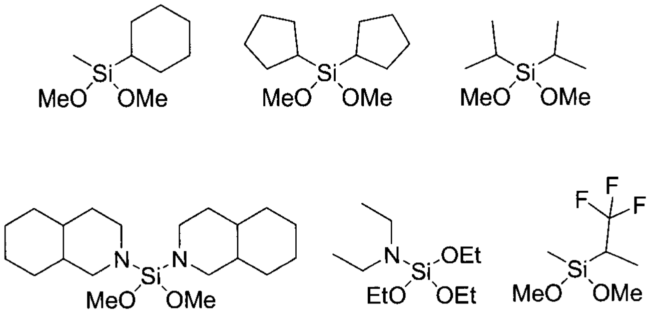

Figure 7.17 Examples of alkoxysilane external donors.

distribution, along with high isotactic stereoregularity, is also beneficial for high crystallinity and therefore high rigidity.

High PP stereoregularity and broad molecular weight distribution have also been obtained by employing dimethoxysilanes containing polycyclic amino groups, as exemplified by di(perhydroisoquinolinyl)dimethoxysilanes.[100] Cyclic amino-substituted silane donors first appeared in a Himont patent application;[101] however, it is the work of scientists in Ube Industries that further developed the potential of these donors.[102,103] Ikeuchi and co-workers reported that dipiperidinyldimethoxysilane, which possesses a similar geometric structure to dicyclopentyldimethoxysilane, yields more isospecific polypropylene and rationalized this increase via interaction of the nitrogen atom of the piperidinyl moiety with the active titanium center, increasing the steric influence at the metal center.[103] The group has also reported the use of amino trialkoxy silane donors, such as diethylaminotriethoxylsilane which yields catalytic systems with an increased hydrogen response. In other words, relatively low concentrations of hydrogen are sufficient to give effective control over polypropylene molecular weight, so that a wide range of polymer grades can be produced.[100,104] From a pratical (process) standpoint (depending on the process conditions), less hydrogen in the reactor keeps the process away from cavitation and bubble formation, which can lead to reactor shutdown.

Mixed External Donors An alkoxysilane external donor can be used to control stereoregularity, molecular weight distribution of a polymer resin, as well as the H_2 response and ethylene copolymerization capability of the catalyst system. However, it is often the case that an external donor that yields desirable control over one polymer property is ineffective or detrimental with respect to additional properties of the polymer. To combat this shortcoming, combinations of external donors have been employed in order to adjust polymer properties either according to an expected average or through the use of multiple reactors in the hope of achieving beneficial effects over an individual external donor.[105–109]

Employing combination of external donors does have some disadvantages. It is not uncommon for one of the external donors to be dominant, so as to exclude the effect of the other(s). As a result, polymerization in single/multistage processes often produces resins whose properties are determined essentially by the dominating external donor. Miro and co-workers at Exxon have exploited the dominant behavior of certain external donors.[108] When the group employed a combination of dicyclopentyldimethoxysilane (D donor) and tetraethoxysilane (TEOS), the D donor acts as the dominant donor-forming resin similar to those produced by the D donor alone, that is, high stereoregularity and low melt flow rate. However, the group discovered that they could take advantage of this dominant effect by using a two-stage polymerization process. The first stage utilized TEOS alone, forming a polymer with a high melt flow rate; the D donor was then added at the second stage. The combination of mixed donor and a two-stage process achieved a final polymer with high stereoregularity, a relatively high melt flow rate, and moderately broad molecular weight distribution. Recently, Chen and Nemzek extensively studied mixed D donor–TEOS systems.[109] The group discovered that at lower total molar ratio of donor to titanium (E.D./Ti = 1–10) it is still possible for the weaker donor TEOS to participate in the reaction, specifically with respect to its effect on the melt flow of the resultant polypropylene resins and hence hydrogen response. Figures 7.18 and 7.19 illustrate that the dominating influ-

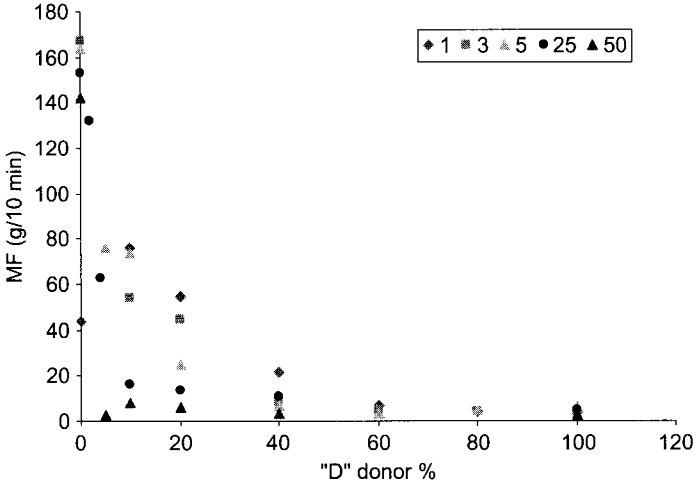

Figure 7.18 Relationship between melt flow (MF) and mole percentage of D donor (D donor/TEOS mixture) at varying molar ratios of total donor to titanium (E.D./Ti = 1, 3, 5, 25, 50).

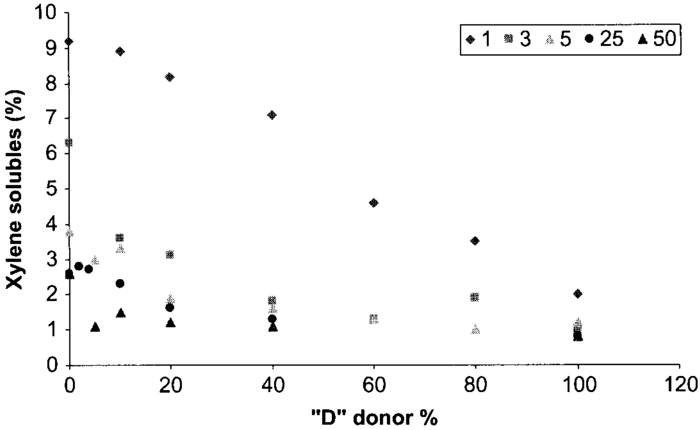

Figure 7.19 Relationship between xylene solubles (%) and mole percentage of D donor (D donor/TEOS mixture) at varying molar ratios of total donor to titanium (E.D./Ti = 1, 3, 5, 25, 50).

ence of the D donor is unsurprisingly related to the total molar ratio of donor to titanium (E.D./Ti) and therefore the total amount of dominant donor. In addition to the increased hydrogen sensitivity, the mixed donor system showed higher incorporation of ethylene in continuous copolymerization experiments with ethylene for a given feed rate.[109]

The main advantage of the fourth-generation catalysts over the third-generation systems is their greater stability during polymerization. The ethyl benzoate–based catalysts exhibit very high initial activity but then decay rapidly, losing around 90% of their activity during the course of a 1-h polymerization. This limits their productivity to around 30 kg PP/g catalyst under typical polymerization conditions (bulk liquid monomer, ~70 °C). In contrast, productivities up to around 70 kg PP/g catalyst are achievable with the fourth-generation, phthalate-based systems. The increased stability also allowed the further development of cascaded process technologies, which has allowed further tailoring of technical polymer resins. However, this increase in activity and stability may lead to operability problems, particularly in gas-phase processes. For example, some of Dow's SHAC™ catalyst systems operating in the Unipol gas-phase process require catalyst kill systems to be installed in the event of a pressure or fluidization loss.[110] This problem has led to the development of the "self-extinguishing/limiting" catalyst concept in which a mixture of external donors [alkyl benzoates (PEEB) and alkoxysilanes] are employed. It is claimed that this results in catalyst systems that are very active at the standard operating conditions but rapidly lose their activity at higher temperatures and therefore prevent the formation of sheets or large polymer chunks in the fluidized-bed reactor. Therefore, if a disruption does occur, the catalyst will deactivate quickly, leaving an intact particle bed. Upon recovery, the bed can be refluidized and reactivated with a minimum of downtime and effort.[110–112]

7.2.5 Fifth-Generation Catalysts

Diethers The search for further catalyst improvements led to the development of internal donors which were not readily removed from the support on contact with the alkylaluminum cocatalyst. It was found that certain diether compounds, in particular 2,2-disubstituted 1,3-dimethoxypropanes with an oxygen–oxygen distance in the range 2.8–3.2 Å (Figure 7.20), similar to those

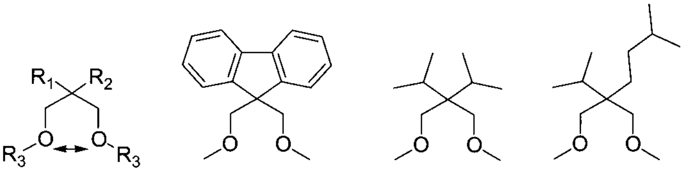

Figure 7.20 Examples of diether internal donors.

of the alkoxysilane external donors, are not extracted when the catalyst is brought into contact with the $AlEt_3$ cocatalyst. As a result high stereospecificity can be obtained even in the absence of external donor.[113–117] Fifth-generation diether catalyst systems show particularly high polymerization activity and good stability, typically giving yields exceeding 100 kg PP/g catalyst. They also give relatively narrow molecular weight distribution and show high sensitivity to hydrogen. Cui et al. recently reported their investigation into the influence of diether donor ratio on the performance of the final catalyst. Experimental data indicate that higher diether loadings cause a decrease in the titanium content of the catalyst, further indicating that the diether is associated with magnesium, not titanium. In addition, an optimum ratio was required for activity and stereoselectivity.[118]

Seminal work by Chadwick and co-workers has shown that the high hydrogen response of fifth-generation, diether-based catalysts arises from chain transfer after the occasional secondary (2,1-) rather than the usual primary (1,2-) monomer insertion.[119] The group rationalized that even the most highly stereospecific active sites are not totally regiospecific. In addition, the broader molecular weight distributions obtained with catalysts containing ester internal donors were attributed to the presence of (some) isospecific active sites having very high regiospecificity and therefore lower hydrogen sensitivity.[120]

There is significant evidence from modeling studies that diether donors preferentially adopt a bidentate coordination mode to the (110) lateral cut of $MgCl_2$.[121,122] Strong evidence points to the fact that donor molecules reside in the vicinity of stereospecific active species. Therefore, the above reports indicate that the likely location of active titanium is also on the (110) lateral cut. In addition, it has also been shown[123,124] that the use of a diether as external donor in combination with a phthalate-based catalyst gives active species which are very similar to those present when the diether is used as internal donor, implying that the active species in phthalate-based catalysts are similarly located on the (110) cut.

Succinates and Polyol Ester Lately, new types of internal donor compounds based on aliphatic dicarboxylic esters such as malonates and glutarates and in particular succinates and polyol esters (Figure 7.21) have been employed. Researchers at Basell developed $MgCl_2$-supported catalysts in which the internal donor is a succinate ester.[125,126] As is the case with phthalate-based

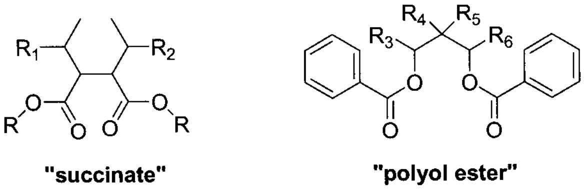

Figure 7.21 Structures of newer internal donor compounds.

catalysts, an alkoxysilane is used as external donor. The essential difference between these catalysts is that the succinate-based systems produce polypropylene having much broader molecular weight distribution. In addition, they also generate ethylene–propylene copolymers having considerably lower glass transition temperature coupled with better inter- and intramolecular comonomer distribution with respect to their conventional counterparts. This has allowed the production of heterophasic copolymers having an improved balance of stiffness and impact strength, taking into account that the incorporation of a rubbery (ethylene/propylene) copolymer phase into a PP homopolymer matrix increases impact strength but leads at the same time to decreased stiffness. Similarly, researchers at BRICI/Sinopec have developed the polyol ester family of internal donors. The catalytic systems resulting from this family of donors have a similar polymerization performance to succinate-based systems. However, unlike the succinates, the polyol ester systems yield high stereoselectivity even in the absence of alkoxysilane external donors.[127]

7.2.6 Discussions on Fourth- and Fifth-Generation Catalysts

Effect of Temperature The ability to run at the highest possible polymerization temperature is extremely important for commercial processes, as it facilitates better temperature control. The highest possible polymerization temperature is intimately linked to the catalyst's ability to withstand the elevated temperature (deactivation) and softening point of the polymer resin that is being produced. Several studies have been undertaken investigating the effect of polymerization temperature on fourth- and fifth generation catalysts. Hsu et al. reported a decrease in the isotactic pentad (*mmmm*) content of the heptane-insoluble polymer fraction (XI) for catalyst systems based on $MgCl_2/TiCl_4$/dioctylphthalate and $AlEt_3$ in the range of 20–70 °C, ascribing the decrease to result from the progressive removal of the internal donor via interaction with the $AlEt_3$ cocatalyst as the polymerization temperature was raised.[128] A further reported effect of the $AlEt_3$ cocatalysts at increased polymerization temperature (70–100 °C) is an increase in the rate of chain transfer to aluminum leading to a reduction in the molar mass of the resultant polymers with a similar $MgCl_2/TiCl_4$/dioctylphthalate (+ alkoxysilane, external donor) system.[129] Kashiwa et al., in a separate communication, also noted a decrease in the melting point of the resin obtained; however, unlike the above, this was ascribed to the formation and copolymerization of traces of ethylene produced by the β-hydride decomposition of $AlEt_3$. Substituting $AlEt_3$ for Al^iBu_3 as the cocatalyst was claimed to avoid the formation of ethylene.[130] Altering the cocatalyst from $AlEt_3$ to ethylaluminoxane has also been claimed to lead to beneficial high-temperature operation.[131]

Kissin and co-workers recently studied the effect that polymerization temperature (40–90 °C) had on polypropylene formed with $MgCl_2/TiCl_4$/dibutylphthalate (Al^iBu_3 or AlEt/silane) using a combination of experimental techniques. They found the crystalline fractions of polypropylene were produced by several "families" of active centers. The centers differed in the average molecular weights and stereospecificity. The average isotacticity of the crystalline fractions increased with polymerization temperature. An effect was attributed to variations in the relative contents of polymer components of low isotacticity in the crystalline fractions prepared at different temperatures. The application of silane external donor was claimed to poison not only aspecific centers but also the centers of reduced isospecificity as well. This effect results in the increase of the average molecular weight of the crystalline fraction, narrowing of its molecular weight distribution, and increase of average isotacticity.[132]

Mao and co-workers have reported on the effect of polymerization temperature on fifth-generation diether-based catalysts. Their initial communication reported that the portion of iPP (heptane insoluble fraction) with a high-crystallization temperature was lower when $AlEt_3$ was compared to Al^iBu_3 at elevated temperatures (70–100 °C). In addition the activity of the $AlEt_3$ was seen to decrease at temperatures approaching 100 °C. The exact reason for this phenomenon could not be elucidated; however, it was hypothesized that Al^iBu_3 is more efficient in the formation of active sites when compared to $AlEt_3$ at elevated temperatures.[133] The group has also reported the generation and incorporation of ethylene resulting from $AlEt_3$ decomposition similar to the Kashiwa et al. report;[120] however, this was noted in donor-free catalysts, suggesting that the decomposition may be donor assisted.[134]

One of the most extensive studies in terms of catalyst families on the effect of temperature (20–80 °C) was reported by Chadwick and co-workers. The group studied $MgCl_2/TiCl_4$ system in combination with a variety of donors. Their results are summarized in Figures 7.22–7.25. As one can see, the effect of polymerization temperature on the performance of a catalyst and the properties of the resultant polymer resin is dependent on the nature of the catalyst. Generally, an increase in polymerization temperature led not only to higher proportions of isotactic polymer but also to an increased stereoregularity of the isotactic fraction (xylene-insoluble fraction). The results indicate a greater relative increase in the productivity of the isospecific sites with increased polymerization temperature as opposed to the moderately isospecific centers. The intrinsic viscosity results reveal a decrease in the molecular weight of the PP carried out in the absence of external donors; however, this decrease is not apparent when the external donor $(c\text{-}C_5H_9)_2SiOMe_2$ is present.[135]

Active-Site Concentration Throughout the years one of the fundamental understandings that has been sought is the active-site concentration (C^*, expressed as a proportion of the total Ti present) for a particular catalyst system. Two basic strategies have been devised to determine C^*: (i) analysis of the time dependence of polymer yield and number average molecular mass at the very early stages of polymerization under *pseudo*-living regimes and stopped-flow conditions pioneered by Keii et al.;[136] (ii) employing labeled "quenching" agents (^{14}CO or CH_3OH^3) which tag the polymer chains with radioactive label at their growing end.[137–139]

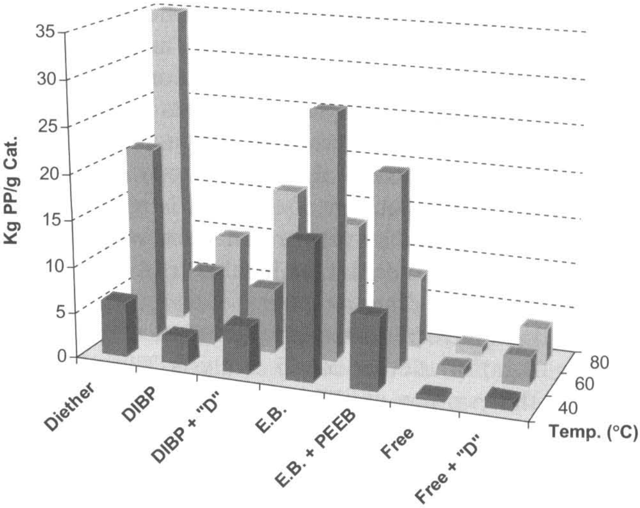

Figure 7.22 Catalyst activity vs. polymerization temperature for range of Ziegler–Natta PP catalysts (diether = 2-fluorenyl-1,3-dimethoxypropane; DIBP = diisobutyl phthalate; D = $(c\text{-}C_5H_9)_2Si(OMe)_2$; E.B. = ethyl benzoate; PEEB = ethyl *p*-ethoxybenzoate; free = no internal donor).

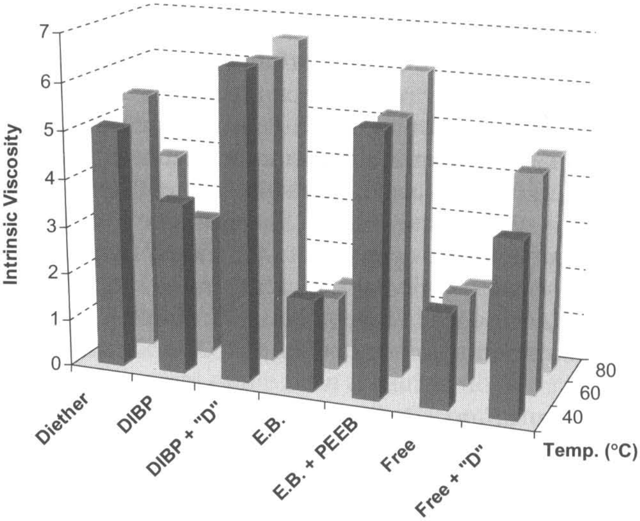

Figure 7.23 Intrinsic viscosity vs. polymerization temperature for range of Ziegler–Natta PP catalysts (diether = 2-fluorenyl-1,3-dimethoxypropane; DIBP = diisobutyl phthalate; D = $(c\text{-}C_5H_9)_2Si(OMe)_2$; E.B. = ethyl benzoate; PEEB = ethyl *p*-ethoxybenzoate; free = no internal donor).

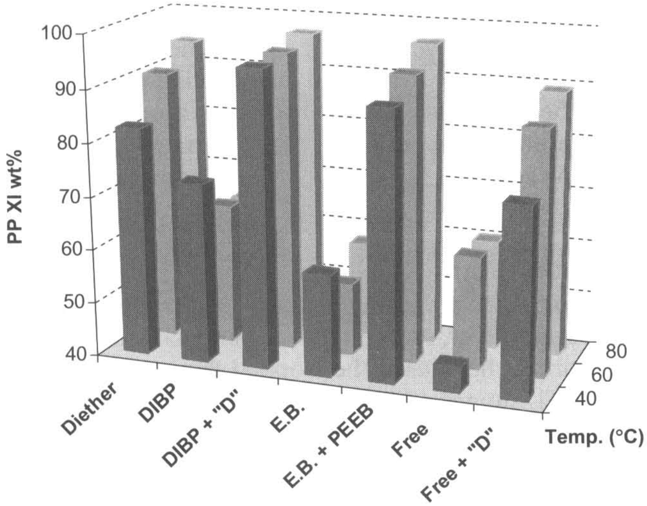

Figure 7.24 Xylene insolubles vs. polymerization temperature for range of Ziegler–Natta PP catalysts (diether = 2-fluorenyl-1,3-dimethoxypropane; DIBP = diisobutyl phthalate; D = $(c\text{-}C_5H_9)_2Si(OMe)_2$; E.B. = ethyl benzoate; PEEB = ethyl *p*-ethoxybenzoate; free = no internal donor).

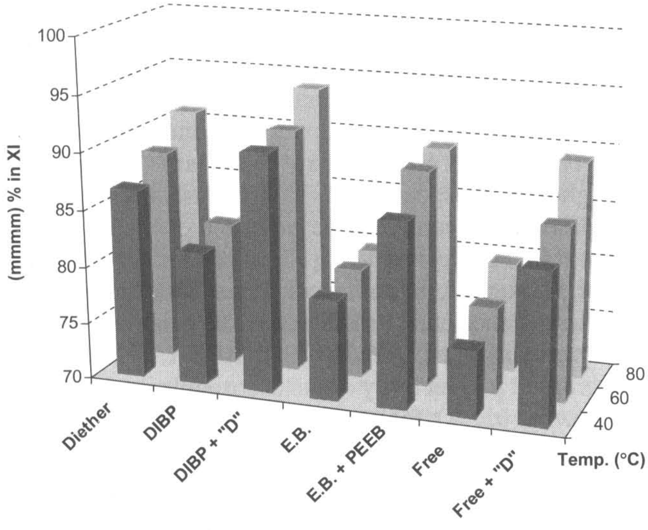

Figure 7.25 (*mmmm*) Percentage in xylene insoluble fraction vs. polymerization temperature for range of Ziegler–Natta PP catalysts (diether = 2-fluorenyl-1,3-dimethoxypropane; DIBP = diisobutyl phthalate; D = $(c\text{-}C_5H_9)_2Si(OMe)_2$; E.B. = ethyl benzoate; PEEB = ethyl *p*-ethoxybenzoate; free = no internal donor).

Both strategies have been applied to fourth- and fifth-generation ZN catalysts. Unfortunately, however, both approaches are potentially flawed: "stopped flow" because there may be an introduction phenomenon occurring; "quenching" to the possibility of incorporating more than one radiolabel per growing chain and/or labeling the "dead/dormant" chain residing as an aluminum alkyl species.[140,141] As a result, there is sometimes substantially different results obtained for C^* depending on the catalyst, approach, and/or quenching agent.

Comparisons of C^* across techniques is therefore tricky and should be restricted to data obtained within single sets of experiments carried out under similar conditions. However, some review is beneficial for "ball-park" figures. Terano and co-workers have used the stopped-flow method to determine C^* values for an $MgCl_2$-supported catalyst containing dibutyl phthalate as an internal donor yielding values of 0.7 and 1.6% for C^* for the systems with or without $AlEt_3$ precontacting, respectively.[142] These results are similar to the values obtained by Zakharov et al. using ^{14}CO quenching techniques with a catalyst with the same internal donor ($C^* = 2.3\%$).[143] Tait and co-workers, on the other hand, measured C^* contents of 8 and 16% for two phthalate-based catalysts using ^{14}CO quenching, while the CH_3O^3H quenching yielded somewhat higher values of 8 and 22%. More recent results by the group have afforded lower values ($C^* = 2.2$–3.9%).[144] Finally, reported values of C^* for diether-based systems have ranged from 1.8 to 7.9%. Despite the differences in the determined values for C^* in fourth- and fifth-generation catalysts, what is clear and generally assumed is that only a limited proportion of the titanium is active in propylene polymerization.

Stereoselectivity and Hydrogen Response The proportions of isospecific and weakly specific active species are of course dependent on catalyst composition and in particular on the internal and external donors present in the system. As mentioned above, the propagation rate constant (k_p) is around an order of magnitude higher for isospecific sites than for weakly specific sites and the value of k_p increases significantly in the presence of hydrogen, in accordance with the reactivation of "dormant" (2,1-inserted) centers by chain transfer with hydrogen. For example, Bukatov et al. reported k_p values of 605 and 2570 L/mol·s in the absence and presence of hydrogen, respectively, for $MgCl_2/TiCl_4$/diisobutyl phthalate–$AlEt_3/PhSi(OEt)_3$ at 70 °C.[145] Figures 7.26 and 7.27 illustrate the increased productivity and stereoregularity in the xylene insoluble fraction (*mmmm* wt %) for the $MgCl_2/TiCl_4$/diether system at various hydrogen levels and polymerization temperatures.[145]

Stopped-flow polymerization studies have shown that hydrogen is only effective as a chain transfer agent when catalyst and cocatalyst have been precontacted, indicating that effective chain transfer with hydrogen requires the presence of species able to promote the dissociation of hydrogen.[146,147] Terano and co-workers have also investigated the formation, variation, and conversion of isospecific active sites on a $MgCl_2$-supported catalyst in the

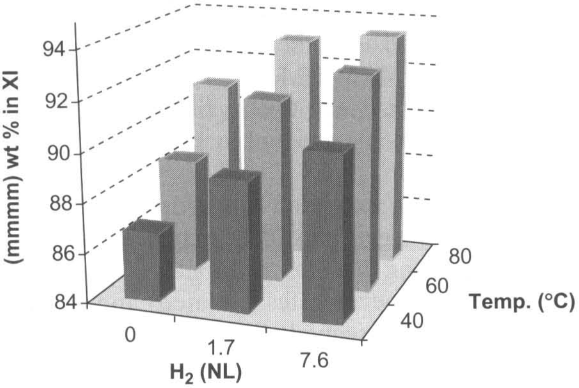

Figure 7.26 (*mmmm*) Percentage in xylene insoluble fraction at varying polymerization temperatures and hydrogen levels for a $MgCl_2/TiCl_4$/diether–$AlEt_3$ system.

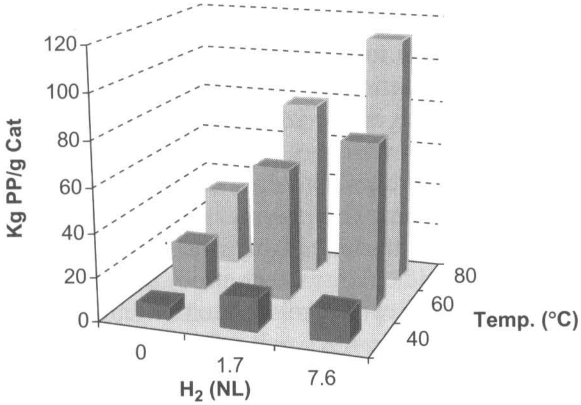

Figure 7.27 Catalyst activity at varying polymerization temperatures and hydrogen levels for $MgCl_2/TiCl_4$/diether–$AlEt_3$ system.

presence and absence of an internal or external donor.[148] Temperature-rising elution fractionation (TREF) analysis of the polypropylenes formed indicated that various kinds of active sites with different isospecificities, including highly isospecific sites, existed even in the absence of internal or external donor. In addition, the effect of titanium loading on stereoselectivity was investigated. The study led the group to propose that these highly isospecific sites may originate from a surface monolayer multinuclear titanium species, namely an "island" of titanium species, taking into account that higher stereoselectivities are found at higher titanium loadings. Furthermore, the addition of an internal donor was proposed to play an important role in creating these islands as well as suppressing the formation of the aspecific sites, while the addition of an external donor was proposed to convert the aspecific and/or low isospecific sites into higher isospecifity. Similar findings have been reported by Soga et al.[149,150] on a catalyst with low titanium content, which presumably yields isolated species. These isolated aspecific sites could be rendered isospecific via addition of donor or the use of Cp_2TiMe_2 as a cocatalyst and led the group to hypothesize that aspecific sites have two available coordination sites, which can be converted to an isospecific site by blocking or coordinating one of the available sites.[42,151]

Terano et al. have recently extended the hydrogen dissociation theory to account for the relative hydrogen sensitivity between aspecific and isospecific sites in their systems, reporting that isospecific sites ("islands") are much more sensitive to hydrogen than aspecific sites (isolated) and by extension must be close to the highly reactive nascent hydrogen-generating sites to facilitate chain transfer (Figure 7.28).[152]

The presence of a donor molecule in the vicinity of isospecific active species is an important feature of a mechanistic model proposed by Busico based on detailed ^{13}C NMR analysis of the polypropylene chain microstructure.[153] This model is based on the fact that defects arising from stereoirregular insertions are not randomly distributed along the chain but are clustered. The chain can therefore contain, in addition to highly isotactic blocks, sequences which can be attributed to weakly isotactic (isotactoid) and to syndiotactic blocks. This implies that the active site can isomerize very rapidly (during the growth time of a single polymer chain) between three different propagating species (Figure 7.29). The same sequences are present, but in different amounts, in both the soluble and insoluble fractions. The polymer can therefore be considered to have a stereoblock structure in which highly isotactic sequences alternate with defective isotactic (isotactoid) and syndiotactoid sequences. The relative contributions of these sequences can be related to site transformations involving

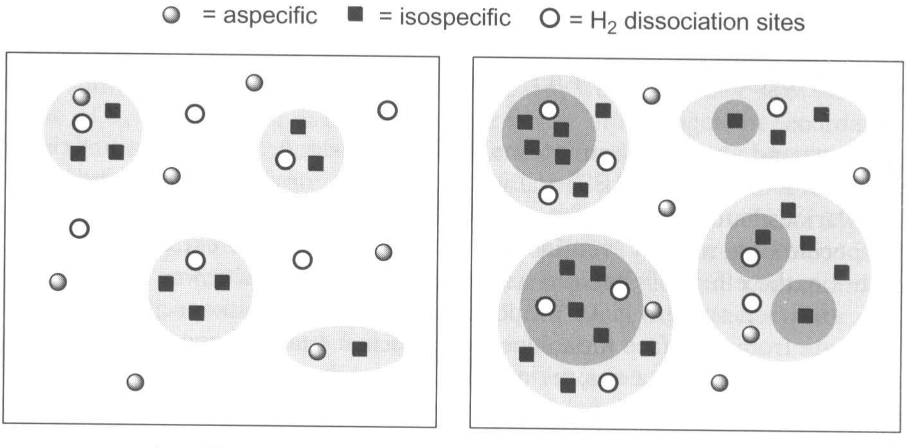

Figure 7.28 Schematic representation of Terano "island" site model for stereoselectivity and hydrogen response.

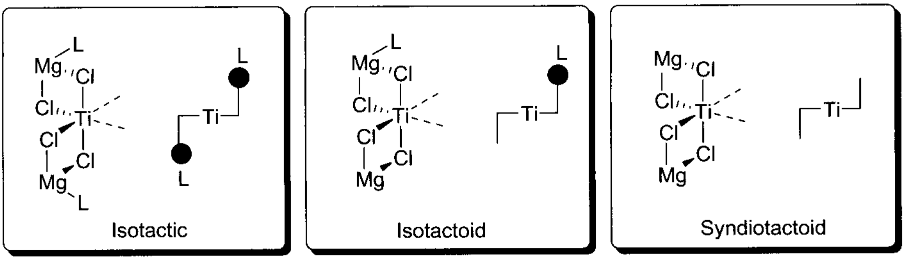

Isotactic

Isotactoid

Syndiotactoid

Figure 7.29 Busico's three-site model.

the presence or absence of steric hindrance in the vicinity of the active species. ^{13}C NMR studies have indicated[154] the presence of C_1-symmetric active species in $MgCl_2$-supported catalysts, with a mechanism of isotactic propagation which is analogous to that for certain C_1-symmetric metallocenes, in the sense that propylene insertion at a highly enantioselective site tends to be followed by chain "back-skip" rather than a less regio- and stereoselective insertion when the chain is in the coordination position previously occupied by the monomer. It is proposed that a (temporary) loss of steric hindrance from one side of an active species with local C_2 symmetry, giving a C_1-symmetric species, may result in a transition from highly isospecific to moderately isospecific propagation. Loss of steric hindrance on both sides can lead to syndiospecific propagation in which chain-end control becomes operative.

If it is considered that the steric hindrance in the vicinity of the active species can result from the presence of a donor molecule and that the coordination of such a donor is reversible, the above model provides us with an explanation for the fact that strongly coordinating, stereorigid donors typically give stereoregular polymers in which the highly isotactic sequences predominate.[155]

Recent Investigations on Magnesium Chloride Donor Interactions Recently extensive molecular modeling studies by Correa and co-workers[156] have indicated that industrially relevant internal and external donors (phthalates, diethers, alkoxy-silanes, and succinates) can be separated into two type classes. The group illustrated that diethers and alkoxysilanes have a short spacer between the coordinating oxygen atoms and coordinate preferentially to the (110) cut of $MgCl_2$. Phthalate and succinate donors have much longer distances between the coordinating oxygen atoms and thus can adopt a variety of coordination modes. In this case, the energies of coordination on the (110) and (100) cuts are much closer and, in addition to bidentate coordination to a single Mg atom on the (110) cut, bridging coordination to Mg atoms on the same or adjacent (110) monolayers is possible. The ability of succinates and phthalates to assume a number of different coordination modes on the (110) cut, adjacent to adsorbed $TiCl_4$, would be expected to lead to the formation of different active sites and is in line with the broader molecular weight distribution of polypropylene produced by catalysts containing phthalates or succinates as internal donors. It should be noted that the majority of investigations have focused on the interaction of the $MgCl_2$–$TiCl_4$ or $MgCl_2$–Lewis base. Cavallo et al. presented the first quantitative evaluation on the interaction of $TiCl_4$ with industrially relevant internal donors. Correlation was drawn between the thermodynamic functions derived from calorimetric experimental data for the complexation of $TiCl_4$ with the internal donors and catalyst efficiency, suggesting that a "somewhat higher affinity" for $TiCl_4$ is a basic requirement of a "well-performing" donor.[157]

7.3 STEREOSPECIFIC SINGLE-SITE CATALYSTS

7.3.1 Introduction

Over the past three decades there have been a large number of industrial and academic publications in the field of single-site polyolefin polymerizations. Equally impressive are the reviews and descriptive protocols for materials preparation and polymerization techniques set forth in patent. Industrial scientists in laboratories all over the world have contributed often without the recognition gained by peer-reviewed publications.[158,159] Indeed, in some instances the true inventors and contributors have been confounded due to the fact that some reviews have concentrated on scientific literature from the academic community. In some descriptions it may be considered tantamount to its rewritting. It is difficult to completely cover all of the literature; what follows is a brief description of the history through some of the major developments in this field. The reader is directed to chapters in the excellent book edited by Baugh and Canich,[160a] along with the recent reviews from Resconi,[160b] Bochmann,[160c] and Kuran[37] for further discussion.

Historical: Development of Stereospecific Metallocene Catalyst Families Stereospecific polypropylene made from single-site catalysts has always been an academic curiosity. In today's world, classic heterogeneous ZN catalysts are beyond compare in performance and cost—thus the quest for understanding the polymerization mechanism and the promise of greater control over the synthetic macromolecular process to produce new materials fuels development. Stereospecific polypropylene and copolymers made with single-site catalysts have been slowly penetrating the market share.

As we have seen above for heterogeneous ZN catalysts, the exact structure of the active species is still by no means fully resolved. What is certain is that the understanding of the underlying mechanisms and results relating catalyst structure and polymer properties have been greatly advanced due to our understanding of homogeneous single-site-catalyzed polyolefin reactions.

Wilkinson and Birmingham synthesized titanocene dichloride in 1954.[161] A single titanium atom wrapped in a defined ligand environment was considered a possible "model" for studying the heterogeneous ZN catalytic mechanism.

Applying polymerization protocols developed and commercialized for the original (ZN) experiments, however, met with limited success.[162] Polymerization reactions of bis-cyclopentadienyl titanium(IV)chloride activated with aluminum alkyls[163] as a model system did not immediately materialize.

It is probable that the metallocenes would not have taken further notice without the *serendipitous* experiments that showed that addition of water to trimethyl aluminum created a complex capable of activating titanocene dichloride. In 1979 Sinn and Kaminsky[164] reported the isolation and characterization of *the* key ingredient in making active metallocene for polyethylene polymerizations: MAO. Kaminsky, noting that Reichert and Meyer[165] and Breslow and Long[163] obtained increases in activity by adding water to Ziegler catalysts, also showed that the same metallocene (Cp_2TiCl_2) makes atactic polypropylene at commercially relevant temperature.[166] In 1982, Kaminsky published again on metallocene ethylene polymerizations and also (notably) the conversion of tires to energy (a concept before its time).[167]

Chiral ansa group IV metallocene derivatives for olefin hydrogenation having three-carbon bridges were produced as early as 1979.[168] In 1982, Wild, Zsolnai, Huttner, and Brintzinger published a paper describing the synthesis of two-carbon-bridged indenyl and tetrahydroindenyl titanium complexes.[169] Immediately after this publication became available in the open literature, interest in this complex for reasons other than for use in chiral synthetic reactions was initiated.

Isotactic Polypropylene Made from Soluble Single-Site Catalysts The first definitive example of isotactic polypropylene obtained with a single-site soluble ZN catalyst was reported in 1984 by John A. Ewen from the exxon long-range polymer group in Baytown, Texas. Discoveries of this magnitude are first reported in patent(s), as indeed this was.[170] Patent coverage using metallocenes in homogeneous olefin polymerizations was broad in scope and application. Indeed, the group of patents using metallocenes were to eventually become known within the "800 patent" family and would prove to be one of the most significant contributions in this field for many years to come.

The 1984 Ewen publication had considerable historical impact. Polymerizing propylene at *subambient temperatures* using unbridged Cp_2TiPh_2 complex activated with Kaminsky's MAO made isotactic polypropylene. This was research not at commercially relevant polymerization conditions. By analyzing the polymer *fractions* with ^{13}C NMR, the microstructure of the isotactic polypropylene was determined. Following with polymerizations using a mixture of newly reported Brintzinger's *rac-/meso-*$Et(Ind)_2TiCl_2$/MAO and by fractionating and analyzing the polymer, the microstructure of the isotactic polypropylene from this catalyst system was determined. Between the two catalytic complexes, the mechanism of polymerization was discriminated: Analysis of the chain microstructure showed a different type of mistake than that found in the conventional ZN-derived polymer which was made by a different polymerization mechanism.

From low-temperature polymerizations using Cp_2TiPh_2, insertions of monomer into the polymer chain were isospecific until a mistake was made: The mistake was propagated. Based on the mistake, the change in the orientation of the monomer being inserted was continued. The information for chirality of insertion originated from the last inserted monomer: *chain-end control.* If a monomer was inserted wrong, the mistake was continued (Figure 7.6). The result is is an example of a stereoblock-type of polymer structure made with a single-site catalyst.

Using *rac-/meso*-$Et(Ind)_2TiCl_2$/ MAO, when a misinsertion was made, the mistake was corrected: A single error in the chain was not propagated. The single isolated error is evident in the ^{13}C NMR pentad analysis which was determined for the various polymer fractions. The mechanism of polymerization for this catalyst system was controlled by the ligand and was termed *site control* (Figure 7.6).

Since this was the *very first available sample of iPP made from a single-site catalyst*, this was the first time a mechanism could be proposed to explain the synthesis of such a structure (Figure 7.30). What followed was a series of papers from the Ewen group that fulfilled the promise of single-site catalysis becoming the vehicle for determining the mechanism of coordinated olefin polymerization.

Kaminsky and others had shown that Cp_2TiCl_2-MAO makes only atactic polypropylene.[171] With the advent of a new description of single-site control from the Exxon group and with the new knowledge that Britzinger's bridged indene ligand could produce site-controlled isotactic sequences, the race to further develop this system was begun. After Ewen discovered that bridged, chiral indenes produced isotactic polymers, the very next year (1985) the laboratories from Kaminsky's group in Hamburg reported an improvement in the stability and activity of the indene complexes by altering the metal from titanium to zirconium: The activity and molecular weight of the polymer made with the *rac*-$Et(Ind)_2ZrCl_2$ catalyst system was increased. This was followed by the logical extension to hafnium as a metal center (being the next metal in

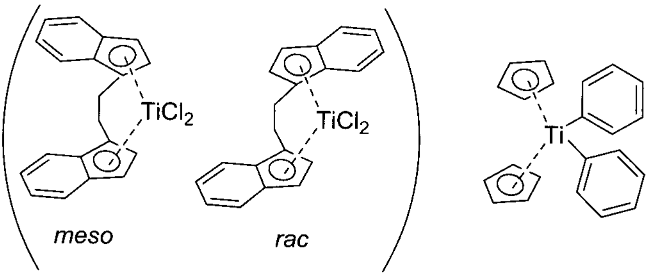

Figure 7.30 Structures of *rac-/meso*-$Et(Ind)_2TiCl_2$.

the series) which also demonstrated high activity and isospecificity. The group IV metals were tested in order. Later criticism of the original Ewen work, such as "the complex had not been cleaned," were moot. The *original* use for the ethylene bridge complex envisioned by Brintzinger was later further developed/realized in a number of synthetic processes: The study of the effectiveness in changing the ligand and modifying it's microarchitecture for controlling polyolefin polymerizations had begun.

In 1989 Mise described the synthesis and propylene polymerization using a series of bridged cyclopentadienyl complexes having methyl and *t*-butyl substitutions in a combinatorial fashion.[172] The results showed that methyl substitutions in the positions adjacent to the bridging carbon created an arrangement that increased polymer melting points. This discovery further showed that tuning the ligand geometry was possible.

In the years that followed stereo- and regiochemical control over monomer insertion into a growing polyolefin chain then achieved a penultimate success through group IV metallocenes. These early studies led to further understanding of the mechanism of polymerization and provided insight into a rational design approach for polyolefin catalyst systems.[173,174] Many modifications to the basic indene ligand were to follow, including changes to the bridging atoms and modifications to the indene structure with alkyl and aryl substituent.

After these early reports there was intense competition between research groups that created a highly motivating and creative environment for synthetic organometallic polyolefin catalysis chemistry, especially in the area of small-molecule/ligand synthesis.

Elaboration of Ansa Indenes: Silicon Bridge Isotactic polymers made in polymerizations using unsubstituted bridged indene metallocenes such as *rac*-Et(Ind)$_2$ZrCl$_2$ or *rac*-Et(H_4-Ind)$_2$ZrCl$_2$ had low melting points and low molecular weight compared to commercially relevant polymers.[175] Indene was a readily available starting material and easily purified by distillation, but synthesis in the bridging step could be complicated by the formation of cyclic by-products requiring additional purification steps. Additionally, 1,2-dibromoethane is toxic and syntheses using this compound eventually became unrecommended. A number of strategies have been put forward to address this,[176,177] and recent strategies for building *ansa* (bridged) metallocenes have been discovered.[178] Erker's group recently made photo-activated ligands capable of closing bridging substitutions in a nonreversible fashion during polymerization.[179] Aleksander, Steinhauser, and Ostoja-Starzewski have made bridging ligands in which a transition metal complexed with two ligand systems can be reversibly connected to one another through a bridge consisting of a donor and an acceptor ion pair.[180]

In the early days of polyolefin metallocene ligand evolution, changes in the basic structural geometry were envisioned where a more accessible metal center could be formed by tying back the indene ligands. The synthesis of these bridged indene complexes was facilitated by changing the bridging atom to silicon (C_2-2, Figure 7.31),[181] which makes the catalyst more rigid and increases catalyst activity. The synthesis of the dimethyl silicon bridged indenyl complexes was first synthesized by Michael Elder and filed in patent with Ewen at Fina Oil and Chemical Company. By treating indene anion with ½ equivalent of dichloro-dimethyl silane rather than 1,2-dibromoethane, the formation of cyclic by-products was avoided and the advantage in catalyst performance was substantial. The *rac*-$Me_2Si(Ind)_2ZrCl_2$ metallocene, when activated with MAO, made a higher melting point polymer and was easier to synthesize than the ethyl-bridged indenyl metallocene. When this finding was coupled with the methyl group on the cyclopentadienyl carbon adjacent to the bridging carbon (C_2-4, Figure 7.31), the activity was decreased slightly, but the polymer molecular weight was significantly increased.[182] Other groups followed with similar teachings;[183] in fact, the germanium-bridged catalyst system results in very high molecular weight polymer.[184] Brintzinger and workers at BASF synthesized a (2-methyl-4,5-benzoindene) containing ligand capable of making high-molecular-weight PP with high melting point (C_2-5, Figure 7.31).[185] This catalyst system has become one of the industry workhorses.

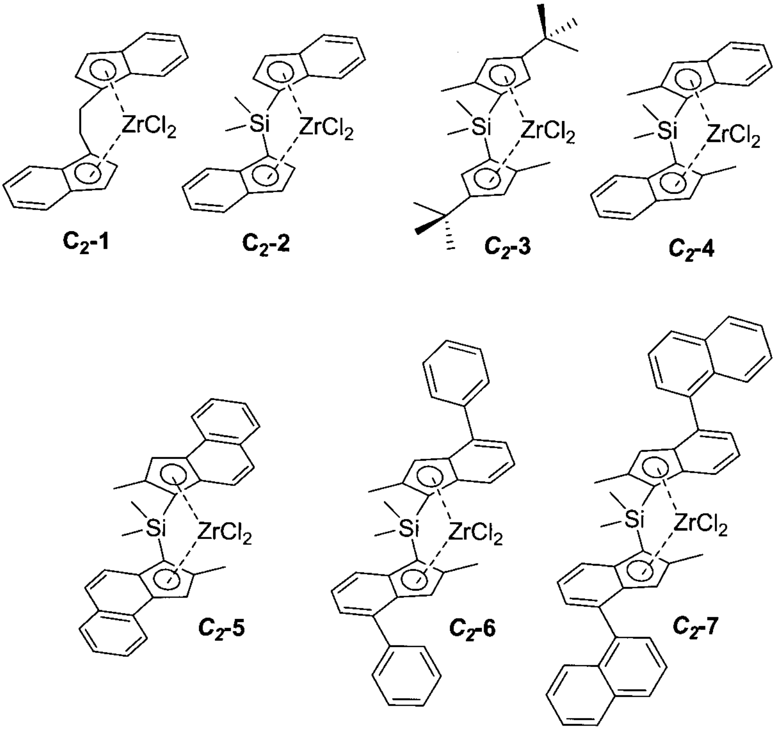

Figure 7.31 C_2-symmetric metallocenes.

Golden Standard(s): Substituted Indene Before there was combinatorial chemistry, there was a remarkable group of synthetic organometallic polyolefin catalyst chemists in the BASF and Hoechst groups in Germany. The challenge was to determine the optimum substitution pattern to produce a catalyst having high activity and making a polymer having high melting point as economically as possible. The synthesis of indenes substituted with all conceivable permutations and combinations having relevant alkyl, aryl, fused benzyl, halogen (etc.) groups eventually revealed key substitution placements providing stereo- and regiocontrol in olefin coordination. Within the decade following Ewen's first reports, Spaleck, Antberg, Rohrmann, Winter, Bachmann, Kiprof, Behm, Herrmann, and co-workers (to mention a few) modified the silyl bridged indenyl ligand framework to include a 2-methyl-4-phenylindenyl substitution pattern.[186–189] The complex containing 2-Me-4-PhInd resulted in a catalyst system that today is still a leading benchmark in metallocene polyolefin catalysis. In addition, the more annulated 2-methyl-4-napthyl indenyl substitution pattern, although more stereospecific, also predominates. Although it is impossible to know the exact structures being developed into heterogeneous commercial single-site catalysts, these types of metallocene structures have now become candidates with high probability (still being selected primary examples in numerous patent applications) and are the direct result of these early investments. The search for copolymerization catalysts which did not terminate with increasing comonomer concentration is an example. Substitution patterns on the ligands were varied strategically, eventually revealing the optimum structure through molecular modeling and testing. Figure 7.32 illustrates some of the structural developments.[190–193]

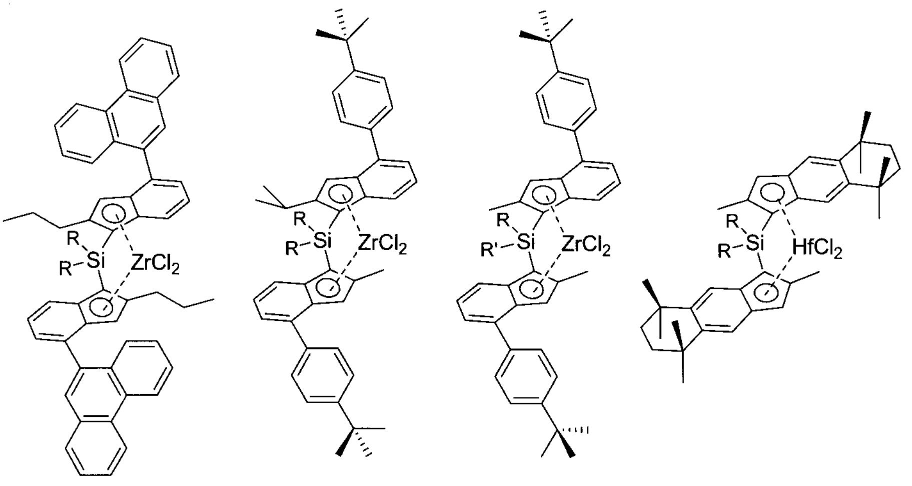

Figure 7.32 Some structural developments of metallocene catalysts.

Heterocenes In 1999, Palo Galli reassembled the team of Ewen (as a consultant), Elder, and Jones in the laboratories at the Giulio Natta Research Center in Ferrara and challenged them with the task of finding a catalyst system "better than and outside of" the 800 umbrella.

The active cationic metal center is extremely electrophilic and the list of materials that can act as catalyst poisons is legion. In the commercial plant environment, a number of tests can be run on the pipeline monomer supply to determine a culprit. Any compound having free electrons is suspect, especially sulfur. In the minds of some chemists at the time, "any compound containing a heteroatom will be stillborn."

Now at first glance, it may not seem obvious: The sulfur electrons can be "tied up" in an aromatic system. In fact, this allows the framework of a heterocycle containing, for example, nitrogen or sulfur to act as an architectural building block rather than an electron sink. Catalysts made with heteroatoms which have their electrons tied up in such a fashion are *not* stillborn (Figures 7.33 and 7.34).

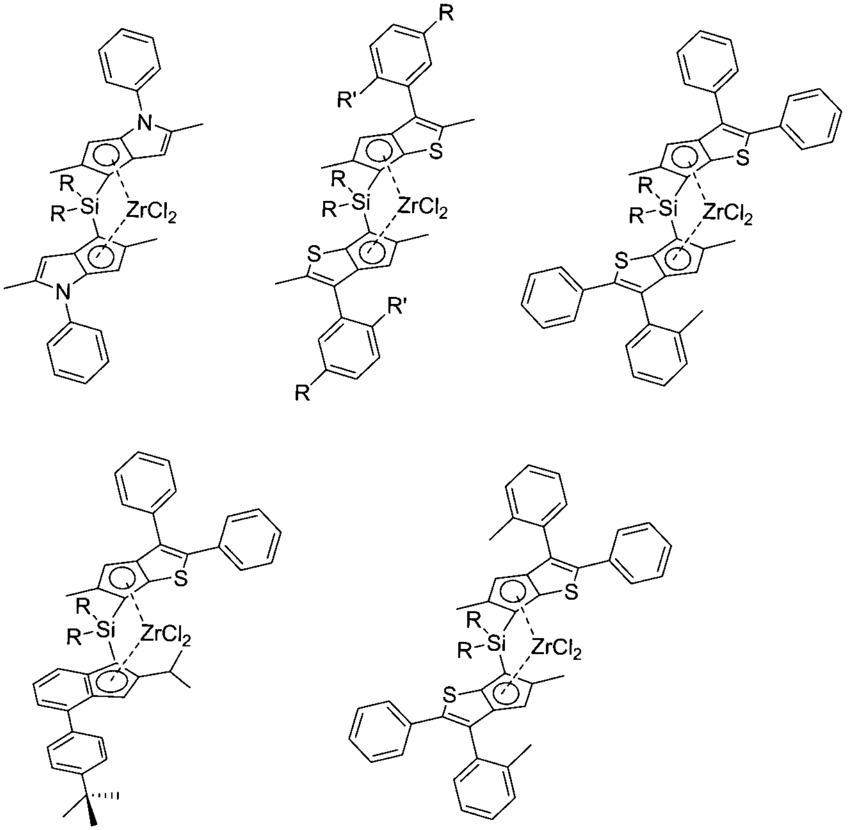

Figure 7.33 Representative heterocenes.

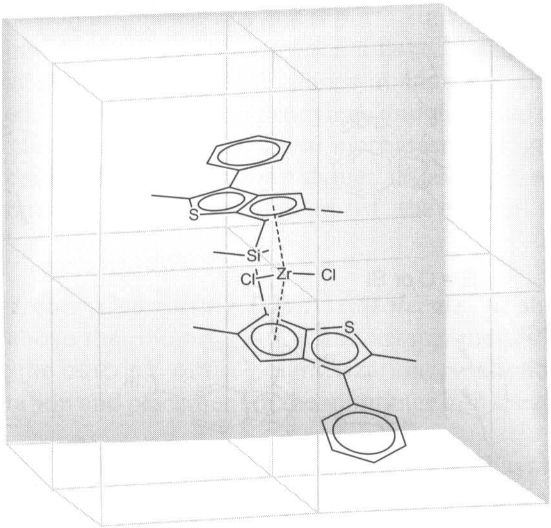

Figure 7.34 Heterocene catalyst containing sulfur.

Cyclopentadiene ring–fused heterocycles were called "heterocenes" and were first synthesized in the Montell Polyolefins Catalyst Laboratories of Albizatti and Resconi at the Giulio Natta Research Center in Ferrara Italy in the fall of 1996. The first heterocene complex was made and tested and the first patents were filed in the fall of that year[194] just months before the competitors filed similar disclosures.[195]

These first complexes were only examples of things to come.[194] After shuffling between the continents and following repatriation of the group to the Montell North American Research and Development center in Elkton, Maryland (prior to the formation of Basell), the team of Ewen, Elder, and Jones synthesized the heterocene analogs of the Hoechst "carbocenes."[196] Results from the polymerizations with these materials proved to have the highest activity and stereospecificities of any known to date,[197–200] including the simpler *t*-butyl-substituted indenes later reported by Resconi.[201]

Syndio- and Hemitactic Polymers In the laboratories of Fina Oil and Chemical Co. in Deer Park, Texas, in 1985, the synthesis of $H_2C(Cp)(Flu)$ ligand was followed in 1986 by the synthesis of the organometallic complex. The ligand was made by the reaction between dimethylfulvene and fluorine anion. The addition of $ZrCl_4$ to the [iPr(Cp)(Flu)] ligand dianion was done under the direction of John Ewen, who conceived it, directed the synthesis of the ligand and catalyst system,[201,202] and was the first to recognize the polymer made from the activated catalytic complex as having syndiotactic sequences. Numerous studies have been done on these polymers, and they have been slowly creeping out of the laboratory into commercial production. They still

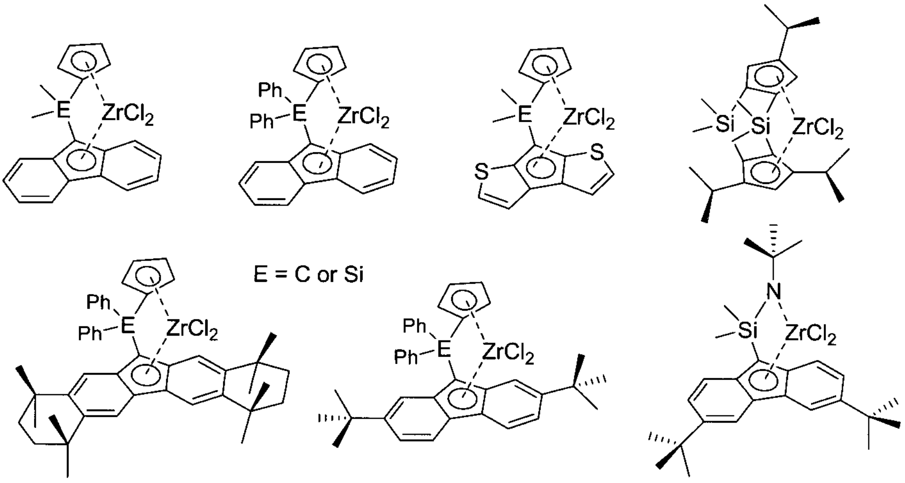

Figure 7.35 C_s-symmetric metallocenes.

remain mostly an intellectual curiosity whose main result was to deepen the understanding of the reaction mechanism.

It was a logical extension to begin substitutions onto the C_s symmetric structure of the iPrCpFluMCl$_2$ syndiospecific catalyst, just as with the indenes (Figure 7.35).[203] Addition of a methyl group in the frontier of the cyclopentadienyl ring produced polypropylene with hemi-isotactic tacticity in which every other stereocenter is random: An isotactic structure is found on every other asymmetric carbon atom.[204]

In substituting phenyl groups onto the bridging carbon, the syndiotactic catalyst became more rigid, producing much higher molecular weight syndiotactic polymer.[205] Substitutions onto the fluorine, such as *tert*-butyl groups, succeded in increasing catalyst solubility and activity.

More recent improvements over and beyond the basic structure of the original iPr(Cp)(Flu)MCl$_2$ complex have made syndiotactic polymer stereosequences of even higher distribution than was originally possible. In an extension of the ring systems, The Miller Group at the University of Florida has been able to produce syndiotactic polymer having elevated (near-theoretical) melting points.[160] Further simple substitutions onto the cyclopentadienyl ring, such as isopropyl, benzyl, or trimethyl-silyl, did not produce dramatic changes in polymer structure;[206] however, substitution onto the cyclopentadienyl group with a *tert*-butyl group (in the 3-position) was shown by Elder and Ewen to produce isotactic polypropylene. By crowding one side of the catalyst so that the growing polymer chain was forced to back-skip without adding a monomer, a predictable result was obtained (isotactic polypropylene). The advantage in this system is that, although the active sites are distereotopic, only iPP is produced: rac–meso isomers are not formed in the synthesis of the complex and therefore no isomer separation is necessary.[207,208]

Hemi-isotactic polypropylene was first reported in 1982 made by a two-step synthesis starting from *trans*-2-methylpentadiene.[209] The C-1 symmetric metallocene first synthesized by R. L. Jones at Fina Oil and Chemical Co. directly produced hemi-isotactic polypropylene and provided further evidence for previously described polymerization mechanisms (Figure 7.36). Basic studies characterizing this interesting polymer followed,[210] while the rest of the work culminated in the assignment of the Ewen symmetry rules (Figure 7.36).[208]

Switches and Motors: Controlling Catalyst Molecule It should be evident from all of the above that the orientation and arrangement of the ligand dramatically affect the outcome of the polymerization: Nonbonding interactions direct the orientation and placement of the monomer into the growing polymer chain.

In a remarkable discovery in 1995, Coates and Waymouth (Stanford University in California) described a catalyst which had the ability to change ligand geometries during the polymerization reaction, thereby affecting monomer placement, that is, the tacticity of the polymer chain was changed during the polymerization reaction.[211] Unbridged oscillating catalysts (Figure 7.37) were made from substituted indenes. The initial mechanism postulated free rotation of the indene ligands during the chain growth, alternating between an isotactic stereospecific catalyst center and an atactic catalyst. The

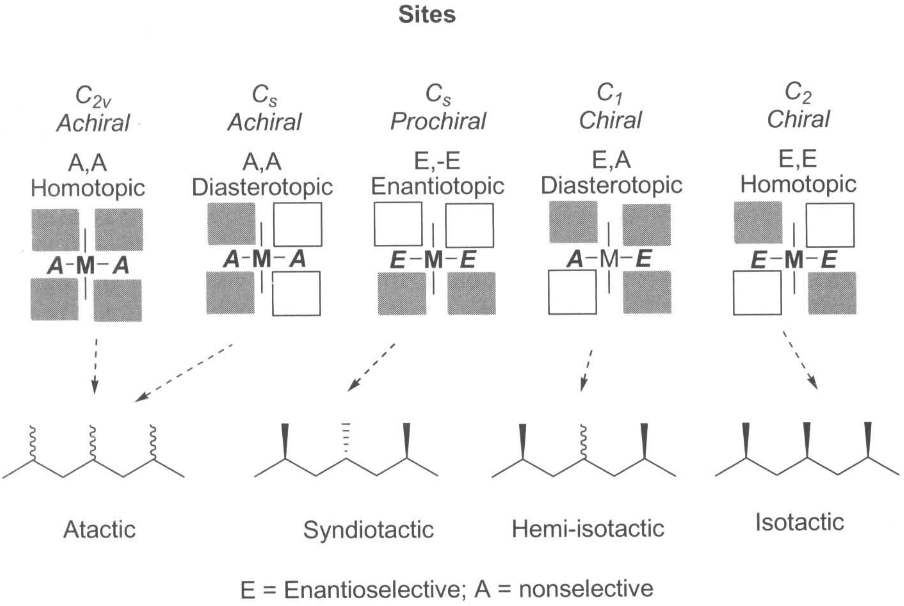

Figure 7.36 Ewen's symmetry rules.

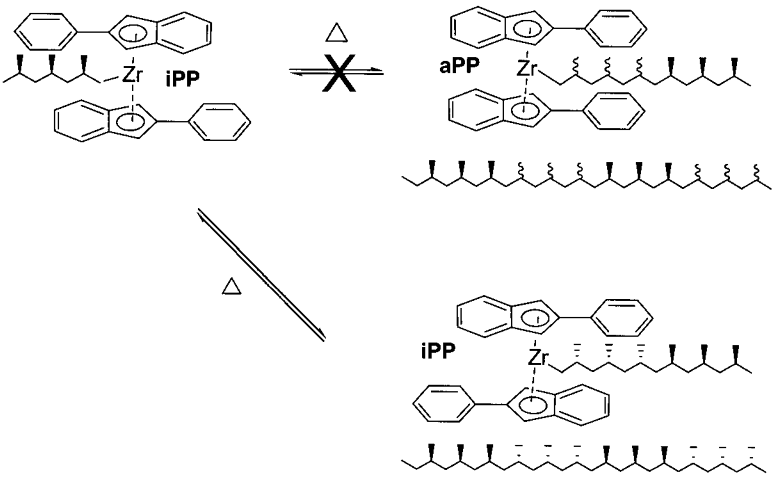

Figure 7.37 Waymouth/Coates oscillating metallocenes.

polymer was believed to have a single chain having isotactic and atactic blocks along the polymer backbone. The resultant polymer was elastomeric. Subsequent studies have shown that the the oscillation is between two racemates forming stereoblocks of isotactic sequences.[212]

Further control and synthesis of stereoblock polymer were demonstrated by Miller and Bercaw, who demonstrated the further utility of the iPrCpFluZrCl$_2$ catalyst system by substituting an adamantyl group onto the Cp ring in the 3-position, attaching the adamantyl group in such a way that it could rotate in and out of the reaction sphere during the polymerization reaction, thereby affecting the polymerization result.[213] In this case, a block isotactic–hemi-isotactic polymer was formed (Figure 7.38). This was further studied in heterocene models.[214]

In neither of the above cases–the Coates–Waymouth *unbridged oscillating aryl substituted indenes* or the Miller–Bercaw *rotating adamantyl-substituted Cp-Flu* complexes—is the orientation of the fluxional portion of the ligand molecule controlled. The control over the rotating (changing) motion is in the hands of statistics: a Boltzmann distribution of the population of molecules which exist in any one configuration at the time of monomer insertion. In order to further exploit the advantage of control over the ligand geometry, a catalyst having a photochromic switch which was capable of geometric changes based on external activation (photon input by choice) was developed at the Basell Polyolefins Molecular Design Laboratories in Höechst, DE, in 2005 (Figure 7.39). For this catalyst system, a change in ligand geometry was controlled by addition of a certain wavelength of radiation (UV or otherwise) to the polymerization reaction, causing predictable changes in the geometry of a ligand via the closing or opening of a photochromic switch.[215]

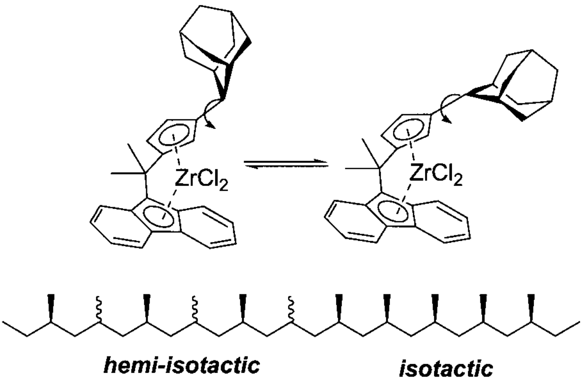

Figure 7.38 Bercaw/Miller oscillating metallocenes.

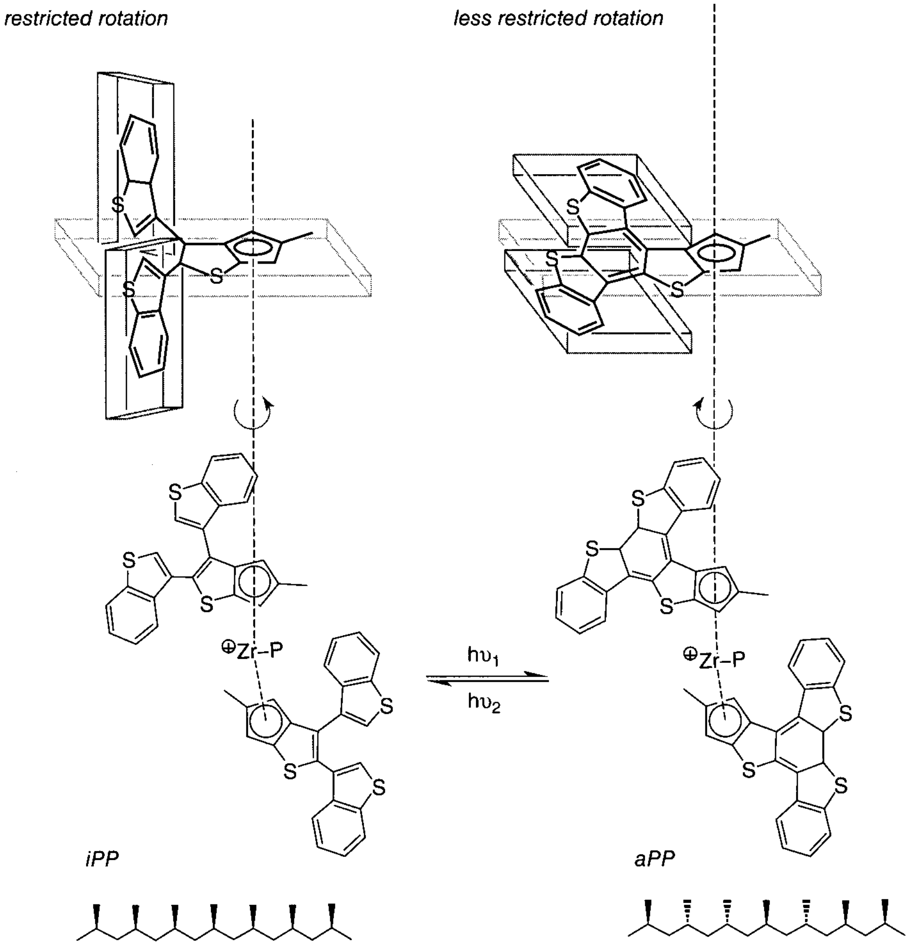

Figure 7.39 Jones photochromic metallocenes.

Postmetallocenes In remarkable discoveries in the advent of postmetallocene catalytic complexes, a group of scientists at Mitsui and simultaneously at Cornell University in New York discovered a phenoxy imine ligand system capable of producing syndiotactic polypropylene. Like the metallocene, versatility in the substitution patterns of the ligand can affect the polymerization result (activity and stereotacticity),[216,217] but the key parameters have been determined. Subsequent developments have led to postmetallocenes capable of producing highly isotactic polypropylene, some with appreciable activity (Figure 7.40).[218–222]

7.3.2 Heterogenization of Single-Site Catalysts

It became evident, during the development of single-site α-olefin polymerization catalysts, that the homogeneous catalysts required heterogenization in such a way as to avoid fouling, allow continuous operation, and retain the desired polymer properties in such processes. As one can imagine, it is quite a challenge to achieve "true" single-site behavior on a heterogeneous catalyst particle, and in practice supported single-site catalysts often give somewhat broader distributions as a result of generating multiple active sites or (co)

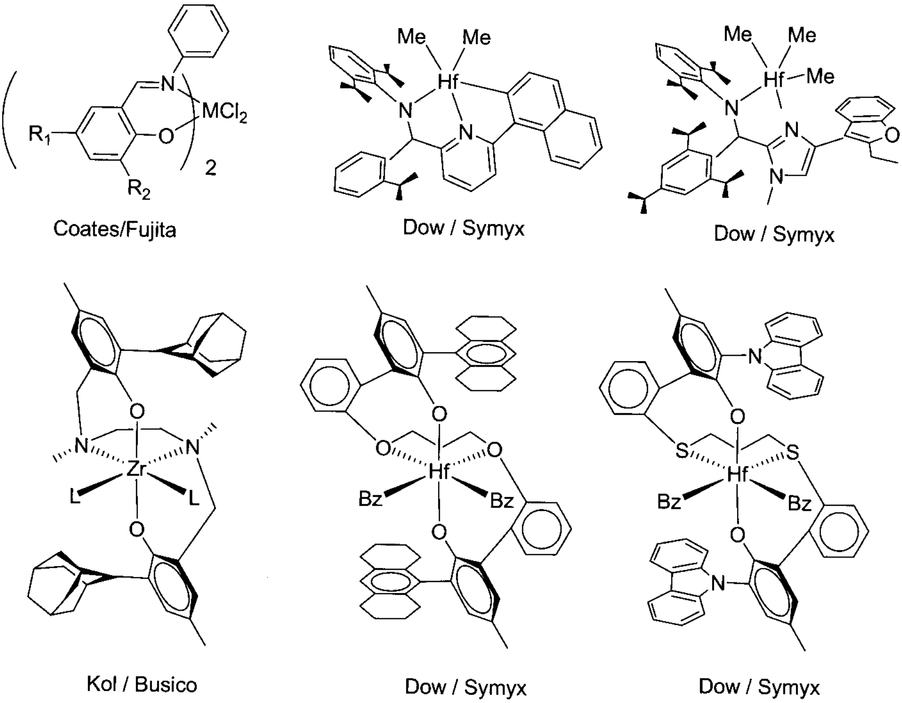

Coates/Fujita

Dow / Symyx

Dow / Symyx

Kol / Busico

Dow / Symyx

Dow / Symyx

Figure 7.40 Selected stereoselective postmetallocenes.

monomer concentration gradients within the particle. However, there may be some tolerance to a deviation from true single-site behavior if it does not adversely affect the desired polymer properties. It is this wish to capture the unique polymer performance package offered by the polymer resin derived from single-site catalyts that has led to the "art" of immobilizing or heterogenizing becoming an area of intense research.[223–225]

At the outset of developing a commercial/industrial immobilization strategy for a single-site PP precatalyst, it is important to take into account and balance several different factors that could affect the success of the intended catalyst. The first consideration is the targeted polymer resin. It is important to consider that the polyolefin industry ultimately sells the property package of a plastic product and not a particular polymer resin. If the property package of the targeted single-site catalyst resin can be achieved at a more economical cost by a traditional ZN-based resin or by blending/additive combination, then it will be. The targeted resin may also put requirements on the polymerization process in terms of multimodal features. The target resin strongly dictates the choice of single-site precatalysts, particularly for PP resins with high molecular weight coupled to good comonomer incorporation (random PP) or isotacticity (PP) demands.

The plethora of recipes and protocols which exist for synthesizing classic heterogeneous ZN catalyst systems is rivaled by the number of combinations possible for single-site catalyst systems. Without insider information it is unlikely that the exact organometallic structure being commercially advanced by any company can be known. Trade secrets and information such as which ligand, metal center, support, and activator system are being used are cards kept close to the chest. Information gleaned from trade journals and scientific and patent literature provides only an overview. It is the goal of this chapter not to fully review every preparation that has been employed but to provide selective illustrative examples of the more relevant supports and synthetic strategies. For more detailed discussion the reader is directed to references 223–225.

There are numerous supports that have been employed in the heterogenization of single-site catalysts. Inorganic supports are typically based on inorganic oxides, such as silica, alumina, and mesoporous material (MCM and SBA) or clays and magnesium chloride. Organic supports are almost exclusively based on a polymer matrix.

The preparation of a heterogeneous single-site PP catalyst is typically achieved by employing one of three basic strategies: grafting, tethering, and physisorbtion. Grafting and tethering can be further broken down depending on whether the precatalyst or cocatalyst is either grafted or tethered (Figure 7.41).

Grafting onto Inorganic Supports There are numerous individual synthetic strategies that have been employed to produce a catalyst from a combination of MAO, silica, and precatalyst complex. Typically, only two routes are

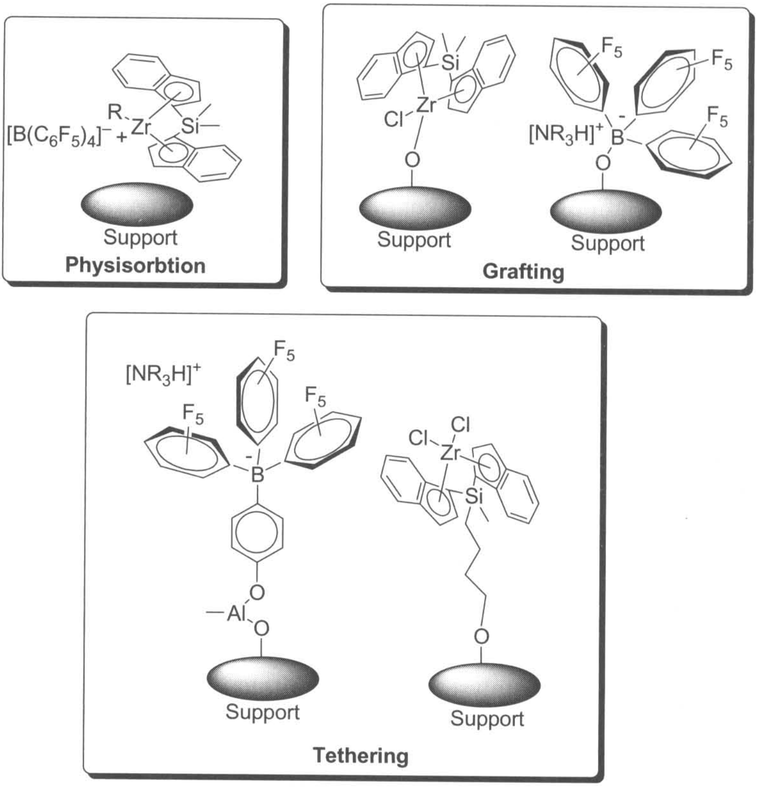

Figure 7.41 Strategies for immobilization of single-site system.

employed in industrial applications. In the first route (**A**, Figure 7.42) the MAO or alkyl aluminum source can first be contacted to the silica, while the precatalyst complex (or MAO-activated precatalyst complex) is introduced in a subsequent step. The second route (**B**, Figure 7.42), involving the activation of the precatalyst with MAO prior to impregnation of the silica, is one of the simplest and most effective methods. There is no universally recommended route for all precatalysts and as a result a considerable amount of investigative research is needed to find the optimum preparation for a particular precatalyst family and polymerization process combination.

In route **A**, as with all synthetic procedures, the target is to effectively immobilize the catalysts onto the surface of the silica and avoid the possibility for the leaching of active species into the polymerization medium. Improving the fixation of MAO to the silica surface is typically accomplished by some form of heat treatment regime and/or washing steps. An example of this can be seen in the work of Gauthier and co-workers at Fina, who disclosed that refluxing the silica/MAO toluene suspension prior to contact with a C_2- or

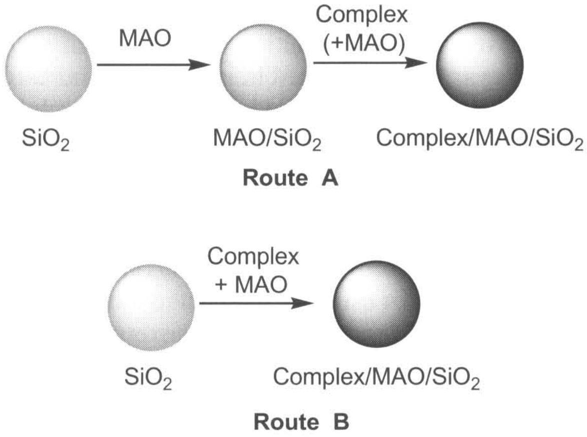

Figure 7.42 Routes to MAO/complex immobilization on inorganic oxide.

C_1-symmetric metallocene improved the fouling tendencies while in addition increasing the stereoselectivity and activity of the finished catalyst and yielding polymer resins with good bulk density and morphology.[226] The catalyst efficiency was strongly related to the temperature used in supporting the metallocene onto the MAO-treated silica. Higher catalytic activities of the finished catalysts were observed when low contact and washing temperatures (–20 to 0 °C) were employed during the fixation of the metallocene. The group also discovered that the silica support plays a crucial role in the final activity of the catalyst system. Interestingly, the group proposed that a large "critical pore diameter" (CPD), defined as the pore volume after contacting the silica pore with MAO and complex, is crucial to achieving high activity and the appropriate CPD is facilitated by a combination of heat fixation of MAO and an appropriate support.

Route **B** has several advantages, particularly from an industrial viewpoint. It reduces the amount of solvent used and by-products produced. It also has limited amount of steps, particularly time- and energy-intensive steps such as drying. All these benefits typically result in a low manufacturing cost. In addition, precontacting allows MAO to solubilize poorly soluble precatalyst prior to impregnation and finally can allow more effective activation of the metal center (for certain complexes) to be carried out in a homogeneous solution rather than a heterogeneous phase, where problems with diffusion or side reaction may occur. A highly successful example of the above procedure was disclosed by Burkhardt and co-workers at Exxon.[227] In this protocol a metallocene precatalyst was initially contacted with a solution of MAO prior to contact with calcined silica (800 °C, 8 h, N_2 flow). The slurry of metallocene/ MAO/SiO_2 was then mixed together, while the temperature was gradually elevated (~50 °C). During heating vacuum is applied above the suspension, while a slight N_2 purge is applied below to remove the solvent and afford a viscous mixture. At this point the heating was gradually increased and the temperature held at ~65 °C for an additional 3 h to afford a dry free-flowing catalyst. The catalyst was then reslurried in isopentane and carefully prepolymerized to yield the finished catalyst. Collaborative research between Exxon and Höechst led to a successful combination of the precatalyst and immobilization technologies.[228–230]

The difficulty in supporting the Spaleck and Brintzinger family of precatalysts was illustrated in subsequent studies by the groups of Mülhaupt[231,232] and Kaminsky.[233] The study investigated and compared the isoselective polymerization of propylene using a supported catalyst, SiO_2/MAO/*rac*-Me_2Si(2-Me-Benz[e]Ind)$_2ZrCl_2$,[232] and the corresponding homogeneous system, concentrating particularly on the influence of monomer concentration, polymerization medium, temperature, and scavenger on polymerization kinetics and polypropylene properties. The supported systems possessed lower activities and yielded resins of lower molecular weight and lower melting point, resulting from an increased number of stereo- and regioerrors—all of which led the group to conclude that mass and heat transfer was important for a supported catalyst when high-bulk-density polypropylene was formed. Similar results were also reported by Kaminsky and co-workers for the polymerization of propylene using *rac*-Me_2Si(2-Me-4-(1-Napth)Ind)$_2ZrCl_2$ as a precatalyst in conjunction with MAO or MAO/SiO_2.[233] In addition the group studied the supported catalyst in various polymerization processes, such as toluene slurry, bulk monomer, and gas phase (NaCl and PE mechanical stirred fluidized bed). The latter gas-phase process resulted in a more stable polymerization, especially at elevated temperatures.

Modifications to the basic procedure of adding a MAO/precatalyst solution to a silica support have been reported to afford dramatic improvements in activity and/or morphological control. Removal of the gel fraction of a MAO solution via decantation or filtration, prior to contact with the metallocene precatalyst, has been claimed to lead to polymer resin of superior morphology and particle size distribution when compared to their gel-containing counterparts.[234,235] Allowing a solution of MAO and *rac*-Me_2Si(2-Me,4-PhInd)$_2ZrCl_2$ to stand in the dark overnight before addition to silica is also reported to lead to an almost doubling of activity of catalysts derived from immediate contact with the support.[236]

Pacification of the silica surface with an alkyl aluminum complex prior to contact with a solution of MAO/precatalyst is commonly encountered, particularly for commercially applicable stereoselective complexes. This is probably due to the fact that the highly tailored metal centers of such complexes can be easily perturbed by steric and/or electronic influences of the support material.[237] Pacification of silica by an alkyl–aluminum complex has also been reported to improve final catalyst performance in the bulk-phase polymerization of propylene. Fritze and co-workers used triethylaluminum (TEA) and triisobutylaluminum (TIBA) treatments to pacify various commercial silica supports that had previously been dried in vacuo at 140 °C. The pacified silica was then treated with a solution of *rac*-$Me_2Si(2\text{-}Me\text{-}4\text{-}PhInd)_2ZrCl_2$ and MAO followed by isolation. The catalysts were then compared in the bulk-phase homopolymerization of propylene to catalyst systems prepared by contact of the precatalyst with commercial or preparative MAO/SiO_2 activator. Higher activity was reported for the catalyst prepared on the pacified supports, affording polymer resins with fewer stereo- and regioerrors, a higher melting point, and similar molecular weight and molecular weight distribution compared to the unpacified system.[238]

If the alkyl aluminum complex is MAO, then one could consider this as a "hybrid" version of routes **A** and **B**. While it may be beneficial, such a route may add further complexity or flexibility, as one has to consider what fraction of the total MAO should be added at the silica and precatalyst steps. The delicate balance has been elegantly demonstrated by Winter and co-workers at NTH.[239] The group started with a set amount of silica, MAO, and *rac*-Me_2Si(2-Me-Benz[*e*]Ind$)_2ZrCl_2$, but differed the fractions of the total MAO to be added to the silica and *rac*-Me_2Si(2-Me-Benz[*e*]Ind$)_2ZrCl_2$ stages to produce a number of catalysts ranging in productivities from 3.3 to 8.7 kg PP/g Cat·h. In addition, the group investigated the effects of heat treatment and washing of the MAO/silica. Once again a heat treatment of the MAO/SiO_2 is extremely beneficial in terms of catalyst productivity when one compares preparations. However, the percentage of the total amount of MAO added to the silica or complex before heat treatment was also critical. The catalyst with the highest productivity demonstrates the potential cumulative benefits of such a route and is achieved by a combination of a high percentage of the total MAO contacted with silica followed by heat treatment and washing of the resultant product before the addition of the complex previously contacted with a low percentage of the total MAO. Those skilled in the art will understand that there may be considerable variation in the SiO_2–MAO–complex ratios found in each of the final catalysts, despite the set ratio used in the total synthesis. However, this example clearly demonstrates the complexity/flexibility one has by combining together a set amount of one complex, one type of MAO [manufacturer, wt %, degree hydrolysis, and residual trimethylaluminum (TMAL)] on one type of silica [pore volume (P.V.), average particle size (APS), surface area (S.A.), and calcination temperature] in various different ways.

Recent efforts to support the metallocene/MAO catalyst have involved to use of silica chemically modified by an inorganic complex. Speca, for example, reported the chemical treatment of silica by solid $[NH_4][X]$ (X = F, SiF_6, PF_6, or BF_4), which followed a heat treatment regime to afford a modified silica.[240] The modified silica was then treated with a metallocene/MAO solution affording catalysts that were up to three times more active than comparative "unmodified" examples in the bulk polymerization of propylene. Similarly, Welch and co-workers pretreated uncalcined silica with borax in methanol.[241] The support was then dried, calcined at 800 °C, and treated with TMA prior to contact with a solution of MAO/Me_2Si(2-Me-Benz[e]Ind$)_2ZrCl_2$ to give systems which were more active in the homopolymerization of propylene.

C_2-symmetric metallocenes confined inside the pores of zeolites (MCM-41 or VPI-5) have been used to prepare isotactic polypropylene with higher stereoregularities, molecular weights, and melting points than the corresponding homogeneous and silica-supported system.[242–245] The pore size of the support has also been shown to strongly influence polymerization stability, molecular weights, and stereoregulaties. Similar increases in stereoregularity, melting points, and molecular weights have also been observed for syndiotactic polypropylene formed with MCM-41-supported $Me_2C(Cp)(Flu)ZrCl_2/MAO$ systems.[246–248] Once again the initial aluminum content of the MCM-41 has a considerable influence on the catalytic performance.[247] Various MCM-41 and SBA 15 materials have been used in the absorptive separation of MAO. Interestingly, the stereoregularity of the polypropylene resins formed by a homogeneous solution of *rac*-$Et(Ind)_2ZrCl_2$ and absorbent (MCM-41s or SBA-15) filtered MAO was markedly dependent on the pore size of the absorbent material.[249,250]

Grafted trispentafluorophenyl borate activators (similar to those outlined in Figure 7.40) have been reported.[251–254] Of note are the disclosures by Vizzini and Chudgar on the silica-supported diethylanilinium borate, which when treated with *rac*-$Me_2Si(2\text{-}Me\text{-}4\text{-}PhInd)ZrMe_2$ polymerized propylene to relatively high activities, 8.6 kg PP/g Cat, and narrow polydispersities, $M_w/M_n = 2.44$.[251] In addition, boralumoxane complexes reported by Kratzer, Fritz, and co-workers have formed silica-supported boralumoxane or anilinium boralumoxate complexes capable of activating dialkyl metallocenes.[255,256]

The physisorption of boron-activated systems on a silica surface, previously pacified by an alkylaluminum or alkylaluminoxane complex, has proven to be an efficient means of producing polymerization systems that operate very effectively in the particle-forming processes. Good morphology, without leaching or reactor fouling, has been observed for the majority of these systems, despite the absence of an apparent link between the support and pre- or cocatalysts. The active species are associated to the surface support via electrostatic or van der Waals interactions. As a result, the polarity of the synthesis solvent and polymerization medium is of critical importance. There are three synthetic protocols to physisorb boron-activated systems. These procedures differ in their order of addition, with the boron-containing cocatalyst, the metal precatalyst, or an activated combination of the two being initially contacted with the pacified surface of the support.

Hlatky et al. reported the use of calcined, TEA-pacified silica in conjunction with $[HNMe_2Ph][B(C_6F_5)_4]$ or $[CPh_3][B(C_6F_5)_4]$ and a dimethylhafnocene complex.[257–259] Calcined silica (800 °C) is treated with TEA to form a pacified silica containing approximately 2 wt % aluminum. Addition of a stoichiometric mixture of dimethylhafnocene and either $[HNMe_2Ph][B(C_6F_5)_4]$ or $[CPh_3][B(C_6F_5)_4]$ in toluene formed a supported ionic catalyst system following removal of toluene in vacuo. However, it was reported to be preferable to first support the borate cocatalyst prior to contact with the dimethylhafnocene. In the latter route the pacified silica is treated with a solution of the cocatalyst dissolved in either CH_2Cl_2 ($[HNMe_2Ph][B(C_6F_5)_4]$) or warm toluene ($[CPh_3][B(C_6F_5)_4]$). The solid activators were analyzed by low-voltage scanning electron microscopy following the removal of the volatiles in vacuo and were found to contain no crystallites of the borate complex (50-Å level) on the surface, suggesting even distribution throughout the support. Pentane slurries of the supported borate could then be treated with Cp_2HfMe_2 or *rac*-$Me_2Si(Ind)_2HfMe_2$, generating an active catalyst. The *rac*-$Me_2Si(Ind)HfMe_2$ system was also used to polymerize propylene with high activities in bulk monomer (80 kg PP/mmol Zr·h) or gas phase (440 g PP/g Cat).

A further example can be seen in the work reported by Fritze and co-workers.[260] Addition of TMA to *rac*-$Me_2Si(2\text{-}Me\text{-}4\text{-}PhInd)_2ZrCl_2$ prior to addition of dimethylanilinium bis(2,2′-octafluorobiphenyl)borate and subsequent admixing with a TIBA-pacified silica led to higher catalyst productivities (48 kg PP/g metallocene·h) in the bulk-phase polymerization of propylene than the corresponding *rac*-$Me_2Si(2\text{-}Me\text{-}4\text{-}PhInd)_2ZrMe_2$ catalyzed species (37 kg PP/g metallocene·h).

Tethering onto Inorganic Supports Tethering of the precatalyst is infrequently employed in the immobilization of single-site PP catalysts. The main drawback of such a procedure is the complicated and numerous synthesis procedure required, which adds substantial expense to an immobilization strategy. Suzuki and co-workers produced a pseudo C_2-symmetric silyl bridged zirconocene compound with a chlorodimethylsilylethyl functional group on the bridging silicon via hydrosilylation of the vinyl-substituted starting material, $(CH_2{=}CH_2)MeSi(1,3\text{-}Me_2Cp)_2ZrCl_2$.[261,262] The chlorosilyl functional group is believed to react selectively with the surface silanol and was supported by a model study carried out using $^tBuMe_2SiOH$ instead of silica, which obtained the expected modified zirconocene compound with a Si–O–Si linkage. Hydroboration of $(CH_2{=}CH_2)MeSi(1,3\text{-}Me_2Cp)_2ZrCl_2$ with BH_3 and subsequent reaction with a vinyl-coated silica, or vice versa, also produced immobilized precatalysts. The precatalyst formed via the hydroboration procedure, when utilized in propylene polymerization, gave higher activity and stereoregularity and a narrower polydispersity than those produced via the hydrosilylation route.

Brintzinger and co-workers reported the pretreatment of dehydroxylated silica with $4\text{-}ClCH_2C_6H_4Si(OMe)_3$ yielding a silica that quartenizes the amino group(s) in $Me_2Si(2\text{-}NMe_2\text{-}Ind)_2ZrCl_2$ to form an ionic metallocene which was active in the polymerization of propylene in combination with MAO.[263]

Polymer Bound There has been considerable interest in polymer-bound α-olefin polymerization precatalysts and this has led to the development of numerous, often elaborate routes to supported pre- and cocatalysts.[264] It is believed by some that polymer supports possess properties ideally suited to the immobilization of single-site α-olefin polymerization catalysts. This derives from the belief that a polymer support is more chemically compatible support relative to silica and other inorganic supports. Additionally, the catalytic species reside within a mobile hydrocarbon-rich matrix, providing a polymerization microenvironment that more closely resembles a homogeneous solution polymerization. Polymer supports are also very versatile materials in terms of the incorporation of functional groups and cross-link densities. Lightly cross-linked polymers can also swell, allowing access to the inner core of the particle during functionalization. A fine line has to be trod, however, when considering cross-link density, as too low a level may lead to formation of a particularly soluble or dimensionally unstable carrier particle and too high a level may hinder particle fragmentation. Typical polymeric supports include polystyrene, polysiloxanes, and polyolefin-based materials.

Resin-bound metallocenes have been produced by the copolymerization of styrene with a vinyl-functionalized ancillary ligand. For example, Alt and coworkers copolymerized 2-vinylfluorene with styrene using a free-radical initiator (AIBN or $BF_3{\cdot}OEt_2$).[265,266] The fluorine-containing copolymers could then be modified to form resin-bound metallocene. Fully formed ligand sets have also been copolymerized with styrene using AIBN as an initiator (Figure 7.43). The zirconocene complexes derived from the copolymers were used to produce syndiotactic polypropylene with relatively high stereospecificity.[267]

Solid ionic cocatalysts have been prepared by covalently binding the anion or cation to a support resin. Covalently bound anions have been prepared by the AIBN-inititated copolymerization of $[Cat][B(C_6F_5)_3(C_6H_4CH{=}CH_2)]$ (Cat = $HNMe_3$ or $HNMe_2Ph$) with styrene or pentafluorostyrene (Figure 7.44).[268] The polymer-bound ionic cocatalyst could then be used to activate and immobilize various zirconocene dichloride/TIBA systems. These activated catalysts were subsequently used to produce iPP resins in a slurry phase, with an absence of reactor fouling.

The use of tertiary amine-functionalized polystyrene as polyionic counterions to $[B(C_6F_5)_4]^-$ has been reported to form immobilized ionic catalyst systems for a range of dimethyl-metallocenes.[269] Roscoe and Fréchet developed a polystyrene-supported trialkylammonium–borate bound to the poly-

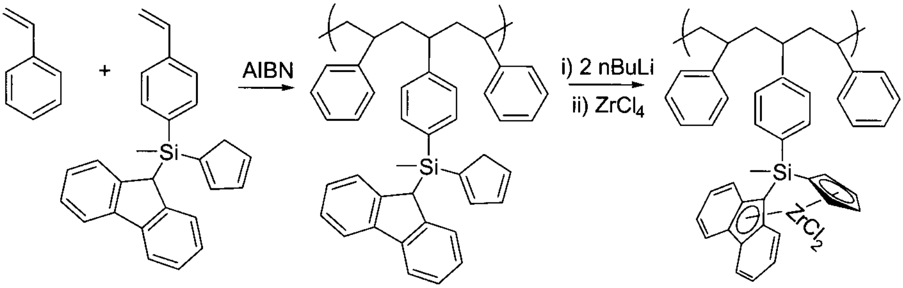

Figure 7.43 Polystyrene-immobilized metallocene.

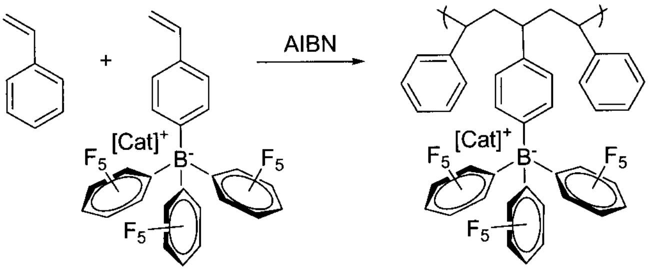

Figure 7.44 Polystyrene-immobilized borate.

styrene via a benzyl-amine group.[269] Treatment of the functionalized support with a solution of a dimethyl metallocene led to an immobilized catalyst system in which the active species is not chemically bound to the support. The polymer support, however, has a higher dielectric constant than the surrounding polymerization medium, discouraging catalyst leaching. High activity was observed for propylene polymerization; however, good morphology was shown to be polymerization temperature and/or metallocene precatalyst dependent.

Resconi et al. reported the introduction of three different polar functionalities to cross-linked polystyrene.[270] Chemical modification of the polystyrene support was performed by either chloromethylation, lithiation, then treatment with CO_2 or acylation with CH_3COCl-$AlCl_3$ followed by reduction with $NaBH_4$ to afford polystyrene supports containing either an acetoxyl, carboxyl, or hydroxyl functional group, respectively. The supports were then used to encapsulate a preactivated *rac*-Et(Ind)$_2$ZrCl$_2$/MAO catalyst. Polymerization experiments with these supported systems demonstrated that sufficient cross-linking of the initial support is required to prevent reactor fouling.

Vizzini used virtually the same supported cocatalysts to activate *rac*-Me$_2$Si(2-Me-4-PhInd)$_2$ZrMe$_2$ for the homopolymerization of propylene.[271] Comparative polymerization experiments were made between the polystyrene-supported borate and a silica-immobilized [HNMe$_2$Ph][B(C$_6$F$_5$)$_4$]. The polystyrene-supported systems were found to be less active than the corresponding silica-supported system. Additionally, the iPP produced had a molecular weight an order of magnitude lower, with a broader molecular weight distribution but a higher melting temperature.

Fait et al. immobilized a C_2-symmetric metallocene system onto porous polyethylene and polypropylene supports.[272] Higher catalyst loadings were achieved for the polyethylene systems, and while this led to a higher catalyst productivity in terms of kg PP/g Cat, the polypropylene-encapsulated catalyst demonstrated greater activity in terms of kg PP/g Zr. The synthesis of functionalized polystyrene capable of immobilizing a metallocene/MAO system can also be achieved by the postmodification of polystyrene resin.

Porous functionalized polyolefin support materials capable of fixating a high loading of metallocene/MAO catalysts have become accessible. One such support material is maleic anhydride–grafted polypropylene, which has been utilized by Sunaga and co-workers to immobilize MAO.[273] Several PP-supported MAO systems with differing MAO loadings dependent on the extent of maleic anhydride grafting were prepared and used as supported activators for various metallocene precatalysts in the polymerization of propylene. Polar functionalized polypropylene-supported catalysts with higher catalyst loading capabilities than the corresponding unfunctionalized support have also been reported.[274]

As mentioned previously, the majority of polystyrene supports are cross-linked with a rigid linker, such as divinylbenzene. Finding the optimal level of cross-link density is therefore important in terms of particle stability and fragmentation. Recently, Klapper and co-workers have proposed the novel solution of reversible cross-links to combat this problem.[275–279] The first strategy developed involved the use of cyclopentadiene-functionalized polystyrene resin in which the cyclopentadiene moieties undergo a Diels–Alder reaction with each other to form a cross-linked support.[275,276] The supports were additionally functionalized with methoxy or PEO groups to noncovalently encapsulate the metallocene/MAO complex. The supported catalysts showed good activity and produced polymer products with improved morphology in propylene homopolymerization. The improvement in morphology was attributed to an enhanced particle fragmentation brought on by the retro-Diels–Alder cleavage of the dicylopentadiene cross-links under polymerization conditions. The protic polymer-bound cyclopentadiene moiety generated during the retro-Diels–Alder reaction has seemingly little effect on the catalytic performance. Further development by the group has led to the synthesis of polystyrene latex nanoparticles containing functionalized PEO or PPO chains on the surface. These uniform and well-defined primary nanoparticles (80–300 nm) were then reversibly aggregated by the interaction of a metallocene/MAO complex to form a secondary catalyst particle.[277–279] The catalyst particles evenly fragmented during polymerization via the production of polyolefins in the boundary between the primary particles (Figure 7.45). The concept has been extended to borate-activated metallocenes, with the incorporation of 4-vinylpyridine groups into the latex particles and pacification and reversible cross-linking of the PEO or PPO chains by AlR_3.[277]

Multicomponent Catalysis Combinations of a ZN catalyst with a metallocene catalyst as well as two or more different metallocenes have been utilized in heterogeneous propylene polymerization and have recently been expertly reviewed by Friederichs and co-workers.[280] As the tacticity and/or comonomer can vary considerably between ZN and single-site catalysts or between single-site catalysts themselves—numerous possible combinations can be imagined. The following section concentrates solely on multicomponent catalysts that are constructed on the same support/carrier.

One of the first examples of a multicomponent system was reported by Dong et al.[281] The group applied a combined ZN/metallocene system in a

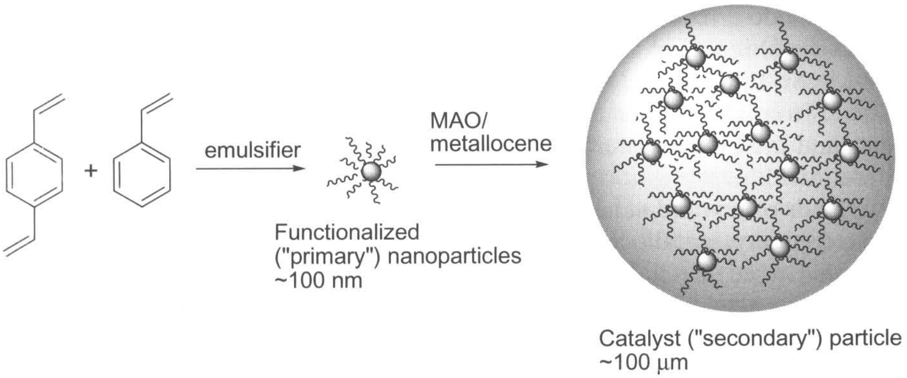

Figure 7.45 Klapper's reversible cross-linking concept.

two-stage process for the production of iPP. The metallocene catalyst was dormant during the first stage and was activated in the second stage by the addition of a suitable cocatalyst. Similiarly, Lee et al. contacted a $MgCl_2/TiCl_4/$ di-isobutylphtalate ZN catalyst with *rac*-$Et(Ind)_2ZrCl_2$.[282] The multicomponent system possessed lower propylene polymerization productivity when compared to the untreated ZN catalyst. However, the isospecificy was higher even in the absence of an external donor.

Speca and McAplin have outlined some of the merits of using mixed metallocenes for iPP.[283] This group illustrates that differences in hydrogen and ethylene response of the individual metallocenes cause, for example, the MWD to respond to different hydrogen or ethylene levels. Whereas narrow MWD m-iPP can have some specific advantages in certain applications, m-iPP prepared using mixed metallocenes might fit better into the broad application window of conventional ZN-iPP. Binary catalysts for obtaining reactor blends of isotactic polypropylenes with broadened MWD have been prepared by the consecutive impregnation of *rac*-$Me_2Si(H_4\text{-}Ind)_2ZrCl_2$ and *rac*-$Me_2Si(2\text{-}Me\text{-}Ind)_2ZrCl_2$ onto MAO-modified silica. Mehta et al. reported an isotactic polypropylene product with broad or bimodal MMD using a dual metallocene catalyst system supported on MAO/SiO_2 in a cascaded process.[284,285] The applied conditions in the cascaded reactors were different with respect to temperature and/or ethylene content. This cascaded procedure resulted in a blend of at least four different polymers which differed in molar mass and/or ethylene content.

Reactor blends of syndiotactic polypropylene with broadened MMD have been formed by coimpregnation of $Ph_2C(Cp)(Flu)ZrCl_2$ and $Me_2C(Cp)(2,7\text{-}{}^tBu_2\text{-}Flu)ZrCl_2$.[286] A dual-supported metallocene catalyst for sPP is reported to increase the activity over that for a single-supported metallocene catalyst and to produce sPP having a relatively broad MWD.[287] In addition, preparation of sPP/iPP reactor blends from a mixture of a stereorigid isospecific metallocene and a stereorigid syndiospecific metallocene on MAO/SiO_2

has been described by Fink et al.[288] and Shamshoum et al.[289] Maques and co-workers reported a binary system based on $Ph_2C(Flu)(Cp)ZrCl_2$ and *rac*-$Me_2Si(2\text{-}Me\text{-}4PhInd)_2ZrCl_2$ cosupported on MAO/SiO_2..[290] They concluded from DSC evaluation of the polymers made with the individual catalysts and the binary system that possible stereoblock formation had occurred (vide infra).

Blends of iso- and atactic polypropylene have also been reported with supported binary metallocene systems based on $Cp_2ZrCl_2/Me_2Si(Ind)_2ZrCl_2$[291] and *rac*-$Et(Ind)_2ZrCl_2/Et(Flu)_2ZrCl_2$ or *rac*-$Me_2Si(Ind)_2ZrCl_2/Et(Flu)_2ZrCl_2$.[292] Similarly, reactor blends of isotactic and elastomeric polypropylene have been reported using a system synthesized by the impregnation of a *rac*-$Et(Ind)_2ZrCl_2$/MAO solution onto $Zr(CH_2{}^tBu)_4/Al_2O_3$.[293]

An interesting development in the polypropylene area has been reported by Zhu et al. Via the combined action of an unsupported aspecific bis(imino) pyridyl iron catalyst and the iso-specific *rac*-Me_2Si(2-MeBenz[*e*]Ind)$_2ZrCl_2$, they obtained a polymer consisting of an iPP backbone with aPP branches.[294] However, in order to obtain branched PP, it was necessary to introduce the bis(imino)pyridyl iron catalyst first followed by the zirconocene being more of a staged process, whereas simultaneous addition of the components did not produce branched PP. The authors hypothesized that the iPP produced by the zirconocene encapsulates the catalyst and forms a kind of diffusion barrier for the aPP produced by the iron catalyst. Another example of in situ versus ex situ grafting is described by Dekmezian et al.[295] They also observed better grafting efficiencies when using a consecutive procedure, which was subsequently rationalized by modeling the concentration of macromers in both procedures.

The novel, emulsion-based heterogenization method has been utilized by Tynys et al. to prepared multicomponent propylene catalysts.[296] The catalyst combinations investigated were *rac*-$Me_2Si(2\text{-}Me,4\text{-}PhInd)_2ZrCl_2$/*rac*-Et(2-$Me_2{}^tBuSiO\text{-}Ind)_2ZrCl_2$/MAO (mix 1) and *rac*-$Me_2Si(2\text{-}{}^iPr\text{-}4\text{-}Ph(3,5\ Me_2)$ $Ind)_2ZrCl_2$/MAO (mix 2). The effects of polymerization temperature and hydrogen on catalyst performance and polymer properties as well as copolymerization with hexene and ethylene were investigated. Depending on the polymerization conditions, the M_w of polypropylene varied considerably and produced broader molecular weight distribution (MWD) for mix 2, and a bimodal MWD with clearly separated low- and high-M_w polymer fractions was observed with mix 1. Additionally the group reported that the catalyst systems showed similar hydrogen and hexene responses. Each metallocene precursor showed individual response toward the polymerization conditions, especially polymerization temperature, suggesting that interaction between the catalyst active sites was negligible in the studied systems.

Multicomponent Catalysts for Block Copolymers Chien et al. postulated alkylaluminum-mediated chain transfer as one of the possible explanations for the presence of stereoblock PP when they used a mixture of *rac*-$Me_2Si(Ind)_2ZrCl_2$

and $Et(Flu)_2ZrCl_2$ cosupported on SiO_2.[297] Fink and co-workers cosupported the syndiospecific *i*-$Pr(Flu)(Cp)ZrCl_2$ and the isospecific *rac*-$Me_2Si(Ind)_2ZrCl_2$ on MAO/SiO_2.[288] They obtained a blend consisting of sPP, iPP, and stereoblock PP. The stereoblock formation was proposed to be mediated by chain transfer via aluminum. They concluded that simultaneous impregnation of the different metallocenes was more effective in generating stereoblocks compared to consecutive impregnation. Brintzinger et al. have shown that stereoblock polypropylene is attainable via a mixture of different unsupported metallocenes using aluminum-mediated chain shuttling and they demonstrated that the rate of chain transfer to aluminum and the back transfer from aluminum to a metallocene cation depend on the steric environment of the metallocene and aluminum compounds.[298]

7.4 CONCLUSION

The dominant position of ZN catalysts in the manufacture of stereospecific polyolefins, in particular PP, is likely to continue for the foreseeable future, despite the extraordinary effort and developments in the field of metallocene and other single-site catalysis. It will hopefully be clear that the composition and characteristics of a traditional ZN catalyst must be tailored to yield systems with the capacity to produce the required polymer molecular structure and properties. The ability to control catalyst particle size, morphology, and porosity has orchestrated the development of advanced and versatile polymerization process technologies to a point where the characteristics of the catalyst can be tuned to both process and product requirements.

Traditional ZN catalysts are complex systems and are still by no means fully understood, but significant advances in their basic understanding are continually being made. The sheer size of the polypropylene market and the ability to extend polypropylene into new areas will ensure that research in this area continues. Developments in the areas of high-throughput experimentation, polymer and catalyst characterization, and molecular modeling studies have and will provide additional mechanistic insight, which in turn can be applied in the further development and implementation of these catalysts.

In single-site catalysis, the structure of the ligands surrounding the metal results in unique monomer placements. The structure of this catalyst in turn strongly influences the structure of the macromolecule one can obtain and consequently the polymer properties of the resultant resin. We have described examples of single-site catalysts that have an enviable ability to impart control over the molecular structure of macromolecular synthesis. From sequence and monomer placement/orientation or with comonomer chemical composition distribution, the final material property originates from controlling the complex interplay of factors surrounding the exploitation of the metal center. Research into stereoregular single-site catalysts continues to generate a great deal of interest in organometallic complexes with the specific purpose of providing well-defined olefin placement. Furthermore, the study of single-site catalysts and the mechanisms of olefin polymerization has opened a Pandora's box to a kalidoscope of kinetically controlled reactions and side reactions most of which can be manipulated, in terms of either catalyst structure or polymerization conditions, to produce a myriad of previously unattainable polymer microstructures.

Despite the fact that single-site catalysts may not become large-volume commodity polyolefin producers, as avenues for producing well-defined stereospecific macromolecules having designed structures, they are currently the method of choice. It is also worth mentioning that there is always something over the horizon: the next generation or the next big discovery. For example, metallocenes have attained a status as a special class of polyolefin catalysts receiving substantial monetary attention. Synthetic chemistries, activators, supports, and reactors have been designed and engineered for making stereoregular polymeric materials using metallocenes. Simpler, equally elegant and effective structures are beginning to enter stage right and it would be brave to predict that commercial stereospecific polymers derived from single-site catalysts will not become more prevalent; after all, the market for designer polymers and copolymers which can only be made from defined catalytic centers is lucrative and substantial: a pirate's trove waiting to be exploited.

In conclusion, if one considers the infinite range of macromolecular structures, for present and future polymer types and grades that can be produced via heterogeneous stereospecific polymerization catalysis, there is ample space for further development and implementation. In this light both ZN and single-site catalyst technologies become complimentary rather than competing catalyst technologies.

REFERENCES

1. Borealis Polymers OY, www.borealisgroup.com.
2. Wikepedia.org, http://en.wikipedia.org/wiki/World_population.
3. Plastic Europe presentation, Resource efficiency: Best Practices for the recovery of plastics waste in Europe, available: http://www.plasticseurope.org/DocShareNoFrame/docs/2/GIIMCBMCEHJFEIMGANJEHFGNKTHNH7V9V6473AR4KL9O/PlasticsEurope/docs/DLS/PresentationASBAPExternalFINALSeptember2007-20071009-007-EN-v1.pdf.
4. Pasquini, N., Ed., *Polypropylene Handbook*, 2nd ed., Hanser Publishers, Munich, 2005, p. 15.
5. Lieberman, R., and Stewart, C., in *Encyclopedia of Polymer Science and Technology*, Wiley, New York, 2002.
6. Arlman, E. J., and Cossee, P., *J. Catal.*, **1964**, 3, 99.
7. Brookhart, M., and Green, M. L. H., *J. Organomet. Chem.*, **1983**, 250, 395.
8. Laverty, D. T., and Rooney, J. J., *J. Chem. Soc. Faraday Trans. I*, **1983**, 79, 869.
9. Resconi, L., Cavallo, L., Fait, A., and Piemontesi, A., *Chem. Rev.*, **2000**, 100, 1253.

10. Busico, V., and Cipullo, R., *Prog. Polym. Sci.*, **2001**, 26, 443.
11. Krentsel, B. A., Kissin, Y. V., Kleiner, V. J., and Stotskaya, L. L., *Polymers and Copolymers of Higher α-Olefins*, Hanser Verlag, New York, 1997.
12. Tullock, C. W., Tebbe, F. N., Mülhaupt, R., Ovenall, D. W., Setterquist, R. A., and Ittel, S. D., *J. Polym. Sci. Pt. A Polym. Chem.*, **1989**, 27, 3063.
13. Nesterov, G. A., Zakharov, V. A., Volkov, V. V., and Myakishev, K. G., *J. Mol. Catal.*, **1986**, 36, 253.
14. King, S. A., and Schwartz, J., *Inorg. Chem.*, **1991**, 30, 3771.
15. (a) Lefebvre, F., Thivolle-Cazat, J., Dufaud, V., Niccolai, G. P., and Basset, J.-M., *Appl. Catal A.*, **1999**, 182, 1; (b) Dufaud, V., and Basset, J.-M., *Angew. Chem.*, **1998**, 37, 806.
16. De Rosa, C., Auriemma, F., Spera, C., Talarico, G., and Gahleitner, M., *Polymer*, **2004**, 45, 5875.
17. Giannetti, E., Nicoletti, G. M., and Mazzocchi, R., *J. Polym. Sci. Polym. Chem. Ed.*, **1985**, 23, 2117.
18. Pellecchia, C., Grassi, A., and Zambelli, A., *J. Mol. Catal.*, **1993**, 82, 57.
19. Simonazzi, T., and Giannini, U., *Gazz. Chim. Ital.*, **1994**, 124, 533.
20. Covezzi, M., and Mei, G., *Chem. Eng. Sci.*, **2001**, 56, 4059.
21. Pitkänen, P., Jääskeläinen, P., Borges, N., and Vestberg, T., *Abstr. Nordic Polym. Days*, Helsinki, Finland, June 24–26, 2000, p. 15.
22. Bartke, M., in *Tailor-Made Polymers: Via Immobilization of Alpha-Olefin Polymerization Catalysts*, Severn, J. R., and Chadwick, J. C., Eds., Wiley-VCH, Weinheim, 2008.
23. McKenna, T. F., and Soares, J. B. P., *Chem. Eng. Sci.*, **2001**, 56, 3931.
24. Ziegler, K., Breil, H., Holzkamp, E., and Martin, H., DE 973626, *Chem. Abstr.*, **1960**, 54, 14794.
25. Natta, G., Pino, P., Corradini, P., Danusso, F., Mantica, E., Mazzanti, G., and Moraglio, G., *J. Am. Chem. Soc.*, **1955**, 77, 1708.
26. (a) Cerruti, L., *HYLE-Int. J. Philos. Chem.*, **1999**, 1, 3; (b) Porri, L., *Macromol. Symp.*, **2004**, 213, 1.
27. Albizzati, E., Cecchin, G., Chadwick, J. C., Collina, G., Giannini, U., Morini, G., and Noristi, L., in *Polypropylene Handbook*, 2nd ed., Pasquini, N., Ed., Hanser Publishers, Munich, 2005, 15.
28. Natta, G., Corradini, P., and Allegra, G., *J. Polym. Sci.*, **1961**, 51, 399.
29. Boor, J., *Ziegler-Natta Catalysts and Polymerizations*, Academic, New York, 1979.
30. Giannini, U., *Makromol. Chem. Phys. Suppl.*, **1981**, 5, 216.
31. Hermans, J. P., and Henrioulle, P., Solvay & Cie., U.S. Patent No. 4,210,738, 1972.
32. Goodall B. L., in *Polypropylene and other Polyolefins. Polymerization and Characterization*, van der Ven, S., Ed., Elsevier, Amsterdam, 1990, p. 1.
33. Bernard, A., and Fiasse, P., in *Catalytic Olefin Polymerization*, Keii, T., and Soga, K., Eds., Elsevier, Amsterdam, 1990, p. 405.
34. Rishina, L. A., Vizen, E. I., and Dyachkovsky, F. S., *Eur. Polym. J.*, **1979**, 15, 93.
35. Van der Ven, S., *Polypropylene and Other Polyolefins: Polymerization and Characterization*, Elsevier, Amsterdam, 1990.

36. Kashiwa, N., *J. Polym. Sci. Pt. A Polym. Chem.*, **2004**, 42, 1.
37. Kuran, W., in *Principles of Coordination Polymerisation*, Wiley, New York, 2001, p. 43.
38. Chadwick, J. C., in *Encyclopedia of Polymer Science and Technology*, Wiley, New York, 2002.
39. Galli, P., Luciani, L., and Cecchin, G., *Angew. Makromol. Chem.*, **1981**, 94, 63.
40. Barbè, P. C., Cecchin, G., and Noristi, L., *Adv. Polym. Sci.*, **1986**, 81, 1.
41. Galli, P., Barbè, P. C., Guidetti, G. P., Zannetti, R., Martorana, A., Marigo, A., Bergozza, M., and Fichera, A., *Eur. Polym. J.*, **1983**, 19, 19–24.
42. Gerbasi, R., Marigo, A., Martorana, A., Zannetti, R., Guidetti, G. P., and Baruzzi, G., *Eur. Polym. J.*, **1984**, 20, 967–970.
43. Giunchi, G., and Allegra, G., *J. Appl. Crystallogr.*, **1984**, 17, 172.
44. Mori, H., Sawada, M., Huguchi, T., Hasebe, K., Otsuka, N., and Terano, M., *Macromol. Rapid Commun.*, **1999**, 20, 245.
45. Marigo, A., Marega, C., Zannetti, R., Morini, G., and Ferrara, G., *Eur. Polym. J.*, **2000**, 36, 1921.
46. Busico, V., Causà, M., Cipullo, R., Credendino, R., Cutillo, F., Friederichs, N., Lamanna, R., Segre, A., and Van Axel Castelli, V., *J. Phys. Chem. C*, **2008**, 112, 1081.
47. Boero, M., Parrinello, M., Weiss, H., and Hueffer, S., *J. Phys. Chem. A*, **2001**, 105, 5096.
48. (a) Corradini, P., Busico, V., and Guerra, G., in *Transition Metals and Organometallics as Catalysts for Olefin Polymerization*, Kaminsky, W., and Sinn, H., Eds., Springer-Verlag, Berlin, 1988, p. 337; (b) Busico, V., Corradini, P., De Martino, L., Proto, A., Savino, V., and Albizzati, E., *Makromol. Chem.*, **1985**, 186, 1279.
49. Lee, J. W., and Jo, W. H., *J. Organomet. Chem.*, **2007**, 692, 4639.
50. Monaco, G., Toto, M., Guerra, G., Corradini, P., and Cavallo, L., *Macromolecules*, **2000**, 33, 8953.
51. Seth, M., Margl, P. M., and Ziegler, T., *Macromolecules*, **2002**, 35, 7815.
52. Brambilla, L., Zerbi, G., Nascetti, S., Piemontesi, F., and Morini, G., *Macromol. Symp.*, **2004**, 213, 287.
53. Brambilla, L., Zerbi, G., Piemontesi, F., Nascetti, S., and Morini, G., *J. Mol. Catal. A Chem.*, **2007**, 263, 103.
54. Sacchi, M. C., Tritto, I., Shan, C., Mendichi, R., and Noristi, L., *Macromolecules*, **1991**, 24, 6823.
55. Liu, B., Nitta, T., Nakatani, H., and Terano, M., *Macromol. Chem. Phys.*, **2002**, 203, 2412.
56. Fregonese, D., Mortara, S., and Bresaola, S., *J. Molec. Catal. A Chem.*, **2001**, 172, 89.
57. Baulin, A. A., Novikova, Y. I., Mal'kova, G. Y., Maksimov, V. L., Vyshinskaya, L. I., and Ivanchev, S. S., *Polym. Sci. USSR*, **1980**, 22, 205.
58. Kashiwa, N., and Yoshitake, J., *Makromol Chem.*, **1984**, 185, 1133.
59. Chien, J. C. W., and Wu, J. C., *J. Polym. Sci. Polym. Chem. Ed.*, **1982**, 20, 2461.
60. Weber, S., Chien, J. C. W., and Hu, Y., *J. Polym. Sci. Pt. A Polym. Chem.*, **1989**, 27, 1499.

61. Sergeev, S. A., Poluboyarov, V. A., Zakharov, V. A., Anufrienko, U. F., and Bukatov, G. D., *Makromol. Chem.*, **1986**, 187, 243.
62. (a) Noristi, L., Barbè, P. C., and Baruzzi, G., *Makromol. Chem.*, 1991, 192, 1115; (b) Parodi, S., Nocci, R., Giannini, U., Barbè, P. C., and Scatà, U., Montedison, European Patent No. 45977, 1982.
63. Spaether, W., Lynch, J., Rösch, J., and Hemmerich, R., ABB Lummus Global, U.S. Patent No. 7,232,785, 2007; (b) Spaether, W., Novolen Tech. Holdings, PCT International application WO 2004016660, 2004; (c) Kerth, J., Zolk, R., and Hemmerich, R., BASF Aktiengesellschaft, U.S. Patent No. 5,162,465 1992; (d) Zolk, R., Kerth, J., and Hemmerich, R., U.S. Patent No. 5,006,620, 1991.
64. Kioka, M., and Kashiwa, N., Mitsui Petrochemical Industries, U.S. Patent No. 4,952,649, 1990.
65. Mao, B., Yang, A., Zheng, Y., Yang, J., and Li, Z., Beijing Inst. Chem., European Patent No. 0,258,485, 1992.
66. (a) Job, R. C., Shell Oil Co., U.S. Patent No. 5,077,357, 1991; (b) Job, R. C., and Goodall, B. L., Shell Oil Co., European Patent No. 0,159,736, 1989.
67. Arzoumanidis, G. G., Johnson, B. V., Karayannis, N. M., Khelghatian, H. M., and Lee, S. S., Amoco Corp., European Patent No. 0,250,230, 2002.
68. Terano, M., Soga, H., and Kimura, K., European Patent No. 0,268,685, 1988.
69. Mao, B., Yang, X., Li, Z., and Yang, A., China Petrochemical, Chinese Patent No. CN 1091748, 1994.
70. Invernizzi, R., and Ligorati, F., Enchimica Secondaria, U.S. Patent No. 4,506,027, 1985.
71. Iiskola, E., and Koskinen, J., Neste Oy, U.S. Patent No. 4,829,034, 1989.
72. Karbasi, A. K., Leinonen, T., and Sormunen, P., European patent application 0,627,449 A1, 1994.
73. Koskinen, J., and Jokinen, P., PCT application 9319100, 1993.
74. Sozzani, P., Bracco, S., Comotti, A., Simonutti, R., and Camurati, I., *J. Am. Chem. Soc.*, **2003**, 125, 12881.
75. Auriemma, F., and De Rosa, C., *Chem. Mater.*, **2007**, 19, 5803.
76. Sacchetti, M., Govoni, G., and Ciarrocci, A., Himont, U.S. Patent No. 5,221,651, 1993.
77. Cecchin, G., Morini, G., and Pelliconi, A., *Macromol. Symp.*, **2001**, 173, 195.
78. Govoni, G., Ciarrocci, A., and Sacchetti, M., U.S. Patent No. 5,231,119, 1993.
79. Cecchin, G., Guglielmi, F., Pellicani, A., and Burgin, E., Himont, U.S. Patent No. 5,286,564, 1994.
80. Garoff, T., Leinonen, T., and Iiskola, E., Neste Oy, European Patent No. 0,586,390, 1992.
81. Leinonen, T., and Denifl, P., Borealis Polymers Oy, European Patent No. 1,273,595, 2003.
82. Rönkkö, H.-L., Knuutilla, H., Denifl, P., Leinonen, T., and Venäläinen, T., *J. Molec. Catal. A Chem.*, **2007**, 278, 127.
83. Abboud, M., Denifl, P., and Reichert, K-H., *Macromol. Mater. Eng.*, **2005**, 290, 1220.
84. Vestberg, T., *Advances in Polyolefins: 2007*, ACS Conference Proceedings, 2007, Santa Rosa, CA.

85. Chang, M., Liu, X., Nelson, P. J., Munzing, G. R., Gegan, T. A., and Kissin, Y. V., *J. Catal.*, **2006**, 239, 347.
86. Härkönen, M., Seppälä, J. V., and Väänänen, T., in *Catalytic Olefin Polymerization*, Keii, T., and Soga, K., Eds., Elsevier, Amsterdam, 1990, p. 87.
87. Proto, A., Oliva, L., Pellecchia, C., Sivak, A. J., and Cullo, L. A., *Macromolecules*, **1990**, 23, 2904.
88. Okano, T., Chida, K., Furuhashi, H., Nakano, A., and Ukei, S., in *Catalytic Olefin Polymerization*, Keii, T., and Soga, K., Eds., Elsevier, Amsterdam, 1990, p. 177.
89. Seppälä, J. V., Härkönen, M., and Luciani, L., *Macromol. Chem.*, **1989**, 190, 2535.
90. Härkönen, M., and Seppälä, J. V., *Stud. Surf. Sci. Catal.*, **1990**, 56, 87.
91. Härkönen, M., Seppälä, J. V., and Väänänen, T., *Macromol. Chem.*, **1991**, 192, 721.
92. Härkönen, M., and Seppälä, J. V., *Macromol. Chem.*, **1992**, 193, 1413.
93. Härkönen, M., Seppälä, J. V., and Salminen, H., *Polym. J.*, **1995**, 27, 256.
94. Härkönen, M., Seppälä, J. V., Chûjô, R., and Kogure, Y., *Polymer*, **1995**, 36, 1499.
95. Kakugo, M., Miyatake, T., Naito, Y., and Mizunuma, K., *Macromolecules*, **1988**, 21, 314.
96. Sacchi, M. C., Forlini, F., Tritto, I., Mendichi, R., Zannoni, G., and Noristi, L., *Macromolecules*, **1992**, 25, 5914.
97. Ishimaru, N., Kioka, M., and Toyota, A., European Patent No. 0,350,170, 1990.
98. Chadwick, J. C., Van Kessel, G. M. M., and Sudmeijer, O., *Macromol. Chem. Phys.*, **1995**, 196, 1431.
99. Chadwick, J. C., *Macromol. Symp.*, **2001**, 173, 21.
100. Yoshikiyo, M., Fukunaga, T., Sato, H., Machida, T., Ikeuchi, H., Yano, T., and Tanaka, Y., Ube Industries, U.S. Patent No. 7,238,758, 2007.
101. Stewart, C. A., Himont, European patent application 0,410,443, 1991.
102. Yao, S., and Tanaka, Y., *Macromol. Theory Simul.*, **2001**, 10, 850.
103. Ikeuchi, H., Yano, T., Ikai, S., Sato, H., and Yamashita, J., *J. Molec. Catal. A Chem.*, **2003**, 193, 207.
104. Tanaka, Y., Sato, H., and Fujita, H., *Stud. Surf. Sci. Catal.*, **2007**, 172, 527.
105. Ishimaru, N., Kioka, M., and Toyota, A., Mitsui Petrochemical Industries, European Patent No. 0,385,765, 1990.
106. Miro, N. D., and Ohkura, M., Exxon Chemical, European Patent No. 1,080,122, 1999.
107. Shamshoum, E., Rauscher, D., and Burmaster, D., Fina Tech., European Patent No. 0,676,419, 2001.
108. Miro, N. D., Georgellis, G. B., and Swei, H., Exxon Chemical, European Patent No. 0,743,960, 1998.
109. Chen, L., and Nemzek, T. L., Union Carbide Chem. and Plastic Tech. Corp., U.S. Patent No. 7,141,635, 2006.
110. Peil, K. P., Neithamer, D. R., Patrick, D. W., Wilson, B. E., and Tucker, C. J., *Macromol. Rapid Commun.*, **2004**, 25, 119.
111. Chen, L., Union Carbide Chem. and Plastic Tech. Corp., U.S. Patent application 2007/0032376, 2007.
112. Campbell, R. E., and Chen, L., Dow Chemical, U.S. Patent application 2007/0032375, 2007.

113. Albizzati, E., Giannini, U., Morini, G., Smith, C. A., and Ziegler, R., in *Ziegler Catalysts. Recent Scientific Innovations and Technological Improvements*, Fink, G., Mülhaupt, R., and Brintzinger, H. H., Eds., Springer-Verlag, Berlin, 1995, p. 413.
114. Albizzati, E., Barbè, P. C., Noristi, L., Scordamaglia, R., Barino, L., Giannini, U., and Morini, G., Himont, European Patent No. 0,361,494, 1989.
115. Morini, G., and Cristofori, A., Montell North America, European Patent No. 0,728,724, 1996.
116. Albizzati, E., Giannini, U., Morini, G., Galimberti, M., Barino, L., and Scordamaglia, R., *Macromol. Symp.*, **1995**, 89, 73.
117. Barino, L., and Scordamaglia, R., *Macromol. Symp.*, **1995**, 89, 101.
118. Cui, N., Ke, Y., Li, H., Zhang, Z., Guo, C., and Lv, Z., *J. Appl. Polym. Sci.*, **2006**, 99, 1399.
119. Chadwick, J. C., Morini, G., Albizzati, E., Balbontin, G., Mingozzi, I., Cristofori, A., Sudmeijer, O., and Van Kessel, G. M. M., *Macromol. Chem. Phys.*, **1996**, 197, 2501.
120. Chadwick, J. C., van der Burgt, F. P. T. J., Rastogi, S., Busico, V., Cipullo, R., Talarico, G., and Heere, J. J. R., *Macromolecules*, **2004**, 37, 9722.
121. Scordamaglia, R., and Barino, L., *Macromol. Theory Simul.*, **1998**, 7, 399.
122. Toto, M., Morini, G., Guerra, G., Corradini, P., and Cavallo, L., *Macromolecules*, **2000**, 33, 1134.
123. Sacchi, M. C., Forlini, F., Tritto, I., Locatelli, P., Morini, G., Noristi, L., and Albizzati, E., *Macromolecules*, **1996**, 29, 3341.
124. Chadwick, J. C., Morini, G., Balbontin, G., Mingozzi, I., and Albizzati, E., *Macromol. Chem. Phys.*, **1997**, 198, 1181.
125. Morini, G., Balbontin, G., Gulevich, Y. V., Kelder, R. T., Duijghuisen, H. P. B., Klusener, P. A. A., and Korndorffer, F. M., Montell Tech., PCT Int. application WO 2000063261, 2000.
126. Cecchin, G., Morini, G., and Pelliconi, A., *Macromol. Symp.*, **2001**, 173, 195.
127. (a) Gao, M., Lui, H., Li, Z., Wang, J., Yang, J., Li, T., Wang, X., Li, C., and Ding, C., China Petroleum Chem., U.S. Patent application 20050239636, 2005; (b) Gao, M., Liu, H., Wang, J., Li, C., Ma, J., and Wei, G., *Polymer*, **2004**, 45, 2175.
128. Yang, C. B., and Hsu, C. C., *J. Appl. Polym. Sci.*, **1995**, 58, 1237.
129. Koyoh, S.-I., Kioka, M., Kashiwa, N., Itoh, M., and Mizuno, A., *Polymer*, **1995**, 36, 5015.
130. Koyoh, S.-I., Kioka, M., and Kashiwa, N., *Eur. Polym. J.*, **1999**, 35, 751.
131. Wang, Q., Lin, Y., Zhang, Z., Liu, B., and Terano, M., *J. Appl. Polym. Sci.*, **2006**, 100, 1978.
132. Kissin, Y. V., Ohnishi, R., and Konakazawa, T., *Macromol. Chem. Phys.*, **2004**, 205, 284.
133. Zhong, C., Gao, M., and Mao, B., *J. Appl. Polym. Sci.*, **2003**, 90, 3980.
134. Zhong, C., Gao, M., and Mao, B., *Macromol. Chem. Phys.*, **2005**, 206, 404.
135. Chadwick, J. C., Morini, G., Balbontin, G., and Sudmeijer, O., *Macromol. Chem. Phys.*, **1998**, 199, 1873.
136. Keii, T., Terano, M., Kimura, K., and Ishii, K., *Makromol. Chem. Rapid Commun.*, **1987**, 8, 583.

137. Yermakov, Y. I., and Zakharov, V. A., in *Coordination Polymerization*, Chien, J. C. W., Ed., Academic, New York, 1975, p. 91.
138. Tait, P., J. T., Zohuri, G. H., Kells, A. M., and McKenzie, I. D., in *Ziegler Catalysts. Recent Scientific Innovations and Technological Improvements*, Fink, G., Mülhaupt, R., and Brintzinger, H. H., Eds., Springer-Verlag, Berlin, 1995, p. 343.
139. Chien, J. C. W., and Kuo, C.-I., *J. Polym. Sci. Polym. Chem. Ed.*, **1985**, 23, 731.
140. Mejzik, J., Lesna, M., and Kratochvila, J., *Adv. Polym. Sci.*, **1986**, 81, 83.
141. Busico, V., Guardasole, M., Margonelli, A., and Segre, A. L., *J. Am. Chem. Soc.*, **2000**, 122, 5226.
142. Mori, H., Yamahiro, M., Terano, M., Takahashi, M., and Matsukawa, T., *Macromol. Chem. Phys.*, **2000**, 201, 289.
143. Zakharov, V. A., Bukatov, G. D., and Barabanov, A. A., *Macromol. Symp.*, **2004**, 213, 19.
144. Yaluma, A. K., Tait, P., J. T., and Chadwick, J. C., *J. Polym. Sci. Pt. A Polym. Chem.*, **2006**, 44, 1635.
145. Bukatov, G. D., Goncharov, V. S., and Zakharov, V. A., *Macromol. Chem. Phys.*, **1995**, 196, 1751.
146. Mori, H., Tashino, K., and Terano, M., *Macromol. Rapid Commun.*, **1995**, 16, 651–657.
147. Liu, B., Murayama, N., and Terano, M., *Ind. Eng. Chem. Res.*, **2005**, 44, 2382.
148. Nishiyama, I., Liu, B., Matsuoka, H., Nakatani, H., and Terano, M., *Macromol. Symp.*, **2003**, 193, 71.
149. Soga, K., Park, J. R., Shiono, T., and Kashiwa, N., *Makromol. Chem. Rapid Commun.*, **1990**, 11, 117.
150. Soga, K., Park, J. R., Uchino, H., Uozumi, T., and Shiono, T., *Macromolecules*, **1989**, 22, 3824.
151. Soga, K., *Makromol. Macromol. Symp.*, **1993**, 66, 43.
152. (a) Kouzai, I., Liu, B., Wada, T., and Terano, M., *Macromol. React. Eng.*, **2007**, 1, 160; (b) Terano, M., *Advances in Polyolefins: 2007*, ACS Conference Proceedings, 2007, Santa Rosa, CA.
153. Busico, V., Cipullo, R., Monaco, G., Talarico, G., Vacatello, M., Chadwick, J. C., Segre, A. L., and Sudmeijer, O., *Macromolecules*, **1999**, 32, 4173.
154. Busico, V., Cipullo, R., Talarico, G., Segre, A. L., and Chadwick, J. C., *Macromolecules*, **1997**, 30, 4786.
155. Chadwick, J. C., Morini, G., Balbontin, G., Camurati, I., Heere, J. J. R., Mingozzi, I., and Testoni, F., *Macromol. Chem. Phys.*, **2001**, 202, 1995.
156. Correa, A., Piemontesi, F., Morini, G., and Cavallo, L., *Macromolecules*, **2007**, 40, 9181.
157. Cavallo, L., Del Piero, S., Ducéré, J.-M., Fedele, R., Melchior, A., Morini, G., Piemontesi, F., and Tolazzi, M., *J. Phys. Chem. C*, **2007**, 111, 4412.
158. American Chemical Society, http://portal.acs.org/portal/acs/corg/content?_nfpb=true&_pageLabel=PP_ARTICLEMAIN&node_id=924&content_id=WPCP_007859&use_sec=true&sec_url_var=region1.
159. "The publication of the industrial scientist is the patent," P. Mueller, Basell Polyolefins, personal communication, 2004.

160. (a) Chapters in *Stereoselective Polymerization with Single-Site Catalysts*, Baugh, L. S., and Canich, J. A. M., CRC Press, Boca Raton, FL, 2007; (b) Wilkinson, G., and Birmingham, J. G., *J. Am. Chem. Soc.*, **1954**, 76, 4281; (c) Bochman, M., in *Mechanism in Homogeneous Catalysis*, Heaton, B., Ed., Wiley-VCH Verlag, Weinheim, 2005.

161. Wilkinson, G., and Birmingham, J. G., *J. Am. Chem. Soc.*, **1954**, 76, 4281.

162. Breslow, D. S., and Newburg, N. R., *J. Am. Chem. Soc.*, **1957**, 79, 5072.

163. Long, W. P., and Breslow, D. S., *Liebigs Ann. Chem.*, **1975**, 463.

164. Sinn, H., and Kaminsky, W., *Adv. Organomet. Chem.*, **1980**, 18, 99.

165. (a) Reichert, K.-H., and Meyer, K. R., *Makromol. Chem.*, **1973**, 169, 163; (b) Long, W. P., and Breslow, D. S., *Liebigs Ann. Chem.*, **1975**, 463.

166. Andersen, A., Cordes, H.-G., Herwig, J., Kaminski, W., Merck, A., Mottweiler, R., Pein, J., Sinn, H., and Vollmer, H.-J., *Angew. Chem.*, **1976**, 88, 689.

167. Sinn, H., Kaminsky, W., and Janning, J., *Angew. Chem. Int. Ed. Engl.*, **1976**, 15, 660.

168. Schnutenhaus, H., and Brintzinger, H.-H., *Angew. Chem. Int. Ed. Engl.*, **1979**, 18, 777.

169. Wild, F. R. W., Zsolnai, L., Huttner, G., and Brintzinger, H.-H., *J. Organomet. Chem.*, **1982**, 232, 233.

170. Ewen, J. A., Exxon Res. Engr. Co., U.S. Patent No. 4,522,982, 1983.

171. (a) Sinn, H., and Kaminsky, W., *Adv. Organomet. Chem.*, **1980**, 18, 99. (b) Pino, P., and Mülhaupt, R., *Angew. Chem. Int. Ed. Engl.*, **1980**, 19, 857.

172. Mise, T., Kageyama, A., Miya, S., and Yamazaki, H., *Chem. Lett.*, **1991**, 20, 1525.

173. Ewen; J. A., *J. Mol. Catal. A. Chem.*, **1998**, 128, 103.

174. Rieger, B., and Chien, J. C. W., *Polym. Bull.*, **1989**, 21, 159–163.

175. Ewen, J. A., Elder, M. J., and Jones, R. L., in *Polypropylene. Past Present and Future: The Challenge Continues*, published by Montell Polyolefins, distributed by Tecnimont, Milan, 1998, p. 191.

176. Collins, S., Hong, Y., and Taylor, N. J., *Organometallics*, **1990**, 9, 2695.

177. Collins, S., Hong, Y., Ramachandran, R., and Taylor, N. J., *Organometallics*, **1991**, 10, 2349.

178. Lensink, C., *Tetrahedron: Asymmetry*, 1995, 6, 2033.

179. (a) Paradies, J., Fröhlich, R., Kehr, G., and Erker, G., *Organometallics*, **2006**, 25, 3920; (b) Chen, L., Nie, W.-L., Paradies, J., Kehr, G., Fröhlich, R., Wedeking, K., and Erker, G., *Organometallics*, **2006**, 25, 5333.

180. (a) Ostoja-Starzewski, K.-H. A., Bayer Aktiengesellschaft, U.S. Patent No. 6,353,064, 2000; (b) Starzewski, K. A. O., Kelly, W. M., Stumpf, A., and Freitag, D., *Angew. Chem. Int. Ed. Engl.*, **1999**, 38, 2439.

181. Ewen, J. A., Fina Tech., U.S. Patentent No. 6,117,957, 2000.

182. Spaleck, W., Antberg, M., Rohrmann, J., Winter, A., Bachmann, B., Kiprof, P., Behm, J., and Herrmann, W. A., *Angew. Chem. Int. Ed. Engl.*, **1992**, 31, 1347.

183. Welborn, H. C., Exxon Chemical, U.S. Patent No. 5,017,714, 1989.

184. Kaminsky, W., Olefin polymerization catalyzed by metallocenes, *Adv. Catal.*, **2001**, 46, 89–159; see Table VII.

185. Stehling, U., Diebold, J., Kirsten, R., Roell, W., Brintzinger, H.-H., Juengling, S., Muelhaupt, R., and Langhauser, F., *Organometallics*, **1994**, 13, 964.
186. Hermann, W. A., Rhormann,. J., Herdtweck, E., Spaleck, W., and Winter, A., *Angew. Chem.*, **1989**, 28, 1511.
187. Spaleck, W., Antberg, M., Rohrmann, J., Winter, A., Bachmann, B., Kiprof, P., Behm, J., and Herrmann, W. A., *Angew. Chem. Int. Ed. Engl.*, **1992**, 31, 1347.
188. Spaleck, W., Kuber, F., Winter, A., Rohrmann, J., Bachmann, B., Antberg, M., Dolle, V., and Paulus, E. F., *Organometallics*, **1994**, 13, 954.
189. Ewen, J. A., Zambelli, A., Longo, P., and Sullivan, J. M., *Macromol. Rapid Commun.*, **1998**, 19, 71.
190. Kashiwa, N., Kojoh, S.-I., Imuta, J.-I., and Tsutsui, T., in *Metalorganic Catalysts for Synthesis and Polymerization*, Kaminsky, W., Ed., Springer, Berlin, 1999, p. 150.
191. Okumura, Y., Sakuragi, T., Ono, M., and Inazawa, S., Japan Polyolefins Co., European Patent No. 0,834,519, 2002.
192. Sell, T., Schottek, J., Paczkowski, N. C., and Winter, A., Novolen Tech. Holdings, U.S. Patent No. 7,232,869, 2007.
193. Rix, F. C., Kacker, S., Datta, S., Zhao, R., and Eswaran, V. R., Exxon/Mobil, U.S. Patent application 20060009595, 2006.
194. Ewen, J. A., Elder, M. J., Jones, Jr., R. L., and Dubitsky, Y. A., Basell Polyolefine GmbH, U.S. Patent No. 7,238,818, 2003.
195. Fisher, R. A., and Temme, R. B., Exxon Mobil Chem., U.S. Patent No. 6,451,938, 2002.
196. Jones, R. L., Elder, M. J., and Ewen, J. A., *Phosphorus, Sulfur, and Silicon and the Related Elements*, **2005**, 180, 827.
197. Ewen, J. A., Elder, M. J., and Jones, R. L., Basell Tech. Co., U.S. Patent No. 6,635,779, 2003.
198. Ewen, J. A., Elder, M. J., and Jones, R. L., Basell Tech. Co., U.S. Patent No. 6,444,833, 2002.
199. Ewen, J. A., Jones, R. L., and Elder, M. J., in *Metalorganic Catalysts for Synthesis and Polymerization*, Kaminsky, W., Ed., Springer, Berlin, 1999, p. 150.
200. Ewen, J. A., in *Metallocene-Based Polyolefins*, Sheirs, J., and Kaminsky, W., Eds., Wiley, Chichester, 2000, pp. 1, 3.
201. Resconi, R., Pietmontesi, F., Camurati, I., Sudmeijer, O., Nifant'ev, I. E., Ivchenko, P. V., and Kuz'mina, L. G., *J. Am. Chem. Soc.*, **1998**, 120, 2308.
202. Ewen, J. A., and Razavi, A., Fina Tech., U.S. Patent No. 4,892,851, 1990.
203. Ewen, J. A., and Razavi, A., Fina Tech., U.S. Patent No. 5,476,914, 1995.
204. (a) Ewen, J. A., Fina Tech., European Patent application EP423101, **1991**; (b) Ewen, J. A., Elder, M. J., Harlan, C. J., Jones, R. L., Atwood, J. L., Bott, S. G., and Robinson, K., *Polymer Preprints*, **1991**, 32, 469; (c) Ewen, J. A., Elder, M. J., Jones, R. L., Haspeslagh, L., Atwood, J. L., Bott, S. G., and Robinson, K., *Makromol. Chem. Macromol. Symp.*, **1991**, 48/49, 253.
205. Winter, A., Rohrmann, J., Antberg, M., Dolle, V., and Spaleck, W., Hoechst, A.-G., European Patent application EP 387690, 1990.
206. Yano, A., Kaneko, T., Sato, M., and Akimoto, A., *Macromol. Chem. Phys.*, **1999**, 200, 2127.

207. Ewen, J. A., and Elder, M. J., Fina Tech., U.S. Patent No. 5,416,228, 1991. This complex was the first working model for the Cossee–Arlman polymerization model.

208. Ewen, J. A., *J. Molec. Catal. A Chem.*, **1998**, 128, 103.

209. Farina, M., Di Silvestro, G., and Sozzani, P., *Macromolecules*, **1982**, 15, 1451.

210. Farina, M., Silvestro, G. D., and Sozzani, P., *Macromolecules*, **1993**, 26, 946.

211. (a) Coates, G. W., and Waymouth, R. M. *Science*, **1995**, 267, 217; (b) Wilmes, G. M., France, M. B., Lynch, S. R., and Waymouth, R. M., *Organometallics*, **2004**, 23, 2405; (c) Lin, S., and Waymouth, R. M., *Acc. Chem. Res.*, **2002**, 35, 765.

212. Busico, V., Cipullo, R., Kretschmer, W. P., Talarico, G., Vacatello, M., and Van Axel Castelli, V., *Angew. Chem. Int. Ed. Engl.*, **2002**, 41, 505.

213. Miller, S. A., and Bercaw, J. E., *Organometallics*, **2002**, 21, 934.

214. Ewen, J. A., Jones, R. L., Elder, M. J., Camurati, I., and Pritzkow, H., *Macromol. Chem. Phys.*, **2004**, 205, 302.

215. Jones, R. L., Bassell Polyolefine, DE Patent application 102005042391, 2005; (b) Jones, R. L., *Photochromic Switches on Polyolefin Catalysts*, dissertation presented to the Faculty at The Technical University of Kaiserslautern, Germany, October 2005.

216. Makio, H., Kashiwa, N., and Fujita, T., *Adv. Synth. Catal.*, **2002**, 344, 477.

217. Tian J., and Coates G. W., *Angew. Chem. Int. Ed. Engl.*, **2000**, 39, 3626.

218. Diamond, G. M., LaPointe, A. M., Leclerc, M. K., Longnire, J., Nava-Salgado, V., Shoemaker, J. A. W., and Sun, P., Symxy Tech., U.S. Patent No. 7,256,296, 2007.

219. Boussie, T. R., Brümmer, O., Diamond, G. M., Goh, C., LaPointe, A. M., Leclerc, M., and Shoemaker, J. A. W., Symxy Tech., U.S. Patent No. 7,241,715, 2007.

220. Segal, S., Goldberg, I., and Kol, M., *Organometallics*, **2005**, 24, 200.

221. Buscio, V., Cipullo, R., Ronca, S., and Budzelaar, P. H. M., *Macromol. Rapid Commun.*, **2001**, 22, 1405.

222. Boussie, T. R., Diamond, G. M., Goh, C., Hall, K. A., LaPointe, A. M., Leclerc, M. K., Murphy, V., Shoemaker, J. A. W., Turner, H., Rosen, R. K., Stevens, J. C., Alfano, F., Busico, V., Cipullo, R., and Talarico, G., *Angew. Chem. Int. Ed. Engl.*, **2006**, 45, 3278.

223. Hlatky, G., *Chem. Rev.*, **2000**, 100, 1347.

224. Severn, J., Chadwick, J. C., Friederichs, N., and Duchateau, R., *Chem. Rev.*, **2005**, 105, 4073.

225. Severn, J., and Chadwick, J. C., Eds., *Tailor-Made Polymers: Via Immobilization of Alpha-Olefin Polymerization Catalysts*, Wiley-VCH, Weinheim, 2008.

226. Tian, J., Gauthier, W. J., Rauscher, D., and Henry, S., Fina Tech., U.S. Patent application 20030236365, 2003.

227. Burkhardt, T. J., Murata, M., and Brandley, W. B., U.S. Patent No. 5,240,894, 1993.

228. Burkhardt, T. J., Brinen, J. L., Hlatky, G. G., Spaleck, W., and Winter, A., Exxon Chemical, PCT Int. application 9428034, 1994.

229. Brinen, J. L., Exxon Chemical, PCT Int. application 9628479, 1996.

230. Speca, A. N., and Tormaschy, K., Exxon Chemical, U.S. Patent No. 5,688,734, 1997.

231. Juengling, S., Koltzenburg, S., and Muelhaupt, R., *J. Polym. Sci. Pt. A Polym. Chem.*, **1997**, 35, 1.

232. Langhauser, F., Kerth, J., Kersting, M., Kölle, P., Lilge, D., and Mueller, P., *Angew. Makromol. Chem.*, **1994**, 223, 155.
233. Arrowsmith, D., Kaminsky, W., Laban, A., and Weingarten, U., *Macromol. Chem. Phys.*, **2001**, 202, 2161.
234. Butler, J. H., and Burkhardt, T., J., Exxon Chemical, U.S. Patent No. 5,902,766; 1999.
235. Burkhardt, J. T., and Brandley, W., Exxon Chemical, PCT Int. application 9518809, 1995.
236. Fraajie, V., B., Bachmann, A., and Winter, A., Hoechst A.-G., European Patent application 780,402, 1997.
237. Severn, J., in *Tailor-Made Polymers: Via Immobilization of Alpha-Olefin Polymerization Catalysts*, Severn, J. R., and Chadwick, J. C., Eds., Wiley-VCH, Weinheim, 2008.
238. Fritze, C., Bachmann, B., and Küber, F., Hoechst A.-G., U.S. Patent No. 6,271,164, 2001.
239. Paczkowski, N., Winter, A., and Langhauser, F., Novolen Tech. Holdings C.V., U.S. Patent No. 7,169,864, 2006.
240. Speca, A., Exxon Chemical, PCT Int. Patent No. 200012565, 2000.
241. Dockter, D. W., Hauger, B. E., Welch, M. B., and Muninger, R. S., Phillips Petroleum Co., U.S. Patent No. 6,239,060, 2001.
242. Tudor, J., and O'Hare, D., *J. Chem. Soc. Chem. Commun.*, **1997**, 603.
243. Ko, Y. S., Han, T. K., Park, J. W., and Woo, S. I., *Macromol. Rapid Commun.*, **1996**, 17, 749.
244. Yorisue, T., and Kanejima, S., Asahi Chemical, Japanese Patent application 08027210, 1996.
245. Hicks, J., and Jones, C. W., in *Tailor-Made Polymers: Via Immobilization of Alpha-Olefin Polymerization Catalysts*, Severn, J. R., and Chadwick, J. C., Eds., Wiley-VCH, Weinheim, 2008.
246. Bastos, Q. C., and Marques, M., de F. V., *J. Polym. Sci. Pt. A Polym. Chem.*, **2005**, 43, 263.
247. Kaminsky, W., Strübel, C., Lechert, H., Genske, D., and Woo, S. I., *Macromol. Rapid Commun.*, **2000**, 21, 909.
248. Shamshoum, E. S., and Lopez, M., Fina Tech., European Patent application 0,857,734, 1998.
249. Sano, T., Hagimoto, H., Sumiya, S., Naito, Y., Oumi, Y., Uozumi, T., and Soga, K., *Micropor. Mesopor. Mat.*, **2001**, 44/45, 557.
250. Sano, T., Hagimoto, H., Jin, J., Oumi, Y., Uozumi, T., and Soga, K., *Macromol. Rapid Commun.*, **2000**, 21, 1191.
251. Vizzini, J. C., and Chudgar, R. K., Exxon Chemical, U.S. Patent No. 6,143,686, 2000.
252. Brant, P., Exxon Chemical, PCT Int. application 200146273, 2001.
253. Chang, M., Exxon Chemical, PCT. Int. application 200136499, 2001.
254. Kwanten, M., Carriere, B. A. M., Grobet, P. J., and Jacobs, P. A., *Chem. Commun.*, **2003**, 1508.
255. Richter, B., Seidel, N., and Kratzer, R., Basell Polyolefine G.m.b.H., German Patent application DE 10,232,082, 2004.
256. Kratzer, R., Fritze, C., and Schottek, J., Targor G.m.b.H., U.S. Patent application 20030008984, 2003.

257. Hlatky, G. G., and Upton, D. J., *Macromolecules*, **1996**, 29, 8019.
258. Hlatky, G. G., and Upton, D., J., Exxon Chemical, PCT Int. application 9403506, 1994.
259. Hlatky, G. G., Upton, D. J., and Turner, H. W., Exxon Chemical, PCT Int. application 9109982, 1991.
260. Bohnen, H., Fritze, C., and Kueber, F., Targor G.m.b.H., U.S. Patent No. 6,391,989, 2002.
261. Suzuki, N., Yu, J., Shioda, N., Asami, H., Nakamura, T., Huhn, T., Fukuoka, A., Ichikawa, M., Saburi, M., and Wakatsuki, Y., *Appl. Catal. A.*, **2002**, 224, 63.
262. Suzuki, N., Asami, H., Nakamura, T., Huhn, T., Fukuoka, A., Ichikawa, M., Saburi, M., and Wakatsuki, Y., *Chem. Lett.*, **1999**, 4, 341.
263. Langhauser, F., Fischer, D., Kerth, J., Schweier, G., Barsties, E., Brintzinger, H.-H., Schaible, S., and Roell, W., BASF A.-G., U.S. Patent No. 5,627,246, 1995.
264. Klapper, M., and Fink, G., in *Tailor-Made Polymers: Via Immobilization of Alpha-Olefin Polymerization Catalysts*, Severn, J. R., and Chadwick, J. C., Eds., Wiley-VCH, Weinheim, 2008.
265. Peifer, B., Milius, W., and Alt, H. G., *J. Organomet. Chem.*, **1998**, 553, 205.
266. Schertl, B., Alt, H. G., Peifer, B., Palackal, S. J., and Welch, M. B., U.S. Patent No. 6,372,930, 2002.
267. Kitagawa, T., Uozumi, T., Soga, K., and Takata, T., *Polymer*, **1997**, 38, 615.
268. Ono, M., Hinokuma, S., Miyake, S., and Inazawa, S., Japan Polyolefins Co., European Patent application 710,663, 1996.
269. Walzer, J. F., Dias, A. J., Fréchet, J. M., and Roscoe, S. B., Exxon Chemical, PCT Int. application 9855518, 1998.
270. Albizzati, E., Resconi, L., Dall'Occo, T., and Piemontesi, F., Sperilene S.r.l., European Patent application 633,272, 1995.
271. Vizzini, J. C., Exxon Chemical, U.S. Patent No. 6,228,795, 2001.
272. Covezzi, M., and Fait, A., Basell Tech. Co., PCT Patent application 200144319, 2001.
273. Sunaga, T., Ishii, Y., and Asanuma, T., Mitsui Toatsu Chemicals, European Patent application 773,237, 1997.
274. Liu, J., Dong, J. Y., Cui, N., and Hu, Y., *Macromolecules*, **2004**, 37, 6275.
275. Koch, M., Stork, M., Klapper, M., Müllen, K., and Gregorius, H., *Macromolecules*, **2000**, 33, 7713.
276. Nenov, N., Koch, M., Klapper, M., and Müllen, K., *Polym. Bull.*, **2002**, 47, 391.
277. Jang, Y.-J., Nenov, N., Klapper, M., and Müllen, K., *Polym. Bull.*, **2003**, 50, 351.
278. Jang, Y.-J., Nenov, N., Klapper, M., and Müllen, K., *Polym. Bull.*, **2003**, 50, 343.
279. Koch, M., Falcuo, A., Nenov, N., Klapper, M., and Müllen, K., *Macromol. Rapid Commun.*, **2001**, 22, 1455.
280. Friederichs, N., Ghalit, N., and Xu, W., in *Tailor-Made Polymers: Via Immobilization of Alpha-Olefin Polymerization Catalysts*, Severn, J. R., and Chadwick, J. C., Eds., Wiley-VCH, Weinheim, 2008.
281. Dong, J., Liu, J., Han, Z., and Wang, D., Chinese Academy of Sciences, PCT Int. application 2006047913, 2005.
282. Ahn, T. O., Hong, S. C., Kim, J. H., and Lee, D-H., *J. Appl. Polym. Sci.*, **1998**, 67, 2213.

283. Speca, A. N., and McAlpin, J. J., in *Metallocene Catalyzed Polymers*, Benedikt, G. M., and Goodall, B. L., Eds., Plastic Design Library, New York, 1998, p. 73.
284. Speca, A. N., Brinen, J. L., and McAlpin, J. J., Exxon Chemical, U.S. Patent No. 5,786,291, 1997.
285. Mehta, A. K., Chen, M. C., McAlpin, J. J., Speca, A. N., Tormaschy, K., and Lin, C. Y., U.S. Patent No. 6,583,227, 2001.
286. Shamshoum, E. S., and Bauch, C. G., Fina Tech., U.S. Patent No. 5,847,059, 1996.
287. Shamshoum, E. S., and Bauch, C. G., Fina Tech., European Patent application 0,849,286, 1998.
288. Przybyla, C., and Fink, G., *Acta Polym.*, **1999**, 50, 77.
289. Shamshoum, E. S., Lopez, M., Harris, T., and Kim, S., Fina Tech., European Patent application 0,870,779, 1998.
290. Marques, M. F. V., and Conte, A., *J. Appl. Polym. Sci.*, **2006**, 99, 628.
291. Marques, M. F. V., Pombo, C. C., Silva, R. A., and Conte, A., *Eur. Polym. J.*, **2003**, 39, 561.
292. Chien, J. C. W., Iwamoto, Y., Rausch, M. D., Wedler, W., and Winter, H. H., *Macromolecules*, **1997**, 30, 3447.
293. Ernst, E., Reussner, J., and Neissl, W., Pcd-Polymere Gesellschaft M.B.H., European Patent application 0,695,765, 1994.
294. Ye, Z., and Zhu, S., *J. Polym. Sci. Pt. A Pol. Chem.*, **2003**, 41, 1152.
295. Dekmezian, A. H., Soares, J. B. P., Jiang, P., Garcia-Franco, C. A., Weng, W., Fruitwala, H., Sun, T., and Sarzotti, D. M., *Macromolecules*, **2002**, 35, 9586.
296. Tynys, A., Saarinen, T., Bartke, M., and Löfgren, B., *Polymer*, **2007**, 48, 1893.
297. Chien, J. C. W., Iwamoto, Y., Ruasch, M. D., Wedler, W., and Winter, H. H., *Macromolecules*, **1997**, 30, 3447.
298. Lieber, S., and Brintzinger, H.-H., *Macromolecules*, **2000**, 33, 9192.

8 $MgCl_2$-Supported $TiCl_4$ Catalysts for Production of Morphology-Controlled Polyethylene

LONG WU and SIEGHARD E. WANKE
Department of Chemical and Materials Engineering, University of Alberta,
Edmonton, Alberta, Canada T6G 2G6

8.1 INTRODUCTION

Karl Ziegler[1] discovered that ethylene was polymerized with a mixture of $TiCl_4$ and triethylaluminum (TEA) as catalyst under mild conditions, and Giulio Natta[2,3] adapted this catalyst for propylene polymerization. With this so-called Ziegler–Natta catalyst, linear polyethylene (PE) was produced at low pressure (<2 MPa) and low temperature (60–110 °C), compared with the already existing process of free-radical ethylene polymerization at high pressure (~300 MPa) and high temperature (~300 °C) for the production of low-density polyethylene (LDPE). The Ziegler–Natta catalyst used in the initial commercial processes consisted of a transition metal compound as an active component and an alkyl or hydride of a main-group element as a cocatalyst. The most often used active component was $TiCl_3$, and the most common cocatalyst was triethylaluminum. The further development of the Ziegler–Natta catalysts is based on these two components.

The original Ziegler catalysts were first improved in the 1960s by introducing a third component, that is, an electron donor (Lewis base) to increase their activity for producing linear polyethylene and to increase both their activity and stereoregularity for producing polypropylene. By the end of the 1970s, the improvement of the Ziegler–Natta catalysts had been extended to the copolymerization ability and morphology, in addition to further increasing catalyst activity, by supporting catalytic sites on such materials as $MgCl_2$ and silica in the commercial processes. With these supported catalysts, a large fraction of titanium is available to take part in the polymerization reaction compared to the unsupported catalysts; that is, less titanium is needed. The

---

Handbook of Transition Metal Polymerization Catalysts Edited by Ray Hoff and Robert T. Mathers
Copyright © 2010 John Wiley & Sons, Inc.

yield of polymer per gram of titanium with these catalysts is sufficiently high so that no removal of catalyst residues from the polymer is required. For polypropylene production, the separation facility for the removal of the atactic polypropylene was also eliminated due to the high stereoregularity and high activity of the supported Ziegler–Natta catalysts. This resulted in a 20% reduction in the capital investment cost and significant reductions in maintenance, labor, raw materials, and utility consumption as well as reduction in potential pollution problems associated with the extraction of solvents.[4]

The improvement in catalyst activity and copolymerization ability of the supported Ziegler–Natta catalysts made the production of polyolefin in the gas phase possible, especially for the production of linear low-density polyethylene (LLDPE). The gas-phase processes offer advantages in investment cost, safety, and environment over other processes;[5] polyolefins with a wide range of properties can be produced in the gas phase without the limitation of viscosity problems encountered in the solution process and solubility problems in the slurry process. The development of spherical $MgCl_2$-supported Ti catalysts led to the production of nascent polyolefin particles with a controlled morphology according to the replication phenomenon.[6] It has been commonly observed that catalysts are capable of replicating their overall morphology into the morphology of polymer particles under proper polymerization conditions in olefin polymerizations.[7] The initial catalyst particles act as a template for the growth of polymer particles. Nascent polymer particles with controlled morphology are polymer particles that have spherical shape, high flowability (i.e., pourability) and high bulk density [see American Society for Testing and Materials (ASTM) D 1895-67], and controlled size with a narrow particle size distribution.

Since the 1980s, the morphology-controlled Ziegler–Natta catalysts have been improved to produce such specialty polyolefins as heterophasic olefin copolymers, reactor blends, multiphase polyolefin alloys, and functionalized polypropylene in commercial processes.[8] With the improved catalysts, each catalyst particle would eventually become a single polymer particle which acts as a polymerization reactor, the so-called reactor granule technology.[9] In this process, olefin polymerization on each catalyst particle is first controlled to give a porous particle growing with a spherical shape (a prepolymerization step). Within the porous reaction bed, the same or other desirable monomers can then be introduced and polymerized. The introduction of other monomers to the internal active sites during the polymerization process can produce a second or third different polymer within the prepolymerized particle to form polyolefins or polyolefin blends. In the final product, different polymers are intimately dispersed among the various preexisting structures of the initially generated polymer. In the middle 1990s, metallocenes and single-site catalysts were subsequently introduced into the porous polyolefin particles which were produced with the $MgCl_2$-supported Ti catalysts.[4,10] The blend of polyolefins made by Ti-based Ziegler–Natta catalysts and metallocene catalysts was obtained directly within a single particle. The intimate mixing of the two different specifically tailored polyolefins in terms of molecular structure and molar mass distribution was achieved as they grew in the same particle. The polymer blends combine the advantages of the polyolefin made by heterogeneous catalysts such as processability and versatility with those by homogeneous catalysts such as mechanical and elastic properties.[11]

Production of nascent polymer particles with controlled morphology eliminates the purchase and operation of the energy-consuming pelletization equipment in the commercial processes.[6,12,13] The deformation of the spherical particles in extrusion devices is easier, and the melt shear starts earlier with the combination of heat and pressure, that is, better processability.[13] Nascent polymer particles have less entangled morphology and are softer than the melt-crystallized pellets, which have a thermal history during the extrusion of melting and cooling in the pelletization process.[14] Due to these physical and morphological properties, the nascent spherical particles can easily be compacted in the solid-conveying section of the extrusion devices under the same conditions as the pelletized resins. During the extrusion of the softer particles, the potential friction-burning and cross-linking phenomena can be reduced, and damaging thermomechanical stresses can be avoided since the softer polymer is extruded at lower temperature. In addition, the direct use of the polymer particles without a thermal history can protect the additive package against degradation that cannot be avoided during pelletization.[15] Consequently, it is possible to reduce the quantity of additives and enhance product purity. Polymers with high purity are better for blending and processing.

Because morphology-controlled polymer particles have the above advantages and can only be made from morphology-controlled catalysts, preparation of morphology-controlled $MgCl_2$-supported Ti catalysts and production of morphology-controlled polyethylene were studied in our laboratory. It is noted that although morphology replication is generally observed in laboratories[7] and commercial processes,[12,16] the operation of laboratory reactors is not trivial. The polymer particles in both morphology-controlled and irregular forms were reported using a similar method of preparing morphology-controlled catalysts and similar polymerization procedures.[17–19] Concerns about the experimental reproducibility in the Ziegler–Natta catalysis and polymerization have been expressed by many researchers.[20–24] Thus, detailed procedures for the reproducible operations of the slurry and gas-phase polymerization reactors will be described. This is followed by the prepolymerization and polymerization results with emphasis on the dependence of the prepolymerization/polymerization activity profiles and prepolymer/polymer properties on the particle sizes. Effects of catalyst and polymer particle sizes on activity profiles and polymer properties have frequently been examined only in the modeling studies of mass and heat transfer limitations in heterogeneous olefin polymerization,[25–27] but not very often in experimental studies. Experimental results on ethylene polymerization and polymer properties are qualitatively compared with model predictions in the literature with an attempt to determine if the mass and heat transfer limitations are significant in reactors.

8.2 PREPARATION OF MORPHOLOGY-CONTROLLED $MgCl_2/TiCl_4$ CATALYSTS

The capability of catalysts to replicate their morphology into the morphology of polymer particles suggests the modification of polymer morphology must begin with the catalyst preparation. Due to the advantages of the morphology-controlled polymer particles, extensive interests have arisen to prepare morphology-controlled catalyst supports which also provide catalysts with high activities. Many materials have been used as catalyst supports and many methods have been applied for preparing the catalysts. For example, ball milling of $MgCl_2$ and $TiCl_4$ with other components was widely used to increase catalyst activities,[21] but it is difficult to control catalyst morphology during ball milling. In the last three decades, many effective materials have been developed for preparing Ziegler–Natta catalysts with high activity for olefin polymerization. These supports include $MgCl_2$, silica,[28,29] and various polymeric materials.[30–32] $MgCl_2$-supported Ti catalysts are currently the major catalysts for the commercial production of morphology-controlled polyolefins.

Ziegler–Natta catalysts supported on spherical $MgCl_2$ particles were discovered by Montedison/Mitsui Petrochemical Industrials for the production of morphology-controlled polypropylene and LLDPE in the slurry reactors in the early 1980s.[12] The spherical $MgCl_2$ support of these catalysts was obtained from solidifying the emulsion of the $MgCl_2$–ethanol complex (or $MgCl_2$–water complex) and an inert liquid to form spherical particles in the liquid[16,33–35] or in the gas phase.[36–40] Another type of morphology-controlled catalyst was developed by BP Chemicals in which nascent $MgCl_2$ particles are formed from a chemical reaction in an inert liquid and precipitated immediately in the liquid phase.[41–43] Both types of catalysts were later used in the two-stage hybrid processes for the production of morphology-controlled polyolefins.

The general procedure of preparing the morphology-controlled $MgCl_2/TiCl_4$ catalysts consists of two steps. The first step is to prepare morphology-controlled $MgCl_2$ supports, and the second step is to treat the $MgCl_2$ support with $TiCl_4$ and an electron donor to obtain active, morphology-controlled catalysts. Very little information on the preparation technique, other than the patent literature, can be found on these morphology-controlled $MgCl_2/TiCl_4$ catalysts; hence, detailed procedures for these two types of catalysts prepared in our laboratory are described below.

8.2.1 Emulsion-Quenching Method

The method of quenching an emulsion in liquid was used to prepare the morphology-controlled $MgCl_2/TiCl_4$ catalyst in our laboratory; this method is similar to that developed by Montedison.[16] In the first step of the emulsion-quenching method, spherical $MgCl_2$ support was prepared by quenching an emulsion of $MgCl_2$–ethanol complex and Vaseline. The specific steps consisted of charging 220 g of Vaseline, 20 g of $MgCl_2$, and 40 mL of ethanol into a 1-L jacketed Pyrex vessel (from Büchi) equipped with a Rushton turbine stirrer and an exit port. The exit port of the 1-L vessel was connected through a valve to Teflon tubing with an inside diameter of 1.5 mm and a length of about 3 m. The other end of the Teflon tubing was dipped into a 3-L vessel containing 1 L of heptane, which was cooled to about −30 °C by an ethylene glycol–water mixture. An emulsion of $MgCl_2$–ethanol complex in Vaseline was formed at 120 °C in the 1-L vessel by stirring at 1000 rpm. The emulsion was then forced out of the 1-L vessel by pressurizing it with nitrogen to 600 kPa. The emulsion flowed through the small-diameter Teflon tubing and then into the cold heptane where it solidified rapidly. After the Vaseline was washed away with heptane, the powder of the $MgCl_2$–ethanol complex was transferred into a glass tube, with a fritted disk at the bottom, for a thermal treatment. The thermal treatment partially dealcoholated the $MgCl_2$–ethanol complex. The temperature for the thermal treatment increased steadily from room temperature to 120 °C over 4 h. After the thermal treatment, about 50% of ethanol was eliminated and the molar ratio of ethanol to $MgCl_2$ was about 1.5 in the partially dealcoholated $MgCl_2$–ethanol complex.

The second step of the preparation of the catalyst consisted of treating the partially dealcoholated $MgCl_2$–ethanol complex with $TiCl_4$ and an electron donor. Special precautions, such as operating environment and purity of all chemicals used, are required for handling toxic and air-sensitive chemicals like $TiCl_4$. About 5 g of the partially dealcoholated $MgCl_2$–ethanol complex, suspended in 150 mL of heptane, was introduced into a 500-mL glass flask equipped with a mechanical agitator. About 150 mL of $TiCl_4$ was slowly added to the flask to remove ethanol in the $MgCl_2$–ethanol complex by reaction with $TiCl_4$ and to fix additional $TiCl_4$ on the $MgCl_2$ support. The temperature of the flask was increased slowly from −20 to 50 °C in about 7 h while stirring slowly at 15 rpm. It is crucial that the stirring be gentle; rapid stirring results in breakup of the $MgCl_2$–ethanol particles. When the temperature reached 50 °C, about 0.6 mL of dibutyl phthalate, an electron donor, was added to the flask. The mixture was then heated to 110 °C in 3 h and kept at 110 °C for 1 h. After the liquid was removed, an additional 150 mL of $TiCl_4$ was added to the flask and the temperature was kept at 110 °C for another 1 h. The reaction product in the flask was then cooled to 50 °C and washed with 100 mL of heptane. The wash was repeated 10 times; hexane was used for the last wash. The particles thus obtained were dried in vacuum at room temperature for 30 min. The dry solid catalyst typically contained 2–4 mass % Ti as determined by a colorimetric analysis method.[44] Examination of the catalyst particles with scanning electron microscopy (SEM) showed that the dry solid catalysts were mostly in spherical form and the particle size is in the range of 25–200 μm in diameter; a sample micrograph is shown in Figure 8.1.

8.2.2 Reactive Precipitation Method

In the reactive precipitation method, morphology-controlled $MgCl_2/TiCl_4$ catalyst was prepared by a procedure similar to that described by BP Chemicals.[41,42] A 1-L jacketed Pyrex reactor, which was equipped with a

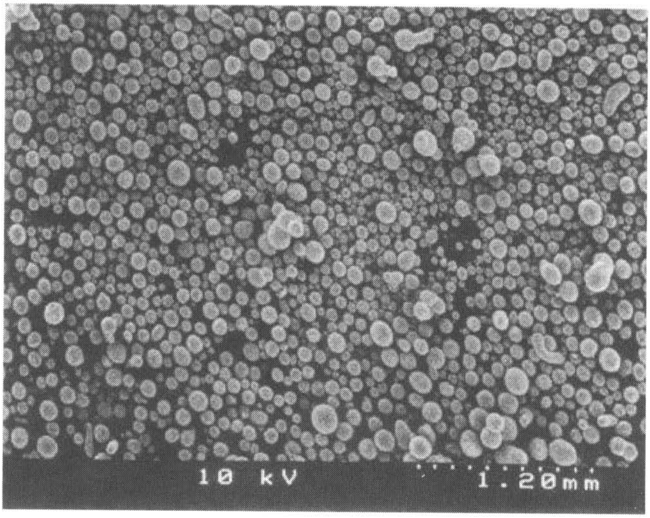

Figure 8.1 SEM micrograph of morphology-controlled $MgCl_2$-supported Ti catalyst ($MgCl_2$ support particles were prepared by emulsion-quenching method).

thermocouple and a stirrer, was used for the catalyst preparation. The temperature in the reactor was controlled by a heating/cooling circulating bath, and the stirring speed in the reactor was kept at 500 rpm in the catalyst preparation. In the first step of the $MgCl_2$ support precipitation, reagents (200 mL of heptane, 16.9 mL of dibutyl ether, and 97 mL of dibutyl magnesium) were introduced into the Pyrex reactor at room temperature under a nitrogen atmosphere. After the temperature in the reactor had been increased to 50 °C, a solution consisting of 24 mL *tert*-butyl chloride in 80 mL of heptane was slowly added into the reactor over 10 h. The temperature in the reactor was kept at 50 °C for an additional 2 h. The solid $MgCl_2$ particles precipitated were washed four times at room temperature; 100 mL of heptane was used for each wash.

In the second step of the catalyst preparation, the $MgCl_2$ particles obtained in the first step were suspended in heptane of 200 mL at 30 °C in the Pyrex reactor. A solution of 9.15 mL *n*-butanol in 20 mL heptane was added to the $MgCl_2$–heptane suspension over a 1-h period. After the addition of *n*-butanol, the reaction mixture in the Pyrex reactor was kept at 30 °C for an additional 0.5 h. The solid particles were washed at 30 °C with 100 mL of heptane; the wash was repeated twice, then the solid particles were suspended in 200 mL of heptane. At 50 °C, 100 mL of triethylaluminum was added to the suspension over a 1-h period. The temperature of the mixture in the reactor was increased to 80 °C and kept at 80 °C for 1 h. The resulting solid particles were washed with 100 mL of heptane at 50 °C, and the wash was repeated twice. At 30 °C, 1.5 mL of $TiCl_4$ in 50 mL of heptane was added to 200 mL of a suspension of the solid particles in heptane in 2 h. The temperature of the mixture in the

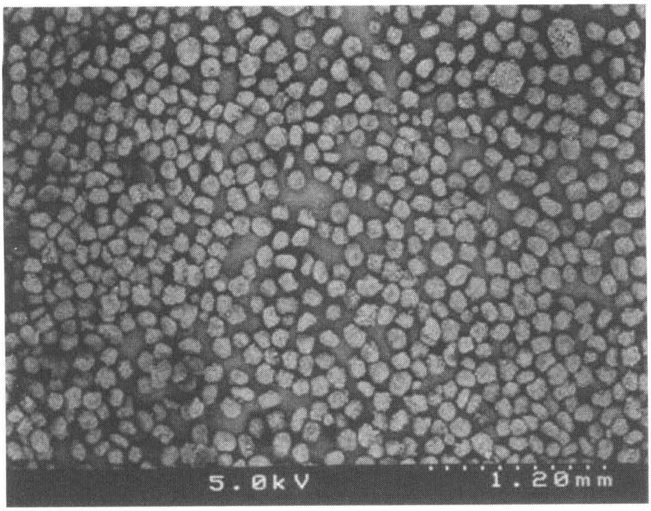

Figure 8.2 SEM micrograph of morphology-controlled $MgCl_2$-supported Ti catalyst ($MgCl_2$ support particles were prepared by reactive precipitation method).

reactor was increased to 80 °C and kept at 80 °C for 1 h. The solid particles were then washed at 50 °C with 100 mL of hexane, and the wash was repeated twice. Finally, the suspension was evacuated at room temperature for 2 h to remove the liquid and obtain dry catalyst particles. The concentration of Ti in the dry solid catalyst determined by a colorimetric analysis method[44] was typically 1–2 mass %. The spheroidal catalyst particles are shown in Figure 8.2; the diameter of the catalyst particles is in the range of 50–170 μm.

8.3 POLYMERIZATION PROCESSES

With the development of the catalysts, the process for polyolefin production has also evolved. The first commercial process was diluent slurry polymerization because of its operational stability. Other industrial processes such as solution- and gas-phase polymerization were also studied but were initially limited by low catalyst activity, which reduced the advantages of these processes. The complexity and versatility of supported Ziegler–Natta catalysts increased, and this made various industrial processes viable, especially the gas-phase processes. Among the gas-phase processes, the UNIPOL process developed by Union Carbide Corporation is one of the most successful gas-phase processes for producing polyolefin in fluidized-bed reactors. However, morphology-controlled polyolefins have not been produced commercially with the UNIPOL process. In 1982, the first commercial process for the production of morphology-controlled polyolefin was jointly developed by ElPaso Polyolefins Co. and Montedison for the production of LLDPE in a liquid-pool slurry reactor.[12] It was reported that this process had similar operating and capital cost advantages as the UNIPOL process, largely due to the elimination of pelletization.[12]

Since 1982, more complicated processes have been developed commercially by Montedison/Himont Incorporated for producing a wide range of morphology-controlled polyolefins.[9,45] Such commercial processes are two-stage hybrid processes which include the SPHERIPOL process for the production of polypropylene, the CATALLOY process for multiphase polyolefinic alloys, the SPHERILENE process for high-density polyethylene (HDPE)/LLDPE, and the HIVALLOY process for non-olefin-grafted polypropylene. The first stage of polymerization (i.e., the prepolymerization step) occurs in a diluent slurry loop reactor. The prepolymer produced in the first stage, as a catalyst, is continuously fed directly into the second stage of polymerization in the gas-phase fluidized-bed reactors. No seed resin is required at the start-up phase; thus, the changes of product grades do not involve extra cost.[13] This also leads to reductions in the capital investment and production costs. Similar two-stage hybrid processes were also developed and reported by BP Chemicals for the production of morphology-controlled polyethylene in the gas-phase fluidized-bed reactors.[41,43] However, the prepolymer is produced in a semibatch slurry reactor.[46,47]

In the commercial processes, prepolymerization is carried out under mild conditions (generally at low monomer concentration and low temperature) to produce a low-yield polymer which is used as a catalyst for the subsequent high-yield polymerization. Under the mild prepolymerization conditions, low polymerization rates in the initial stage are obtained; this reduces particle overheating, allows full activation of the catalyst, and protects polymer particles from uncontrollable fragmentation during the initial stage of polymerization.[48,49] Thus, the overall activities of catalysts and the bulk density of final polymer particles can be increased;[50–54] the increases in polymerization rate and polymer bulk density are more pronounced at higher polymerization temperatures.[53] However, no effects on the nature of catalytic sites and molar mass distribution of final polymer products were observed.[51,54–56]

Reactor operations in our laboratory for the production of morphology-controlled polyethylene are similar to that of the two-stage industrial process in which the prepolymerization takes place in a slurry reactor followed by polymerization in a gas-phase reactor. However, both reactors were operated in the semibatch mode under a constant total pressure and temperature throughout a run. The two reactors shared a common series of gas purification columns and data acquisition system.[57] A 1-L jacketed Pyrex reactor was used for the ethylene prepolymerization in the slurry mode, and a 1-L stainless steel reactor was used for the ethylene homopolymerization and ethylene/1-butene copolymerization in the gas phase. The procedure of the overnight treatment of the reactors developed by Lynch and Wanke[57] was adopted before each run was performed. Ethylene was fed into the reactor to keep the reactor pressure at the desired operating pressure; this measured feed rate is equal to the rate for ethylene polymerization because the change in the reactor void volume is negligible. Additional details on the reactor systems have been previously described.[57] The specific procedures for the slurry and gas-phase operations are described below.

8.3.1 Slurry Polymerization Procedure

At the beginning of each slurry run, the clean and empty reactor was leak tested with nitrogen of 0.7 MPa before it was evacuated at 90 °C overnight. After the reactor reached the required reaction temperature, the catalyst injector, in which the desired amount of solid catalyst particles were suspended in 1 mL of heptane, was connected to the reactor under nitrogen flow. The reactor was charged with 300 mL of heptane using a 100-mL Hamilton gas-tight syringe and with 0.25 mL of neat triethylaluminum as cocatalyst using a 1-mL Hamilton gas-tight syringe under the nitrogen flow. After the cocatalyst injection, the data acquisition system was started and data were recorded at 10-s intervals. During the stirring, the desired amount of hydrogen was introduced into the reactor. Hydrogen was used for all the prepolymerization runs. Ethylene was added to the reactor from the top of the flange until the desired total pressure in the reactor was reached. The catalyst suspension was injected into the reactor with a small amount of nitrogen so that the increase in the total pressure in the reactor was less than 30 kPa after the catalyst injection. After the catalyst injection, the valve for the catalyst injection port was immediately closed. The time at which the catalyst was injected was the start of a run. Ethylene was fed into the reactor at a rate required to maintain the reactor at the desired operating pressure. The polymerization was terminated by stopping the ethylene feed, venting the reactor, and slowly admitting air to the reactor. Heptane was separated from the polymer particles under nitrogen flow and residual heptane was removed under vacuum at room temperature for 30 min. For the prepolymerization run, the dry prepolymer particles were stored in the glove box for the subsequent use as polymerization catalysts.

8.3.2 Gas-Phase Polymerization Procedure

For the gas-phase operation, 80–200 g of NaCl seedbed particles (0.5 mm) was placed into a thoroughly cleaned reactor before the reactor assembly was sealed and leak tested at 2.0 MPa with nitrogen. The leak-free reactor was evacuated at 90 °C overnight. The reactor was cooled to the desired temperature and was filled with nitrogen to 140 kPa. The catalyst injector, containing the catalyst particles sandwiched by NaCl particles, was connected to the catalyst injection port under the nitrogen flow. Then, the reactor was evacuated for 10 min before it was filled with ethylene to 140 kPa. After the ethylene addition, the data acquisition system was started and data were recorded at 10-s intervals. The cocatalyst was injected into the reactor with a Hamilton gas-tight syringe and the comonomer (1-butene or 1-hexene), in a copolymerization run, was added to the reactor with an ISCO model 500D syringe pump. This was followed by the addition of a desired amount of hydrogen to the reactor. Ethylene was added to the reactor to a pressure that is 350 kPa below the desired operating pressure before stirring the reactor. After the reactor was stirred for 30 min, polymerization was started by flowing ethylene through the catalyst injector to inject the catalyst particles into the reactor. It is noted that the valve for the catalyst injection port was immediately closed and the pressure in the reactor must not exceed the desired operating pressure. Ethylene was fed into the reactor from the top of the flange at a rate required to maintain the reactor at the desired operating pressure. The polymerization run was terminated by stopping the ethylene feed, venting the reactor, and slowly admitting air to the reactor. Product was washed repeatedly with water to remove salt and was dried in an air oven at 60 °C for 24–72 h. The dried product was stored in plastic bags until analysis.

Following the above operation procedures, reproducible results can be obtained. Typical morphology replication from catalyst to prepolymer to polymer particles is illustrated in Figure 8.3, with little fines in the final polymer particles. The catalyst particles shown in Figure 8.3*a*1 were prepared by the emulsion-quenching method (shown in Figure 8.1) and the catalyst particles shown in Figure 8.3*a*2 were prepared by the reactive precipitation method (shown in Figure 8.2). The prepolymer particles shown in Figures 8.3*b*1 and *b*2 were homopolyethylene obtained under the mild conditions in the slurry reactors. The polymer particles shown in Figure 8.3*c*1 were obtained in the gas-phase operation, and the polymer particles shown in Figure 8.3*c*2 were obtained in the slurry operation. It can be seen that the cracks on the catalyst surface shown in Figures 8.3*a* are similar to the cracks on the polymer surface shown in Figures 8.3*c*; the similarity of the cracks is especially striking for the catalyst prepared by the reactive precipitation method while no cracks were found on the surface of prepolymer particles shown in Figure 8.3*b*.

8.4 EFFECT OF PREPOLYMERIZATION ON ACTIVITY PROFILES AND PREPOLYMER PROPERTIES

Polymerization conditions affect polymerization profiles and polymer properties such as morphology and bulk density.[50,53] The morphology and bulk density are important properties for nascent prepolymer particles, and they are difficult to control and reproduce in Ziegler–Natta polymerization. The typical rate profiles of ethylene prepolymerization in the gas-phase and slurry reactors are shown in Figure 8.4. The catalyst consisting of spherical particles prepared by the emulsion-quenching method, as shown in Figure 8.1, was used for the prepolymerization runs; hydrogen was added to the reactors. The run conditions are listed in Table 8.1. It is shown in Figure 8.4 that the rate profile

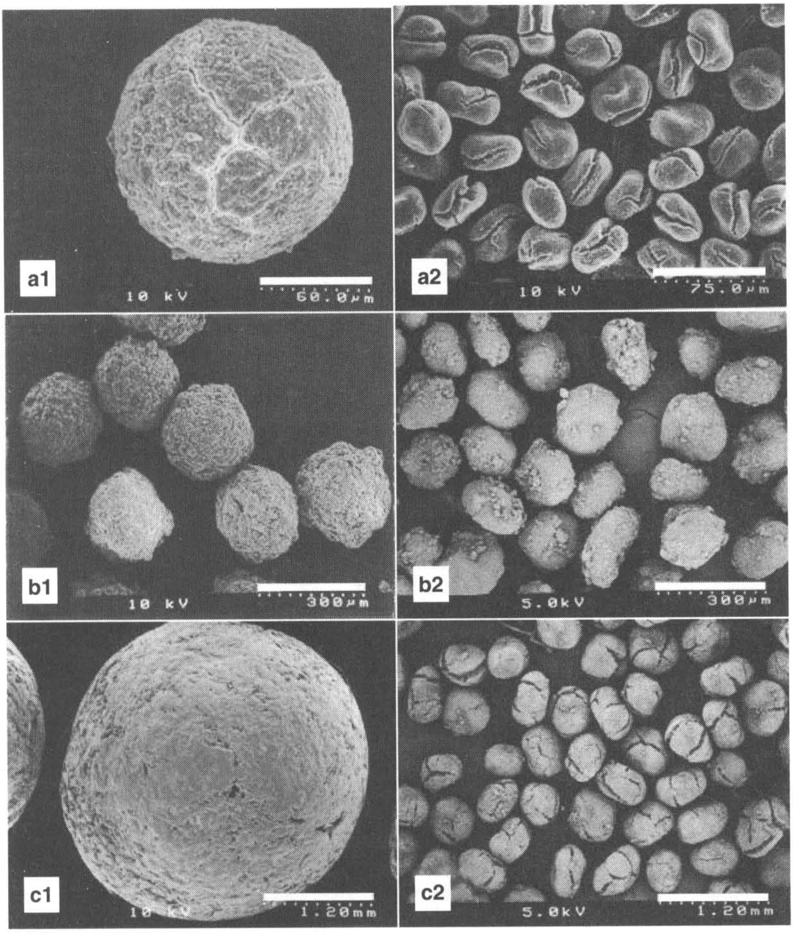

Figure 8.3 SEM micrographs: (*a*) catalyst particles (*a*1: bar = 60 µm; *a*2: bar = 75 µm); (*b*) prepolymer particles (bar = 300 µm); (*c*) polymer particles (bar = 1.2 mm).

in the gas-phase reactor is of the decay type (run P1) but of the acceleration type for the slurry operation (run P2) at a low temperature of 30 °C; at a high temperature of 70 °C, the rate profile in the slurry reactor is of the hybrid type (run P3) according to the classification of the rate profile types generalized by Kissin.[21]

The bulk density and morphology of nascent prepolymer particles are shown in Table 8.1 and Figure 8.5, respectively. It is seen in Figure 8.5 that prepolymer particles were totally broken down into fine powders and flakes in the gas-phase reactor (Figure 8.5*a* for run P1), even under the lowest ethylene pressure. For the prepolymerization in the slurry reactors, the spherical shape of catalysts was basically replicated into the shape of prepolymer particles (see Figures 8.5*b* and *c*). However, the bulk density of the prepolymer

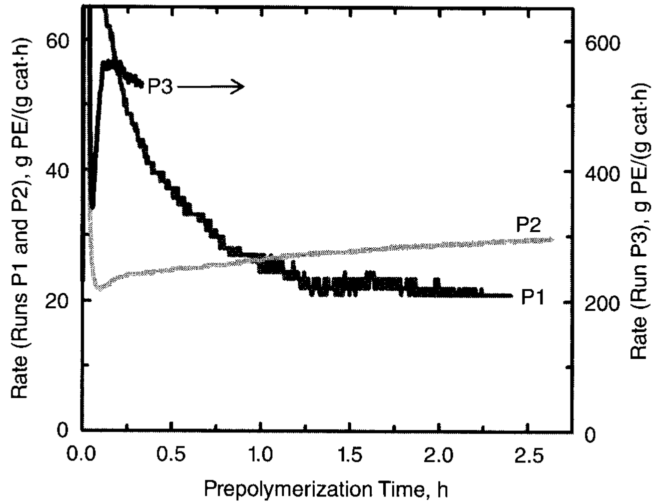

Figure 8.4 Typical rate profiles for ethylene prepolymerization in gas-phase (Run P1) and slurry (runs P2 and P3) reactors.

TABLE 8.1 Prepolymerization Conditions and Bulk Density of Prepolymer

Run No.	Reactor Type	*T*, °C	PH_2, kPa	PC_2H_4, kPa	Time, h	Yield, g PE/g Cat	Bulk Density, g/cm^3
P1	Gas phase[a]	30.0	89.8	36.2	2.43	75	n.m.[b]
P2	Slurry	29.6	86.2	61.6	2.64	73	0.34
P3	Slurry	72.6	85.4	342.9	0.33	160	0.29

[a] Rulon LR particles (35 g, 2 × 2 × 2 mm by size) were used as seedbeds.

[b] n.m. = not measured for broken gas-phase products.

produced at lower ethylene pressure (run P2) is higher, as seen in Table 8.1, probably due to the longer polymerization time. This indicated that prepolymerization in the slurry reactors is the critical process for the production of morphology-controlled polyethylene particles.

Since the yield of the prepolymerization at low temperatures and low ethylene pressures in slurry reactors is easy to control, prepolymer particles produced at 30 °C and ethylene pressure <70 kPa in slurry reactors were used as catalysts for the subsequent polymerization. This ensures the morphology replication for the production of morphology-controlled polymer particles. Such morphology replication is unique in that activity profiles and polymer properties can be examined as a function of catalyst/prepolymer and polymer particle sizes. This allows the direct comparison of experimental result with model predictions in the literature.

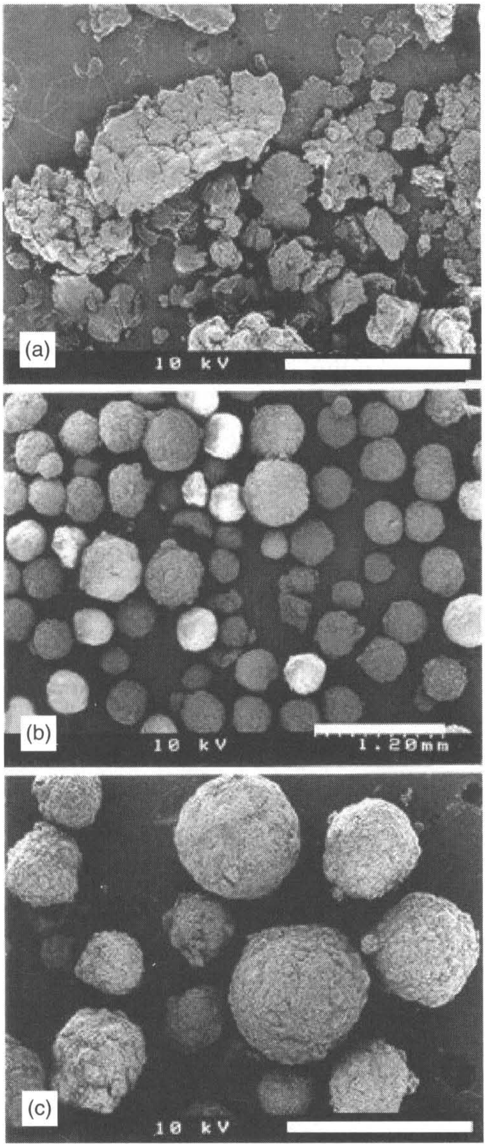

Figure 8.5 Typical morphologies of nascent prepolymer particles: (*a*) gas-phase product run P1; (*b*) slurry product run P2; (*c*) slurry product run P3 (all bars = 1.2 mm).

8.4.1 Effect of Prepolymer Particle Size on Its Properties

Nascent prepolymer particles produced in run P2 were sieved and their properties as a function of the prepolymer size were measured. Molar masses of polyethylene were measured by size exclusion chromatography with a Waters 150C GPC equipped with a differential refractometer and a series of four

Shodex GPC/UT-800M columns. The effects of prepolymer particle sizes on molar masses are shown in Figure 8.6. The results of Brunauer–Emmett–Teller (BET) surface areas as a function of the prepolymer particle size are shown in Table 8.2; the mesopore size distribution of the prepolymer particle was independent of particle size. The BET measurements were done using an OMNISORP 360 with nitrogen as the adsorbate.[58]

Assuming that initial catalyst particles are equally porous and active, large catalyst particle will produce large polyethylene particle.[7] Thus, the properties of the prepolymer particles should be independent of particle sizes if catalyst particles of different sizes undergo an even fragmentation. It is seen from Figure 8.6 that molar masses decrease with increasing nascent prepolymer particle size. The decrease in molar masses with increasing particle size indicated that the ethylene concentration inside the large particles is lower than

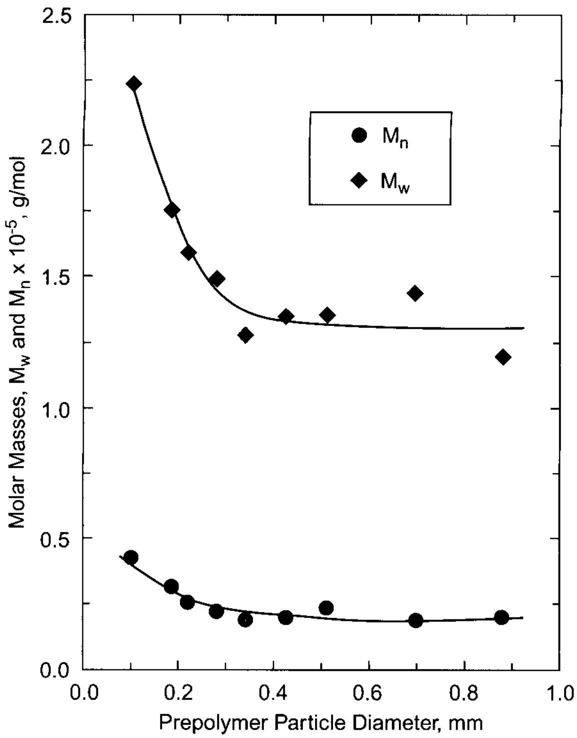

Figure 8.6 Effect of particle size on molar masses for prepolymer from run P2.

TABLE 8.2 Effect of Particle Size on BET Surface Area for Prepolymer Produced in Run P2

Particle diameter, mm	0.15	0.24	0.35	0.60
BET surface area, m^2/g	<1.0	1.9	2.3	3.8

that in small particles; this is predicted by the multigrain model; that is, intraparticle mass transfer limitations increase with increasing catalyst particle size for slurry polymerization under mass transfer limitations.[25] Mass transfer limitations will also lead to increases of the intraparticle void fraction with increasing particle size.[59] The increases in the BET surface areas (i.e., the void fraction since the pore sizes are independent of the particle sizes) with increasing prepolymer particle size are seen in Table 8.2. The uneven fragmentation and mass transfer limitations are further discussed in the following SEM studies of prepolymer morphology.

8.4.2 Initial Prepolymer Growth on Catalyst Particles

The first step of particle growth in heterogeneous olefin polymerization is catalyst fragmentation. The initial fragmentation of catalyst particles to the subsequent growth of polymer particles is dependent on the type of catalysts, the nature of the support materials, and the polymerization conditions.[24] Various microscopic techniques have been used to study the fragmentation process of the commercial $MgCl_2$-supoprted Ti catalysts for propylene polymerization.[24,49,60–62] However, little information is available on the fragmentation of catalyst particles and their growth to polymer particles at the early stages of ethylene polymerization.

A series of prepolymers with different polymerization yields from 1 to 16g PE/g catalyst was produced under the same mild conditions in the slurry reactor with the catalyst shown in Figure 8.1. The prepolymerization profiles of this series of runs are of the acceleration type, which is similar to that of run P2, as shown in Figure 8.4. The particles of the catalyst and prepolymer were imbedded in epoxy and microtomed before they were coated with a thin layer of carbon for the examination of their cross sections with SEM and energy-dispersive X-ray (EDX) analysis.[63] The cross-sectional images and elemental mapping of the catalyst and prepolymer particles are shown in Figures 8.7 and 8.8. It can be seen in Figure 8.7 that the active elements Cl, Mg, and Ti are evenly distributed throughout the cross section of the solid catalyst particle. For prepolymer particles, only Mg signals are shown in Figure 8.8 because of the weak Ti signals at higher prepolymerization yields. After 3min of prepolymerization with a yield of 1g PE/g catalyst, a continual layer of polyethylene shell of 10–30μm, as indicated in Figure 8.8*a*, was formed at the outer surface of the particle. The signals of all the elements in the X-ray mapping were also weaker toward the edge of the particle. This indicated that the catalyst particles did not completely fracture immediately after the polymerization started; a greater amount of polymer was formed at the outer layer due to the higher degree of particle fragmentation close to the surface of the particle. Inside the polymer shell, large pores were developed due to the rapid expansion of the growing shell within a short time. Similar uneven expansion was observed at a higher prepolymerization yield of 4.6g PE/g catalyst, as shown in Figure 8.8*b*, except that the outer polymer shell had grown thicker.

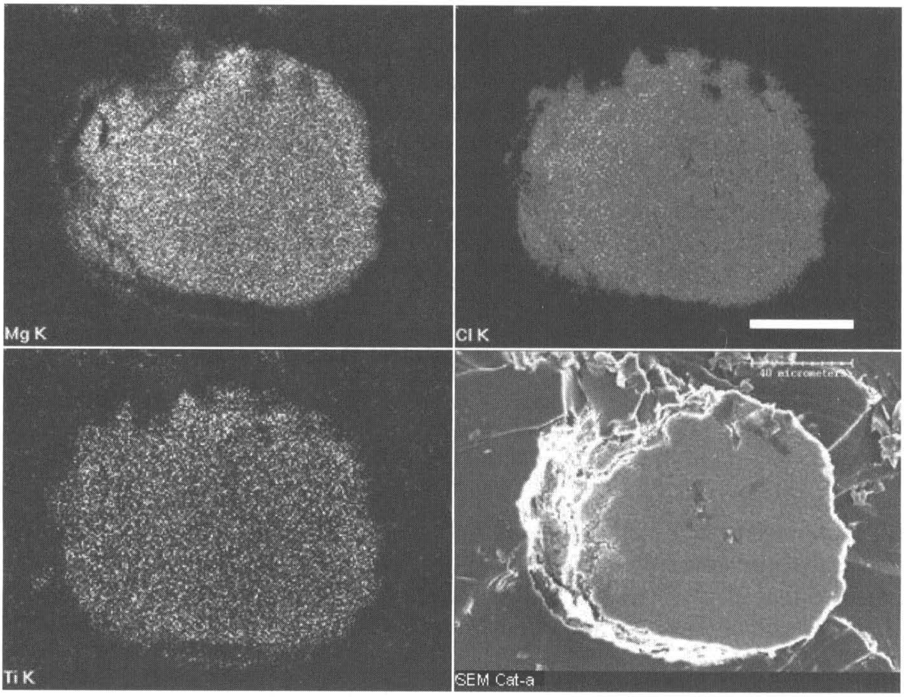

Figure 8.7 Dispersive X-ray analysis for Mg, Cl, and Ti and SEM image of cross-sectioned particle of $MgCl_2$-supported Ti catalyst (Cat-a) prepared by emulsion-quenching method (bar = 40 μm).

At higher yields of 9.3–16 g PE/g catalyst, more polymer was formed inside the particle to fill up the pores, as shown in Figures 8.8*c* and *d*. The filling of pores with the progress of polymerization was also reported for olefin polymerization over various Ziegler–Natta catalysts.[50,64–66] This result is in agreement with the prediction of the multigrain model that mass transfer limitations are most severe during the initial stages of particle growth.[26]

To further determine the spatial variation in composition across the particles, quantitative EDX analyses were performed at the central area and close to the edge of the particle cross sections shown in Figures 8.7 and 8.8. The concentrations of elements Cl, Mg, and Ti are listed in Table 8.3. It should be noted that the values listed in Table 8.3 may not be accurate because of the variations in the thickness of the carbon coating on the surface of the samples, the flatness and selection of the specific areas used for the analysis, and the disturbance of the background noise for the low-concentration elements. For example, the Ti concentration, as shown in Table 8.3, was 2.9 mass %; this is equivalent to 4.7 mass % on the carbon-free basis while the Ti concentration in the catalyst determined by the colorimetric analysis method was 3.5 mass %. However, the Cl, Mg, and Ti concentrations in the catalyst

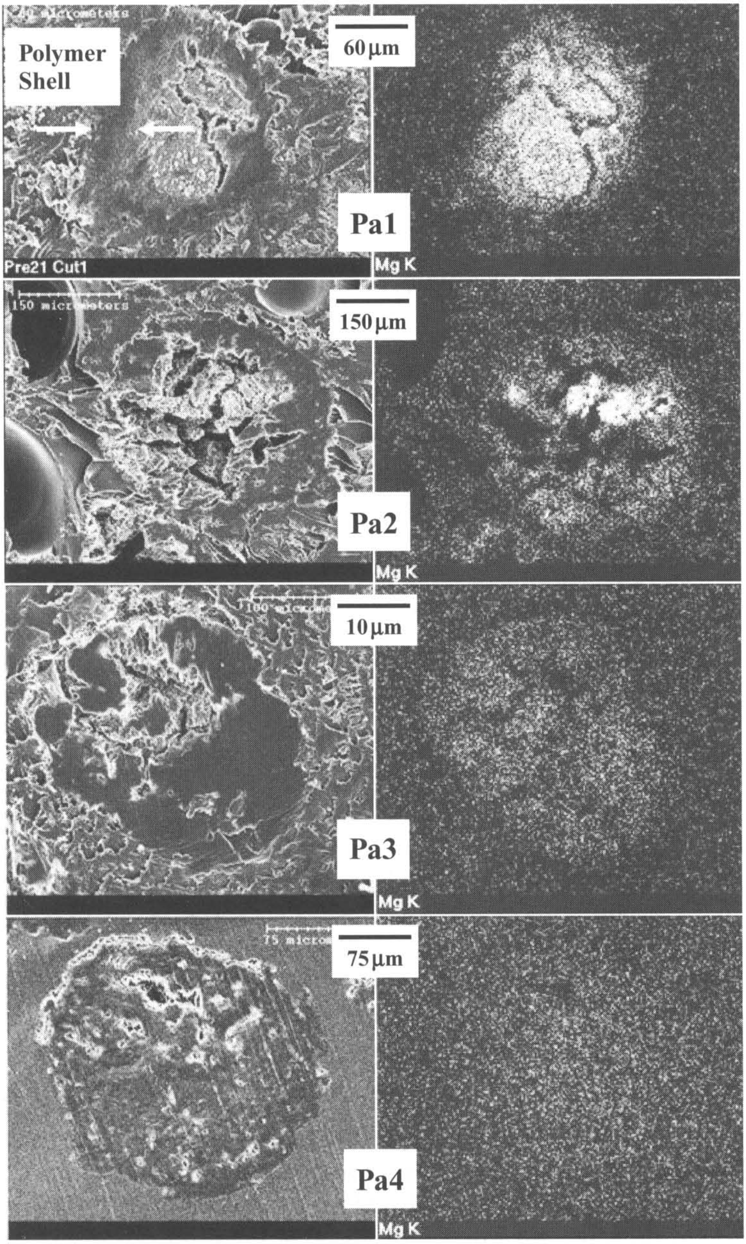

Figure 8.8 SEM images (left) and dispersive X-ray analyses for Mg (right) of cross-sectioned prepolymer particles after initial stages of prepolymerization in slurries.

TABLE 8.3 Quantitative EDX Analyses of Catalyst and Prepolymers with Different Yields

		Element Concentration, mass %								
		Center			Edge			Overall		
Sample	Yield, g PE/g Cat	Cl	Mg	Ti	Cl	Mg	Ti	Cl	Mg	Ti
Cat-a	0	43	15	3.1	44	17	2.8	43	16	2.9
Pa1	1.0	32	7.0	1.6	6.5	1.4	0.4	21	5.2	1.0
Pa2	4.6	10	2.1	0.8	1.7	0.4	0.1	3.7	0.8	0.2
Pa3	9.3	3.3	0.7	0.2	1.0	0.2	0.04	2.6	0.6	0.1
Pa4	16.0	1.7	0.5	0.1	0.5	0.2	0.04	1.0	0.3	0.1

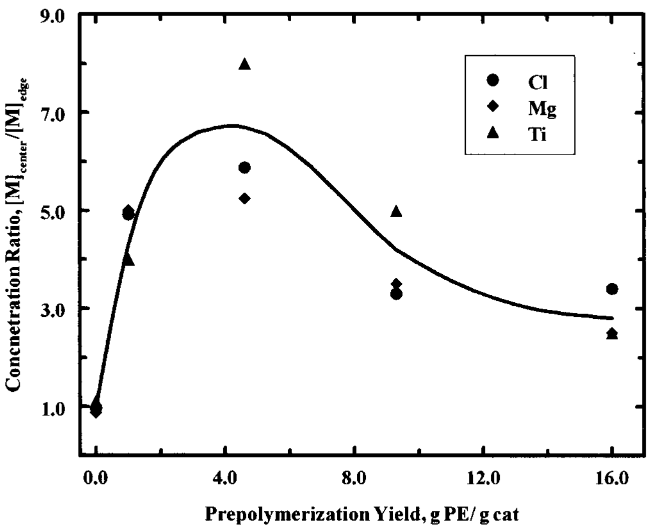

Figure 8.9 Center-to-edge ratios of Cl, Mg, and Ti concentration for catalyst and prepolymer particles as function of prepolymerization yield.

are higher than those in the prepolymer particles; the concentrations decrease with increasing polymerization yield, and the overall concentrations are higher than those at the edge but lower than those at the center of the prepolymer particles. This indicated that the data provided general trends of element distributions with respect to the position, polymerization time, or yield.

From the data in Table 8.3, the ratio of the concentrations of the three elements at the center to that at the edge can be calculated and is plotted in Figure 8.9 as a function of prepolymerization yield. For the catalyst (Cat-a), there is very little difference in elemental concentrations with position in the pellet, that is, the ratios of the concentrations at the center of the pellet to that at the edge of the pellet were close to unity for Cl, Mg, and Ti. The ratios for all of the prepolymerization yields are much greater than 1, that is, the polymerization rate at the outer surface of the particle was much higher than that at the center. The ratios increased with increasing prepolymerization yield and reached a maximum at the yield of 4.6 g PE/g catalyst. As the yield increased from 4.6 to 16 g PE/g catalyst, the ratios decreased. This observation indicated that the catalyst fragmentation started from outside progressively toward its interior of the particle. The interior of the catalyst particle also fragmented, but to a lesser degree, because Cl, Mg, and Ti concentrations at the center of the prepolymer particle with a low yield of 1 g PE/g catalyst were lower than those of the catalyst (see Table 8.3). At the very beginning, an uneven expansion of the particle, as indicated by the increasing ratios in Figure 8.9, resulted in the open structure inside the growing particle. As prepolymerization continued, catalyst fragmentation inside the particle took place to a greater degree, as shown by the decreases in the concentration ratios at higher prepolymerization yields (Figure 8.9).

The catalyst fragmentation in ethylene polymerization observed in Figure 8.8 is different from the previously reported fragmentation types for the propylene polymerization; the fragmentation in the sequential formation of concentric layers of the onion-skin type starting from the external surface toward the center of the particle was reported by several investigators.[15,45,49,67] The other type of reported fragmentation is the uniform particle fragmentation immediately after the beginning of the propylene polymerization.[24,49,61,62] According to Zheng and Loos[49] and Zheng et al.,[68] the different fragmentation types in the early stages of propylene polymerization are influenced by the porosity of the $MgCl_2$-supported Ti catalysts. For low-porosity catalysts, the polymerization is under mass transfer limitations; this will cause layer-by-layer fragmentation. For highly porous catalyst, the monomer has easy access into the pores of the catalyst/polymer particle, which will result in an almost instantaneous fragmentation. The single-shell formation observed in Figure 8.8 seems to indicate that mass transfer was slightly limiting during the early stages of catalyst fragmentation in ethylene polymerization in our studies.

8.5 POLYMERIZATION BEHAVIOR

Activity profiles and polymer properties are valuable parameters in evaluating catalysts and resolving mass and heat transfer limitations during the polymerization. Activity profiles for slurry and gas-phase operations are presented for ethylene polymerization over morphology-controlled $MgCl_2$-supported Ti catalysts. The properties of polymer products were measured, particularly as a function of particle sizes. Comparison of these results with model predictions in the literature will be made in terms of mass and heat transfer limitations.

8.5.1 Activity Profiles in Gas-Phase Reactors

Activity profiles as a function of ethylene pressures at 70 °C are shown in Figure 8.10 for ethylene homopolymerization and ethylene/1-hexene copolymerization in the gas-phase reactors. Prepolymer particles, such as those shown in Figure 8.3*b*1, were used as the catalyst for the runs; the molar ratio of 1-hexene to ethylene in the gas phase was 0.055 for all the copolymerization runs shown in Figure 8.10*b*. The polymerization activities shown in Figure 8.10 were normalized with respect to ethylene pressure. The increases in normalized activities with increasing ethylene pressure indicate that the polymerization orders with respect to ethylene concentration are >1 for the prepolymerized catalyst.

Mass transfer limitations of ethylene can cause polymerization orders >1 because mass transfer limitations are more severe at lower ethylene pressures.[59] However, mass transfer limitations were unlikely for these runs because mass transfer limitations can lengthen the acceleration period at lower ethylene pressure, and this was not observed in Figure 8.10. Heat transfer limitations for which the particle temperature would be significantly higher than the gas temperature can also lead to the higher polymerization orders if the polymerization rate increased with increasing temperature. However, the effect of polymerization temperature on the activity profiles shown in Figure 8.11 indicated that the polymerization rate decreases from 60 to 90 °C due to the catalyst deactivation at higher temperatures. The decrease in activities with increasing temperature from 50 to 80 °C was reported for

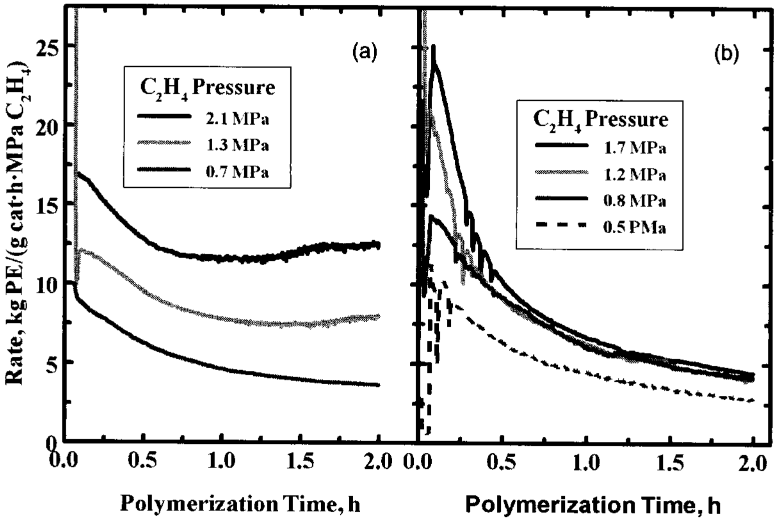

Figure 8.10 Effect of ethylene pressure on activity profiles: (*a*) ethylene homopolymerization; (*b*) ethylene/1-hexene copolymerization at 1-hexene/ethylene molar ratio of 0.055.

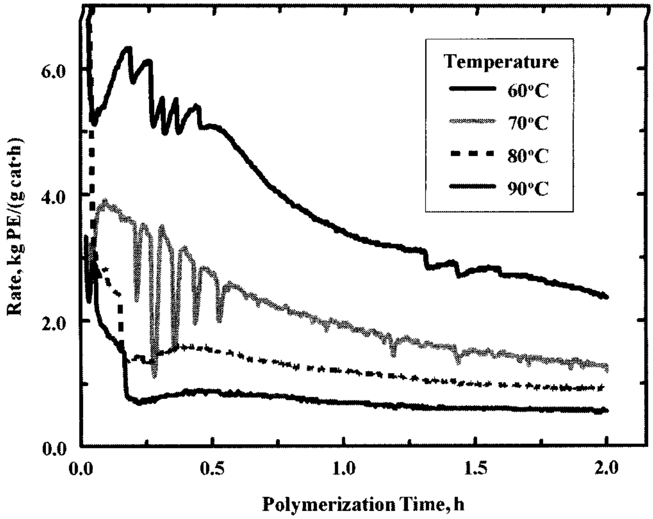

Figure 8.11 Effect of polymerization temperature on activity profiles for ethylene/1-hexene copolymerization.

gas-phase ethylene homopolymerization over a silica/$MgCl_2$-supported Ti catalyst.[69] It was also reported that the maximum activity for $MgCl_2$-supported Ti catalysts was around 60 °C for ethylene homopolymerization[17] and propylene polymerization.[6,70]

Particle fragmentation can cause a higher polymerization order if the fragmentation rates increase more rapidly than the increases in the polymerization rates due to the increases in ethylene pressure. The high polymerization orders were attributed to the presence of two different types of catalytic sites for which the polymerization rates were first and second order to the ethylene concentration.[17] Nevertheless, the above results on the activity profiles indicated the absence of mass and heat transfer limitations during ethylene polymerization in the gas-phase reactors.

8.5.2 Activity Profiles in Slurry Reactors

Activity profiles as a function of catalyst size are shown in Figure 8.12 for ethylene homopolymerization under the conditions of ethylene pressure of 965 kPa, hydrogen pressure of 276 kPa, and reactor temperature of 70 °C in the stainless steel reactor operated in the slurry mode.[63] The nascent particles from a prepolymerization run were separated into several fractions according to the particle sizes by sieving in the glove box, and prepolymer particles of each fraction were used as catalysts for each run. It can be seen in Figure 8.12 that the rate increases in the activity profiles at the beginning of polymerization were independent of prepolymer size. This indicates that concentration of active sites is similar in catalyst particles of different sizes. After 30 min of

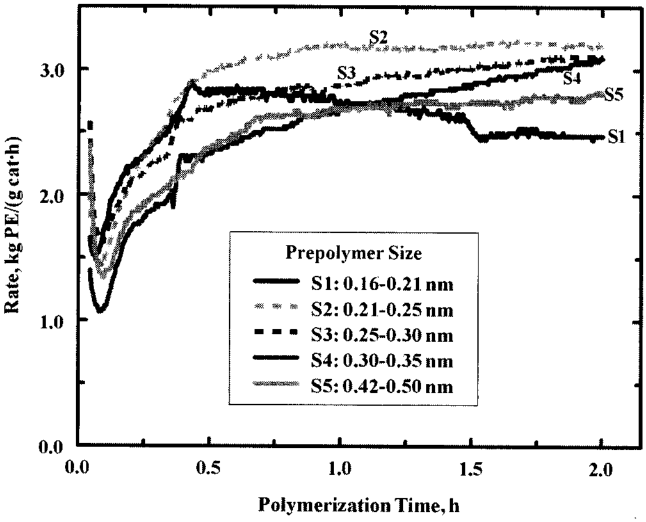

Figure 8.12 Activity profiles for ethylene polymerization in slurry reactors using prepolymerized catalyst of different sizes.

polymerization, the increases in polymerization rates started to slow down for larger particles and even decrease for smaller sizes. The change of activity profiles from the acceleration type to hybrid type with decreasing particle sizes is in agreement with the effects of different catalyst particle sizes on activity profiles of olefin polymerization under the mass transfer limitations.[25,71] It is noted that the lowest activity observed for the smallest prepolymer particles is probably due to the catalyst deactivation by impurities because the larger surface–volume ratio makes smaller particles more vulnerable to poisoning.

8.5.3 Effect of Polymer Particle Size on Its Properties

The results of polymer properties such as densities and molar masses are presented for polymer particles made in slurry and gas-phase reactors at two different ethylene pressures. The run conditions are listed in Table 8.4. The bulk densities of the polyethylene products are also listed in Table 8.4. The bulk density is an important parameter for product handling and transportation. The bulk density ρ_b is the mass per unit volume of a bed of all the particles (see ASTM D1895–67):

$$\rho_b = \frac{W}{V} \tag{8.1}$$

where W and V are the mass and volume, respectively, of all the particles obtained in a run; V includes intraparticle porosities and interparticle voids.

TABLE 8.4 Polymerization Conditions and Bulk Density of Polymer Products

Run No.	Reactor Type	T, °C	PH_2, MPa	PC_2H_4 MPa	Yield, kg PE/g Cat	Bulk Density, g/cm^3
S1	Slurry	68.3	0.33	1.38	8.53	0.40
S2	Slurry	68.9	0.35	0.66	2.77	0.32
G1	Gas phase[a]	70.5	0.31	1.37	10.03	0.45
G2	Gas phase	67.9	0.35	0.69	2.39	0.42

[a] Rulon LR particles (35 g, 2 × 2 × 2 mm by size) were used as seedbeds.

It can be seen in Table 8.4 that the bulk densities of the polyethylene products are as high as 0.4 g/cm^3 for slurry operations; typical gas-phase products have bulk densities of up to 0.45 g/cm^3. These bulk densities of polymer, especially for the gas-phase products, are higher than those of prepolymer particles (see Table 8.1).

Assuming the void fraction of the interparticle bed is ε_b, the bulk density ρ_b is related to the particle density ρ_p as

$$\rho_b = (1-\varepsilon_b)\rho_p \tag{8.2}$$

For the morphology-controlled particles, the particle density can be calculated. This is done by manually sorting the nascent polymer particles of each run into several sets of particle sizes. The diameter of each individual particle is measured under an optical microscope.[17] The individual particle diameter d_i is taken as the average of the diameters measured at different positions. Since density is related to the volume number average diameter (d_{30}), the volume number average diameter of each set can be calculated according to the equation 3

$$d_{30} = \left(\frac{\sum_i n_i d_i^3}{n_i} \right)^{1/3} \tag{8.3}$$

where n_i is the number of particles with a diameter d_i and n_t is the total number of particles in each set. The particle density ρ_p is then calculated as

$$\rho_p = \frac{6W_t}{\pi n_t d_{30}^3} \tag{8.4}$$

where W_t is the total mass of particles in each set.

The particle densities of each set of polymer particles as a function of particle size are shown in Figure 8.13. For a typical interparticle void fraction of 0.37, the results shown in Figure 8.13 are in agreement with the bulk density

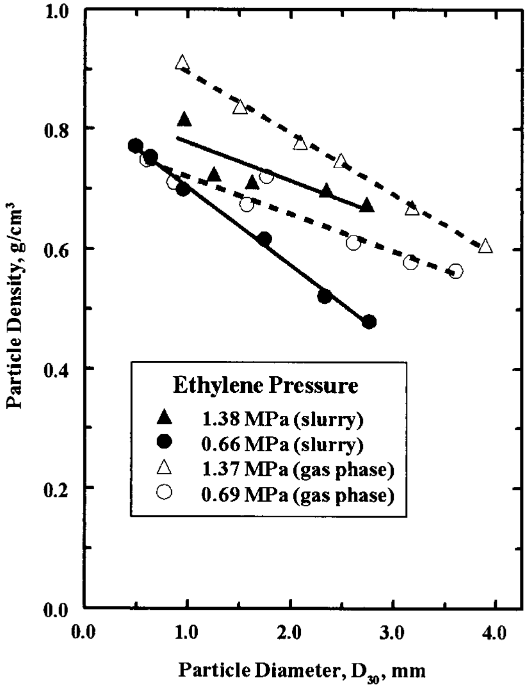

Figure 8.13 Effect of particle size on particle density for products from slurry and gas-phase operations.

data listed in Table 8.4. The effect of polymer particle size on the weight average molar masses is shown in Figure 8.14 for nascent polyethylene particles produced in slurry and gas-phase reactors under the two different ethylene pressures. The following general observations can be made from the results of particle densities (see Figure 8.13) and molar masses (see Figure 8.14):

1. The bulk densities and particle densities of polymer made in the gas-phase reactor are higher than those made in the slurry reactor.
2. The bulk densities, particle densities, and molar masses are higher at higher ethylene pressure for both slurry and gas-phase operations.
3. The particle densities decrease with increasing particle size for both slurry and gas-phase operations.
4. For the slurry operation, the molar masses decrease with increasing particle size, and the decrease is more pronounced at the lower ethylene pressure.
5. For the gas-phase operation, the molar masses are independent of particle size.

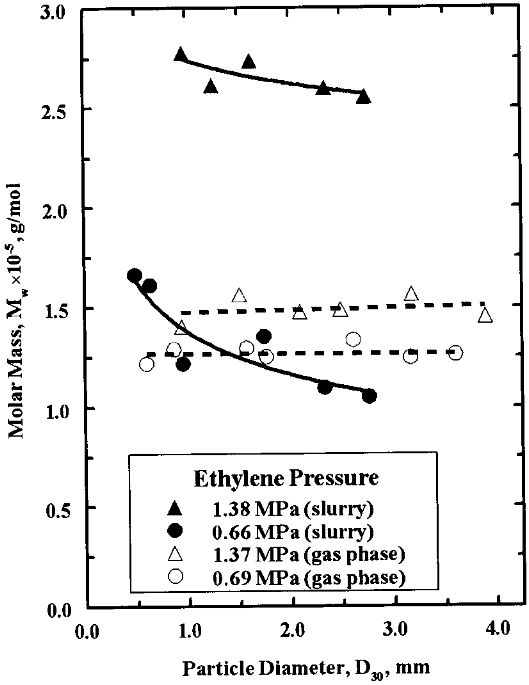

Figure 8.14 Effect of particle size on molar masses for products from slurry and gas-phase operations.

The dependencies of molar masses on particle size and ethylene pressure in slurry operations are probably caused by the presence of mass transfer limitations because mass transfer limitations are more severe at lower monomer pressures and for larger particles in slurry reactors.[26] The decreases in molar masses with increasing sizes of polyethylene particles produced in slurry reactors were also reported by McKenna et al.[27] The lower bulk densities and particle densities in the slurry operations are likely caused by mass transfer limitations because polymer grows faster in the outer layer than in the inner core, and larger pores are more likely to develop inside the larger particles, as already seen in the effect of particle sizes on the BET surface areas of prepolymer particles (see Table 8.2). The higher porosity of larger prepolymer particles was replicated to the polymer particles, as seen in the decreases in polymer particle density with increasing size for the slurry and gas-phase operations in Figure 8.13. The independence of molar masses on size as shown in Figure 8.14 indicated that mass transfer limitations are less severe for gas-phase operations. The interior of the typical particles produced in the slurry and gas-phase reactors is shown in Figure 8.15. The hollow structure for the slurry particle from run S2 is in contrast with the solid gas-phase product from run G1.

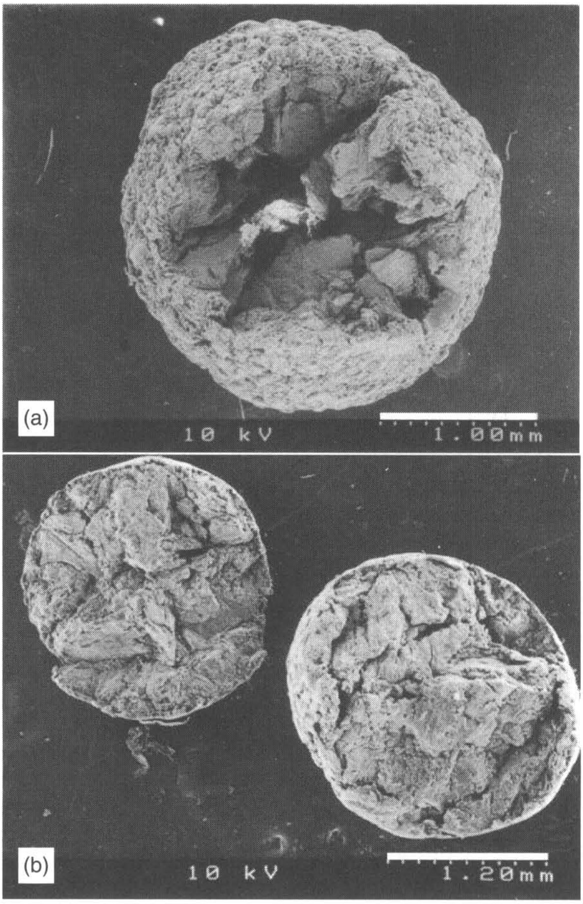

Figure 8.15 Interior of polymer particles: (*a*) slurry product from run S2 (bar = 1.0 mm); (*b*) gas-phase product from run G1 (bar = 1.2 mm).

The lower densities of the slurry products could also be due to the swelling effect of heptane used for the polymerization medium. Heptane, which essentially consists of the same chemical structure as polyethylene, can swell the polymer particles. Removal of heptane will result in particles with higher porosity.

8.6 SUMMARY AND CONCLUSIONS

Morphology-controlled polyethylene particles with little fines were produced in our laboratory in a two-stage polymerization over $MgCl_2$-supported Ti catalysts. Prepolymerization in slurry reactors prior to the high-yield polymerization is essential in the production of morphology-controlled polyethylene.

Mass transfer limitations were present during prepolymerization in slurry reactors. The properties of prepolymers varied with prepolymer particle sizes; this variation did not affect the molar masses of polymer products from the subsequent gas-phase operation. Mass and heat transfer limitations are unlikely in gas-phase polymerization reactors with prepolymerized catalysts.

REFERENCES

1. Ziegler, K., Breil, H., Holzkamp, E., and Martin, H., K. Ziegler, DE Patent No. 973,626, **1953**. See also U.S. Patent No. 3,257,332, 1954.
2. Natta, G., Pino, P., and Mazzanti, G., Montecatini, U.S. Patent No. 3,112,300, 1955.
3. Natta, G., Pino, P., Corradini, P., Danusso, F., Mantica, E., Mazzanti, G., and Moraglio, G., *J. Am. Chem. Soc.*, **1955**, 77, 1708–1710.
4. Galli, P., *Macromol. Symp.*, **1996**, 112, 1–16.
5. Haggin, J., *Chem. Eng. News*, **1992**, 70(13), 17–18.
6. Galli, P., Luciani, L., and Cecchin, G., *Angew. Makromol. Chem.*, **1981**, 94, 63–89.
7. Boor, Jr., J., *Ziegler-Natta Catalysts and Polymerizations*, Academic, New York, 1979.
8. Galli, P., Milani, F., and Simonazzi, T., *Polym. J.*, **1985**, 17, 37–55.
9. Galli, P., *Macromol. Symp.*, **1994**, 78, 269–284.
10. Galli, P., Collina, G., Sgarzi, P., Baruzzi, G., and Marchetti, E., *J. Appl. Polym. Sci.*, **1997**, 66, 1831–1837.
11. Galli, P., *J. Macromol.Sci. Pure Appl. Chem.*, **1999**, A36, 1561–1586.
12. Cipriani, C., and Trischman, Jr., C. A., *Chem. Eng.*, **1982**, 89(10), 66–67.
13. Galli, P., *Popular Plastics & Packaging*, **1993**, 38, 71–80.
14. Smith, P., Chanzy, H. D., and Rotzinger, B. P., *J. Mater. Sci.*, **1987**, 22, 523–531.
15. Galli, P., and Haylock, J. C., *Prog. Polym. Sci.*, **1991**, 16, 443–462.
16. Ferraris, M., Rosati, F., Parodi, S., Giannetti, E., Albizzati, E., Motroni, G., and Albizzati, E., Montedison S.p.A., U.S. Patent No. 4,339,054, 1981.
17. Wu, L., Lynch, D. T., and Wanke, S. E., *Macromolecules*, **1999**, 32, 7990–7998.
18. Jamjah, R., Zohuri, G. H., Vaezi, J., Ahmadjo, S., Nekomanesh, M., and Pouryari, M., *J. Appl. Polym. Sci.*, **2006**, 101, 3829–3834.
19. Mirzaei, A., Vakili, M., and Tafi, N., *J. Appl. Polym. Sci.*, **2007**, 105, 2703–2711.
20. Keii, T., *Kinetics of Ziegler-Natta Polymerization*, Kodansha, Tokyo, and Chapman & Hall, London, 1972.
21. Kissin, Y. V., *Isospecific Polymerization of Olefins with Heterogeneous Ziegler-Natta Catalysts*, Springer-Verlag, New York, 1985.
22. McKenna, T. F., DuPuy, J., and Spitz, R., *J. Appl. Polym. Sci.*, **1995**, 57, 371–384.
23. Bu, N., Lynch, D. T., and Wanke, S. E., *Polym. React. Eng.*, **1995**, 3, 1–22.
24. Pater, J. T. M., Weickert, G., Loos, J., and van Swaaij, W. P. M., *Chem. Eng. Sci.*, **2001**, 56, 4107–4120.
25. Floyd, S., Choi, K. Y., Taylor, T. W., and Ray, W. H., *J. Appl. Polym. Sci.*, **1986**, 32, 2935–2960.

26. Floyd, S., Heiskanen, T. W., Taylor, T. W., Mann, G. E., and Ray, W. H., *J. Appl. Polym. Sci.*, **1987**, 33, 1021–1065.
27. McKenna, T. F., Barbotin, F., and Spitz, R., *J. Appl. Polym. Sci.*, **1996**, 62, 1835–1841.
28. Luciani, L., Milani, F., Invernizzi, R., Borghi, I., and Labianco, A., ECP Enichem Polimeri S.r.l, Canadian Patent No. 2,073,723, 1992.
29. Luciani, L., Milani, F., and Zannetti, R., *Macromol. Symp.*, **1995**, 89, 139–149.
30. Ran, R., *J. Polym. Sci. Pt. A Polym. Chem.*, **1993**, 31, 1561–1569.
31. Sun, L., Hsu, C. C., and Bacon, D. W., *J. Polym. Sci. Pt. A Polym. Chem.*, **1994**, 32, 2127–2134.
32. Jericó, S., Schuchardt, U., Joekes, I., Kaminsky, W., and Noll, A., *J. Molec. Catal. A Chem.*, **1995**, 99, 167–173.
33. Ushida, Y., Amimoto, Y., Toyota, A., and Kashiwa, N., Mitsui Petrochemical Industries, U.S. Patent No. 4,315,847, 1980.
34. Toyato, A., and Kashiwa, N., Mitsui Petrochemical Industries, U.S. Patent No. 4,547,522, 1984.
35. Sacchetti, M., Govoni, G., and Clarrocchi, A., Himont, U.S. Patent No. 5,221,651, 1992.
36. Galli, P., Di Drusco, G., and De Bartolo, S., Montecatini Edison S.p.A., U.S. Patent No. 3,953,414, 1974.
37. Iikolan, E., and Koskinen, J., Neste Oy, U.S. Patent No. 4,829,034, 1987.
38. Miya, S., Tachibana, M., and Karasawa, Y., Chisso, U.S. Patent No. 5,100,849, 1990.
39. Masi, F., Moalli, A., Invernizzi, R., Menconi, F., Ferrero, F., Malquori, S., Barazzoni, L., and Polesello, M., Enichem Anic S.p.A., U.S. Patent No. 5,070,051, 1991.
40. Pentti, I., and Leskinen, P., Neste Oy, European Patent No. 607,703, 1993.
41. Bailly, J.-C. A., and Behue, P., BP Chemicals, U.S. Patent No. 5,106,805, 1990.
42. Bailly, J.-C. A., BP Chemicals, U.S. Patent No. 5,208,303, 1991.
43. Jenny, C., and Lalanne-Magne, C., BP Chemicals, European Patent No. 570,199, 1993.
44. Vogel, A. I., *A Text-Book of Quantitative Inorganic Analysis Including Elementary Instrumental Analysis*, 3rd ed., Longmans, London, **1961**, pp. 788–790.
45. Covezzi, M., *Macromol. Symp.*, **1995**, 89, 577–586.
46. Roger, D., Havas, L. J., and Mangin, P., Naphtachimie, U.S. Patent No. 3,922,322, 1973.
47. Havas, L. J., and Mangin, P. M., Naphtachimie, U.S. Patent No. 3,954,909, 1976.
48. Carson, I. G., *Angew. Makromol. Chem.*, **1988**, 16, 145–156.
49. Zheng, X. J., and Loos, J., *Macromol. Symp.*, **2006**, 236, 249–258.
50. Tang, S. P., *Stud. Surf. Sci. Catal.*, **1986**, 25, 165–179.
51. Yano, T., Inoeu, T., Ikai, S., Kai, Y., Tamura, M., and Shimizu, M., *Makromol. Chem. Rapid Commun.*, **1986**, 7, 491–495.
52. Xu, Z. K., Zhu, Q. Q., Feng, L. X., and Yang, S. L., *Makromol. Chem. Rapid Commun.*, **1990**, 11, 79–81.
53. Hutchinson, R. A., and Ray, W. H., *J. Appl. Polym. Sci.*, **1991**, 43, 1271–1285.
54. Czaja, K., and Krol, B., *Macromol. Chem. Phys.*, **1998**, 199, 451–455.

55. Soares, J. B. P., and Hamielec, A. E., *Polymer*, **1996**, 37, 4599–4605.
56. Chu, K. J., Soares, J. B. P., Penlidis, A, and Ihm, S.-K., *Eur. Polym. J.*, **2000**, 36, 3–11.
57. Lynch, D. T., and Wanke, S. E., *Can. J. Chem. Eng.*, **1991**, 69, 332–339.
58. Pieters, W. J. M., and Venero, A. F., *Stud. Surf. Sci. Catal.*, **1984**, 19, 155–163.
59. Hutchinson, R. A., Chen, C. M., and Ray, W. H., *J. Appl. Polym. Sci.*, **1992**, 44, 1389–1414.
60. Kakugo, M., Sadatoshi, H., Sakai, J., and Yokoyama, M., *Macromolecules*, **1989**, 22, 3172–3177.
61. Noristi, L., Marchetti, E., Baruzzi, G., and Sgarzi, P., *J. Polym. Sci. Pt. A Polym. Chem.*, **1994**, 32, 3047–3059.
62. Abboud, M., Denifl, P., and Reichert, K.-H., *Macromol. Mater. Eng.*, **2005**, 290, 558–564.
63. Liu, W., Gas-phase ethylene/1-hexene copolymerization over $MgCl_2$-supported Ziegler-Natta catalysts, Ph.D. Thesis, University of Alberta, Edmonton, Canada, 2002.
64. Baker, R. T. K., Harris, P. S., Waite, R. J., and Roper, A. N., *J. Polym. Sci. Polym. Lett. Ed.*, **1973**, 11, 45–53.
65. Galli, P., Barbè, P. C., and Noristi, L., *Angew. Makromol. Chem.*, **1984**, 120, 73–90.
66. Conner, W. C., Ferrero, M., Webb, S., Sommer, R., Chiovetta, M., Jones, K., and Spanne, P., *Stud. Surf. Sci. Catal.*, **1993**, 75, 1827–1830.
67. Simonazzi, T., Cecchin, G., and Mazzullo, S., *Prog. Polym. Sci.*, **1991**, 16, 303–329.
68. Zheng, X. J., Pimplapure, M. S., Weickert, G., and Loos, J., *e-Polym.*, **2006**, no. 028, 1–10.
69. Jejelowo, M. O., Lynch, D. T., and Wanke, S. E., *Macromolecules*, **1991**, 24, 1755–1761.
70. Dusseault, J. J., and Hsu, C. C., *J. Appl. Polym. Sci.*, **1993**, 50, 431–447.
71. McKenna, T. F., DuPuy, J., and Spitz, R., *J. Appl. Polym. Sci.*, **1997**, 63, 315–322.

9 Product Morphology in Olefin Polymerization with Polymer Supported Metallocene Catalysts

LONG WU and SIEGHARD E. WANKE
Department of Chemical and Materials Engineering, University of Alberta,
Edmonton, Alberta, Canada T6G 2G6

9.1 INTRODUCTION

The discovery in the 1950s that transition metal compounds, the Ziegler and Phillips catalysts, were capable of catalyzing olefin polymerization at mild conditions, even at room temperature and atmospheric pressure, revolutionized the production of polyethylene (PE).[1–3] The discovery by Natta[4] that Ziegler's catalysts polymerized propylene to produce product with high fractions of stereoregular polypropylene ushered in the large-scale polypropylene industry. A third major advance in olefin polymerization was the development of gas-phase olefin polymerization processes in the 1970s.[5] All of these discoveries and developments were applied to large-scale polyolefin production within a few years of their announcement.

Another major milestone in polyolefin catalysis was the serendipitous discovery by Sinn and Kaminsky[6] that the combination of methylaluminoxane (MAO) and metallocenes was much more active for olefin polymerization than Ziegler–Natta catalysts. Not only were the metallocene/MAO catalysts more active than previous polymerization catalysts but also the properties of the copolymers of ethylene with α-olefins produced with metallocene/MAO catalysts were very different than the product produced with conventional Ziegler–Natta catalysts. Metallocene/MAO catalysts produced copolymers with narrow molar mass distribution (polydispersities of 2–3) and relative uniform comonomer incorporation. The metallocene/MAO systems showed great promise, and a tremendous amount of academic and industrial research has been done on these systems in the past 25 years. A very large number

---

Handbook of Transition Metal Polymerization Catalysts Edited by Ray Hoff and Robert T. Mathers
Copyright © 2010 John Wiley & Sons, Inc.

of metallocenes have been synthesized and shown to be extremely active polymerization catalysts with exceptional abilities to manipulate stereospecificity.[7–11] Numerous patents have been applied and granted for metallocene polymerization catalysts; Hlatky[12] lists over 250 patents, applications, and disclosures in his review. However, metallocenes have not replaced most of the conventional Ziegler–Natta or Phillips catalysts in commercial production of commodity polyolefins. One of the reasons for the failure of metallocene/MAO to replace conventional polymerization catalysts in commercial applications is the incompatibility of homogeneous metallocene/MAO catalyst with current polyolefin production facilities.

Industrial slurry and gas-phase olefin polymerization processes require solid (heterogeneous) catalysts. Homogeneous catalysts, although very active, cannot be used in slurry processes because the product morphology is unacceptable. The poor product morphology results in product with low bulk densities, typically about 0.15 g/cm^3, making post–reactor processing difficult; bulk densities of at least 0.35 or 0.40 g/cm^3 are required.[13,14] Poor product morphology also results in reactor fouling because products adhere to the reactor walls.[12,15] The requirement of a large amount of cocatalyst, commonly MAO with an aluminum-to-metallocene metal atomic ratio >1000, is another barrier to the use of homogeneous metallocenes in commercial processes.[16,17] Homogeneous catalysts are obviously unsuitable for gas-phase processes because fluidized- and stirred-bed reactors require solid catalysts.

The most common method of converting a homogeneous metallocene into a solid catalyst is to immobilize the metallocene onto a solid carrier (support), although other methods, which will be discussed later, have also been proposed. Some of the required properties of supported metallocene catalysts have been enumerated by various investigators[17–20]; the requirements include the following:

1. Heterogeneous catalysts should have activities comparable to those of their homogeneous counterparts.
2. Heterogeneous catalysts should not deactivate rapidly.
3. The supported catalysts should require much less cocatalyst (MAO) than the homogenous metallocenes.
4. The supported catalysts must be free-flowing solids.
5. The shape and size of polymer product particles should be controllable, that is, morphology control.
6. The product should not contain significant amounts of fines (particles <0.1 mm in size).
7. Reactor fouling should not occur; this is related to morphology control.
8. The product particles must have a high bulk density, preferably above 0.4 g/cm^3.

A large number of studies on the preparation and use of heterogenized metallocene catalysts have appeared; several reviews have been published on the topic and many patents have been granted for such catalysts.[10,12,16,17] By far the most commonly studied supports for the metallocenes are inorganic supports[15] with silica gel (SiO_2) being the most commonly used support.[12,16,17] Silica is used so frequently because of the controllability of surface hydroxyls by thermal treatment[12,18] and its availability with a wide range of porosities and surface areas. The great success of silica as a support for Ziegler–Natta catalysts has also contributed to its popularity as a support for metallocenes. However, silica and other inorganic supports are not the best suited supports for metallocenes because the polar nature of inorganic surfaces results in the deactivation of metallocenes[12,22–24]; hence, modifications of the inorganic surfaces are required before the metallocenes can be added.[18,24] Many polymeric materials can also be used and these do not have the drawback of having reactive surfaces; that is, polymeric surfaces can provide an environment which is closer to that encountered by metallocenes in solution.[25,26] Polymeric supports have the additional advantage of reducing the inorganic residue in the product.[27,28]

Methods used to prepare polymer-supported metallocene catalysts and the product morphologies obtained with these catalysts are discussed in this chapter. Preparation and use of these catalysts for both slurry and gas-phase operations will be described, but the examples for morphology control will be taken from results obtained in our laboratory, which mainly studies gas-phase polymerization. No detailed review of the patent literature is included because the claims are much too broad and the examples too narrow. For example, one of the early patents granted in the area of polymer-supported catalysts claims the invention of olefin polymerization catalysts which are a combination of a porous polymer (support), an aluminum alkyl, and a group IVB-to-VIB transition metal compound which has at least one conjugated five-membered cyclic ligand.[29] Essentially all porous polymers are claimed and over 100 metallocene or metallocene-like compounds are listed; although several metallocenes were included in the examples, the only polymer support used in the examples was polypropylene.

9.2 PREPARATION OF POLYMER-SUPPORTED METALLOCENE CATALYSTS

The heterogeneous metallocene catalysis literature, including patents and disclosures, has been reviewed by Ribeiro et al.[16] and Hlatky.[8] However, the majority of the reviewed work deals with metallocenes on inorganic supports, but many of the methods used for supporting metallocenes on inorganic supports have been adopted for polymer supports. We have categorized the common methods of preparing polymer-supported metallocene into three general methods. Specific examples of these methods are listed in Table 9.1, but different investigators use wide variants of these methods and the specific papers should be consulted for details.

TABLE 9.1 Examples of Polymer-Supported Metallocene Catalysts

Support	Catalyst	Preparation Method, Properties, and Observations	References
p(S–4VPy–5% DVB); p(S–4VPy–10% DVB)[a]	Cp_2ZrCl_2; 0.11–1.14 mass % Zr; Al:Zr = 50–65	Method A1; catalytic activity increases with increasing cross-linking; marked comonomer effect; max activity = 3400 kg PE/(mol Zr·h·bar)[b]	27, 28
p(S–AM–5% DVB); 250-μm particles	Cp_2ZrCl_2; 0.35–0.48 mass % Zr	Method A1; Al:Zr = 60–70; no comonomer effect; max activity = 2000 kg PE/(mol Zr·h·bar)	30
p(S–2% DVB)	*rac*-Et[Ind]$_2$ZrCl$_2$; 0.14 mmol Zr/g support	Method A2; borate cocatalyst; max activity = 180 kg PE/(mol Zr·h·bar)	34
p(S–4VPy–2% DVB)	Cp_2ZrMe_2; 0.083 mmol Zr/g	Method A2; borate cocatalyst; 1250 kg PE/(mol Zr·h·bar)	35
CpMeO–p(S); p(S)	$Me_2Si[2\text{-}MeBenzInd]_2ZrCl_2$; 0.017–0.044 mmol Zr/g support	Method A2; Diels–Alder Cp cross-linked support; max activity = 8100 kg PP/(mol Zr·h·bar)	24
p(S–10% DVB); primary particles of 0.16 and 0.3 μm	$Me_2Si[2\text{-}MeBenzInd]_2ZrCl_2$; 0.027–0.044 mmol Zr/g support	Method A2; max activity = 880 kg PE/(mol Zr·h·bar) at total pressure of 40 bars	21
Cl–p(S–1% DVB)	Cp_2ZrCl_2; $[Ind]_2ZrCl_2$; $Me_2Si[Ind]_2ZrCl_2$; 0.17 mass % Zr	Method A1; gas-phase operation; max activity = 4000 kg PE/(mol Zr·h·bar)	31, 32
p(S–AA–EA–DVB); 0.3-μm particles	Cp_2ZrCl_2; 0.08–0.12 and 0.025 and 0.036 mmol Zr/g for porous and nonporous, respectively	Method A1; max activity porous = 430 kg PE/(mol Zr·h·bar); max activity nonporous = 125 kg PE/(mol Zr·h·bar)	36, 37
p(HEMA–ES–DVB); p(HEMA–S–ES–DVB); p(4VPy–DVB); p(ES–55% DVB); p(EGDM); p(EI–DVB); p(NV2P–DVB)	(*n*-BuCp)$_2$ZrCl$_2$; 0.06–0.24 mass % Zr; support particle sizes 30–400 μm; Al:Zr = 100–435	Methods A2 and A3; gas phase; max activity = 14,000 kg PE/(mol Zr·h·bar); activity was not a function of degree of cross-linking; strong comonomer effect for some catalysts and not for others	38–42

p(S–1% DVB); p(HEMA–S–ES–DVB)	(n-BuCp)$_2$ZrCl$_2$; 0.13 and 0.15 mass % Zr	Method A2; gas phase; max activity = 1500 kg PE/(mol Zr·h·bar)	43
OH–p(P)	Cp$_2$ZrCl$_2$; 0.002–0.004 mmol Zr/g	Method A1; max activity = 7400 kg PE/(mol Zr·h·bar)	23
p(P)	*rac*-Et[Ind]$_2$ZrCl$_2$; *meso*-Et[Me$_2$Ind]$_2$ZrCl$_2$	Method A2; gas phase; max activity = 4600 kg PE/(mol Zr·h·bar)	44
Li–p(S–2% DVB)	Various supported Si-bridged indenyl zirconocenes	Method B2; max activity = 640 kg PE/(mol Zr·h·bar); max activity = 720 kg PP/(mol Zr·h·bar)	45–47
Br–p(S); 40–150-μm particles	Cp$_2$ZrCl$_2$ attached via a spacer to the support	Method B2; activity = 41 kg PE/(mol Zr·h·bar)	48
Cl–p(S–1–12% DVB); 35–75-μm particles	(CpMe$_4$)$_2$HfMe$_2$ after support was aminated and borated; 0.14–0.7 mmol Hf/g	Method B1; borate cocatalyst; max activity = 630 kg PE/(mol Hf·h·bar); activity decreased with increasing cross-linking	22, 25
Cl–p(S)	Cp$_2$ZrCl$_2$; 0.17–0.82 mmol Zr/g	Method B1; Diels–Alder Cp cross-linked support; max activity = 1850 kg PE/(mol Zr·h·bar)	26
	Cp$_2$ZrCl$_2$	Method B2; Diels–Alder Cp cross-linked support; max activity = 170 kg PE/(mol Zr·h·bar) at 40 bars	49
Cl–p(S) (porous) Cl–p(S–1% DVB); Cl–p(S–2% DVB); 75–150-μm particles and 35–75-μm particles	Cp$_2$ZrCl$_2$ and Cp$_2$TiCl$_2$; 0.11–0.51 mmol Zr/g resin; 0.13–0.47 mmol Ti/g resin	Method B2; max activity = 63 kg PE/(mol Ti·h·bar); max activity = 160 kg PE/(mol Zr·h·bar)	50
None	Various zirconocene dichloride complexes with alkenyl substituents	Method C1; max activity for PE = 20,000 kg PE/(mol Zr·h·bar) at 10 bars; max activity for PP = 62,200 kg PP/(mol Zr·h) in bulk polymerization at 60 °C	51–53
None	Et[Ind]$_2$ZrCl$_2$; Cp$_2$ZrCl$_2$	Method C2; max activity = 994 kg PE/(mol Zr·h·bar)	54–56

---

[a] p(X–Y–n% Z) = polymer made from monomers X, Y, and Z with n% of monomer Z; see Table 9.2 for definition of abbreviations.

[b] The maximum activity is the highest average activity in the paper. All polymerizations were done in slurry operation unless indicated otherwise.

1. *Method A* In this preparation method the polymeric support is usually dried, then suspended in a solvent, then treated with an aluminum alkyl solution, typically MAO, or reacted with a borate complex to incorporate a borate cocatalyst, followed by the addition of a metallocene-containing solution and ending with a vacuum-drying step which results in a free-flowing solid. The main variations in this procedure are the treatments between cocatalyst addition and metallocene addition and the temperatures and durations for the cocatalyst and metallocene addition. Three subcategories of method A are described below.

Method A1 The solution after the addition of the cocatalyst is removed by filtration or decantation and the solids are thoroughly washed before the addition of the metallocene solution. After a desired time of reaction between the metallocene solution with the treated support, the solution is removed by filtering or decantation and the resulting solid is again washed thoroughly to remove all weakly bound metallocene; that is, in this method the cocatalyst is reacted with the polymeric support and the metallocene is reacted with the cocatalyst-treated support. Conditions for reaction with the cocatalysts and metallocene varied widely. For example, Liu et al.[30] contacted the p(S–AM–5% DVB) support with a MAO–toluene solution for 1 h at room temperature before filtering and washing, while Hsu and co-workers[31,32] contacted hydroxylated p(S–1% DVB) with a MAO–toluene solution for 20 h at 50 °C before filtering and washing. (See Table 9.2 for polymer and monomer notation.)

Method A2 No washing of the solids occurs before the addition of the metallocene solution or after addition of the metallocene. In some of these cases, the solutions were removed by filtration or decantation, but in other cases the solutions were not removed at all and the metallocene solution was added directly to the cocatalyst solution and all the solvent was removed by evaporation during the final step in the catalyst preparation. Method A2 is a typical impregnation method where all the cocatalyst and metallocene in solution is deposited on the support. Variations of this method appear to be the choice for commercial preparations of supported metallocene catalysts.[12]

Method A3 In this variation, a second addition of cocatalyst, usually MAO, is carried out after the metallocene addition; this method produces a "sandwich-like" catalyst phase; that is, it is assumed that the metallocene is sandwiched between two layers of MAO in the pores of the support.[33] This method results in increased Al–metallocene ratios.

2. *Method B* The surface of the polymeric support is functionalized and the most common starting materials for this method are chloromethylated polystyrenes with and without cross-linking. There are many variations of this method and frequently many reaction steps are required to convert the

TABLE 9.2 List of Abbreviations for Monomers and Polymers

Abbreviation	Definition of Abbreviations	References
AA	Acrylic acid	36, 37
AM	Acrylamide	30
Br–p(S)	*p*-Bromopolystyrene	48
Cl–p(S)	Chloromethylated polystyrene	21, 25, 26, 31, 32, 48, 50
CpMeO–p(S)	Cp-methoxy-functionalized polystyrene	24
DVB	Divinylbenzene	21, 22, 25, 27, 28, 30, 31, 32, 35–47, 50
EA	Ethyl acrylate	36, 37
EGDM	Ethylene glycol dimethacrylate	39, 41, 47
EI	Ethyleneimine	41
ES	Ethylstyrene	38–43
HEMA	2-Hydroxyethyl methacrylate	38–43
Li–p(S)	Lithiated polystyrene	45, 46
NV2P	*N*-Vinyl-2-pyrrolidinone	39, 41, 42
OH–p(P)	Hydroxylated polypropylene	23
P	Propylene	44
p(P) or pp	Polypropylene	44
S	Styrene	21, 22, 24–28, 30–32, 34–43, 45–50
4VPy	4-Vinylpyridine	27, 28, 35, 41, 43

starting polymer to the functionalized form suitable for the attachment of the cocatalyst and/or the metallocene. Two common variants are described below.

Method B1 The metallocene is reacted with the functionalized support; that is, the metallocene is tethered to the support. The support may already contain a borate cocatalyst.

Method B2 The functionalized support, usually containing attached cyclopentadienyl groups, is reacted with a metal halide to form the attached metallocene complex.

3. *Method C* In this method the heterogeneous catalyst is formed inside the reactor; that is, a homogeneous catalyst is injected into the reactor and a solid catalyst is formed in the reactor. This type of catalyst heterogenization is only useful for slurry operation because gas-phase operation requires injection of solid catalysts. There are two variations of this method.

Method C1 Alkenyl or alkyne functions are added to fluorenylidene, indenylidene, or bis(fluorenylidene) metal dichlorides, and these homogeneous metallocenes are injected into the slurry reactor containing the diluent, MAO, and ethylene or propylene. The alkenyl or alkyne groups participate in the polymerization and become part of the growing solid polymer particles; that is, the catalysts act as comonomers. This method, developed by Alt and co-workers,[51–53] is referred to as self-immobilization and does not result in reactor fouling.[51]

Method C2 The metallocene is injected into a slurry reactor containing the diluent, for example, hexane, and suspended MAO-treated SiO_2, particles; no external MAO is added to the diluent. This in situ immobilization method, developed by Soares and co-workers,[54–58] has only been used with MAO-treated SiO_2, but there is no reason why this method should not work with MAO-treated polymer supports.

Several other techniques have been used to prepare polymer-containing supported metallocenes. Kamfjord et al.[19] used the incipient-wetness impregnation method to add Cp_2ZrCl_2 and $(n\text{-BuCp})_2ZrCl_2$ to MAO-treated silica and then added this catalyst to a solution containing 1-hexene, styrene, or 1,7-octadiene at low temperature (–50 to –30 °C). Slowly warming the suspension to 25 °C resulted in a slow polymerization of the monomer and the formation of a polymer–SiO_2–metallocene catalyst. These catalysts were subsequently used for ethylene polymerization in a heptane slurry and had activities ranging from 120 to 3550 kg PE/(mol Zr·h·bar). These polymer-coated catalysts also retained up to 30% of their activity after being exposed to air for 5 h. Another class of supported catalysts is the metallocenes supported on polysiloxane derivatives synthesized by Soga and co-workers.[22,59–61] However, these catalysts are not true heterogeneous catalysts because many are soluble, or at least partially soluble, in organic diluents used in slurry polymerizations.

Many types of polymers have been used in the preparation of supported metallocene catalysts (see Table 9.1). Both laboratory-synthesized and commercially available polymers have been used as supports. Emulsion and suspension polymerization are the most common methods used to prepare the custom-made polymer supports (e.g., refs. 21, 27, 30, and 38–43). Arshady[62] has compared these polymerization methods. Most of the polymer supports used were spherical, and the particle diameters were usually in the 40–300-μm range (see refs. 23, 25, 30, 42, 43, 45–48, 50, and 55), but support particles as small as 0.3 μm[36,37] and as large as 400 μm[38,40] have been used. Most of the supports used were porous; unfortunately, surface areas, pore volumes, and pore sizes were usually not reported. Wanke and co-workers[40–42] used porous supports with surface areas of 7–640 m^2/g, mesopore volumes of 0.13–0.98 cm^3/g, and average mesopore diameters of 8–16 nm. Qin et al.[37] synthesized 0.3-μm polystyrene particles with areas of 750–800 m^2/g and used these particles as supports for Cp_2ZrCl_2.

It is commonly accepted that good product morphology requires good catalyst morphology if product particles are formed by replication of the catalyst particles; that is, spherical catalyst particles and even distributions of catalyst and cocatalyst throughout catalyst pellets are prerequisites for obtaining product particles with good morphology. Catalysts with these properties are relatively easy to prepare. Figure 9.1 shows examples of two supports

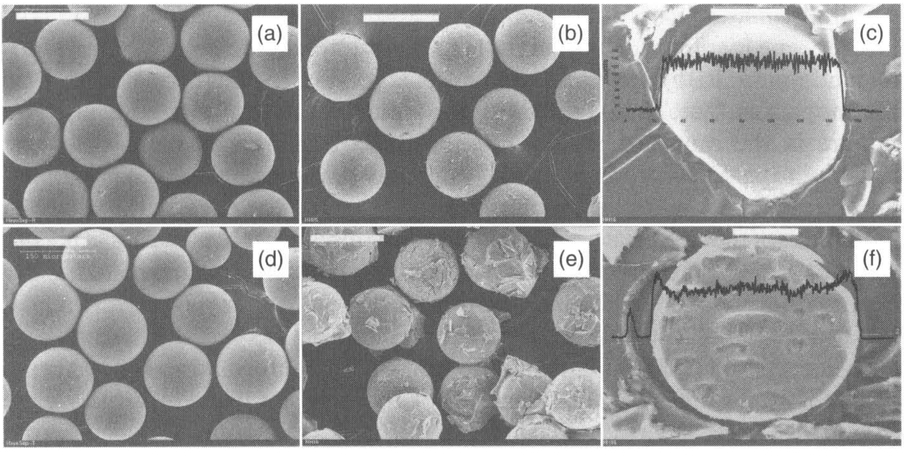

Figure 9.1 SEM images of supports (*a* and *d*), catalysts (*b* and *e*), and catalyst cross sections with EDX analysis for aluminum (*c* and *f*). (The size bars are 150 μm in *a*, *b*, *d*, and *e*; 50 μm in *c*; and 40 μm in *f*.)

and catalysts prepared by impregnation of supports with toluene solutions of MAO and (n-BuCp)$_2$ZrCl$_2$ (method A2). The support shown in Figure 9.1*a* is a commercial p(NV2P–DVB) porous resin and the support shown in Figure 9.1*d* is a commercial p(EGDM) porous resin; the mesopore volumes of these two supports were 0.96 and 0.46 cm^3/g. Figures 9.1*b* and *e* show the catalysts made with the supports. The Zr contents of the catalysts in Figures 9.1*b* and *e* were 0.16 and 0.13 mass % Zr, and the Al–Zr ratios for these catalysts were 171 and 286, respectively. Figures 9.1*c* and *f* show cross sections of catalyst pellets and concentration profiles of aluminum obtained by energy-dispersive X-ray (EDX) line-scan analyses. For the catalyst shown in Figure 9.1*c*, the aluminum concentration across the interior of the pellet was constant while for the catalyst shown in Figure 9.1*f* the aluminum concentration was higher on the outer surface of the catalyst particles than on the inside of the particles. The flaky appearance of the exterior of the catalyst in Figure 9.1*e* was probably due to MAO which precipitated on the external surface of the catalyst. Zirconium concentration profiles could not be measured by EDX due to the low concentration of zirconium, but it is likely that the Zr concentrations were proportional to the Al concentrations. The amount of MAO which can be accommodated by a support before deposition occurs on the external surface of the support particles depends on the pore volume and the pore size.

Different methods of preparation by different researchers resulted in different metallocene loadings and different cocatalyst–catalyst ratios. The metal loadings and Al–Zr ratios can be easily adjusted for catalyst prepared by impregnation (method A2) since all the MAO and metallocene in the impregnation solutions end up in the catalyst, while the MAO and metallocene loadings for the catalysts prepared by surface reactions (methods A1 and method B) depend on the concentration of the functional groups on the support surface. The Al–Zr ratios for typical catalysts prepared by method A1 are in the range of 30–70,[27,30] while those prepared by method A2 are usually in the 100–400 range.[39–41] It is difficult to compare the metal loadings reported in the various studies because some of the loadings are reported in *millimoles of metallocene per gram of support (e.g., millimoles of Zr/g support)*, while others are reported in mass percentage of metal (e.g., mass % Zr). The former does not include the mass of the cocatalyst. In order to convert one of the compositions to the other, the mass percentage of cocatalysts, or at least the Al–metal or B–M ratio, has to be known. This information is not always provided. The ranges of metal content for the catalysts listed in Table 9.1 are 0.06 to 0.48 mass % Zr[39,30] and 0.002 to 0.82 mmol Zr/g support.[23,26] The boron-to-metallocene ratio in the borate-activated catalysts is usually about 1[34] but may be slightly <1[35] or slightly >1.[25]

The specific activities of supported metal catalysts vary over several orders of magnitude. The various maximum values of the average rates normalized with respect to monomer pressure are listed in Table 9.1. The highest average rate for ethylene polymerizations was 20,000 kg PE/(mol Zr·h·bar) reported by Alt[53] for self-immobilized (preparation method C1) metallocenes in pentane slurries at 60 °C for 1 h and ethylene pressures of 10 bars. Hammawa et al.[39] reported an average activity of 14,000 kg PE/(mol Zr·h·bar) for a $(n\text{-BuCp})_2ZrCl_2$–p(HEMA–DVB)–MAO catalyst, containing 0.06 mass % Zr, for gas-phase ethylene polymerization at 80 °C for 1 h and ethylene pressures of 1.4 bars. Most of the average activities reported in Table 9.1 are not as high, but values of 1000–8000 kg PE/(mol Zr·h·bar) are not uncommon (see refs. 23, 24, 26–28, 30–32, 35, and 38–44). These activities are not as high as the record of 2×10^6 kg PE/(mol Zr·h·bar) reported by Alt[53] for a homogeneous bridge $Et[Flu]_2ZrCl_2$ catalyst, but they are comparable to the activities of many homogeneous metallocene catalysts.[18,24,55,56] Most of the polymer-supported metallocene catalysts maintain their activity for an hour or more and frequently have activity profiles superior to those of homogeneous metallocenes (see refs. 19, 31, 32, 39, 40, 43, and 56).

High activities for homogeneous MAO-activated catalysts usually require large amounts of MAO and Al–Zr ratios ≥1000 are commonly used.[18,49] Unfortunately, additional external MAO is added in most of the slurry studies with polymer-supported metallocene catalysts in order to get high activities (see refs. 26, 30, 36, 45, 46, and 49). This practice totally negates one of the objectives for the development of supported-metallocene catalysts. Fortunately, many polymer-supported catalysts with incorporated MAO have high activities without the further addition of MAO. For example, the high-activity $(n\text{-BuCp})_2ZrCl_2$–p(HEMA–DVB)–MAO catalyst mentioned above[39] had an Al–Zr ratio of 375 and no additional MAO was added during the polymerization. Another catalyst in the same study[39] with an Al–Zr ratio of 215 had an activity of 4600 kg PE/(mol Zr·h·bar) during gas-phase ethylene/1-hexene copolymerization.

The above results demonstrate that stable and high-activity polymer-supported metallocene catalysts, consisting of spherical free-flowing particles, can be prepared by a variety of methods. The catalyst synthesis techniques vary in complexity, the simplest being impregnation using unfunctionalized supports (method A2). The remaining requirements for industrial use of polymer-supported catalysts are that they produce products which have acceptable bulk density and morphology so that reactor fouling does not occur and fines are not produced. The elimination of fines is especially important for gas-phase operations. These product properties are addressed below.

9.3 FACTORS AFFECTING MORPHOLOGY OF PRODUCT PARTICLES

Most studies dealing with supported metallocene catalysts mention the requirement for good product morphology (e.g., refs. 12, 15–19, 21, 23, 24, 26, 32, 36, 38–43, 45–47, and 49), and only a few of the studies mentioned in Table 9.1 do not specifically address product morphology in their discussion. Scanning electron microscopy (SEM) is the most commonly used tool for studying the particle morphology, although transmission electron microscopy has also been used occasionally.[37,44] The various general types of product morphologies that we have observed in our laboratory in studies of gas-phase ethylene homopolymerization and ethylene/1-hexene copolymerizations with polymer-supported $(n\text{-BuCp})_2ZrCl_2$ catalysts will be presented before discussing the factors which affect the morphology of product particles.[38–43,63,64] Morphology control is usually more difficult in gas-phase operation and gas-phase processes offer many advantages over slurry operation.[65]

9.4 TYPES OF PRODUCT MORPHOLOGIES

The various types of product particle morphologies we have observed can be divided into five general categories: fines, cauliflower external appearance, empty shells, concentric shells and uniform porosity.

9.4.1 Fines

The two types of fines which we have observed were those resulting from uncontrolled fracturing of growing polymer particles (type 1 fines) and those fines coming from the detachment of growing globules from the external surface of growing polymer particles (type 2 fines). Type 1 fines are illustrated in Figures 9.2*a* and *b*. Type 1 fines are the result of breaking particles rather than the formation of polymer around catalytic sites; this is clearly shown by the sharp and ragged edges of the particles shown in the larger magnification

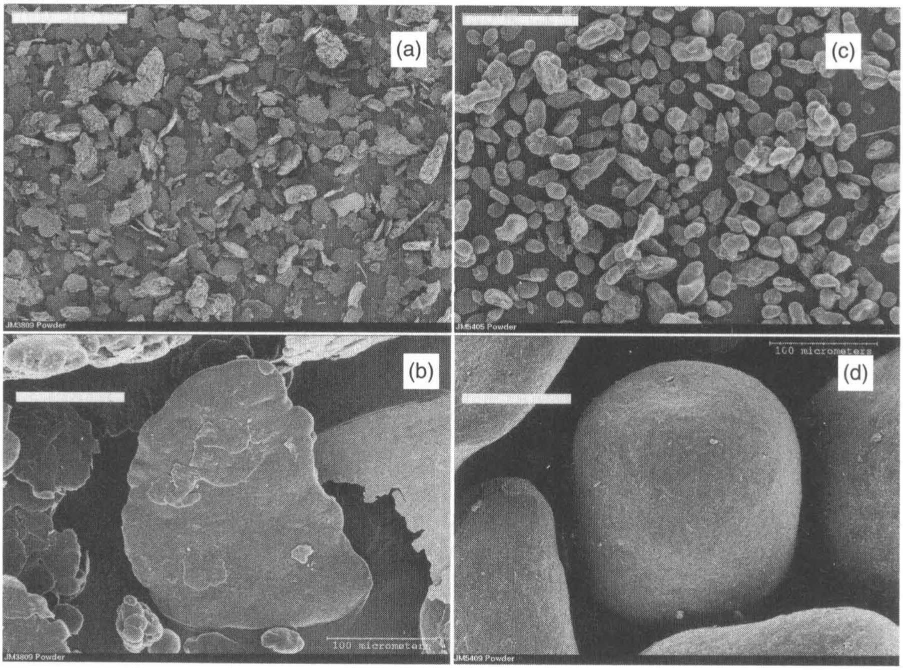

Figure 9.2 Fines obtained during gas-phase polymerization. (The bars are 1.2 mm in *a* and *c*, and 0.1 mm in *b* and *d*.)

image in Figure 9.2*b*. Type 1 fines have a broad size distribution, varying in size from a few micrometers to >0.5 mm. The smooth external surface of type 2 fines shows that these fines are not the result of uncontrolled particle breakup but result from the growth and subsequent detachment of these small particles from the external surface of the growing polymer particles.[40] Type 2 fines tend to be more uniform in size and shape than type 1 fines.

9.4.2 Cauliflower-Like Particles

Particle shapes similar to those shown in Figure 9.3*a* have been observed for polymer-supported metallocene catalysts used in slurries[24,36,49] and gas-phase operation[41–43] and for polymerization using the in situ immobilization method (method C2).[56] It is claimed that these particles are spherical particles[24,36,56] with good morphology.[56] It is usually assumed that particles such as those shown in Figure 9.3*a* are the result of catalyst particle fragmentation.[24,36,49] However, one cannot determine the degree of catalyst particle fracturing by the overall shape of the product particles. This is clearly shown by the image of a cross section of such a particle in Figure 9.3*b*. This sectioned particle came from the same run as the particles shown in Figure 9.3*a* and clearly shows an unfragmented catalyst core at the center of the particle. All sectioned particles

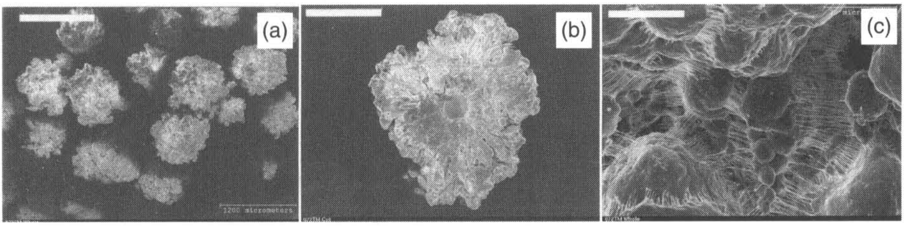

Figure 9.3 Cauliflower-shaped particles: (*a*) whole particles (bar = 1.2 mm); (*b*) cross-section of particle (bar = 0.5 mm); (*c*) high magnification of external surface of polymer (bar = 0.03 mm).

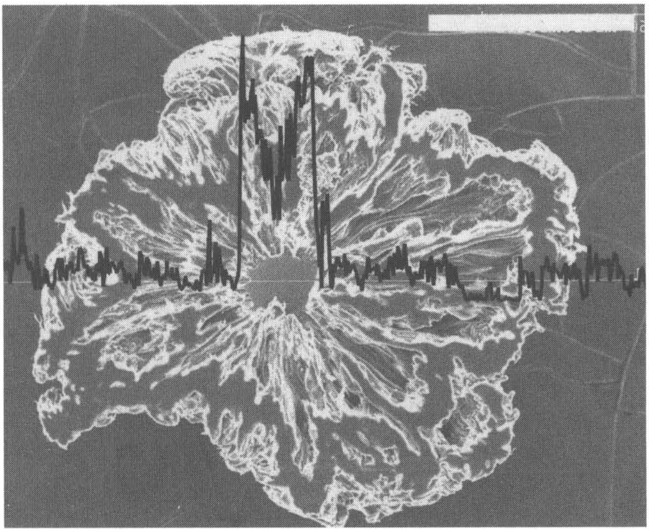

Figure 9.4 Cross section of polymer particle with Al concentration profile by EDX (bar = 0.5 mm).

from this run showed such unfragmented catalyst cores and the sizes of these central cores are essentially the same as the initial catalyst particles. The proof that the core is a catalyst particle is shown in Figure 9.4. (*Note*: The polymerization conditions for the products shown in Figures 9.2–9.11 are listed in Table 9.3.)

Figure 9.4 shows a cross section of another product particle with the cauliflower morphology which also shows an unfragmented catalyst particle at the center. The EDX line scan for aluminum is also shown in this figure. The aluminum concentration was high in the central core and no aluminum was detected in the polymer product surrounding the unfractured core. The size of the core and the high Al content of the core provide very strong evidence that little or no fracturing of the catalyst particles occurred even though polymerization rate was reasonably high (275 kg PE·(h·bar·mol Zr)$^{-1}$). The

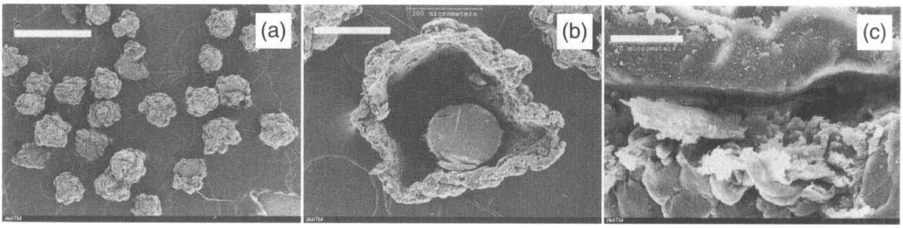

Figure 9.5 Empty-shell particles: (*a*) whole particles (bar = 1.2 mm); (*b*) cross section of empty-shell particle (bar = 0.3 mm); (*c*) high magnification of shell (bar = 0.02 mm).

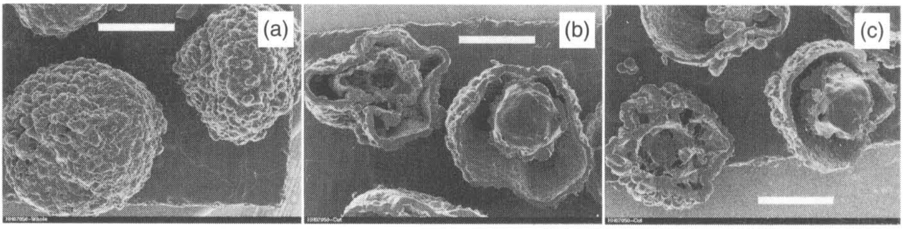

Figure 9.6 Hollow-shell particles: (*a*) whole particles (bar = 1.2 mm); (*b*) cross section of empty-shell particle (bar = 1.2 mm); (*c*) high magnification of shell (bar = 1.2 mm).

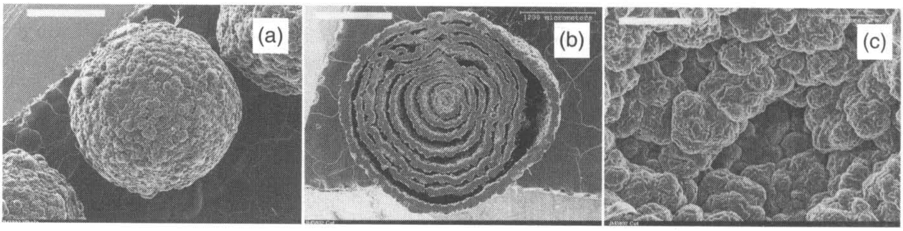

Figure 9.7 Concentric-shell particles: (*a*) whole particles (bar = 1.2 mm); (*b*) cross section of empty-shell particle (bar = 1.2 mm); (*c*) high magnification of shell (bar = 0.06 mm).

structure of the polymer surrounding the catalyst core contains macropores (see Figure 9.3*c*) which allow ready access of the monomer to the unfractured catalyst core. It appears that polymer is formed on the external surface of the catalyst pellets and then is pushed outward resulting in the fibers seen in Figure 9.3*c*; the fibers are possibly due to the cold drawing of the polymer particles. The bulk densities of these particles are typically 0.2–0.3 g/cm^3.

9.4.3 Hollow-Shell Particles

The formation of hollow shells such as those shown in Figures 9.5 and 9.6 has been reported for polymer-supported metallocene catalysts[23,41] as well as for $MgCl_2$-supported $TiCl_4$ catalysts.[66] The external surfaces of the hollow particles look similar to the cauliflower-like particles, but the interior is totally different.

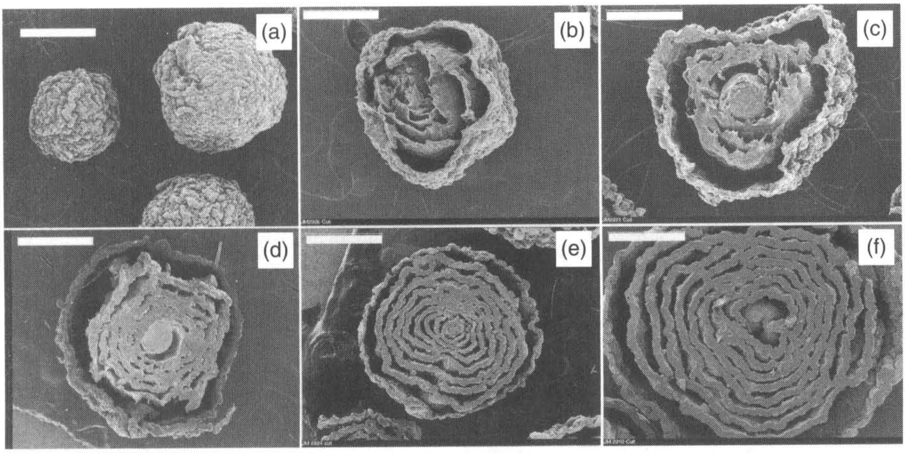

Figure 9.8 Particle morphology as function of polymerization time: (*a*) whole particles after 2 min (bar = 0.6 mm); (*b*) cross section after 2 min (bar = 0.6 mm); (*c*) cross section after 5 min (bar = 0.6 mm); (*d*) cross section after 10 min (bar = 0.8 mm); (*e*) cross section after 20 min (bar = 1.2 mm); (*f*) cross section after 60 min (bar = 1.2 mm).

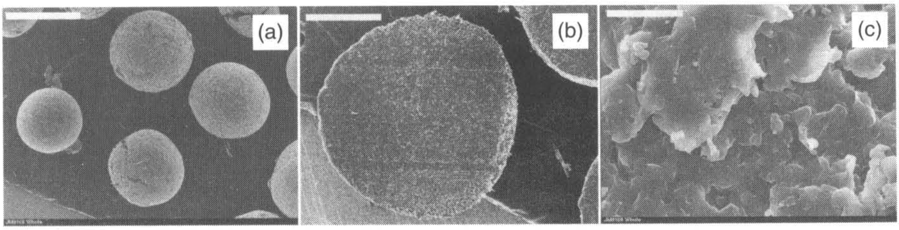

Figure 9.9 Uniformly porous homo-polyethylene particles: (*a*) whole particles (bar = 1.2 mm); (*b*) cross section of particle (bar = 0.5 mm); (*c*) high magnification of external surface of particle (bar = 0.008 mm).

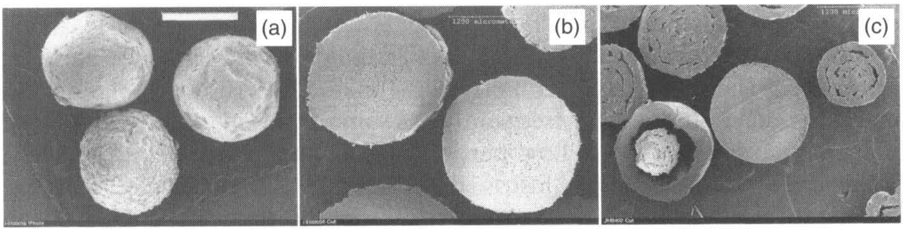

Figure 9.10 Uniformly porous ethylene/1-hexene co-polymers: (*a*) whole particles (bar = 1.2 mm); (*b*) cross section of particles (bar = 1.2 mm); (*c*) cross section of particles from different run (see Table 9.3; bar = 1.2 mm).

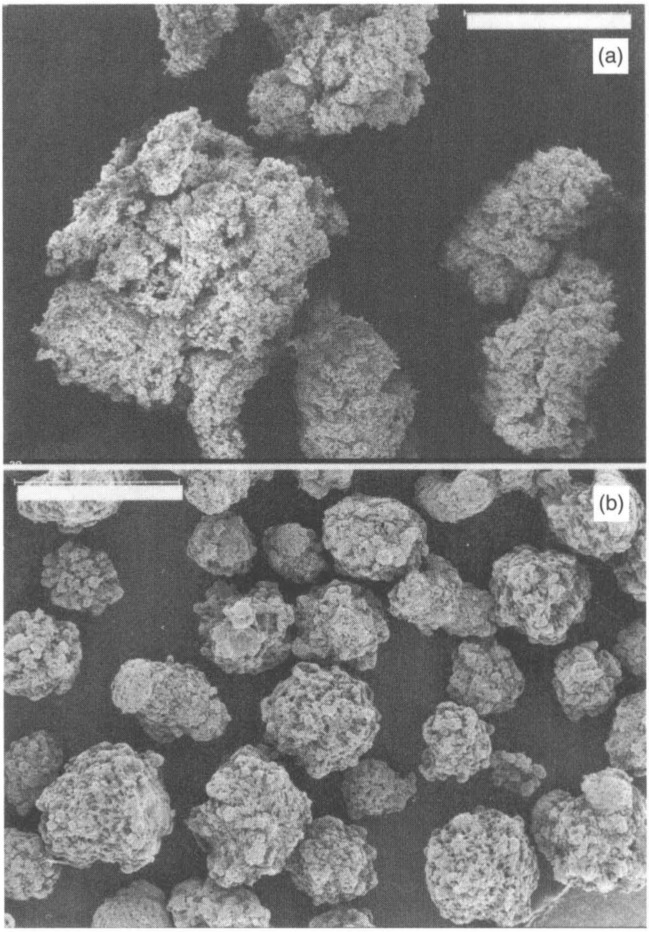

Figure 9.11 SEM images of whole particles: (*a*) slurry polymerization; (*b*) gas-phase polymerization (bars = 1.2 mm; see Table 9.3 for details).

The hollow particles usually contain a loosely attached or detached catalyst particle; this can be seen in Figure 9.5*b*. In most cases the catalyst particle falls out when the polymer particle is sectioned; however, the loose particles in the hollow spheres are easily detected by the rattling when unsectioned particles are shaken. The shell consists of fairly dense material as shown in Figure 9.5*c*, and the inside of these shells frequently has some attached loosely aggregated polymer particles. Some hollow particles have other fairly detached shells inside the outer shell. This is illustrated in Figure 9.6. These particles look very spherical (Figure 9.6*a*). The distorted shapes of the particles in Figure 9.6*b* were due to the sectioning process; the particles were spherical before being cut in half with a surgical scalpel. The bulk density of these particles was typically 0.2–0.3 g/cm^3; the bulk density increased with the number of shells.

TABLE 9.3 Description of Catalysts and Rates for Gas-Phase Ethylene or Ethylene/1-Hexene Copolymerizations for Products Shown in Figures 9.2–9.11[a]

Figure Numbers	Support	Support Area, m^2/g	Zr Content, mass %	Al:Zr Ratio	[1-C_6H_{12}], mol/m^3	Average Rate[b]	Bulk Density, g/cm^3
9.2*a* and *b*	p(HEMA–S–ES–22% DVB)[c,d]	107	0.27	170	0	260	n.m.[g]
9.2*c* and *d*	p(HEMA–S–ES–22% DVB)	280	0.21	370	15	2300	0.39
9.3*a*, *b*, and *c*	p(HEMA–S–ES–22% DVB)	168	0.23	285	0	80	n.m.
9.4	p(DVB)	592	0.11	150	0	275	0.29
9.5*a*, *b*, and *c*	P(NV2P–DVB)	620	0.24	200	0	95	0.23
9.6*a*, *b*, and *c*	p(EGDM)	313	0.13	435	14	3400	0.27
9.7*a*, *b*, and *c*	p(HEMA–S–ES–22% DVB)[c,d]	107	0.27	170	14	2800	0.27
9.8*a*–*f*	p(HEMA–S–ES–25% DVB)	44	0.28	135	23	1650[e]	0.23[e]
9.9*a*, *b*, and *c*	p(HEMA–S–ES–22% DVB)	430	0.39	100	0	1400	0.42
9.10*a* and *b*	p(HEMA–ES–27% DVB)	375	0.06	375	15	7900	0.43
9.10*c*	p(HEMA–S–ES–22% DVB)[c,f]	107	0.26	130	14	3490	0.42
9.11*a*	p(HEMA–S–ES–22% DVB)[c,f]	107	0.26	130	0	1550	<0.1
9.11*b*	p(HEMA–S–ES–22% DVB)[c,f]	107	0.26	130	0	270	0.37

[a] Polymerization conditions: Catalyst: (n-BuCp)$_2$ZrCl$_2$; co-catalyst: MAO; temperature 80°C; ethylene pressure 14 bars; length of runs 1h except for Figure 9.8.

[b] Average rate in kg PE/(mol Zr·bar·h).

[c] Same support used for these catalysts.

[d] Same catalysts for these runs.

[e] Average rate and bulk density for Figure 9.8*f*.

[f] Same catalysts for these runs.

[g] n.m. = not measured.

9.4.4 Concentric-Shell Particles

One of the most common internal morphologies which we observed for ethylene/1-hexene gas-phase copolymerization with polymer-supported (n-BuCp)$_2$ZrCl$_2$ catalysts was the concentric-shell morphology shown in Figure 9.7.[38,40,42,43] This is a continuation of the one- and two-shell hollow particles shown in Figures 9.5 and 9.6. Similar concentric-shell structures (onionlike morphology) have been reported by Galli and Haylock[66] for MgCl$_2$-supported TiCl$_4$ catalysts. The microstructure of these particles is much denser than that of particles having the cauliflower morphology (cf. Figures 9.3*c* and 9.7*c*). The formation of this concentric-shell structure with polymerization time is shown in Figure 9.8. For the case shown in Figure 9.8, the shell structure forms very rapidly; that is, in less than 2 min the catalyst particle was totally fractured and subsequent polymerization resulted in increases in the thickness of the shells and the size of the product particles. Excellent sphericity is maintained as the particles grow. The bulk densities of these types of particles, after 60 min of polymerization, are in the range 0.20–0.43 g/cm^3 depending on the number and thickness of the concentric shells.

In other cases, the fracturing proceeded much more slowly. At reaction conditions similar to those used to produce the particles in Figure 9.8, but for different supports, the unfractured catalyst cores were still present after 20 min even though a multishell structure had formed.[64] Long fracturing times for polymer-supported metallocene catalysts have also been reported by Koch et al.[21]; their styrene–divinylbenzene copolymer support required over 2 h to fracture. Fink et al.[17,67] also show that fracturing of silica-supported metallocene catalysts can exceed 30 min.

9.4.5 Uniformly Porous Product Particles

The final general type of morphology which we observed was spherical particles with uniform internal structure. Such particles are shown in Figures 9.9 and 9.10. The products have excellent sphericity and density (usually in the range 0.4–0.48 g/cm^3). The microstructure of these homopolymer particles, shown in Figure 9.9*c*, is similar to that of the concentric-shell structure for copolymers shown in Figure 9.7*c*. (*Note*: The magnifications in Figures 9.7*c* and 9.9*c* are different.) The image in Figure 9.9*c* is of the external surface of the particles; the microstructure in the interior is similar to that on the external surface.[63]

Figure 9.10*c* shows cross sections of various particles from a single copolymerization run. All the particles are spherical, but their internal morphology varies from particle to particle. There is one particle with uniform porosity, several particles with concentric-shell morphology, and even a single-shell particle. The particles imaged in Figure 9.10*c* were chosen randomly; that is, the internal morphology was not known before the sectioned particles were placed on the SEM specimen stub. An additional 15 SEM stubs were prepared and a total of 56 sectioned particles were imaged; of these 49 were concentric-shell particles, 5 were uniform-porosity particles, and 2 were single-shell particles. A total of 56 particles is not sufficient for statistical analysis, but the results clearly show that particles with significantly varying morphology can be produced under the same reaction conditions. This is probably due to spatial variations in the concentrations of cocatalyst and metallocene among catalyst pellets. Variations in temperatures with position in the reactor could also cause a difference in fragmentation behavior among particles. Zöllner and Reichert[68] have shown, by using videomicroscopy, that the activity of individual catalyst particles differs significantly for gas-phase butadiene polymerization over a silica-supported neodymium catalyst. Mannan,[64] using a similar technique for ethylene polymerization over a (n-BuCp)$_2$ZrCl$_2$ supported on MAO-treated polymer support, also observed the different fracturing behavior among catalyst particles from the same batch of catalyst.

9.4.6 Models for Product Morphology

Various models have been proposed for the growth of polymer particles.[69–80] The aim of this brief section is not to review models for the fragmentation of catalyst particles and growth of polymer particles but to indicate that considerable progress has been made since the early polymer flow[69,70] and multigrain models.[71,72] Hollow single-shell particles, multishell particles, and uniform-porosity particles are predicted by current models (e.g., M-2 and M-7). Horáčková et al.[80] recently proposed "shrinking core" and "continuous bisection" as two extremes for modeling the fragmentation of catalyst particles during polymerization. These two extremes deal with the case of the gradual shrinking of the unfragmented catalyst core and the uniform fragmentation of the catalyst particles, permitting various product morphologies to be modeled. Prediction of product morphologies is possible, but detailed information about the pore structure and active catalyst distribution in the initial catalyst particle is required. It is likely that, in the future, prediction of polymer morphology will be possible; however, all the key factors which affect product morphology will first have to be identified and quantified. In the next section some of the main factors which affect product morphology are discussed.

9.5 FACTORS AFFECTING PRODUCT MORPHOLOGY

Numerous factors—such as reactor operating conditions; polymerization rates and shapes of activity profiles; type of monomers; structure, composition, and porosity of support; and distribution of the active species throughout the support—all can affect the product morphology. The influence of these factors, with emphasis on gas-phase ethylene and ethylene/1-hexene polymerization, is discussed below.

9.5.1 Slurry versus Gas-Phase Polymerization

Very few data are available which compare morphology of products obtained by slurry polymerization with those obtained by gas-phase polymerization for the same catalyst. We have done a limited amount of work on slurry polymerization with $(n\text{-BuCp})_2\text{ZrCl}_2$ supported on MAO-treated polymer supports. Figure 9.11*a* shows an SEM image of the product obtained by homopolymerization of ethylene in 400 mL of heptane diluent at 80 °C and 14 bars ethylene pressure; no additional MAO was added to the slurry (other information is given in Table 9.3). The product from gas-phase ethylene homopolymerization, also at 80 °C and 14 bars ethylene pressure, is shown in Figure 9.11*b*. The product particle morphologies and bulk densities (see Table 9.3) are drastically different. The gas-phase product has the cauliflower structure discussed above while the slurry product consists of irregularly shaped, highly porous particles. The catalyst used for these experiments was prepared by impregnation (method A2 described above). Excess MAO and metallocene were not removed by washing the impregnated catalyst before drying the solid. This results in precipitated MAO and $(n\text{-BuCp})_2\text{ZrCl}_2$ in the pores of the support which are probably leached from the catalyst particles during slurry polymerization.

The possibility of leaching catalyst and cocatalyst is one of the main differences between slurry and gas-phase operation with supported catalysts. Leaching is not possible in gas-phase operations because there is no liquid present. Leaching of both MAO and metallocene in slurry operation has been reported by some researchers while others observed no leaching.[18] Even for the in situ immobilization technique, preparation method C2, leaching did not seem to be a problem.[54,57] Leaching will be a problem for catalysts in which the MAO or metallocene is not strongly bound to the support, for example, catalyst preparation method A2 and to a lesser degree method A1. The leaching problem will be increased if external MAO is added to the slurry diluent liquid and if toluene is used rather than paraffinic diluents such as isobutane, hexane, or heptane. Leaching will be much less likely for catalysts prepared by reacting of functionalized supports with the cocatalyst and/or the metallocene (method B).

9.5.2 Polymerization Rates and Shapes of Activity Profiles

High initial reaction rates can result in uncontrolled catalyst fragmentation causing the formation of fines, such as those shown in Figure 9.2*a*. Large temperature increases frequently occur during the initial stages of polymerization and these are difficult to control in gas-phase laboratory reactors,[81,82] but such temperature excursions, resulting in undesirable poor product morphology, can also occur in slurry polymerization.[22,25] Roscoe et al.[25] point out that there is a balance between temperature/rate and product morphology. Prepolymerization under mild conditions (low temperature and low monomer concentration) is one technique used to improve product morphology by reducing uncontrolled catalyst particle fragmentation due to high initial activities.[12] The use of different and varying amounts of aluminum alkyls as scavengers/cocatalysts can also be used to alter the activity profile and reduce initial high activities.[39] While high rates of polymerization can result in undesirable particle fragmentation, low rates may result in only limited fragmentation.[37]

9.5.3 Homopolymerization versus Copolymerization

The presence of a 1-alkene comonomer, such as 1-hexene, can have a major effect on product morphology. This can be due to an effect of the comonomer on the activity profile; the presence of a comonomer can reduce the high initial activity frequently observed during ethylene homopolymerization.[43] However, some polymer-supported metallocene catalysts fracture in the presence of a comonomer but do not fracture during homopolymerization. Particles with the cauliflower morphology, as shown in Figure 9.3, were most commonly observed with ethylene homopolymers; occasionally copolymers made with low 1-hexene concentration also had the cauliflower structure, but most of the catalysts which failed to fracture during homopolymerization did fracture during copolymerization with a 1-alkene, resulting in hollow-shell, concentric-shell, and occasionally uniformly porous morphologies, shown in Figures 9.5–9.8.[63,64] The most likely cause for this behavior is that during homopolymerization the pores in the support particles are filled with highly crystalline polyethylene without fracturing the particles and subsequent access to the catalytic sites is blocked by the crystalline ethylene due to the low solubility of ethylene in crystalline polyethylene. Hence, polymerization stops or is greatly reduced.[25,83] The addition of a 1-alkene to the reactor results in the filling of pores with linear low-density polyethylene, in which ethylene is much more soluble,[84] resulting in access of monomers to the active sites, continued polymerization, and catalyst particle fragmentation. However, the rate of this process may be controlled by diffusion of monomer to the active sites, and such diffusion-controlled polymerization can, according to models,[74] result in hollow- and concentric-shell morphologies. Surface area measurements on products with cauliflower morphology showed that the pores in the unfractured catalyst particles are filled with polymer, and the addition of 1-hexene to the reactor after a period of ethylene homopolymerization does not change the cauliflower morphology.[63] These observations support the idea that the absences of catalyst particle fracturing for some catalyst is due to the filling of the pores with crystalline polyethylene.

9.5.4 Distribution of Active Phases in Polymer Support

Uniform distribution of the catalyst and cocatalyst throughout the support particles is a prerequisite for good product morphology.[21,24,36,49] The most common type of maldistribution of the active phase in catalyst particles is the high concentrations of active material on the external surface of the catalyst particles. Reasons for high concentration of catalyst and cocatalyst on the external surface of the support particle include the use of nonporous supports[47] and high catalyst/cocatalyst loading which exceed the pore volume of the support.[40] If the metallocene is only located on the exterior surface of the support particles, then fines will form by attrition, especially in gas-phase operation using stirred- and fluidized-bed reactors where there are many particle–particle collisions. The fines shown in Figures 9.2*c* and *d* were formed by this mechanism. Maldistribution of the metallocene inside porous supports can result in shell-like structures, shown in Figures 9.5 and 9.6, and voids inside product particles.

9.5.5 Structure and Properties of the Support

The shape, porosity, and friability of the support particles are the most important properties of the polymer support related to producing products with controlled particle morphology. If growth of product polymer particles occurs by replication, then irregularly shaped support particles will result in irregularly shaped product particles. Irregularly shaped particles are not suitable for fluidized-bed operation, and they are also more prone to formation of fines by attrition. Musikabhumma et al.[35] blamed the poor product morphology on the nonuniformity of the support particles. Hence, good support particles should be spherical with a narrow size distribution.

Support particles with high and low porosity have been used to synthesize catalysts which are very active and yield products with good morphology.[43] However, nonporous catalysts must be soluble or swellable during the addition of cocatalyst and metallocene so that these components are evenly distributed throughout the support particles. Some investigators believe that soluble polymers are the best because the catalysts and cocatalysts can be attached to the polymer molecules in solution before cross-linking,[24,49] others believe that nonporous, swellable supports are preferable,[25] and still other investigators prefer and use porous supports (e.g., refs. 36–38, 41, and 44). Qin et al.[37] found that for ethylene polymerization with Cp_2ZrCl_2 supported on nonporous p(S–AA–EA–DVB) reactor fouling occurred and all the product consisted of dust. However, with the same supports which had been made porous by alkali and acid treatment, before addition of Cp_2ZrCl_2, the product consisted of hard polyethylene particles without any dust formation. Hence, porous supports are generally preferable to nonporous supports, and preparation by impregnation, the preferred method for commercial preparation of supported metallocene catalysts,[12] can only be done with porous catalysts. Many porous cross-linked polymers are available commercially, and others with desired micro-, meso-, and macroporosity can be synthesized easily.[38]

The final requirement of support particles is friability, that is, the property of being easily broken into small pieces. Friability is obviously related to catalyst particle fragmentation, but it is not directly related to the degree of cross-linking. Some investigators believe that cross-linking supports with DVB will result in catalysts with poor fracturing characteristics.[23–26,49] These investigators prepared solid supports by weakly cross-linking cyclopentadiene functionalized polystyrene [Cp–p(S)] by the Diels–Alder reaction after the metallocene had been introduced to the dissolved Cp–p(S). Some of these reversibly cross-linked supported catalysts were relatively active, that is, up to about 2000 kg PE/(mol Zr·h·bar), and they produced product with good morphology. However, the activities and product morphology were not superior to many of the catalysts made with cross-linked polymers. Roscoe et al.[25] report that increasing the degree of cross-linking with DVB from 3 to 12% resulted in a very large decrease in activity, while Meng et al.[27] report that increasing the degree of cross-linking with DVB from 5 to 10% resulted in increases in activity by a factor of 1.3–2.4. Hence, something other than the degree of cross-linking is responsible for the changes in activity.

We have studied over 20 cross-linked polymers in our laboratory with different degrees of cross-linking from 1% DVB to pure polydivinylbenzene p(DVB) as supports for $(n\text{-BuCp})_2\text{ZrCl}_2$.[38–42,63,64] Surface areas, micropore volumes, and mesopore volumes of the supports and catalysts, after impregnation with MAO and $(n\text{-BuCp})_2\text{ZrCl}_2$, were determined by the Brunauer–Emmett–Teller (BET), *t*-plot, and Barrett–Joyner–Halenda (BJH) methods.[85] No correlations could be found between the degree of cross-linking and activity or between the degree of cross-linking and product morphology. The activity and morphology of $(n\text{-BuCp})_2\text{ZrCl}_2$-supported p(S–1% DVB) and p(HEMA–S–ES–25% DVB) was compared by Hammawa and Wanke.[43] The catalyst made with the more heavily cross-linked polymer was more active than the catalyst made with the lightly cross-linked polymer for both homopolymerization of ethylene and copolymerization of ethylene/1-hexene. The morphology of the copolymer products was good for both catalysts, consisting of thick concentric shells or uniformly porous product particles (such as Figures 9.7 and 9.10) with bulk densities of 0.36–0.43 g/cm^3. However, the homopolymerization products had different morphologies. Contrary to expectations, the morphology of the homopolymer made with the lightly cross-linked polymer had the cauliflower structure (such as Figures 9.3 and 9.4) with unfragmented catalyst cores at the center of the product particles, while the product made with the more heavily cross-linked support resulted in uniformly porous particles (such as Figure 9.9); that is, the heavily cross-linked support fractured more easily than the lightly cross-linked support. Highly cross-linked supports, such as p(DVB), can fracture readily if they are made up of submicrometer primary particles which are weakly interconnected.[41]

Micro- and mesopore volumes also did not correlate with activity and product morphology, but there was an unexpected correlation between support surface area and activity. For homopolymerization, the activity for catalysts made with supports having surface areas <200 m^2/g were severalfold higher than those for catalysts made with supports having surface areas

>200 m^2/g.[41] Higher macropore volumes for low-surface-area supports are the probable cause for this unexpected behavior. Higher macropore volume would result in more friable particles. Friability measurements of support particles showed that activities and product morphology were correlated with support friability. Highly friable supports resulted in high activities and uniformly porous product morphologies for both homo- and copolymerizations[41]; these catalysts did not show the commonly observed comonomer effect.[86] Low-friability catalysts had low ethylene homopolymerization activity and produced product particles with the cauliflower or empty-shell morphologies (such as Figures 9.3 and 9.5). These catalyst had a very significant comonomer effect; that is, the rates increased by a factor of 20 and 50 when 1-hexene or propylene was added to the feed.[41] The morphology for most of these copolymers was of the concentric-shell type. These results indicate that good polymer supports should have high friability and the degree of cross-linking is only important if it affects the friability.

9.6 PRODUCT FINES AND DENSITIES

The absence of fines or dust is frequently mentioned when the nature of the products obtained with polymer-supported metallocenes is discussed (see refs. 21, 22, 24, 25, 36, 38, 40, and 50). The absence of fines has been reported for both slurry and gas-phase operations as well as ethylene and propylene homopolymerization and ethylene/α-olefin copolymerization. The main causes for the production of fines are uncontrolled fragmentation of catalyst particles, attrition of loosely held polymer product on the exterior of the growing polymer pellet, and leaching of catalyst in slurry operation resulting in homogeneously catalyzed polymerization. Causes of fine production have been discussed above; however, it should be emphasized that many catalysts have been synthesized which do not produce fines and the associated fouling of reactors or heat exchangers in gas-phase operation.

Results of studies which report bulk densities of products are summarized in Table 9.4; bulk density is addressed much less frequently in studies than product morphology even though bulk density is an important property for commercial operation. Most of the densities reported are less than the minimum density of 0.35 or 0.4 g/cm^3 desired by industry.[13,14] The need for improved density is recognized by some investigators.[49] Sometimes the claim is made that products with high density were made; however, the claim of high densities is relative to the density of products made with homogeneous catalysts[54,55] and not high compared to the industrially desired bulk densities.

Products with bulk densities exceeding 0.35 g/cm^3 have been made in both slurry and gas-phase operation; in general, gas-phase operation results in higher bulk densities than slurry operation. However, no definite trends in bulk density with operating temperature and overall productivity were dis-

TABLE 9.4 Bulk Densities of Nascent Polyolefin Products Made with Polymer-Supported Metallocene Catalysts

Mode of Operation	Temperature, °C	Pressure, bars	Productivity, g product/ (g cat·h)	Bulk Density, g/cm^3	References
Slurry-isobutane	70	40	690–1320	0.37–0.42	21
Slurry-hexane[a]	40–60	4	440–1440	0.18–0.20	24
Slurry-hexane	40–60	—	10–100	0.12–0.17	35
Slurry-toluene	60	1.2	90–100	0.10–0.13	36
Slurry-hexane	60	5	—	0.17[b] 0.26[c]	54
Gas phase	50–90	14	3–790	0.23–0.39	38
Gas phase	50–100	14	50–1120	0.23–0.49	40
Gas phase	80	14	60–350	0.36–0.43	43

[a] Propylene polymerization; all others are ethylene or ethylene/1-hexene polymerizations.
[b] $Et[Ind]_2ZrCl_2$-supported MAO-treated SiO_2.
[c] In situ supporting of $Et[Ind]_2ZrCl_2$ on MAO-treated SiO_2.

cernable in the studies cited in Table 9.4. For example, no correlation between productivity and bulk density were apparent in the results obtained by Koch et al.[21] and Hammawa and Wanke.[43] The results of Musikabhumma[35] and Wu et al.[40] do show a trend of increasing bulk densities with increasing polymerization temperatures, but no such correlation was observed by Zhou et al.[38] The Al–Zr ratio also does not seem to be correlated with bulk density.[35] Additional research is required to determine the effects of catalyst type, support properties, and operating conditions on the bulk density of product for polymer-supported metallocenes which produce particles with good morphology.

9.7 CONCLUSIONS

Various polymer-supported metallocene catalysts have been reported in the literature which have high activity [well over 5000 kg of polymer/(mol metallocene·h·bar of olefin)] and produce products with excellent particle morphology and density (>0.4 g/cm^3) without the production of fines during both slurry and gas-phase polymerizations. Catalysts which are to be used in slurry applications require that the catalyst and cocatalyst be anchored to the support to prevent leaching (preparation by method A1 or B) while catalysts for gas-phase use can be prepared by the simpler impregnation method

(method A2). Many of these catalysts are very easy to prepare and require low cocatalyst–metal ratios; MAO-activated catalysts with Al–Zr ratios <200 have high activity without further addition of MAO to the reactor. Such catalysts have the potential for industrial use to manufacture commodity resins with excellent morphology, high bulk density, and very low inorganic content.

REFERENCES

1. Ziegler, K., Holzkamp, E., Breil, H., and Martin, H., *Angew. Chem. Int. Ed.*, **1955**, 67, 541–547.
2. Clark, A., Hogan, J. P., Banks, R. L., and Lanning, W. C., *Ind. Eng. Chem.*, **1956**, 48, 1152–1155.
3. Hogan, J. P., and Banks, R. L., Phillips Petroleum Co., U.S. Patent No. 2,825,721, **1958**.
4. Natta, G., *Angew. Chem. Int. Ed.*, **1956**, 68, 393–403.
5. Karol, F. J., *Chemtech*, **1983**, 13, 222–228.
6. Sinn, H., and Kaminsky, W., *Adv. Organometal. Chem.*, **1980**, 18, 99–149.
7. Brintzinger, H. H., Fischer, D., Mülhaupt, R., Rieger, B., and Waymouth, R. M., *Angew. Chem. Int. Ed. English*, **1995**, 34, 1143–1170.
8. Hlatky, G. G., *Coordinat. Chem. Rev.*, **2000**, 199, 235–329.
9. Alt, H. G., and Köppl, A., *Chem. Rev.*, **2000**, 100, 1205–1221.
10. Alt, H. G., *Coordinat. Chem. Rev.*, **2006**, 250, 1.
11. Kaminsky, W., *Adv. Catal.*, **2001**, 46, 89–159.
12. Hlatky, G. G., *Chem. Rev.*, **2000**, 100, 1347–1376.
13. Herrmann, H.-F., and Böhm, L. L., *Polym. Commun.*, **1991**, 32, 58–61.
14. Antberg, M., Dolle, V., Haftka, S., Rohrmann, J., Spaleck, W., Winter, A., and Zimmermann, H. J., *Macromol. Chem. Macromol. Symp.*, **1991**, 48/49, 333–347.
15. Ciardelli, F., Altomare, A., and Michelotti, M., *Catal. Today*, **1998**, 41, 149–157.
16. Ribeiro, M. R., Deffieux, A., and Portela, M. F., *Ind. Eng. Chem. Res.*, **1997**, 36, 1224–1237.
17. Fink, G., Steinmetz, B., Zechlin, J., Przybyla, C., and Tesche, B., *Chem. Rev.*, **2000**, 100, 1377–1390.
18. Chien, J. C. W., *Top. Catal.*, **1999**, 7, 23–36.
19. Kamfjord, T., Wester, T. S., and Rytter, E., *Macromol. Rapid Commun.*, **1998**, 19, 505–509.
20. Langhauser, F., Derth, J., Kersting, M., Kölle, P., Lilge, D., and Müller, P., *Die Angew. Makromol. Chem.*, **1994**, 223, 155–164.
21. Koch, M., Falcou, A., Nenov, N., Klapper, M., and Müllen, K., *Macromol. Rapid Commun.*, **2001**, 22, 1455–1462.
22. Roscoe, S. B., Fréchet, J. M. J., Walzer, J. F., and Dias, A. J., *Science*, **1998**, 280, 270–273.
23. Liu, J., Dong, J.-Y., Cui, N., and Hu, Y., *Macromolecules*, **2004**, 37, 6275–6282.

24. Koch, M., Stork, M., Klapper, M., Müllen, K., and Gregoroius, H., *Macromolecules*, **2000**, 33, 7713–7717.
25. Roscoe, S. B., Gong, C., Fréchet, J. M. J., and Walzer, J. F., *J. Polym. Chem. P. A Polym. Chem.*, **2000**, 38, 2979–2992.
26. Wang, W., Wang, L., Wang, J., Wang, J., and Ma, Z., *J. Polym. Chem. P. A Polym. Chem.*, **2005**, 43, 2650–2656.
27. Meng, F., Yu, G., and Huang, B., *J. Polym. Chem. P. A Polym. Chem.*, **1999**, 37, 37–46.
28. Yu, G. Q., Zhang, D. Z., Shun, F., Qiao, L. J., Tang, T., and Huang, B. T., *Chin. Chem. Lett.*, **2001**, 12, 257–260.
29. Sugano, T., Fujita, T., and Kuwaba, K., Mitsubishi Petrochemical Company, U.S. Patent No. 5,346,925, **1994**.
30. Liu, S., Meng, F., Yu, G., and Huang, B., *J. Appl. Polym. Sci.*, **1999**, 71, 2253–2258.
31. Chung, J. S., and Hsu, J. C., *Polymer*, **2002**, 43, 1307–1311.
32. Chung, J. S., Tairova, G., Zhang, Y., Hsu, J. C., McAuley, K. B., and Bacon, D. W., *Korean J. Chem. Eng.*, **2002**, 19, 597–600.
33. Janiak, C., and Rieger, B., *Die Angew. Makromol. Chem.*, **1994**, 215, 47–57.
34. Kishi, N., Ahn, C.-H., Jin, J., Uozumi, T., Sano, T., and Soga, K., *Polymer*, **2000**, 41, 4005–4012.
35. Musikahumma, K., Uozumi, T., Sano, T., and Soga, K., *Macromol. Rapid Commun.*, **2000**, 21, 675–679.
36. Qin, Y., Tang, T., Zhao, Z., and Huang, B., *J. Polym. Sci. P. A Polym. Chem.*, **2003**, 41, 3313–3319.
37. Qin, Y., Tang, T., and Zhao, Z., *Chem. Commun.*, **2004**, 222–223.
38. Zhou, J.-M., Li, N.-H., Bu, N.-Y., Lynch, D. T., and Wanke, S. E., *J. Appl. Polym. Sci.*, **2003**, 90, 1319–1330.
39. Hammawa, H., Mannan, T. M., Lynch, D. T., and Wanke, S. E., *J. Appl. Polym. Sci.*, **2004**, 92, 3549–3560.
40. Wu, L., Zhou, J.-M., Lynch, D. T., and Wanke, S. E., *Appl. Catal.*, **2005**, 293, 180–191.
41. Hammawa, H., and Wanke, S. E., *J. Appl. Polym. Sci.*, **2007**, 104, 514–527.
42. Hammawa, H., and Wanke, S. E., *Recent Res. Devel. Appl. Polym. Sci.*, **2006**, 3, 175–204.
43. Hammawa, H., and Wanke, S. E., *Polym. Int.*, **2006**, 55, 426–434.
44. Galli, P., Collina, G., Sgarzi, P., Baruzzi, C., and Marchetti, E., *J. Appl. Polym. Sci.*, **1997**, 66, 1831–1837.
45. Nishida, H., Uozumi, T., Arai, T., and Soga, K., *Macromol. Rapid Commun.*, **1995**, 16, 821–830.
46. Hong, S. C., Ban, H. T., Kishi, N., Jin, J., Uozumi, T., and Soga, K., *Macromol. Chem. Phys.*, **1998**, 199, 1393–1397.
47. Hong, S. C., Teranishi, T., and Soga, K., *Polymer*, **1998**, 39, 7153–7157.
48. Barrett, A. G. M., and de Miguel, Y. R., *Chem. Commun.*, **1998**, 2079–2080.
49. Stork, M., Koch, H., Klapper, M., Müllen, K., Gregorius, H., and Rief, U., *Macromol. Rapid Commun.*, **1999**, 20, 210–213.

50. Shearer, A. S., de Miguel, Y. R., Minich, E. A., Pochan, D., and Jenny, C., *Inorg. Chem. Commun.*, **2007**, 10, 262–264.
51. Peifer, B., Milius, W., and Alt, H. G., *J. Organometal. Chem.*, **1998**, 553, 205–220.
52. Alt, H. G., and Jung, M., *J. Organometal. Chem.*, **1999**, 580, 1–16.
53. Alt, H. G., *J. Chem. Soci. Dalton Trans.*, **1999**, 1703–1709.
54. Chu, K. J., Soares, J. B. P., and Penlidis, A., *J. Polym. Chem. P. A Polym. Chem.*, **2000**, 38, 462–468.
55. Chu, K. J., Soares, J. B. P., and Penlidis, A., *J. Polym. Chem. P. A Polym. Chem.*, **2000**, 38, 1803–1810.
56. Lee, H.-W., and Park, Y.-H., *Catal. Today*, **2002**, 74, 309–320.
57. Franceschini, F. C., Tavares, T. T. R., dos Santos, J. H. Z., and Soares, J. B. P., *Macromol. Mater. Eng.*, **2006**, 291, 279–287.
58. Franceschini, F. C., Tavares, T. T. R., dos Santos, J. H. Z., and Soares, J. B. P., *Macromol. Chem. Phys.*, **2004**, 205, 1525–1529.
59. Soga, K., Arai, T., Hoang, B. T., and Uozumi, T., *Macromol. Rapid Commun.*, **1995**, 16, 905–911.
60. Arai, T., Ban, H. T., Uozumi, T., and Soga, K., *Macromol. Chem. Phys.*, **1997**, 198, 229–237.
61. Soga, T., Ban, H. T., Arai, T., and Uozumi, T., *Macromol. Chem. Phys.*, **1997**, 198, 2779–2787.
62. Arshady, R., *Colloid Polym. Sci.*, **1992**, 270, 717–732.
63. Hammawa, H., Influence of supports on gas-phase olefin polymerization over polymer-supported (n-BuCp)$_2$ZrCl$_2$/MAO catalysts, PhD Thesis, University of Alberta, **2004**.
64. Mannan, T. M., Influence of polymerization conditions on activities and product properties of polymer supported (n-BuCp)$_2$ZrCl$_2$/MAO catalysts, PhD Thesis, University of Alberta, **2006**.
65. Haggin, J., *Chem. Eng. News*, **1992**, 70(13), 17–18.
66. Galli, P., and Haylock, J. C., *Makromol. Chem. Macromol. Symp.*, **1992**, 63, 19–54.
67. Knoke, S., Korber, F., Fink, G., and Tesche, B., *Macromol. Chem. Phys.*, **2003**, 204, 607–617.
68. Zöllner, K., and Reichert, K.-H., *Chem. Eng. Technol.*, **2002**, 25, 707–710.
69. Singh, D., and Merrill, R. P., *Macromolecules*, **1971**, 4, 599–604.
70. Schmeal, W. R., and Street, J. R., *J. Polym. Sci. P. B Polym. Phys.*, **1972**, 10, 2173–2187.
71. Crabtree, J. R., Grimsby, F. N., Nummelin, A. J., and Sketchley, J. M., *J. Appl. Polym. Sci.*, **1973**, 17, 959–976.
72. Floyd, S., Choi, K. Y., Taylor, T. W., and Ray, W. H., *J. Appl. Polym. Sci.*, **1986**, 32, 2935–2960.
73. McKenna, T. F., and Soares, J. B. P., *Chem. Eng. Sci.*, **2001**, 56, 3931–3949.
74. Kittilsen, P., McKenna, T. F., Svendsen, H., Jakobson, H. A., and Fredriksen, S. B., *Chem. Eng. Sci.*, **2001**, 56, 4015–4028.
75. Naik, S. D., and Ray, W. H., *J. Appl. Polym. Sci.*, **2001**, 79, 2565–2579.

76. Alexiadis, A., Andes, C., Ferrari, D., Korber, F., Hauschild, K., Bochmann, M., and Fink, G., *Macromol. Mater. Eng.*, **2004**, 289, 457–466.
77. Merquior, D. M., Lima, E. L., and Pinto, J. C., *Macromol. Mater. Eng.*, **2005**, 290, 511–524.
78. Grof, Z., Kosek, J., Marek, M., and Adler, P. M., *AIChE J.*, **2003**, 49, 1002–1013.
79. Grof, Z., Kosek, J., and Marek, M., *AIChE J.*, **2005**, 51, 2048–2067.
80. Horáčková, B., Grof, Z., and Kosek, J., *Chem. Eng. Sci.*, **2007**, 62, 5264–5270.
81. Lynch, D. T., and Wanke, S. E., *Can. J. Chem. Eng.*, **1991**, 69, 332–339.
82. Mannan, T. M., Hammawa, H., Lynch, D. T., and Wanke, S. E., *Can. J. Chem. Eng.*, **2004**, 82, 371–381.
83. Webb, S. W., Weist, E. L., Chiovetta, M. G., Laurence, R. L., and Conner, W. C., *Can. J. Chem. Eng.*, **1991**, 69, 665–681.
84. Moore, S. J., and Wanke, S. E., *Chem. Eng. Sci.*, **2001**, 56, 4121–4129.
85. Gregg, S. J., and Sing, K. S. W., *Adsorption, Surface Area and Porosity*, 2nd ed., Academic, New York, **1982**.
86. Koivumäki, J., and Seppälä, J. V., *Macromolecules*, **1993**, 26, 5535–5538.

10 Review of Phillips Chromium Catalyst for Ethylene Polymerization

MAX P. McDANIEL
Phillips Research Center, Highways 60 and 123A, Bartlesville,
Okhahoma 74004

Commercial linear polyethylene (PE), the most commonly used type of plastic, was born over half a century ago with the accidental discovery at Phillips Petroleum Company that chromium oxide supported on silica can polymerize α-olefins.* That same catalyst system, modified and evolved, is still used today by many companies worldwide and accounts for one-third to one-half of the world's high-density polyethylene (HDPE) supply and some linear low-density polyethylene (LLDPE) polymers as well. The catalyst is now more active and has been tailored in numerous ways for many specialized modern applications. This chapter reviews our understanding of the complex chemistry associated with that catalyst system, and it provides examples of how that chemistry is controlled and exploited commercially to produce a wide variety of polymer grades. It is written from an industrial perspective, drawing on the experience of numerous scientists working at Phillips Petroleum and other companies over 50 years, many of whom this author was fortunate to know and work with.

10.1 HISTORICAL AND COMMERCIAL BACKGROUND

Linear or high-density PE was invented in the early 1950s as a result of three independent catalyst discoveries in three separate locations using three differ-

*The inventors J. P. Hogan and R. L. Banks were inducted into the National Inventors Hall of Fame, in Akron, Ohio, in 2001, to join other distinguished inventors spanning two centuries who have shaped our world. The Oklahoma building in which the discovery took place, and in which this author still works, was designated as a "historic landmark" by the American Chemical Society.

Handbook of Transition Metal Polymerization Catalysts Edited by Ray Hoff and Robert T. Mathers
Copyright © 2010 John Wiley & Sons, Inc.

ent transition metals.[1–8] It is interesting to compare the directions these inventors and their companies took, which J. Paul Hogan, one of the inventors, later summarized.[1]

The chromium catalyst was discovered in 1951 and immediately Phillips developed a commercial process which was being licensed in less than four years. The Phillips license included all information and technical aid needed, including plant design, polyethylene in 1000-lb quantities for market development, on-site plant start-up assistance, and complete on-going information exchange. By 1955, a 1000-lb/day semiworks plant was on stream, and in that same year Phillips management approved building a commercial 75-million-lb/year HDPE plant and an accompanying 180-million-lb/year ethylene plant. It was concluded that no one manufacturer could develop the full market potential of the Phillips HPDE process, and therefore Phillips decided to license. Between 1955 and 1956 nine companies in seven countries signed up.[1,9] These earliest licensees included Union Carbide (U.S.), Allied (U.S.), Pullman (U.S.), British Petroleum (U.K.), Soltex-Celanese (U.S.), Rhone Poulenc (France), Solvay (Italy), Eletroteno (Brazil), BASF (Germany), and Showa Denko (Japan). The Phillips plant came on stream in 1956 and licensee plants were not far behind.

Karl Ziegler discovered a catalyst based on titanium two years later in 1953 and began licensing it within a year. He could offer only a laboratory method that each licensee then had to develop and scale up independently.[11] Apparently the license did not include adequate information on how to control the molecular weight of the polymer.[1]

Standard Oil of Indiana discovered yet another catalyst in 1950 based on molybdenum. This system took a still different direction. The company hired an outside consultant to evaluate their new linear PE and obtained a negative report. This discouragement apparently caused a delay in plans for commercialization until after the early Phillips and Ziegler commercial successes had occurred.[1,10] The first plant using Standard Oil technology only went on stream in 1961 in Japan.[1] Consequently the early Standard Oil of Indiana discovery had little impact on the linear PE industry. Within a few years the process was dead.

For the first four years production was entirely from a solution form (SF) process, in which the polymer dissolves in a good PE solvent.[11] Cyclohexane was used along with ethylene and 1-butene as needed at 125–175 °C under pressures of 400–500 psig. However, laboratory discoveries at Phillips in the early 1950s led to another, more efficient process in which the polymer does not go into solution but instead forms insoluble particles in a hydrocarbon slurry. This slurry, or "particle form" (PF), process[12,13] was commercialized in early 1961 and was then quickly adopted by licensees. A jacketed pipe-loop-shaped reactor was chosen because of the larger cooling surface provided per unit volume and the reduced tendency for dead spaces and consequent polymer build-up. Soon the loop-slurry process overtook the solution process because of its simplicity and reliability. A low-boiling liquid paraffin was used as the diluent (pentane, isopentane, and finally isobutane) at 70–110 °C and about

600 psig. Since catalyst activity was high, no catalyst removal was ever required in the slurry process. The megaloop reactors of today, modified and improved in numerous ways, have output rates of over a billion pounds PE per year.

The first grades of HDPE by the Phillips process were homopolymers of less than 1 melt index. Ethylene–butene copolymers were introduced in 1958[14] and soon other polymer parameters were utilized to extend the choice of polymer types. New copolymers containing 1-hexene and having improved properties were introduced in 1968. In 1969 Phillips announced a new process to produce LLDPE.[15,16] Beginning in 1969 polymers with density as low as 0.925 were produced in a modified PF process using chromium catalysts. For the most part, however, polymers below 0.93 were not common among Phillips licensees due to the tendency of low-density polymer to swell, which limited reactor output. The introduction of gas-phase technology by Union Carbide in the 1970s filled this requirement well. Further developments in the late 1980s now also make it possible to produce HDPE or LLDPE in the loop reactor with equal ease.[17–20] Commercial transitions between HDPE and LLDPE require only a few hours.

HDPE is the most widely used form of polyethylene, and the Phillips catalyst is used in many different forms and processes to produce a large fraction (~40–50%) of the world's HDPE. It is used in solution, slurry, and gas-phase processes. The Phillips catalyst is only used commercially to produce PE because these catalysts do not provide a high level of stereoregulation like some Ziegler–Natta catalysts. Even so, they do produce a significant proportion of isotactic polymer and this was the basis for awarding Phillips the crystalline polypropylene composition of matter U.S. Patent in 1983.[1,21,22]

Today three main types of transition metal catalysts are used commercially to make linear polyethylenes (HDPE and LLDPE): (1) Phillips chromium oxide–based catalysts, (2) Ziegler titanium or vanadium halide catalysts, and (3) metallocene catalysts. These differ in many ways, most notably in the molecular weight distribution that each delivers to the polymer. Figure 10.1 illustrates these differences by plotting the molecular weight (MW) distribution from each catalyst type. The Phillips catalyst produces the broadest MW distribution; in this case the polydispersity (M_w/M_n) was about 20. Ziegler is narrow, with M_w/M_n of about 4 and metallocene about 2.

These catalysts also differ in other ways, such as the amount of long-chain branching each imparts to the polymer and in the extent and distribution of comonomer incorporation. These molecular characteristics in turn impart different flow characteristics to the molten resins and physical properties to the final molded parts. Polymers derived from the Phillips catalyst are usually more "shear thinning" than from the other two, meaning that the polymer flows more easily under pressure. These different characteristics mean that these three catalysts do not usually compete with each other in the market, but instead each serves a different part of the market's diverse needs. Phillips- and Ziegler-based resins together comprise most of the linear PE market, perhaps 95%, but metallocene catalysts are slowly gaining acceptance for certain specialty applications, especially in low-density film.

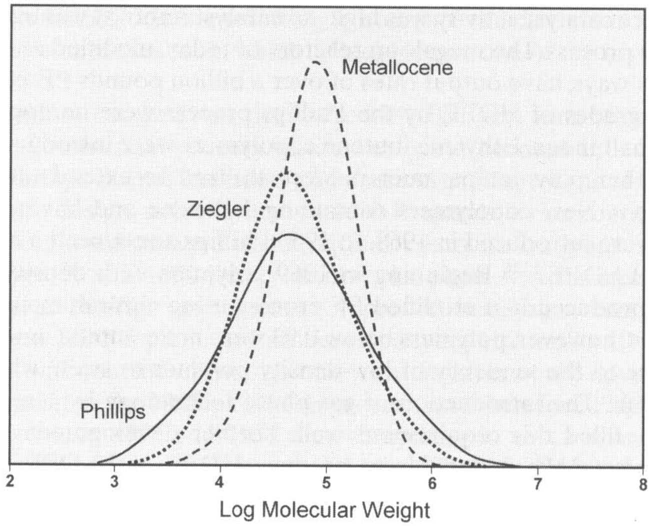

Figure 10.1 Molecular weight distribution of three LLDPE polymers made from three common linear PE catalysts.

10.2 CATALYST PREPARATION

To make the Phillips polymerization catalyst, a wide pore carrier, usually silica, is impregnated with a chromium compound followed by calcination in dry air or oxygen to "activate" the catalyst.[23,24] This stabilizes at least some of the chromium in the hexavalent state, where it becomes dispersed and "anchored" to the carrier surface. Almost any other source of chromium can also be used because oxidation to Cr(VI) occurs readily during calcining. Basic Cr(III) acetate is the most common commercial source of chromium.[25–28] Typical commercial loading ranges from 0.2 to 2 wt % Cr.

Although bulk CrO_3 begins to decompose above 200 °C into O_2 and Cr_2O_3, a certain amount is stabilized on silica even up to 1000 °C.[24,29–48] This "anchoring" is due to the formation of surface chromate and perhaps also dichromate species at 150–350 °C in which each chromium atom is directly linked to the support, as shown in Scheme 10.1.[30,49–55]

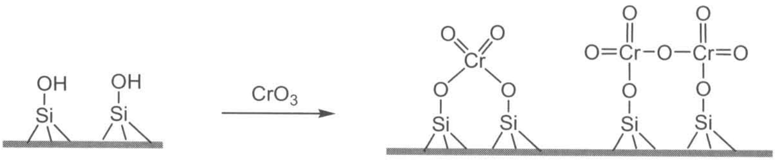

Scheme 10.1

Even though oxidation and subsequent "anchoring" of the chromium occur below 350 °C, respectable polymerization activity does not develop until the catalyst has been calcined at much higher temperatures, such as 600–900 °C. As the temperature is raised, surface silanols condense to release moisture. At first the so-called paired silanols condense, but above 600 °C only "isolated" silanols remain.*[,56–62] As the temperature is further raised, surface annealing permits condensation of some of these hydroxyls, but the silanol population never quite reaches zero, even as sintering begins around 900 °C. During activation, the stability of surface Cr(VI) at high temperature depends on minimizing its exposure to this same moisture, especially above 600 °C. Traces of water vapor can hydrolyze the Si–O–Cr attachment, which at high temperatures results in the decomposition of Cr(VI) to Cr_2O_3.[59,60]

Whether the anchored chromium atoms are isolated as chromate or exist in pairs as dichromate (or perhaps as higher polychromates) has proven a difficult problem despite its importance to our understanding of the catalyst. Some researchers have suggested that polymerization can occur only when the chromium atoms are paired, and they have sometimes proposed polymerization mechanisms involving two chromium atoms.[63–78] This was once advanced as the reason why unsupported organic Cr(VI) esters have failed to exhibit activity because they are always chromate-like structures.[63] The initial Cr compound used makes no difference. Catalysts made from ammonium chromate or ammonium dichromate or CrO_3 or Cr(III) acetate behave identically after being calcined.

Numerous authors have utilized many different sophisticated techniques to determine what Cr(VI) species exist on the commercial catalyst. Recently the Turin group has published an excellent review of this work.[79] Various types of spectroscopy were initially attempted but often proved contradictory or inconclusive.[27,51,70,80–86] In recent years exhaustive studies have been undertaken of the binding of CrO_3 on silica, alumina, and other oxides and mixed oxides over a wide range of metal loadings using Raman, infrared (IR), diffuse-reflectance IR, electron spin resonance (ESR), X-ray adsorption fine structure (EXAFS-XANES), and temperature-programmed reduction.[87–107] A summary of these studies has been published which provides a useful background when considering the behavior of commercial polymerization catalysts.[63] Despite some disagreement among researchers, most of the literature studies conclude that both chromate and dichromate can exist on these surfaces and the support, loading, and calcining history can determine which species is favored. A recent exception to that generalization is Thune et al., who created a Si(100) model and, using a combination of X-ray photoelectron spectroscopy, secondary ion mass spectrometry, and Rutherford backscattering, concluded that chromate is the only species detected at all loadings and up to 730 °C.[108–110]

---

*The designation of surface silanols as "paired" or "isolated" refers to their reactivity with such compounds as $SiCl_4$, $TiCl_4$, BCl_3, etc. Two silanols are considered as paired if they are close enough to both react with a single reactant molecule.

In another approach Krauss and co-workers carefully studied the luminescence of Cr/silica and concluded that at least a portion of the chromium is present as chromate.[111] Others have examined the geometry of the chromate and dichromate ions and compared them to models of the silica surface.[80] Again, however, the uncertainty is significant due to the lack of precise models. Hydroxyl spacings derived from a particular face of cristobalite or tridymite may or may not have relevance to amorphous, high-surface-area silica gels.

Other researchers approached the question by measuring the change in hydroxyl population when CrO_3 attaches to the surface.[112] A chromate species was expected to yield a loss of 2 OH/Cr whereas dichromate would lose only 1. Hogan, working from gravimetric measurements after calcination at 150 °C, concluded that CrO_3 attaches as mainly chromate.[29–31] Zecchina[80] and Krauss,[81] working from IR measurements of OH groups on catalysts calcined at 500–600 °C, reported that dichromate was the dominant species. Later Hierl and Krauss, in another type of gravimetric study using CO reduction, concluded that chromate is the dominant species.[113]

However, even this seemingly straightforward approach requires some interpretation, which may help rationalize these contradictory results. In yet another study, OH groups on silicas with and without Cr and calcined between 200 °C and 800 °C were measured by reaction with methylmagnesium iodide.[114] The ΔOH/Cr replacement ratio was found to be near 2 at 200 °C, in agreement with Hogan,[29–31] and near 1 at 500 °C, in agreement with Zecchina[80] and Krauss.[81] At still higher temperatures the observed ΔOH/Cr dropped even below 1, which would not seem to correspond to either species. In fact, the ΔOH/Cr replacement ratio was found to be proportional to the silica OH population itself at the temperature in question. This is shown in Figure 10.2, and it suggests that the chromium is occupying a section of surface that would be hydroxylated or not to about the same extent as the original silica. This is in contrast to the previous studies which carried implied assumptions that those unreacted

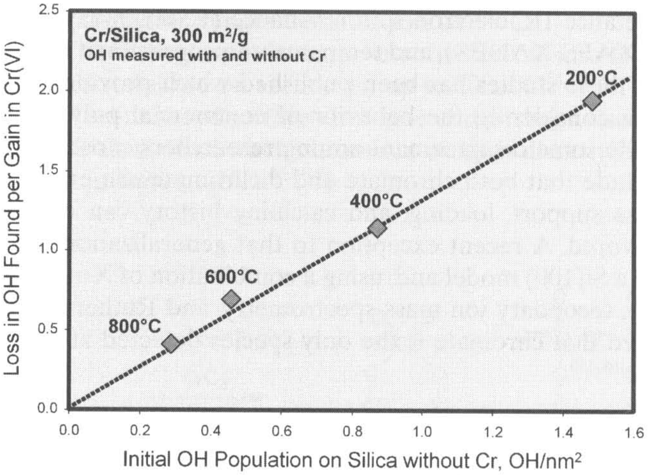

Figure 10.2 ΔOH/Cr replacement ratio is proportional to original OH population.

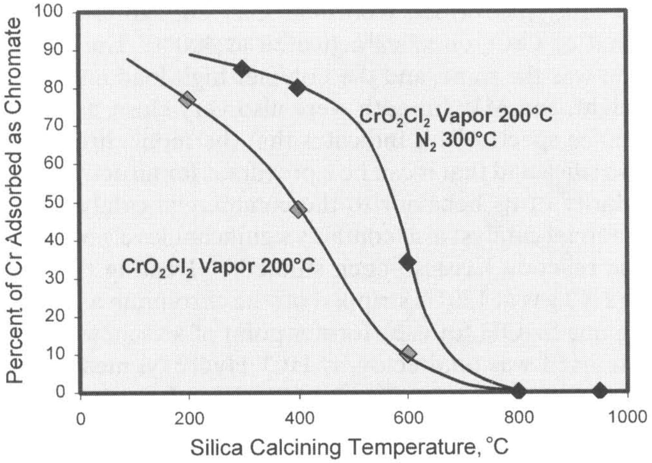

Figure 10.3 Reaction of CrO_2Cl_2 with silica to form chromate species.

hydroxyls on virgin silica would remain unaffected during the calcining step. In fact this is most likely not the case. Therefore the most that might be concluded from such ΔOH/Cr displacement measurements is that CrO_3 initially attaches to the hydrated surface as chromate at lower temperatures.

In perhaps the most direct approach, silica calcined at various temperatures was treated with chromyl chloride vapor in nitrogen at 200 °C.[115–117] The adsorbed chromium was then encouraged to further react by subjecting the catalyst to nitrogen at 300 °C for 30 min. When the silica was first calcined at 400 °C or lower, most or even all of the chromyl chloride was found to attach as chromate, losing two chlorides per Cr, as shown in Scheme 10.2. When the silica had been calcined at higher temperatures much of the chromium became attached by losing only one chloride, yielding a chlorochromate species. This is shown in Figure 10.3. All of the chromium remained hexavalent. Presumably adsorption as dichromate would not be possible in nitrogen at 300 °C or below. Thus chromyl chloride behaved like chlorosilanes, $TiCl_4$, BCl_3, and other reagents that have been used to determine the extent of hydroxyl pairing on silicas[56,57,61,62]:

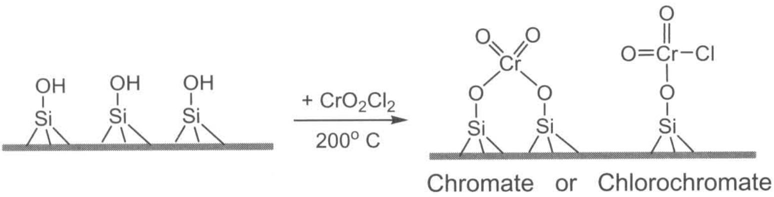

Scheme 10.2

The chlorochromate catalysts did not polymerize ethylene under the usual commercial conditions (100 °C at 14 mol % ethylene, no cocatalyst). However, the chromate catalysts, formed from 400 °C silica, exhibited activity nearly identical to that of CrO_3 on silica activated at 400 °C. The kinetic profile of polymerization was the same, and the polymer high-load melt index (HLMI), molecular weight, and MW breadth were also very close, as well as the UV–visible reflectance spectra. This indicates that the monochromate species can indeed exist on silica and that it can be a precursor for an active polymerization site. The similarity of its behavior to the commercial catalyst makes it likely that the commercial catalyst also contains significant levels of monochromate.

The reverse reaction has also been studied.[118] Treating the calcined CrO_3/silica with dry HCl gas at 130 °C stripped off the chromium as chromyl chloride vapor, leaving one Si–OH for each former point of attachment (Scheme 10.3). The silica base itself was unaffected by HCl. Hydroxyl measurements before and after the stripping gave a direct indication of the bonding of Cr(VI). Figure 10.4 shows the results of a single typical experiment in which the calcining temperature was 400 °C before treatment with HCl gas. At low loadings all of the chromium was found attached as chromate, generating two silanol groups for each lost Cr. At higher loadings, however, the ratio decreased, suggesting the development of some dichromate:

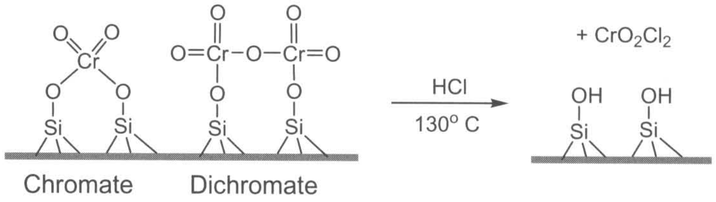

Scheme 10.3

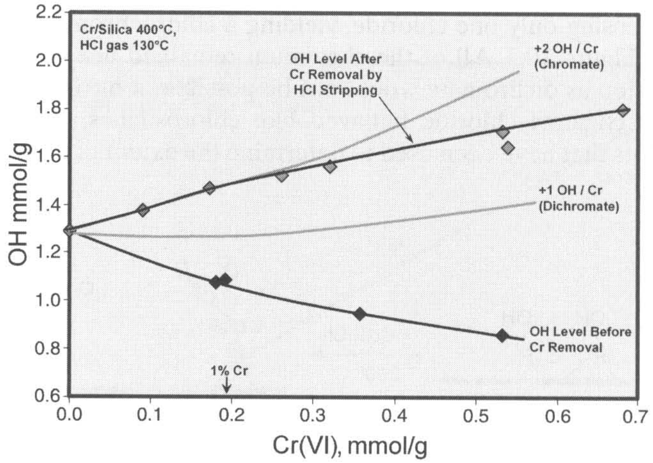

Figure 10.4 Removal of a Cr(VI) from a Cr/silica catalyst (300 m^2/g) as CrO_2Cl_2 vapor by reaction with dry HCl gas at 130 °C.

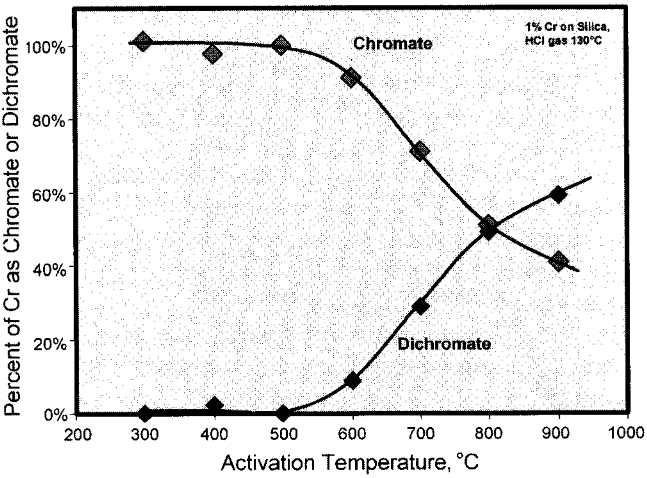

Figure 10.5 Chromate–dichromate partition found by HCl stripping of commercial 1% Cr catalyst.

These results were fairly typical when the experiment was repeated at other calcining temperatures. The overall results suggested that both the temperature and chromium loading are important in determining the form of Cr(VI) present.[118] Low temperatures and low loadings usually favored chromate, but even after calcination at 700–900 °C, considerable chromate was found. At high loadings and high temperatures lower ΔOH/Cr ratios were measured, suggesting formation of some dichromate. Figure 10.5 shows this trend. It plots the amount of chromium found as dichromate for a typical commercial catalyst containing 1% Cr on a silica having a surface area of 300 m^2/g. Again significant polymerization activity was obtained from catalysts that were found by this technique to contain only chromate, which provides a second confirmation that chromate can serve as an active precursor.

One curiosity of stripping off Cr(VI), whether chromate or dichromate, was that it left pairs of hydroxyls, even when the catalyst had been previously calcined at 800 °C, which would normally remove such closely spaced OH pairs. Despite being paired, these hydroxyls did not condense so easily when reheated; 800 °C was required to remove all of them. Nevertheless, they did react with chromyl chloride vapor at 200 °C to generate (regenerate) a good deal of chromate. (In contrast, virgin silica calcined at 800 °C formed no chromate when reacted with chromyl chloride.) This suggested that even after activation at 800 °C CrO_3/silica contained a considerable amount of chromate.

The maximum amount of chromium that can be stabilized as Cr(VI) depends on the calcination atmosphere and temperature.[119,120] Figure 10.6 shows the amount of Cr(VI) stabilized when CrO_3/silica was calcined as a function of the overall chromium loading. When the calcination was done in dry oxygen, all of the chromium remained hexavalent at the lowest loadings. However, at some point, as the Cr loading was increased, saturation occurred,

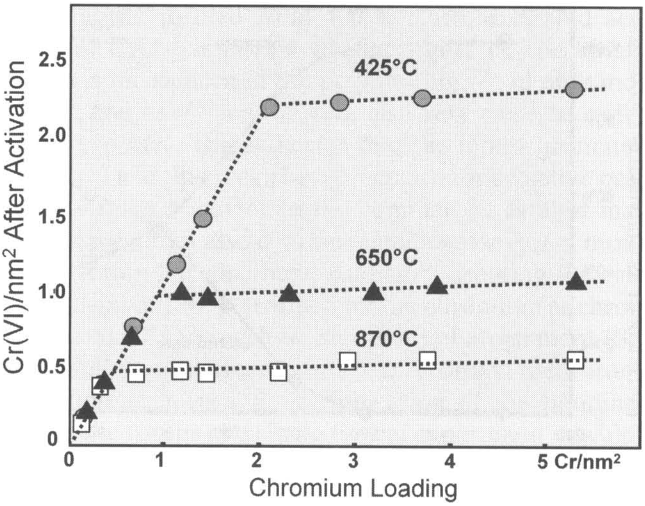

Figure 10.6 Stabilization of Cr(VI) during activation.

and beyond that limit the excess CrO_3 decomposed into the trivalent oxide α-chromia.[114,119,121,122] This limit was often a sharply defined one that varied with temperature but not with the total chromium loading or the source of chromium. In these experiments, trivalent chromium salts were used in addition to CrO_3 as well as ammonium chromate and ammonium dichromate. All behaved similarly.

The maximum Cr(VI) coverage also depends on the calcination atmosphere. In the absence of oxygen, almost all of the CrO_3 eventually decomposed to Cr_2O_3, usually above 600 °C, whatever the loading. The higher the oxygen content of the gas, the more effective it was at stabilizing Cr(VI). Traces of moisture in the gas stream were found to inhibit the stabilization of Cr(VI) due to hydrolysis of the Cr–O–Si linkage.[59,60] Therefore the depth of the fluidized bed during activation can be important in commercial activations as well as the rate of heat-up and the purity of the gas. All of these variables can affect the moisture level during activation.

A fully hydrated silica contains about 4.5 OH/nm^2.[56] Therefore saturation of sites by chromate could yield no more than 2.2 Cr/nm^2, whereas dichromate could give up to 4.5 Cr/nm^2. The highest Cr(VI) saturation coverage actually found, after calcination at 425 °C, was 1.8–2.3 Cr(VI)/nm^2.* This is consistent with mainly monochromate, as indicated by other evidence. Saturating the surface with chromyl chloride vapor yielded 1.6 chromates/nm^2.

It is interesting that the saturation coverage noted above is not reversible. That is, if a catalyst that has undergone saturation at 900 °C is then reactivated for 24 h at 400 °C, the chromium does not redistribute. The original saturation value characteristic of 900 °C is retained. This suggests that it is the dehydra-

*Higher amounts of Cr(VI) can be obtained at still lower calcining temperatures, but it is uncertain in those cases to what extent the chromium is fully attached to or stabilized by the silica.

tion or annealing of the silica surface that determines the saturation coverage, and not the temperature itself. Indeed, applying Cr anhydrously to a silica already calcined at 900 °C followed by a second calcining at 400 °C yields the Cr(VI) level characteristic of 900 °C even though the Cr has only experienced 400 °C.[119,123–126]

Hexavalent chromium has a high degree of mobility on the silica surface during activation.[43,63,125,126] Transport of Cr(VI) between silica particles is easy to demonstrate experimentally because of the saturation coverage behavior described above. For example, if a Cr/silica containing a high level of CrO_3 (5% Cr) is mixed with plain silica and then activated in oxygen, one obtains a saturation curve such as that shown in Figure 10.7. Although the catalyst initially contains 5% Cr(VI), it cannot maintain that amount in the hexavalent state at higher levels of dehydroxylation. Thus Cr(VI) decomposes into Cr(III) with ever higher activation temperatures, and the lower curve in Figure 10.7 is obtained. The curve plots the amount of Cr(VI) as a percentage of the total Cr.

The upper curve in Figure 10.7 represents the hexavalent Cr content of the same Cr/silica catalyst, but dry mixed with silica before activation. The hexavalent Cr content found in the mixture is much higher than could be supported by the original parent catalyst at each temperature tested. This can only mean that the plain silica has adsorbed some of the excess chromium and maintained it in the hexavalent form. By continuing to raise the temperature, one eventually reaches the point where even the two combined silica sources also become saturated with Cr(VI). Then the excess decomposes into the trivalent oxide, as would be expected. High mobility is detected even at 400 °C, the lowest activation temperature tested by this technique.

One could imagine several different mechanisms that might allow Cr(VI) transfer. It is not from the movement of free pore water, because both source and recipient were individually dried at 200 °C or higher before mixing in all

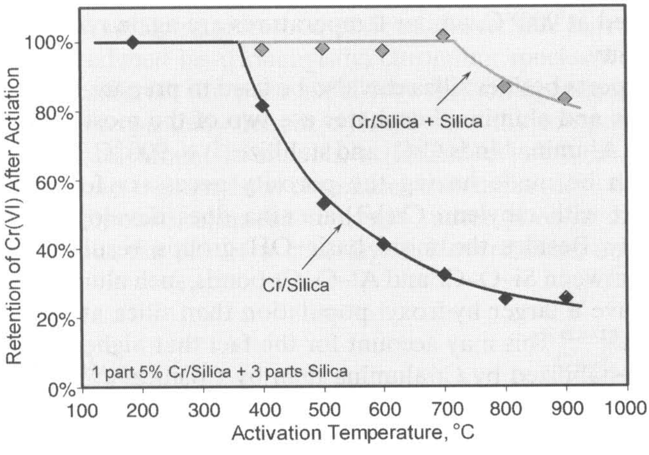

Figure 10.7 Conversion to Cr(VI) of a 5% Cr/silica catalyst during activation at the indicated temperatures, alone (lower line) and as part of a dry mixture with 75% silica (upper curve). Divergence of the two lines indicates movement of the Cr.

experiments. Another possibility is the evaporation of Cr(VI).[45,53,109,110] However, Cr could not be transported by a gas stream moving sequentially through the Cr/silica source and then the silica recipient, when the two beds were separated by a sintered quartz frit only 2 mm apart. This suggests that the transfer must occur through particle-to-particle solids contact. One mechanism that could allow surface mobility during activation is rapid chromium cycling between Cr(VI) and Cr(III). Each redox cycle could break and reconnect bonds with the silica surface, resulting in Cr mobility. Oxygen is released during the reduction and adsorbed during oxidation. However, Cr transfer was found to occur even in the absence of oxygen, which should stop the redox cycling. Thus the transfer mechanism does not seem to be solely dependent on redox cycling.

A third possibility is that Cr(VI) moves about the surface through hydrolysis of Cr–O–Si bonds followed by reconnection. This could involve hydrolysis by moisture vapor or by surface silanols, such as shown in Scheme 10.4, for example:

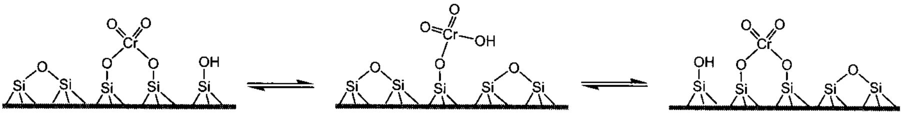

Scheme 10.4

When the Cr/silica donor and silica recipient were first dehydroxylated by calcination at 900 °C, before mixing and coactivation, no transfer of Cr was observed at 400 °C. In fact, transfer did not resume until the mixture was coactivated at 800–900 °C. Thus the degree of dehydroxylation, or surface annealing, does determine the extent of Cr transfer. This suggests that silanols could be involved in the transfer, or at least that surface mobility is required for Cr mobility, and this is determined by the degree of surface annealing. Once annealed at 900 °C, similar temperatures are again required for surface and Cr mobility.

Other supports besides silica can also be used to prepare Phillips-type catalysts. Alumina and aluminophosphates are two of the most common alternatives to silica. Alumina binds CrO_3 and stabilizes it to 900 °C. High-surface-area γ-alumina can be made having the porosity necessary for polymerization. Upon contact with ethylene Cr(VI)/alumina does develop weak polymerization activity. Besides the more basic OH groups, resulting in electronic differences between Si–O–Cr and Al–O–Cr bonds, such alumina catalysts also frequently have a larger hydroxyl population than silica at normal calcining temperatures.[127–129] This may account for the fact that higher levels of Cr(VI) can often be stabilized by Cr/alumina than by Cr/silica.[114,119,128,130–132] Hexavalent chromium was also found to be mobile on alumina carriers. Transfer was observed from alumina to alumina, from silica to alumina, and from alumina to silica. Again no transfer was observed between 900 °C Cr/alumina and 900 °C alumina when coactivated at 400 °C.

Aluminum phosphate, $AlPO_4$, is isoelectronic and isostructural with silica. The phase diagrams are nearly identical, and even the transition temperatures are similar. Si^{4+} in the silica matrix is replaced by alternating Al^{3+} and P^{5+}. Therefore aluminum phosphate can replace silica as a support to form an active polymerization catalyst.[133–136] However, it makes a profound difference in the catalyst behavior because the two supports exhibit somewhat different surface chemistry. Hydroxyls on $AlPO_4$ are more varied (P–OH and Al–OH) and more acidic than those on silica. The OH population measured by reaction with methyl magnesium iodide would seem to be slightly lower on $AlPO_4$ than on silica. Perhaps this is due to the presence of terminating P=O groups. The saturation coverage of Cr(VI) on Cr/$AlPO_4$ appears to be very similar to that of Cr/silica at all temperatures.

$AlPO_4$ is just one member in the broader aluminophosphate family. Stoichiometric $AlPO_4$ (P/Al = 1.0) precipitated from acidic aqueous solutions containing Al^{3+} and PO_4^{-3} ions tends to be crystalline, which lowers its surface area. Other aluminophosphates of P/Al < 1.0 display considerable surface area and porosity. These supports are not just intimate mixtures of Al_2O_3 and $AlPO_4$, but instead they form amorphous uniform compositions. X-ray diffraction and solid-state nuclear magnetic resonance (NMR) find no evidence of domains of either alumina or aluminum phosphate.[128] For polymerization-grade supports, the preferred P/Al ratio is usually 0.4–0.8. Highest activity occurs at around P/Al of 0.6–0.8.

Organic chromate esters have also been investigated as a chromium source. One in particular, bis-triphenylsilyl chromate, was first studied by Baker and Carrick as a homogeneous model for the surface chromate structures postulated on the Phillips catalyst.[137] The compound is quite stable but is reduced by olefins under polymerization conditions to Cr(II) or Cr(III) and to the corresponding aldehyde, which mimics the behavior of Cr(VI)/silica.[138] The homogeneous compound does polymerize ethylene, although at a much slower rate than the supported surface structures described above. Side reactions between reduced and nonreduced bis-triphenylsilyl chromium species were suggested as the probable reason for this poor activity by the homogeneous model.

Upon exposure to partially dehydroxylated silica the compound gradually adsorbs through attachment to silanols, as indicated below in Scheme 10.5. This supported mono-triphenylsilyl chromate structure is more active than the homogeneous compound, although it is still rather poor in comparison to CrO_3/silica (without the aid of a cocatalyst). Nevertheless, it demonstrates

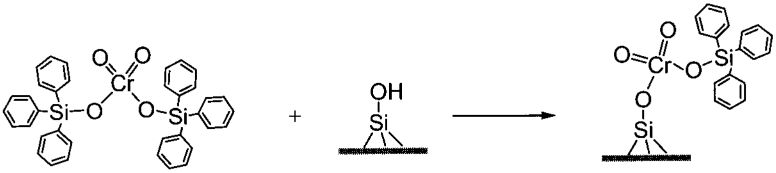

Scheme 10.5

again that polymerization can take place in the absence of a dichromate structure. Chromium oxide–based catalysts could be converted to silyl chromate catalysts by the addition of triphenylsilanol.[139] Other organic chromate esters, such as bis-adamantyl chromate or bis-triphenyltin chromate, have also been used successfully in this way[140,141]:

Supported bis-triphenylsilyl chromate is widely used commercially as a substitute for chromium oxide in gas-phase processes. However, in order to generate acceptable activity, an organoaluminum compound (e.g., $AlEt_3$ or $AlEt_2OEt$) is usually impregnated onto the silica-supported bis-triphenylsilyl chromate. The polymerization behavior is then dominated by the presence of the aluminum alkyl. The well-known broad MW breadth from the silyl chromate catalyst can be attributed mostly to the presence of this cocatalyst. Impregnating such cocatalysts onto Cr oxide catalysts produce similar polymers.[139]

10.3 CONTROL OF CATALYST ACTIVITY

10.3.1 Porosity

The observed activity from Phillips catalysts is the result of many influences, both chemical and physical, and therefore many commercial variations exist.[142] Perhaps the first consideration is the porosity of the support. Polymerization poses a special problem in catalysis because the polymer molecule is often hundreds of times longer than the average pore diameter of the catalyst in which it is formed. Commercial polyethylene having a weight average MW of 100,000–500,000 is typical, and a good fraction of these chains have MW in the millions. Some grades have even higher average MW. Thus, for example, a 100,000-Å chain could be formed in a 100-Å silica pore in the interior of a 100-μm catalyst particle. If the polymer is in solution (SF process), the chains may be able to escape the pores. In a slurry or gas-phase process, however, the solid polymer is trapped in the pore structure. The chains fold on themselves as they are formed, clogging the internal pores, which can potentially stop the reaction except on the exterior surface of each catalyst particle, representing less than 1% of the total surface area.

If the silica is chosen well, however, polymer formation can exert enough pressure in the pores to rupture them, and the catalyst particle "explodes" into billions of smaller fragments, exposing fresh exterior catalyst surface.[41,143–166] These fragments then become buried in the polymer that they subsequently produce. This fragmentation occurs only on certain polymerization-grade silicas that are designed to be friable. In addition to having a high surface area, these silicas must be fragile enough to fragment during polymerization, yet sturdy enough for handling during processing prior to reaction.

For silicas, fragility generally requires high pore volume (PV) and most commercial silicas sold as adsorbents or zeolites, or supports for other catalytic applications, cannot be used for polymerization because their PV is too low.[41,167–169,223–225] For other supports this principle may or may not apply depending on their structure and inherent strength. For silicas, the dependence on PV is illustrated in Table 10.1, where six commercial silicas and one made in this laboratory are compared.[41] Each was impregnated with 1% Cr, calcined at 700 °C, and tested for polymerization activity. Although all six had a high surface area, two of them were unsuitable for polymerization, including the one of highest surface area.

Usually the silica must have a PV of at least about 1 mL/g in order to be fragile enough for commercial polymerization. One can see that from the trend in Table 10.1. Activity usually comes on rather suddenly as PV is increased to around 1 mL/g. Further increases in PV, above about 3 mL/g, do not always have the same impact on activity. However, once friability is obtained from a sufficiently high PV, activity can still be influenced by the surface area.

The LPS silica in Table 10.1 was prepared by extracting the water from a low-solids hydrogel first with an organic solvent before final drying in order to avoid the compression caused by the surface tension of water.[162] This leaves a fragile catalyst of very high PV. Such preparations often provide dramatic examples of the effect of PV because if the same hydogel is dried directly in an oven, it will usually be less active or even completely dead.[41,145,170] Figure 10.8 provides a summary of this effect. In this series of experiments, samples

TABLE 10.1 Dependence of Polymerization Activity on Porosity of Silica Support

Silica Grade	Surface Area (m^2/g)	Pore Volume (mL/g)	Activity (g/g·h)
Grace 35	740	0.43	20
Grace 81	600	0.60	300
Grace 951	600	0.97	2500
Grace 56	300	1.2	2400
Grace 952	300	1.6	2500
Phillips LPS	300	2.5	2600

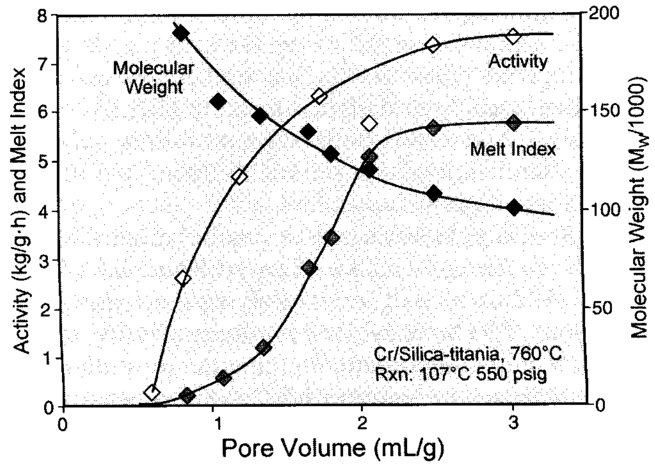

Figure 10.8 Influence of mesoporosity on activity.

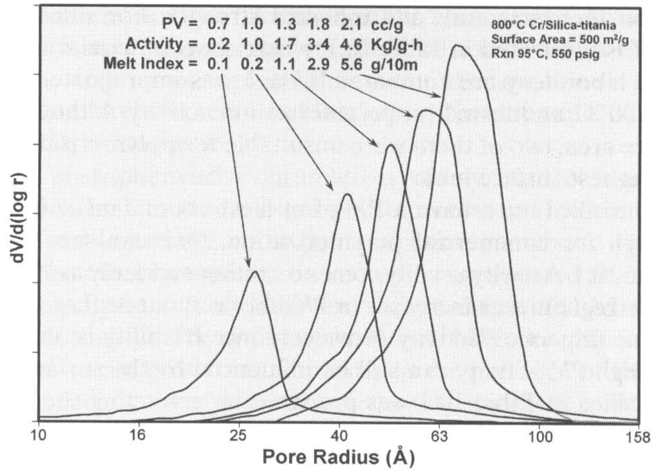

Figure 10.9 Influence of PV on activity.

of hydrogel were dried by extracting the pore water using various solvents and techniques designed to give varying PV. This happens without affecting the chemical composition or surface area of these catalysts. The activity of the finished catalyst is plotted against total PV.

Inevitably, nitrogen sorption shows the inactive silica to contain a low PV mainly inside small pores of less than 60 Å diameter. In contrast, the active samples dried by organic solvent extraction usually have greater total volume and most of that is inside much larger (meso) pores. An example of the pore size distributions of these extremes is shown in Figure 10.9. In this series a Cr/silica–titania hydrogel was dried in various ways, from direct oven drying to more elaborate azeotropic extraction methods in organic solvents of progressively lower surface and interfacial tension, which compress the pores to varying degrees during drying. Again all samples had the same chemical composition and the same high surface area. Only the PV and pore size were different and these are shown in the figure. One can see that as PV (or pore size—they move together when the surface area is held constant) increased, the activity also increased from marginal to quite high. This is attributed to the varying ability of these catalysts to fragment during polymerization—an indirect consequence of manipulating the PV. This principle applies to alumina and aluminophosphate supports as well.

That the catalyst really does fracture during polymerization can be easily demonstrated. When a Cr/silica catalyst of say 60–80 mesh (~200 μm) polymerizes ethylene to a yield of 1000 g/g, each catalyst particle produces a polymer particle that is about 1000 times larger by volume. Cutting into the polymer granule will not expose the original catalyst particle. Even under a microscope the fragments are too small to be seen easily in the polymer background. But gently burning away the polymer leaves catalyst ash, a loose agglomerate of extremely fine dust. Often the original polymer particle shape and dimensions are still visible, but it crumbles at the slightest touch. The average particle size in this dust can be measured by Microtrac to be no more than 7 μm.[145,146] However, even this is an agglomerate particle, and the ultimate fragment size has been demonstrated to be much smaller. The work of Conner,[154–160,171] Wagner,[172,173] and others,[147–151,174,175] using specialized techniques, has done much to shed light on the details of the fragmentation process. The ultimate catalyst fragment size has been reported to be as small as 0.01–0.1 μm.[164,165,172,173] Thus the average catalyst particle fractures into approximately 1 billion to 1 trillion fragments.

One vital question is whether the interior of the fragments can participate in the activity or whether they remain blocked as some believe.[176] If the interior of the fragments do not contribute to the activity, then the effective surface area (the external area of each fragment) could be reduced significantly from the measured Brunauer–Emmett–Teller (BET) surface area. However, pyrogenic silicas like Cabosil have no such pore structure and therefore all of the BET area should be accessible. Yet these pyrogenic silicas do not show improved activity over the normal commercial high-activity silica gel supports. This suggests that the interior of the fragments does indeed participate in the polymerization. All silicas fracture down to the point where internal pressure cannot cause further fragmentation.[176] By computing the number of primary silica particles expected in fragments of 0.01–0.1 μm, one sees that for the best silicas the fracturing probably takes place down to the point where egress is permitted, that is, where each fragment consists of only a few primary particles. Recent work with mesoporous zeolites also suggests that a certain amount of egress from pores is possible.[177,178]

10.3.2 Kinetic Profile

Once introduced into the reactor with ethylene, the Cr(VI) on the activated catalyst does not itself polymerize ethylene, but must first be reduced to a lower valent active form.[28,122,179–184] This reduction is accompanied by an expansion in the allowed coordination number from tetrahedral before reduction, to potentially octahedral afterward. The process of active-site formation includes reduction of Cr(VI) by monomer, desorption of redox products, and self-alkylation (that is, without a metal alkyl cocatalyst). The alkylation step is particularly obscure. Therefore Cr(VI)/silica normally develops polymerization activity only gradually after being introduced into the reactor at 80–100 °C. First it undergoes a dormant period or induction time, then the rate of polymerization increases during the rest of the run, or eventually it levels out. Usually the induction time lasts a few minutes, but it can also extend to an hour or more, depending on reaction conditions.[41,185]

The induction time is thought to be due in part to the slow reduction of Cr(VI) by ethylene to a lower valent species and subsequent alkylation or, perhaps, to the desorption of organic redox by-products.[29–32,35,36,186,187,265] Baker and Carrick, and later others, determined that the hexavalent species is converted cleanly to Cr(II), perhaps passing through Cr(IV), while the ethylene is converted to formaldehyde.[29,30,182,188,189] Krauss performed similar experiments, again claiming Cr(II) as the valence obtained. However, his redox by-products were slightly different from those of Baker and Carrick. Instead of formaldehyde, Krauss reported methyl ketone end groups on the first polymer chains.[190] Even when cleanly reduced to Cr(II), subsequent oxidative alkylation by ethylene probably means that polymerization occurs on a Cr(IV) or perhaps Cr(III) species. Krauss and others have also suggested that the reduction goes to or through Cr(IV).[186,188,191–198]

Thus the concentration of active sites would be expected to increase with time. Below 100 °C the induction time becomes longer until by about 60 °C there is little polymerization activity in comparison to the commercial process. Conversely, increasing the reaction temperature shortens the induction time. At 150 °C Cr(VI)/silica exhibits an immediate and constant activity in solution-phase polymerization. Likewise the induction time is also dependent on ethylene concentration. Thus vacuum line experiments on Cr(VI)/silica often have little resemblance to commercial conditions, a fact not always appreciated in the earlier literature.

One common belief about the fragmentation process is that the rising kinetic profile of Cr(VI)/silica is the result of the disintegration of the silica particle.[30,152] That fragmentation can affect activity is beyond question, but certain facts do nevertheless contradict the notion that the well-known rising profile of Cr(VI)/silica is due to fragmentation:

(1) Although disintegration occurs during the first minute or two of polymerization (first few g PE/g cat yield),[145,151] the rising kinetic profile often extends out beyond an hour.
(2) Ziegler, Ballard, or metallocene catalysts made on the same supports often display totally different kinetic profiles without a gradual rise in activity.
(3) The kinetic profile of a single Cr/silica can be widely manipulated through reaction and activation temperature, CO reduction (see Figure 10.18 later), metal alkyls, and poisons.
(4) Catalyst ash, already fragmented, can be recovered, reactivated, and tested again for polymerization activity. Its second kinetic profile is like the first.
(5) Pyrogenic silicas, which presumably do not fragment, display similar kinetic profiles.

10.3.3 Reactor Conditions

The activity of Cr/silica catalyst generally increases with reactor temperature, up to the point at which the polymer begins to swell or anneal. An example of the changing kinetic profile is shown in Figure 10.10 for a series of homo-

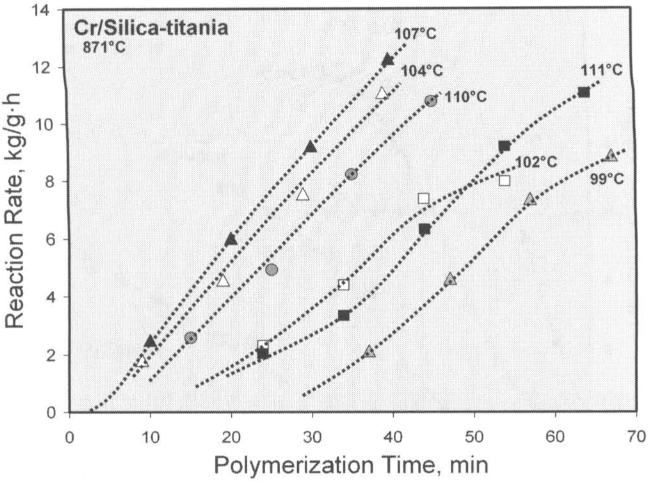

Figure 10.10 Influence of reactor temperature on activity.

polymers made at varying reactor temperatures. Induction time is usually shortened with increasing reactor temperature. In this example activity improves up to about 107 °C. Above that temperature the activity starts to decline, even though the polymer was not technically fouled. At the higher temperatures it anneals enough to retard monomer flow. The annealing temperature of the polymer is determined by the solvent (diluent) used and by the character of the polymer itself.

The polymerization activity under commercial conditions is usually considered to be near first order in ethylene.[36,41,199–202] However, the true relationship is a bit more complicated because, in addition to the insertion reaction, the observed activity is also a function of the induction time, which involves reduction and alkylation of the site. These reactions also have a strong dependence on ethylene concentration, and therefore the observed rate is often more sensitive to ethylene than first order.[201] In fact, the overall observed activity, when measured over a wider ethylene range than used commercially, can indeed exhibit a higher dependence than first order. An example of the change in kinetic profile with ethylene concentration for Cr/silica is shown in Figure 10.11. The activity develops more quickly at high ethylene concentration. While it is easy to imagine the final rate being proportional to ethylene concentration in Figure 10.11, clearly the amount of polymer made during 120 min, for example, would show a higher order.

Cr/silica catalysts run in the solution process, where the activity develops very quickly, do not show the same sensitivity to ethylene concentration. An example is shown in Figure 10.12, where ethylene concentration was varied over a very wide range, extending both above and below the typical commercial range. At lower ethylene concentration the reaction does appear to be first order. The activity varies in direct proportion to ethylene concentra-

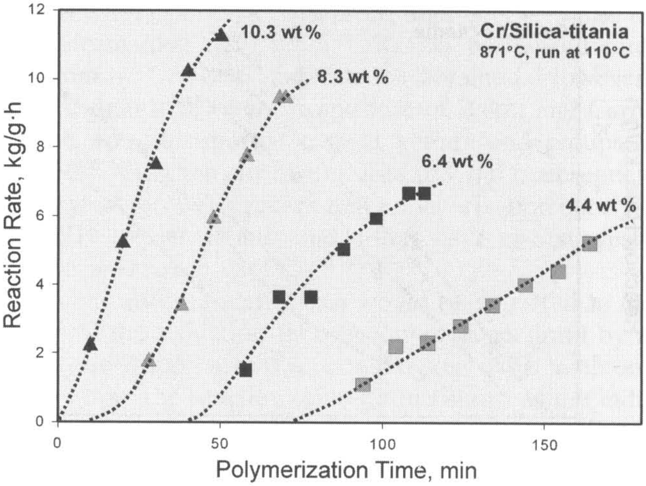

Figure 10.11 Reduction and initiation also exhibit dependence on ethylene concentration.

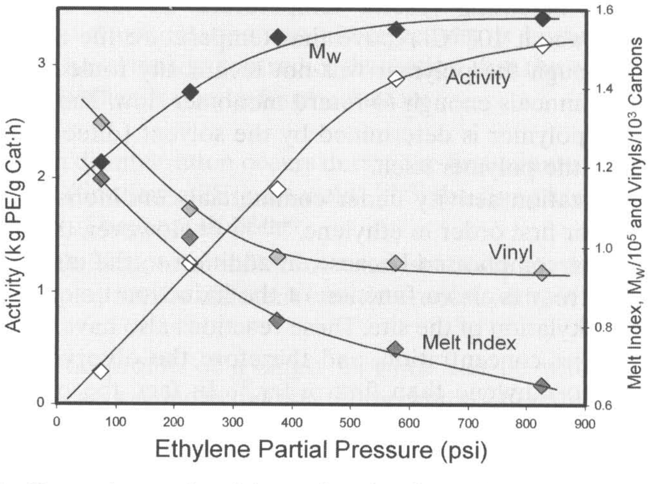

Figure 10.12 Dependence of activity and molecular weight on ethylene concentration. Cr/silica–alumina, 538 °C, reaction at 138 °C.

tion. At very high concentrations, however, the observed activity becomes less sensitive, and the curve bends over, seemingly approaching zero-order dependence. This is an indication that the polymerization may actually proceed through a Langmuir–Hinshelwood mechanism (Scheme 10.6). That is, a slow adsorption of ethylene onto the active site is followed by a fast insertion step.[7,199,201,203–205] As ethylene concentration is increased, the rate-limiting step changes from adsorption to insertion.

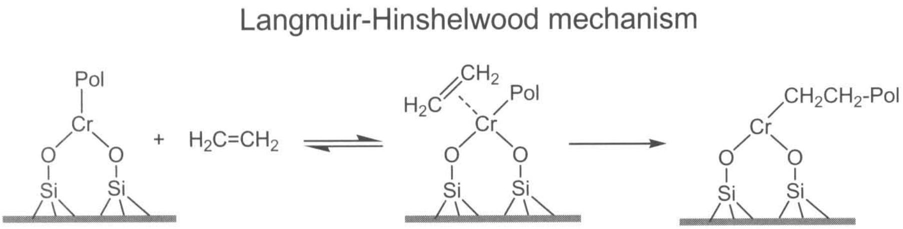

Scheme 10.6

10.3.4 Reactor Poisons

Chromium catalysts tend to be extremely sensitive to trace impurities in the ethylene or diluent feedstocks. Any oxidant or Lewis base is strongly coordinated and inhibits polymerization. Sub-ppm levels in the reactor can be enough to bring it down, corresponding to stoichiometries of less than one poison molecule per chromium. An example is shown in Figure 10.13 where three different poisons were added to the reactor in different amounts. The two most abundant and common contaminants, water and oxygen, are unfortunately also among the strongest.

Poisons retard polymerization activity in two ways. Predictably they can decrease the maximum polymerization rate achieved, probably due to the irreversible blocking of sites. However, poisons can also inhibit the creation of active sites, and this avenue is usually the most damaging. Small amounts of poisons usually slow down the initiation reactions, thus lengthening the induction period, and this has a much more profound effect on the average observed activity in a commercial reactor. An example is shown in Figure

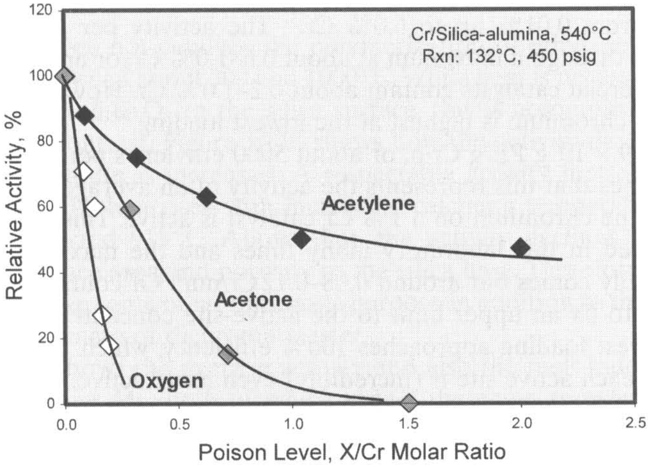

Figure 10.13 Poisoning by various compounds.

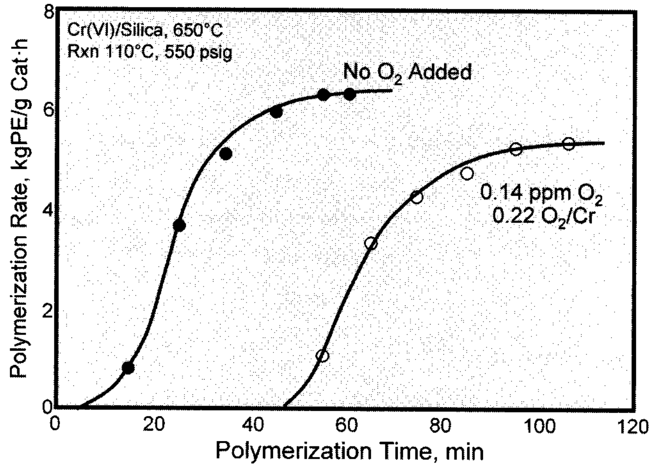

Figure 10.14 Poisoning of Cr/(VI)/silica by oxygen.

10.14 where a trace of oxygen was added to the reactor with a Cr/silica–titania catalyst.[206] One can see the lengthening induction time, even though the final rate is less affected. Therefore commercial operations always require a high degree of feedstock purification.

10.3.5 Cr Loading

Naturally the catalyst activity is influenced by the Cr loading on the catalyst, and this variable is used commercially to control activity. One might suppose that highest activity would always be preferred, but in some cases it is desirable to lower the activity to avoid fouling, such as in gas-phase polymerization. Figure 10.15 shows the result of varying the Cr loading using commercial conditions from 0.01% up to 6.0% Cr.[31] The activity per gram of catalyst usually goes through a maximum at about 0.6–1.0% Cr, or around 0.4 Cr/nm^2. Most commercial catalysts contain about 0.2–1.0% Cr. However, the activity per gram of chromium is highest at the lowest loading.[30,183,207] At 0.01% Cr, it approaches 9 × 10^6 g PE/g Cr·h, or about 5000 ethylenes per Cr per second.* If one assumes that this represents the activity of an average site, then about 10–25% of the chromium on a 1% Cr catalyst is active. This experiment has been repeated in this laboratory many times and the maximum active-site density usually comes out around 0.08–0.12 Cr/nm^2. Of course, this approach serves only to fix an upper limit to the active-site concentration. It assumes that the lowest loading approaches 100% efficiency, which may not be true. If not, then each active site is (incredibly) even more active.

The reason for the behavior in Figure 10.15 is not clear, although a few comments can be made. First, the leveling of catalyst activity with increased

---

*This activity clearly rivals metallocene catalysts.

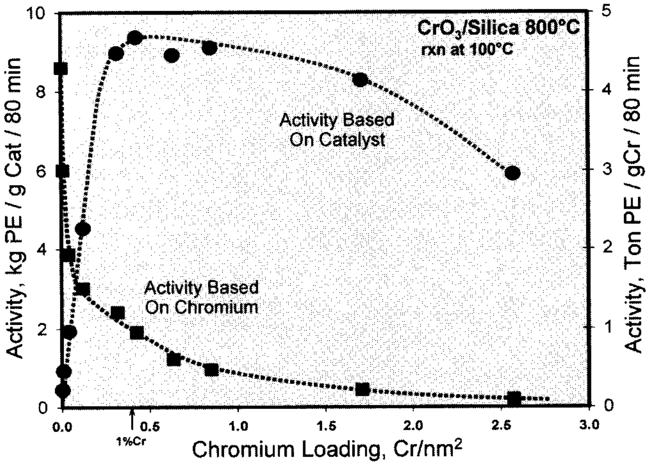

Figure 10.15 Activity versus Cr loading for Cr/silica.

loading is not due to some diffusional barrier being reached, because activity can still be improved by increasing activation temperature, adding cocatalyst, or CO reducing the catalyst, to name a few possibilities. Instead, the behavior above, which is fairly common in catalysis reactions in general, is usually explained in one of the following ways: (1) Only the first sites occupied on the silica are capable of activating Cr (or the first are more active than those occupied later), perhaps because of special surface geometry (2) Chromium centers with close neighbors tend to become deactivated through their mutual interaction.

10.3.6 Activation Temperature

CrO_3 on silica does not catalyze the polymerization of ethylene until it has been calcined between about 300 and 1000 °C. While heat is necessary to cause the esterification of CrO_3 to the silica surface, this is accomplished at 150–350 °C.[51,53,114] In contrast, Figure 10.16 shows how the activity develops as the calcining temperature is increased. A respectable activity first appears only at about 500 °C. It then rises with increasing calcining temperature up to a maximum at around 925 °C. Above that, the activity declines as sintering destroys the surface area and porosity of the silica base. Therefore the calcining step must serve some other necessary purpose in addition to the formation of a surface chromate or dichromate ester.

Figure 10.17 shows the average activity and also the melt index (MI) and the weight average M_W, both of which reflect the chain transfer rate. They indicate that MW decreases with increasing activation temperature up to the point of sintering. No obvious chemical changes occur during this temperature range. All of the chromium remains hexavalent and no major changes are

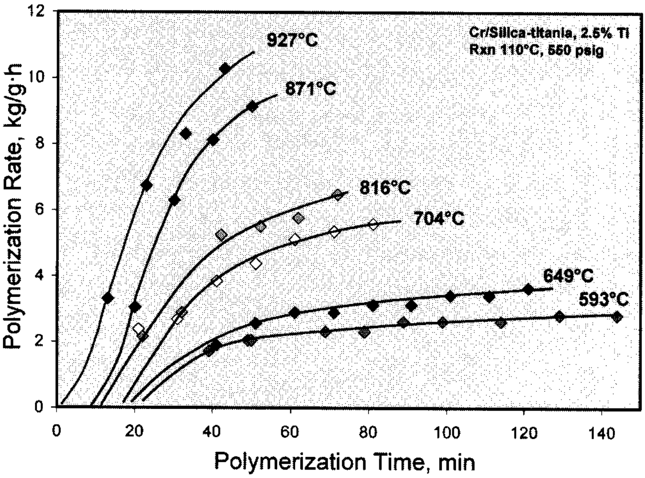

Figure 10.16 Influence of activation temperature on development of activity.

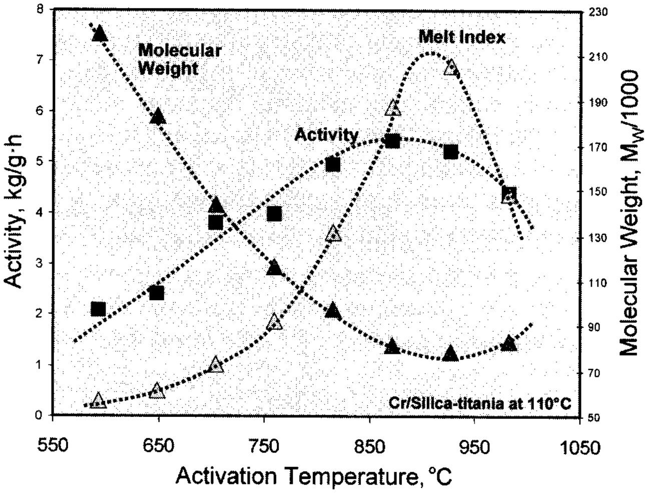

Figure 10.17 Influence of activation temperature on activity and MW.

observed in the crystallinity or porosity of the support, just a gradual dehydration of the silica surface as hydroxyl groups condense to release water.

As the calcining temperature is raised, Cr(VI)/silica changes from yellow to a deeper orange color. This may reflect increased dehydration or even the formation of some dichromate[118] that might also contribute to site diversity. On exposure to moisture in the atmosphere the orange catalyst immediately reverts back to yellow and loses its polymerization activity. A second calcining step then restores the activity and the orange color.

At least two reasons have been proposed to explain the strong effect of activation temperature. One suggests that dehydroxylation creates active sites because neighboring surface hydroxyl groups coordinate to the Cr active center and thereby interfere with polymerization. The other possibility is that dehydroxylation merely accompanies an annealing of the surface that perhaps changes the bonding of the Cr and introduces strain into the Si–O–Cr–O–Si bonds, making the Cr more electron deficient and thus more reactive.[127,220] There is considerable evidence for the former and also some for the latter.

For example, Krauss has shown that the degree of coordinative unsaturation of Cr(II)/silica, as measured by chemisorption of various ligands, chemiluminescense, and other techniques, follows a similar dependence on activation temperature.[41,51,81,111,120,208–214] Likewise, the Turin group has found spectroscopic evidence for different types of sites which differ in their coordination number (CN) with surface groups.[208–212,215,216] One type of site, having CN of only 2, was identified as a site from which polymerization is initiated. Evidence from Fourier transform IR (FTIR) also suggests that coordination to silanols is possible.[216] Thus it seems likely that as the silica support becomes increasingly dehydroxylated at higher temperatures, more Cr sites become exposed.

On the other hand recent studies with X-ray photoelectron spectroscopy (XPS), XANES, and EXAFS indicate that the surface Cr(VI) becomes increasingly electron deficient with increasing calcining temperature.[53,218,219] This was attributed to a change in the Si–O–Cr–O–Si bond angle, perhaps analogous to tight bridging in metallocenes. And there is other evidence that the geometry of binding could indeed determine subtle aspects of the site's chemistry.[220,221] However, it should also be noted that the catalytic activity and the effects of activation temperature are not limited to just silicas. For example, active catalysts can be made from amorphous aluminophosphates, γ-alumina, stoichiometric $AlPO_4$, and zeolites.[168,169,178,223–225] It is unclear whether these other supports, some of which are crystalline, would undergo a similar kind of annealing as amorphous silica.

10.3.7 Reduction in CO

One commercial method of increasing the activity of the catalyst is to reduce the Cr(VI) before the catalyst is contacted with ethylene. Krauss and Stach[226–228] demonstrated that the hexavalent catalyst can be quantitatively reduced by CO at 350 °C to divalent chromium (Scheme 10.7).* The resulting CO_2 by-product is removed at 350 °C by the CO activation gas, and while still at 350 °C the carbon monoxide is then also removed. Titration by pulses of

*Although not published externally, Phillips research reports from as early as 1959 and 1962 indicate that Hogan and co-workers had already discovered that CO reduction yields an active catalyst of valence Cr(II).

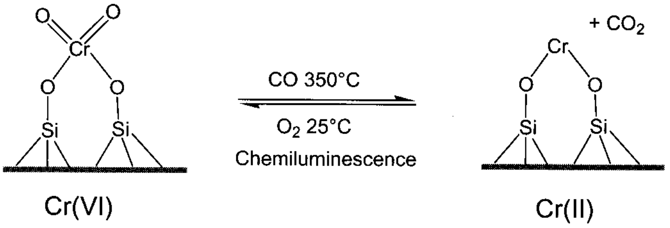

Reduction of Cr(VI) to Cr(II) by Carbon Monoxide

Scheme 10.7

CO or measurement of evolved CO_2 indicated near-quantitative conversion to Cr(II). The surface-bound Cr(II) species is left highly coordinatively unsaturated and exhibits some unusual chemistry.[41,99,190–192,208,209,211–214,229–249] The Turin group has recently published an excellent review of its reactions.[79] The reduced catalyst has a light green color but quickly turns blue when exposed to N_2, indicating a weak 2:1 chemisorption.[229,246] CO is adsorbed to yield a violet color. Olefins are reported to adsorb in a 2:1 ratio, and acetylene is converted cleanly to benzene.[226,227,250,251] Polar compounds like alcohols, ethers, or amines are strongly held. Oxygen is instantly adsorbed, converting the divalent chromium back to its original orange hexavalent state with a brilliant flash of chemiluminescense.[29–31,42,111,191,192,213,214,229–238] The light emitted has a wavelength centered around 650 nm, characteristic of oxygen.[252] The ease of this reversal suggests that there is little rearrangement during reduction at 350 °C or during reoxidation. Ligands, such as olefins, can interfere with the reoxidation.

The divalent catalyst is quite active for olefin polymerization, which indicates that Cr(II) is definitely an active precursor. The quantitative reduction to Cr(II) has since been confirmed by many other laboratories, including this one.[35,41,46,122,184,193,208,209,211,212,253–259] Such divalent catalysts can initiate polymerization at much lower temperatures, such as 25 °C or lower.[34] They polymerize ethylene under commercial conditions much like their hexavalent parents, producing very similar polymer, except that the induction time is eliminated, giving overall higher activity. An example is shown in Figure 10.18. Subsequent oxidative alkylation of Cr(II) to Cr(IV) by olefin during the initiation of polymerization, along the lines suggested by Scott and many others, is a reasonable hypothesis from our present state of knowledge.[41,192,194–197,260–266] This probably explains why the kinetic profile of Cr(II)/silica still rises with time.

The use of reducing agents other than CO did not reduce the chromium as cleanly to Cr(II). Hydrogen was tried along with various hydrocarbons and NH_3 at 200–500 °C.[29–31,35,226–228,267–270] Usually the resulting catalyst was green and did not have the reactivity of CO-reduced samples, and the measured oxidation number never went entirely to 2.0. This is probably because water

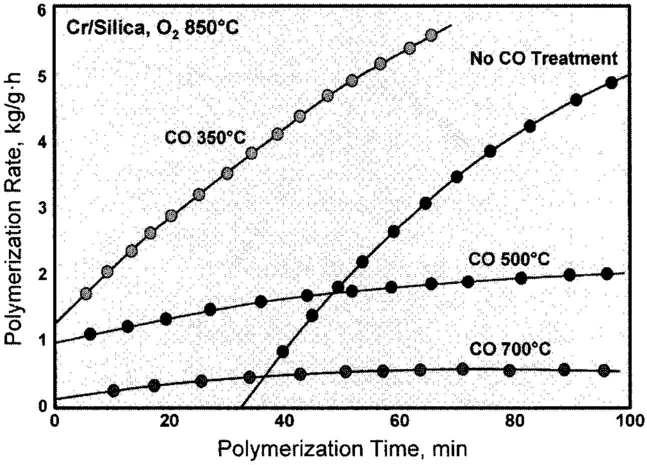

Figure 10.18 Ethylene polymerization kinetics over Cr/silica: (*a*) calcined in air at 850 °C, (*b*) then reduced in CO at 350 °C, (*c*) at 500 °C, and (*d*) at 700 °C.

is a by-product from these other reducing agents. Water destabilizes Cr(VI) and can oxidize Cr(II) to Cr(III).

During reduction in CO, temperatures higher than 350 °C or vacuum treatment of the Cr(II)/silica often causes a deactivation (rearrangement) even though no further reduction is observed.[42,51,122,203,230,231] This is shown in Figure 10.18. When the catalyst has been reduced in CO at 800–900 °C, the subsequent reoxidation at 25 °C to Cr(VI) can be less complete, sometimes also yielding Cr(III). The result of this rearrangement by high-temperature reduction in CO is decreased coordinative unsaturation. This phenomenon might represent a clustering of the chromium, although no CrO crystallites have been detected by X-ray diffraction.[231] The chromium may also find a better position on the surface so that it can coordinate with more oxide or hydroxyl ligands.[51,211]

Hogan has observed that catalysts activated at lower temperatures are more likely to display this thermal instability after reduction.[271] An example of this behavior is shown in Figure 10.19. Cr/silica–titania was calcined in air at either 540 or 760 °C, then reduced in CO at increasingly severe conditions. The initial reduction at 316 °C increased the activity. More severe reduction greatly diminished the activity of the catalyst calcined at 540 °C but had no effect on the one calcined at 760 °C. Hogan attributed this result to oxidation of Cr(II) by silanol groups.

Krauss and others detected several types of Cr(II) species after reduction in CO which differ in their reactivities.[111,237,238,271] He noted that hydroxyls on the silica can interfere with the reduction to Cr(II) and diminish the "quality" (i.e., the coordinative unsaturation) of the resultant catalyst.[90,213,231–233] The Turin group has studied the coordination chemistry of Cr(II)/silica catalysts most extensively over a number of years. Using spectroscopy with a number

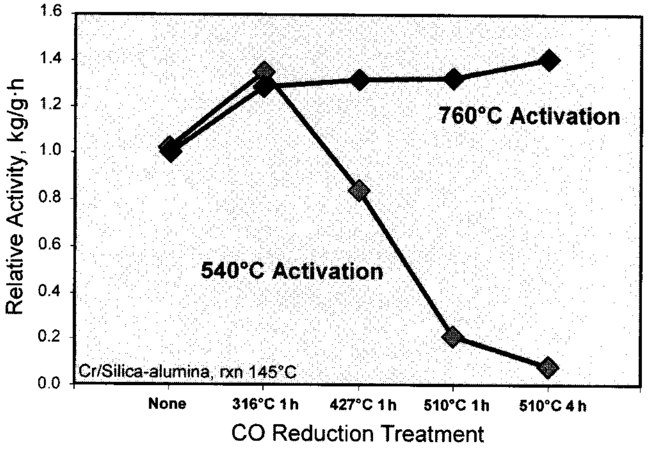

Figure 10.19 Effect of reduction severity on activity of two catalysts.

of probe molecules,[51,208,209,211,212,254,273] their preferred "best catalyst" corresponded well to commercial experience from this laboratory. They chose a 0.5% Cr catalyst calcined at 750 °C and reduced at 350 °C. On this catalyst they identified three major types of Cr(II) species, designated Cr_A, Cr_B, and Cr_C, the latter being later subdivided into Cr_{C1} and Cr_{C2}. These species differed in their coordinative unsaturation. Cr_A sites, which were found to be most unsaturated, were said to be coordinated to only two surface oxide ligands, Cr_B to three, and Cr_C to four. Thus from their behavior, Cr_A and Cr_B ions were thought to be active while Cr_C ions were "shielded" and thus inactive.

Cr_A sites, the most numerous of the three on this preparation, were identified as the most reactive species and thought to comprise the sites active in ethylene polymerization, while Cr_C ions were found to be inactive. Cr_B sites were also thought to exhibit polymerization activity, but distinctions were made. The concentration of these surface species could be varied with the Cr content and with the conditions of the thermal pretreatments.[274] Heating the Cr(II) catalyst under vacuum at 700 °C, which causes a deactivation for ethylene polymerization, was found to convert Cr_A into Cr_C while Cr_B remained unaffected.

10.3.8 Cocatalysts

Another way of eliminating the induction time, and thus increasing the average activity, is to add a cocatalyst to the reactor. Reducing agents like the alkyls or hydrides of aluminum, boron, zinc, lithium, and magnesium eliminate the induction time of Cr(VI)/silica. These reducing "cocatalysts" may contain other groups as well, such as alkoxides or halides. For example, diethyl aluminum ethoxide is a common cocatalyst used since the 1960s. These compounds usually significantly increase the activity of Cr(VI)/silica through several possible mechanisms: (1) They can act as scavengers, removing minute amounts of poisons from the reactor, such as oxygen and moisture, and possibly including redox by-products generated from the catalyst itself during its reduction by ethylene. (2) They can reduce Cr(VI) to lower valent species, thus accelerating the onset of activity. (3) In some cases, they may even be able to act as alkylating agents, again accelerating the development of polymerization activity or changing the polymer produced. (4) They can become a part of, and thus transform, the site itself.

Krauss and others have postulated that, when a cocatalyst functions as a reducing agent for Cr(VI), the extent of reduction can vary and the valence can go though a Cr(IV) intermediate to ultimately Cr(II). It was suggested that the result can vary with the type and level of cocatalyst and also the exposure to olefins.[195–197,275] This picture agrees with behavior noted in this laboratory and in commercial operations. Under certain conditions activity could conceivably develop without going through Cr(II), such as shown in Scheme 10.8.

In commercial operations the cocatalyst can be contacted with the catalyst in several ways. One method is to impregnate a metal alkyl directly onto the silica-supported catalyst and then (usually) dry it for subsequent introduction into the reactor. Both Cr(VI) oxide catalysts and triphenylsilyl chromate catalysts can be reduced in this way. Curiously they both produce very similar catalysts after reduction with diethylaluminum ethoxide. In slurry polymerization the metal can also be added to the reactor as an independent feed stream. Cocatalysts are usually added as 0.5–5 ppm of the diluent, although somewhat greater concentrations, even up to 10 ppm, can be used occasionally. This range usually corresponds to a cocatalyst/Cr mole ratio of close to unity or less. Much larger amounts can sometimes diminish activity or even kill the catalyst. This may indicate an attack on the Cr–O–Si anchoring bonds. In some commercial operations a "precontacting vessel" is used in which the catalyst is exposed directly to the cocatalyst in a concentrated slurry before being added to the reactor. This precontacting step may last from a minute up to an hour, and it generally exaggerates the effect of the cocatalyst by permitting greater reaction concentrations and longer reaction times. Furthermore, if the catalyst contacts cocatalyst before contact with monomer, the cocatalyst sometimes has a more pronounced effect, indicating that the olefin can have a protective effect.[270,276]

Cocatalysts change the kinetic profile of Cr(VI)/silica by shortening or eliminating the induction time.[41,277–280] Thus activity develops much more

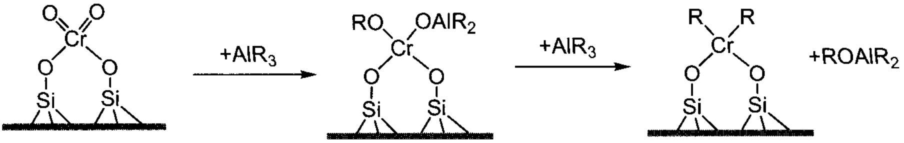

Scheme 10.8

rapidly, often rivaling some of the better organochromium catalysts, which are already reduced and alkylated. The maximum attainable rate may also be increased, suggesting that some sites are activated that would not otherwise become active. Although cocatalysts usually promote the activity of any Cr(VI) catalyst, they are most effective on those catalysts activated at low temperatures. This is shown in Figure 10.20, where Cr/silica–titania was activated in air at various temperatures and then tested with and without 10 ppm of triethylboron cocatalyst in the reactor. The activities are plotted against activation temperature. BEt_3 enhanced the activity of all catalysts, regardless of the activation temperature. However, on closer inspection one can see that the low-temperature samples are enhanced proportionally more. This is shown by the other line in Figure 10.20, which represents the ratio of the activity with BEt_3 to the activity without BEt_3. This ratio shows that the benefit of the cocatalyst on activity decreased as the activation temperature was raised. This is consistent with a more diverse population of sites at the lower activation temperature, some more difficult to reduce.[206,276]

The activity is usually improved most when the stoichiometry (cocatalyst/Cr) is low, around unity. At very high levels of cocatalyst the activity is actually depressed. An example is shown in Figure 10.21 where triethylboron is again added to the reactor with the catalyst. Activity increases with stoichiometry up to around B/Cr = 2, and then it begins to decline. By a stoichiometry of B/Cr = 10 the catalyst is actually *less* active than it was without cocatalyst. This is usually interpreted as evidence that the cocatalyst begins to attack Si–O–Cr linkages or coordinate to the active site.

The alkyls of boron are considered to be mild reducing agents. The alkyls of aluminum are stronger. Figure 10.22 shows a similar plot but the cocatalyst used was triethylaluminum. Again the activity went through a maximum, this time at a stoichiometry near unity. The chart covers a wider range of stoichi-

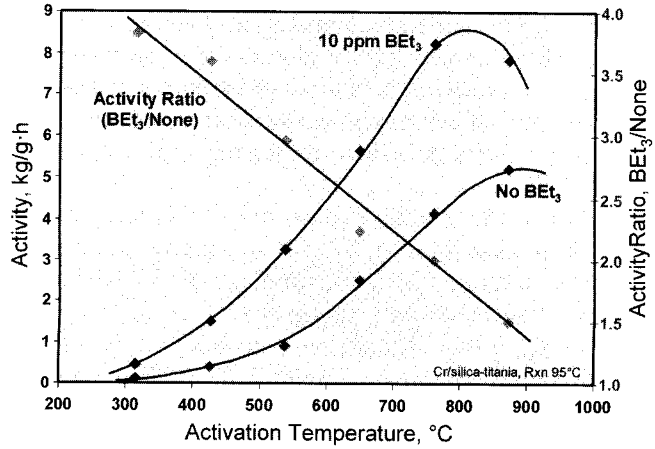

Figure 10.20 Cr/Silica–titania calcined at various temperatures and tested with and without triethylborane cocatalyst.

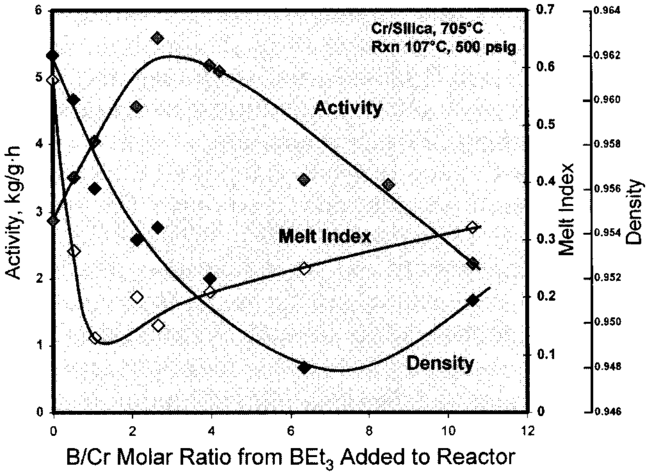

Figure 10.21 Influence of triethylboron cocatalyst.

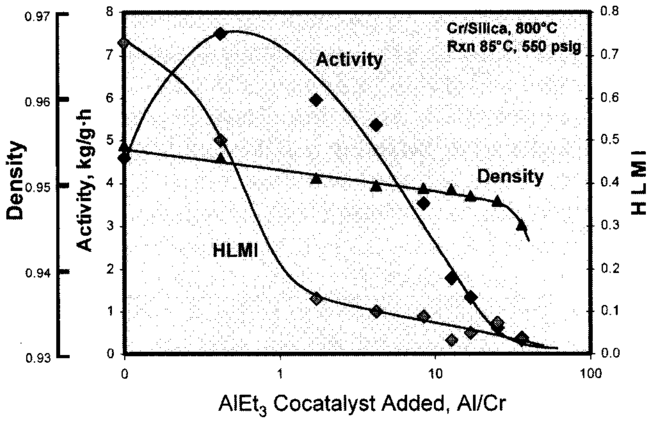

Figure 10.22 Influence of triethylaluminum cocatalyst.

ometry than Figure 10.21 and clearly shows the loss of nearly all activity at high Al/Cr ratios. By Cr/Al = 7 the activity is less than obtained without cocatalyst. By a stoichiometry of Cr/Al = 35, the activity was almost gone. Again this may indicate that when an excess of cocatalyst is added the connecting bonds with the surface Cr–O–Si may be vulnerable to attack. Coordination of the cocatalyst with the reduced Cr has also been suggested as a possible reason for the loss in activity.

10.3.9 Promotion by Titania

The Phillips chromium-based catalyst is extremely sensitive to minor changes in the silica preparation or calcining history. The active sites no doubt respond to the local electronic and structural environment. Creating higher acidity on the support often increases the activity of the catalyst. This may happen because Cr(VI) attaches to Brönsted sites, which then decrease the electron density on the Cr. This may either increase the activity of sites or generate sites that would not otherwise become active.

Adding titania to a Cr/silica recipe is one powerful method of modifying the catalyst's performance and the resins it produces. The presence of titania in small amounts on Cr/silica catalysts has a strong promotional effect on chromium, for both the activity and the termination rate.[41,199,281–291] Adding titania to a silica surface is known to increase its Brönsted acidity, and it is possible that Cr binds to these acidic sites, which render the Cr more electron deficient.[292,293] In fact, some of the behavior modification that accompanies addition of titania is shared with other acidic supports as well. This would agree with recent XPS reports that titania, like calcination, increases the electron deficiency on the chromium.[294] The presence of titania may also influence the chromate–dichromate distribution.[63,87] Whether titania causes an increased site population, as seems likely, or just increases the activity of each site is not known.

Figure 10.23 demonstrates the promotional effect of titania on the activity of Cr/silica catalysts. These samples were made by coprecipitation. The chromium was then added and each sample was calcined at 760 °C to form surface-attached Cr(VI). Figure 10.23 shows that titania increases the activity of the catalyst, first by shortening the induction time and then by allowing higher polymerization rates. The shortened induction time suggests that titania makes Cr(VI) more easily reducible because the lower valent active sites come to life

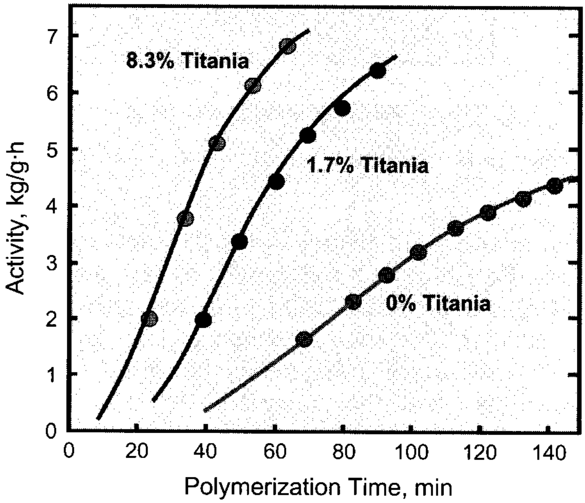

Figure 10.23 Increase in polymerization rate when titania is added to Cr/silica catalyst.

more quickly. This coincides with other evidence that Cr(VI) may be less stable when attached to titania.[89,95,281] In addition temperature programmed reduction (TPR) experiments by Marsden indicate that titania addition creates a second, more easily reducible species.[167] The higher maximum rate may indicate an increase in the active-site population, although this is not certain.

10.3.10 Promotion by Other Additives

In addition to modification by titania, several other additives are known to enhance the activity of chromium catalysts. Again this is a direct consequence of the fact that the chromium is directly attached to the support and derives a considerable amount of its "character" from those support-derived ligands. Fluoride is one such agent. Some PE applications require very high molecular weight polymer. To make these grades commercially catalysts must be activated at low temperatures, 400–600 °C, which can also result in low activity. One solution is to impregnate the catalyst with an ammonium fluoride salt such as NH_4F, NH_4HF_2, NH_4BF_4, $(NH_4)_2SiF_6$, and NH_4PF_6.[41,119,288,295–297] During the calcining step the salt, which is typically loaded at 1–5% of the catalyst, decomposes and thereby imparts a surface fluoride treatment in which silanols, and perhaps even some siloxanes, are replaced by F. This can greatly increase activity, presumably by removing ligands from the Cr coordination sphere or even by adding an inductive electron-withdrawing effect through F–Si–O–Cr attachments. It has been recently reported that fluoride, like titania, decreases the electron density on the chromium.[294] But apart from increased activity, fluoride does not behave like titania. The ammonium salt need not be impregnated onto the catalyst. It can also be dry mixed. During calcining it decomposes into HF or other fluoride vapors which can then react with the catalyst. Alternatively, a fluoride-containing gas such as HF and F_2 or a fluorocarbon vapor can be added in the appropriate amount to the activation gas during calcining. An example of the increase in activity brought about by fluoride addition is shown in Figure 10.24.

Fluoriding profoundly accelerates sintering. This is demonstrated in Figure 10.25 by the major surface area collapse obtained when Cr/silica was exposed to a combination of fluoride and high temperature. Fluoride acts as a flux at high temperature, accelerating the annealing process. Thus, when fluorided, Cr/silica should not be calcined at very high temperatures, typically not above 600 °C. Otherwise catalyst porosity is likely to be destroyed. The interaction between temperature and fluoride content is also evident in Figure 10.24. However, the promotion of sintering by fluoride is much less pronounced on Cr/silica–titania or Cr/silica-alumina, suggesting that the titania or alumina strongly adsorbs the fluoride as Ti–F or Al–F and renders it less destructive on the silica matrix.

Cr/alumina is only weakly active for ethylene polymerization, perhaps reflecting its lower Brönsted acidity. However, adding acidic anions like fluoride or sulfate to Cr/alumina boosts the activity by as much as 10-fold.[298,299]

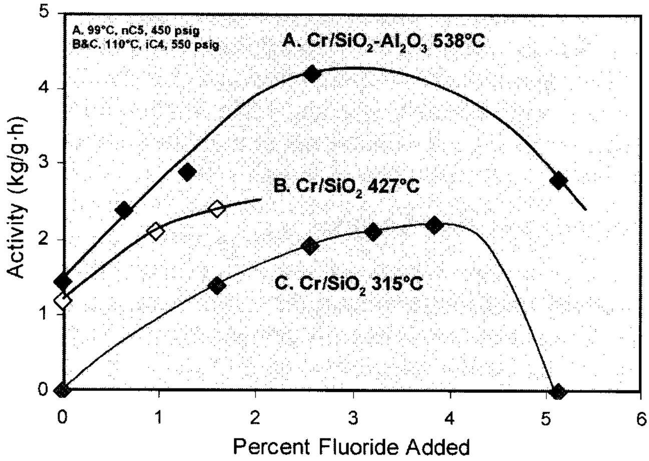

Figure 10.24 Effect of fluoride on activity of Phillips catalysts.

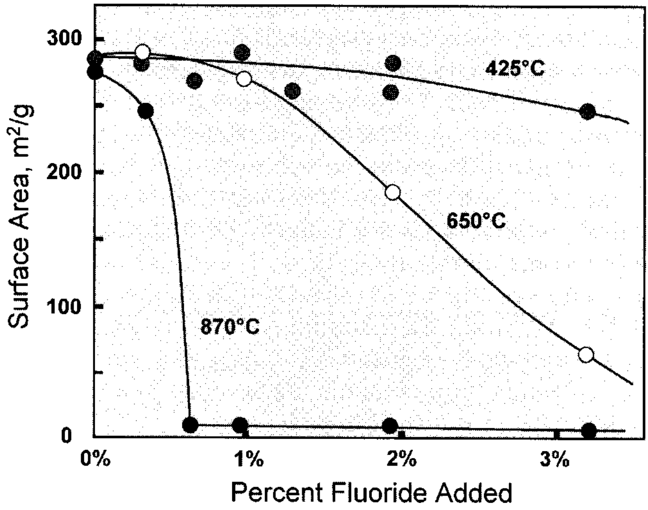

Figure 10.25 Influence of fluoride on Cr/silica sintering.

The effect of both fluoride and sulfate on alumina may be due to formation of stronger Brönsted sites on which the Cr attaches. As with silica, a fluoride salt such as NH_4F can be impregnated onto Cr/alumina, which reacts with the surface or releases HF during calcining that reacts with the surface. Alternatively, unusual aluminum oxy-fluoride supports (AlO_xF_y) of high fluoride content can also be cogelled having high surface area.[300–303] An example of fluoride promoting activity is shown in Figure 10.26 where both activity and surface area are plotted against the amount of fluoride impregnated onto a highly porous γ-alumina. Fluoride is effective at low activation temperatures

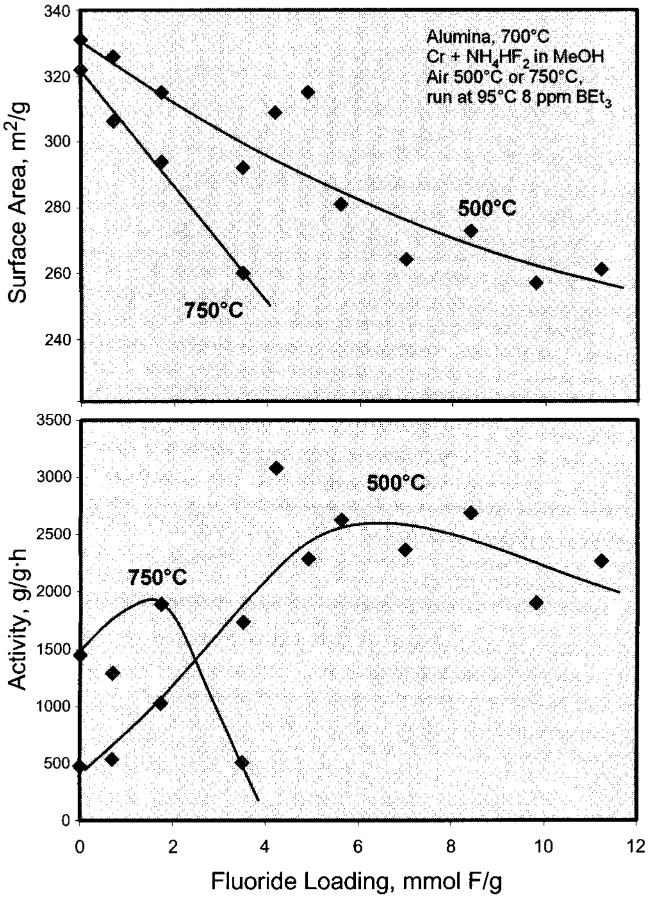

Figure 10.26 Effect of fluoride on Cr/alumina.

but accelerates sintering at higher temperatures. However, calcining the alumina at 600 °C, which converts it from bohemite (AlOOH) to γ-alumina, before treating it with fluoride, improves its resistance to sintering by fluoride later. At 500–600 °C activation temperature, it is often possible to add up to 10% fluoride without damage to the porosity or activity, many times more than silica can adsorb.

Another useful acidic treatment is the addition of sulfate to Cr/alumina. As with fluoride, it increases activity, sometimes by almost an order of magnitude.[299] Figure 10.27 shows an example of sulfate treatment increasing activity. Ammonium sulfate, aluminum sulfate, or sulfuric acid can be easily impregnated aqueously onto the alumina. Ammonia is driven off during the calcining, but sulfate survives the 600 °C calcining, at least up to a loading of about 2–3 mmol SO_4/g Al_2O_3, for materials having a surface area of 300–400 m^2/g. In this example activity goes through a maximum at about 1.5 mmol SO_4/g. The

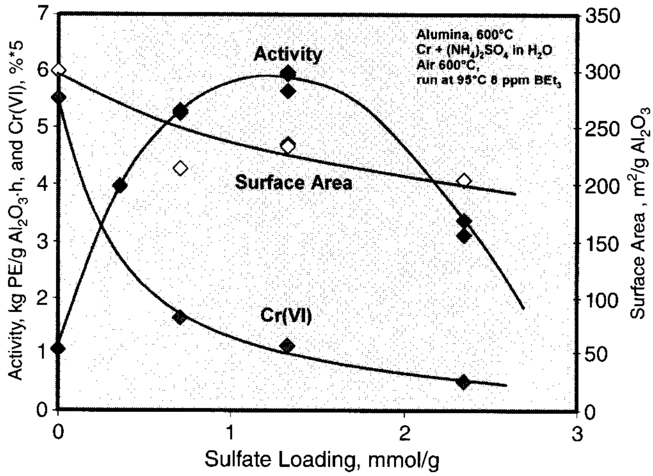

Figure 10.27 Effect of sulfate loading on activity and surface area of Cr/alumina catalyst.

TABLE 10.2 Increase in Cr/Alumina Activity by Adding Brönsted-Enhancing Oxides

Additive to Cr/alumina (then 600 °C)	Activity (g/g·h)
None	1200
1.5 mmol/g SO_4	3600
1 mmol/g H_3BO_3	4150
1 mmol/g H_3PO_4	3800
10% SiO_2	2820

decrease in activity at higher sulfate loadings is not due to sintering because the surface area is not affected greatly by the sulfate. Instead the amount of chromium stabilized as Cr(VI) during activation is greatly diminished by sulfate, starting at about 1.2% Cr(VI) without sulfate and ending at about 0.1% Cr(VI) at a loading of 2.3 mmol SO_4/g Al_2O_3. This suggests that at higher loadings sulfate may displace Cr(VI) from the surface, resulting in lower activity. Again, if the alumina hydrate is first calcined at 600 °C to convert it into γ-alumina before treatment with the sulfate, the surface area and porosity are not seriously harmed by the sulfate, although sulfate does contribute additional mass to the final catalyst.

Cr/alumina can also be modified by a small amount of silica applied as a surface layer.[304] Treating the alumina with an organic silicate, yielding 5–10% SiO_2 after calcining, will result in a substantial improvement in activity, perhaps up to fourfold. Again this is attributed to a strong increase in Brönsted acidity, which decreases electron density on the attached Cr. Adding other tetrahedral oxides, like phosphate or boria, which are also known to greatly enhance Brönsted acidity on alumina, likewise produces a large boost in activity for Cr/alumina, but not to Cr/silica. Table 10.2 compares these activity results.

10.4 CONTROL OF MOLECULAR WEIGHT AND MW DISTRIBUTION

10.4.1 Site Initiation and Chain Formation

The chain growth that follows initiation is most often thought to proceed through the classical Cossee mechanism, in which coordinated monomer inserts into an alkyl group.[29–31,221,305–307] Termination of the chain, or chain transfer, then follows and is usually thought to proceed through elimination of an agostic β-hydride to yield a vinyl end group. A new chain then begins the cycle again on the same site with a methyl end group, and the process repeats, so that each chain has a vinyl on one end and a methyl on the other.[31,308,309] The molecular weight of the polymer is determined by the rate of chain growth relative to the rate of chain termination or transfer, each of which can have a dependence on ethylene concentration if ethylene is involved in the step.

Unlike Ziegler, Ballard, or metallocene catalysts, chromium somehow "self-alkylates" upon exposure to ethylene. Although the starting valence of the catalyst may be Cr(II), the initiation step could involve a formal oxidation by ethylene[41,122,191,192,195–197,236,265,310–317] possibly to Cr(IV).[41,122,191,192,195–197,200,236,265,266,313,317–319] The first chain on a site is formed much more slowly than later chains. Even a bare Cr(II) site formed by CO reduction is slow to form the first chain, and it may take 20 min on most sites.

And yet those same sites then produce an average of about seven chains per second during the rest of the 1-h run (~5000 ethylene molecules per site per second, assuming 10% of Cr is active and $M_n = 20{,}000$). Thus the initiation of a site must not be confused with normal chain transfer, and the termination of a typical chain does not leave the site in the original state.

One puzzle associated with the initiation step on Phillips and other non-alkylated catalysts is the problem of the missing hydrogen. The growing polymer chain is usually considered to be a linear alkyl, that is $Cr–(CH_2)_n–CH_3$, thus containing one more hydrogen than the equivalent number of ethylene molecules from which it was formed. The extra H is assumed to have come from the previous chain, which ended in vinyl. Unfortunately this does not explain from where the first chain obtained its hydrogen. The many possibilities that have been proposed to address this H deficiency can be classified into four generic cases:

1. *Two Bonds to Cr* It has been suggested that all polymer chains grow in such a way that it contains two, not one, attachments to the active Cr complex. The simplest example is polymer growing in a loop,[244,317] with both ends connected to the Cr center (or pair of Cr ions) as shown in Scheme 10.9. Termination removes H from one end, supplying it to the other. Unfortunately this idea makes no distinction between the first and later chains, or between initiation of the site and of each chain.

Another variation is the Green–Rooney mechanism. Many have found evidence for carbene species on chromium polymerization

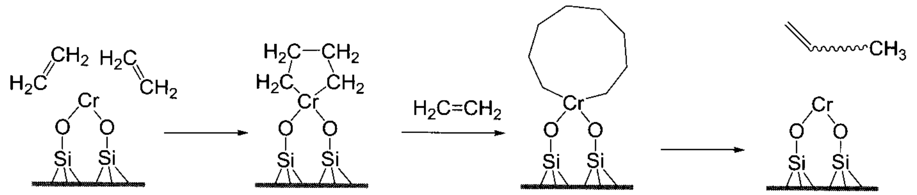

Scheme 10.9

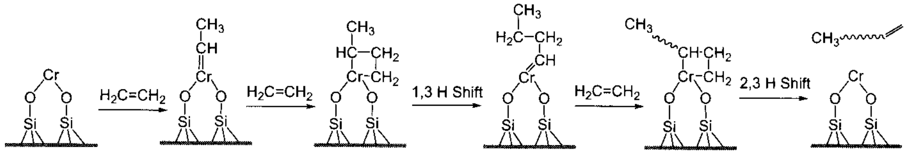

Scheme 10.10

catalysts,[191,192,194,196,200,236,260–265,319–321] prompting suggestions that alkylidenes are involved in the propagation step.[191,192,195–197,200,236,265,310,313] The usual expression of this idea is the Green–Rooney mechanism in which ethylene inserts to form chromacyclobutane (Scheme 10.10). A 1,3 hydride shift then restores the original alkylidene species only one unit longer. Presumably termination must occur through a 2,3 hydrogen shift.

Again this makes no distinction between the first and later chains. In addition the Green–Rooney mechanism requires hydrogen scrambling as ethylene is polymerized, due to the 1,3 H shift. Polymers made in this laboratory using mixtures of normal and deuterated ethylene failed to exhibit any scrambling.[322] Recent kinetic studies are also inconsistent with Green–Rooney.[260,262–264] The Turin group has suggested other ways of alkylidene participation without scrambling. However, these do not address the missing H problem.[317] It is important to remember that the existence of alkylidene species does not necessarily imply that they are involved in the polymerization. They may be only resting states, or necessary for initiation only, or unrelated side reactions.

2. *From Silanol* Some researchers have proposed that the first hydrogen atom is contributed by the silica surface.[70–74,217,272,323–328] However, this goes against the general trend of growing activity with dehydroxylation. In fact, completely dehydroxylated catalysts made in this laboratory (by reaction at 400 °C with $TiCl_4$, $AlCl_3$, $SiCl_4$, $ZrCl_4$, $SnCl_4$, etc.) have displayed high activity. Attempts to find deuterium exchange with the support have yielded contradictory results.[70–74,313]

3. *First Chain Different* Another possibility is that the first chain is different from succeeding ones and has less than the usual H/C ratio of 2.[29,41] The initial formation of chromacycloalkane has been proposed, either through a conventional pathway or from an alkylidene.[41,63,191,192,195–197,212,228,236,265,310,313,329]

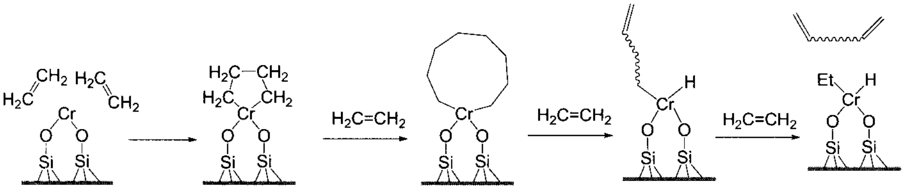

Scheme 10.11

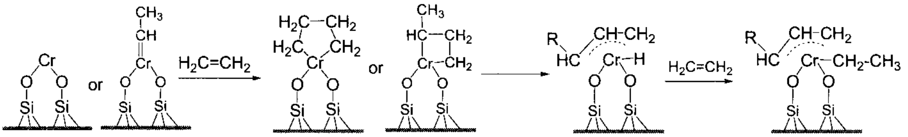

Scheme 10.12

Most recently the Turin group has actually found spectroscopic evidence for the formation of chromacycloalkane.[314] From there, the first chain could contain a vinyl on both ends, as shown in Scheme 10.11, for example. Further reaction of the chromium hydride with the silica surface is also possible for example to yield Si–H and a third Si-O–Cr link.

4. *From Ligand* Still another possibility is that the first product species formed is a ligand, such as allyl, which donates the hydrogen.[41] An example is shown in Scheme 10.12. Chain growth could proceed from the hydride as shown, or from the allyl group by rearrangement into its mono-hapto form. This latter pathway would be a variant of option 3 above, since the first chain would have two unsaturated groups. Again the chromium hydride could further react with the surface, perhaps to Si–H.[331]

5. *Vinyl First* It has also sometimes been proposed that chain growth starts with the vinyl end first, by abstraction of a vinylic H from ethylene that is later added back to yield the terminating methyl group.[194] However, this seems inconsistent with the many chain transfer responses, and has been reported to be at odds with hydrogen response, 1-butene formation, and some kinetic features.[331] It also fails to distinguish between the first and subsequent chains formed on a site.

Finally it should also be remembered that, in addition to chromium oxide catalysts, many other diverse catalyst systems also polymerize ethylene in a similar fashion. They too produce linear polymer with first-order kinetics, exhibit very similar activity, transfer primarily to monomer, respond to H_2, insert comonomer in a 1,2 orientation with accompanying acceleration of chain transfer, produce vinyl and methyl end groups, and exhibit other behavioral similarities. Examples include Ziegler catalysts based on titanium or vanadium, Ballard-type catalysts[332–345] based on zirconium, titanium, yttrium or scandium, lanthanides, certain nickel catalysts,[346] divalent and zerovalent

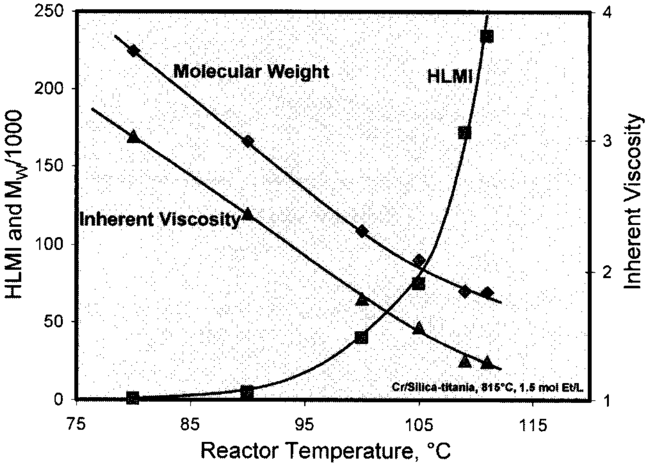

Figure 10.28 Influence of reactor temperature on polymer molecular weight and its derivatives, high load melt index and inherent viscosity.

organotitanium compounds,[303,347] chromocene,[348,353] chromium (II, III, or VI) alkyls or allyls,[301,422] diarene Cr(O) compounds,[422] and many others. Although not known with certainty, it is reasonable to suspect some common underlying mechanistic principles behind all these systems. Thus it is also reasonable to ask whether any mechanism proposed for one system, such as those requiring alkylidenes or surface silanols or chains in loops, would be applicable to the other systems.

10.4.2 Reactor Variables

Molecular weight is governed by the rate of termination of chains relative to the rate of propagation. Instead of molecular weight itself, most commercial manufacturers use melt index (MI) as the primary production variable. Melt index, or high-load melt index (another variant called HLMI), is a measure of the flow of the molten polymer under a specified shear stress. It is a more consistent and easier measurement to make in a plant environment than molecular weight. Therefore it is the primary specification under which commercial grades of PE are made and sold. The MI is inversely related to molecular weight; high MI means low MW.*

Reactor temperature is the main variable for controlling molecular weight or melt index in commercial operations. Increasing the reactor temperature even a degree or two decreases the stability of the Cr–polymer bond, thus accelerating chain transfer. An example of this response is shown in Figure 10.28, where the weight average MW is plotted. As the reactor temperature was increased over the typical commercial range, the MW decreased. The inherent viscosity of the polymer in solution is also plotted and it also decreased because of its dependence on MW. And the HLMI is likewise plotted in Figure 10.28 as a function of reactor temperature. The HLMI increases exponentially as the reactor temperature increases.

---

*Melt index is also affected by MW distribution and by long-chain branching. However, in the typical comparison of commercial PE grades these other parameters are usually similar.

Ethylene concentration is also sometimes used as a production variable to control MI. The dependence of chain transfer on ethylene concentration is a result of two independent mechanisms of agostic β-H transfer. As shown in Scheme 10.13, it can occur either (1) to Cr or (2) directly to incoming monomer.[29–31,36,41,204,324,354–357] In the first case, H elimination to Cr is not dependent on ethylene concentration but chain growth is. Therefore MW (more accurately M_n, the number average) should be proportional to monomer concentration. In the latter case, H elimination to monomer *is* dependent on monomer concentration, and since propagation is also first order in ethylene, there is no net dependence of MW on monomer concentration.

On the Phillips catalyst MW does increase with ethylene pressure, but it is not proportional. That is, doubling the ethylene pressure does not double the MW. If chain transfer occurred entirely by H transfer to Cr, then the MW should be proportional and should extrapolate to zero at zero ethylene pressure. It does not. On the other hand, if chain transfer were entirely through the second method, H transfer to monomer, then MW should remain constant. Again it does not. The behavior actually represents an intermediate case, where both chain transfer reactions probably contribute, although clearly it is the second reaction, H transfer to monomer, which dominates, as on many other industrial catalysts.

Figure 10.12 shows the response of MI as ethylene concentration is varied over a wide range. Also plotted are the weight average MW and the vinyl end-group concentration in the polymer, which indicates the number average MW. These three independent measurements each indicate increasing MW as

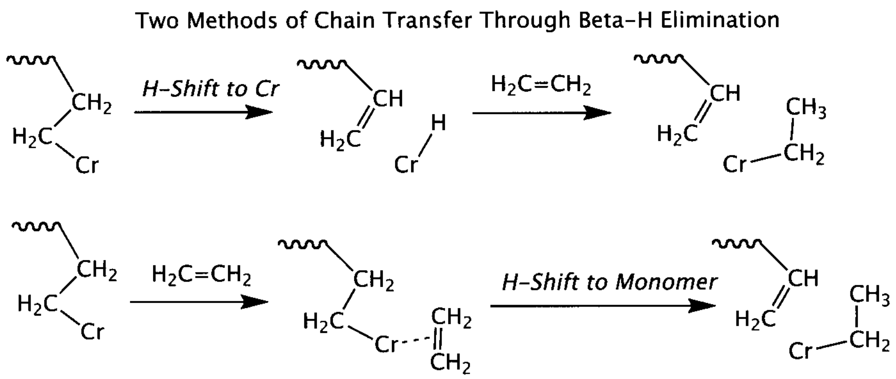

Scheme 10.13

ethylene concentration in the reactor was raised. This is because the termination of chains involves at least some hydride transfer to chromium, rather than to the incoming ethylene.

H_2 is also added to the reactor to lower the MW via hydrogenolysis. Chromium oxide on silica is not as sensitive to H_2 as some other catalysts, such as Ziegler or chromocene. However, its H_2 sensitivity is also not unusual, as many zirconium- or titanium-based Ballard catalysts fall into the same category.[303,347] In fact, the sensitivity of chromium oxide catalysts can vary considerably depending on the support. Cr/alumina and Cr/aluminophosphate catalysts tend to be much more responsive than Cr/silica. There are some indications that hydrogen, even in small amounts, removes the highest MW tail from the MW distribution. This does not imply any selectivity between sites. Instead, it is a natural consequence of the fact that the MW from high-MW sites, is affected disproportionally more than other sites if all sites consume the same level of H_2. Thus certain polymer behavior is noticeably changed by hydrogen.

10.4.3 Site Heterogeneity

The broad MW distribution from chromium oxide catalysts is due to a diverse population of sites, each producing its own characteristic chain length. The diversity of sites is a result of the heterogeneity of the amorphous support, which produces a spectrum of different geometric and ligand environments for the Cr. Thus any variable that can affect the site population is also likely to affect the average MW produced and the MW distribution.

That Cr/silica catalysts have a diverse population of sites is immediately apparent from the polymer MW distribution, shown in Figure 10.1, which is usually much broader than that from metallocenes or Ziegler catalysts. Breadth is usually measured by the polydispersity index (PDI), which is the ratio of the weight average MW to the number average MW (M_w/M_n). A single type of active site produces a PDI near 2.0 from a nonliving system, such as is produced by some metallocenes. Chromium oxide on silica catalysts, on the other hand, produce polymer with M_w/M_n typically ranging from 6 to 20, and special catalyst treatments can provide polymers of PDI as low as 4.0 or as high as 100. This is because the catalyst contains a heterogeneous population of sites differing in propagation and termination rate constants. Each site type generates polymer with its own characteristic molecular weight, and consequently the polymer breadth reflects the heterogeneity of the site population. Differences in site reactivity no doubt derive from the amorphous support surface. Depending on how the support dehydrates, each chromium site can have variations in the angle and strain of attachment and in the number and distance to the nearest oxide or hydroxide ligands. Using supports other than silica also has a profound impact on the polymer, indicating that the support is much more than an inert carrier. Instead, it affects the reactivity of the chromium.

10.4.4 Reaction Time

Another manufacturing variable that influences MW is the reactor residence time. This also derives from site diversity. A typical polymerization reaction might last 1 h and yield 5000–10,000 g PE/g catalyst·h. Measuring the average molecular weight M_n by gel permeation chromatography (GPC) or by end-group analysis through IR or NMR, one finds that the number of chains produced far exceeds the number of chromium atoms on the catalyst. During its 1-h lifetime in the reactor each chromium site must yield thousands of chains. This is in contrast to a "living" system, where the longer the polymerization is allowed to continue, the longer the chains will grow. In fact, the lifetime of each PE chain on the Phillips catalyst is only a fraction of a second, so any change in the MW over an hour cannot be ascribed to simple chain growth with time.

Actually the MW usually does increase with polymerization time out to several hours when run in a slurry process.[41,206,358] Figure 10.29 shows a typical kinetic profile for Cr(VI)/silica. The polymerization rate increases for a time and then levels out at a constant activity for as long as it can be measured before the reactor overfills. This gradual rise in rate is thought to be due to slow reduction and alkylation of Cr sites, and it is evidence that different chromium sites become active at different times due to inherent differences in their reactivity with ethylene. As it turns out, those sites that come on stream first also produce lower MW polymer. Thus the average MI, measured by sampling the polymer at different times during the reaction, also decreases with time as more sites come on stream that produce ever higher MW polymer. This also is shown in Figure 10.29. Figure 10.30 shows the MW distribution from Cr/silica and how it can vary with time. The first polymer formed tends to have a low-MW shoulder that quickly fades away

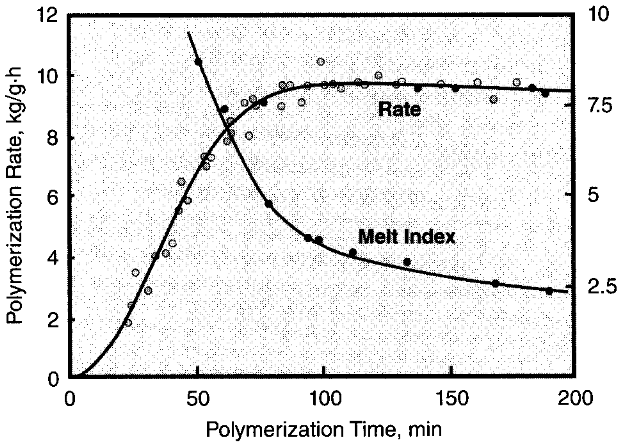

Figure 10.29 MW of polymer changes with reaction time.

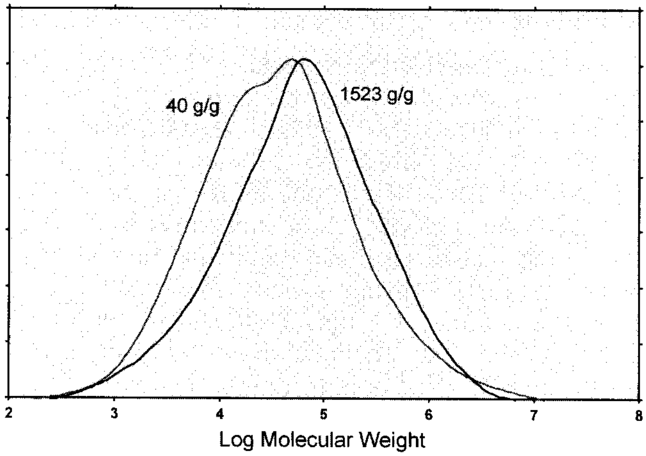

Figure 10.30 Polymer MW distribution change with reaction time (Cr/silica, 700 °C, reaction at 85 °C, 50 mL 1-hexene, 550 psig).

with increasing polymer yield. Therefore the first polymer formed is clearly lower in MW.

Reducing the Cr(VI) to Cr(II) in CO at 350 °C, which accelerates the development of activity, also reduces the initial MI, because the higher MW sites are already reduced prior to ethylene contact. Thus CO-reduced catalysts produce a flatter MI response with time. Similarly, this MI dependence on polymer yield does not exist when these same catalysts are allowed to polymerize ethylene in a solution process at much higher reaction temperatures. Activity develops immediately at such high temperatures. All sites come on stream at roughly the same time, which results in a lack of MI dependence on polymer yield.

The exact cause of the MI dependence on reaction time is still debated. It has been argued that the MW change with time could be due to the initial overheating of the catalyst particle until it develops more mass. Other facts seem to contradict that interpretation, however. First, the amount of temperature rise in a slurry process is not calculated to be very severe, and not nearly enough to account for such large changes in MW. Second, decreasing ethylene concentration, which should diminish the heat release, does not remove the connection and in fact lower ethylene *further decreases* MW. Also, the relationship seems to be most pronounced when there is a slow buildup of activity and less when the activity is fast. Finally, the relationship does not seem to hold for other supported catalysts (metallocenes) that are also sensitive to temperature.*

---

*Another piece of information that, although difficult to explain, might have relevance is the ^{14}CO-labeling experiments by Tait et al. (see ref. 175), who found a constant number of active sites with time. The matter waits for an explanation.

That some sites are reduced more easily than others was initially reported by Holm and Clark, who used hydrogen as the reducing agent and monitored its uptake while the temperature was raised.[30,35] It is also possible to demonstrate this spectrum of sites using carbon monoxide.[206] CO reduction yields highly coordinatively unsaturated Cr(II).[41,191,192,195–197,208,209,211,236,265,310,318] By partially reducing a catalyst in CO and then cooling it in CO, reduced sites, which are Cr(II), chemisorb CO and are subsequently inactive for polymerization. In contrast, the Cr(VI) sites that were not reduced do not chemisorb CO and thus do become active for polymerization upon later exposure to ethylene. In this way it is possible to selectively inhibit certain sites. The process is illustrated in Scheme 10.14 below.

Figure 10.31 shows the result of such site discrimination. A Cr(VI) catalyst, calcined in dry air at 600 °C, was then exposed to CO at various temperatures, cooled to 25 °C in CO, then flushed with nitrogen. When the treatment with CO occurred at 25 °C, the resulting catalyst was orange, indicating no reduction had taken place, and there was no loss in activity. When the exposure to CO occurred at 300 °C, the resulting catalyst was violet, due to full reduction

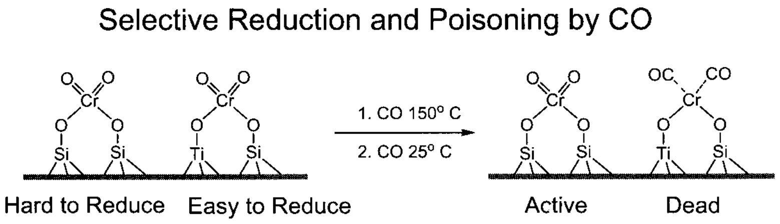

Scheme 10.14

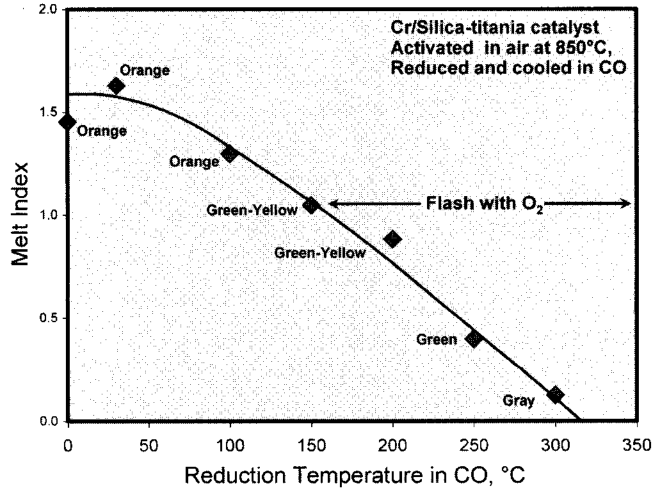

Figure 10.31 Partial reduction and poisoning by CO.

and subsequent adsorption of CO. This sample had almost no activity because of the chemisorbed CO. Between those two extremes the color and the activity of the catalyst was intermediate, indicating that some sites reduced more easily than others. Figure 10.31 shows the MI obtained from the polymer these catalysts produced. Notice that the MI of the first point (25 °C exposure to CO), in which all of the sites participated, was high. However, the MI dropped as more of the low-temperature reduced sites were removed from the catalyst. This indicates that the sites that are most difficult to reduce also produce the highest MW (lowest MI).

10.4.5 Activation Conditions

Figure 10.17 shows that activation temperature is another powerful variable for controlling MW or MI. As the surface becomes increasingly dehydroxylated, activity improves and the MW declines, both because of a changing site population. It is unclear whether this is due to less ligation from neighboring oxide or hydroxide species or to a difference in bond angle that comes from annealing the surface. This apparently results from a more electron deficient Cr center.[53,218,219] Other polymer changes also seem to suggest this.

Figure 10.32 shows the GPC of polymers made from chromium catalysts activated at various temperatures from 400 to 800 °C. During this range the MW distribution of the polymer narrows and the activity increases with rising activation temperature. This again suggests that the site population during this temperature range is growing and changing and these new sites contribute to the mid-MW region. Notice in Figure 10.32 that the MW distribution narrows by removal of both the high- and low-MW tails. These two effects combined

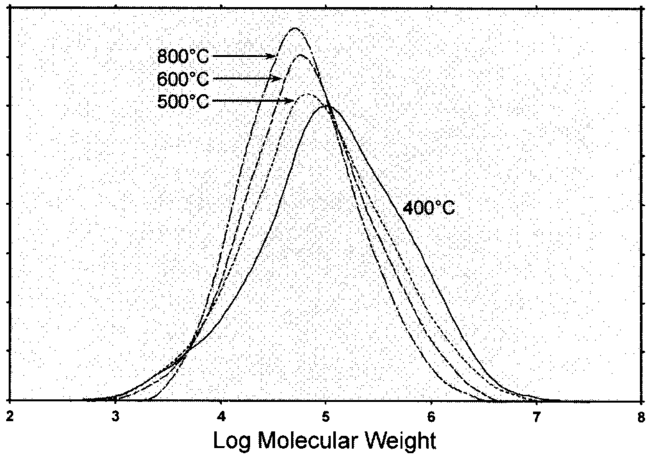

Figure 10.32 MW distribution of polymers made from C/silica activated at various temperatures.

(removal of tails and enhanced mid-MW production) result in a significant narrowing of the MW distribution at higher activation temperatures. A removal of some of the high-MW polymer would be consistent with the MI change observed in Figure 10.17 as the activation temperature was increased. It suggests that dehydration is converting the high-MW sites into more coordinatively unsaturated and more reactive lower MW sites. That the lowest MW side is also diminished, however, suggests that some of the most reactive sites are not stable at the highest activation temperatures and redistribute themselves into other, more stable, medium-MW sites.

This dependence of the MW distribution on activation temperature is partly responsible for some of the major differences in polymer properties produced, and therefore activation temperature is widely used as a commercial variable to manipulate product quality. For example, as the activation temperature is increased, these physical characteristics are diminished: (1) impact and tear resistance in film, (2) hoop stress and creep resistance in pipe, (3) toughness in sheet, and (4) resistance to chemical attack or ESCR (environmental stress crack resistance) in blow molding. An example of dependence of ESCR on activation temperature is shown in Figure 10.33, where polymers of constant MI, but varying MW distribution, were made from Cr/silica catalyst activated at different temperatures. They were then evaluated in a laboratory ESCR test. That is, strips of the molded polymers were stressed (bent) and then submerged in hot surfactant solution until they cracked. The time to failure is recorded in hours. ESCR and the other properties listed above are usually improved at higher MW. Hence ESCR is plotted in Figure 10.33 against MI. A broader MW distribution provides higher MW when compared at equivalent MI. Therefore broader MW distributions (low activation temperature) tend to provide better polymer properties.

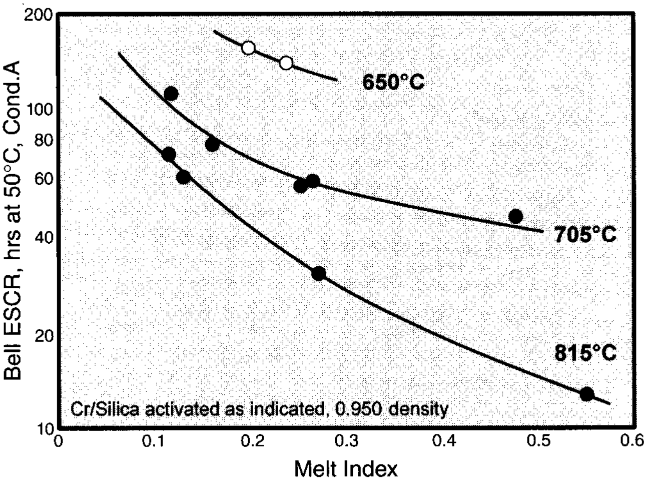

Figure 10.33 Dependence of ESCR on activation temperature.

10.4.6 Poisons

Poisons can sometimes also affect the MW or the MW distribution. Presumably this happens because some sites are selectively poisoned before others. When small amounts of CO are added the MI decreases. This suggests that CO is preferentially adsorbed on the low-MW-producing sites. An example is shown in Figure 10.34. Small amounts of CO caused a strong inhibition of activity, indicating a highly selective poison. Activity was almost gone by addition of 0.25 CO/Cr. However, the shape of the curve shows the classical response in a poisoning experiment. As the first increments of poison were added, activity declined rapidly. Then with later increments the effect of the CO was less severe. This behavior suggests that chemisorption of the first increments of CO is highly selective on the most coordinatively unsaturated sites followed by declining selectivity. These first increments presumably correspond to some of the Cr_A population identified by the Turin group.[208–212] If this explanation is correct, then extrapolating down the initial slope of the curve indicates that 6–7% of the Cr on a 1% Cr catalyst was active, or in this case 0.02 Cr/nm^2. Alternatively, if one concludes that later CO adsorption is equally selective but the later sites to be poisoned are just less active, then about 30% of the chromium is active, or about 0.10 Cr/nm^2, which coincides with the Turin group's measure of Cr_A.[208,209,211,212] The true active-site density may lie somewhere between these two extremes.

Poisoning by methanol also lowered the MI. Oxygen has the opposite effect. Gas-phase reactors tend to produce high yields at low MI because of their very long residence times. One way of overcoming this problem is to deliberately add oxygen in small amounts to the reactor. Figure 10.35 shows an example of this response. Adding a small amount of oxygen to the

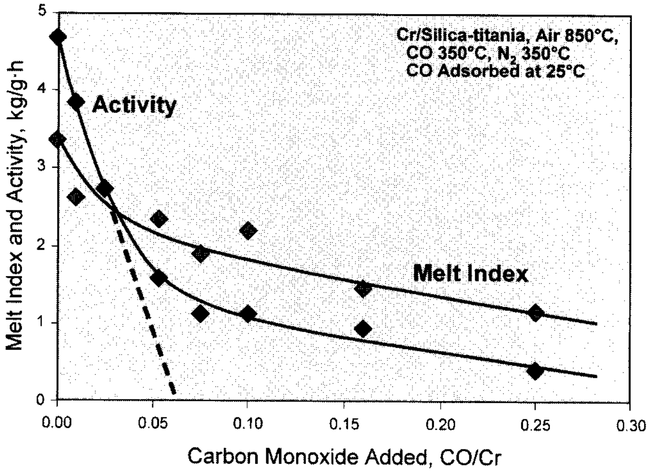

Figure 10.34 Titration of Cr(II) activity by preadsorbed CO.

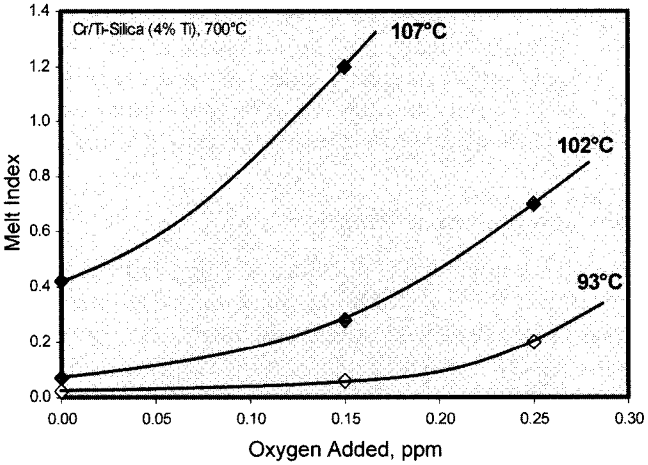

Figure 10.35 MI control by adding O_2 to reactor.

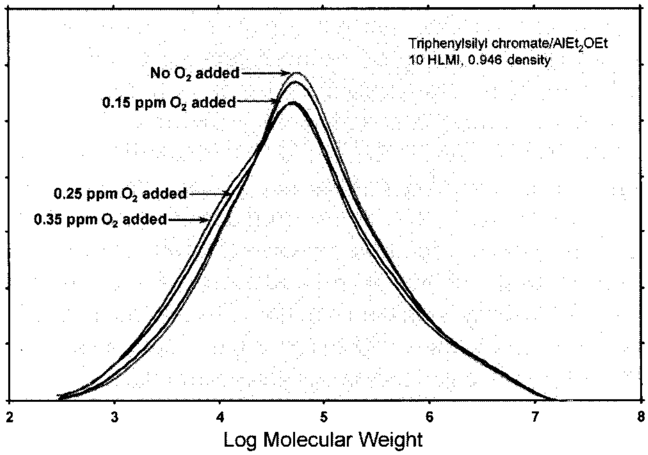

Figure 10.36 Effect of O_2 poisoning on MW distribution.

reactor often embellishes the low-MW side of the MW distribution, thereby raising the overall MI obtained. The MW distribution from this interaction is shown in Figure 10.36, where up to 0.35 ppm O_2 was added to the ethylene stream. This response is sometimes used commercially to improve the flow of the molten polymer, or shear response, because of the increased MW breadth. Unfortunately the change is accompanied by a loss of up to 50% of the catalyst activity.[143,144]

The effect of oxygen can perhaps be explained in two possible ways. First, one might suppose that the sites that were last (most difficult) to reduce, which also produce high-MW polymer, would be most reactive with oxygen. Therefore the adsorption of O_2 might be considered as selectively poisoning the high-MW sites. Or, alternatively, one might consider all sites to be equally reactive with oxygen, but after being killed the more easily reducible sites, which produce low-MW polymer, tend to come back on stream more quickly. So, again, the high-MW sites are in effect selectively poisoned.

10.4.7 Porosity and Molecular Weight

The porosity of Cr/silica catalysts also has a strong influence on the MW of the polymer produced.[31,41,145,359,360] The larger the pore volume of the silica (or alternatively, the larger the average pore diameter), the lower the MW. This was shown in Figures 10.8 and 10.9 where a hydrogel was dried by extraction with several different organics varying in surface tension. All these catalysts had the same chemical composition and the same surface area, but the pore volume varied from as little as 0.7 mL/g to over 3.0 mL/g. All catalysts were allowed to polymerize ethylene under the same conditions. Notice in these figures that the MW decreased with increasing pore volume and that the MI, which is inversely related to MW, increased.

Experience such as this example suggests that the mesopores greater than 100 Å diameter can be important for the development of activity and MI.[41,145,160] When the packing between primary silica particles is loose enough to generate pores of this size, the overall matrix becomes friable during polymerization. Apparently these pores can be susceptible to crushing by aqueous surface tension during drying and also to rupture during polymerization. Mercury porosimetry is a technique better suited to measuring such large pores. One often obtains a very good correlation between catalyst activity and the volume of mercury penetrating this mesopore size range. An example is shown in Figure 10.37, where activity is plotted against pore volume inside 100–10,000 Å for another such series of catalysts. Other mesopore ranges, such as 100–1000 Å, also correlate well. As the mesopore volume decreases to near zero, the activity does also. Most likely, the mercury "penetration" being measured here is also the result of the matrix collapsing under increasing pressure, which likewise indicates the fragility. This is why, at the highest pressure, associated with pores <100 Å in diameter, all of the samples had the same penetration volume. Notice in Figure 10.37 that the principle applies to aluminphosphate-, as well as silica-, based catalysts, and that both MI and activity are affected similarly.

It is important to keep in mind that these preferred pore diameters are probably important only because they reflect the strength of the catalyst matrix. For a uniform, narrow pore size distribution such as that shown in Figure 10.9 the average pore size usually does correlate well, suggesting that pores of 100–1000 Å in diameter produce optimum fragility. For a broad or bimodal distribution of pores, however, it is the small ones that seem to dominate in determining catalyst character.[143,144] This is where most of the surface area is, and hence the Cr, and it probably determines the pore size of the fragments.

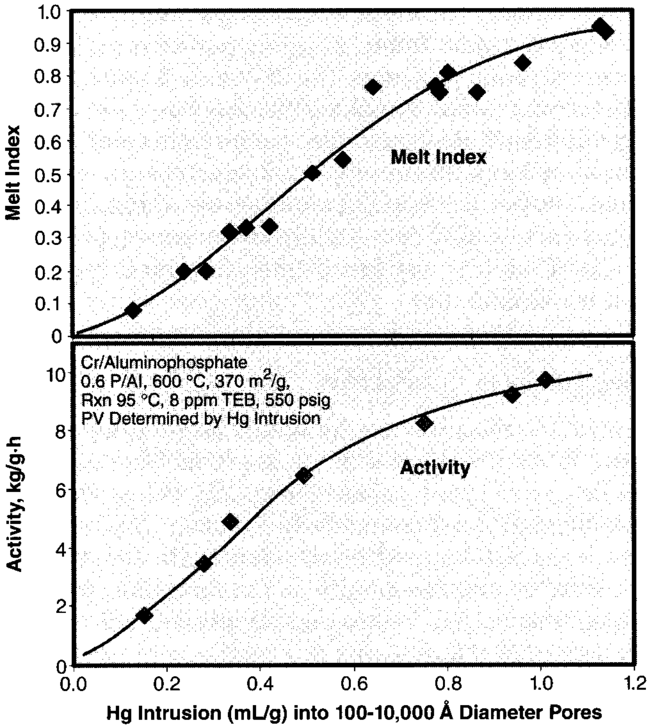

Figure 10.37 Influence of mesoporosity on activity and MI.

Although exploited commercially for nearly 50 years, the mechanism by which porosity affects molecular weight is still not clear. One can understand how porosity controls activity, but its influence on MW is not intuitive. Diffusion of ethylene into the pores fails to explain it, because the trend actually runs opposite to what would be expected. Starving the catalyst of ethylene, which presumably might happen in small pores or large fragments, is known to decrease MW, not increase it. Another proposal is that lower PV results in larger fragments, less activity, and thus less local heat generation. This might make more sense for gas-phase processes, where heat removal can be problematic, but in a slurry process or even a solution process, it is not very satisfying. To our knowledge this relationship is common to no other catalyst system. Ziegler and metallocene catalysts do not seem to follow it, although this point has not been fully investigated.

It has also been proposed in some early modeling papers that diffusional restrictions can account for the broad MW distribution from Cr/silica. This is usually imagined to occur through ethylene concentration gradients within the macroparticle. For Cr/silica catalysts, however, this would require chain transfer to metal, or perhaps mostly to hydrogen, neither of which is the case. Stated another way, the dependence of MW on ethylene concentration is not great enough to account for much broadening, even if the gradients were extreme. Another clue comes from comparing polymers made in slurry versus gas-phase or even solution processes. The MW distributions from Cr/silica are approximately the same even though the mechanisms of mass transport must be completely different. Still another clue comes from comparing metallocene catalysts which were run in the unsupported state (catalyst in solution) versus those supported on silica. Both produce homogeneous branch profiles in copolymers and quite narrow MW distributions, sometimes approaching the theoretical PDI = 2.0. Therefore any broadening that comes from concentration gradients must be insignificant.

10.4.8 Adding Titania to Control MW

Closely related to its effect on activity, titania also has a powerful influence on the MW produced. The beneficial effect probably results from a change in the electronic environment on the chromium, which becomes associated with (perhaps linked to) the titania during calcining. The formation of strong Brönsted sites on silica–titania, which may react with and attach the Cr as in Scheme 10.15 decrease electron density on the chromium, increasing its reactivity. That the addition of titania increases the average chain transfer rate can be seen in Figure 10.38. Here a Cr/silica catalyst was dried at 250 °C, then impregnated with various amounts of titanium isopropoxide in heptane solvent. After evaporating the heptane, these catalysts were then activated at 650 °C and tested for polymerization. Melt index increased substantially with the first additions of titania, indicating an acceleration of chain transfer. At higher levels of titania the slope begins to level as the silica surface becomes saturated near 6–8% Ti. Also shown in Figure 10.38 is the weight average MW

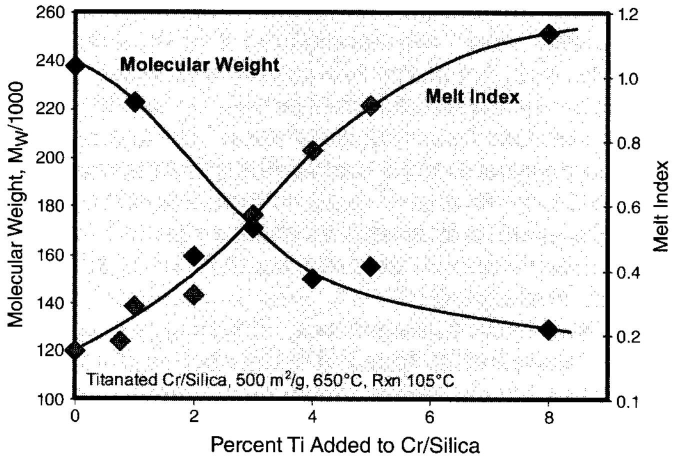

Figure 10.38 Influence of titania on MI and MW.

obtained from these same catalysts. As would be expected, MW decreases with increasing MI. In other words, the addition of titania tends to lower the average MW.

Titania decreases the average MW of the polymer by broadening the MW distribution on the low-MW side. This probably means that a significant new population of sites has been created by the addition of titania which produce mainly low-MW polymer. An example is shown in Figure 10.39 where the GPC curves of four polymers are shown. One is from Cr/silica, activated at 650 °C; the others are from that same Cr/silica except treated with various amounts of titanium isopropoxide. Unlike normal GPC curves, these four curves have been normalized according to the catalyst activity. This makes it very apparent that the effect of titania is mainly on the low-MW side of the distribution. The more titania added to the catalyst, the higher the activity becomes and the more low-MW polymer is made. Special "two-step" activation techniques (described in Section 10.4.9) can be used to greatly exaggerate the effect of titania on the MW distribution.

Thus titania broadens the MW distribution by adding low-MW polymer, which increases the MI. In commercial operations, however, when titania is added to a catalyst recipe, the reactor or activation conditions are usually readjusted to shift the MI back to its original target. This shifts the entire distribution to higher MW, resulting in a broadening on both the low *and* the high end of the distribution. The broader MW distribution so produced can be very useful in many commercial applications, such as blow molding, film, sheeting, and pipe. In general, it causes improved flow properties at high shear rates, and it also improves polymer toughness due to the longer chains in the broadened distribution. Environmental stress crack resistance and creep resistance can all be enhanced from this broadening.

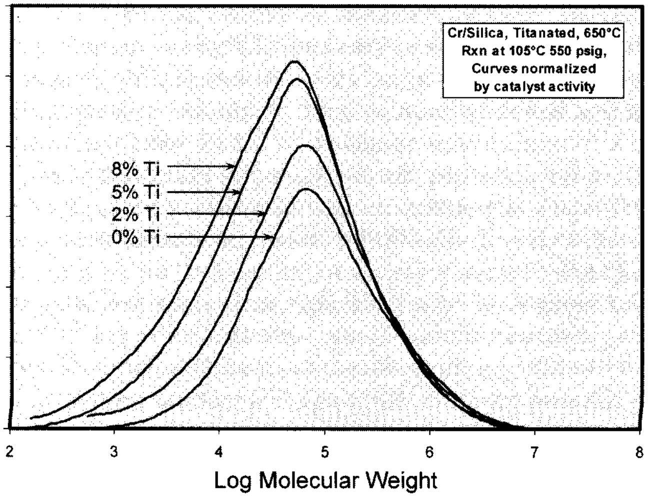

Figure 10.39 GPC curves from Cr/silica–titania.

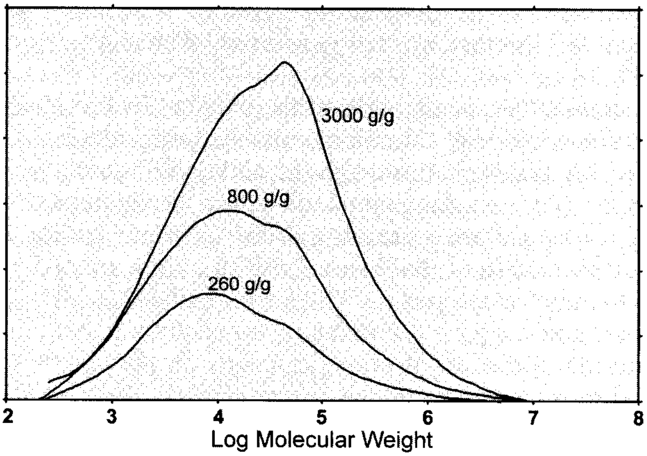

Figure 10.40 MW distribution of Cr/silica–titania as function of reaction time (Cr/silica–titania, 8% Ti, 500 °C, reaction at 105 °C, 550 psig).

That titania seems to make the Cr(VI) more easily reducible can also be seen in the MW distribution. In Figure 10.40, a silica was titanated to 8% Ti and calcined at 500 °C. Then it was impregnated with chromium acetylacetonate in toluene and activated at 500 °C. Polymerization was carried out at 105 °C and stopped at various times to yield different amounts of polymer as more sites came on stream. The resulting MW distributions are shown in the figure. It is clear that the low-MW, presumably Ti-associated, sites came on stream first. The MW gradually shifts upward with time. Even catalysts containing no titania show an increase in MW with time, as different sites come on stream (see Figure 10.29), but the presence of titania exaggerates the effect, suggesting that the Ti-associated sites are more reactive.

Two ways of incorporating titania onto Cr/silica catalysts are commonly used commercially, and each has certain advantages. In the simplest method the silica surface is coated with a layer of titania by reacting the hydroxyl groups with a titanium ester or halide.[281,282,285,286] Unreacted ester or halide groups are then burned away during the subsequent calcining. Owing to its simplicity this method permits commercial silicas to be treated with any amount of titania up to 5–8% Ti, depending on surface area, at which point saturation is reached.

The second method of incorporating titania onto the catalyst consists of coprecipitating hydrous titania along with the silica gel.[281,287] This can be accomplished by adding sodium silicate to an acidic solution of a water-soluble titanium salt to cause gellation. Although this method probably gives a higher degree of dispersion throughout the catalyst bulk, much of the titania is exposed on the surface and during later calcining chromium may attach to it. Specialty catalysts have been developed through coprecipitation of titania to impart high ESCR to the polymer.

Despite the many benefits of adding titania to Cr/silica, it does not promote Cr/alumina, nor does pure titania function well as a support in itself. This is partly because TiO_2 does not form the correct porosity for fragmentation. However, some Cr(VI) is stabilized by TiO_2 at 400 °C, and small amounts of polymer can be made and analyzed. Curiously, Cr/titania itself produces extremely high MW polymer, in complete contrast to its effect on Cr/silica catalysts, where titania is noted for adding low-MW polymer to the MW distribution. This probably indicates that it is not the presence of Ti itself that is important, but the combination of Si and Ti. That is, the capability of titania to influence polymerization may derive from an ability of Ti(IV) to assume a tetrahedral coordination and fit in with the silica lattice, increasing the acidity of Brönsted hydroxyls used for Cr(VI) attachment.[361]

10.4.9 "Two-Step" Activation of Cr/Silica–Titania

Ordinarily chromium is impregnated aqueously onto the silica–titania support and then calcined, which means that Cr(VI) binds to the support by reacting with hydroxyls on a hydrated surface. However, a different catalyst results if the chromium attaches instead to a surface already dehydrated by calcining. A large promotional effect, particularly on the termination rate, can be obtained.[123–124,127] To do this a "two-step" activation procedure is used in which the silica–titania is first dehydrated at 800–900 °C, then impregnated with chromium anhydrously so that the surface is not rehydrated. A secondary calcining step at a lower temperature, such as 300–600 °C, then fixes the Cr(VI) to the silica. The MI enhancement is especially pronounced if the support contains titania. One interpretation is that this preparation selectively inserts Cr(VI) into strained Ti oxide surface bridges (Scheme 10.15).

Any aprotic chromium solution can be used. CrO_3 in acetonitrile or organic chromate esters in hexane are good candidates. Lower valent compounds, such as diarene chromium in hexane, can also be used because they are oxidized to the same Cr(VI) surface species during the secondary calcining in air. Even chromyl chloride vapor can be used without a solvent. Residual chloride is burned away during the secondary calcining step.

An example is shown in Figure 10.41. Here silica–titania dehydrated at 820 °C was impregnated with 0.5% Cr as dicumene chromium in hexane and then calcined in air at the temperatures listed. Ordinarily MI increases with calcining temperature up to the point of sintering at about 900 °C, as is shown in Figure 10.17. However, the two-step activated catalyst goes through a much

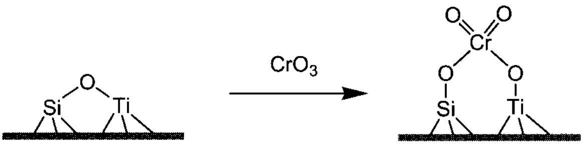

Scheme 10.15

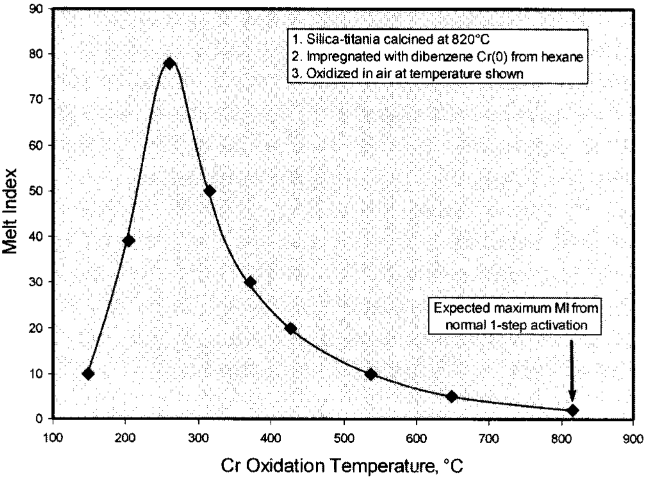

Figure 10.41 Anhydrous impregnation of Cr onto precalcined silica–titania.

higher maximum at less than 300 °C. In fact this maximum can be orders of magnitude higher than that obtained at 900 °C from the one-step activation. After being activated at 870 °C during the secondary calcining, however, the promotional effect vanishes.

The reason for the extreme promotional effect may be that the Cr(VI) species associated with titania and high MI is not very thermally stable. This way of impregnation allows the support to be fully dehydrated without exposing the chromium to high temperatures. In this way, the chromium is more selectively placed in contact with/on the surface titania. Once formed, however, these high-MI sites are clearly not thermally stable because calcining at higher temperatures than 300 °C brings down the MI. By 870 °C only the ordinary sites are left, like those made aqueously in Figure 10.17. This is no doubt the same instability that was observed in the low-MW narrowing in Figure 10.32 with increasing calcining temperature.

That this promotional effect (and subsequent loss of it at high temperature) are due to a repositioning of the chromium (first on and then off the titania) is apparent in another curious experiment.[362] Titanated Cr/silica was first calcined in air at 800 °C, leaving the usual hexavalent catalyst. The catalyst produced the expected low MI of 0.22. Then the catalyst was slurried in hexane, to which 1 mol of *t*-butanol per mole of chromium was added. After being stirred for a few minutes, the hexane was evaporated away, and the catalyst was calcined again in air at 300 °C. When retested for polymerization activity, the catalyst produced 2.0 MI polymer, indicating a significant promotional effect. The *t*-butanol apparently reacted with some of the bound Cr(VI) to form *t*-butyl ester linkages. This gave the Cr enough mobility to allow repositioning during the second, 300 °C activation.

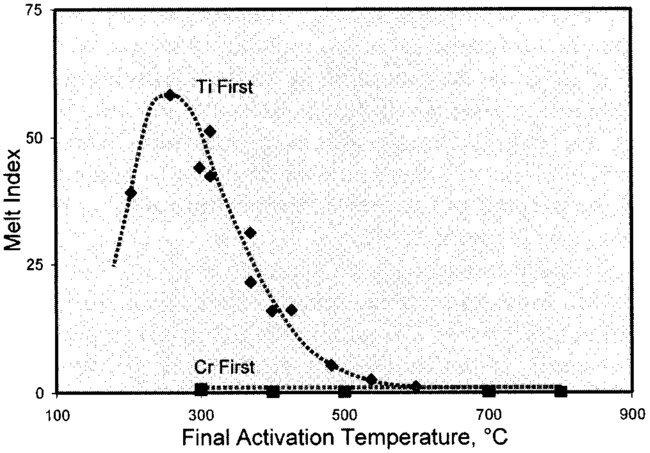

Figure 10.42 The order of impregnation is important. In one series TI was added to Cr, and in the other the order was reversed.

The order of addition can also influence the Cr positioning, and Figure 10.42 illustrates this. The melt indices from two series of catalysts are plotted against the activation temperature. In one case chromium was added first, then titanium, and in the other series the order was reversed. In the first series Cr/silica was calcined in air at 800 °C, impregnated with titanium isopropoxide in hexane to equal 8.3% titania, then activated at the temperatures indicated. In the second case, the silica alone was impregnated with the same amount of titania in the same way, calcined at 820 °C, and then anhydrously impregnated with 0.5% Cr as CrO_3 in acetonitrile. Finally it was activated at the temperature shown. There is a major difference in MI between the two series. MI peaked at about 60 when titania was added first, but at less than 1.0 when chromium was added first. This suggests that in the first case the chromium was already attached to silica and adding titania afterward did produce the desired species.* Notice also in Figure 10.42 that, even though the titania-first catalyst yielded much higher MI values at low activation temperatures, the advantage was again lost with continued activation at 800 °C. The two curves merge together at high temperatures, suggesting a migration off of the titania.

The sensitivity of the two-step activation to titania is demonstrated in the following experiment. Silica was dried at 260 °C, then titanated with titanium isopropoxide to various levels of titania. These samples were calcined at 815 °C followed by anhydrous impregnation of chromium as *t*-butyl chromate in

*The Cr first catalyst was dehydrated at 800 °C before reacting with titanium isopropoxide, whereas the Ti-first sample was fully hydrated when treated with titanium isopropoxide. One could argue that this favors the latter, since silanols help anchor and disperse the titanium. Thus the Ti-first experiment was repeated except using a silica previously calcined at 820 °C. A curve very similar to that in Figure 4.15 was again generated. The melt index peaked at 25.

hexane and a final activation at 260 °C. The melt indices and activities obtained from this series are listed in Table 10.3, under "two-step activation." Notice that the MI and even the activity increase as the titanium level increases. For comparison the same silica catalyst, this time already containing chromium, was titanated and simply given a one-step activation. These data are also shown in the table. The difference in MI response is remarkable and again indicates that the purpose of the two-step procedure is to preserve a thermally unstable species associated with titania.

This two-step procedure also shows some sensitivity to the amount of chromium added. Melt index often goes though a sharp peak during the first additions of chromium. As more Cr is added, the MI drops somewhat and usually levels out. An example is shown in Figure 10.43 where the catalyst was a silica–titania cogel calcined at 871 °C and then impregnated with a hexane solution of dicumene chromium(0). This behavior could suggest that the most reactive surface oxide binding sites, perhaps strained Si–O–Ti links generated by high-

TABLE 10.3 Sensitivity of Two-Step Activation to Titania Level

Two-Step Activation			One-Step Activation	
Ti/nm^2	MI	Activity (g/g·h)	Ti/nm^2	MI
0	0.4	2500	0	0.48
0.4	0.6	2740	1.3	2.07
0.8	4.7	2950	2.1	2.4
1.0	25	5980	2.5	2.85
1.3	40	6400	3.3	2.28
2.1	77	7554		
2.9	85	7080		

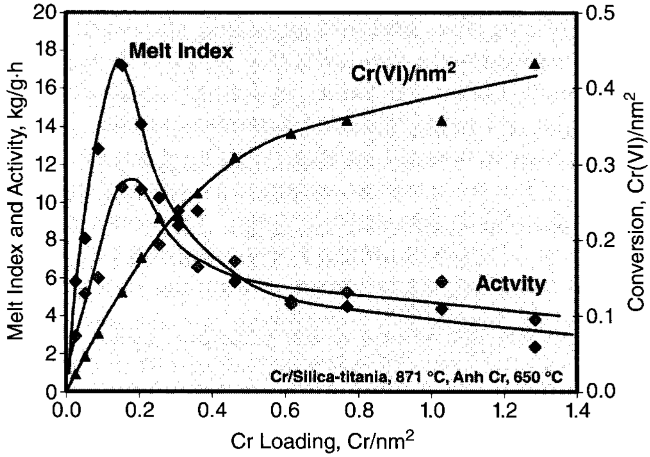

Figure 10.43 Effect of Cr loading in two-step activation.

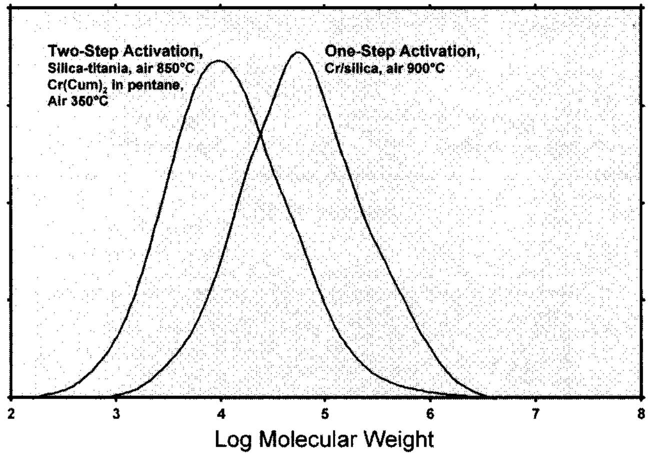

Figure 10.44 Shift in MW from two-step activation (reaction at 85 °C, 50 mL 1-hexene, 450 psig).

temperature calcining, are responsible for much of the "high-MI" orientation of surface Cr(VI). When these sites are occupied, excess Cr goes on in more conventional modes. It is also conceivable that an excess of Cr changes the earlier Cr binding, such as to dichromate. The more titania the support contains, the less Cr(VI) that can be stabilized when Cr is applied in the two-step way. This suggests again that Cr(VI) is unstable on the titania.

An example of the extreme molecular weight shift that is brought about by the two-step impregnation of chromium onto calcined titania is shown in Figure 10.44. In this example a silica–titania cogel, containing 8% Ti, was calcined at 850 °C in air, then the chromium was impregnated anhydrously onto the support as dicumene chromium(0) in pentane. After evaporating the solvent off, the catalyst was reoxidized in dry air at 350 °C in order to convert and attach the chromium as Cr(VI). For comparison a Cr/silica catalyst was calcined in a one-step approach (without titania) at a similar temperature. The former catalyst produced a 360 MI, whereas the latter catalyst produced a MI less than 1. The MW shift is shown in Figure 10.44. The former catalyst produced an average MW of less than one-third that of the former.

Dehydration by Chemical Means The extent of dehydroxylation of the surface seems to exert a powerful influence on the activity and MI potential of the Phillips catalyst. MI increases with increasing temperature up to about 900 °C where sintering begins. Even at 900 °C, however, the OH population does not drop to zero, but some residual hydroxyls remain. A further lowering of the OH population can be accomplished by calcining not in air, but in carbon monoxide.[26,123] This is shown in Figure 10.45. The effect is probably due to the water gas shift reaction in which water (hydroxyls) is converted to hydrogen and carbon dioxide as depicted in Scheme 10.16.

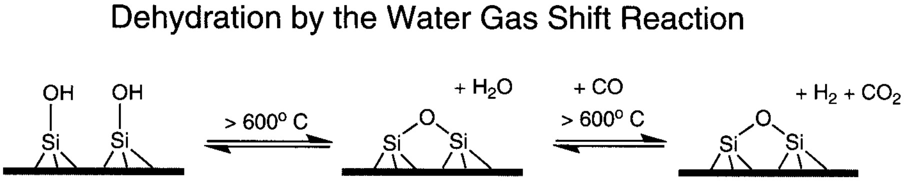

Scheme 10.16

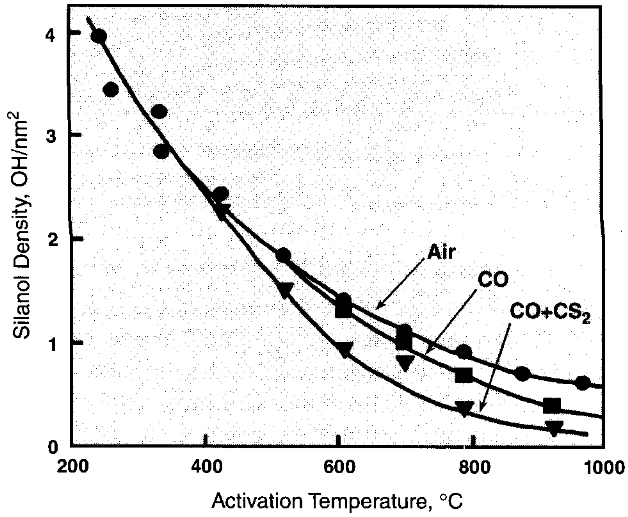

Figure 10.45 Hydroxyl concentrations on silicas treated in various gases at high temperature. Measurements made by reaction with CH_3MgI.

Sulfur compounds like COS or CS_2 are even more effective than CO for removal of hydroxyls and for improving the MI. Sulfur-containing reducing agents which do not contain carbon, like S, SO_2, or H_2S are ineffective. Again this is probably due to a variation of the water gas shift reaction producing CO or CO_2 and H_2S since sulfur is not left on the support. Table 10.4 shows the effect on MI of dehydration by chemical means. Silica–titania samples were calcined at 870 °C in various gases, then impregnated anhydrously with 0.5% Cr, and finally calcined in air at 650 °C to convert the chromium to Cr(VI). Only the support was exposed to the reducing treatment, not the chromium. Even so, CO treatment more than doubled the MI potential and COS improved it by a factor of 60. Activity was also increased.[363,364]

In the latter two examples in Table 10.4, the hydroxyls were replaced by halide groups.[57,365,366] Bromide and iodide were particularly interesting. Subsequent exposure to air at 600–870 °C then removed these groups by oxidation to I_2 or Br_2, which could be seen leaving the support as a colored vapor. This treatment yielded a highly dehydroxylated support which produced a powerful

TABLE 10.4 Dehydroxylation by Various Chemical Means

Treatment[a]	Melt Index
Air or N_2	2.5
CO	6.0
COS	150
CO + I_2, then air	12
CO + Br_2, then air	21

[a] Silica–titania was calcined at 870 °C in composition shown, impregnated with 0.5% Cr as dicumene Cr(0) in hexane, and then calcined in air at 300–600 °C.

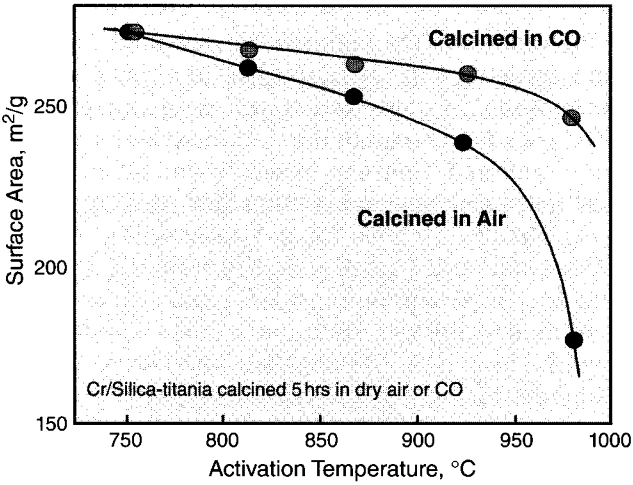

Figure 10.46 Carbon monoxide inhibits sintering.

promotional effect on MI.[124,364–366] Curiously some of the iodide is oxidized to a yellow-colored, highly reactive, and paramagnetic surface species. Reacting the silanol groups with silanes has also been reported to promote the chromocene catalyst.[367]

Calcining the support in carbon monoxide benefits the catalyst in another way too, by protecting it from sintering. Probably minute amounts of moisture in the gas stream during calcining encourage sintering at the high temperatures by acting as a flux, encouraging the opening and closing of Si–O–Si bonds. This water is probably evolved from the silica itself. When the support is calcined in carbon monoxide instead of predried air or nitrogen, sintering is shifted to higher temperatures. This is shown in Figure 10.46, where a loss in surface area indicates sintering. The protective effect of CO is most pronounced on samples being calcined close to the sintering temperature. Table 10.5 provides an example that contained high levels of titania, which also has

TABLE 10.5 Calcining in CO Protects High-Titania Cogels from Sintering

	Pore Volume (mL/g)		
Titania (Ti/nm^2)	Initially	CO, 870 °C	Air, 870 °C
0.4	2.64	2.48	2.43
0.9	2.90	2.76	2.61
1.1	2.58	2.37	1.78
1.5	2.55	2.33	1.59

a tendency to accelerate sintering. Here the pore volume was used as a measure of sintering. The porosity of high-titania samples was badly damaged by heating in air at 870 °C, but not when heated in CO.

Activation by Reduction and Reoxidation It is possible to obtain the benefit of the two-step anhydrous impregnation procedure described above without going to the expense and trouble of two activations or of using anhydrous solvents.[123,368] The trick is to separate the dehydroxylation step, in which high temperatures are preferred, from the oxidation and attachment of the chromium, in which low calcining temperatures are preferred. Starting with a silica–titania that already contains Cr, dehydroxylation is accomplished at 800–900 °C in CO. Under these conditions the chromium is in a reduced state, probably in islands or small crystallites, but not attached to the support in the desired way, and almost inactive. Then the catalyst is cooled to 300–600 °C, where it is exposed to dry air. This oxidizes the chromium to Cr(VI) and causes its attachment to the dehydroxylated support in the same way that happens through anhydrous impregnation. The result is a catalyst of greatly improved MI potential and often better activity too.

A strong promotional effect is obtained from a combination of chemical dehydration and two-step activation. As in the anhydrous impregnation procedure, raising the secondary oxidation step to high temperatures removes the promotional effect and restores the ordinary Cr(VI) catalyst. This again probably signifies that the chromium migrates back to the usual state. However, even when the final oxidation is at 870 °C, the MI obtained is still increased over that from a simple one-step activation in air at the same temperature due to enhanced dehydroxylation from CO.

This behavior is shown in Figure 10.47, in which a Cr/silica–titania was activated in three different ways. Catalyst series A was simply calcined in air at the temperatures shown. Series B was calcined in CO, then air, both at the temperature shown. The promotional effect on MI is due mainly to dehydration by CO because the temperature of attachment is identical to series A. Finally series C was calcined in CO at the temperature shown, then oxidized in air at 760 °C. It exhibits a double promotional effect, caused by dehydration in CO and also by the low temperature of attachment. Commercially, this type of activation is referred to as "reduction/reoxidation" or sometimes just R&R.[369–371]

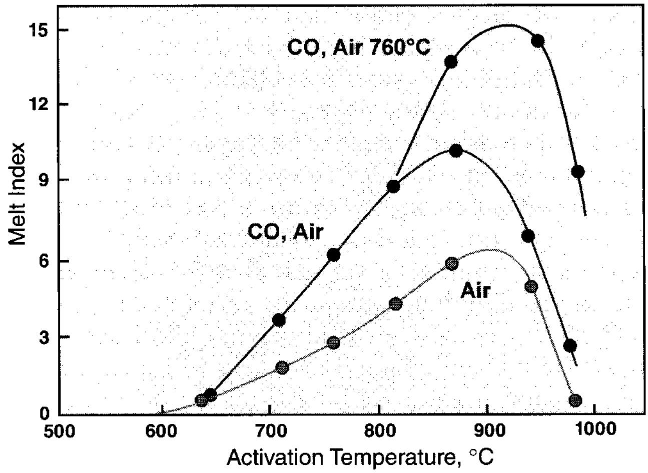

Figure 10.47 Three series using Cr/silica–titania: (*a*) calcined in air only; (*b*) calcined in CO, then air at same temperature; (*c*) calcined in CO at temperature indicated, then in air at 760 °C.

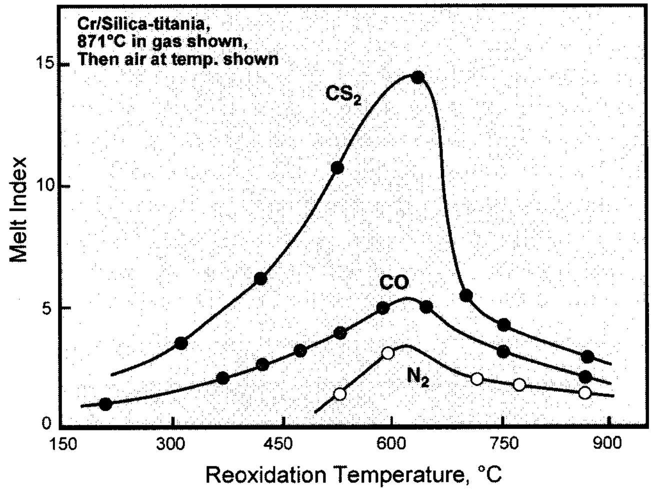

Figure 10.48 R&R activation in N_2, CO, or CS_2.

The optimum reoxidation temperature is illustrated in Figure 10.48. In this experiment the same Cr/silica–titania was calcined at 870 °C in CO, then reoxidized at the temperature shown. In this case the peak occurred at about 600 °C, but this can depend on the type of support and how easily oxidized the chromium is. If the reduced catalyst is left with large crystallites of α-Cr_2O_3 (detectable by X-ray diffraction) reoxidation at 760 °C or higher may be required. Above this peak the activity remains high, but the advantage of low-temperature attachment is lost, and the MI drops.

Sulfur compounds perform better than CO because they are better dehydrating agents, as shown in Figure 10.48. When Cr/silica–titania is reduced by CO+H_2S, COS, or CS_2, a black chromium sulfide forms.[124,372] Reoxidation then converts it back to the hexavalent oxide. The catalyst retains no sulfur, but it often takes on a new reddish hue and the activity and MI are greatly improved. The origin of the unusual red color is unknown; dichromate has been suggested as one possibility. It is noted that with increasing dehydroxylation the catalyst color changes from yellow to orange and then, for sulfided catalysts, to red. Adding water vapor to a sulfided catalyst completely reversed the benefit. Selenium and tellurium compounds performed similarly.[373]

Although much less effective, even nitrogen, which is also shown in Figure 10.48, can be used in this procedure. If one starts with a trivalent catalyst, such as $Cr(OAc)_3$/silica–titania, calcining in nitrogen at 900 °C dehydroxylates the surface and leaves the chromium as amorphous islands of Cr_2O_3.[124,374,375] Then air at 600 °C oxidizes and redisperses the chromium as Cr(VI), giving the promotional effect expected from low-temperature attachment onto a dehydrated surface. However, since nitrogen does not assist in the dehydration of silica as does CO or CS_2, a smaller promotional effect is obtained.

If the N_2 experiment is repeated but starting with a hexavalent catalyst, such as CrO_3/silica–titania, then calcining as before in nitrogen at 900 °C again generates Cr_2O_3, because Cr(VI) is not stable in the absence of oxygen. This time, however, large crystallites of α-Cr_2O_3 are obtained, because the crystallization is encouraged by even a trace of Cr(VI) to act as flux.[376,377] These crystallites are more difficult to reoxidize and consequently the optimum promotional effect is now found at 750 °C rather than at 600 °C. The higher temperature, of course, diminishes the magnitude of the effect.

Like anhydrous impregnation, the R&R activation technique is extremely sensitive to the presence of titania because, as noted above, the procedure is thought to maximize the Cr–Ti interaction. Figure 10.49 provides an example

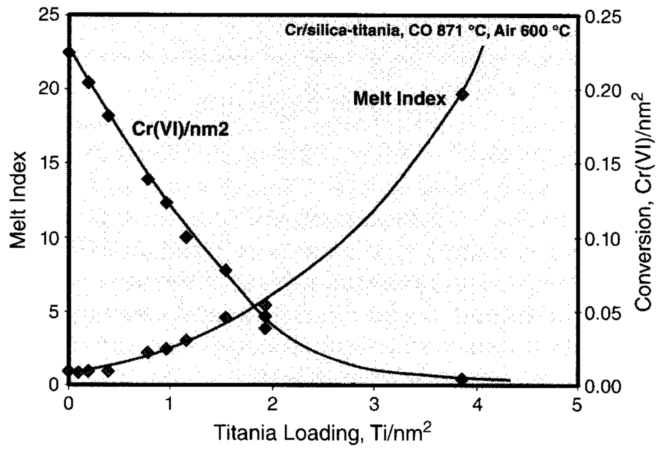

Figure 10.49 Effect of Ti loading on R&R activation.

of the MI response to titania. These catalysts were made by titanation of a Cr/silica base followed by activation at 871 °C in CO, then 600 °C in air. MI increases exponentially with titania level. Notice also that, as titania is increased, the stability of Cr(VI) in decreased so that at full titania loading hardly any Cr is reoxidized into the hexavalent state. This is another indication that the high-MI Cr(VI) species is thermally unstable. Despite the decreasing Cr(VI), however, the activity remained strong even approaching the highest loadings.

10.4.10 Treatment with Alkali Metals

Traces of alkali metals can promote sintering of silica by acting as a flux at high temperatures.[378,379] This is why silica manufacturers, who typically use sodium silicate as a feedstock, take great care to wash, or ion exchange, out the last traces of residual sodium ions. To fail to do so would be to risk sintering during calcinations. Typical specifications for polymerization-grade silicas call for less than around 0.1% Na_2O. The effect of sodium ion is to promote the making and breaking of Si–O–Si bonds, which increases the mobility of the structural elements. The higher the level of sodium (or other alkali metal ions) on the silica, the lower the temperature at which sintering is observed.

Thus it may seem strange that another way of promoting Cr/silica catalysts involves doping it with alkali metal ions. If done correctly, this treatment can enhance both activity and particularly the MI potential. It works because it causes the Cr/silica activity and MI curve of Figure 10.17 to be shifted to lower temperatures.[380–383] For example, the presence of 0.8 mmol of extra alkali metal per gram of catalyst shifts the sintering process and the polymerization response about 300–400 °C lower in temperature.

The response to alkali metal is shown in Figure 10.50, in which pore volume reflects the sintering process, and in Figure 10.51, which shows the MI response of those same catalysts. The activity response was much like the MI response.

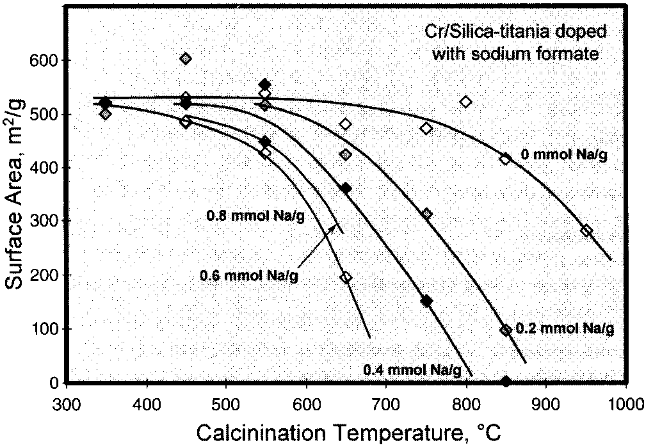

Figure 10.50 Surface area of Cr/silica–titania doped with sodium formate and calcined at various temperatures.

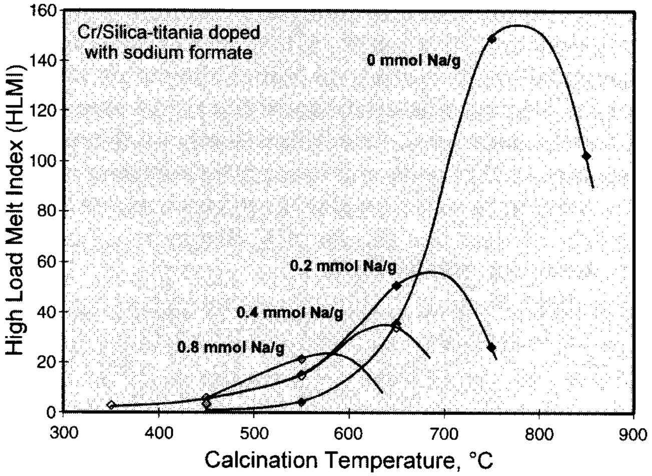

Figure 10.51 Melt index response of Cr/silica–titania doped with sodium formate and calcined at various temperatures.

Doping a Cr/silica catalyst with alkali metal followed by calcination at low temperatures yielded many of the same effects on porosity and polymerization performance that calcining the undoped catalyst has at higher temperatures. The shift in the MW distribution and the MI response as sintering is approached are observed in both cases. This response, like earlier observations, again suggests that some kind of silica annealing process occurs at the highest activation temperatures and that this process influences the chromium, probably by determining how it attaches.

There are also differences between sodium-induced and normal sintering. The maximum MI response to alkali metal at 600 °C does not come close to matching that of the undoped catalyst calcined at 850 °C. This may suggest that, although sintering is definitely enhanced by alkali ions, it may not be accompanied by exactly the same extent of dehydration that would result from higher temperatures. However, if the comparison is made at one temperature, 600 °C, then one can say that adding sodium significantly improves the activity and MI potential of the catalyst. There are occasions when this property can be useful.

10.4.11 Cr/Alumina

Chain transfer rates are extremely depressed on Cr/alumina, and polymers typically have average MW in the commercial "ultrahigh" (UHMW) range of 1–4 million when made in the absence of hydrogen. Perhaps this reflects its less acidic nature. The depressed termination rate is desirable for some applications, which require high MW, such as pipe and large part blow molding.[384] In contrast, Cr/silica is not well suited to make ultrahigh MW polyethylene. Figure 10.52 compares the MW distribution obtained from the three major

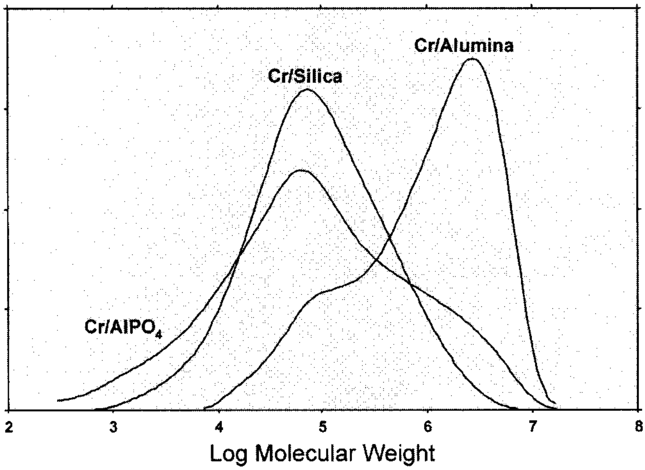

Figure 10.52 MW distribution from three catalysts (700 °C, reaction at 95 °C, 550 psig).

support types, Cr/Al_2O_3, Cr/SiO_2, and $Cr/AlPO_4$, all tested under the same conditions. Notice that Cr/Al_2O_3 yields much higher MW.

One major difference between Cr/alumina and Cr/silica is the sensitivity to hydrogen. Cr/alumina catalysts tend to incorporate hydrogen much more effectively, often producing low-MW waxy material along with a significant portion greater than one million. An example is shown in Figure 10.53, where the three catalysts, including Cr/alumina and Cr/silica, were tested alone and then again with hydrogen. Cr/alumina exhibits a major shift from very high to very low MW. This change is also detected by a large increase in the methyl-to-vinyl end-group ratio. When used commercially, Cr/alumina can also hydrogenate ethylene to produce small amounts of ethane.

Figure 10.54 shows the MW distribution from Cr/alumina doped with various modifiers. When tested in the presence of H_2, adding a sulfate to the alumina causes a loss of the lowest MW polymer, significantly narrowing the MW distribution and raising the average MW. Adding boria tends to increase activity and embellish the high-MW side of the MW distribution. Adding zinc oxide and magnesium oxide, on the other hand, shifts the distribution to the low-MW side. Phosphate greatly increases activity and introduces a low-MW peak, with corresponding increase in long-chain branching (LCB).[298,385] There are many other examples as well. It is curious that the MW distribution from Cr/alumina is so easily modified compared to Cr/silica, of which few examples are known. This may reflect the greater compatibility that the octahedral alumina lattice has with other metal ions compared to tetrahedral silica. It must be remembered that these runs had to be made with H_2 in the reactor in order to obtain reasonable MW for measurement. Consequently the observed responses in Figure 10.54 include changes in the sensitivity to H_2, as well as inherent MW changes.

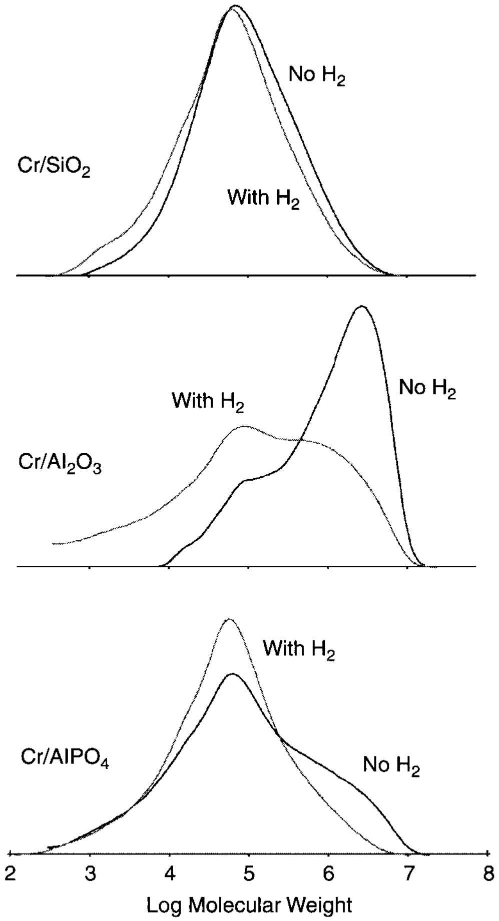

Figure 10.53 Effect of H_2 on MW distribution.

The alumina can also be treated with a layer of silica, which greatly increases its acidity and consequently its activity. Curiously these changes occur without a loss in molecular weight. That is, the polymer so obtained is not typical of Cr/silica but is more like Cr/alumina, despite the fact that most of the activity was the result of adding the silica. Figure 10.55 shows the unusual effect that a surface silica coating has on the MW distribution. It creates a second, very high MW peak. Since these runs were made with hydrogen in the reactor, it is possible that the silica-affected sites lost their ability to respond to H_2, in contrast to the alumina-associated sites. It is interesting that adding a small coating of silica to alumina had a different effect from adding Al^{3+} ions to silica. Both treatments increased activity, but while the former increased MW, the latter decreased it.

Like Cr/silica, treating Cr(VI)/alumina catalyst with carbon monoxide at 350 °C yields a catalyst with a substantial portion of the chromium coordina-

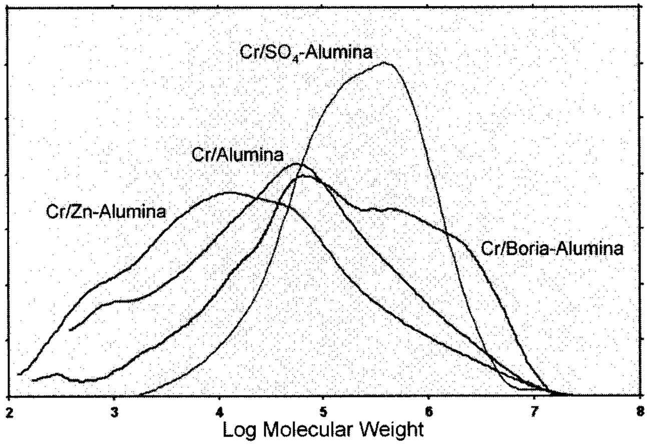

Figure 10.54 MW distribution from modified Cr/alumina (600 °C, reaction at 95 °C, 150 psi H_2, 8 ppm BEt_3).

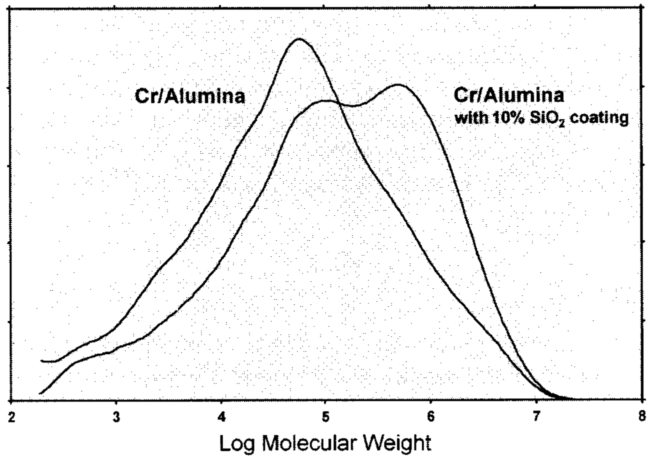

Figure 10.55 MW distribution from Cr on SiO_2-coated alumina (10% SiO_2, 600 °C, reaction at 95 °C, 8 ppm BEt_3, 150 psi H_2).

tively unsaturated and in the divalent state. The reduction is not as clean as on silica, however, and considerable Cr(III) is also obtained. The reduced catalyst exhibits chemiluminescence upon exposure to air, and the wavelength of light emitted, characteristic of oxygen, is not much different from that emitted by Cr(II)/silica.[252] Unlike Cr/silica, reducing Cr/alumina increases its (already higher) sensitivity to hydrogen as a chain-terminating agent. This results in a considerable amount of low-MW waxy material which can be the cause of excessive "smoke" during molding operations. An example is shown in Figure 10.56. Adding sulfate to the catalyst before activation and reduction removes this tendency and also removes most of the hydrogen sensitivity.

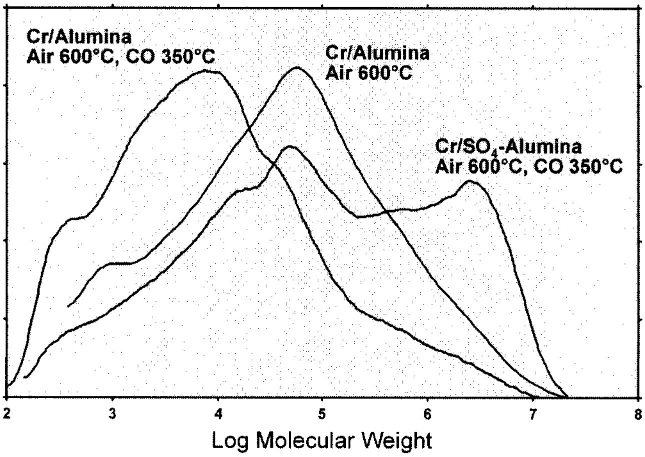

Figure 10.56 MW distribution from reduced Cr/Alumina (reaction at 95 °C, 8 ppm BEt_3, 150 psi H_2).

Alternatively the Cr/alumina catalyst can be given a "two-step" activation as described above in Section 14.4.9. For example, Cr/alumina can be calcined in carbon monoxide at 800 °C for several hours followed by reoxidation in air at 600 °C (the R&R activation procedure). Unlike Cr/silica–titania, when this treatment is performed on Cr/alumina, it has very little effect. The shape of the MW distribution is not changed significantly. Only a very slight shift to lower MW is observed.

10.4.12 Cr/AlPO$_4$

One of the more useful treatments that can be applied to Cr/alumina catalysts is impregnation of a small amount of phosphate. H_3PO_4 reacts with the alumina surface to create acidic phosphate groups that can affect the chromium in profound ways. Most notably it creates a low-MW peak that, if enough phosphate is added, can dominate the MW distribution. An example of this is given in Figure 10.57, which shows the GPC curves obtained from a series of Cr/alumina catalysts treated with varying amounts of H_3PO_4. The treatment is more effective if the alumina is calcined before contact with phosphate. This converts the original bohemite (AlOOH) or aluminum hydroxide into alumina (usually the γ-form). Notice in Figure 10.57 that only a small amount of phosphate is needed to produce the effect, indicating that the reaction is primarily with the surface.

The MW distribution from Cr/AlPO$_4$, compared in Figure 10.52 with silica and alumina, also reflects the different character in surface OH. The OH population measured by reaction with methyl magnesium iodide would seem to be slightly lower on AlPO$_4$ than on silica. Perhaps this is due to the presence of terminating P=O groups. Cr/AlPO$_4$ is somewhat more active than Cr/

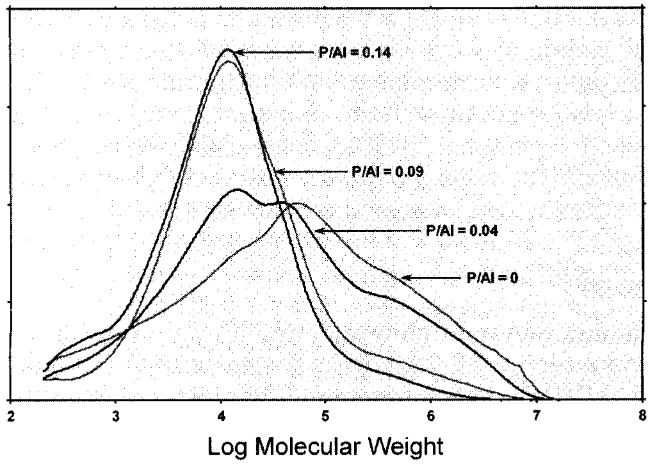

Figure 10.57 MW distribution from Cr/alumina treated with H_3PO_4 (650 °C, reaction at 100 °C, 8 ppm BEt_3, 150 psi H_2).

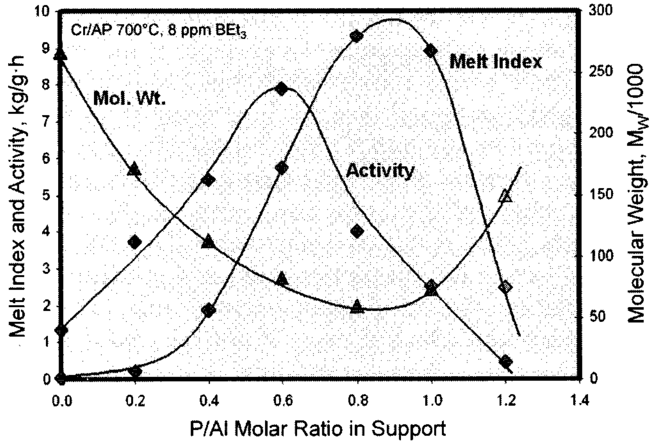

Figure 10.58 Melt index, inherent viscosity, and activity dependence on P/A1 ratio.

silica at the lowest calcining temperatures and is considerably more active than Cr/alumina. The saturation coverages for $Cr/AlPO_4$ appear to be very similar to that of Cr/silica at all temperatures. Activity and MI are similarly affected, as Figure 10.58 shows. The preferred P/Al ratio for polymerization-grade supports is usually 0.4–0.8, when the phosphate and aluminum ions are coprecipitated or cogelled into the structure. Highest activity occurs at around P/Al of 0.6–0.8. The chain transfer rate constant on chromium oxide sites varies with the local ligand field and geometry of attachment. Because the aluminophosphate surface contains a more varied assortment of hydroxyls than silica,[386] it also tends to produce a broader MW distribution, as shown in Figure 10.52.[201,221,387–389] This fact makes it useful in commercial operations, where a broad MW distribution can impart improved molding and better mechanical properties to certain applications. Melt index potential is dependent on the amount of phosphate in the support. The higher the P/Al ratio, the greater the MI potential of the catalyst. This is also shown in Figure 10.58 and suggests that Cr attached to phosphate produces lower MW polymer than Cr attached to aluminum ions. The activity of all the Cr/aluminophosphate catalysts also varies with activation temperature, much like Cr/silica catalysts.

10.4.13 Fluoride

Fluoride increases acidity on many supports, thereby changing the site population. It also interferes with chromium attachment to the surface, resulting in a diminshed Cr(VI) saturation coverage.[119] Because the early solution process polymerized ethylene at much higher temperatures than the current slurry process (125–160 °C vs 70–110 °C), catalysts of low MI potential were needed. Fluorided Cr/silica, activated at low temperatures, provided that benefit. It also provided a narrow MW distribution, producing polymers very similar to the narrow Ziegler polymers sold today. To accomplish this, fluoride probably decreases the heterogeneity of the site population by replacing coordinating ligands and by relieving surface strain. An example of the effect of fluoride is shown in Figure 10.59, where a series of Phillips catalysts were treated with varying levels of $(NH_4)_2SiF_6$ and then calcined at 540 °C before being tested in a solution process at 120–140 °C. The HLMI/MI ratio of the resultant polymer, or shear response, is plotted against its MI. Shear response is an indication of elasticity, and the lower shear response brought about by the addition of fluoride is the result of it narrowing the MW distribution. This influence is highly valued for injection molding resins, because melt elasticity can introduce stresses into the flowing polymer that become frozen into the solidified molded item. Such stresses, if not relieved during cooling, can

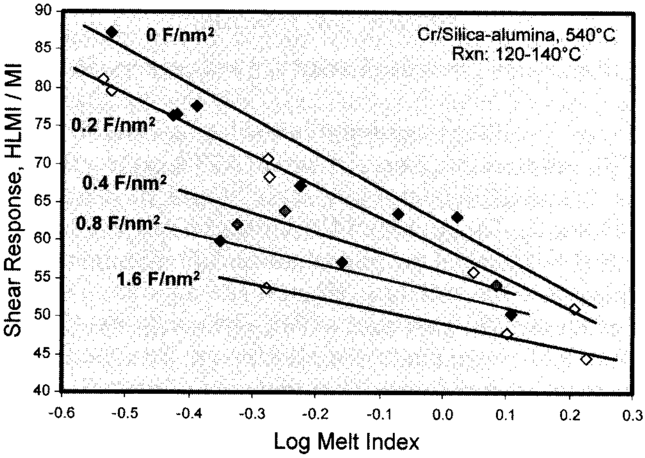

Figure 10.59 Effect of fluoriding on shear response.

cause warpage of the item. A narrow MW distribution tends to minimize such frozen-in stresses by reducing the number of very long chains. These longest chains introduce stress during flow and resist melt relaxation during cooling. Polymers made from fluorided catalysts used in the slurry process also display a slightly narrower MW distribution.

Adding fluoride to a Cr/silica–titania catalyst made by the two-step method of activation described above, which normally produces extremely high MI polymer, completely destroyed the MI enhancement. For example, a catalyst was made by impregnating titanium isopropoxide onto silica to equal 8.3% titania. It was calcined at 820 °C, anhydrously impregnated with 0.5% Cr, then activated in dry air at 315 °C. When tested the catalyst produced a 77 MI polymer, which compares to only 0.4 MI when the same catalyst was made but without titania. Then 1% ammonium hexafluorosilicate was dry mixed with the titanated catalyst to equal 1% of the mixture, and it was reactivated in air at 315 °C. When retested, it produced only a 0.54 MI polymer, equivalent to the nontitanated catalyst. This is taken as evidence that fluoride becomes attached to the titania, displacing the Cr from this special, perhaps unstable, type of Cr bonding to the titania.

10.4.14 Adding Cocatalysts to Broaden MW Distribution

Another common reason for employing cocatalyst is not to improve activity but rather to tailor the polymer MW distribution.[390–395] There is evidence that some cocatalysts may activate sites that would not ordinarily become active under the conditions chosen. This may be due to assistance in reducing Cr(VI), or in alkylation, or by removal of ligands from the coordination sphere (surface OH or oxide groups, redox by-products, etc.). For example, catalysts activated at low temperature (500–600 °C) and run at low temperature (say 80–90 °C) often come on stream very slowly, and the kinetic profile may not have fully developed the maximum possible rate by the time the catalyst is discharged from the reactor (usually after about an hour). Adding a cocatalyst accelerates the reduction and activation of those slow sites. As noted above, those sites that are most difficult to reduce also produce the highest MW polymer. Thus, adding cocatalyst activates high-MW sites that might otherwise contribute little or nothing to the total polymer. Consequently the MW distribution is often significantly embellished on the high-MW side.

Sometimes the MW distribution continues to broaden as the cocatalyst concentration in the reactor is increased even after the maximum activity is achieved. In such cases it is clear that the cocatalyst is doing more than activating reluctant sites. Chemical modification of sites by the cocatalyst is a possible explanation, such as an attack on the Cr–O–Si surface attachments. Another mechanism has been proposed for boron cocatalysts which can embellish the low-MW side of the distribution. The mechanism must involve some very specific (perhaps acidic) sites because the effect is most pronounced with Cr/silica–titania or Cr/aluminophosphate but less with Cr/silica or Cr/alumina. Two possible explanations have been proposed, both relating to those more reactive sites associated with titania or phosphate, which already have a tendency to produce fairly low MW polymer.[42,220,274] One is that the boron adsorbs onto the site, perhaps breaking one link to the surface and alkylating it, and thus influencing its behavior.

Alternatively, it is possible that these sites participate in an alkyl exchange between boron and chromium, which would prematurely terminate the growing chain and enhance the low-MW side of the distribution. However, this would take the boron out of solution along with the polymer chain. Since the amount of boron in the reactor is negligible compared to the number of polymer chains formed, BEt_3 would be quickly exhausted. However, one can further postulate that the boron–polymer bond then exchanges with ethylene in the reactor to regenerate the original soluble BEt_3 cocatalyst. Thus the mechanism would be catalytic, consuming and regenerating triethylboron (Scheme 10.17). If true, this would be another termination mechanism, prematurely shortening polymer chains and broadening the MW distribution on the low-MW side.

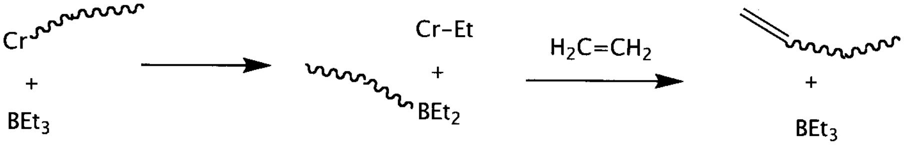

Scheme 10.17

An example of the effect of cocatalysts on MW distribution is shown in Figure 10.60. A 600 °C Cr/silica–titania was run first without cocatalyst, then with triethylaluminum, and finally with triethylboron. Notice that the distribution is broadened on both sides when a cocatalyst is used and that BEt_3 has a greater effect than $AlEt_3$ on the low-MW side. When the catalyst is activated at a high temperature, such as 800–900 °C, the low-MW embellishment is

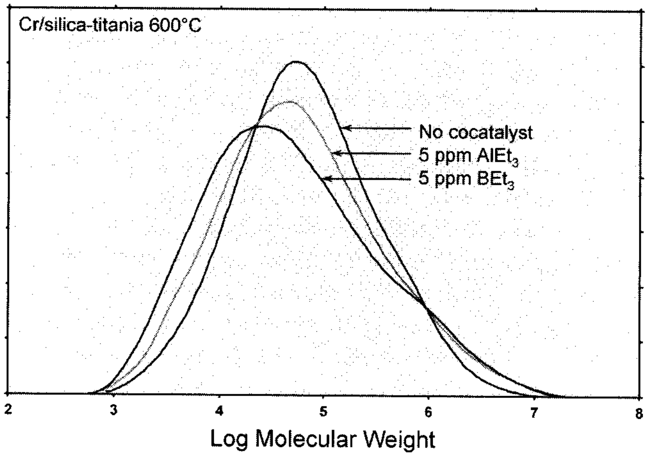

Figure 10.60 Effect of cocatalyst on MW distribution.

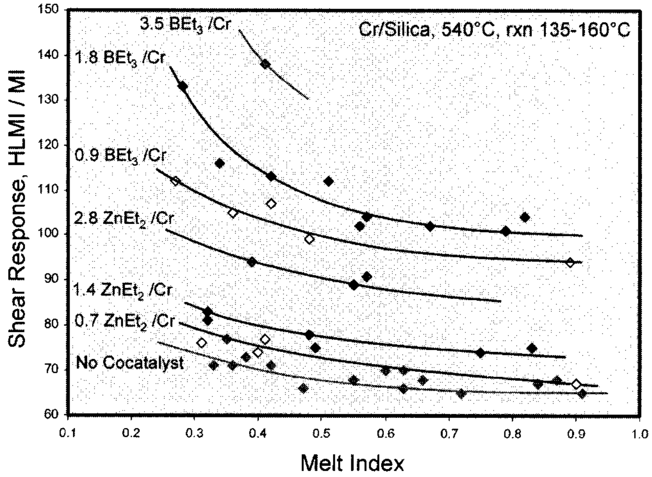

Figure 10.61 Effect of cocatalyst type and amount on shear response.

not as pronounced. Likewise when the catalyst contains no titania, the effect is also diminished. This suggests that the alkyl exchange, or whatever mechanism is responsible for low-MW embellishment, occurs mainly on certain low-MW-producing sites, such as those associated with titania at low activation temperature.

Broadening the MW distribution through the use of cocatalysts is a very useful commercial method of enhancing polymer quality. Broadening means that the polymer becomes more "shear thinning"—that is, the molten polymer flows more easily when molded under pressure. As an example of this behavior Figure 10.61 shows this shear-thinning ability, or shear response (HLMI/MI is one measure), plotted against the MI. Reactor temperature was varied to yield an assortment of polymers having different molecular weights (or MI values) under certain conditions. First the Cr/silica catalyst was run without cocatalyst, then it was tested again with different levels of diethylzinc and triethylboron cocatalyst. One can see that the zinc alkyl increases the shear response, but not as much as the boron alkyl. In fact, the highest level of zinc used (~3 Zn/Cr) was not as effective as the lowest level of boron used (~1 B/Cr).

As noted above, the increased breadth of the MW distribution also means that the polymer physical characteristics are often improved. This includes toughness, impact, and tear resistance in film, creep and hoop stress resistance in pipe, and ESCR in blow molding. This is most often the main reason for adding cocatalyst to the reactor, and it can be a very useful way of controlling product quality. An example of the effect these same two cocatalysts have on the ESCR is shown in Figure 10.62. Again Cr/silica was tested without cocatalyst and again with different levels of diethylzinc or triethylboron cocatalyst. These were copolymers of 0.950 density. ESCR is plotted against HLMI because ESCR is highly dependent on MW. One can see that for a given

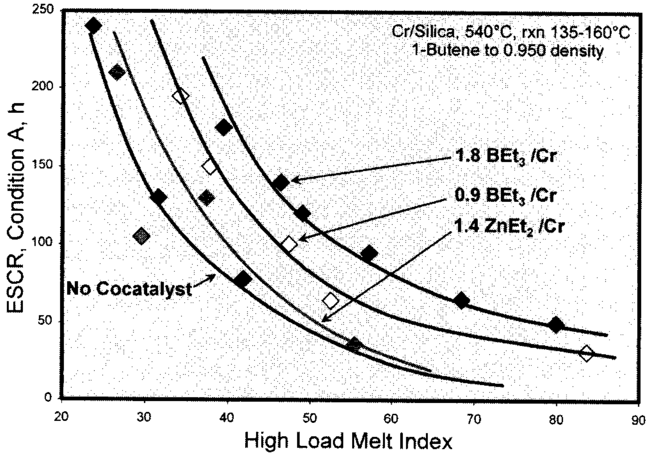

Figure 10.62 Effect of cocatalyst type and amount on ESCR.

HLMI (which is usually specified by the molding application) polymers made with cocatalyst in the reactor offer higher ESCR. And again boron seems to be much more effective than zinc.

One can also see these effects in Figures 10.21 and 10.22. Notice that MI goes through a minimum with BEt_3 in Figure 10.21 with increasing cocatalyst amount. This is the effect of the alkyl exchange at high BEt_3 concentrations embellishing the low-MW side of the MW distribution. Clearly the alkyl exchange effect cannot become significant until the redox reaction has taken place. Now consider Figure 10.22. The minimum in MI does not appear with $AlEt_3$ or $ZnEt_2$. The HLMI continues to drop even out to Al/Cr = 35. $AlEt_3$ does not have the same effect on the low-MW side.

Catalysts based on triphenylsilyl chromate ester instead of chromium oxide (see Section 10.3) behave in much the same way. After adsorption of the triphenylsilyl chromate they must be reduced by treatment with an aluminum alkyl, often $AlEt_2OEt$. These catalysts usually provide a broader MW distribution than simple catalysts made from chromium oxide on silica, and the two types are often contrasted.[139] However, the additional MW breadth is the result of the cocatalyst addition, rather than the use of bis-triphenylsilyl chromate. Catalysts made from chromium oxide on silica can be similarly impregnated with such cocatalysts and they then produce the same broad MW distribution.[396]

Figure 10.63 shows the change in MW distribution obtained from $Cr/AlPO_4$ catalyst when triethylborane was added as cocatalyst. BEt_3 cocatalyst greatly enhances the activity. The curves in Figure 10.63 have been normalized according to the activity of the catalyst, so that one can see where the extra polymer from BEt_3 is added. The high-MW part of the distribution is mostly unaffected, whereas the low-MW part is greatly enhanced. This suggests that it is the phosphate-associated sites that are most affected by the cocatalyst.

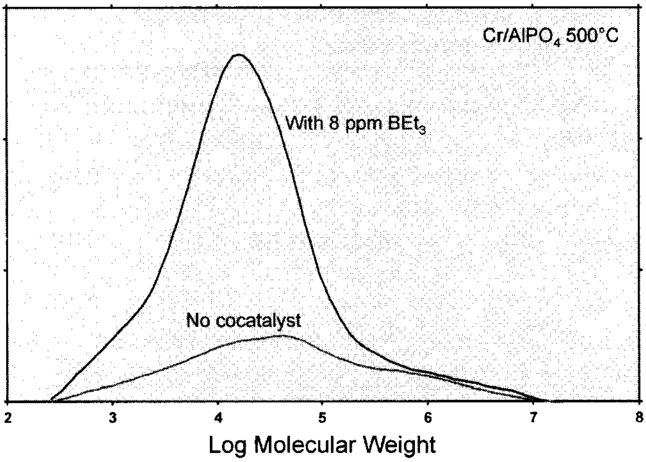

Figure 10.63 MW distribution from Cr/AlPO$_4$ run with and without BEt$_3$ cocatalyst (normalized by activity).

10.5 CONTROL OF CRYSTALLINITY

10.5.1 Copolymerization Mechanism

Most commercial grades of polyethylene are actually copolymers of ethylene and other α-olefins. Comonomers, such as 1-butene, 1-hexene, 1-octene, and 4-methyl 1-pentene are commonly used in commercial polymers in the 0–5 mol % range to add side branching to the otherwise linear polymer chain. Such branching decreases polymer crystallinity and thereby increases flexibility, toughness, and other mechanical properties.[6,30,31,397–402] As the crystallinity decreases the density of the polymer also decreases, and in commercial operations the amount of comonomer incorporated is typically monitored by measuring the density.*

Insertion usually occurs almost entirely in a 1,2-orientation, as evidenced by (1) the lack of head-to-tail orientation of branches in the NMR and (2) the appearance of vinylidene end groups, but little internal unsaturation, when 1-hexene is added to the reactor with ethylene.[29–31,354] The preference for 1,2-insertion is usually attributed to steric restrictions around the site. However, another possibility is an electronic preference dictated by the dipole moment of 1-hexene and the polarization of the Cr–polymer bond.

Secondary olefins like 2-butene are not incorporated well and may even tend to retard polymerization. Neither does isobutene react well, nor α-olefins with a branch in the 3-position.[403] An example of the difference in reactivity

*Neither is density a perfect indicator of branching, because molecular weight and MW breadth can also affect it to a lesser degree. These variables must be held approximately constant for the relationship between density and branching to strictly hold.

TABLE 10.6 Reactivity of Various α-Olefins (At 5 mol % Ethylene Feed)

Comonomer	Density
None	0.963
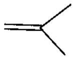	0.965
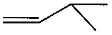	0.945
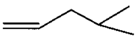	0.941
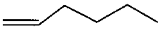	0.935

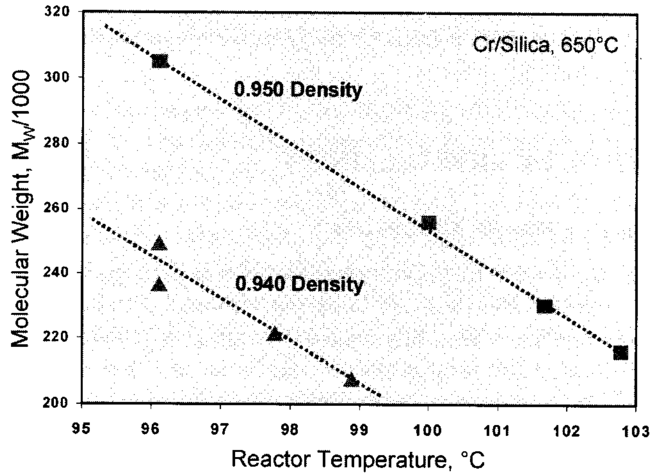

Figure 10.64 Influence of reactor temperature and 1-hexene on molecular weight (M_W).

of the various olefins is shown in Table 10.6. As more of the olefin is incorporated, the density of the resin drops.

Once inserted, comonomer tends to increase the chain transfer rate, as indicated by lower MW, and a disproportional amount of vinylidene end groups. Beta-H elimination is thought to be more easily accomplished from the tertiary carbon of an incorporated branch, rather than the secondary carbon of a linear chain (see Scheme 10.18).[29–31,404] An example is shown in Figure 10.64, where the MW from Cr/silica is plotted against reactor temperature for two branching levels. The more comonomer that is added (lower density), the lower the M_w. Sometimes activity is also enhanced slightly by comonomer owing to the increased ability of higher olefins to reduce Cr(VI)/silica.[29–31,400,404]

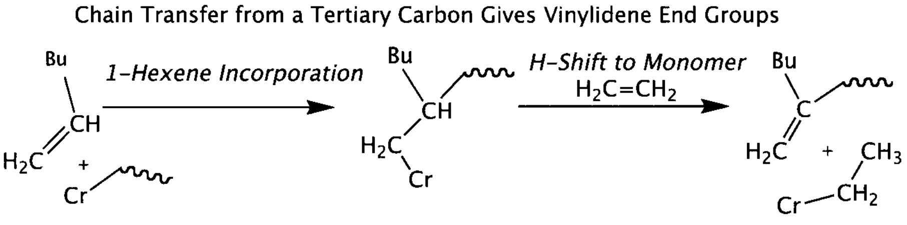
Chain Transfer from a Tertiary Carbon Gives Vinylidene End Groups

Scheme 10.18

Table 10.7 shows a typical end-group analysis and how this composition is changed by the presence of comonomer. Three polymers were made from Cr/silica–alumina catalyst having approximately the same average MW. In the first case only ethylene was added to the reactor so that homopolymer was obtained containing only methyl and terminal vinyl groups in approximate equal amounts, corresponding to polymer molecules of the formula $CH_2{=}CH{-}(CH_2)_n{-}CH_3$. The second polymer was made by adding propylene to the reactor along with ethylene. Reactor temperature was lowered to maintain approximately the same molecular weight. Now one can see a sharp increase in methyl groups from branches due to propylene incorporation. Vinylidene groups now appear as well, indicating that for many chains propylene was the last monomer added before termination. That propylene was added strictly in a 1,2-orientation is indicated by the lack of internal unsaturation. The number of terminal vinyls actually decreased due to the lowered reactor temperature (maintaining approximately the same amount of total unsaturation). In the third example the reactor temperature was lowered further and still more propylene was added to the reactor. The same trends noted above were found

TABLE 10.7 Infrared Analysis of Three Polymers of Similar MW from Cr/Silica-Alumina

	All Methyls, 1000 °C	All Double Bonds, 1000 °C	Percent of Total Unsaturation		
			Term-vinyl	Trans-internal	Vinylidene
Monomer	$-CH_3$	C=C	$H_2C{=}CH$∿	$\mathrm{R(H)C{=}C(H)R}$	$H_2C{=}C(R)$∿
Ethylene	1	0.8	98	<2	<1
Ethylene–propylene	25	0.7	85	<2	15
Ethylene–propylene	44	0.8	75	<2	25

Source: From J. P. Hogan, in G. E. Ham, Ed., *Copolymerization*, Vol. 18, Interscience Publishers, New York, 1964, Chapter 3.

to continue. Once propylene is added to the reactor, one would expect (from a statistical view) to find a certain number chains ending with propylene. However, the number of vinylidene ends, relative to the amount of propylene in the reactor, indicates a preference for ending the chain with propylene. That is, once incorporated, propylene has a stronger tendency to terminate the chain than ethylene. This is why the reactor temperature had to be lowered to maintain a similar MW.

The primary commercial use of the Phillips catalyst is for the polymerization of ethylene and α-olefins with ethylene. Nevertheless other olefins can also be homopolymerized over Cr/silica, although their reactivity is much lower than that of ethylene. This includes acetylenes[226,227,250] and various branched and unbranched α-olefins, such as propylene, all butenes, 1-pentene isomers, and 1-hexene.[1,6,30,405–413] For example, Cr/silica–alumina polymerizes 1-hexene at about 1% of the rate that ethylene reacts. Although Phillips catalysts do not provide a high level of stereoregulation, they do produce a significant proportion of isotactic polymer. Like Ziegler–Natta catalysts, certain adjuvants can be used with Cr/silica to improve the stereoselectivity.[414]

10.5.2 Incorporation Efficiency

α-Olefins incorporate into the PE chain with less reactivity than ethylene, so that much higher concentrations of α-olefin than ethylene are required in the reactor to achieve a similar level of incorporation. For example, equal molar concentrations of ethylene and 1-hexene in the reactor may result in only 2–3 mol % 1-hexene in the polymer. Nevertheless, the incorporation of α-olefins into polyethylene is also usually considered to be first order in olefin, so that the amount of branching incorporated is dictated by the comonomer/ethylene ratio of concentrations in the reactor.

Originally 1-butene was the most widely used comonomer for linear PE, but today 1-hexene is preferred with Cr/silica catalysts because the longer branch length generally gives better polymer properties. Different chromium catalysts display widely different reactivity to 1-hexene. For example, Cr(II) incorporates it quite well, and several times better than similar Cr(VI) catalysts, implying that the two are not entirely identical. Both Cr(VI) and Cr(II) are much better than common Ziegler catalysts. In contrast, chromocene catalysts almost completely reject 1-hexene under ordinary commercial conditions. Whether these differences are due to steric or electronic variations at the active metal is uncertain. Steric factors are most often cited, particularly for metallocenes. However, in addition to the larger size of the comonomer, the higher polarity of the α-olefin double bond, relative to ethylene, could also serve as a basis for discrimination. By that reasoning it would be expected that catalyst environments that place more positive charge on the metal, such as through strained bonding (or tight metallocene bridging), could be better at comonomer incorporation.

Incorporation efficiency is also influenced by the polymerization process. In gas-phase processes, for example, hexene incorporation is usually more efficient than in a slurry-phase reactor being run with the same catalyst at the same reactant concentrations and at the same temperature. This is thought to be due to the fact that hexene dissolves or condenses in the amorphous polymer phase and is therefore partitioned more favorably between the vapor and the polymer in a gas-phase reactor than between the hydrocarbon solvent and the polymer in a slurry-phase reactor. This partition can greatly affect local concentrations around the site and therefore it can affect perceived incorporation efficiency. In fact the local concentration of hexene near the active site can be much higher than exists in the reactor as a whole.

10.5.3 Comonomer Distribution

Another consequence of the diversity of active sites on Cr/silica is that those more reactive sites which come on stream first and produce lower MW polymer are also more efficient at copolymerization of hexene. Coincidentally, when these sites accept comonomer, the chain transfer rate is further increased due to the increased level of tertiary hydride. The result is that ethylene–hexene copolymers made over Cr/silica have a tendency for the hexene to be disproportionately represented in the low-MW side of the MW distribution. Ziegler catalysts also share this natural tendency and without proper tailoring can be much worse than Cr/silica.

Unfortunately the preferred orientation for polymer properties is to place the branching in the opposite pattern in the high-MW side of the distribution. Concentrating the branching on the longest chains tends to force them selectively into the amorphous regions of the polymer, where they can serve as "tie molecules" bridging the different crystalline regions and holding them together. It is from these tie molecules that the polymer derives its toughness and environmental stress crack resistance. Reversing this natural tendency of branch placement is what "bimodal" technology has accomplished by sequentially allowing the catalyst to progress through two reaction zones in which the MW and branching levels are deliberately manipulated in a two-step reaction.

Figure 10.65 shows a branch profile of two ethylene–hexene copolymers derived from two Cr/silica catalysts.[415,416] It plots the short-chain branching (SCB) concentration, in branches per 1000 carbons, within each segment of the MW distribution. These two polymers were made from Cr/silica activated at 600 °C and at 900 °C, each run under identical conditions, resulting in a density around 0.935. Also shown in the plot is the GPC curve for each polymer. One can see in the chart that for both polymers the branching is concentrated into the low-MW side of the distribution.

One can also see in Figure 10.65 that the catalyst activated at 900 °C incorporated a little more 1-hexene than the one activated at 600 °C, although both have a similar pattern. In fact, it is interesting to break down the MW

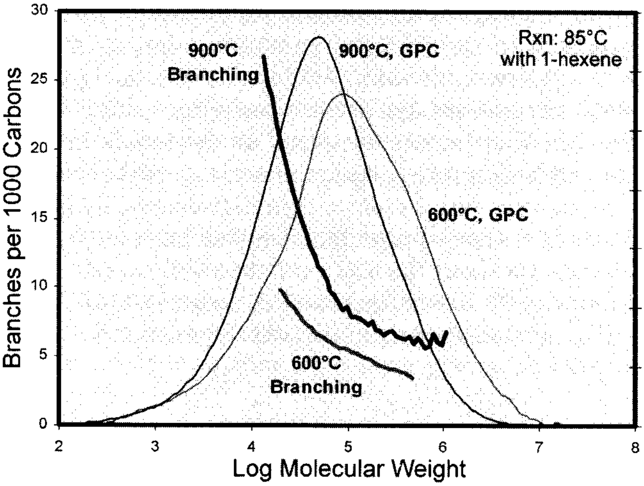

Figure 10.65 GPC with branch profiles from Cr/silica.

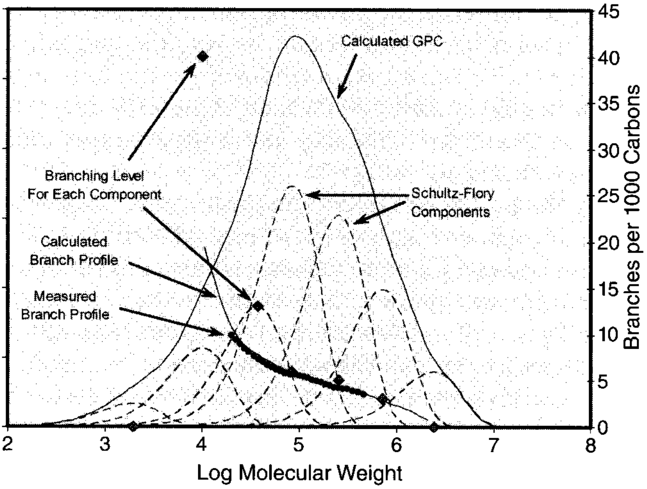

Figure 10.66 Deconvolution of MW distribution into seven Schultz–Flory components.

distribution from the 600 °C catalyst into seven Schultz–Flory (single-site) distributions of PDI = 2.0, as would be produced by seven types of active sites, as shown in Figure 10.66. This is not to suggest that there are actually seven types of sites but rather that seven is the minimum number needed to faithfully represent the observed MW distribution. Then branching content was assigned to each of these components in order to reproduce the observed overall branch profile from the 600 °C catalyst. These levels are also shown in Figure 10.66. Having done this, one then finds that the MW distribution and the

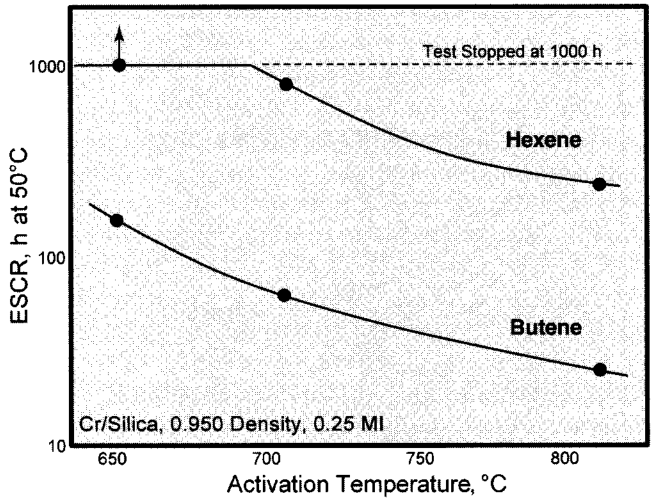

Figure 10.67 Dependence of ESCR on activation temperature.

branch profile from the 900 °C catalyst can be synthesized from those same components by only changing the amount of each. Stated another way, higher activation temperature does not seem to create completely new site types but only repopulates some of the existing site types at the expense of others.

As a result of this redistribution of sites, lower activation temperatures are often preferred commercially for producing superior polymer physical properties, including film puncture and tear resistance, and crack and creep resistance in blow molding and pipe resins. An example is shown in Figure 10.67, which plots the resistance to chemical attack (ESCR) of ethylene–butene and ethylene–hexene copolymers made from Cr/silica catalyst activated at various temperatures. At constant MI and density, the ESCR decreases as the activation temperature is raised. This is in part because the MW distribution is narrowed and also because of the change in branch distribution.*

Sometimes additives applied to the catalyst or to the reactor can change the branch profile. This no doubt results from a modification of the active-site distribution. An example is shown in Figure 10.68, where methanol was added to the reactor as a poison to titrate the activity of an 850 °C Cr/silica–titania catalyst. The activity of the catalyst and the MI of the polymer obtained are plotted against the amount of methanol added to the reactor. As methanol killed active sites, activity decreased and the MI also dropped significantly. As noted above, this suggests that some sites, the more reactive sites that produce low-MW polymer, were to some degree preferentially poisoned first. Actually these polymers were ethylene-hexene copolymers and the density is also plotted in Figure 10.68. The density increased as methanol was added to the

*A third reason is the increasing long-chain branching brought about by higher activation temperature (see Section 10.6).

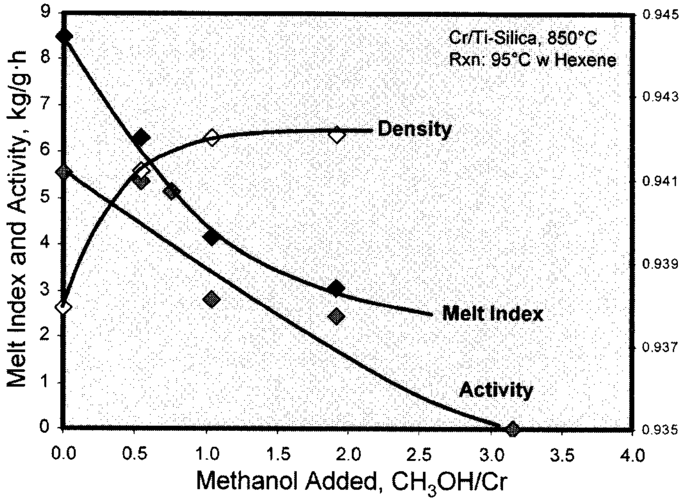

Figure 10.68 Effect of poisoning by methanol.

reactor, which would be another indication that the low-MW-producing sites, those that also incorporate most of the hexene, were to some extent poisoned first.

In recent years much industrial research has gone toward finding ways of reversing this natural tendency to put branching in the low-MW side of the distribution. Certain chromium catalysts and treatments have been discovered that do provide a flat branch profile, showing little or no preference for either side of the MW distribution.[384]

Another type of branch distribution is called "blocking," which is illustrated in Scheme 10.19 below. Each branch off the linear backbone disrupts crystallization and thus lowers polymer density. However two neighboring branches are no more effective than one isolated branch. This is called blocking and is usually regarded as undesirable, first because the comonomer is wasted and second because a high degree of blocking is often associated with poor polymer performance. Blocking is most critical in the lowest density resins, around 0.92, which are most often used in film applications.

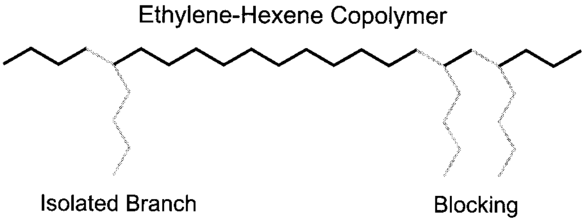

Scheme 10.19

Blocking is measured by ^{13}C NMR. The measured number of blocked branches is then compared to the number of paired branches predicted from a purely random statistical distribution of the same number of branches. A branch dispersion index (BDI) of 100% indicates that the branch distribution is random. However, most commercial polymers have a BDI of less than 100%,[417] which unfortunately means that they contain more blocking than a statistical distribution would deliver. In other words, this would seem to indicate that Cr/silica catalysts have a natural preference to create blocks of branches.

But this would also seem to contradict the known chemistry of Cr/silica catalysts. Even the catalysts that incorporate hexene most willingly still have a natural reluctance to incorporate hexene versus ethylene. In fact, one can get an idea of the relative rates of monomer sequence additions by measuring incorporation rates during the production of various polymers. For example, 1-hexene homopolymerization may be up to two orders of magnitude slower than ethylene homopolymerization, indicating that the addition sequence E–E is much faster than H–H. Likewise the E–H rate can be estimated by adding small amounts of hexene into a primarily ethylene polymerization. The E–H rate is usually found to be intermediate between E–E and H–H. Calculation of these "reactivity ratios" makes it very clear that Cr/silica should have a preference for producing isolated, not blocked, hexene incorporation. Therefore, contrary to what is actually found from most commercial polymers, one should never find more than the statistical amount of blocking from any one chromium site.

This dilemma is resolved if one remembers that Cr catalysts contain a variety of site types. The real reason for the BDI to be less than 100% comes from the branch distribution across the MW distribution. If a polymer concentrates most of the branching into the low-MW fraction, then the BDI will usually be <100% (high blocking) because there are more blocks than would be expected in a uniform distribution having the same branch content. This is true even though each individual site may yield a BDI equal to or higher than 100%. In other words, it is a mathematical artifact.[418] The well-known correlation between blocking and poor physical properties is therefore not a result of blocking itself, because blocking probably has no effect whatever on physical properties when compared at similar density. Instead it is because of the tendency of blocking to indicate a high degree of branching in the low-MW side of the distribution, which is definitely known to be harmful to physical properties when compared at the same density, because of its connection with tie molecules.

10.5.4 Branch Length

Each branch from incorporated 1-butene or 1-hexene is almost equivalent in its ability to disrupt crystallinity. Nevertheless, there is a clear advantage by incorporating the longer branch from hexene even when compared at identical

TABLE 10.8 Effect of Branch Length on Environmental Stress Crack Resistance

Comonomer	Melt Index	Density (g/mL)	ESCR (Bell Lab., 50%)
Propylene	0.32	0.937	250
1-Butene	0.31	0.937	435
1-Pentene	0.27	0.940	600
1-Hexene	0.30	0.940	>1000
1-Octene	0.29	0.939	>1000

crystallinity. Polymer properties are enhanced. This becomes evident, for example, in increased tear resistance in film or increased creep resistance in pipe (ductile distortion from cold flow under pressure) or increased resistance in bottles to impact or to chemical attack (ESCR). An example was shown in Figure 10.67. Further lengthening of the branch by copolymerization of 1-octene gives additional improvement, although not as large as the change from butene to hexene. An example of the dependence on branch length is shown in Table 10.8, where copolymers were made from Cr/silica to have the same approximate density and MI. Different comonomers were used, ranging from propylene to 1-octene. The ESCR of each polymer was then determined. There is a clear advantage for longer branch length. Although not documented in the table, a small increase in properties is also usually seen on going from ethylene–hexene to ethylene–octene polymers.

Unfortunately, such comparisons usually suffer from some uncertainty because they normally compare resins made with different comonomer but from different catalysts and even under different processes (gas-phase vs. solution process). Furthermore, 1-octene is incorporated more reluctantly than 1-hexene, and that more reluctantly than 1-butene, each requiring more in the reactor to achieve a similar incorporation. Even on the same catalyst, not all sites respond to different comonomers to the same extent. Therefore changing the comonomer may also change the comonomer distribution slightly, further confusing the comparison. One way of clarifying the question is to use a "single-site" catalyst such as metallocene, where the branch distribution is constant. A definite benefit is again seen on going from 1-butene to 1-hexene, and an additional benefit, although smaller, is also seen on going from 1-hexene to 1-octene comonomer.[419,420] Thus, there is a real advantage for the longer branch length in itself. To date, this response has not been adequately explained in terms of polymer mechanics.

10.5.5 Influence of Titania on Copolymerization

Adding titania to a catalyst, particularly one activated at lower temperature, decreases hexene incorporation (raises density). An example of this typical response is shown in Table 10.9, where a Cr/silica catalyst was treated with different amounts of titanium ester and calcined at 550 and 650 °C. Each run

TABLE 10.9 Density of Copolymers from Titanated Cr/Silica Catalysts

Ti Content (%)	550 °C	650 °C
0	0.9395	0.9384
2	0.9448	0.9471
3	0.9469	0.9478
6	0.9501	0.9483

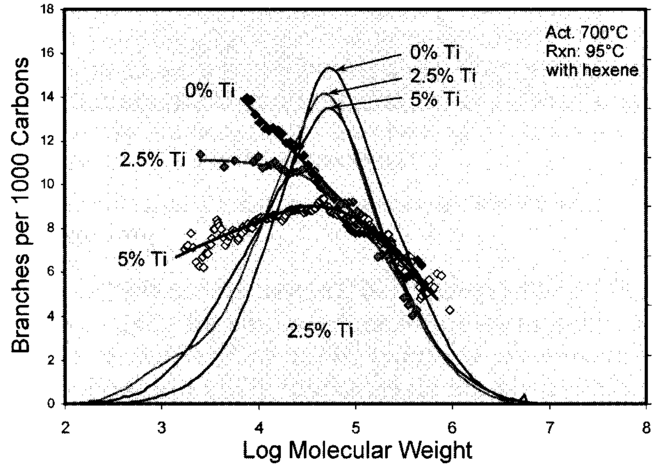

Figure 10.69 Branch profiles from three catalysts varying in titania.

was made at 85 °C, 450 psig, and 50 mL hexene. Notice that, as the titania was increased, less hexene was incorporated, causing the rise in resin density.

Although one might first think of less efficient hexene incorporation as a disadvantage, it is actually a positive trait for resin producers. This is because the addition of titania promotes polymer properties for two reasons. First it broadens the MW distribution, as noted above. Second, and at least as important, it inhibits hexene incorporation by the sites that are associated with titania. Since these sites are concentrated in the low-MW side of the distribution, this has the effect of stopping the usual high concentration of branching in the low-MW side. An example is given in Figure 10.69, which shows the branch profiles from three catalysts of varying titania content, all activated at 700 °C. As titania is added, incorporation in the low-MW end is retarded, causing a flattening of the overall branch profile. It is this flattening of the branch profile at the low-MW end that is responsible for the well-known density response of titania-containing catalysts shown in Table 10.9.

Another example of branch profiles from Cr/silica–titania catalysts is shown in Figure 10.70 where a catalyst containing 2.5% Ti was activated at three different temperatures. First consider the polymer made from

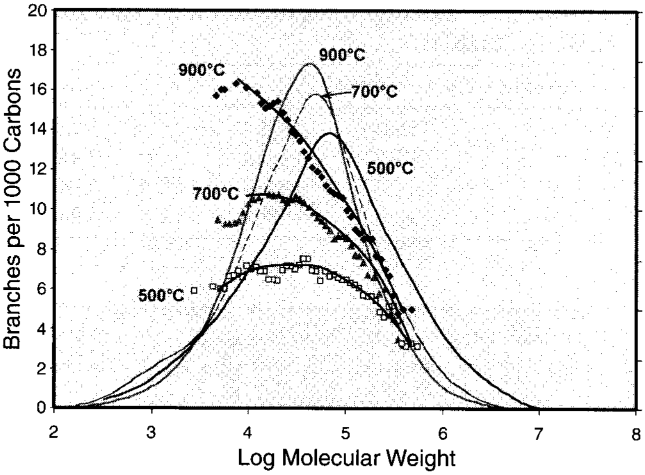

Figure 10.70 Branch profiles from Cr/silica–titania.

low-temperature (500 °C) activated catalyst. Notice that, unlike the branch profiles for Cr/silica in Figure 10.66, the profile for Cr/silica–titania is almost flat at low activation temperatures. When this polymer in Figure 10.70 was deconvoluted into the same seven Schultz–Flory distributions described for Figure 10.66, the GPC curve could be fit nicely, as would be expected (seven peaks would fit almost any curve), but the seven branching constants that had to be assigned to these peaks to fit the branch profile in Figure 10.70 were nowhere close to those for Cr/silica. This indicates that the sites on Cr/silica–titania are completely different in their branching behavior. One cannot simply redistribute the same sites used for Cr/silica to obtain the information in Figure 10.70. Again this is not to say that there are exactly seven types of sites—only that seven is the minimum number needed to represent the curves faithfully.

Now consider the branch profile in Figure 10.70 corresponding to the Cr/silica–titania activated at high temperature, 900 °C. Notice that it again concentrates the branches into the low-MW side of the distribution, like Cr/silica in Figure 10.66. In fact, this profile could now be reproduced by redistributing the same seven Schultz–Flory peaks obtained from Cr/silica. This indicates that the sites on high-temperature Cr/silica–titania are similar in their branching behavior to those on Cr/silica. In other words it is yet another indication that at high temperature the titania-associated sites are unstable and the chromium tends to migrate.

Since for Cr/silica catalysts it is the highly reactive low-MW sites that incorporate comonomer most efficiently, and since titania greatly increases the contribution from low-MW sites, it seems surprising that titania inhibits hexene incorporation in the low-MW region. Another seeming contradiction is the fact that the MI response to hexene by Cr/silica–titania catalysts is much greater than that from Cr/silica catalysts. This would seem to suggest that Cr/silica–titania catalysts do incorporate hexene, because incorporation of comonomer is known to increase chain transfer (raise MI). One possible explanation, which would contribute to these observed trends, could be that the titania-associated sites do incorporate comonomer but then have a stronger tendency to terminate the chain immediately. This would produce the observed chain transfer response, but a branch at the end of a chain would not be effective for density suppression. In fact, Cr/silica–titania does often produce a large vinylidene concentration and even increased trans-internal unsaturation upon addition of hexene, larger than that obtained from Cr/silica. This suggests that much of the incorporated hexene does help terminate the chain. Internal unsaturation sometimes even suggests increased incorporation in a 2,1-orientation as well. This probably stops propagation, since the chain would then be attached through a secondary carbon. Incorporation followed by termination would not account for the entire effect but could contribute to the observed trend.

10.5.6 CO Reduction

Although the hexavalent catalyst is normally reduced in the reactor by ethylene, sometimes it is preferable to reduce the catalyst prior to the reactor. Treatment in CO at about 350 °C followed by flushing in nitrogen at 350 °C cleanly converts the surface Cr(VI) into the divalent form and eliminates the induction time. This is helpful when low reactor temperatures must be used or when higher activity is desired. In addition to the faster kinetic profile, Cr(II)/silica also displays a few other slight differences in its behavior compared to Cr(VI)/silica. The MI potential of the catalyst is usually decreased some. This is because the MW distribution is usually narrowed by removal of some of the lowest MW polymer. An example is shown in Figure 10.71. This

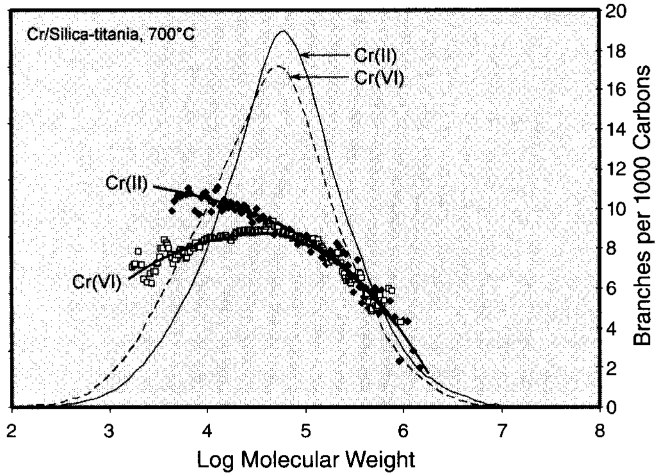

Figure 10.71 Effect of CO reduction on MW and branch distribution.

may indicate that some of the most reactive species are not very stable after reduction and therefore they redistribute at the 350 °C reduction temperature. This is quite noticeable if the catalyst contains Ti and especially if it has undergone a two-step activation designed to amplify the effect of the titania. Comonomer incorporation is also increased significantly by CO reduction. The short-chain branch distribution, also shown in Figure 10.71, shows that the extra comonomer is added to the low-MW part of the MW distribution. This again suggests that the effect of the titania is curtailed, perhaps indicating that CO reduction (like fluoride) causes a redistribution of the Cr away from the titania.

10.5.7 Partial CO Reduction and Selective Poisoning

In Figure 10.31 an experiment was performed in which a Cr/silica–titania catalyst was partially reduced in carbon monoxide at various temperatures. By choosing a low reduction temperature, only a portion of the hexavalent chromium was reduced, in fact, that portion that was most reactive (most easily reduced). Afterward the catalyst was cooled to room temperature in CO so that the reduced sites adsorbed CO and were therefore poisoned. Any remaining activity would most likely come from sites that were not reduced and consequently did not adsorb CO. In this way some distinction can be made between sites based on their reactivity. This process was depicted in Scheme 10.14.

Figure 10.72 shows the MW distribution obtained from such a series, where the curves are normalized according to the amount of polymer made. The catalyst used in this series was Cr/silica–titania, containing 5% Ti and calcined

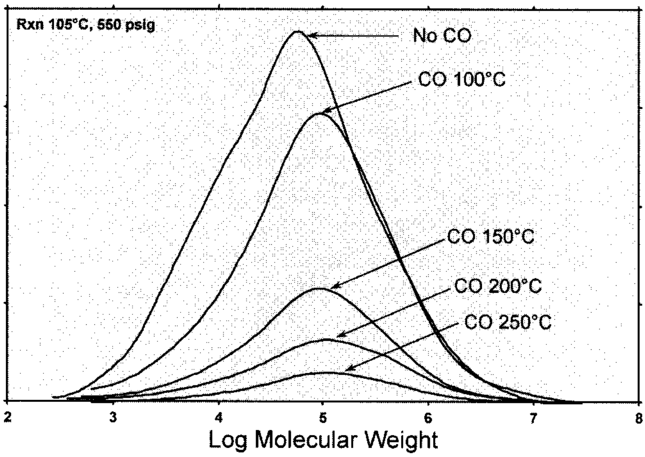

Figure 10.72 Partial CO reduction and kill of Cr/silica–titania.

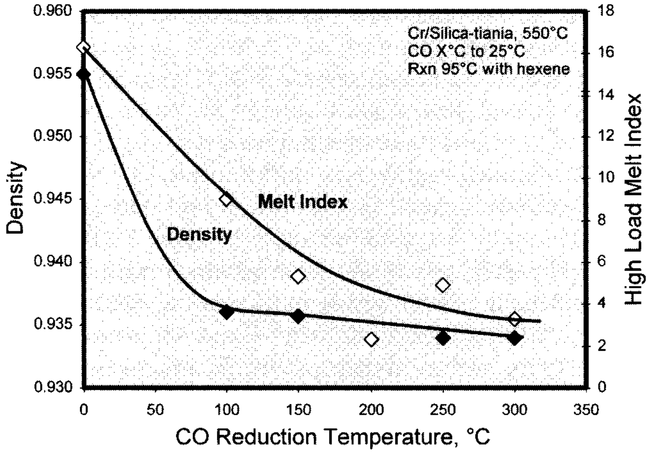

Figure 10.73 Partial CO reduction and kill of Cr/silica–titania.

at the low temperature of 550 °C in order to obtain a broad distribution of sites. It is clear from the chart that the first exposure to CO at 100 °C preferentially takes out the high-MI sites that were probably associated with titania. In contrast, there is no mass subtracted from the high-MW side of the distribution by CO at 100 °C. Further treatment in CO at higher temperatures followed by CO adsorption at 25 °C destroys more of the MW distribution, but without the same concentration on the low-MW side. Once these sites have reacted, further reduction is less discriminating.

Figure 10.73 shows the other results of this experiment. Melt index dropped as the more reactive (titania-associated) sites were eliminated, also indicating that they tend to make low-MW polymer. These were copolymers, all made with the same amount of hexene added to the reactor. However, the density dropped significantly with the first elimination of reactive sites in CO at 100 °C. This also confirms the conclusion from branching studies that those titania-associated sites inhibit hexene incorporation.

Similar experiments were then performed on a Cr/silica sample calcined at high temperature, 875 °C in order to homogenize the side diversity. Some of these trends were again visible but much more subdued. For example, there was little change in density with such partial CO reduction and killing. Hexene incorporation started high and remained almost constant with temperature of CO reduction and poisoning. In fact, the 550 °C titanated catalyst delivered exactly the same density after the first reduction treatment as the nontitanated samples had produced. This again suggests that the most reactive Ti-associated sites inhibit incorporation. The shift in the MW distribution for Cr/silica was almost imperceptible in comparison to Figure 10.72. So the 875 °C Cr/silica catalyst did not seem to produce the same broad dispersion of site types that 550 °C Cr/silica–titania did.

10.5.8 Fluoride

One common commercial practice is to add fluoride to Cr/silica–titania catalysts in order to increase hexene incorporation and decrease the amount of very low MW material.[421] A typical example in Table 10.10 shows two catalysts, a Cr/silica and a Cr/silica–titania, both of which were activated at 600 °C with and without fluoride. The flouride level was adjusted for the difference surface areas to yield a constant 1.5 F/nm^2. Then they were each tested for polymerization activity with a given amount of hexene in the reactor. The density of the polymer obtained is shown in Table 10.10. Notice that while fluoride had little effect on the density from Cr/silica, there was a major suppression of density from Cr/silica–titania. Thus fluoride seems to have greatly enhanced the hexene incorporation efficiency of Cr/silica–titania.

Figure 10.74 shows why fluoride had this effect. It shows the MW distribution of the same two polymers from Cr/silica–titania. Again the MW distribution has been narrowed, but this time the low-MW portion, from the

TABLE 10.10 Effect of Fluoride on Density

Catalyst	Density
Cr/silica	0.9364
Cr/silica + 1.3% F	0.9372
Cr/silica–titania	0.9413
Cr/silica–titania + 2.7% F	0.9317

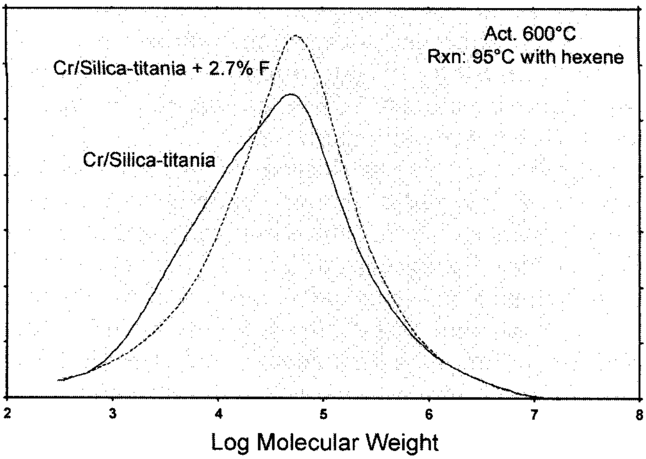

Figure 10.74 Effect of fluoride on MW distribution from Cr/silica–titania.

titania-associated sites, has been completely removed by fluoride. This is an indication that fluoride is adsorbed on these catalysts as Ti–F, displacing the Cr associated with titania. Thus the suppression of hexene incorporation by titania is also removed and the density drops. Much the same effect could have been obtained by simply decreasing the titania level.

10.5.9 Cr/Alumina

Cr/alumina does not incorporate hexene very efficiently compared to Cr/silica. Instead it is similar to Ziegler catalysts in its ability to incorporate comonomer. This means that larger amounts of hexene are required in the reactor to achieve density suppression. However, one very useful attribute of Cr/alumina is in the placement of comonomer. Although the MW distribution from Cr/alumina can be extremely broad if H_2 is added to the reactor, the catalyst does not have the same low-MW sites found on Cr/silica. These are the sites that tend to incorporate hexene most efficiently, leading to the skewed branch profile shown in Figure 10.66 in which most of the branches fall into the low-MW side of the distribution. In contrast, the branch profile from Cr/alumina can be quite uniform, as shown in the example in Figure 10.75.[384] Placing a significant degree of branching in the very high MW region imparts extreme toughness and ESCR to the polymer.

10.5.10 Cr/AlPO$_4$

Cr/aluminophosphate catalysts do not incorporate 1-hexene very efficiently compared to Cr/silica. Nevertheless, comonomer has a strong effect on the

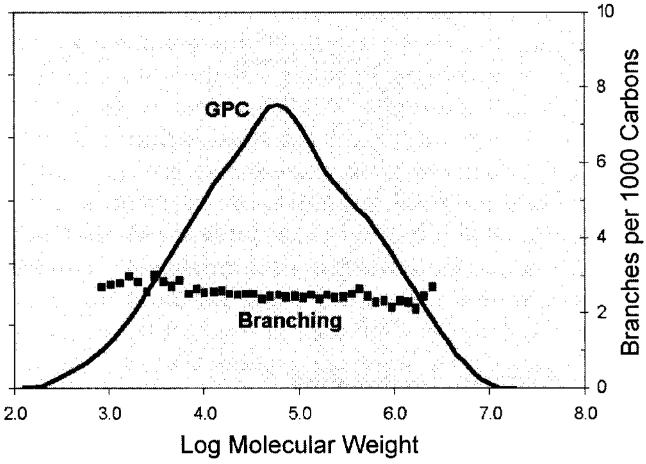

Figure 10.75 Branch profile of polymer from fluorided Cr/alumina.

chain transfer rate. These Cr–O–P sites not only produce lower MW polymer than other sites, but they also make the catalyst more sensitive to certain chain transfer agents, including 1-hexene. Adding just 20 mL of 1-hexene to the reactor increased the HLMI 13-fold when the support was $AlPO_4$, compared to 3 fold when it was silica. This behavior is beyond that usually expected due to H elimination from the tertiary branch carbon because for $Cr/AlPO_4$ the density hardly changed with the added 1-hexene. As expected, vinylidene appeared in the polymer upon addition of 1-hexene to any of the catalysts. However, the vinyl concentration also increased significantly using Cr/aluminophosphate. Possibly 1-hexene may accelerate chain transfer by acting as a better H receptor than ethylene on the high-phosphate catalysts or incorporation of hexene may immediately cause termination. Initiation or termination of a chain by 1-hexene would not be detectable as a branch. 1-Hexene addition also caused the appearance of significant amounts of internal unsaturation using high-phosphate catalysts, suggesting 2,1-addition followed by elimination. This may account for the fact that 1-hexene tended to inhibit the activity of the high-phosphate catalysts.

All this together suggests that, far from being nonreactive with 1-hexene, $Cr/AlPO_4$ catalysts tend to incorporate it but then terminate immediately so that the branches are ineffective. This response is almost certainly due to the influence of the phosphate, perhaps to the formation of P–O–Cr bonds. Alumina can be treated with phosphoric acid to produce the same effect, and the more phosphate added, the more sensitivity. Even silica can be impregnated with phosphoric acid, or a phosphate, to increase its sensitivity.[221,422,423]

10.5.11 Porosity and Copolymerization

It has been observed in the past that catalysts having wide pores incorporate hexene better than those with narrow pores, other factors being equal.[424] An example is shown in Figure 10.76. In this case a single hydrogel was again dried by different techniques to obtain catalysts of identical composition and surface area but varying in pore volume. Polymer was then made in the presence of hexene and the density is plotted against pore volume. In this example there is quite a change in density from these catalysts. However, it should be noted that this also affects the activity of the catalyst and thus the size of the polymer particles. Ethylene concentration gradients can sometimes develop through large polymer particles that increase hexene incorporation.[425] Ethylene, rather than hexene, gradients are more likely to develop due to the much higher rate of consumption.

10.5.12 In Situ Comonomer Generation

One of the unique characteristics of most organochromium catalysts is a production of olefins, either as the only or main product or at a low level along with high-MW polymer. This is attributed to a monoattached Cr species (prob-

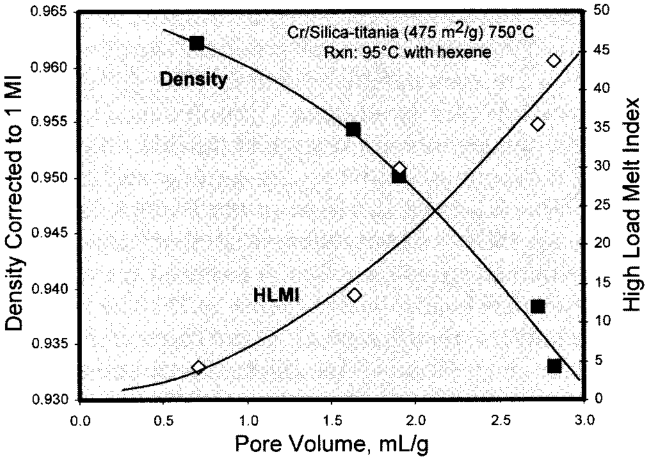

Figure 10.76 Influence of catalyst porosity on 1-hexene incorporation.

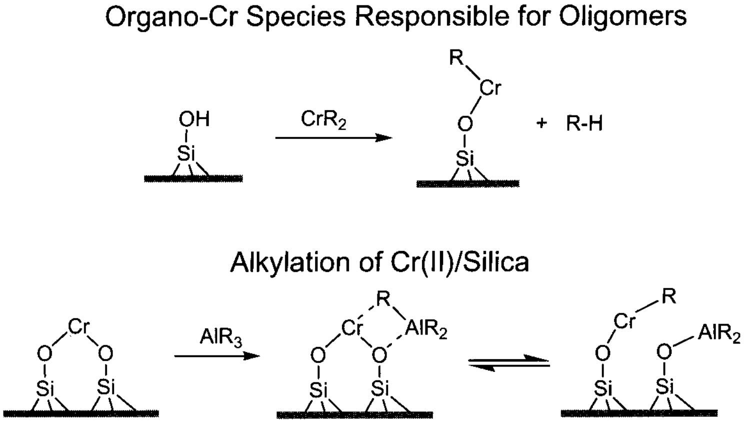
Organo-Cr Species Responsible for Oligomers
OH
Si
CrR2
R
Cr
O
Si
+ R-H
Alkylation of Cr(II)/Silica
Cr
O
O
Si
Si
AlR3
R
Cr
AlR2
O
O
Si
Si
R
Cr
AlR2
O
O
Si
Si

Scheme 10.20

ably of very low CN), in which isolated hydoxyls react with one Cr alkyl or other ligand described in Scheme 10.20.[20,300,301,303,304,352,422] These olefins are then simultaneously copolymerized with ethylene to produce branched polymer. Since most commercial polyethylene grades are actually copolymers of ethylene and another α-olefin, these in situ–derived copolymers can be of commercial interest. The most commonly used commercial comonomers are 1-butene, 1-hexene, and 1-octene, all of which are more expensive than ethylene by weight. Therefore the cost incentive and the simplification of plant investment have served to fuel commercial interest in olefin production from organochromium and related catalyst systems.

The composition of these oligomers can be tailored in part by the choice of organochromium compound, the support, and the run conditions. In general, the olefins produced are even numbered and follow a Schultz–Flory distribution, with one exception. Nearly all these Cr compounds have a tendency to produce disproportionately more hexene than the other olefins. In fact, some organochromium compounds produce only hexene and no other olefin or polymer product. This has been the basis of the Phillips commercial hexene process discovered in 1989.[426] Clearly there is another mechanism involved in addition to the traditional growth reaction. It has been suggested that a metallocyclic intermediate may be involved (Scheme 10.21). The key to the selectivity lies in the relative stability toward intramolecular H transfer of the chromacyclopentane ring relative to the chromacycloheptane ring, and this is consistent with the known behavior of other metallocyclics.[427–430] This in situ olefin generation is usually enough to drop the resin density to a large, sometimes too large, extent. This also makes it difficult to produce homopolymers from the organo-Cr catalysts. Chromocene is the exception, not generating olefins and not incorporating them well either.

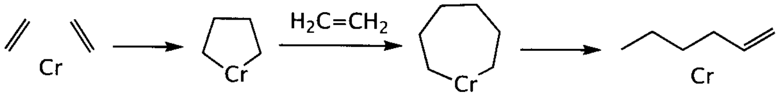

Scheme 10.21

In addition to incorporated oligomers, which produce even-numbered branches, methyl branching is also detected in small amounts from some organochromium (but not chromium oxide) catalysts. Chromocene is especially known for this behavior.[350,431–433] It is usually thought to be from β-H elimination to Cr, followed by reinsertion of the same chain or (perhaps a comonomer) in the 2,1-position. The amounts are usually not large enough to have a major effect on the resin density.

Cocatalysts can be used to alkylate chromium oxide catalysts and thus also produce this same in situ olefin generation. Figures 10.21 and 10.22 show the effect of adding BEt_3 or $AlEt_3$ cocatalyst to a Cr(VI) oxide/silica catalyst. At the lowest cocatalyst levels there is a significant increase in activity with very little change in the polymer. However, at higher cocatalyst levels, something different begins to happen. Activity decreases and polymer molecular weight can change significantly (initially the MI or HLMI went down, indicating increasing MW, but in the presence of H_2 it might have gone up). Most noticeably, one sees generation of 1-butene 1-hexene, 1-octene, and higher oligomers. These become incorporated as comonomers, and there is a corresponding decrease in resin density from incorporation of these oligomers. This drop in density can be seen clearly in Figures 10.21 and 10.22.* This response is attrib-

---

*In Figure 10.21 density goes through a minimum because of the broadening MW distribution.

TABLE 10.11 Density of Polymer Obtained with and without BEt_3 Cocatalyst Using Normal Cr(VI) and CO-Reduced Catalyst, Cr(II)

Valence	No Cocatalyst	4 ppm BEt_3
Cr(VI)	0.963	0.959
Cr(II)	0.962	0.928

Note: Catalyst was Cr/silica–titania activated at 800 °C.

uted to the breaking of surface–O–Cr bonds to create "bare" monoattached sites like those formed on organo–Cr catalysts.

If a Cr(II)/silica catalyst, one already reduced by carbon monoxide at 350 °C, is used with low levels of cocatalyst, there is little or no enhancement in activity because the catalyst is already reduced. Instead there is a sudden generation of large quantities of these same light α-olefins, 1-hexene in particular. Suppression of the resin density is observed in response to the 1-hexene generation, signifying copolymerization of those olefins. An example is shown in Table 10.11. The resin density drops profoundly only when cocatalyst and Cr(II) are used together. On these catalysts there seem to be sharply distinct product profiles—first α-olefins, mainly hexene, sometimes only hexene, and second, a polymer with normal MW distribution. Usually only 1–10 ppm of cocatalyst is enough to accomplish this in situ hexene generation.[17–19,270,276,434–439] In this example the olefin produced was about 90% 1-hexene.

This behavior is similar to the organochromium catalysts which contain monoattached uncoordinated species on silica. A similar site is probably also formed on these Cr(II) oxide catalysts treated with cocatalyst.[20,276,422,440,441] In both cases, olefin generation probably happens only on the most bare, ligand-poor surfaces.[422] The conversion of surface Cr(II) oxide to this species probably accounts for only a small portion of the total chromium present, as only a few especially strained or reactive sites are transformed. This is why polymer continues to be the main product. Apparently Cr(VI) catalysts can also, but less cleanly, yield some of these olefin-producing sites, under very high concentrations of cocatalyst.

Just as silica is the best support for organochromium compounds to produce the monoattached site for olefin generation, so it is also for the in situ hexene generation over chromium oxide catalysts. Cr(II) oxide on silica does best, although silica–titania and silica–alumina can also be used as supports. This agrees with the findings for organo-Cr catalysts, where silica was found to be most efficient at producing this "bare" site that produces mainly liquids. On alumina and aluminophosphates the response almost disappears. This may reflect the known inability of these catalysts to incorporate higher olefins very well or it may also indicate a smaller amount of olefin-generating sites.

Treatment in CO at 350 °C gives the cleanest conversion to Cr(II) of any reducing treatments studied. Hogan and others have noted that reducing treatments like hydrogen or alkanes can generate water as a by-product. Water can then destabilize the surface–Cr attachment during calcining and cause decomposition or oxidation to Cr(III).[29,84,270,276,442,443] Many reducing treatments have been tested in this laboratory, including methane, other hydrocarbons, SO_2, methanol, carbon disulfide, acetylene, and hydrogen. However, only CO-reduced catalyst produced high activity and a strong lowering of density due to in situ hexene generation when tested in the presence of 8 ppm BEt_3.

The temperature of reduction in carbon monoxide is also important in determining the in situ hexene response. It was noted earlier that Cr(VI) is reduced cleanly to Cr(II) at about 300–350 °C and that higher temperatures do not further reduce the chromium but do perhaps provide the opportunity for it to rearrange and become less coordinatively unsaturated. This may explain why 300–350 °C was also the preferred reduction temperature for the in situ hexene response.

The in situ hexene response is governed by many variables. Among the most effective cocatalysts were boron alkyls and dialkylaluminum alkoxides. Aluminum trialkyls were also quite effective, but one halide added, such as $AlEt_2Cl$, diminished the response greatly. Alkyls of lithium, magnesium, zinc, and others were effective to varying degrees.

The in situ density suppression was found not to be very dependent on ethylene concentration. This near-zero-order dependence may perhaps be explained in this way: Both the hexene generation and the copolymerization exhibit first-order dependence on ethylene concentration. Thus, as ethylene concentration is increased, hexene generation increases, but copolymerization also increases proportionally. More hexene is generated, but more hexene is also consumed, so that the net result is little or no change in density.

The order in which the ingredients are contacted also influences how effective the in situ hexene generation will be. For example, in one series of experiments a Cr/silica–titania was calcined at 650 °C and then reduced in CO at 350 °C. In the first polymerization run, the catalyst was added to the reactor first, then the ethylene monomer, and finally BEt_3 cocatalyst was introduced about 3 min later. This run produced polyethylene of 0.9470 g/cm^3 density. Then the experiment was repeated, except the catalyst was added first, then the BEt_3, and about 3 min later the ethylene was added. This run produced a polymer of 0.9276 g/cm^3 density. Clearly the presence of olefin coordinated to the Cr(II) slows down the formation of the species that generates the olefins. Recently others have also noted the importance of contact order.[444]

For any given Cr(II) catalyst the degree of density suppression can be controlled to make different resin grades by varying the amount of cocatalyst used in the recipe. Rather than impregnate the catalyst with metal alkyl in a fixed ratio, the metal alkyl is instead fed directly to the reactor or to a premixing vessel that continuously feeds the reactor after a short residence time. The premixing vessel permits the cocatalyst and catalyst to react before exposure to ethylene. In this way the cocatalyst-to-catalyst ratio can be finely adjusted hourly during production. Thus the in situ hexene generation is easily controlled by varying the amount of cocatalyst added to the reactor. This technique has been used commercially for almost two decades by this company and licensees to control density down to 0.918. Figure 10.77 shows the wide range of density that can be achieved by varying the triethylboron concentration over a fairly narrow range.

Like the organochromium compounds, the cocatalyst method of producing in situ olefins can also yield a Schultz–Flory distribution of even-numbered olefins, although the exact olefin distribution can be very sensitive to cocatalyst type and reaction conditions. Two examples are shown in Figure 10.78, in which two different cocatalysts were used at 8 ppm with a CO-reduced, 650 °C Cr/silica–titania. Often a prominent hexene spike is superimposed onto the Schultz–Flory distribution. This indicates two independent mechanisms of

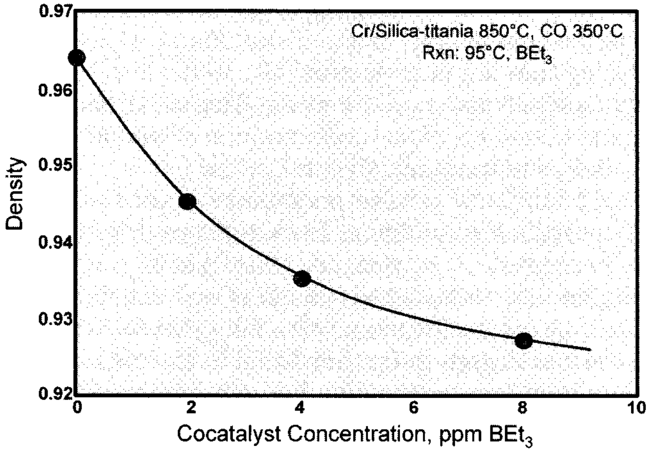

Figure 10.77 Control of resin density by variation of cocatalyst concentratin.

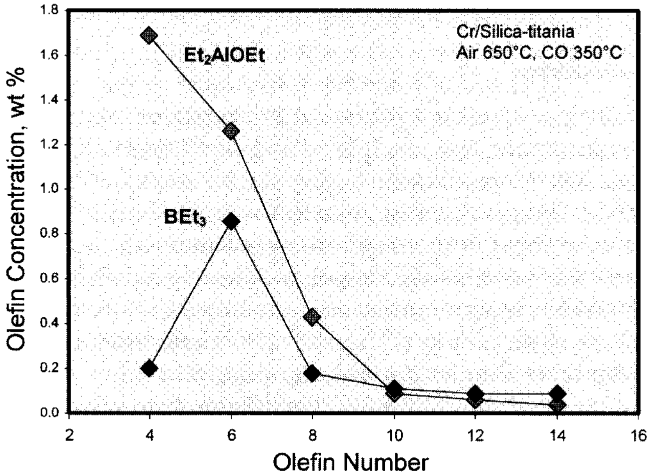

Figure 10.78 Olefin distributions 650 °C Cr(II)/silica–titania and either 10 ppm $AlEt_2OEt$ or 12 ppm BEt_3.

olefin generation in operation. The former obviously comes from an ethylene growth reaction on some sites that have a strong disposition to terminate. The latter, producing hexene only, probably comes from formation of chromacycloheptane, as has been observed from other chromium catalysts.[426] Thus different cocatalysts and other conditions can change the olefin distribution produced considerably. The hexene spike can become more or less prominent relative to the Schultz–Flory background, and the Schultz–Flory contribution can become sharp or extended. In some cases it was possible to obtain hexene exclusively along with the polymer.

In commercial operations the in situ hexene incorporation is up to four times more efficient than ordinary Cr(VI)/silica catalysts. That is, in the reactor it may take only about 25–30% of the hexene normally needed to make the same density. This probably derives from two causes. First, as noted above, Cr(II)/silica itself is considerably more efficient than Cr(VI)/silica. Second, the hexene-producing sites are in close proximity to the hexene-consuming sites within the catalyst/polymer pore structure. Therefore the consuming sites probably experience a higher local concentration of hexene than exists in the reactor as a whole, and consequently it takes less.

The increased efficiency of incorporation is a great advantage in commercial loop operations. In addition, 1-hexene is usually considerably more expensive by weight than ethylene, so that the in situ hexene reaction brings a significant feedstock cost advantage as well. Capital costs can also be reduced because the usual purification of incoming hexene is no longer needed. Thus the process has proven to be very useful in commercial operations and has become the basis for some unique low-density commercial resins introduced during the early 1990s.[17,19,434,435] Over a billion pounds of polyethylene products have now been manufactured by this process for film and other applications. The process is also helpful in remote locations where hexene is less easily obtained.

10.5.13 Hydrosilanes

Perhaps the most powerful class of cocatalysts found for in situ hexene production are the hydrosilanes. For example, in one experiment a Cr(VI)/silica catalyst activated at 600 °C was allowed to polymerize ethylene at 95 °C, producing a 0.961-density polymer. The same catalyst was then exposed to SiH_4 gas at room temperature for a few minutes, then flushed with nitrogen and tested again. The treated catalyst produced polymer having a density of 0.9287. Thus even the hexavalent catalyst was transformed by exposure to SiH_4. The CO-reduced catalysts were even more sensitive. Organic hydrosilanes could also be added to the reactor to accomplish the same effect. For example, diethylsilane, triethylsilane, phenylsilane, diphenylsilane, hexylsilane, and just SiH_4 were extremely powerful.[445] These silane compounds even rendered Cr(VI) catalysts as efficient olefin generators. However, the response was only observed if the silane contained at least one Si–H bond. Otherwise it was inert.

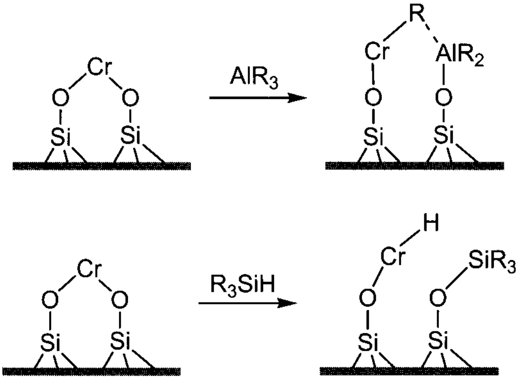

Scheme 10.22

The surprisingly effective response from the hydrosilanes is hard to explain. Many of these compounds are not strong reducing agents, and some of them can even be handled in the air. Presumably the reaction with Cr(II) involves the transfer of a hydride to the chromium (see Scheme 10.22). Why silicon hydrides are so much more effective than other metal alkyls is not clear, but it could be related to the inability of silicon to coordinate or bridge with the transferred ligand, in contrast to some other cocatalysts. The hydrides of aluminum or boron did not have this same powerful effect.

The potent reactivity of the hydrosilanes is apparent from the amount needed to affect the catalyst. Both divalent and hexavalent catalyst activity was improved by the addition of silane. However, the optimum stoichiometry was much lower than observed from the other cocatalysts. The highest activity was usually achieved at Si/Cr ratios of 0.3 or less. Likewise the density suppression from the silanes occurs at very low stoichiometries. In most cases a respectable effect on activity and density is observed with just 100 ppb in the reactor! This can only mean that the silane is very selective in its reaction with the catalyst, preferring to react with potentially active sites.

Like the other cocatalysts, the hydrosilanes seem to transform the chromium into sites not unlike those produced from organochromium compounds. This is apparent from the characteristic olefin generation and branching content of the polymer. It is also evident from the change in the MW distribution. An example is shown in Figure 10.79, which shows the activity increase upon adding diethylsilane in minute amounts. Both liquid and solid products were obtained. The MW distribution is shown in Figure 10.80, from Cr(II)/silica run alone, and then again with two levels of phenylsilane. The first addition of the silane creates a separate small low-MW peak at 2.5, which is identical to that from the monoattached "bare" Cr species of the organo-Cr catalysts. The second addition of silane, which is only a Si/Cr stoichiometry of 2.1, transforms almost all of the Cr into this species and there is very little original species left. This reactivity is remarkable.

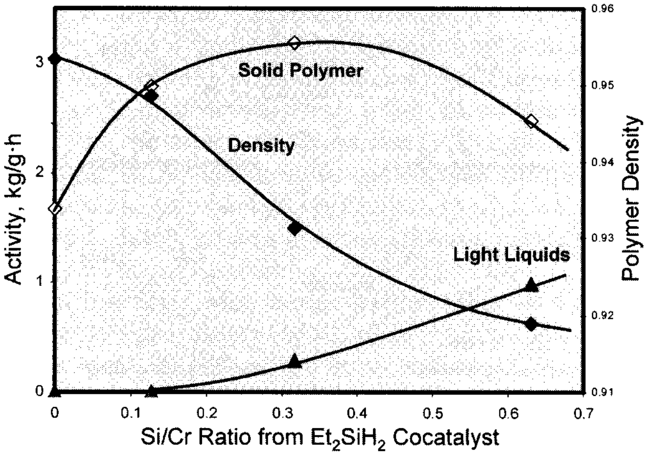

Figure 10.79 Influence of diethylsilane on activity and distribution of products.

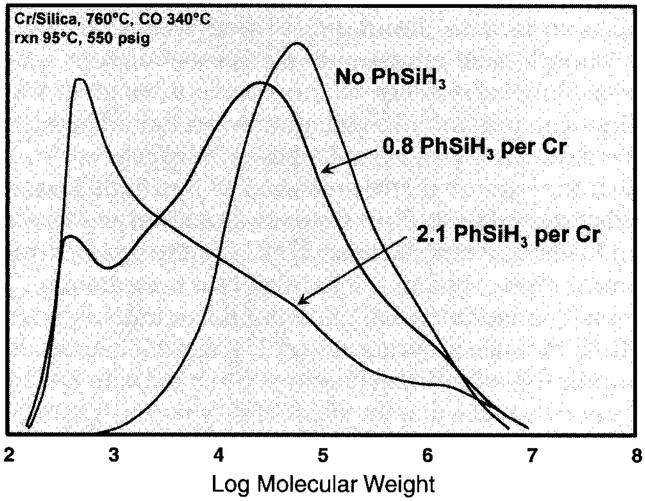

Figure 10.80 Influence of phenylsilane on MW distribution.

10.6 CONTROL OF ELASTICITY

10.6.1 Importance of LCB

The elasticity of the molten polymer is very important during molding applications because it determines melt strength, flow properties, and relaxation times. Elasticity can be considered as the amount of "memory" in the polymer as it flows due to orientation of polymer chains. Therefore long chains obviously make a big contribution to elasticity, making it dependent on the average molecular weight and also the high-MW part of the MW distribution. However, another and perhaps more potent contributor is long-chain branching. This is because chain entanglement and disentanglement are highly influenced by the long-chain branch points, each one of which serves as an "anchor point" or "knot."

Although more often associated with metallocene catalysts in recent years, in fact for four decades the Phillips catalyst has been known to produce LCB.[29,30,41,207,446–449] Although present in only trace amounts, less than one branch per 10,000 carbons, LCB still exerts enormous influence on polymer-molding characteristics.[450] For example, LCB levels are thought to influence (1) swell during blow molding; (2) bubble stability, orientation, melt fracture, and extensional viscosity in film blowing; (3) melt strength in geomembrane resins; (4) sag during large-diameter pipe extrusion; (5) flow characteristics in all kinds of extrusion equipment; and (6) even various mechanical properties in the finished articles. Much industrial effort has been expended to develop proprietary catalysts that exploit or limit these LCB-related characteristics.

10.6.2 Mechanism of LCB Generation

The most commonly cited mechanism for LCB formation is macromonomer incorporation.[451,452] The liberated vinyl end group of one terminated chain is thought, through random motion, to become copolymerized into another growing chain (Scheme 10.23).

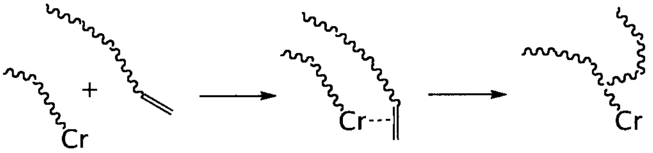

Scheme 10.23

Since typical Ziegler catalysts do not usually generate vinyl end groups to a significant degree and do not incorporate comonomer well either, their polymers do not normally contain measurable LCB levels. However, chromium oxide catalysts do produce one vinyl per chain and do incorporate comonomer well. Therefore they tend to impart LCB into the polymer, although usually at low levels. One problem with this mechanism is that in slurry- and gas-phase processes the polymer chains are not in solution but rather have been "frozen out" into a solid phase immediately as they are formed. Therefore one could question whether these chain ends are really available for subsequent reaction. The usual explanation given is that the active sites are embedded in the amorphous polymer phase where chain ends reside and do have some degree of limited motion.

Such LCB formation is usually regarded as a random process in which a Cr site draws its feed, including the macromonomer vinyl group, from its immediate environment. The level of LCB would then be determined only by the local concentration of macromonomer and ethylene around the site. However, this view has problems, which are summarized below:

1. Catalysts which incorporate comonomer well, such as Cr(II)/silica, are expected to also incorporate macromonomer more efficiently too, thus giving the highest levels of LCB. Such reasoning should apply to other catalyst types as well, such as metallocenes. In practice, however, we have not seen this correlation, and there are many glaring counterexamples. For example, catalysts are known which incorporate comonomer very well, produce vinyl end groups, but do not make LCB. Others incorporate comonomer relatively poorly but produce high LCB levels.
2. Given a constant vinyl end-group concentration within the amorphous phase, the LCB level should be inversely proportional to ethylene concentration. For chromium catalysts this relationship is often weak or not present.
3. Mobility within the amorphous phase, and thus LCB, should vary considerably with reactor temperature. Again, this correlation has not been observed in this laboratory.
4. Many catalyst and reactor variables have a strong influence on LCB, with no clear connection to random macromonomer insertion.

These problems suggest that macromonomer insertion, even if the mechanism is basically correct, is not entirely a random process. Chemistry and even physical considerations seem to impose preferences that cannot be accounted for by the purely statistical approach.

10.6.3 Definition and Measurement of LCB

To be rheologically significant, a branch must be longer than the critical entanglement length, which for polyethylene is known to be about 140 carbons.[450,453] However, there is currently no convenient way of directly measuring low LCB levels, position, or length in commercial PE products. Obviously NMR cannot be used for this purpose.

Size exclusion chromatography multiangle light scattering (SEC-MALS) is one method of detecting LCB and can even provide a limited LCB distribution within the MW distribution. It compares the radius of gyration for PE in solution to that of linear PE references having the same MW. Unfortunately this method is not usually sensitive enough to pick up the low LCB levels in most Cr/silica-derived polymers. In our experience at this laboratory so far, the presence of LCB can sometimes be detected, but the sensitivity is not great enough to make judgments concerning relative levels between polymers SEC-MALS is also not very sensitive to LCB in the low MW part of the MW distribution.

Rheology is very sensitive to the effects of LCB. Currently the most useful method of detecting LCB in Cr/silica-derived polymers is to look for increases in low shear melt viscosity that go beyond what would be expected from linear polymers of the same molecular weight.[207,450,454] Polymers containing trace levels of LCB are more likely to entangle in the melt phase, causing extreme changes in (especially low-shear) melt viscosity. As with many other polymers, if the log of the extrapolated zero-shear viscosity (designated η_0) is plotted against the log of the weight average MW, a straight line is obtained for linear polymers having a slope of 3.4. This is called an Arnett plot,[455] and deviations from the line indicate LCB. An example is shown in Figure 10.82 below.

The effect of LCB on viscosity is more pronounced at high MW than at low MW, because entanglements are less easily overcome during flow. This relationship was defined by Janzen and Colby, giving rise to the curved grid lines for given LCB levels in Figure 10.82 below.[450] This insight provides a reference to compare LCB levels in polymers at different molecular weights. At very low MW, say M_w of 10,000, the effects of LCB become much less pronounced. The Janzen–Colby grid lines were derived based on a monodisperse MW distribution. A broad MW distribution may produce different lines, but the general relationship is still expected to hold. Therefore, in comparing different polymers using the Janzen–Colby equation, one should stipulate that the MW breadth is similar. It is a qualitative relationship only.

One curious result of the Janzen–Colby relationship is that at very high LCB levels, for example, above about 1 branch per 10^4 carbons, the effect on low-shear melt viscosity reverses and it begins to become less pronounced. That is, viscosity begins to decline with increasing LCB until, at very high LCB levels like those found in commercial LDPE, the zero-shear viscosity can be even less than that of a linear polymer. This is usually interpreted to mean that very high levels of LCB actually interfere with entanglements, because the polymer becomes more spherical in shape. Fortunately Cr/silica-derived PE does not normally reach such high LCB levels.

10.6.4 LCB Placement within MW Distribution

Unfortunately the effect of MW breadth and LCB distribution within the MW distribution can be a complicating factor in the interpretation of Arnett/Janzen-Colby data. The Janzen–Colby relationship was derived for a monodisperse distribution, and although the Arnett relationship (for linear polymers) is not greatly affected by MW breadth, the Janzen–Colby response could be influenced by where the LCB falls within that distribution. For example, consider two polymers both having a broad MW distribution and one LCB per 10^5 carbons. The zero-shear melt viscosity must be higher if the branches are in the long chains versus if they are in the short chains, even though the weight average MW M_w is unchanged. This amounts to two different points on the Arnett plot for the same level of LCB. Thus caution must be exercised in drawing conclusions about LCB levels from this technique in some experiments. In this chapter we define the LCB level as the "effective average" LCB level measured from the Arnett/Janzen–Colby plots.

For example, this issue frequently arises when evaluating the effect of certain experimental variables on LCB levels. If the MW distribution is broadened on the low-MW side by introduction of linear molecules, the average MW decreases accordingly but the zero-shear viscosity may be less affected if the long chains contain the LCB. This amounts to a shift in the LCB distribution and could give the appearance on a Janzen–Colby grid that the LCB level has increased, whereas in fact it really decreased. Nevertheless, one could still say that the elasticity or "effective LCB" (relative to the MW) did increase, and this definition has meaning from a commercial viewpoint. To follow what happened on a molecular level, however, it is often necessary to consider which response may have changed most—M_w or η_0.

Finally three additional points should perhaps be mentioned to understand the significance of LCB. First, even when the LCB distribution is flat within the MW distribution, in terms of LCBs per carbon, the longer chains must receive more branches *per chain*. Second, two branch points on one chain are thought to be much more effective than the same two branches each on a separate chain. This is because the branches become "anchor points" which resist relaxation in the melt. These two effects tend to make the high-MW portion of the MW distribution much more influential in determining the zero-shear viscosity.

Third, even a single-site distribution, that is, with $M_w/M_n = 2$, is still expected, from random statistical incorporation, to put more branches *per carbon* into the long chains.[456,457] This is simply because the act of incorporating a long branch into a chain increases the MW of that chain. In other words, from statistics alone and without invoking any chemical selection, the branching tends to be disproportional in the higher MW chains. An example of this behavior is shown in Figure 10.81, where the branch level derived from

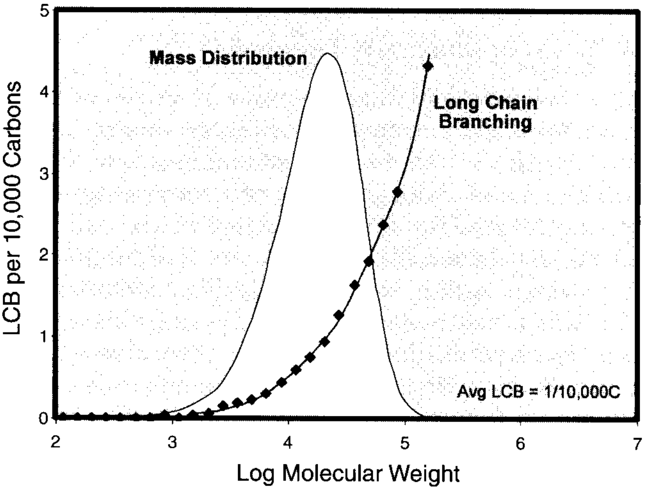

Figure 10.81 Statistical distribution of LCB within MW distribution of single-site catalyst determined from model calculations based on random incorporation.

computer modeling of random incorporation is plotted against MW. This is the behavior expected, from statistics only, from a metallocene-derived polymer containing LCB.

In such polymers these three influences of the MW on LCB combine to yield extreme relaxation times and thus some very powerful and unusual effects. For example, such polymers can become almost or completely insoluble. Or they can produce strange instabilities during extrusion, such as flat strands coming from round holes. Or the physical properties of the molded polymer part can become very poor, even resembling oxidative embrittlement. Fortunately Cr/silica-derived PE does not usually display such behavior. Phillips catalysts contain a variety of site types that yield a broad MW distribution. Much evidence suggests that in Cr/silica-derived PE the LCB level is not concentrated into the higher MW part of the distribution. Rather, it is likely in the 10^4–10^5 region.

10.6.5 Activation Temperature

Major differences can be seen in LCB levels (or elasticity) derived from one Cr/silica catalyst versus another. One of the most potent methods of manipulating LCB is by adjustment of the catalyst activation temperature. Table 10.12 shows some seemingly contradictory trends, first observed in the early 1960s, that can only be resolved by postulating changing LCB levels.[207] When the activation temperature was increased, varying reactor temperature to hold a constant 0.35 melt index, these trends were observed: (1) the MI is constant whereas the M_w declines, (2) the solution viscosity decreases but the melt viscosity increases; and (3) the chromatographic breadth (the polydispersity) narrows while the rheological breadth (HLMI/MI or other measurements) broadens, indicating increasing elasticity. These opposing trends can only be rationalized by concluding that the LCB level in the polymer increases with increasing activation temperature. Arnett plots confirm this view. Other important commercial variables also change, including swell (a function of LCB and elasticity) and environmental stress crack resistance (a function of MW).

Between 500 and 800 °C no phase transitions are known to occur on Cr/silica catalysts, and the surface area and pore volume remain almost constant.

TABLE 10.12 Influence of Activation Temperature on LCB at Constant MI

Parameter	593 °C	677 °C	760 °C
Melt Index	0.35	0.35	0.35
$M_W/1000$	171	153	118
Solution viscosity (inherent viscosity)	1.92	1.82	1.64
Melt viscosity (at $0.1\,s^{-1}$)	4.20	4.59	4.73
Chromatographic breadth (M_W/M_n)	10	8.2	6.1
Rheological breadth (HLMI/MI)	75	92	110
Parison swell, %	40	34	28
Environmental stress crack resistance, h	85	65	43

TABLE 10.13 Effect of Activation Temperature, Constant Reaction Conditions

Calcining Temperature (°C)	HLMI	Density	Eta(0)	CY-tau	CY-a	M_W	GPC Breadth
500	1.7	0.9354	2.54×10^7	301	0.2225	374.4	1.853
600	2.1	0.9349	1.67×10^7	166	0.2022	370.6	1.773
700	13.9	0.9326	8.69×10^7	83	0.1655	190.1	1.641
800	21.9	0.9325	6.94×10^7	657	0.1175	142.0	1.537
900	10.1	0.9327	8.41×10^7	14,720	0.1070	148.1	1.408

Note: Catalyst: Cr/silica, reaction at 85 °C with 50 mL hexene and 450 psig.

Only a gradual annealing and dehydration of the silica surface is observed, with an accompanying rise in activity from a changing and probably increasing site population. The changing site population results in a slight improvement in comonomer incorporation efficiency, but not enough to account for the large increase in LCB. Therefore the increase in LCB does not suggest a random process. It indicates that the change in either type or number of sites must somehow promote macromonomer incorporation.

Another example is shown in Table 10.13. In this case the reactor conditions were held constant as the activation temperature was increased from 500 up to 900 °C. HLMI rose and then fell while M_w went through a minimum, both trend reversals indicating the onset of sintering, as shown above in Figure 10.17. Density decreased as shown in Figure 10.66. Most significantly, zero-shear viscosity and relaxation time (CY-tau) first drop with M_w but then rise sharply. The Carreau–Yasuda "*a*" parameter* decreases, indicating steady rheological broadening,[454] whereas the GPC integral breadth narrows. Again these are seemingly contradictory trends that signify increasing levels of long-chain branching with rising activation temperature.

A common method of detecting and quantifying small amounts of long chain in PE is called an Arnett plot,[455] which graphs the log of the zero-shear viscosity against the log of the weight average MW. An example of such a plot is shown in Figure 10.82. Longer chains are more prone to entanglements, which increase their ultimate (zero-shear) melt viscosity. For linear polymers this relationship is expressed as the "Arnett line," the bottom line in Figure 10.82. Deviations from the line indicate contributions to the viscosity from increased entanglements due to the presence of LCB. LCB is indicated then by high melt viscosity that is not accompanied by high MW. The contribution to the viscosity of each level of LCB, say one LCB per million carbons, for example, is also dependent on the overall MW, and this relationship is expressed by the Janzen–Colby curved grid lines that are also shown in Figure 10.82.[450] Each curved line represents a different level of LCB in the polymer. Thus the amount of LCB in the polymer may be roughly gauged by its position on this graph.

*CY-a indicates the distribution of relaxation times in the polymer. A high CY-a indicates a narrow distribution. LCB typically broadens the relaxation time distribution.

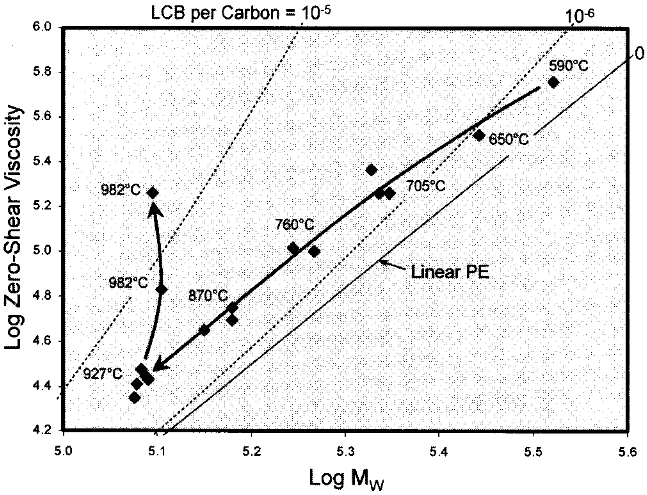

Figure 10.82 Arnett plot, showing effect of varying activation temperature of Cr/silica–titania catalyst.

Figure 10.82 shows a series of polymer points representing different catalyst activation temperatures. As the activation temperature was raised, M_w decreased and log η_0 moved farther away from the linear reference line, indicating increasing LCB. At the very highest temperatures, one can see the effect of sintering of the silica support. The sample line suddenly reverses direction (log M_w goes up, not down) and log η_0 moves still farther away from the linear reference line. This suggests that sintering greatly increases LCB compared to lower temperatures.

These relationships have been reduced to a simpler graph in Figure 10.83, which plots the level of LCB found in these same series of polymers against activation temperature. These numbers were taken from the Janzen–Colby equation, which was derived for a monodisperse MW distribution. Since the effect of MW breadth on viscosity is unquantified when LCB is present, these numbers should not be taken literally, but only as an indicator of the direction of LCB content. There is a steady rise in LCB level with activation temperature up until the point of sintering; then the rise accelerates. Also plotted on this chart are the activity and MI potential, which likewise show a transition (downturn) due to sintering, as well as the surface area of the catalyst—a direct measure of sintering. Weight average MW is shown for comparison. All these charts merely confirm that LCB increases as the catalyst activation temperature is raised.[207]

10.6.6 Chromium Loading

Raising the activation temperature increases the number of active sites. A more direct way of varying active-site density is to vary the chromium loading

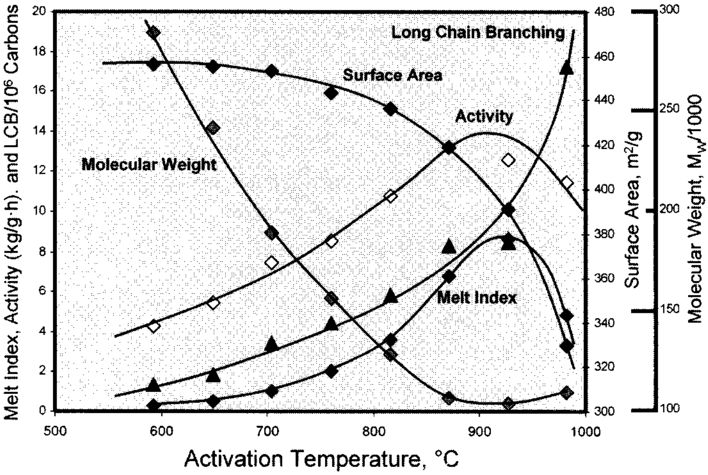

Figure 10.83 Influence of activation temperature on LCB level from Cr/silica–titania catalyst.

on the catalyst. This was done in a number of experiments using many different types of silica and silica–titania supports calcined at different temperatures and run under different reaction conditions.[207] Chromium loadings were varied from as little as 0.01 wt % Cr to as much as 3.0 wt % Cr. Again it was found that increasing the site density tends to increase the elasticity of the polymer. Increasing the Cr loading increased rheological breadth while the chromatographic breadth remained constant. Likewise melt viscosity increased without an accompanying increase in MW, as was described above to indicate increasing LCB. The Arnett plot is shown in Figure 10.84. Notice that as the Cr loading was increased, the points move away from the linear reference line, indicating increasing LCB.[207] This plot has been converted into LCB per million carbons in Figure 10.85, again using the Janzen–Colby equation so that the numbers reflect the direction of LCB content but should not be taken as quantitative. The catalyst activity is also plotted against chromium loading. Again one sees that LCB increases with Cr loading. In fact, this relationship is not a strict function of activity, because LCB continues to go up even after activity has stopped rising. This may reflect changes in the Cr species obtained at higher loadings.

10.6.7 Other Reactor Variables

Some other variables that affected the active-site population were also found to influence the elasticity.[207] For example, adding cocatalysts to the reactor to improve activity or adding titania to the surface usually increased the elasticity of the polymer. An example is shown in Figure 10.86, where two different Cr/silica–titania catalysts were tested with and without cocatalyst. Figure 10.86 is another Arnett plot where zero-shear viscosity is graphed against MW. For

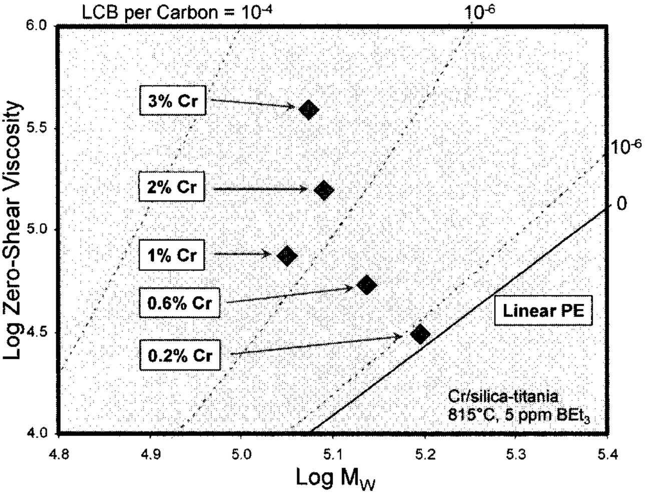

Figure 10.84 Influence of Cr loading on LCB.

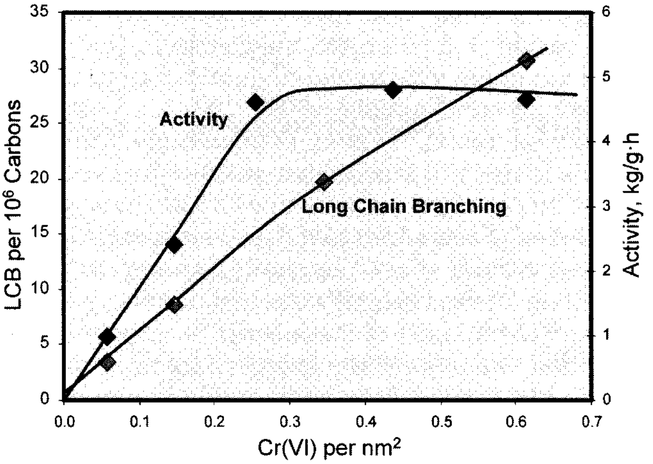

Figure 10.85 Influence of Cr loading on LCB.

both catalysts the use of cocatalyst increased the viscosity, implying an increase in LCB or at least an increase in the effectiveness of the LCB. Triethylboron seemed to have a stronger effect than triethylaluminum, even though it did not provide any more activity.

That the use of cocatalysts could increase the level of LCB is a strong possibility since the active-site density probably did increase. However, another possible contribution to the elasticity must also be considered. Because these cocatalysts can significantly broaden the MW distribution, particularly the borane cocatalyst, it is conceivable that the LCB distribution within the MW distribution has changed. In Figure 10.86 one sees that cocatalyst moves

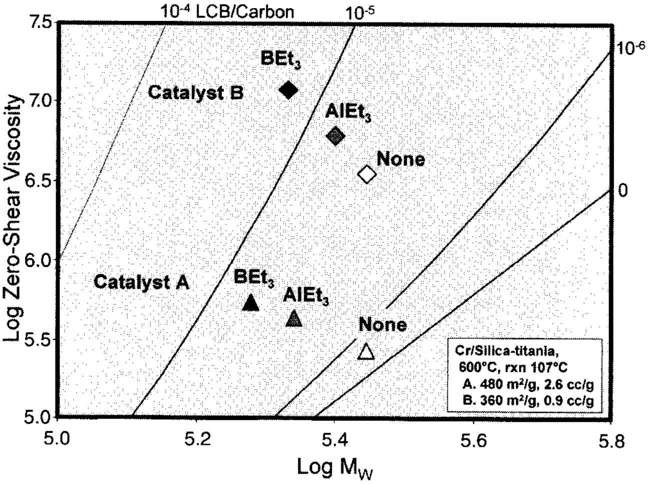

Figure 10.86 Influence of cocatalysts on LCB levels from Cr/silica–titania.

$\log M_w$ to the left, indicating an increased concentration of low-MW chains. However, $\log \eta_0$ also moved up on the chart, suggesting at least some additional LCB, perhaps in the mid- to mid–high-MW region. The net effect is a major increase in the elasticity of the resin.

Conversely, adding certain poisons to the reactor decreased elasticity. Carbon monoxide is effective as a catalyst modifier to decrease the elasticity of the polymer.[458] In one experiment up to 0.2 CO/Cr was added to poison a Cr/silica catalyst. As CO was added to the reactor, the activity decreased and the polymer also changed. First, the shear response, or HLMI/MI ratio, decreased, indicating lowered elasticity due to a narrowing of the rheological and/or chromatographic breadth of the polymer. Second, an increase was seen in the melt–solution viscosity (MSV) index, a ratio that compares the melt viscosity, which is highly affected by LCB, to the solution viscosity, which is little affected by LCB. This indicates decreasing LCB, as CO was added to the reactor.

The apparent connection with active-site density clearly does not fit with the normal view of macromonomer insertion, because none of these variables is known to increase comonomer incorporation efficiency. Increasing the ethylene concentration, which should compete with vinyl end groups to lower LCB, usually did not have a strong effect. But increasing the ethylene concentration *is* known to increase site density, suggesting the possibility that the two opposing forces may counteract each other.

Reactor temperature, often used to control MW in commercial operations, seems to have little effect on the LCB level, at least in the usual commercial range. One does, however, often observe a sharp drop in LCB level when the reactor temperature is raised until swelling of the polymer results. This is discussed in more detail below.

10.6.8 Speculation on Mechanism of LCB Generation

It is hard to explain these phenomena (and others described below) based on a purely random approach. Therefore many avenues of speculation open up. For example, one possible explanation for these LCB preferences is that, once terminated, the polymer tail containing the vinyl end group does quickly become immobilized, but it may have some limited freedom during a short time after its formation. During this time and before a new chain can grow on the parent site, it may be able to reach neighboring sites and become incorporated there as a long-chain branch. Thus the closer the active sites are to each other (e.g., the higher the active-site density), the greater the likelihood of LCB formation, as illustrated in Scheme 10.24.

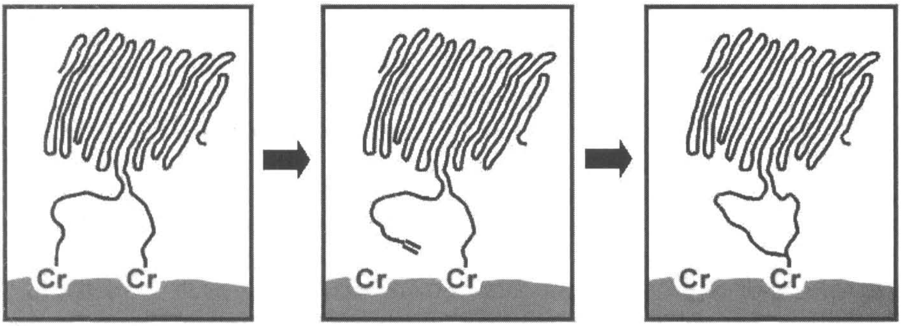

Scheme 10.24

In Figure 10.87 the degree of LCB is plotted against the average separation between active sites. As a surrogate for LCB, the shear response is plotted as measured in two ways. First, the ratio of low-shear melt viscosity to high-shear melt viscosity is plotted. Second was the simple HLMI/MI ratio. Both these ratios are a measure of melt elasticity, and because the MW distribution did not change, it indicates LCB in this case. The *X* axis is the distance between active sites calculated using the method of Hogan (Figure 10.17) in which the measured activity is compared to the activity per Cr at extremely low Cr loadings. The shape of the curve in Figure 10.87 is obtained from many other indicators of LCB as well. It is usually flat when the Cr–Cr separation distance is high, but when site distances come within some value, in this case about 4 nm, the LCB indicator climbs steeply. It causes one to wonder if this separation corresponds to something real, such as the degree of mobility that chain ends have.

In a related but alternative idea, LCB might come from certain special sites that do not liberate the chain after termination but remain coordinated to it while another chain grows. In fact, certain observations from metallocene work strongly suggest that sites do hold on to the terminated chain while another chain is growing. This idea might be considered as a modification of the "trigger mechanism" proposed for Ziegler catalysts.[459] It is conceivable

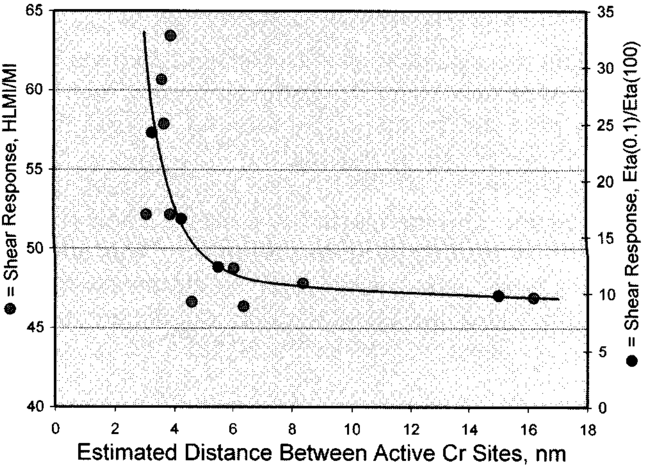

Figure 10.87 Influence of Cr content on LCB.

that some sites are more prone to hold the terminated chain than others, and the differences in LCB propensity between catalysts merely reflect the degree to which these special sites have formed. The distance between sites might also be important should terminated chains become displaced.

Still another possibility is that LCB comes from dichromate (as opposed to chromate) species in which the neighboring Cr(II) either is also active or at least serves as a coordinative "parking" place for a macromonomer generated by its neighbor. Increasing activation temperature and chromium loading have both been shown to increase dichromate content, as in Figures 10.4 and 10.5. One interesting observation is that, when raising the Cr loading, the LCB level continues to increase even after the activity stops rising. This indicates that the additional Cr, which is probably not active, still plays a role in LCB formation. The additional Cr might serve to increase the dichromate level or otherwise be the neighboring "parking place." Other factors, like metal alkyls or higher ethylene, could help activate these dichromate sites.

Thus, for now, there are many ways to speculate on LCB formation but little reason to believe in a purely random process. No doubt future work will shed light on this important area, as tools for detecting LCB in polymer continue to improve.

10.6.9 LCB and Porosity

Perhaps the most powerful commercial variable for controlling LCB is the porosity of the support.[59,60] For three decades it has been known that higher surface area tends to lower the elasticity of the polymer. One possible explanation is that the typical fixed 1% Cr loading is spread out over more surface, thereby lowering the active-site density, which in turn tends to lower LCB, as noted above. However, often it is found that lowering the surface area has a much more profound effect on LCB than one might expect from the resultant small change in chromium spacing (which can be checked by merely varying the Cr loading).

Another clue comes from a closer inspection of the effect of activation temperature on LCB. Figure 10.82 is an Arnett plot of polymers made from catalysts in which the activation temperature was varied. Because the effect of LCB on melt viscosity is also related to the molecular weight, the Janzen–Colby grid lines are shown, indicating the viscosity expected for various levels of LCB.[450] Notice that as the activation temperature is increased the points move away from the linear reference line and across the Janzen–Colby grid, indicating increasing LCB. At around 900 °C there is a sudden shift back in molecular weight and a large increase in melt viscosity. This is typical of most catalysts and indicates a disproportional increase in LCB associated with reaching the sintering temperature.

Sintering does lower the porosity of the catalyst. Figure 10.83 shows the sudden increase in LCB as a function of temperature along with the change in surface area, which drops precipitously at the same temperature. Figure 10.88 shows the change in pore size distribution, determined by nitrogen sorption, which accompanies the typical sintering of a catalyst. Although surface area is reduced, it is not enough to account for this large change in LCB based on the increase in Cr density. In fact, the Cr(VI)/nm^2 level is usually saturated at this temperature and does not change (Figure 10.6). Instead, the silica structure begins to exhibit the early stages of melting. The primary silica particles (typically about 3–8 nm diameter) begin to fuse together (Figure 10.89), suggesting that this new architecture somehow influences later LCB formation.

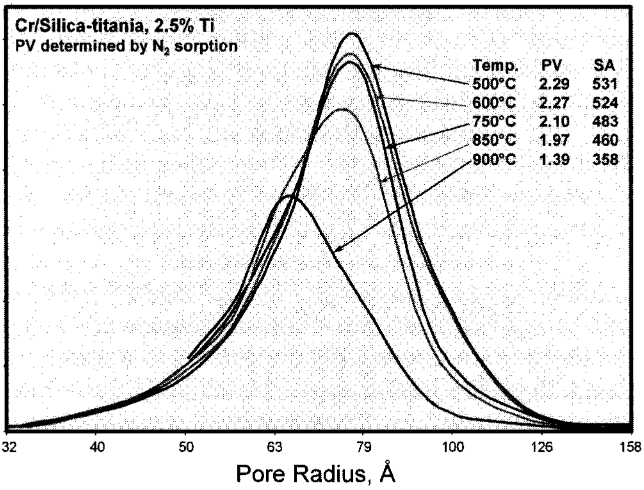

Figure 10.88 Decrease in porosity from sintering.

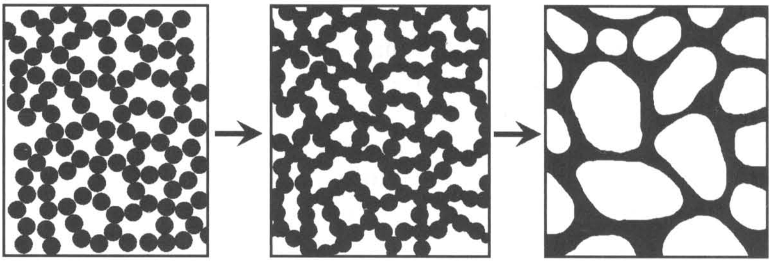

Figure 10.89 Coalescence of silica gel primary particles during sintering or through Oswald ripening during alkaline aging.

It is interesting to separate these two coexisting but independent influences on LCB: (1) the effect of calcining the chromium at high temperature versus (2) the effect of the structural changes to the silica that accompany the high temperature. To do this, many experiments were done in which the silica support alone was sintered, or "fused," in different ways.[59,60] For example, in one series of experiments a high-surface-area (600-m^2/g) silica obtained from W. R. Grace as grade 951 was treated with steam at high temperatures in order to cause primary particle fusion. Such hydrothermal treatments are well-known methods of lowering the surface area of silicas through coalescing of their fine structure. Afterward the silica was rehydrated in liquid water, impregnated with 1% Cr, and activated at 700 °C. When tested, these catalysts produced LCB levels that increased profoundly with the severity of the steam treatment, as measured by surface area loss.

In a similar experiment another silica, lower in surface area (300 m^2/g), was obtained from W. R. Grace as grade 952 and it also was steam treated. The natural LCB level from this silica was higher than from the grade 951 used above. Nevertheless steaming further increased the LCB level to some extraordinarily high values even at the low activation temperatures. It is interesting that the LCB level from all these steamed samples, from both the 951 and 952 series, can be plotted against surface area to yield a single line. This is shown in Figure 10.90. This is because both grades 951 and 952 are made from the same silica hydrogel. The 952 grade has been chemically treated during its manufacture to cause fusion of the primary particles into a stronger gel network with lower surface area. Thus the process is very similar in its result to steaming.

This process is called alkaline aging of the hydrogel.[167,460] The fine structure of the silica is fused as it is soaked in a basic solution at 60–90 °C. Apparently small amounts of silica are temporarily dissolved in the alkaline solution and then redeposited along the primary particle contact points, thus welding the primary particles together into a stronger network but also removing some of the fine structure. In one series of experiments a silica–titania–chromia hydrogel, known for its low LCB potential, was soaked for varying times at 80 °C in water to which NH_4OH was added to maintain a high pH. After the aging

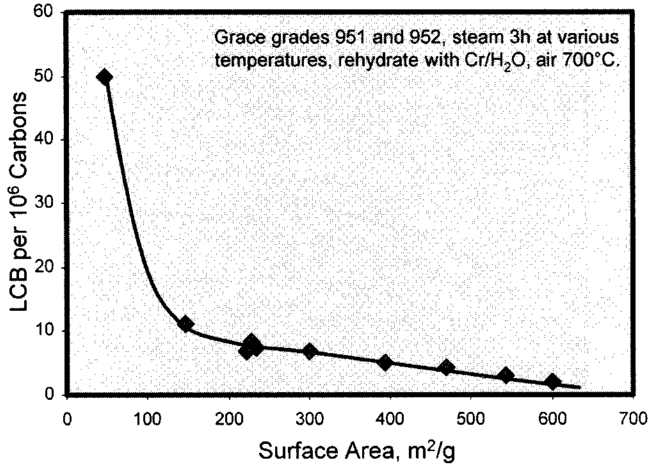

Figure 10.90 Raising LCB by steam-produced fusion of base silica.

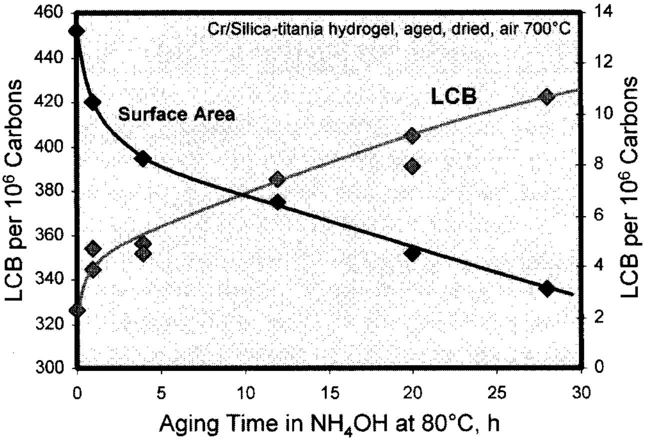

Figure 10.91 Alkaline aging increases LCB.

treatment each sample was alcohol washed, dried, and then activated at 700 °C. When tested for polymerization the LCB level was found to increase as the surface area decreased. This is shown in Figure 10.91.

Another example of the effect of alkaline aging is shown in Figure 10.92, where blow-molding resins were made from two Cr/silica–titania catalysts, one alkaline aged and the other not aged.[207] These two catalysts differed only in their pore structure. The chemical composition, Cr loading, and activation were identical. In this application high LCB is usually associated with low parison swell, an important characteristic in many commercial molding operations. Notice in Figure 10.92 that for a given MI (or HLMI) swell decreases with increasing activation temperature and more significantly with alkaline

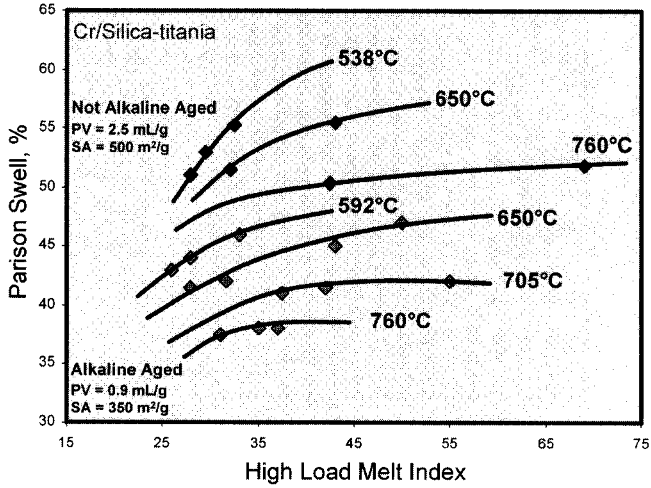

Figure 10.92 Influence of alkaline aging on PE swell.

TABLE 10.14 Effect of Catalyst Pore Structure on Product Behavior

Application	Catalyst	
	Alkaline Aged	Not Aged
Blow molding		
Flow at high shear	High	Low
Die swell	Very low	Very high
Environmental stress crack resistance	Low	High
Film		
Bubble stability	Excellent	Poor
Transverse tear resistance	Poor	Good
Sheeting		
Head pressure	Low	High
Melt strength	High	Poor

aging. Such considerations are very important in determining which catalyst will be used commercially to make a given resin grade.

Table 10.14 summarizes the behavior of resins from these two catalysts in three applications. Some of the differences were profound. In blow molding, polymers from the aged catalyst exhibited lower viscosity at high shear (easy molding), higher viscosity at low shear (better melt strength), and very low swell, even at low activation temperatures. The lower molecular weight decreased the resistance to chemical attack (ESCR). In film blowing the aged catalyst yielded much better bubble stability but poorer transverse direction tear resistance due to slow relaxation and consequent orientation. In geomembrane sheeting the aged catalyst yielded lower pressure on the die during blowing, and the melt strength was much better compared to the unaged cata-

TABLE 10.15 Commercial Silica Grades Varying in Degree to Which They Have Been Alkaline Aged

Grace Silica Type[a]	Surface Area (m^2/g)	LCB per Million Carbons
968MS	600	3.9
969MPI	300	6.5
Low SA 969MS	240	10.4
250A Carrier	175	12.8
350A Carrier	130	23.3
1000A Carrier	45	25.5

[a] Grace commercial silicas: Each sample was impregnated with CrO_3 aqueous solution, then activated at 700 °C. Polymerization was at 105 °C and 550 psig.

lyst. This latter trait is particularly important in geomembrane molding, where the film bubble is 22.5 ft wide, rises eight stories into the air, and weighs 2.5 tons. All these traits are characteristics of higher LCB levels. It is remarkable that the porosity of the silica imparts such profound differences in the polymer.

For many decades HDPE manufacturers have unknowingly used the principle of alkaline aging to control polymer properties through the selection of different commercially available base silicas. Table 10.15 lists some common silica grades made by W. R. Grace from the same hydrogel type and the LCB level they produced when activated at 700 °C. One can see that LCB goes up as surface area goes down due to particle fusion. HDPE producers have long connected surface area with resin swell and made their selection accordingly, perhaps without realizing the actual underlying variable.

Exactly why fusion of primary silica particles should increase LCB is unclear, but given this connection, it is not surprising that lower surface area silicas should tend to give highest LCB levels. One possibility is that the bonding with Cr is somehow affected by the curvature of the silica surface.[461] Another idea is that the reinforced structure results in less fragmentation during polymerization, and larger fragments mean proportionally more polymer formed inside pores (as opposed to the exterior of each fragment). Large polymer chains formed inside much smaller pores probably would not have the freedom to fold in the normal way and could be left in an unnatural or activated state until they can escape from the pore. Speculating further, perhaps during this time they have a higher probability of being incorporated by a neighboring site within the pore.

Other methods of fusing the primary particles also increased LCB. For example, in one experiment a high-surface-area (450-m^2/g) Cr/silica–titania catalyst was sprinkled through the high-temperature zone of a laboratory torch used for glass blowing.[462] Thus, for a brief instant, the catalyst was exposed to a very high temperature, high enough to approach the melting point. In fact, given the good insulating properties of the catalyst and its extremely brief passage through the flame, it is likely that the exterior of each particle received a more severe treatment than the center. This "flame-treated" silica–titania cogel was found to have diminished surface area of 257 m^2/g. It was then activated at 870 °C in the normal way and tested for polymerization. The flame-treated catalyst produced much higher elasticity (LCB) than its untreated parent.

In yet another way of fusing catalyst particles, a small amount of sodium (0.3 mmol/g) was added to silica so that it would act as a flux during subsequent calcining steps at 700–800 °C.[59,60] This treatment reduced the surface area from 300 down to 200, then further to 140, and finally to only 25 m^2/g. Afterward the sodium was washed off of each silica sample and chromium was impregnated from aqueous solution. A final activation at 700 °C resulted in catalysts that again produced high levels of LCB according to the level of surface area loss.

Precipitated silicas (as opposed to the gelled silicas used for polymerization) are usually of lower surface area, and these also provided high LCB levels when converted into Cr/silica catalysts.[59,60] In fact, some of the highest levels of LCB that we have observed in this laboratory from a Cr/silica catalyst came from an unusual silica grade called Sylox from W. R. Grace Company. According to Grace researchers, it is a hybrid structure between gelled and precipitated and made by a kind of double-precipitation reinforcement.

Still other support structures produced very low LCB levels. For example, pillared bentonite yields low LCB if activated below the fusion temperature. Bentonite consists of large sheets that could easily separate to accommodate growing polymer. However, if taken to 600–700 °C, where the structure rearranges, high LCB levels are found. Alumina, which is quite unlike silica in its structure, provides very low levels of LCB. Alumina consists of crystallites or platelets rather than a gel network.

10.6.10 LCB and Polymer Yield

It was postulated above that particle fusion might influence the extent of fragmentation during polymerization, which in turn determines how much polymer is formed inside pores versus on the surface of the fragments. If polymer formed in pores is more likely to contain LCB, then one might expect that the first polymer chains formed from a catalyst particle would have the highest level of LCB, because before fracturing, all polymer chains are formed inside pores. To test this idea, several catalyst types were charged to the reactor, but the run was stopped at various times to yield different amounts of polymer.[207] Those polymers were then analyzed for LCB by an Arnett plot. Two examples are shown in Figure 10.93. In one case a Cr/silica–titania containing 5% Ti and activated at 650 °C was allowed to make polymers varying in yield from as little as about 25 g PE/g catalyst to about 5000 g PE/g catalyst. The viscosity/MW points on the graph make a zone for each catalyst, and the arrows point in the direction of higher polymer yield with time. It can be seen that there is a large difference, almost two orders of magnitude, between the melt viscosity at the earliest stages of production compared to the last stages of polymerization. In this example, for instance, the starting LCB level was about 25 branches per million carbons, but at the end of the run (at 5000 g PE yield/g catalyst) the average LCB level

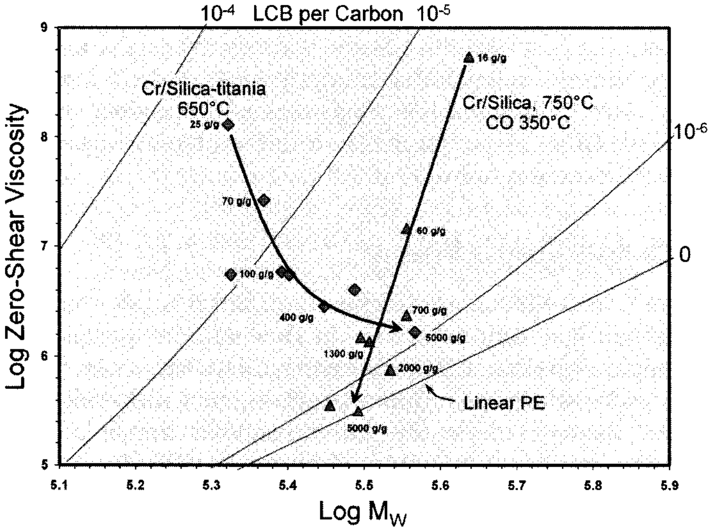

Figure 10.93 Arnett plot, highest LCB at lowest yields.

had dropped to 2 branches in 10^6 carbons. Thus it is clear that the first chains formed contain the highest levels of LCB.

Why the first polymer chains formed contain more LCB could be related to pore rupture, as noted above, but another possibility considered was that the first sites to be reduced by ethylene, being the most reactive, also naturally incorporate LCB more efficiently. To probe that possibility, another series of runs was made, varying in polymer yield, but the catalyst was a Cr/silica rather than a Cr/silica–titania and activated at a higher temperature, 750 °C, in order to have a more uniform distribution of sites. Then this catalyst was also CO reduced at 350 °C so that all sites would already be reduced. These results are also plotted in Figure 10.93. They exhibited the same trend of increasing LCB with decreasing polymer yield. However, because of inherent differences between the two catalysts, this catalyst produced somewhat less LCB at the beginning and at the end of its polymerization runs.

For both catalyst types, there was a sharp increase in LCB level during the first 100 g/g polymer yield, as if the first polymer made were somehow different from later polymer made. Obviously this is the time when polymer is primarily made inside pores before their complete rupture. The experiment above was repeated except with a Ziegler catalyst supported on the same silica. Identical runs were made and stopped to various yields similar to those in Figure 10.93. In this case, however, there was no movement away from the linear polymer reference line. These Ziegler polymers were all the same and all unbranched. This was partly expected because these Ziegler catalysts produced few vinyl end groups, making incorporation of macromonomer much less likely. Nevertheless we wanted to make sure that the silica impurity left in the polymer did not artificially raise the viscosity and give misleading results. These Ziegler "blanks" with similar silica levels indicated no significant contribution to the measured viscosity from the silica at these levels. When the experiment was repeated with certain metallocene catalysts supported on silica, which are known to produce LCB, again low yields seemed to produce more LCB. On the other hand, Cr/alumina, which has a different pore structure, was not found to follow the same trend.

10.6.11 LCB from Solution Process

In the slurry process the reactor temperature, which is often used to control molecular weight, has little effect on LCB within the normal commercial operating range. However, if the reaction is allowed to cross the foul curve, the temperature at which the polymer begins to melt and swell in the hydrocarbon diluent, then one frequently observes a major drop in LCB level. Even a degree or two can result in a large decrease in LCB. An example of this behavior is shown in Figure 10.94, which is another Arnett plot. The zero-shear viscosity of polymers made from 815 °C Cr/silica–titania is plotted against log M_w. These polymers were made at different temperatures in order to vary the molecular weight. As reactor temperature was increased from 80 up to 109 °C, the viscosity of these polymers resulted in a line that paralleled the Janzen–Colby LCB lines, indicating a constant LCB level (about 13 branches per million carbons on the chart). However, as the temperature was increased another two degrees to 111 °C, the foul curve was crossed, resulting in partial melting and swelling of the polymer. Notice that this also caused a rather sharp drop in LCB level, down to about 4 branches per million carbons.

This is because there is a major difference in LCB level from Cr/silica catalysts according to which polymerization process is used. Polymers made in the solution process, where the polymer dissolves as it is formed, contain much less LCB than polymers made in the slurry- or gas-phase processes.[207] The

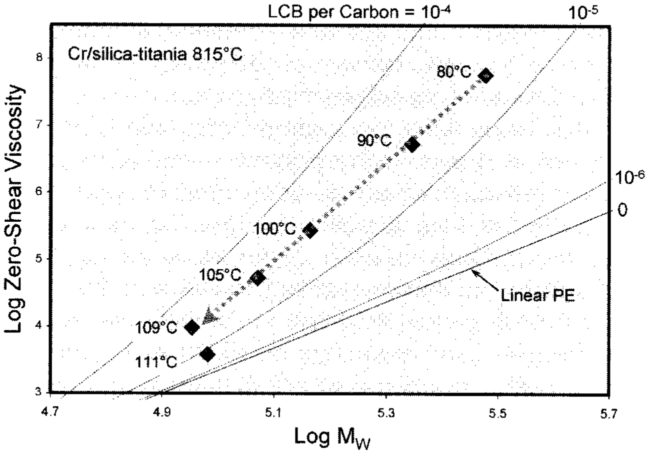

Figure 10.94 Arnett plot showing effect of crossing foul curve on LCB level.

solution process runs at much higher reactor temperatures, so that Cr/silica catalysts are traditionally activated at lower temperatures in order to lower the MI potential. Lower activation temperatures tend to produce lower LCB, as noted above. Nevertheless, even Cr/silica catalysts activated at the same temperature tend to yield much lower LCB when run in the solution process.

One possible explanation is that in the solution process each chain is dissolved and carried away from the active site as it is formed, in contrast to the slurry- or gas-phase processes where the chains remain in the vicinity of the active site. Stated another way, the concentration of chain ends in the amorphous phase of a polymer particle (which surrounds the active site) would be considerably higher than exists when those same chain ends are dissolved and dispersed throughout the entire reactor space. Of course, the chains in solution should be more mobile and therefore possibly more reactive than when frozen out in a polymer particle. Nevertheless, this effect might not be significant enough to overcome the concentration difference, and the net result is that polymers made in solution generally contain less LCB. Another possible reason for lower LCB from the solution process is the higher temperatures involved. If some LCB does result from the site holding onto a vinyl end group while a second chain grows, the higher temperatures, as well as the greater mobility, may help the macromer to desorb.

This response is responsible for some interesting contrasts in catalyst behavior between the two polymerization processes. As noted in Table 10.12, at constant MI, the rheological breadth of the polymer broadens with rising activation temperature in the slurry process. This is evident in many resin characteristics, including its shear thinning behavior, which is very important in determining how the molten polymer will flow during molding. One common measure of the shear-thinning ability of a polymer is the ratio of the high-load MI to the MI. In Table 10.12 the HLMI/MI ratio can be seen rising with activation temperature. Since the MW distribution is actually narrowing, the shear-thinning behavior here is the result of increasing LCB.

In the solution process, however, this relationship is reversed. The polymer becomes less shear thinning as the activation temperature is raised. This is because polymers made in the solution process contain little or no LCB and therefore the shear-thinning behavior reflects only the chromatographic breadth or MW distribution. Since the polydispersity actually narrows with rising activation temperature (M_w/M_n in Table 10.12), the solution-derived polymers become *less* shear thinning.

The HLMI/MI ratio (or other viscosity ratios) is usually also dependent on the MW if the polymer contains at least a low level of LCB. Thus the HLMI/MI ratio is often plotted against MI to compare different families of polymers or catalysts. An example is shown in Figure 10.95 for polymers made from Cr/silica–titania in the slurry process. Notice that each increment of higher activation temperature generates a new curve that lies above the preceding one. Thus the polymer is becoming *more* shear thinning with rising activation temperature. The same kinds of data are plotted in Figure 10.96, but from poly-

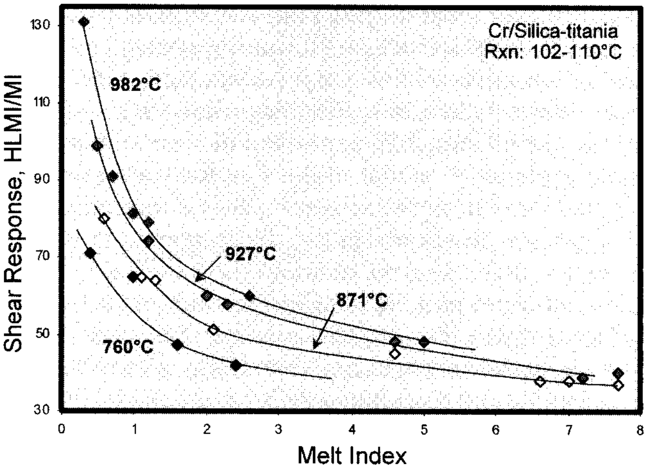

Figure 10.95 Influence of activation temperature on shear response of PE from slurry process.

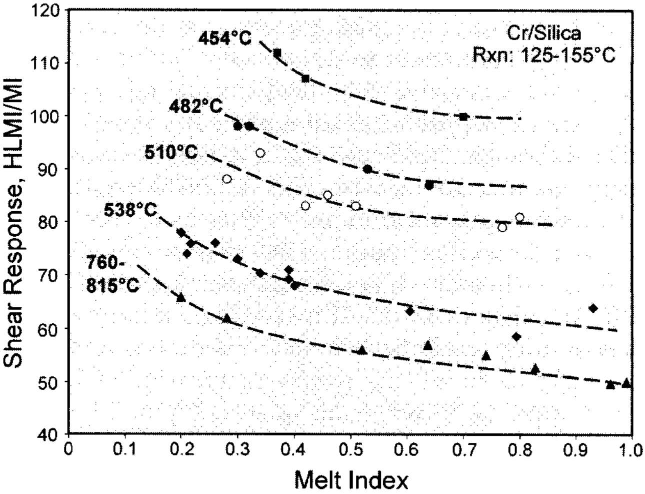

Figure 10.96 Influence of activation temperature on shear response of PE from solution process.

mers made in the solution process. Now each higher activation temperature generates a new line below the preceding one. These polymers are becoming *less* shear thinning with rising activation temperature.

For many years a goal of catalyst research at Phillips was to use the more economical slurry process to make the same high-MI injection- and roto-molding polymers that were normally made in the solution process. At first, it was difficult just to achieve the required high MI at the lower slurry reactor temperatures. Eventually catalysts were developed to deliver high MI, but the polymers still often had problems, such as higher warpage during cooling and sometimes more brittle impact behavior. These undesirable characteristics

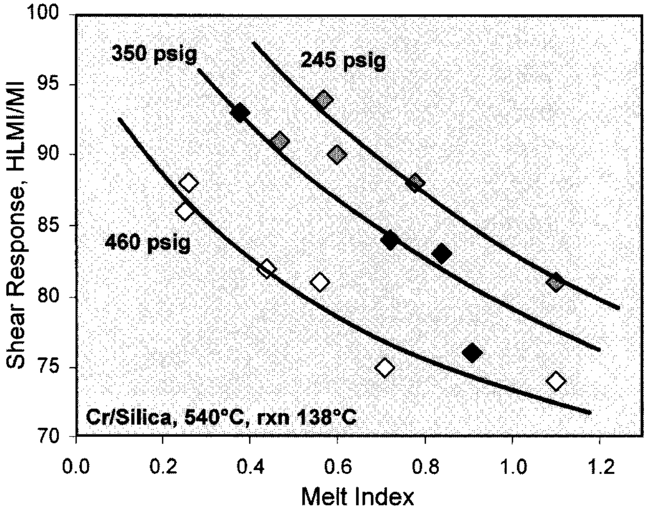

Figure 10.97 Shear response as function of ethylene concentration in solution process.

resulted from the naturally higher LCB level that the slurry process tends to produce from Cr/silica. Thus higher MI potential was not enough. To fully satisfy these applications, it was also necessary to minimize LCB.

Ethylene concentration does exhibit a clear influence on melt elasticity in the solution process. As might be expected, increasing ethylene decreases elasticity. Since the MW distribution is little affected, this suggests that the already low levels of LCB may indeed be influenced slightly, due to competition between ethylene and chain ends. This shows up frequently in the shear response of the polymer, or HLMI/MI ratio, which is known to increase with both LCB and MW breadth. An example is shown in Figure 10.97. Cr/silica activated at 540 °C was tested at 138 °C in cyclohexane solvent at three different reaction pressures. The HLMI/MI ratio for each polymer was plotted against its MI. A line is formed for each pressure which moves lower on the graph as pressure was increased. This indicates less elasticity.

Other variables that affect elasticity in the slurry process seemed to perform similarly in the solution process. This included chromium concentration and reactor residence time. Figures 10.98 and 10.99 show two typical plots of shear response against MI, in which the chromium loading or the residence time was varied. These plots, obtained in 1961, show the characteristics that were valued most at the time, namely low MI potential and low shear response. The latter was considered important in the prevention of warpage during cooling, which can be brought on by frozen residual stresses caused by high melt elasticity.

10.6.12 Alpha–Omega Dienes

One method of sharply increasing LCB in PE derived from Cr/silica catalyst is to increase the vinyl concentration of the polymer by copolymerizing dienes that contain two terminal vinyl end groups. For example, a small amount of

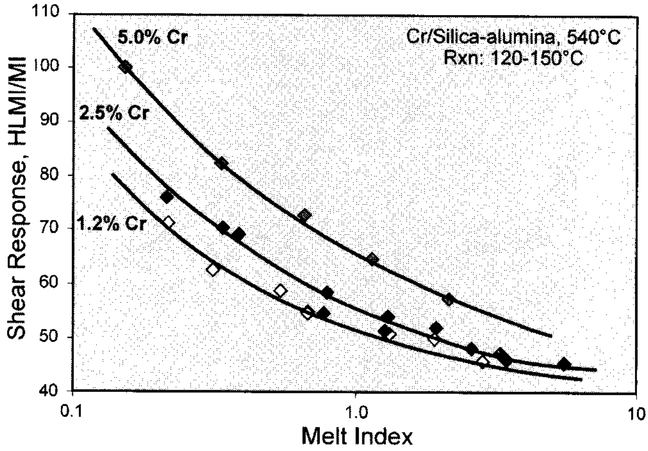

Figure 10.98 Shear response as function of chromium loading in solution process.

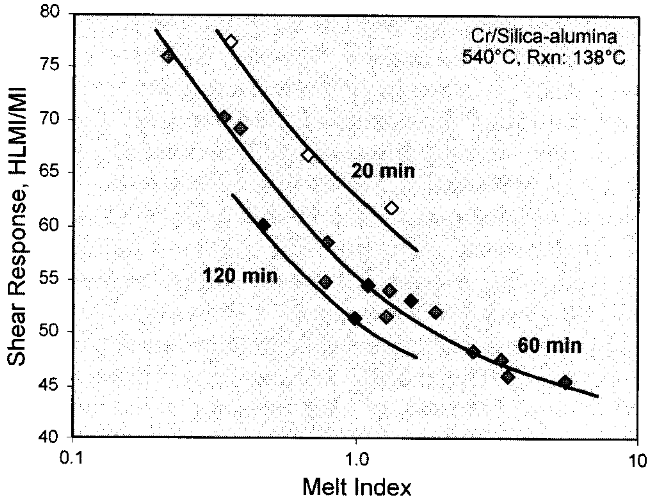

Figure 10.99 Shear response as function of polymerization time in solution process.

1,9-decadiene added to the reactor with Cr/silica catalyst greatly increases the LCB content, as measured by melt viscosity. Polymers also quickly become insoluble due to excessive cross-linking. In fact, the approach seems to work for many other catalysts as well. Even Ziegler catalysts, which are not known for producing LCB (presumably due to lack of vinyls), develop very high levels of LCB when such dienes are used. It is unclear whether this is simply the result of increasing vinyl concentration in the polymer or whether it occurs by some other mechanism such as shown in Scheme 10.25.[463]

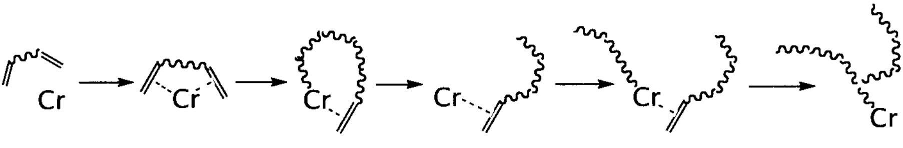

Scheme 10.25

This mechanism assumes that one end of the diene remains coordinated, but passive, during the growth of a chain from the other end on the same site. This idea, which requires coordination to two olefins in addition to the growing alkyl, is similar to the "trigger mechanism" proposed for Ziegler catalysts.[459]

10.6.13 LCB Distribution from Cr/Silica

Chromium catalysts contain a distribution of site types differing in the chain length they produce and the degree of ease of comonomer incorporation. It is interesting to consider for Cr/silica what the LCB distribution would be, within the MW distribution, under the usual assumption of a random process. This can be calculated if one assumes that sites would incorporate macromonomer with the same relative ease or difficulty that they incorporate SCBs, an assumption that is usually made in the literature. The SCB distribution breakdown was indicated in Figure 10.66. Superimposed on this distribution, however, is the fact that LCB from each single site can also be skewed toward the high-MW side, because the act of adding a long chain branch to a chain can significantly increase the MW of that chain (Figure 10.81). Combining these two trends yields the LCB distribution shown in Figure 10.100. LCB is concentrated not in the lowest or highest MW region but in the mid–low- to

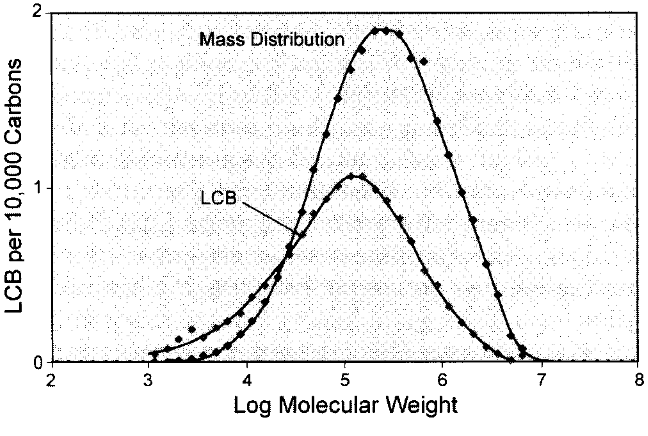

Figure 10.100 Theoretical LCB distribution from Cr/silica assuming sites incorporate macromonomer in relative proportion to that measured for 1-hexene.

mid-MW part of the MW distribution.[457] This treatment also assumes that vinyls generated by one site are available for incorporation by another.

Experimentally, several observations suggest that this picture is probably not too unrealistic. For example, one very broad MW distribution polymer from modified Cr/alumina was fractionated in this laboratory in order to determine the LCB distribution. LCB was indeed found to be mainly in the mid- to low-MW portion of the MW distribution, as predicted, and not in the lowest MW portion. Similarly the LCB level from Cr/aluminophosphate catalysts strongly follows the phosphate contribution, which is in this same 10^4–10^5-MW range. Titania, which can also increase elasticity, likewise tends to add polymer in this range. Thus the distribution in Figure 10.100 would seem to be in rough agreement with what experimental data are available.

However, it should be pointed out that some of these examples violate the very assumptions on which Figure 10.100 was based. For example, Cr/alumina produces a fairly flat SCB profile even though the LCB profile was not flat. Thus another mechanism could also be proposed to give the same experimental result: That is, some sites produce more LCB than others, quite independently of SCB incorporation, because they tend to hold onto the last chain terminated. This ability of a site may have little connection with its ability to incorporate SCB. These very reactive sites may be the same ones that produce mid–low-MW polymer.

10.6.14 Low-LCB Catalysts

Many ways of tailoring catalysts have been developed to increase or decrease LCB for special polymer applications. One such treatment involves another alkaline modification of Cr/silica, a treatment with magnesium hydroxide, which has just the opposite effect on surface area as that described above.[464] When applied to a commercial preformed silica or silica–titania, the resulting acid–base reaction, possibly producing a magnesium silicate species, changes the structure and greatly increases the surface area, sometimes doubling it or more. The MW of the polymer is increased, sometimes by up to twofold. These trends are shown in Figure 10.101 for a series of silica–magnesia cogels containing various amounts of magnesia. These were activated at 600 °C and then run at 98 °C. It is unclear whether any of the polymer changes are the result of electronic influences on the chromium, but it seems fairly certain that the new physical matrix plays a strong role to minimize LCB. Other metal hydroxides were less or not effective. The effect of magnesia is very useful in commercial production settings because of its ability to diminish LCB, especially in pipe and film.

Cr/alumina also produces polymers of extremely low LCB content.[384] When activated at 700 °C polymers from Cr/SiO_2 and $Cr/AlPO_4$ contained about 30 long-chain branches per million carbons, whereas the polymers from Cr/Al_2O_3 contained about one LCB per million carbons, over an order of magnitude less. In addition the LCB level from Cr/alumina does not display the usual

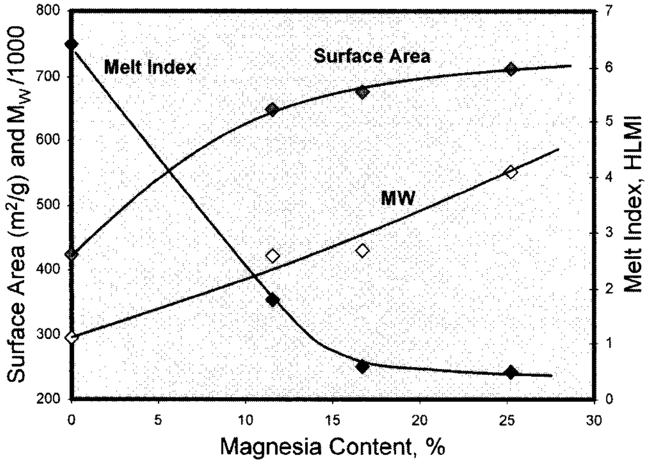

Figure 10.101 Effect of magnesia on Cr/silica.

dependence on polymer yield. Even polymers made at very low yields exhibit extremely low LCB levels. Whether these variations are due to a chemical difference, such as the well-documented domination of chromate species on alumina (little or no dichromate), or to a difference in catalyst structure is not clear. Both may be important. Although high-porosity aluminas are available (400–500 m^2/g, 1.5 mL/g) and comparable in porosity to the best polymerization-grade silicas, the skeletal density of alumina can be nearly twice (~4 g/mL) that of silica (2.2 g/mL). This means that alumina must have a more finely divided microstructure for the same surface area and pore volume. Actually the porosity of alumina is considered to be qualitatively different from that of silica. Silica develops its microstructure due to the coagulation and fusion of primary particles that (baring sintering) do not change during calcining. In contrast, alumina develops much of its pore structure as a result of the loss of bulk water during calcining from the conversion of the trihydroxide or bohemite (AlOOH) form into γ-alumina crystallites. These differences may contribute to the differences seen in activity and in LCB between silica- and alumina-based catalysts.

Adding sulfate to the alumina causes a loss of the lowest MW polymer, significantly narrowing the MW distribution and raising the average MW.[298] It also results in a further lowering of the elasticity. For example, in one series of experiments, shown in Table 10.16, increasing the sulfate level on 600 °C Cr/alumina catalyst from 0 up to 3.0 mmol SO_4/g Al_2O_3 decreased the already low LCB level from 2 down to about 0.5 LCB per million carbons. This may further suggest that most LCB-producing sites on this catalyst also produce low MW.[384]

The combination of properties listed for these polymers in Table 10.16 is truly unique from chromium oxide–based catalysts. Sulfate increases the

TABLE 10.16 PE from Sulfated Cr/Alumina

	By Sulfate Added			
Parameter	0 mmol/g	0.8 mmol/g	1.5 mmol/g	3.0 mmol/g
H_2 Added, psi	50	175	175	175
$M_W/1000$	459	329	368	521
M_W/M_n	105	13.5	11.4	8.0
M_z/M_W	7.8	4.1	4.2	4.4
HLMI	4.7	3.0	2.1	0.3
HLMI/MI	>200	45	43	33
CY relaxation time, s	137	2.1	3.1	5.5
LCB/million carbons	2.3	1.5	1.2	0.5

Note: Cr/alumina, 600 °C, reaction at 95 °C, 5 ppm TEB, 550 psig.

molecular weight (H_2 was altered in the control run so that it would produce a comparable MW) and also narrows the polydispersity. In fact, the distribution becomes surprisingly narrow for Cr oxide–derived catalyst of such high MW and made with a cocatalyst. Even more remarkable, however, is the low shear response (HLMI/MI). HLMI is inversely related to MW, but shear response decreases to that expected from Ziegler catalysts. Despite the higher MW, the Carreau–Yasuda relaxation time actually *decreased* to about 5 s—incredible for a 0.3-HLMI chromium-based PE. This unusual combination of properties is the result of an exceptionally low (for chromium oxide) level of LCB and a narrow MW distribution.

10.6.15 Cr/Aluminophosphate

Cr/$AlPO_4$ catalysts tend to impart higher levels of LCB much like that of Cr/silica. In one series of experiments Cr/alumina catalyst was doped with various levels of phosphoric acid, then calcined at 650 °C, and finally tested for polymerization activity with 5 ppm of either triethylboron or triethylaluminum cocatalyst. The degree of LCB found in the polymer was then measured by Arnett plot using the Janzen–Colby gridlines, as described above. One plot is shown in Figure 10.102, where the two effects of increasing phosphate are apparent—first a declining average molecular weight and second the development of higher levels of LCB. Trialkylboranes have a strong interaction with the phosphate-associated sites on Cr/aluminophosphate catalysts, increasing the activity, MI, and level of LCB imparted to the polymer.[384] This observation, coupled with the fact that the cocatalyst greatly increased the phosphate contribution to the MW distribution (Figure 10.63), again suggests that LCB comes primarily from phosphate-associated sites and may be concentrated in the low-MW part of the distribution.

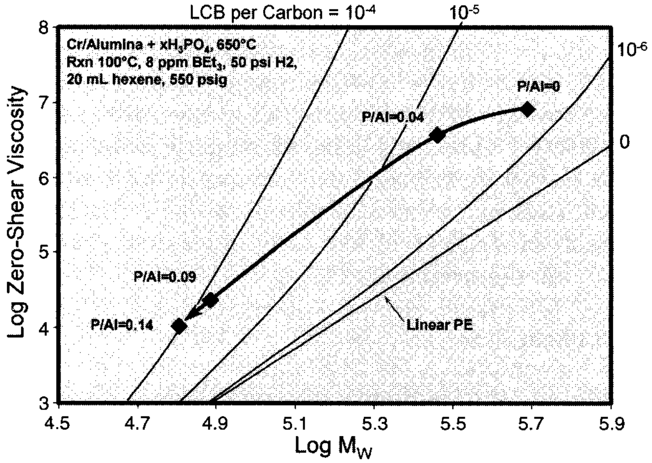

Figure 10.102 Arnett plot showing decrease in M_W and increase in LCB with increasing phosphate.

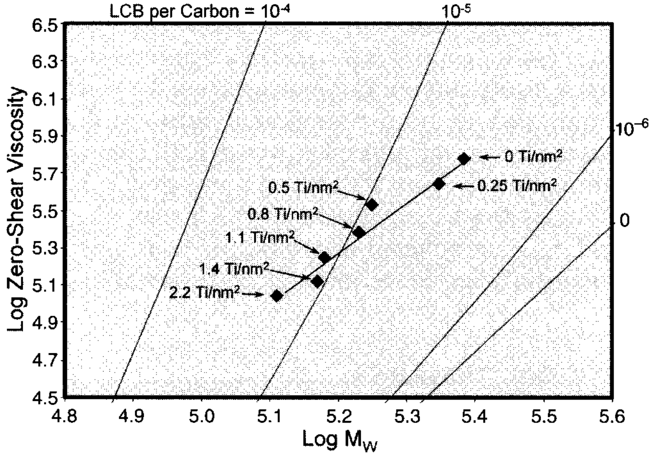

Figure 10.103 Arnett plot from titanated Cr/silica.

10.6.16 Influence of Titania on LCB

Figure 10.103 shows an Arnett plot in which Cr/silica was titanated to various levels, activated at 650 °C, and tested for polymerization. It is clear in the figure that the zero-shear viscosity moves away from the linear reference line as the titania loading is increased, indicating increased elasticity. At face value this would suggest an increasing LCB level. However, this is another case where the MW distribution broadens as the points move away from the reference line, even though the viscosity itself does not increase. Therefore, the possibility exists in this case that the LCB population has shifted within the

MW distribution relative to the average MW. Titania expanded the low-MW region of the distribution. In these examples the zero-shear viscosity did not increase, as might be expected from a major increase in LCB. Rather, it appears that the average MW has shifted to lower values while maintaining much of the viscosity. Figure 10.82 behaved similarly, however, there the MW distribution was narrowing as the line moved away, whereas for Figure 10.103 it has broadened. Thus, in this instance, one cannot tell with certainty whether or to what extent the LCB level has really increased, even though titania clearly does increase the overall elasticity.

10.6.17 LCB Conclusions

Despite the occasional discussion of possible competing mechanisms, it seems likely that Cr/silica catalysts do produce LCB through the copolymerization of vinyl chain end groups. However, the available data do not always fit the usual view of macromonomer incorporation, in which active sites are surrounded by mobile vinyl chain ends within an amorphous phase that are incorporated randomly. In this picture, selectivity happens only when some sites are more reluctant than others to incorporate α-olefins of any kind. To the contrary, as we have noted above, LCB levels can be controlled over a wide range using catalyst and reactor variables that have no obvious connection to comonomer incorporation. This indicates that the mechanism of macromonomer incorporation is more complicated than usually imagined. This observation also applies to metallocenes, where both comonomer incorporation and LCB formation can vary widely and completely independently. There are some suggestions from metallocene research that sites may be able to temporarily hold on to terminated macromer, even as a new chain grows. If true this could explain some of the unexpected behavior of these catalysts.

10.7 CONCLUDING REMARKS

10.7.1 Tailoring Catalysts for Specific Applications

Catalyst activity is valued, but during commercial PE manufacturing it is even more important to be able to control and deliver certain polymer properties. Such features as toughness, flexibility, impact and tear resistance, creep resistance, and resistance to chemical attack are determined by the MW of the polymer, the MW distribution, the short-chain branch content and distribution, and the amount of LCB. As mentioned above, these polymer properties are controlled by choice of (1) catalyst type, (2) activation temperature, (3) cocatalyst, and finally (4) reactor conditions. Many different principles, some outlined in this chapter, are used simultaneously to maximize or minimize various polymer responses. In fact, most polymer grades have been developed as a complex compromise between many different competing and opposing variables.

An example is shown in Figure 10.104. Environmental stress crack resistance (ESCR) is a property highly valued in bottle resins. ESCR is a measure of how long the morphology of the polymer will resist unraveling when lubricated by certain chemicals, especially surfactants, at elevated temperature. Measured in hours, ESCR is plotted in Figure 10.104 for resins made from two catalysts. One was simple Cr/silica activated at 800 °C to achieve high activity. The other was Cr/silica–titania activated at 600 °C and run with 8 ppm BEt_3, all to achieve a high degree of MW breadth. ESCR is helped by the broader MW distribution and flatter branch profile achieved by adding titania, and the lower activation temperature and cocatalyst provide an additional boost in ESCR due to further broadening. ESCR is also affected by density, so the results are plotted against density for a constant MI. Thus Cr/silica–titania provides considerably higher ESCR than Cr/silica catalyst. However, other properties like swell and extrusion output had to be compromised by this catalyst change because the LCB content is not equivalent.

Another example of using multiple variables to achieve broadening is shown in Figure 10.105 where the MW distribution is plotted for three 0.3-MI, 0.958-density resins. One is made from Cr/silica again activated at 800 °C. This resin had an ESCR (condition A) of 20 h. The second resin is from a Cr/silica–titania catalyst activated at a lower temperature, 650 °C, and run with a triethylboron cocatalyst to achieve further broadening. It is much broader and produced an ESCR (condition A) of 400 h. The last sample was also from a Cr/silica–titania catalyst, but activated at a still lower temperature, 540 °C, to achieve still further broadening. It also was used with a triethylboron cocatalyst and yielded an ESCR value greater than 1000 h.

As another example one of the effects of MW breadth is shown in Figure 10.106. This graph compares two series of polymers, each made with

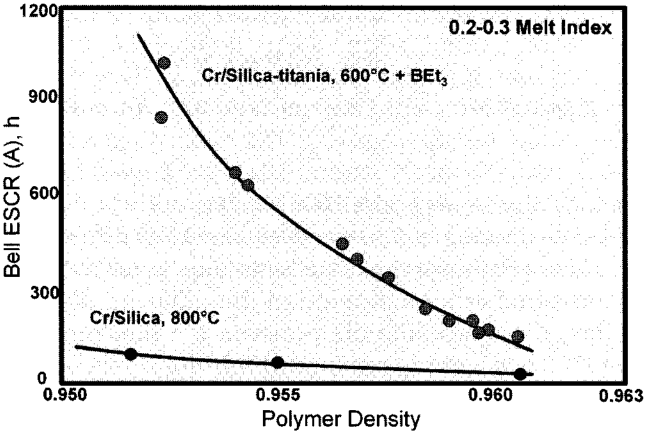

Figure 10.104 Control of environmental stress crack resistance.

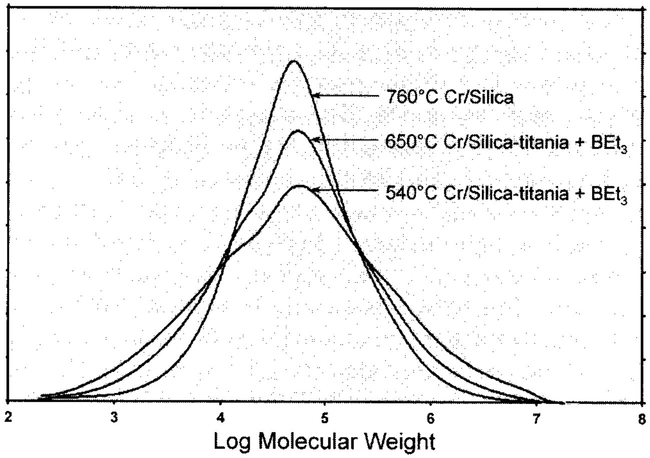

Figure 10.105 Example of utilizing several variables to precisely control breadth of MW distribution.

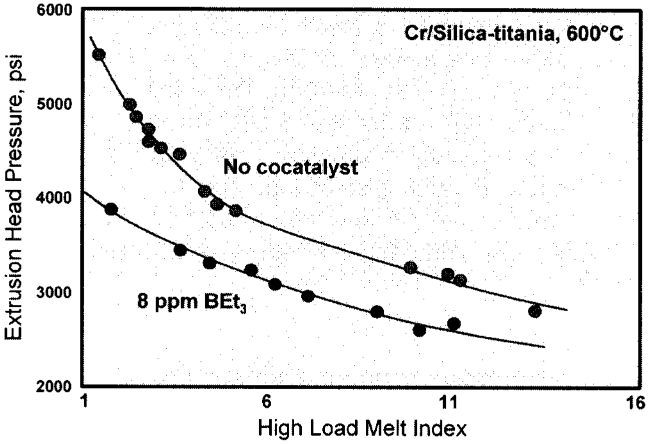

Figure 10.106 Shear thinning from BEt_3 cocatalyst.

Cr/silica–titania catalyst activated at 600 °C. One set also had triethylboron cocatalyst added to the reactor to broaden the MW distribution while the other did not. These resins were extruded into pipe at a fixed rate and the die pressure was measured as an indication of the difficulty of extrusion or the resistance to flow. Of course, the die pressure is a function of MW, so it is plotted against HLMI, which is a convenient substitute. Notice that when BEt_3 cocatalyst is added, the head pressure drops considerably, indicating that the polymer has become more "shear thinning," that is, easier to flow, as a result of the broader MW distribution.

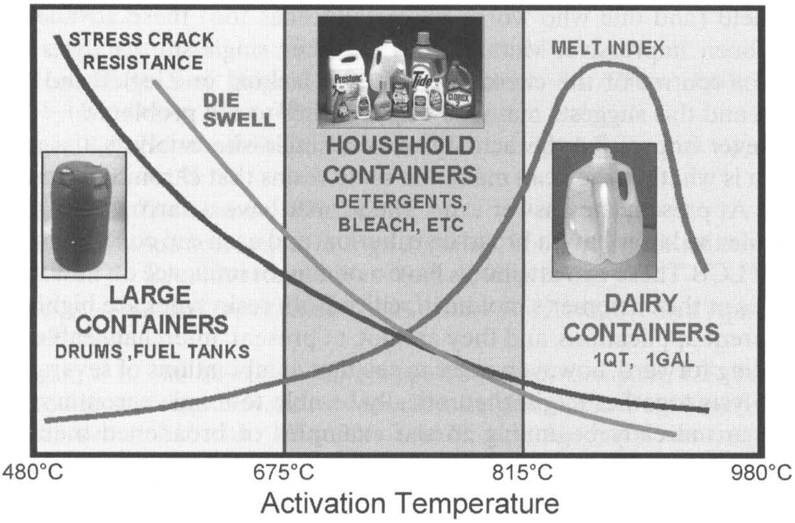

Figure 10.107 Tailoring blow-molding grades by varying catalyst activation temperature.

Because the level of LCB controls the polymer's relaxation time, it is extremely important in determining how the molten polymer flows during molding and how much "memory" it carries when forced through a die at high shear. In blow-molding resins high LCB levels are usually associated with low parison swell, an important characteristic during molding. As the molten polymer exits the die, it flares. If it flares too much or too little, mold closure results in waste or defective bottles.

Thus the variations in resin characteristics that accompany the activation temperature change provide the basis for different grades of polymers. For example, this behavior is summarized for blow molding in Figure 10.107. Low activation temperature produces high MW (low MI) that provides toughness and high resistance to chemical attack (ESCR). This is ideal for large blow-molded containers such as drums and fuel tanks. On the other extreme, high activation temperatures are ideal for the high-speed molding of disposable milk bottles. In this application ESCR is not required, but high MI is needed for molding speed. Low swell is also critical. Between these two extremes are small household containers such as food, detergent, and bleach bottles. These require some ESCR, intermediate MI for molding ease, and swell is a consideration, although of less importance than in milk bottles.

10.7.2 The Future

During the 1990s the industry publications and even the popular press continually announced advances in metallocene catalysts and often suggested that they would replace the "traditional" Ziegler or Phillips catalysts. To a chemist in the field (and one who works on metallocenes too) these advances have indeed been impressive. Metallocenes or other single-site catalysts offer a degree of control of the chemistry that was lacking in Ziegler and Phillips systems, and this suggests many new approaches to old problems.

However impressive the activity of new single-site catalysts, the relevant question is whether they can make the same resins that chromium oxide catalysts do. At present the answer is no. The former have a narrow MW distribution, while the latter have a broad distribution, and each can contain significant levels of LCB. These two attributes have a dominant influence on how the resin processes at the customer's molding facility. Both resin types are highly useful for different applications, and they are not, at present, interchangeable.

Looking forward, however, one can see that combinations of several single-site catalysts together might theoretically be able to mimic chromium behavior. We are already beginning to see examples of broadened metallocene resins displacing Ziegler resins in the film market. However, reproducing chromium resin flow behavior from single-site catalysts can be much more difficult than reproducing that of a Ziegler resin. This is because there is a limited number of ways to make a narrow Ziegler distribution with no LCB, whereas for chromium-based resins the number of possible variations goes up geometrically with the breadth. There is also a distribution of LCB within the MW distribution to be considered. To some extent, MW breadth and LCB can even substitute for each other.

Therefore, single-site-based resins must exhibit molding behavior like chromium based catalysts in order to compete in the same markets. Better physical properties will not mean much if a molder cannot use his or her equipment or must run at a slower rate. This is already evident by the meager penetration of metallocene resins into all PE markets during the 1990s. The most common complaint was that metallocene-derived resins do not process as easily, due to a MW distribution even narrower than the Ziegler resins.* Due to this inertia, the odds are always against a completely new type of resin displacing popular existing resins in established markets. However, just like Ziegler LLDPE, which was supposed to replace LDPE but did not, it is certain that new applications will develop to take advantage of the new possibilities offered by metallocene catalysts, even if they do not displace Cr-based resins in the foreseeable future.

Finally, it is perhaps a mistake to think of the Phillips catalyst as if it were a single static entity. Actually the early chromium oxide catalysts were indeed replaced—by other chromium catalysts. And this trend will likely continue. Some of the new single-site catalysts are even based on chromium. Furthermore, this laboratory and others continue to explore "hybrid" combinations of traditional Phillips catalyst with metallocene and other catalysts. Therefore the lines between various catalyst types have become blurred and will no doubt continue to become less distinct in the future.

---

*Another handicap was the higher cost of metallocene catalysts, but we do not believe this is an inherent problem.

REFERENCES

1. Sailors, H. R., and Hogan, J. P., *J. Macromolec. Sci. Chem.*, **1981**, A15 (7), 1375–1400; *Polym. News.*, **1981**, 7(4), 152–167.
2. Hogan, J. P., Norwood, D. D., and Ayres, C. A., *J. Appl. Polym. Sci. Appl. Polym. Symp.*, **1981**, 36, 49–60.
3. Hogan, J. P., *The Chemist*, **1973**, L(2), 46.
4. Doak, K. W., and Schrage, A., in *High Polymers*, Vol. 20, Part I, Raff, R. A. V., and Doak, K. W., Eds., Interscience, New York, 1965, p. 351.
5. Zletz, A., Standard Oil of Indiana, U.S. Patent No. 2,692,257, filed Apr. 28, 1951, issued 1954.
6. Hogan, J. P., and Banks, R. L., Phillips Petroleum Company, U.S. Patent No. 2,825,721 filed Aug. 1954, issued Mar.1958; Belgian Patent No. 530,617, filed Jan, 1955, filed in U.S. Jan. 1953, S.N. 333,576; also Austrian Patent Application 864/54, filed Aug 6, 1954.
7. Clark, A. Hogan, J. P., Banks, R. L., and Lanning, W. C., *Ind. Eng. Chem.*, **1956**, 48, 1152–1155.
8. Ziegler, K., Breil, H., Martin, H., and Holzkamp, E., to Ziegler, K., German Patent No. 973,626, filed Nov. 17, 1953, issued Apr. 14, 1960; see also U.S. Patent No. 3,257,332, filed Nov. 15, 1954, issued June 21, 1966.
9. Hogan, J. P., in *High Polymers*, Vol. 18, Ham, G., Ed., Interscience, New York, 1964.
10. Harris, M., and Tishler, M., *Chemistry in the Economy*, American Chemical Society, Washington, DC, 1973, pp. 70–71.
11. Clark, A., and Hogan, J. P., in *Polythene*, 2nd ed., Renfrew, A., and Morgan, P., Eds., Interscience, New York, 1960, p. 29.
12. Rohlfing, R. G., Phillips Petroleum Co., U.S. Patent No. 3,226,205, 1965.
13. Norwood, D. D., Phillips Petroleum Co., U.S. Patent Nos. 3,248,179 and 3,257,362, 1966.
14. Pritchard, E., McGlamery, R. M., and Boeke, P. J., *Modern Plastics*, **1959**, 37, 132.
15. Josephs, M. J., *Chem. Eng. News*, **1969**, 47(17), 15.
16. Hogan, J. P., Phillips Petroleum Co., U.S. Patent No. 3,666,736, 1972.
17. Phillips Novel Linear Grade, *Chem. Week*, **1993**, May 5 (Review of low density linear PE development).
18. Benham, E. A., McDaniel, M. P., Smith, M. A., Whitte, W. M., and Ratzlaff, J. D., A low density linear polyethylene by the Phillips slurry process, *SPO-93*, paper presented at the Scotland International Business Forum on Specialty Polyolefins, Houston, TX, Sept. 23, 1993.
19. Smith, M. A., Benham, E. A., Didier, C. M., McDaniel, M. P., Ratzlaff, J., and Whitte, W. M., Novel low density linear polyethylene (LDLPE) made via the Phillips process, paper presented at the MAACK Conference, Zurich, Switzerland, Oct. 5, 1993.
20. Benham, E. A., Smith, P. D., and McDaniel, M. P., *Polym. Eng. Sci. (SPE)*, **1988**, 28(22), 1469–1472.
21. Hogan, J. P., and Banks, R. L., Phillips Petroleum Company, U.S. Patent No. 4,376,851, Mar. 15, 1983.

22. Hogan, J. P., and Banks, R. L., History of polypropylene, in *History of Polyolefins*, Seymour, R., and Cheng, T., Eds., Reidel Publishing Co., Dordrecht, The Netherlands, 1986, pp. 103–115.
23. McDaniel, M. P., The Phillips process for ethylene polymerization, in *Handbook of Heterogeneous Catalysis*, Ertl et al., Ed., VCH Verlagsgesellschaft, Weinheim, Germany, 1995.
24. Clark, A., Hogan, J. P., Banks, R. L., and Lanning, W. C., *Ind. Eng. Chem.*, **1956**, 48, 1152.
25. Augustine, S. M., and Blitz, J. P., *J. Catal.*, **1996**, 161, 641.
26. Ruddick, V. J., Dyer, P. W., Bell, G., Gibson, V. C., and Badyal, J. P. S., *J. Phys. Chem.*, **1996**, 100(26), 11062–11066.
27. Kim, C. S., and Woo, S. I., *J. Mol. Catal.*, **1992**, 73, 249.
28. Chudek, J. A., Hunter, G., McQuire, G. W., Rochester, C. H., and Smith, T. F. S., *J. Chem. Soc. Faraday Trans.*, **1996**, 92(3), 453–460.
29. Hogan, J. P., *J. Polym. Sci.* P. A-1, **1970**, 8, 2637.
30. Hogan, J. P., in *Applied Industrial Catalysis*, Vol. 1, Leach, B. E., Ed., Academic, New York, 1983, p. 149.
31. Hogan, J. P., and Witt, D. R., Prepr., *Div. Pet. Chem., Am. Chem. Soc.*, **1979**, 24(2), 377–387.
32. Witt, D. R., in *Reactivity, Mechanism, and Structure in Polymer Chemistry*, Jenkins, A. D., and Ledwith, A., Eds., Wiley, Chichester, 1974, pp. 431–445.
33. Holm, V. C. F., and Clark, A., *J. Catal.*, **1968**, 11, 305.
34. Clark, A., Finch, J. N., and Ashe, B. H., *Proc. Third Int. Cong. Cat., Amsterdam*, **1964**, 1010.
35. Finch, J. N., *J. Catal.*, **1976**, 43, 111.
36. Clark, A., *Catal. Rev.*, **1969**, 3(2), 145.
37. Vuillaume, G., Spitz, R., Revillon, A., Charcosset, H., Turlier, P., and Guyot, A., *J. Catal.*, **1971**, 21(2), 159–163.
38. Charcosset, H., Revillon, A., and Guyot, A., *J. Catal.*, **1967**, 8(4), 334–339.
39. Charcosset, H., Revillon, A., and Guyot, A., *J. Catal.*, **1967**, 8(4), 326–333.
40. Krauss, H. L., Weber, E., and Moevik, N., *Z. Anorg. Allgem. Chem.*, **1965**, 338(3/4), 121–133.
41. McDaniel, M. P., *Adv. Catal.*, **1985**, 33, 47–98.
42. Hierl, C., and Krauss, H. L., *Z. Anorg. Allg. Chem.*, **1973**, 401(3), 263; *React. Kinet. Catal. Lett.*, **1975**, 3(1), 48.
43. Jozwiak, W. K., and Dalla Lana, I. G., *J. Chem. Soc. Faraday Trans.*, **1997**, 93(15), 2583–2589.
44. Liu, B., and Terano, M., *J. Molec. Catal. A. Chem.*, **2001**, 172, 227–240.
45. Thune, P. C., Verhagen, C. P. J., van den Boer, M. J. G., and Niemantsverdriet, J. W., *J. Phys. Chem. B.*, **1997**, 101, 8559–8563.
46. Jozwiak, W. K., Ignaczak, W., Kincel, D., Goralski, J., and Paryjczak, T., *Polish J. Chem.*, **2002**, 76, 857–873.
47. Moisii, C., Stiegman, A. E., Callahan, S. D., and Lita, A., *Abstracts of Papers, 231st ACS National Meeting*, Atlanta, GA, March 26–30, 2006, INOR-826.

48. Fouad, N. E., and Knozinger, H., *Zeits. Physikal. Chem. Bd.*, **1991**, 171, 75–96.
49. Chudek, J. A., Hunter, G., Rochester, C. H., and Smith, T. F. S., *J. Catal.*, **1992**, 136(1), 246–251.
50. Chudek, J. A., Hunter, G., Geoffrey, G., McQuire, G. W., Rochester, C. H., Smith, T. F. S., and Terence F. S., *J. Chem. Soc. Faraday Trans.*, **1996**, 92(3), 453–460.
51. Krauss, H. L., Surface compounds of transition metals, XXXIII. Phillips-like systems and their reaction with olefins, in *Transition Metal and Organometal Catalyzed Olefin Polymerization, Proceedings of the International Symposium*, Kaminsky, W., and Sinn, H., Eds., Springer, Berlin, 1988, pp. 163–168.
52. Fubini, B., Ghiotti, G., Stradella, G. St. L., Garonne, E., and Morterra, C., *J. Catal.*, **1980**, 66, 200.
53. Liu, B., Fang, Y., and Terano M., *J. Molec. Catal. A Chem.*, **2004**, 219, 165–173.
54. Callahan, S., and Stiegman, A. E., Studies of silica supported Cr(VI) sites, paper presented at the 223rd ACS National Meeting, Orlando, FL, April 7–11, 2002, INOR-286.
55. Moisii, C., Deguns, E. W., Lita, A., Callahan, S. D., van de Burgt, L. J., Magana, D., and Stiegman, A. E., *Chem. Mat.*, **2006**, 18(17), 3965–3975.
56. Armistead, C. G., Tyler, A. J., Hambleton, F. H., Mitchell, S. A., and Hockey, J. A., *J. Phys. Chem.*, **1969**, 73(11), 3947.
57. McDaniel, M. P., *J. Phys. Chem.*, **1981**, 85, 532.
58. McDaniel, M. P., Martin, J. L., Smith, P. D., and Fahey, D. R., Polyolefin catalysts based on titanium and vanadium chlorides, in *Advances in Polyolefins*, Seymour, R. B., and Cheng, T., Eds., Plenum, New York, 1987, p.153.
59. McDaniel, M. P., Collins, K. S., Benham, E. A., and Cymbaluk, T. H., *Appl. Catal. A General*, **2008**, 335, 252–261.
60. McDaniel, M. P., Collins, K. S., Benham, E. A., and Cymbaluk, T. H., *Appl. Catal. A General*, **2008**, 335, 180–186.
61. Pegler, R. J., Hambleton, F. H., and Hockey, J. A., *J. Catal.*, **1971**, 20, 309.
62. Kunawicz, J., Jones, J., and Hockey, J. A., *Trans. Faraday Soc.*, **1971**, 67(3), 848.
63. Weckhuysen, B. M., Wachs, I, E., and Schoonheydt, R. A., *Chem. Rev.*, **1996**, 96, 3327–3349.
64. Rebenstorf, B., and Larsson, R., *J. Molec. Catal.*, **1981**, 11, 247.
65. Rebenstorf, B., and Larsson, R., *Z. Phys. Chem.* (Wiesbaden), **1982**, 133(1), 119–127.
66. Rebenstorf, B., and Larsson, R., *Z. Anorg. Allg. Chem.*, **1981**, 478, 119–138.
67. Rebenstorf, B., *J. Molec. Catal.*, **1989**, 56(1–3), 170–182.
68. Rebenstorf, B., *J. Catal.*, **1989**, 117(1), 71–77.
69. Rebenstorf, B., *Acta Chem. Scand*, **1989**, 43(5), 413–416.
70. Groeneveld, C., Wittgen, P. P. M. M., Kersbergen, A. M., Mestrom, P. L. M., Nuijten, C. E., and Schuit, G. C. A., *J. Catal.*, **1979**, 59, 153.
71. Wittgen, P. P. M. M., Groeneveld, C., Janssens, J. H. G. J., Wetzels, M. L. J. A., and Schuit, G. C. A., *J. Catal.*, **1979**, 59, 168.

72. Wittgen, P. P. M. M., Groeneveld, C., Zwaans, P. J. C. J. M., Morgenstern, H. J. B., van Heugten, A. H., van Heumen, C. J. M., and Schuit, G. C. A., *J. Catal.*, **1982**, 77, 360.
73. Groeneveld, C., Wittgen, P. P. M. M., Lavrijsen, J. P. M., and Schuit, G. C. A., *J. Catal.*, **1983**, 82, 77.
74. Groeneveld, C., Wittgen, P. P. M. M., Swinnen, H. P. M., Wernsen, A. and Schuit, G. C. A., *J. Catal.*, **1983**, 83, 346.
75. Spitz, R., Revillon, A., and Guyot, A., *J. Catal.*, **1974**, 35, 335.
76. Spitz, R., *J. Catal.*, **1974**, 35, 345.
77. Espelid, O., and Borve, K. J., *J. Catal.*, **2002**, 206(2), 331–338.
78. Rebenstorf, B., *J. Polym. Sci. Pt A. Polym. Chem.*, **1991**, 29(13), 1949–1953.
79. Groppo, E., Lamberti, C., Bordiga, S., Spoto, G., and Zecchina, A., *Chem. Rev.*, **2005**, 105, 115–183.
80. Groppo, E., Lamberti, C., Bordiga, S., Spoto G., and Zecchina, A., *Chem. Rev.*, **2005**, 105, 115–183.
81. Krauss, H. L., in *Proceedings, 5th International Congress on Catalysis, 1972*, Vol. 1, Hightower, J. W., Ed., North Holland, Amsterdam, 1973, p. 207.
82. Karakchiev, I. G., Brmakov Yu. I., and Kolovertnov, G. D., *Kinet. Catal.*, **1967**, 8(1), 156.
83. Iannibello, A., Marengo, S., Tittarelli, P., Morelli, G., and Zecchina, A., *J. Chem. Soc. Faraday Trans.*, **1984**, 80(8), 2209–2223.
84. Ellison, A., Overton, T. L., and Bencze, L., *J. Chem. Soc. Faraday Trans.*, **1993**, 89(5), 843–849.
85. Hill, W., Shelimov, B. N., Kibardina, I. R., and Kazanskii, V. B., *React. Kinet. Catal. Lett.*, **1986**, 31(2), 315–320.
86. Espelid, O., and Borve, K. J., *Catal. Lett.*, **2001**, 75(1/2), 49–54.
87. Weckhuysen, B. M., and Wachs, I. E., *J. Phys. Chem.*, **1996**, 100(34), 14437–14442.
88. Weckhuysen, B. M., Schoonheydt, R. A., Jehna, J., Wachs, I. E., Cho, S. J., Ryoo, R., Kijlstra, S., and Poels, E., *J. Chem. Soc. Faraday Trans*, **1995**, 91(18), 3245–3253.
89. Weckhuysen, B. M., Wachs, I. E., and Schoonheydt, R. A., *Stud. Surf. Sci. Catal.*, **1995**, 91(Preparation of Catalysts VI), 151–158.
90. Weckhuysen, B. M., Verberckmoes, A. A., Buttiens, A. L., and Schoonheydt, R. A., *J. Phys. Chem.*, **1994**, 98, 579.
91. Jehng, J., Wachs, I. E., Weckhuysen, B. M., and Schoonheydt, R. A., *J. Chem. Soc. Faraday Trans.*, **1995**, 91(5), 953–961.
92. Kim, D. S., Wachs, I. E., and Israel, E., *J. Catal.*, **1993**, 142(1), 166–171.
93. Vuurman, M. A., Wachs, I. E., Stufkens, D. J., and Oskam, A., *J. Molec. Catal.*, **1993**, 80(2), 209–227.
94. Kim, D. S., Tatibouet, J. M., and Wachs, I. E., *J. Catal.*, **1992**, 136(1), 209–221.
95. Hardcastle, F. D., and Wachs, I. E., *J. Molec. Catal.*, **1988**, Vol. 1987, 46(1–3), 173–186.
96. Ellison, A., Diakun, G., and Worthington, P., *J. Molec. Catal.*, **1988**, 46, 131.

97. Wekhuysen, B. M., Veberckmoes, A. A., De Baets, A. R., and Schoonheydt, R. A., *J. Catal.*, **1997**, 166, 160.
98. Zaki, M. I., Fouad, N. E., Leyrer, J. and Knozinger, H., *Appl. Catal.*, **1986**, 21, 359–377.
99. Groppo, E., Damin, A., Bonino, F., Zecchina, A., Bordiga, S., and Lamberti, C., *Chem. Mater.*, **2005**, 17, 2019–2027.
100. DiCroce, P. G., Aubriet, F., Chety-Gimondo, R., Muller, J. F., and Grange, P., *Rapid Commun. Mass Spectrom.*, **2004**, 18, 601–608.
101. Weckbuysen, B. M., DeRidder, L. M., and Schoonheydt, R. A., *J. Phys. Chem.*, **1993**, 97, 4756–4763.
102. Weckbuysen, B. B. M., DeRidder, L. M., and Schoonheydt, R. A., *J. Phys. Chem.*, **1993**, 97, 4156–4163.
103. Gaspar, A. B., Perez, C. A. C., and Dieguez, L. C., *Appl. Surf. Sci.*, **2005**, 252(4), 939–949.
104. Rahman, A., Mohammed, M. H., Ahmed, M., and Aitrani, A. M., *Appl. Catal. A. Gen.*, **1995**, 121, 203–216.
105. Weckhuysen, B. M., and Wachs, I. E., *J. Phys. Chem. B*, **1997**, 101, 2793.
106. Chua, Y. T., Stair, P. C., and Wachs, I. E., *J. Phys. Chem. B*, **2001**, 105, 8600.
107. Yim, S. D. and Nam, I.-S., *J. Catal.*, **2004**, 221, 601–611.
108. Thune, P. C., Linke, R., van Gennip, W. J. H., deJong, A. M., and Niemantsverdriet, J. W., *J. Phys. Chem. B*, **2001**, 105, 3073–3078.
109. Thüne, P. C., Loos, J., Wouters, D., Lemstra, P. J., and Niemantsverdriet, J. W., *Macromol. Symp.*, **2001**, 173, 37.
110. Thune, P. C., Loos, J., deJong, A. M., Lemstra, P. J., and Niemantsverdriet, J. W., *Topics Catal.*, **2000**, 13, 67–74.
111. Morys, P., Gorges, U., and Krauss, H. L., *Z. Naturforsch. B Anorg. Chem. Org. Chem.*, **1984**, 39b, 458.
112. Topchiev, A. V., Krentsel, B. A., Perelman, A. I., and Miesserov, K. G., *J. Polym. Sci.*, **1959**, 34, 129–137.
113. Hierl, G., and Krauss, H. L., *Z. Anorg. Allg. Chem.*, **1975**, 415(1), 57.
114. McDaniel, M. P., *J. Catal.*, **1981**, 67, 71.
115. McDaniel, M. P., *J. Catal.*, **1982**, 76, 17.
116. Demmelmaier, C. A., White, R. E., van Bokhoven, J. A., and Scott, S. L., *J. Phys. Chem. C*, **2008**, 112, 6439–6449.
117. Demmelmaier, C. A., White, R. E., van Bokhoven, J. A., and Scott, S. L., *J. Catal.*, **2009**, 262(1), 44–56.
118. McDaniel, M. P., *J. Catal.*, **1982**, 76, 29.
119. McDaniel, M. P., *J. Catal.*, **1982**, 76, 37.
120. Krauss, H. L., and Westphal, U., *Z. Anorg. Allg. Chem.*, **1977**, 430, 218.
121. Liu, B., Shimizu, T., and Terano, M., Surface analytical approaches for the Phillips catalyst by EPMA and XPS, in *Organometallic Catalysts and Olefin Polymerization*, Blom, R., Ed., Springer, Berlin, 2001, pp. 206–216.
122. Merryfield, R., McDaniel, M. P., and Parks, G., *J. Catal.*, **1982**, 77, 348.
123. McDaniel, M. P., and Welch, M. B., *J. Catal.*, **1983**, 82, 98.

124. McDaniel, M. P., and Welch, M. B., *J. Catal.*, **1983**, 82, 110.
125. McDaniel, M. P., Collins, K. S., and Benham, E. A., *J. Catal.*, **2007**, 252(2), 281–295.
126. McDaniel, M. P., Welch, M. B., and Dreiling, M. J., *J. Catal.*, **1983**, 82, 118.
127. McDaniel, M. P., and Welch, M. B., in *Initiation of Polymerization*, Bailey, Jr., F. E., Ed., ACS Symposium Series 212, Paper 15, Las Vegas, 1983; p. 191; *Org. Coat. Appl. Polym. Sci. Proc.*, **1981**, 46, 708–713.
128. Schreiber, L. B., and Vaughn, R. W., *J. Catal.*, **1975**, 40, 226.
129. Cheung, T. T. P., Willcox, K. W., McDaniel, M. P., and Johnson, M. M., *J. Catal.*, **1986**, 102, 10–20.
130. Shiba, T., Shih, C. C., and Takashima, K., *J. Chem. Soc. Jpn. Ind. Chem. Sec.*, **1966**, 69, 1003–1006.
131. McDaniel, M. P., Phillips Petroleum, unpublished results, 1983.
132. Vuurman, M. A., Hardcastle, F. D., and Wachs, I. E., *J. Molec. Catal.*, **1993**, 84(2), 193–205.
133. Hill, R. W., Kehl, W. L., and Lynch, T. J., Gulf Petroleum Co., U.S. Patent No. 4,219,444, Aug. 1980.
134. McDaniel, M. P., and Johnson, M. M., Phillips Petroleum Co., U.S. Patent Nos. 4,444,965, issued Apr. 24, 1984; 4,364,855, issued Dec. 21, 1982; and 4,364,842, issued Dec. 21, 1982.
135. McDaniel, M. P., and Johnson, M. M., Phillips Petroleum Co., U.S. Patent Nos. 4,444,962, issued Apr. 24, 1984; and 4,364,854, issued Dec. 21, 1982.
136. Kerber, N., BASF, U.S. Patent No. 2,930,789, Mar. 30, 1960.
137. Carrick, W. L., Turbett, R. J., Karol, F. J., Karapinka, G. L., Fox, A. S., and Johnson, R. N., *J. Polym. Sci. Pt. A-1*, **1972**, 10(9), 2609–2620.
138. Baker, L. M., and Carrick, W. L., *J. Org. Chem.*, **1970**, 35(3), 775.
139. Cann, K., Apecetche, M., and Zhang, M., Comparison of silyl chromate and chromium oxide based olefin polymerization catalysts, in *Stereospecific Polymerization and Stereoregular Polymers*, Wiley-VCH, Weinheim, 2004, pp. 29–36.
140. Johnson, R. N., Ridge, B., Karol, F. J., and Fulton, L. A., Union Carbide, U.S. Patent No. 3,642,749, Feb. 15, 1972.
141. Pullukat, T., Chemplex Company, U.S. Patent No. 3,928,304, Dec. 23, 1975.
142. Marsden, C. E., *Plastics Rubber Composites Process. Appl.*, **1994**, 21, 193–200.
143. McDaniel, M. P., and Collins, K. S., *J. Catal.*, **2009**, 261, 34–49.
144. McDaniel, M. P., and Collins, K. S., *J. Polym. Science, Part 1: Chemistry*, **2009**, 47(3), 845–865.
145. McDaniel, M. P., *J. Polym. Sci. Polym. Chem. Ed.*, **1981**, 19, 1967.
146. Whitacker, H. L., and Wills, G. B., *J. Appl. Pol. Sci.*, **1969**, 13, 1921.
147. Ruddick, V. J., and Badyal, J. P. S., *J. Phys. Chem. B.*, **1997**, 101, 1791.
148. Dalla Lana, I. G., Szymura, J. A., and Zielinski, P. A., *Stud. Surf. Sci. Catal.*, **1993**, 75 (New Frontiers in Catalysis, Pt. C), 2329–2332.
149. Szymura, J. A., Zielinski, P. A., and Dalla Lana, I. G., *Catal. Lett.*, **1992**, 15(1/2), 145–153.
150. Szymura, J. A., Zielinski, P. A., and Dalla Lana, I. G., *Stud. Surf. Sci. Catal.*, **1992**, 73 (Prog. Catal.), 69–75.

151. Szymura, J. A., Dalla Lana, I. G., Fiedorow, R., Zielinski, P. A., *Macromolecules*, **1996**, 29(9), 3103–3110.
152. Follestad, A., Helleborg, S., and Almquist, V., *Stud. Surf. Sci. Catal.*, **1990**, 56 (Catal. Olefin Polym.), 63–85.
153. Davidson, T., *Polym. Lett.*, **1970**, 8, 855.
154. Conner, W. C., Ferrero, M., Webb, S., Sommer, R., Chiovetta, M., Jones, K., and Spanne, P., *Stud. Surf. Sci. Catal.*, **1993**, 75 (New Frontiers in Catalysis, Pt. B), 1827–1830.
155. Jones, K. W., Spanne, P., Lindquist, W. B., Conner, W. C., and Ferrero, M., *Nucl. Instrum. Methods Phys. Res. Sect. B*, **1992**, B68(1–4), 105–110.
156. Webb, S. W., Weist, E. L., Chiovetta, M. G., Laurence, R. L., and Conner, W. C., *Can. J. Chem. Eng.*, **1991**, 69(3), 665–681.
157. Conner, W. C., Webb, S. W., Spanne, P., and Jones, K. W., *Macromolecules*, **1990**, 23(22), 4742–4747.
158. Conner, W. C., Weist, E. L., Ali, A. H., Chiovetta, M., and Laurence, R. L., in *Transition Metal Catalyzed Polymerization, Proceedings of the International Symposium, 2nd*, Akron, OH. Quirk, R. P., Ed., Cambridge University Press, Cambridge, 1988, pp. 417–427.
159. Webb, S. W., Conner, W. C., and Laurence, R. L., *Macromolecules*, **1989**, 22(7), 2885–2894.
160. Weist, E. L., Ali, A. H., and Conner, W. C., *Macromolecules*, **1987**, 20(3), *689–693*.
161. Jones, K. W., Spanne, P., Webb, S. W., Conner, W. C., Beyerlein, R. A., Reagan, W. J., and Dautzenberg, F. M., *Nucl. Instrum. Methods Phys. Res. Sect. B*, **1991**, B56–B57(Pt. 1), 427–432.
162. Witt, D. R., U.S. Patent No. 3,900,457, Aug. 19, 1975; Short, J. N., and Witt, D. R., U.S. Patent No. 4,081,407, Mar. 28, 1978; and Short, J. N., and Witt, D. R., U.S. Patent No. 4,152,503, May 1, 1979, all assigned to Phillips Petroleum Co.
163. Schmidt, H., Riederer, W., and Krauss, H. L., *J. Prakt. Chem./Chem.-Ztg.* **1996**, 338(7), 627–633.
164. Ballard, D. G. H., *J. Polym. Sci. Polym. Chem. Ed.*, **1975**, 13(10), 2191–2212.
165. Ballard, D. G. H., Jones, E., Wyatt, R. J., Murray, R. T., and Robinson, P. A., *Polymer*, **1974**, 15(3), 169–174.
166. Calleja, G., Aguado, J., Carrero, A., and Moreno, J., *Catal. Commun.*, **2005**, 6, 153–157 (MCM-41).
167. Marsden, C. E., *Stud. Surf. Sci. Catal.*, **1991**, 63 (Prep. Catal. 5), 215–227.
168. Wichterlova, B., Traruzkova, Z., Krajcikova, L., and Novakova, J., *Structure and Activity of Modified Zeolites*, Elsevier, Amsterdam, 1984, p. 246.
169. Wang, J. K., Komatsu, T., Namba, S., and Yashima, T., *J. Molec. Catal.*, **1986**, 37, 327.
170. McDaniel, M. P., Knudsen, R. D., Benham, E. A., and Bailey, F. W., Phillips Petroleum Co., U.S. Patent No. 4,981,831, Jan. 1, 1991.
171. Weist, E. L., Ali, A. H., Naik, B. G., and Conner, W. C., *Macromolecules*, **1989**, 22(8), 3244.
172. Niegisch, W. D., Crisafulli, S. T., Nagel, T. S., and Wagner, B. E., *Macromolecules*, **1992**, 25(15), 3910–3916.

173. Wagner, B. E., and Niegisch, W. D., *Polym. Mater. Sci. Eng.*, **1991**, 64, 139–141.
174. Kakugo, M., Sadatosi, H., Yokoyama, M., and Kojima, K., in *Transition Metals and Organometallics as Catalysts for Polymerization*, Kaminsky, W., and Sinn, H., Eds., Springer-Verlag, Berlin, 1988, p. 433.
175. Wang, S., Tait, P. J. T., and Marsden, C. E., *J. Molec. Catal.*, **1991**, 65, 237–252.
176. Estinoz, D. A., and Chiovetta, M. G., *Polym. Eng. Sci.*, **1996**, 36(17), 2208–2228, 2229–2240.
177. Mokaya, R., and Jones, W., *Chem. Commun.*, **1997**, 22, 2185.
178. Weckhuysen, B. M., Ramachandra, R. R., Pelgrims, J., Schoonheydt, R. A., Bodart, P., Debras, G., Collart, O., Van der Voort, P., and Vansant, E. F., *Chem. Eur. J.*, **2000**, 6(16), 2960–2970.
179. Cimino, A., DeAngelis, B. A., Luchetti, A., and Minelli, G., *J. Catal.*, **1976**, 45, 316.
180. Best, S. A., Squires, R. G., and Walton, R. A., *J. Catal.*, **1977**, 47, 292.
181. Groppo, E., Prestipino, C., Cesano, F., Bonino, F., Bordiga, S., Lamberti, C., Thüne, P. C., Niemantsverdriet, J. W., and Zecchina, A., *J. Catal.*, **2005**, 230, 98–108.
182. Lui, B., Nakatani, H., and Terano, M, *J. Molec. Catal. A Chem.*, **2002**, 184, 387.
183. van Kimmenade, E. M. E., Kuiper, A. E. T., Tamminga, Y., Thune, P. C., and Niemantsverdriet, J. W., *J. Catal.*, **2004**, 223, 134–141.
184. Liu, B., Sindel, P. L., Fang, Y., Hasebe, K., and Terano, M., *J. Molec. Catal. A Chem.*, **2005**, 238, 142–150.
185. Krauss, H. L., and Langstein, G., *J. Molec. Catal.*, **1991**, 65(1/2), 101–112.
186. Choi, K. Y., and Tang, S., *J. Appl. Polym. Sci.*, **2003**, 91, 2923.
187. Choi, K. Y., Tang, S., and Yoon, W. J., *Macromol. Theory Simul.*, **2004**, 13, 169–177.
188. Baker, L. M., and Carrick, W. L., *J. Org. Chem.*, **1968**, 33(2), 616.
189. Liu, B., Fang, Y., and Terano, M., *Molec. Simul.*, **2004**, 30(13–15), 963–971.
190. Krauss, H. L., and Schmidt, H., *Z. Anorg. Allg. Chem.*, **1972**, 392(3), 258–270.
191. Ellermann, V. J., Hagen, K., and Krauss, H. L., *Z. Anorg. Allg. Chem.*, **1982**, 487, 130.
192. Krauss, H. L., Hagen, K., and Hums, E., *J. Molec. Catal.*, **1985**, 28, 233.
193. Brown, C. E., Stiegman, A. E., Callahan, S., Achey, R. M., and Fu, R., Direct characterization of the active site in the Phillips ethylene polymerization catalys, paper presented at the Meeting of the American Chemical Society, Atlanta, 2006.
194. Scott, S. L., and Ajjou, J. A. N., *Chem. Eng. Sci.*, **2001**, 56, 4155–4168.
195. Krauss, H. L., and Hanke, B., *Z. Anorg. Allg. Chem.*, **1985**, 521, 111.
196. Krauss, H. L., *Proceedings of the 28th Macromoleculor Symposium of IUPAC*, 1982, p. 238.
197. Krauss, H. L., *J. Molec. Catal.*, **1988**, 46, 97.
198. Xing, Q., Milius, W., Krauss, H. L., Bluemel, J., Hilbig, H., Koehler, F. H., Strauss, W., and Bayreuther, G., *Z. Anorg. Allg. Chem.*, **1999**, 625(3),521–529.
199. Conway, S. J., Falconer, J. W., and Rochester, C. H., *J. Chem. Soc. Faraday Trans. 1*, **1989**, 85(1), 71.

200. Rebenstorf, B., *J. Molec. Catal.*, **1988**, 45(2), 263–274 (Carbene).
201. McDaniel, M. P., and Johnson, M. M., *J. Catal.*, **1986**, 101, 446–457.
202. Clark, A., and Bailey, G. C., *J. Catal.*, **1963**, 2, 230, 241.
203. Ruddick, V. J., and Badyal, J. P. S., *Langmuir*, **1997**, 13(3), 469–472.
204. Saito, T., Motegi, M., Furuhashi, H., and Ueki, S., *Sci. Technol. Catal.*, **1998**, 477.
205. Spitz, R., *J. Macromol. Sci., Chem.*, **1972**, 6(1), 169–176.
206. McDaniel, M. P., and Martin, S. J., *J. Phys. Chem.*, **1991**, 95, 3289.
207. McDaniel, M. P., Rohlfing, D. C., and Benham, E. A., *Polym. React. Eng.*, **2003**, 11(2), 101–132.
208. Zecchina, A., Garrone, E., Ghiotti, G., and Coluccia, S., *J. Phys. Chem.*, **1975**, 79(10), 972.
209. Zecchina, A., Garrone, E., Morterra, C., and Coluccia, S., *J. Phys. Chem.*, **1975**, 79(10), 984.
210. Krauss, H. L., Rebenstorf, B., Westphal, U., and Schneeweiss, D., The influence of preparation parameters on the reactivity of chromium(II) surface compounds (modified Phillips catalysts), in *Proceedings of the International Symposium on Preparation of Catalysts*, Delmon, B., Jacobs, P. A., and Poncelet, G., Ed., Elsevier, Amsterdam, 1976, pp. 489–495.
211. Ghiotti, G., Garrone, E., Della Gatta, G., Fubini, B., and Giamello, E., *J. Catal.*, **1983**, 80, 249.
212. Zecchina, A., Spoto, G., Ghiotti, G., and Garrone, E., *J. Molec. Catal.*, **1994**, 86, 423.
213. Krauss, H. L., Rebenstorf, B., Westphal, U., and Schneeweiss, D., in *Preparation of Catalysts*, Delmon, B., Jacobs, P. A., and Poncelet, G., Eds., Elsevier, Amsterdam, 1976.
214. Krauss, H. L., and Naumann, D., *Z. Anorg. Allg. Chem.*, **1978**, 446, 23.
215. Garrone, E., Abello, S., Borello, E., Ghiotti, G., and Zecchina, A., *Mater. Chem. Phys.*, **1991**, 29(1–4), 369–378.
216. Garrone, E., Ghiotti, G., and Zecchina, A., *NATO ASI Ser., Ser. C*, **1990**, 326 (Olefin Metathesis Polym. Catal.), 393–406.
217. Nishimura, M., and Thomas, J. M., *Catal. Lett.*, **1993**, 21, 149.
218. Fang, Y., Liu, B., and Terano, M., *Appl. Catal. A Gen.*, **2005**, 279, 131–138.
219. Demmelmaier, C. A., and Scott, S. L., XAS investigation of the precursor to the Phillips catalyst, Presentation at ACS Meeting, San Francisco, Sept. 13, 2006, American Chemical Society, Washington, D.C.
220. Parks, G. D., Phillips Petroleum, March 1996, unpublished calculations indicating that different angles of attachment can strongly affect the electron density on the chromium center.
221. McDaniel, M. P., and Johnson, M. M., *Macromolecules*, **1987**, 20, 773.
222. Espelid, O., and Borve, K. J., *J. Catal.*, **2000**, 195(1), 125–139.
223. Weckhuysen, B. M., and Schoonheydt, R. A., *Stud. Surf. Sci. Catal.*, **1994**, 84, 965.
224. Zhang, Y., Matos, I., Lemos, M., Freire, F., Nunes, T., Botelho do Rego, A., Henriques, R. T., Fonseca, F., Marques, M., and Lemos, F., *J. Polym. Sci. Pt. A Polym. Chem.*, **2003**, 41, 3768–3780.
225. Kippenberger, D. J., Vansant, E. F., and Lunsford, J. H., *J. Catal.*, **1974**, 35(3), 447–451.

226. Krauss, H. L., and Stach, H., *Inorg. Nucl. Chem.*, **1968**, 4, 393.
227. Krauss, H. L., and Stach, H., *Z. Anorg. Chem.*, **1969**, 366, 280.
228. Krauss, H. L., Reactions of unsaturated coordination surface compounds. Elucidation of Phillip's polyethylene synthesis, in *Jahre Fonds Chem. Ind. Foerder. Forsch. Wiss. Lehre Beitr. Wiss. Veranst.,* Fond Chem. Ind, Frankfurt am Main, Germany, 1970, pp. 113–120.
229. Krauss, H. L., and Rebenstorf, B., *Z. Anorg. Allg. Chem.*, **1973**, 402(1), 113.
230. Krauss, H. L., and Weisser, B., *Z. Anorg. Allg. Chem.*, **1975**, 412(1), 82.
231. Krauss, H. L., Rebenstorf, B., and Westphal, U., *Z. Anorg. Allg. Chem.*, **1975**, 414(2), 97.
232. Krauss, H. L., and Westphal, U., *Z. Naturforsch. B Anorg. Chem. Org. Chem.*, **1978**, 33B(11), 1278.
233. Krauss, H. L., and Westphal, U., *Z. Anorg. Allg. Chem.*, **1977**, 430, 218.
234. Morys, P., Gerritzen, R., and Krauss, H. L., *Z. Naturforsch. B Anorg. Chem. Org. Chem.*, **1976**, 31B(6), 774.
235. Moeseler, R., Horvath, B., Lindenau, D., Horvath, E. G., and Krauss, H. L., *Z. Naturforsch. B Anorg. Chem. Org. Chem.*, **1976**, 31B(6), 22.
236. Hums, E., *Ind. Eng. Chem. Prod. Res. Dev.*, **1985**, 24, 517.
237. Krauss, H. L., *Angew. Chem. Int. Ed. Engl.*, **1973**, 12(10), 861.
238. Krauss, H. L., and Hopf, R., *Proc. Eur. Symp. Therm. Anal. (PESAG)*, **1981**, 2, 175.
239. Krauss, H. L., Frank, B., Hanke, B., Hums, E., Langstein, D., Naumann, D., Siebenhaar, B., and Weiss, K., *NATO ASI Ser., Ser. C*, **1990**, 326 (Olefin Metathesis Polym. Catal.), 375–384.
240. Hums, E., and Krauss, H. L., *Z. Anorg. Allg. Chem.*, **1986**, 537, 154–162.
241. Krauss, H. L., Reactions of coordinatively unsaturated surface compounds and the Phillips polyethylene synthesis process, in *Jahre Fonds Chem. Ind. Beitr. Wiss. Veranst.*, Fonds der Chem. Ind., Frankfurt am Main, Germany, 1970, pp. 31–38.
242. Rebenstorf, B., Larsson, L., and Larsson, R., *Acta Chem. Scand. Ser. A*, **1977**, A31(10), 877–883.
243. Rebenstorf, B., Larsson, L., and Larsson, R., *Acta Chem. Scand. Ser. A*, **1978**, A32(5), 461–465.
244. Ghiotti, G., Garrone, E., and Zecchina, A., *J. Molec. Catal.*, **1991**, 65(1/2), 73–83.
245. Zecchina, A., Garrone, E., Ghiotti, G., and Borello, E., Three-ligand complexes of surface chromium ions, in *Proceedings of the International Congress on Catalysis*, Delmon, B., and Jannes, G., Eds., Elsevier, Amsterdam, 1975, pp. 243–252.
246. Groppo, E., Lamberti, C., Bordiga, S., Spoto, G., Damin, A., and Zecchina, A., *J. Phys. Chem. B.*, **2005**, 109(31), 15024–15031.
247. Spoto, G., Bordiga, S., Garonne, E., Ghiotti, G., Damin, A., Zecchina, A, Petrini, G., and Leofanti, G., *J. Molec. Catal.*, **1992**, 74, 175–184.
248. Espelid, O., and Borve, K. J., *J. Catal.*, **2002**, 205, 177–190.
249. Rebenstorf, B., and Larsson, R., *Inorg. Nucl. Chem. Lett.*, **1978**, 14(11), 381–388.
250. Clark, A., Hogan, J. P., Witt, D. R., and Lanning, W. C., *World Petrol. Congr. Proc. 5th.*, **1960**, 4, 267–273.

251. Zecchina, A., Bertarione, S., Damin, A., Scarano, D., Lamberti, C., Prestipino, C., Spoto, G., and Bordiga, S., *Phys. Chem. Chem. Phys.*, **2003**, 5(20), 4414–4417.
252. Figard, J., and McDaniel, M. P., Phillips Petroleum Company, unpublished results, 1986.
253. Zecchina, A., Garrone, E., Morterra, C., and Coluccia, S., *J. Phys. Chem.*, **1975**, 79(10), 978.
254. Vikulov, K., Spoto, G., Coluccia, S., and Zecchina, A., *Catal. Lett.*, **1992**, 16(1/2), 117–122.
255. Peri, J. B., *J. Phys. Chem.*, **1974**, 78(6), 588.
256. Gaspar, A. B., and Dieguez, L. C., *J. Molec. Catal. A Chem.*, **2004**, 219, 357–362.
257. Gaspar, A. B., Brito, J. L. F., and Dieguez, L. C., *J. Molec. Catal. A Chem.*, **2003**, 203, 251–266.
258. Gaspar, A. B., and Dieguez, L. C., *Appl. Catal. A Gen.*, **2002**, 227, 241–254.
259. Bensalem, A., Weckhuysen, B. M., and Schoonheydt, R. A., *J. Chem. Soc. Faraday Trans.*, **1997**, 93, 4065–4069.
260. Ajjou, J. A. N., Scott, S. L., and Paquet, V., *J. Am. Chem. Soc.*, **1998**, 120(2), 415–416.
261. Beaudoin, M. C., Womiloju, O., Fu, A., Ajjou, J. A. N., Rice, G. L., and Scott, S. L., *J. Molec. Catal. A Chem.*, **2002**, 190(1/2), 159–169.
262. Ajjou, J. A. N., Rice, G. L., and Scott, S. L., *J. Am. Chem. Soc.*, **1998**, 120(51), 13436–13443.
263. Ajjou, J. A. N., and Scott, S. L., *J. Am. Chem. Soc.*, **2000**, 122, 8968.
264. Ajjou, J. A. N., and Scott, S. L., *Organometallics*, **1997**, 16(1), 86–92.
265. Beaudoin, M. C., Womiloju, O., Fu, A., Ajjou, J. A. N., Rice, G. L., and Scott, S. L., *J. Molec. Catal. A Chem.*, **2002**, 3676, 1–11.
266. Krauss, H. L., Schmidt, H. A., Siebenhaar, B., Wolff, P., and Xing, Q., *Stud. Surf. Sci. Catal.*, **1993**, 75, 2325 (New Frontiers in Catalysis, Pt. C).
267. Spitz, R., Vuillaume, G., Revillon, A., and Guyot, A., *J. Macromol. Sci., Chem.*, **1972**, 6(1), 153–168. (Reduction with ethylene)
268. Guyot, A., and Durrieu, M., *J. Chim. Phys. Physicochim. Biol.*, **1968**, 65(5), 863–869.
269. Krauss, H. L., and Stach, H., *Z. Anorg. Allg. Chem.*, **1969**, 366(1/2), 34–42.
270. McDaniel, M. P., Benham, E. A., Norwood, D. D., Klendworth, D. D., and Hsieh, E. T., Phillips Petroleum Company, U.S. Patent Nos. 4,735,931, Apr. 5, 1988, and 4,820,785, Apr. 11, 1989.
271. Hogan, J. P., unpublished data from Phillips Petroleum Company internal research report No. 3827, 1964.
272. Gaspar, A. B., Martins, R. L., Schmal, M., and Dieguez, L. C., *J. Molec. Catal. A Chem.*, **2001**, 169, 105–112.
273. Garrone, E., Ghiotti, G., Morterra, C., and Zecchina, A., *Z. Naturforsch. B Chem. Sci.*, **1987**, 42(6), 728–738.
274. Groppo, E., Lamberti, C., Spoto, G., Bordiga, S., Magnacca, G., and Zecchina, A., *J. Catal.*, **2005**, 236(2), 233–244.

275. Liu, B., Sindel, P., Fang, Y., Hasebe, K., and Terano, M., *J. Molec. Catal. A Chem.*, **2005**, 238, 142–150.
276. McDaniel, M. P., Benham, E. A., and Smith, P. D., A catalyst system for the production of hexene-ethylene copolymers by the in-situ generation of hexene, paper presented at the SPO-92 Schotland Business and Technical Conference on Polyolefins, Houston, TX, Sept. 1992.
277. McDaniel, M. P., *Ind. Eng. Chem. Res.*, **1988**, 27, 559–1564.
278. Woo, T. W., and Woo, S. I., *J. Catal.*, **1990**, 123(1), 215–227.
279. Spitz, R., Florin, B. and Guyot, A., *Eur. Polym. J.*, **1979**, 15(5), 441–444.
280. Stricklen, P. M., and Hogan, J. P., Phillips Petroleum Co., U.S. Patent No. 4,374,234, Feb. 15, 1983.
281. McDaniel, M. P., Welch, M. B., and Dreiling, M. J., *J. Catal.*, **1983**, 82, 118.
282. Pullukat, T. J., Hoff, R. E., and Shida, M., Titanium modified chromium catalysts for ethylene polymerization, paper presented at the Symposium on Transition Metal Catalyst Polymerization, Michigan Molecular Institute, Aug. 1981.
283. Pullukat, T. J., Hoff, R. E., and Shida, M., *J. Polym. Sci. Polym. Chem. Ed.*, **1980**, 18, 2857.
284. Conway, S. J., Falconer, J. W., Rochester, C. H., and Downs, G. W., *J. Chem. Soc. Faraday Trans. 1*, **1989**, 85(7), 1841.
285. Hogan, J. P., and Witt, D. R., Phillips Petroleum Co., U.S. Patent No. 3,622,521, filed Aug. 1967, issued Nov. 1971.
286. Bouh, A. O., Rice, G. L., and Scott, S. L., *J. Am. Chem. Soc.*, **1999**, 121, 7201.
287. Deitz, R. E., Phillips Petroleum Co., U.S. Patent No. 3,887,494, June 3, 1975.
288. Rebenstorf, B., and Sheng, T. C., *Langmuir*, **1991**, 7(10), 2160–2165.
289. Conway, S. J., Falconer, J. W., Rochester, C. H., and Downs, G. W., *J. Chem. Soc. Faraday Trans. 1*, **1989**, 85(7), 1841–1851.
290. Conway, S. J., Falconer, J. W., and Rochester, C. H., *J. Chem. Soc. Faraday Trans. 1*, **1989**, 85(1), 79–90.
291. Mabilon, G., and Spitz, R., *Eur. Polym. J.*, **1985**, 21(3), 245–249.
292. Ellison, A., and Overton, T. L., *J. Molec. Catal.*, **1994**, 90(1/2), 81–86.
293. Ellison, A., and Overton, T. L., *J. Chem. Soc. Faraday Trans.*, **1993**, 89(24), 4393–4395.
294. Liu, B., and Terano, M., in *Advances in Polyolefins*, Sonoma, CA, Sept. **2005**.
295. Hogan, J. P., Phillips Petroleum, U.S. Patent No. 3,130,188, Apr. 21, 1964.
296. Kallenbach, L. R., Phillips Petroleum Co., U.S. Patent No. 3,445,367, filed Nov. 1965, issued May 1969.
297. Rebenstorf, B., *J. Molec. Catal.*, **1991**, 66(1), 59–71.
298. McDaniel, M. P., Phillips Petroleum Co., U.S. Patent No. 4,397,765, Aug. 1983.
299. McDaniel, M. P., Collins, K. S., Benham, E. A., Deslauriers, P. J., Chevron-Phillips Chemical Co., U.S. Patent 7,122,643 issued Sept. 26, 2006; 7,214,642 issued May 8, 2007.
300. McDaniel, M. P., and Smith, P. D., Phillips Petroleum Co., U.S. Patent Nos. 5,075,394, Dec. 24, 1991, and 5,200,379, Apr. 6, 1993.
301. Smith, P. D., and McDaniel, M. P., *J. Polym. Sci. Polym. Chem. Ed.*, **1990**, 28, 3587.

302. McDaniel, M. P., Klendworth, D. D., and Johnson, M. M., Phillips Petroleum Co., U.S. Patent Nos. 5,171,798, Dec. 15, 1992; 5,221,654, June 22, 1993; 5,221,655, June 22, 1993; 5,221,720, June 22, 1993; 5,219,817, June 15, 1993; and 5,219,962, June 15, 1993.
303. Smith, P. D., and McDaniel, M. P., *J. Polym. Sci. Polym. Chem. Ed.*, **1989**, 27, 2695.
304. McDaniel, M. P., Smith, P. D., and Norwood, D. D., Phillips Petroleum Co., U.S. Patent Nos. 5,401,820, Mar. 28, 1995; 5,037,911, Aug. 6, 1991; and 4,806,513, Feb. 21, 1989.
305. Cossee, P., *J. Catal.*, **1964**, 3, 80.
306. Banks, R. L., and Bailey, G. C., *J. Catal.*, **1969**, 14(3), 276–278.
307. Espelid, O., and Borve, K. J., *J. Catal.*, **2000**, 195(1), 125–139.
308. Smith, D. C., *Ind. Eng. Chem.*, **1956**, 48(7), 1161.
309. Witt, D. R., and Hogan, J. P., *J. Polym. Sci. Polym. Chem. Ed.*, **1970**, 8(9), 2689–2701.
310. Krauss, H. L., and Hums, E., *Z. Naturforsch. B Anorg. Chem. Org. Chem.*, **1979**, 34b, 1628.
311. Krauss, H. L., and Hums, E., *Z. Naturforsch. B Anorg. Chem. Org. Chem.*, **1980**, 35b(7), 848.
312. Krauss, H. L., and Hums, E., *Z. Naturforsch. B Anorg. Chem. Org. Chem.*, **1983**, 38b(11), 1412.
313. Ruddick, V. J., and Badyal, J. P. S., *J. Phys. Chem. B*, **1998**, 102(16), 2991–2994.
314. Groppo, E., Lamberti, C., Bordiga, S., Spoto, G., and Zecchina, A., *J. Catal.*, **2006**, 240, 172–181.
315. Bordiga, S., Bertarione, S., Damin, A., Prestipino, C., Spoto, G., Lamberti, C., and Zecchina, A., *J. Molec. Catal. A Chem.*, **2003**, 204/205, 527–534.
316. Krauss, H. L., and Schmidt, H., *React. Kinet. Catal. Lett.*, **1975**, 3(1), 83–88.
317. Ghiotti, G., Garrone, E., and Zecchina, A., *J. Molec. Catal.*, **1988**, 46, 61.
318. Ghiotti, G., Garrone, E., Coluccia, S., Morterra, C., and Zecchina, A., *J. Chem. Soc. Chem. Commun.*, **1970**, 801, 1032.
319. Krauss, H. L., Hums, E., and Weiss, K., *NATO ASI Ser. C*, **1987**, 215 (Recent Adv. Mech. Synth. Aspects Polym.), 353–362.
320. Terano, M., Liu, B., and Fang, Y., *Polym. Prepr.*, **2003**, 44(2), 22.
321. Lieu, B., Nakatani, H., and Terano, M., *J. Molec. Catal.*, **2003**, 201, 189–197.
322. McDaniel, M. P., and Cantor, D. M., *J. Polym. Sci. Polym. Chem. Ed.*, **1983**, 21, 1217.
323. Jozwiak, W. K., Dalla Lana, I. G., and Fiederow, R., *J. Catal.*, **1990**, 121, 183.
324. Jozwiak, W. K., Dalla Lana, I. G., Przystajko, W., and Fiedorow, R., in *Proceeding of the International Congress on Catalysis*, Vol. 3. Phillips, M. J., and Ternan, M., Eds., Chemical Institute of Canada, Ottawa, 1988, pp. 1340–1346.
325. Kantcheva, M., Dalla Lana, I. G., and Szymura, J. A., *J. Catal.*, **1995**, 154, 329.
326. Zielinski, P., and Dalla Lana, I. G., *J. Catal.*, **1992**, 137, 368.
327. Habeshaw, J., and Hill, T., in *Proceedings of the Third International Congress on Catalysis, July 20–25, 1964, Amsterdam*, Sochtler, W. M. H., Schuit, G. C. A., and Zwietering, P., Eds., North Holland Publishing, Amsterdam, 1965, p. 975.

328. Espelid, O., and Borve, K. J., *J. Catal.*, **2002**, 205, 366–374.
329. Krauss, H. L., *J. Molec. Catal.*, **1988**, 46, 97.
330. Wasserman, E., Hsi, E., and Young, W. T., *Polym. Prepr.*, **1998**, 39(1), 201–202.
331. Kissin, Y. V., and Brandolini, A. J., *J. Polym. Sci., A: Polym. Chem.*, **2008**, 46, 5330–5347.
332. Ballard, D. G. H., *Adv. Catal.*, **1973**, 22, 263.
333. Ballard, D. G. H., Jones, E., Pioli, A. J. P., Robinson, P. A., and Wyatt, R. J., U.S. Patent No. 3,840,508, Oct. 1974.
334. Ballard, D. G. H., Parkins, A. W., Robinson, P. A., Ibekwe, S. D., Lappert, M. F., and Pearce, R., Imperial Chemical Industries, U.S. Patent No. 3,969,386, 1976.
335. McDaniel, M. P., and Smith, P. D., Phillips Petroleum Co., U.S. Patent Nos. 5,075,394, Dec. 24, 1991; and 5,200,379, Apr. 6, 1993.
336. McDaniel, M. P., Klendworth, D. D., and Johnson, M. M., Phillips Petroleum Co., U.S. Patent Nos. 5,171,798, Dec. 15, 1992; 5,221,654, June 22, 1993; 5,221,655, June 22, 1993; 5,221,720, June 22, 1993; 5,219,817, June 15, 1993; and 5,219,962, June 15, 1993.
337. Smith, P. D., and McDaniel, M. P., *J. Polym. Sci. Polym. Chem. Ed.*, **1989**, 27, 2695.
338. Yermakov, Y., and Zakharov, V., *Adv. Catal.*, **1975**, 24, 173.
339. Yermakov, Y., and Zakharov, V., *Catal. Rev. Sci. Eng.*, **1979**, 19(1), 67.
340. Yermakov, Y., *Catal. Rev.*, **1976**, 13(1), 77.
341. Zakharov, V., and Yermakov, Y. I., *J. Polym. Sci. A-1*, **1971**, 9, 3129.
342. Zakharov, V., and Yermakov, Y. I., paper presented, at the *Proc. IV Int. Cong. Catal.*, Moscow, 1968, p. 232, paper 16.
343. Zakharov, V., Yermakov, Y. I., and Kushnareva, E. G., *Kinet. Catal.*, **1967**, 8(6), 1181; *J. Polym. Sci. A-1*, **1971**, 9, 771.
344. Martin, S. J., McDaniel, M. P., Conroy, B. K., and Martin, J. L., Phillips Petroleum Co., U.S. Patent Nos. 5,021,379 (June 4, 1991); and 5,104,950 (Apr. 14, 1992); Geerts, R. L., Benham, E. A., and McDaniel, M. P., Phillips Petroleum Co., U.S. Patent Nos. 5,399,622 and 5,459,203, Mar. 21, 1995.
345. Ballard, D. G. H., Courtis, A., Holton, J., McMeeking, J., and Pearce, R., *J. Chem. Soc. Chem. Commun.*, **1978**, 22, 994–995; Ballard, D. G. H., Courtis, A., Holton, J., McMeeking, J., and Pearce, R., Lanthanide catalysts for the polymerization of olefins., paper presented at the 5th Conf. Eur. Plast. Caoutch., 1978.
346. Jackson, M. F., Knudsen, R. D., and Shveima, J. S., Phillips Petroleum Co., U.S. Patent No. 5,198,512, Mar. 30, 1993; Knudsen, R. D., Hawley, G. R., and Jackson, M. F., Phillips Petroleum Co., U.S. Patent No. 5,332,708, July 26, 1994.
347. Unpublished experiments in this laboratory with cyclooctatrienyl Ti and other compounds.
348. Karol, F. J., and Johnson, R. N., *J. Polym. Sci. Polym. Chem. Ed.*, **1975**, 13, 607.
349. Karol, F. J., Brown, G. L., and Davison, J. M., *J. Polym. Sci. Polym. Chem. Ed.*, **1973**, 11, 413.
350. Karol, F. J., Karapinka, G. L., Wu, C., Dow, A. W., Johnson, R. N., and Carrick, W. L., *J. Polym. Sci. A-1*, **1972**, 10, 2621.

351. Karol, F. J., Wu, C., Reichle, W. T., and Maraschin, N. J., *J. Catal.*, **1979**, 60, 68.
352. Freeman, J. W., Wilson, D. R., Ernst, R. D., Smith, P. D., Klendworth, D. D., and McDaniel, M. P., *J. Polym. Sci. A, Polym. Chem.*, **1987**, 25, 2063.
353. McDaniel, M. P., and Short, J. N., Phillips Petroleum Co., U.S. Patent Nos. 4,424,139, Jan. 3, 1984; 4,690,990, Sept. 1, 1987; and 4,803,253, Feb. 7, 1989.
354. Karol, F. J., *Catal. Rev. Sci. Eng.*, **1984**, 26(3/4), 557.
355. Blom, R., Follestad, A., and Noel, O., *J. Molec. Catal.*, **1994**, 91(2), 237–249 (mainly transfer to monomer).
356. Ermakov, Y. I., Ivanov, L. P., and Gel'bshtein, A. I., *Kinet. Katal.*, **1969**, 10(1), 183 (Eng. 146).
357. Ivonov, L. P., Yermakov, Y. I., and Gellbshtein, A. I., *Vysokomol. Soedin. Siberian Acad. Sci. USSR*, **1967**, Ser. A9, No. 11, 2422.
358. Kim, C. S., Woo, S. I., Seong Ihl, J., Jeong, D. J., and Oh, J. S., *Polym. Bull. (Berlin)*, **1992**, 29(1/2), 205–212.
359. Hogan, J. P., and Kitchen, A. G., Phillips Petroleum Co., U.S. Patent No. 3,225,023, Dec. 21, 1965.
360. McDaniel, M. P., and Hottovy, T. D., *J. Colloid Interf. Sci.*, **1980**, 78(1), 31–36.
361. Soult, A. S., Carter, D. F., Schreiber, H. D., van de Burgt, L. J., and Stiegman, A. E., *J. Phys. Chem. B*, **2002**, 106(36), 9266–9273.
362. McDaniel, M. P., Phillips Petroleum Co., U.S. Patent Nos. 4,489,172, Dec. 18, 1984; 4,559,394, Dec. 17, 1985.
363. McDaniel, M. P., and Welch, M. B., Phillips Petroleum Co., U.S. Patent Nos. 4,177,162, Dec. 4, 1979, and 4,277,587, July 7, 1981.
364. McDaniel, M. P., Phillips Petroleum Co., U.S. Patent Nos. 4,248,735, Feb. 3, 1981, 4,297,460, Oct. 27, 1981.
365. McDaniel, M. P., *J. Phys. Chem.*, **1981**, 85, 537.
366. McDaniel, M. P., Phillips Petroleum Co., U.S. Patent Nos. 4,308,172, Dec. 29, 1981, and 4,357,451, Nov. 2, 1982.
367. Noshay, A., and Karol, F. J., in *Transition Metal Catalyzed Polymerization, Proceedings of the International Symposium, II*, June 16–20, 1986, Akron, OH, Qurik, R. P., Ed., Cambridge University Press, Cambridge, 1988, pp. 396–416.
368. Pullukat, T. J., Hoff, R. E., and Shida, M., *J. Appl. Polym. Sci.*, **1981**, 26, 2927.
369. McDaniel, M. P., and Welch, M. B., Phillips Petroleum Co., U.S. Patent Nos. 4,151,122, Apr. 24, 1979, 4,182,815, Jan. 8, 1980.
370. McDaniel, M. P., Sanbrano, J. A., and Johnson, M. M., Phillips Petroleum Co., U.S. Patent Nos. 4,397,769, Aug. 9, 1983, and 4,460,756, July 17, 1984.
371. McDaniel, M. P., and Welch, M. B., Phillips Petroleum Co., U.S. Patent No. 4,247,421, Jan. 27, 1981.
372. Mangnus, P. J., Ellison, A., Scheffer, B., and Moulijn, J. A., *Bull. Soc. Chim. Belg.*, **1987**, 96(11/12), 977–983.
373. Hawley, G. R., Phillips Petroleum, U.S. Patent Nos. 4,295,998, Oct. 1981, and 4,331,789, May 1982.
374. Burwell, R. L., Haller, G. L., Taylor, K. C., and Read, J. F., *Adv. Catal.*, **1969**, 20, 1.
375. Cornet, D., and Burwell, R. L., *J. Am. Chem. Soc.*, **1968**, 90, 2489.

376. McDaniel, M. P., and Burwell, R. L., *J. Catal.*, **1975**, 36, 394.

377. McDaniel, M. P., and Burwell, R. L., *J. Catal.*, **1975**, 36, 404.

378. Iler, R. K., *The Chemistry of Silica: Solubility, Polymerization, Colloid and Surface Properties, and Biochemistry*, Wiley, New York, 1979.

379. Ries, H. E., *Advances in Catalysis and Related Subjects*, Vol. 4, Academic, New York, 1950, p. 87.

380. McDaniel, M. P., Witt, D. R., and Benham, E. A., *J. Catal.*, 1998, 176, 344–351.

381. Witt, D. R., Benham, E. A., and McDaniel, M. P., Phillips Petroleum Co., U.S. Patent No. 5,444,132, Aug. 22, 1995.

382. Rebenstorf, B., *Acta Chem. Scand.*, **1991**, 45(10), 1012–1017.

383. Rebenstorf, B., *Z. Anorg. Allg. Chem.*, **1985**, 531, 41–51.

384. Deslauriers, P. J., McDaniel, M. P., Rohlfing, D. C., Krishnaswamy, R. K., Secora, S. J., Benham, E. A., Maeger, P. L., Wolfe, A. R., Sukhadia, A. M., and Beaulieu, W. B., *Polym. Eng. and Sci.*, **2005**, 45(9), 1203–1213; Society of Plastics Engineers, International Conference on Polyolefins, Houston, TX, Feb. 24, 2004; *ANTEC* 2005, *Proceedings of the 63rd SPE Annual Conference*, Boston, MA, May 1–5, 2005.

385. McDaniel, M. P., Pitzer, E. W., and Farha, F. E., Phillips Petroleum Co., U.S. Patent Nos. 4,900,704, Feb. 13, 1990, and 5,026,796, June 25, 1991.

386. Conway, S. J., Falconer, J. W., and Rochester, C. H., *J. Chem. Soc., Faraday Trans.*, **1990**, 86(3), 577–580.

387. Wharry, S. M., Martin, S. J., and McDaniel, M. P., *J. Catal.*, **1989**, 115, 463.

388. McDaniel, M. P., Cheung, T. T. P., and Johnson, M. M., Ethylene Polymerization over Cr/aluminophosphate catalysts, in *Transition Metal Catalyzed Polymerization, Proceedings of the International Symposium, II*, June 16–20, 1986, Akron, OH, and Qurik, R. P., Eds., Cambridge University Press, Cambridge, 1988, pp. 382–395.

389. Rebenstorf, B., Lindblad, T., Andersson, T., and Lars, S., *J. Catal.*, **1991**, 128(2), 293–302, 303–310.

390. Witt, D. R., Phillips Petroleum Co., U.S. Patent No. 3,947,433, Mar. 1976.

391. Bergmeister, J. J., Wolfe, A. R., Secora, S. J., Benham, E. A., Coutant, W. R., and McDaniel, M. P., Phillips Petroleum Co., U.S. Patent No. 6,174,981, Jan. 16, 2001.

392. Bergmeister, J. J., Secora, S. J., Guenther, G., Benham, E. A., and McDaniel, M. P., Phillips Petroleum Co., U.S. Patent Nos. 6,201,077, Mar. 13, 2001; 6,204,346, Mar. 20, 2001; and 6,642,324, Nov. 4, 2003.

393. Sukhadia, A. M., Benham, E. A., Bergmeister, J. J., Bobsein, R. L., Guenther, G., Hsieh, E. T., McDaniel, M. P., Secora, S. J., Shveima, J. S., and Stewart, J. D., Phillips Petroleum Co., U.S. Patent No. 6,617,403, Sep. 9 2003.

394. Bergmeister, J. J., Secora, S. J., Benham, E. A., and McDaniel, M. P., Phillips Petroleum Co., U.S. Patent Nos. 6,569,960, May 27, 2003, and 6,855,781, Feb. 15, 2005.

395. McDaniel, M. P., and Short, J. N., Phillips Petroleum Co., U.S. Patent Nos. 4,818,800, Apr. 4, 1989; and 4,877,763, Oct. 31, 1989.

396. Hogan, J. P., Phillips Petroleum Co., U.S. Patent Nos. 4,025,707, May 1977, and 3,959,178, May 1976.
397. Hogan, J. P., in *Copolymerization*, Vol. 18, Ham, G. E., Ed., Interscience, New York, 1964, Chapter 3.
398. Benham, E. A., and McDaniel, M. P., *High density polyethylene, in Encyclopedia of Polymer Science and Technology*, 3rd ed., Wiley, New York, 2001.
399. Hogan, J. P., Ethylene alpha-olefin copolymers made in gas phase process, in *Proc. IUPAC, Macromol. Symp.*, International Union of Pure and Applied Chemistry, Oxford, 1982, p. 251.
400. Rangwala, H. A., Dalla Lana, I. G., Szymura, J. A., and Fiedorow, R. M., *J. Polym. Sci. Pt. A Polym. Chem.*, **1996**, 34, 3379–3387.
401. Zakharov, V. A., Echevskaya, L. G., and Bukatov, G. D., *Makromol. Chem.*, **1989**, 190(3), 559–566.
402. Bukatov, G. D., Yechevskaya, L. G., and Zakharov, V. A., Copolymerization of ethylene with α-olefins by highly active supported catalysts of various composition, in *Transition Metal and Organometallic Catalyzed Olefin Polymerization, Proceedings of the International Symposium*, Kaminsky, W., and Sinn, H., Eds., Springer, Berlin, 1988, pp. 101–108.
403. Bade, O. M., Blom, R., Dahl, I. M., and Karlsson, A., *J. Catal.*, **1998**, 173(2), 460–469.
404. Fenogenova, L. T., Zakharov, V. A., Buniyat-Zade, A. A., Bukatov, G. D., and Plaksunov, T. K., *Polym. Sci. U.S.S.R.*, **1979**, 22, 448.
405. Weiss, K., and Krauss, H. L., *J. Catal.*, **1984**, 88, 424.
406. Spitz, R., Revillon, A., and Guyot, A., *J. Macromol. Sci. Chem.*, **1974**, A8(6), 1129–1136.
407. Vuillaume, G., Spitz, R., Revillon, A., and Guyot, A., *J. Macromol. Sci. Chem.*, **1974**, A8(6), 1117–1128.
408. Vuillaume, G., Revillon, A., Spitz, R., and Guyot, A., *J. Macromol. Sci. Chem.*, **1971**, 5(3), 557–571.
409. Revillon, A., Daniel, J. C., and Guyot, A., *J. Chim. Phys. Physicochim. Biol.*, **1968**, 65(5), 857–862.
410. Revillon, A., Guyot, A., and Trambouze, Y., *J. Chim. Phys. Physicochim. Biol.*, **1968**, 65(5), 849–856.
411. Revillon, A., and Guyot, A., *J. Chim. Phys. Physicochim. Biol.*, **1968**, 65(5), 845–848.
412. Soga, K., Chen, S. I., Doi, Y., and Shiono, T., *Macromolecules*, **1986**, 19(12), 2893.
413. Gan, S. N., Chen, S. I., Ohnishi, R., and Soga, K., *Polymer*, **1987**, 28, 1391.
414. Hogan, J. P., Phillips Petroleum Co., U.S. Patent No. 3,098,062, July 1963.
415. DesLauriers, P. J., Rohlfing, D. C., and Hsieh, E. T., *Polymer*, **2002**, 43, 159–170.
416. Deslauriers, P. J., and McDaniel, M. P., Short chain branch distributions from the Phillips Cr/silica catalysts, paper presented at the Oklahoma ACS Pentasectional Meeting, Stillwater, OK, Apr. 2005.
417. Hogan, J. P., Hsieh, E. T., and Randall, J. C., Phillips Petroleum Co., U.S. Patent No. 4,522,987, June 11, 1985.

418. Wharry, S. M., *Polymer*, **2004**, 45, 2985–2989.

419. Gupta, P., Wilkes, G. L., Sukhadia, A. M., Krishnaswamy, R. K., Lamborn, M. J., Wharry, S. M., Tso, C. C., DesLauriers, P. J., Mansfield, T., and Beyer, F. L., *Polymer*, **2005**, 46, 8819–8837.

420. Sukhadia, A. M., Welch, M. B., Krishnaswamy, R. K., and Palackal, S. J., The effects of comonomer type on the blown film performance LLDPE resins made using a metallocene single-site catalyst. *Soc. Plastics Eng. ANTEC Conf. Proc.*, **2000**, 58, 1578–1582.

421. Levine, I. J., and Karol, F. J., Union Carbide Corp., U.S. Patent No. 4,011,382, Mar. 8, 1977.

422. McDaniel, M. P., Leigh, C. H., and Wharry, S. M., *J. Catal.*, **1989**, 120, 170.

423. McDaniel, M. P., and Johnson, M. M., Phillips Petroleum Co., U.S. Patent Nos. 4,364,840, Dec. 21, 1982, and 4,398,004, Aug. 9, 1983.

424. Badley, R. D., The influence of catalyst pore size on 1-hexene incorporation, Phillips Petroleum Company, unpublished reports, 1993.

425. McDaniel, M. P., Badley, R. D., Kreischer, B. F., and Shveima, J. S., Phillips Petroleum, U.S. Patent No. 5,641,842, June 1997.

426. (a) Reagan, W. K., Phillips Petroleum Co., European Patent No. EP 0417477, 1991. (b) Reagen, W. K., and McDaniel, M. P., Phillips Petroleum Co., U.S. Patent Nos. 5,438,027, Aug. 1, 1995, and 5,382,738, Jan. 17 1995. (c) Conroy, B. K., Pettijohn, T. M., and Benham, E. A., Phillips Petroleum Co., European Patent No. EP 0608447, 1994; Reagen, W. K., and Conroy, B. K., Phillips Petroleum Co., U.S. Patent Nos. 5,331,104 and 5,198,563, Mar. 30, 1993. (c) Freeman, J. W., Buster, J. L., and Knudsen, R. D., Phillips Petroleum Co., U.S. Patent No. 5,856,257, 1999. (d) Reagan, W. K., Freeman, J. W., Conroy, B. K., Pettijohn, T. M., and Benham, E. A., Phillips Petroleum Company, U.S. Patent No. 5,451,645, 1995.

427. Emrich, R., Heinemann, O., Jolly, P. W., Kruger, C., and Verhovnik, G. P. J., *Organometallics*, **1997**, 16(8), 1514.

428. Briggs, J. R., *J. Chem. Soc. Chem. Commun.*, **1989**, 1(11), 674.

429. Meijboom, N., Schaverien, C. J., and Orpen, A. G., *Organometallics*, **1990**, 9, 774.

430. Manyik, R. M., Walker, W. E., and Wilson, T. P., *J. Catal.*, **1977**, 47, 197.

431. Karol, F. J., Copolymerization and chain-branching studies with high-activity chromium and titanium catalysts, in *Transition Metal Catalyzed Polymerization, Proceedings of the International Symposium, II*, June 16–20, 1986, Akron, OH, and Qurik, R. P., Eds., Cambridge University Press, Cambridge, 1988, pp. 702–718.

432. Blom, R., Dahl, I. M., and Swang, O., *J. Catal.*, **2000**, 194(2), 352–363.

433. Blom, R., Dahl, I. M., Follestad, A., and Jens, K. J., *J. Molec. Catal. A Chem.*, **1999**, 138(1), 97–102.

434. Benham, E. A., McDaniel, M. P., and Bailey, F. W., Phillips Petroleum Co., U.S. Patent Nos. 4,966,951, Oct. 30, 1990, and 5,115,068, May 19, 1992.

435. McDaniel, M. P., and Benham, E. A., Phillips Petroleum Co., U.S. Patent Nos. 5,208,309, May 4, 1993, and 5,274,056, Dec. 28, 1993.

436. Bade, O. M., and Blom, R., *Appl. Catal. A. Gen.*, **1997**, 161, 249.

437. Bade, O. M., Blom, R., and Ystenes, M., *J. Molec. Catal. A Chem.*, **1998**, 135(2), 163–179.

438. Fang, Y., Liu, B., Hasebe, K., and Terano, M., *J. Polym. Sci. Pt. A Polym. Chem.*, **2005**, 43, 4632–4641.

439. Liu, B., Fang, Y., Nakatani, H., and Terano, M., *Macromol. Symp.*, **2004**, 213, 37–46.

440. Benham, E. A., Smith, P. D., Hsieh, E. T., and McDaniel, M. P., *J. Macromole. Sci. Chem.*, **1988**, A25(3), 259–283.

441. Monoi, T., Ikeda, H., Sasaki, Y., Matsumoto, Y., *Polym. J.*, **2003**, 35(7), 608.

442. Miesserov, K. G., *J. Polym. Sci. A-1*, **1966**, 4, 3047.

443. Miesserov, K. G., *J. Catal.*, **1971**, 22, 340.

444. Xia, W., Liu, B., Fang, Y., Hasebe, K., and Terano, M., *J. Molec. Catal. A Chem.*, **2006**, 256, 301–308.

445. McDaniel, M. P., Benham, E. A., and Martin, S. J., Phillips Petroleum Co., U.S. Patent Nos. 4,988,657, Jan. 29, 1991, and 5,171,801, Dec. 15, 1992.

446. Tung, L. H., *J. Polym. Sci.*, **1960**, 46, 409–422.

447. Hogan, J. P., Levett, C. T., and Werkman, R. T., *SPE J.*, **1967**, 23(11) 87.

448. Arnett, T., Long chain branching in PE from the PF process, Phillips Petroleum Company, internal research reports, 1963; Hogan, J. P., and Werkman, R. T., Effects of long chain branching in determining melt processing, Phillips Petroleum Company, internal research reports, 1966.

449. vanKimmenade, E. M. E., Loos, J., Niemantsverdriet, J. W., and Thüne, P. C., *J. Catal.*, **2006**, 240, 39–46.

450. Janzen, J., and Colby, R. H., *J. Molec. Struct.*, **1999**, 485/486, 569.

451. Reinking, M. K., Orf, G., and McFaddin, D., *J. Polym. Sci. A Polym. Chem.*, **1998**, 36, 2889.

452. Reinking, M. K., Orf, G., and McFaddin, D., Novel mechanism for the formation of long-chain branching in polyethylene, paper presented at *SPE Polyolefins XII, International Conference on Polyolefins*, Houston, TX, Feb. 27–March 1, 2000.

453. Fetters, J., Lohse, D. J., and Colby, R. H., in *Physical Properties of Polymers Handbook*, Mark, J. E., Ed., AIP Press, New York, 1996, p. 335.

454. Bird, R. B., Armstrong, R. C., and Hassager, O., *Dynamics of Polymeric Liquids*, Vol. 1: *Fluid Mechanics*, Wiley, New York, 1987.

455. Arnett, R. L., and Thomas, C. P., *J. Phys. Chem.*, **1980**, 84, 649.

456. Yiannoulakis, H., Yiagopoulos, A., Pladis, P., and Kiparissides, C., *Macromolecules*, **2000**, 33, 2757–2766.

457. Computer simulation by McDaniel, M. P., Chevron-Phillips Chemical Company, 2004.

458. Hogan, J. P., and Nease, C. R., Phillips Petroleum Co., U.S. Patent No. 5,155,186, Oct. 13, 1992.

459. Ystenes, M., *J. Catal.*, **1991**, 129(2), 383–401.

460. Patterson, R. E., *Kirk-Othmer Encyclopedia of Chemical Technology*, Vol. 21, 4th ed., Howe-Grant, M., Ed., Wiley, New York, 1997, p. 977.

461. Suggested in 2004 by Dr. R. Glemza of W. R. Grace Company.

462. McDaniel, M. P., and Welch, M. B., Phillips Petroleum Co., U.S. Patent Nos. 4,378,306, Mar. 29, 1983, and 4,434,280, Feb. 28, 1984.

463. Jensen, M., Chevron-Phillips Chemical Company, private communication, 2004.

464. Shveima, J. S., McDaniel, M. P., Martin, S. J., Collins, K. S., Benham, E. A., Eaton, A. P., and Sukhadia, A. M., Phillips Petroleum Co., U.S. Patent Nos. 6,538,077, Nov. 1999, and 6,716,938, Apr. 2004.

11 Silica-Supported Silyl Chromate–Based Ethylene Polymerization Catalysts

KEVIN CANN
Univation Technologies, Bound Brook Technical Center, Piscataway,
New Jersey 08854

11.1 INTRODUCTION

Polymerization of ethylene with supported chromium-based catalysts has been known for over 40 years. Most of the chromium-based catalyst work has focused on oxo chromium systems, commonly referred to as the Phillips-type catalyst (Cr/SiO_2).[1,2] There has also been a significant amount of work based on the organochromium systems, chromocene[3] and organosilyl chromate. Of the organochrome-based systems, silyl chromate–derived catalysts are used in gas-phase polyethylene (PE) production primarily for high-density applications.[4–7]

11.2 CATALYST DEVELOPMENT

Ethylene polymerization with organo silyl chromate catalysts was first reported in 1967 by Union Carbide.[4–6] Unsupported silyl chromate catalyst in conjunction with an aluminum alkyl cocatalyst was found to polymerize ethylene only under very high ethylene partial pressure conditions. Chemisorption of silyl chromate on alumina improved catalyst productivity significantly allowing for the use of low-pressure ethylene conditions. Alkyl aluminum reagents were introduced into the catalyst formulations to increase catalyst productivity and control polymer molecular weight.[7] In the early literature, supported catalysts were prepared without isolation (Figure 11.1).

Handbook of Transition Metal Polymerization Catalysts Edited by Ray Hoff and Robert T. Mathers
Copyright © 2010 John Wiley & Sons, Inc.

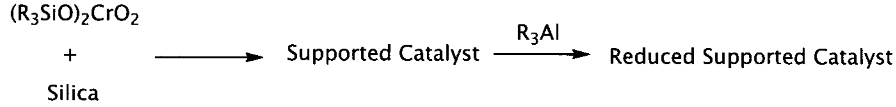

$$\begin{matrix} (R_3SiO)_2CrO_2 \\ + \\ \text{Silica} \end{matrix} \longrightarrow \text{Supported Catalyst} \xrightarrow{R_3Al} \text{Reduced Supported Catalyst}$$

Figure 11.1 Nonseparated silica-supported reduced silyl chromate catalyst sequence.

The silyl chromate precursor was allowed to chemisorb on dehydrated silica in hydrocarbon for a number of hours followed by addition of the aluminum alkyl reagent. The entire slurry was then added to the polymerization reactor followed by hydrogen and monomers. In most examples the supported catalyst was formed in the polymerization reactor prior to monomer introduction.

Early work examined a variety of different organo groups on the silyl chromate catalysts and different aluminum alkyl reducing agents. Although many different organo polyalicyclic chromate ester derivatives (U.S. 3,642,749)[8] were examined, organosilyl derivatives and in particular bis-triphenylsilyl chromate (BPSC) have become the preferential derivative used in the patent literature. This derivative[6,9] is easy to make and has good stability, which is an issue for many of the other derivatives.[10–12] Dialkyl aluminum alkoxides are the preferred reducing agents. Diethyl aluminum ethoxide (DEALE) is commercially available and is cited frequently in the patent literature. While both the trialkyl and dialkyl-ethoxy aluminum compounds increase the productivity of the catalyst, dialkyl aluminum alkoxides[3] lower the molecular weight of the polyethylene polymers made with silyl chromate catalysts. The trialkyl aluminum reducing agents increase the polymer molecular weight. Reduction with DEALE produces a catalyst that makes polymers, in both slurry and gas-phase processes, that have molecular weights that are useful for many high-density PE (HDPE) applications.

Chromium catalysts are often characterized by the polymer molecular weight made under a certain set of conditions. Polymer molecular weight can be measured indirectly by measuring the flow index (FI) [American Society for Testing and Materials (ASTM) D-1238] of the polymer, which is the time for a certain amount of polymer to pass through a die in the molten state at 190 °C under a certain weight. The FI is inversely related to polymer molecular weight. Thus, a catalyst will have a certain FI response. A catalyst can be constructed to give a certain FI response, which means it will make the desired polymer molecular weight under the most economical process conditions.

The earliest published supported formulations can be found in U.S. patents 4,003,712[13] and 4,065,612,[14] where BPSC is added to a silica support (300 M^2/g, 200 Å pore diameter, <100 µm particle size) in hydrocarbon. The chromium loading can be between 0.01 and 0.1 mmol Cr/g silica (0.05 mmol Cr/g silica is typical) and complete chemisorption of the BPSC takes several hours followed by DEALE addition. The ratio of aluminum reducing agents to chromium can be between 1 and 16, although Al/Cr ratios between 1.5 and 6.0 are more typical. In addition to DEALE, triethyl aluminum may also be added. The preceding catalysts were employed in fluid bed gas-phase ethylene polymerization reactions found in U.S. patent 4,003,712.

Later publications[15–17] have focused on more specific formulations. BPSC is mixed at 45 °C for 5–10 h with 600 °C dehydrated silica (0.05 mmol Cr/g silica) in hydrocarbon. DEALE is added and the mixture is stirred for 0.5–2 h prior to drying via a nitrogen purge for 10 h or more at elevated temperatures.

11.3 CATALYST STRUCTURE

Over the years there have been several proposals for the structure of the silica-supported silylchromate precursor and the reduced version. Carrick et al.[7] proposed that the silica-supported catalysts consisted of a transesterification reaction between bistriphenylsilyl chromate and the surface silanols of dehydrated silica. One or both triphenylsilyl groups could be displaced by silica; both structures are shown in Figure 11.2. Later, Sindelar et al.[18] proposed that both triphenylsilyl groups are displaced when the silica is dehydrated under a certain set of conditions.

Zakharov et al.[19] proposed that the silyl chromate does not react in a transesterification reaction with the silica silanols. Using fourier transform infrared (FTIR) spectroscopy, it was concluded that the silyl chromate adsorbs on the surface and the aluminum alkyl reacts with the surface silanols and the silyl chromate, as shown in Figure 11.3.

Regardless of the proposed structure of the silyl chromate on silica, it is believed that the addition of aluminum alkyl results in significant reduction of the chromium oxide. Zakharov proposed that chromium IV and V complexes are formed, while Johnson[12] proposed the final chromium oxidation state is less than IV. Carrick[7] showed that at high aluminum-to-chromium ratios essentially no chromium VI remains. A more recent study[20] by X-ray photoelectron spectroscopy (XPS) found that at a 5/1 DEALE-to-chromium

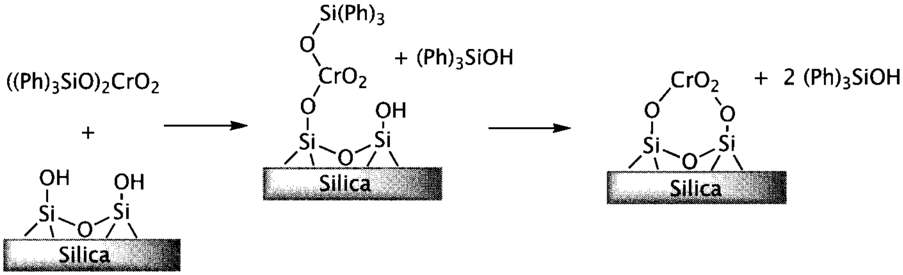

Figure 11.2 Structure of silica-supported silyl chromate precursor.

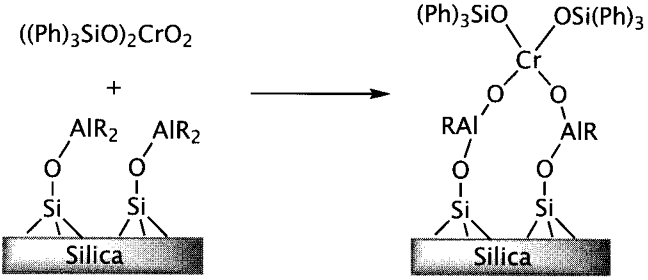

Figure 11.3 Structure of aluminum-bridged silica-supported silyl chromate catalyst.

TABLE 11.1 Oxidation States of Silica-Supported Silyl Chromate Catalysts by XPS

Sample Davison 955 Silica	XPS Measurement Time (min)	Binding Energy (eV) Cr2p(3/2)		Content of Cr^{6+} (%)
		Cr^{6+}	Cr^{2+}	
Bis-triphenylsilyl chromate	10	579.82	—	100
Bis-triphenylsilyl chromate + 5 eq. DEALE	10	579.81	576.35	63

ratio only 63% of the chromium VI is reduced (Table 11.1). This study also found that the reduced product is a chromium II complex. The mechanism by which ethylene polymerization is initiated on the reduced silica-supported silyl chromate catalyst is not understood.

11.4 POLYMERIZATION PROCESS

There are many examples in the patent literature of polymerization reactions in both slurry and gas-phase processes to make HDPE with silica-supported silyl chromate catalysts.

11.4.1 Slurry Polymerizations

In a typical slurry polymerization,[21] catalyst is charged to a reactor equipped with a mechanical stirrer and a jacket for internal temperature control. The catalyst is introduced followed by dry purified hexane or isobutane. The reactor is brought up to reaction temperature (85–100 °C), hydrogen batch charged, ethylene feed started, and 1-hexene is batch charged. The ethylene is fed con-

TABLE 11.2 Slurry Polymerizations with Silyl Chromate Catalysts

DEALE/Cr in Catalyst	FI (I_{21}) (dg/10 min)	Activity (g PE/g Cat·h)	BBF[a]	Density (g/mL)
0	13.6	133	2.0	0.9504
1.5	16.6	252	2.0	0.9501
5	67.8	388	1.0	0.9561
10	296	789	0.6	0.9633

Note: Reaction conditions: 500 mL hexane slurry; 10 mL 1-hexene; 85 °C; 200 psi C_2.

[a] Butyl branches/1000 CH2.

tinuously upon demand to maintain an ethylene partial pressure of 200 psi. Polymerization results in a slurry reaction are shown in Table 11.2 for catalysts with different degrees of DEALE reduction.[22,23] Polymer density and butyl branching frequency measurements show the amount of comonomer (hexene) incorporated into the polymer.

The unreduced silica supported silyl chromate has poor polymerization activity. Like chromium oxide–based catalysts, it is assumed that ethylene functions as the reducing agent for the unreduced silica-supported silyl chromate catalyst. Addition of increasing amounts of DEALE to the catalyst increases catalyst activity, lowers polymer molecular weight (increasing FI values), and decreases comonomer incorporation (density increases and incorporated branching decreases).

11.4.2 Gas-Phase Polymerizations

Silica-supported reduced silyl chromate catalysts are used in fluid bed gas-phase polymerization reactions. A description of a fluid bed polymerization reaction can be found in U.S. 4,482,687.[24] Gas-phase process conditions to make HDPE can be found in U.S. 5,034,364[15] to Mobil and U.S. 6,022,933[25] to Union Carbide. Reaction conditions are dictated by the choice of catalyst formulation and final product specifications (FI and density). Table 11.3 shows gas-phase polymerization reaction conditions for two of the main HDPE products made with silyl chromate catalysts.

Typical reaction temperatures are between 92 and 110 °C with ethylene partial pressures of 175–250 psi and catalyst residence times from 2 to 6 h. Hydrogen-to-ethylene ratios can vary from 0.02 to 0.20. Polymer molecular weight is controlled by reaction temperature, hydrogen-to-ethylene ratio, and or oxygen add-back. Polymer density is primarily controlled by varying the comonomer-to-ethylene ratio. This catalyst system produces granular polymer with very high bulk densities, generates very few polymer fines, and has excellent reactor operability.

TABLE 11.3 Fluidized-Bed HDPE Process Conditions for Silica-Supported Reduced Silyl Chromate Catalysts

Reaction Conditions	Film	Pipe
Reactor temperature, °C	95	106
C_6/C_2	0.0049	0.0086
H_2/C_2	0.039	0.05
O_2, ppmv	0	0.04
Production rate (lb/h)	30	—
C_2 partial pressure (psi)	215	248
Product properties		
Flow index (FI), I_{21}, pellets (g/10 min)	9	10.1
Melt flow ratio (MFR), I_{21}/I_2, pellets	122	118
Resin density, g/cm^3	0.948	0.945
Dart drop F50 (g)	139	—
Elmendorf tear (g/mil)		
Machine direction (MD)	15	—
Transverse direction (TD)	161	—
Bubble stability/extrudability	Good	Good
Pennsylvania Notched Test (PENT) (ASTM-1 1473) slow crack growth resistance	—	74–90

11.5 PRODUCT CHARACTERIZATION AND APPLICATIONS

Silica-supported reduced silyl chromate catalysts are used primarily in gas-phase reactions to make polymers for HDPE applications. Specific applications include pipe, film, large-part blow molding, and conduit. These applications are large-volume markets requiring polymers that are extremely tough. All HDPE chromium catalysts, including the Phillips chromium oxide catalysts, make PE with broad molecular distributions. Using the most simplistic models for Cr^{6+} catalysts based on the oxo[26] and organosilanol[7] (triphenylsilanol) derivatives, it can be seen that the structural features of these catalyst precursors are quite similar (Figure 11.4). However, the polymer molecular weight distributions (MWDs) are very different for the chromium oxo and the silyl chromate systems[22] (Figure 11.5). Both catalysts produce broad MWD polymers, but the silyl chromate catalyst produces broader polymer distributions (broader on both the high- and low-molecular-weight ends) with a pronounced high-molecular-weight tail, almost indicative of a second type of active site.

The increased amount of polymer chains with higher molecular weight[24,25] leads to improved application attributes[27,28] such as higher environmental stress crack resistance (ESCR), high film puncture resistance, good film bubble stability, high swell polymer for large-part blow-molding applications, and high slow crack growth resistance for high-pressure pipe.

The extra broadening of the MWD with the high-molecular-weight shoulder is the result of the presence of the organo silyl chromate ligand on the

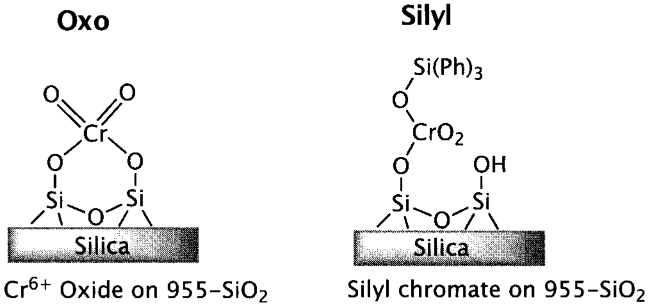

Figure 11.4 Possible structures of oxo and silyl chromate catalysts on silica.

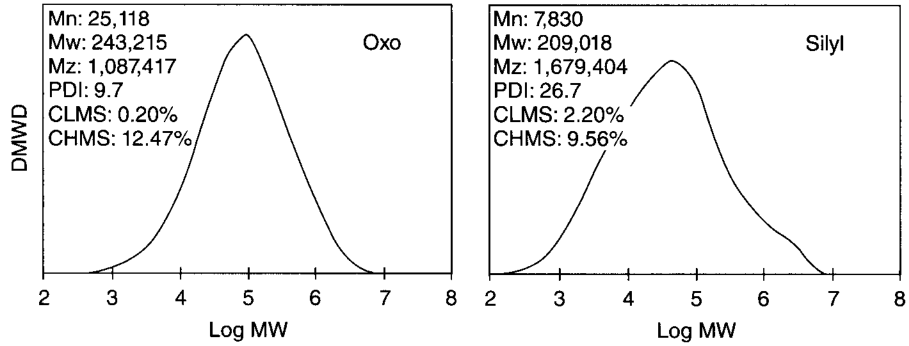

Figure 11.5 MWD of polymer made with oxo and silyl chromate catalysts.

TABLE 11.4 Size Exclusion Chromatography Data for Polymers Made with Silica-Supported Silyl Chromate Catalysts

DEALE/Cr	M_n	M_w	M_z	M_w/M_n
0	7.8×10^3	209×10^3	1.68×10^6	26.7
5	11×10^3	233×10^3	1.49×10^6	21.1
10	8.3×10^3	167×10^3	1.88×10^6	26.3

chromium oxide precursor. From the size exclusion chromatography (SEC) data (Table 11.4 for polymers made in slurry polymerizations shown in Table 11.2), it can be seen that MWD broadening occurs with or without aluminum alkyl reduction. The addition of aluminum alkyl may influence catalyst productivity and polymer molecular weight but the polymer MWD is intrinsic to the silica-supported organo silyl chromate precursor structure.

In addition to the characteristic broad MWD polymer made with chromium catalysts, the silyl chromate catalyst produces a significant amount of unsaturation in polymers compared to Ziegler–Natta catalyst produced polymers. The unsaturation is believed to be the result of a β-hydride elimination chain termination mechanism[7] (Figure 11.6).

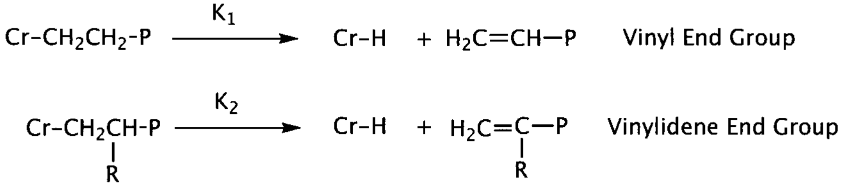

Figure 11.6 Chain termination for silyl chromate polymers.

11.6 PRODUCT PHYSICAL PROPERTY ATTRIBUTES

Film is a key application for HDPE products made with silyl chromate catalysts. Typical applications include bags and agricultural cover. Due to the broad molecular weight distribution of the polymers, these products are easy to extrude (good processability, low melt fracture) and have excellent bubble stability and very good puncture resistance and tear. The dart drop and Elmendorf tear data shown in Table 11.3 are for 1.0-mil film. Films can be drawn down to thin gauge and run at very high rates.

Large-part blow molding is another high-volume application. Silyl chromate–catalyzed HDPE products have very high ESCR, impact resistance, and swell, which are key properties in this area. Applications include 5–55-gal drums and large tanks.

Pipe (both high and low pressure) is another application for silyl chromate–catalyzed HDPE products. Good processing, melt strength, slow crack growth resistance, and hydrostatic pressure are the key property requirements of pipe products. In Table 11.3 the Pennsylvania Notched Test (PENT) value reported indicates that the slow crack growth resistance is very good for silyl chromate HDPE.

In summary the broad molecular weight distribution with the high-molecular-weight shoulder found in the MWD measurements by SEC is believed to be a key macrostructural feature of the polymer that allows high impact resistance, good bubble stability, high ESCR, high PENT values, and good melt strength.[27,28]

11.7 SILICA-SUPPORTED REDUCED SILYL CHROMATE CATALYST ADVANCEMENTS

Even though the silyl chromate catalyst has been used for HDPE production for more than 30 years, a number of improvement patent and patent applications continue to be published. A representative list of these patents and patent applications along with their corresponding abstract of inventions is provided below.

11.7.1 EP0931797 (1999) to Showa Denko

A polymerization catalyst suitable for the production of an ethylene polymer having a wide molecular weight distribution range by virtue of its high catalytic activity and hydrogen response can be prepared by using a chromium compound, an organoaluminum compound, and a carrier in a process comprising the steps of (a) bringing the chromium compound into contact with the carrier in the presence or absence of a solvent; (b) adding the organoaluminum compound to the resultant material so as to satisfy the following relationship at 60 °C or below in a mixing ratio of the organoaluminum compound to the chromium compound of 0.5:1–100:1 in terms of the ratio of aluminum atoms to chromium atoms (Al-to-Cr molar ratio):

$$\log_{10} t \leq 0.33 \log_{10} C + 0.35 \tag{11.1}$$

where t represents the time (min) necessary for the organoaluminum compound to be added to give an Al-to-Cr molar ratio of 10:1 and C represents the amount (kg) of the carrier; (c) stirring, after the addition of the organoaluminum compound, at a temperature of 0–60 °C for 0.5–4 h; and (d) removing the solvent used, the material remaining unreacted, and reaction by-products at 60 °C or below so as to satisfy the relationship

$$\log_{10} T \leq 0.23 \log_{10} C + 1.10 \tag{11.2}$$

where T represents the time (h) necessary for the removal and C represents the amount (kg) of the carrier.

11.7.2 U.S. 6,569,966 (2003) to Chemopetrol

In the method of preparation of ethylene copolymers suitable for manufacturing films or pipes for the initiation of polymerization of ethylene and 1-alkene monomer a substantially innovated catalyst system containing silyl chromate compound is used. The catalyst system is prepared by a sequential interaction of the following components: (a) a silyl chromate compound completely freed from water and oxygen prior to its contact with the porous support, (b) a support containing a suitable type and optimum concentration of hydroxyl groups, and (c) an alkylating agent, being a combination of organometal compounds of aluminum [$(RO)AlR_2$] and magnesium (R^1MgR^2), where the ratios between the components in the catalyst vary in the following ranges: content of silyl chromate on the support varies from 0.05 to 0.35% of the support weight, molar ratio between the total amount of organometals (ORG) to silyl chromate (expressed in terms of ORG/Cr) varies between 0.5 and 20, and the mutual molar ratio of organoaluminum compound and organomagnesium compound (Al–Mg) varies between 10:0.1 and 0.1:10.

11.7.3 U.S. 6,673,736 (2004) to Chevron

An improved chromate catalyst is used on a highly porous silica support having high surface area and total pore volume, and high-performance polyethylene products, such as polyethylene pipe, are produced as a result.

11.7.4 WO 2007/112919 A1 (2007) to SABIC

The invention is directed to a process for the preparation of a silyl chromate catalyst comprising the following steps: (1) depositing silyl chromate on a support at a deposition temperature of at least 55 °C during a deposition time of less than 6 h; (2) reducing the supported silyl chromate by addition of a reducing agent at a reduction temperature of at least 15 °C during a reduction time of less than 1.5 h; and (3) drying of the reduced silyl chromate at a temperature of at least 25 °C during a drying time of less than 8 h. The invention also relates to a process for the production of an ethylene homopolymer or an ethylene copolymer in the presence of the silyl chromate catalyst obtained with the process according to the invention.

ACKNOWLEDGMENTS

The author would like to thank Univation Technologies for permission to publish this chapter. Special thanks to John Moorhouse of Univation Technologies for his many helpful discussions.

REFERENCES

1. McDaniel, M. P., *Adv. Catal.*, **1985**, 33, 47.
2. Hogan, J. P., J. *Polym. Sci.*, **1970**, 8, 2637.
3. Karol, F., Karapinka, G., Wu, C., Dow, A., Johnson, R., and Carrick, W., *J. Polym. Sci: Part A1*, **1972**, 10, 2621.
4. Carrick, W. L., Karapinka, G. L., and Turbett, R. J., U.S. Patent No. 3,324,095, June 6, 1967.
5. Baker, L. M., and Carrick, W. L., U.S. Patent No. 3,324,101, June 6, 1967.
6. Baker, L. M., and Carrick, W. L., *J. Org. Chem.*, **1970**, 35, 775.
7. Carrick, W., Turbett, R., Karol, F., Karapinka, G., Fox, A., and Johnson, R., *J. Polym. Sci., Part A1*, **1972**, 10, 2609.
8. Johnson, R. N., Karol, K. J., and Pilato, L. A., U.S. Patent No. 3,642,749, Feb. 15, 1972.
9. Granchelli, F. E., and Walker, G. B., U.S. Patent No. 2,863,891, Dec. 9, 1958.
10. Bretherick, L., *Handbook of Reactive Chemical Hazards*, 2nd ed., Butterworth, London, 1979, p. 611.
11. Sax, N. Irving, *Dangerous Properties of Industrial Materials*, 6th ed., Van Nostrand Reinhold, New York, 1984, p. 506.

12. Johnson, R. N., U.S. Patent No. 3,704,287, Nov. 28, 1972.
13. Miller, A. R., U.S. Patent No. 4,003,712, Jan. 18, 1977.
14. Hamer, A. D., and Karol, F. J., U.S. Patent No. 4,065,612, Dec. 27, 1977.
15. Kral, B. V., Tsien, G. O., and Wu, C., U.S. Patent No. 5,034,364, July 23, 1991.
16. Goode, M. G., Spriggs, T. E., Levine, I. J., Wildner, W. R., and Edwards, C. L., U.S. Patent No. 5,137,994, Aug. 11, 1992.
17. Palackal, S., Hazra, S., Hamed, O., and Al-Anazi, PCT WO 2007/112919 A1, March 29, 2007.
18. Sindlelar, P., Havranek, M., Salajka, Z., Pesta, P., Stepankova, K., and Jansa, L., U.S. Patent No. 6,569,966 B1, May 27, 2003.
19. Lesnikova, N. P., Zakharova, V. A., Paukshtls, E. A., Yurchenko, E. N., Demin, E. A., and Ermakov, Y. I., *Kinetika Kataliz*, **1979**, 20(6), 1533.
20. Cann, K. J., Apecetche, M. A., Liu, B., and Terano, M., *Polymerization Performance and Characterization of Reduced Silyl Chromate and Chromium Oxide Based Olefin Polymerization Catalysis*, Presentation at Mospol 2004, International Olefin Polymerization Conference, Moscow, June 22–25, **2004**.
21. Monoi, T., Yamamoto, M., Torigoe, H., Ishihara, Y., and Inazawa, S., U.S. Patent No. 6,326,443, Dec. 4, 2001.
22. Cann, K. J., Apecetche, M. A., and Zhang, M., *Macromol. Symp.*, **2004**, 213(1), 29–36.
23. Cann, K. J., Apecetche, M. A., and Zhang, M., *Comparison of Silyl Chromate and Chromium Oxide Based Olefin Polymerization Catalysts*, Presentation at EUPOC 2003, Stereospecific Polymerization and Stereoregular Polymers Conference, Milan, June 8–12, **2003**.
24. Noshay, A., Karol, F. J., and Jorgensen, R. J., U.S. Patent No. 4,482,687, Nov. 13, 1984.
25. Wright, D. A., Engelmann, T. R., Nicholas, A., and Alexandre, F., U.S. Patent No. 6,022,933, Feb. 8, 2000.
26. Liu, B., Nakatani, H., and Terano, M., *J. Mol. Catal. A Chem.*, **2002**, 184, 387.
27. Patterson, R. E., and Pullukat, T. J., *High Performance Silica-Chrome Catalysts for High-Density Polyethylene Production*, Presentation at Specialty Silica Summit, Bangkok, Thailand, Oct. 17, **2007**.
28. Kellen, G. E., and Maeger, P. M., PCT WO 00/39173, Dec. 21, 1999.

12 Ethylene Polymerization and α-Olefin Oligomerization Using Catalysts Derived from Phosphoranes and Ni(II) or Ni(0) Precursors

SCOTT COLLINS*
Department of Polymer Science, University of Akron, Akron,
Ohio 44325-3909

12.1 INTRODUCTION

The first synthesis of branched poly(ethylene) solely from ethylene monomer using a nickel catalyst was reported in 1981 by W. Keim and co-workers,[1] 14 years prior to the disclosure of practical catalysts based on Ni–α-diimine complexes.[2] The catalyst discovered by Keim and co-workers was derived from the reaction of either $Ni(COD)_2$ or $Ni(\eta^3\text{-}C_3H_5)_2$ with the sterically hindered phosphorane **1** *in the presence of ethylene* (Eq. 12.1). In the absence of ethylene, $Ni(\eta^3\text{-}C_3H_5)_2$ and compound **1** reacted to form a π-allylnickel iminophosphonamide (PN_2) complex **2**.

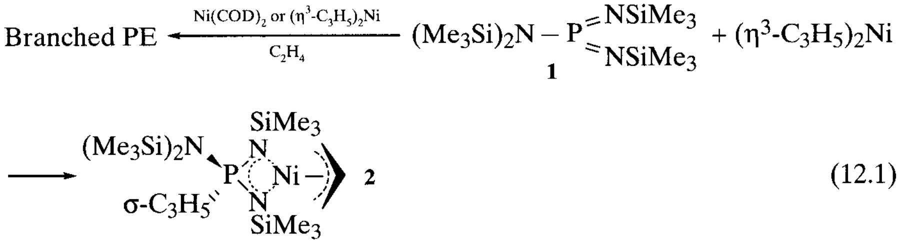

$$\text{Branched PE} \xleftarrow[C_2H_4]{Ni(COD)_2 \text{ or } (\eta^3\text{-}C_3H_5)_2Ni} (Me_3Si)_2N-P\begin{smallmatrix}=NSiMe_3\\=NSiMe_3\end{smallmatrix} + (\eta^3\text{-}C_3H_5)_2Ni$$

1

2

(12.1)

---

*Current address: Instituto Universitario de Catálisis Homogénea, Facultad de Ciencias, Universidad de Zaragoza, Pedro Cerbuna 12, 50009 Zaragozo, España

Handbook of Transition Metal Polymerization Catalysts Edited by Ray Hoff and Robert T. Mathers
Copyright © 2010 John Wiley & Sons, Inc.

Subsequent work from the group of Fink and co-workers established that the combination of $Ni(COD)_2$ and phosphoranes analogous to and including **1** were competent for the oligomerization of α-olefins at low temperature to form "chain-straightened" materials with variable amounts of Me branching.[3] Here we find the first proposal for 2,ω-olefin enchainment to explain the unique microstructure of these materials; at the time, the proposal was both revolutionary and somewhat controversial.

Scientists at Tosoh, under the direction of A. Yano, evaluated these catalysts for commercial use in ethylene polymerization. Their work is disclosed in a number of patent filings,[4] but regrettably they have not published detailed interpretations of their important work in broadly accessible journals.[5] They discovered that the activity of the Ni(0) formulations was considerably enhanced if an α-olefin was present though there was little evidence for incorporation of α-olefin through copolymerization. They were also able to show through ^{13}C nuclear magnetic resonance (NMR) spectra that the poly(ethylene) formed contained approximately equal amounts of Me branches and branches ≥6 C atoms (Hx^+) in length. Finally, they established that the polymers also contained much longer branches through solution viscosity measurements where $g' = [\eta]_{br}/[\eta]_{lin}$ values varied between 0.6 and 0.8. In subsequent work they showed that the combination of $Ni(acac)_2$ [or related Ni(II) salts], phosphorane **1**, and alkylaluminum compounds were also competent catalysts; here it was unnecessary to add α-olefin to observe enhanced activity.

Mechanistic work from the group of Fink is summarized in a German paper which appeared in 1995,[6] the same year in which Ni–α-diimine catalysts were initially disclosed in the primary literature by Brookhart and co-workers.[2] In this work, Fink and co-workers examined the reactions of phosphorane **1** with both $Ni(CH_2{=}CH_2)_3$ and $Ni(acac)_2$ and characterized the products formed by X-ray crystallography (Scheme 12.1). In the former case a stable nickelacycle,

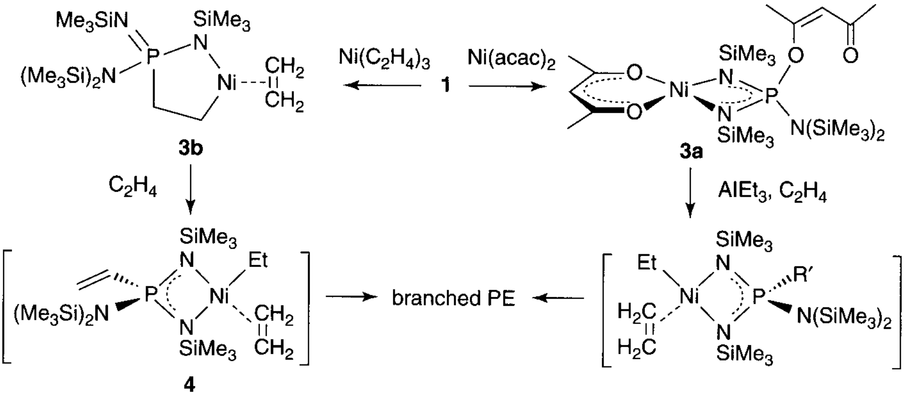

Scheme 12.1

ethylene complex **3a**, was formed, while in the latter case a (acac)NiPN$_2$ complex **3b** was produced.

The latter product could be activated for ethylene polymerization using AlEt$_3$ while the former complex was suggested to rearrange to NiPN$_2$ **4** complex in situ. This work also demonstrated that the capability of these catalysts for ethylene polymerization versus α-olefin oligomerization was a function of both phosphorane structure and Ni(0) precursor. In particular, Ni(CH$_2$=CH$_2$)$_3$ gave rise to the most active catalysts compared with other stable Ni(0) alkene precursors and increasing steric hindrance at *P*(*V*) in the phosphorane led to catalysts that were only competent for ethylene polymerization.

Aside from mention of this work at the end of a general review which appeared in 2000,[7] this area lay largely dormant for a period of about 10 years. We had been studying the ethylene polymerization chemistry of group 4 PN$_2$ complexes[8] and decided to also investigate a direct synthesis of Ni complexes of this type. We prepared a number of π-allylNiPN$_2$ complexes and also two examples of stable PN$_2$NiPh(L) complexes (**4a**: PN$_2$ = Ph$_2$P(NSiMe$_3$)$_2$; L = PPh$_3$; **4b**: PN$_2$ = (Me$_3$Si)$_2$N–[PMe(NSiMe$_3$)$_2$]; L = PPh$_3$).[9] Only the latter complexes provided branched poly(ethylene) in the presence of phosphine scavengers; in particular, the sterically hindered complex **4b** provides poly (ethylene) with basically an identical microstructure to that produced using *either* of the original Keim formulations.[9a] It is thus clear that the active catalyst in these polymerizations is a PN$_2$NiR(L) complex, although it is interesting to note that the actual structure of the PN$_2$ complex(es) formed in situ from phosphoranes and Ni(0)–olefin complexes is still unknown and these formulations are still the most active!

The polyethylene materials formed using the Keim catalyst appear somewhat unique. Because of the unusual branching distribution, density and T_m are mainly determined by the levels of Hx+ branches present (typically 15–20 Hx+ branches/1000 C atoms) in materials of sufficiently high molecular weight (MW). The MW distribution (MWD) of the materials formed in the absence of α-olefin is typically narrow (PDI 2–3 under conditions where the catalysts are more stable), and thus the properties of these materials are somewhat akin to linear low-density polyethylene (LLDPE) prepared using Insite™ constrained geometry catalyst technology[10] but without the need for 1-octene (or another α-olefin) for lowering of density. The drawbacks to these catalyst systems are their low activity/stability, particularly at higher temperature under commercially applicable conditions, and that the branching distribution is largely insensitive to changes in T or P,[4,9] in contrast to behavior observed with Ni–α-diimine catalysts.[7] Finally, the Keim catalysts are not competent for α-olefin homo- or even copolymerization with ethylene at conventional polymerization temperatures; instead α-olefins act as potent chain transfer agents and are found exclusively at chain ends.[9a]

12.2 STARTING MATERIALS

Ni(COD)$_2$ was either obtained from Strem Chemicals or prepared as described in the literature.[11] Phosphorane **1** was prepared from [(Me$_3$Si)$_2$N–P=NSiMe$_3$][12] and Me$_3$SiN$_3$ (Aldrich) as described in the literature.[13] Since compound **1** is prone to degradation on prolonged storage, it is best to isolate the intermediate adduct formed from these two starting materials[13] and convert this material to the final product as needed by heating in vacuo.

12.3 BIS(η^3-ALLYL)-NICKEL

The (η^3-C$_3$H$_5$)$_2$Ni was prepared using a modified literature method of Wilke.[14] A mixture of NiCl$_2$ (10.0g, 77.2mmol) and 150mL of ether was cooled to –80°C. Two equivalents of allylMgBr in ether (0.35M) was then added via cannula. This solution was allowed to warm to 20°C. The resulting dark solution was vacuum transferred into a new flask. Using a distillation column packed with glass helices, the ether was distilled off at 20°C and reduced pressure. The liquid residue was cooled to 0°C and residual ether removed by vacuum. The product was crystallized from hexane at –40°C to give light orange crystals. The product (1.0g, 10%) was a light orange liquid at room temperature that could be stored for several weeks below 0°C in the dark. Spectroscopic data were consistent with that reported in the literature.

12.4 (η^3-ALLYL)(σ-ALLYL-[BIS(TRIMETHYLSILYL)AMINO]-BIS(TRIMETHYLSILYLIMINO)PHOSPHORATO)-NICKEL (2)

A modified procedure, based on that previously reported by Keim, was used to synthesize (TMS$_2$N)(σ-C$_3$H$_5$)P(N-TMS)$_2$Ni(η^3-C$_3$H$_5$) **2**. Phosphorane **1** (1.00g, 2.73mmol) was dissolved into 4.5mL of hexane. In a separate flask 1eq. of (η^3-C$_3$H$_5$)$_2$Ni was dissolved into 4.5mL of hexane. The two solutions were mixed to form a deep red solution, which upon evacuation at 0.01mmHg yielded an orange powder (1.5g, 95% yield of the title compound). Deep red and cubic crystals were grown from evaporation of hexane. ^{1}H NMR (300MHz, benzene-d$_6$, 298K): major isomer: δ 0.21 (s, 18H, NSiCH$_3$), 0.52 (s, 18H, N(SiCH$_3$)$_2$), 1.49 (dd, J = 12.7Hz, 2H, anti-1/3-allyl-CH$_2$), 2.51 (ddt, J = 14.3, 6.6, 1.7Hz, 2H, P-CH$_2$), 2.81 (dd, J = 12.7Hz, 2H, syn-1/3-allyl-CH$_2$), 5.05–4.85 (tt, J = 6.7, 12.7Hz, 1H, allyl-CH), 5.05–4.85 (dt, 1H, P-allyl-cis-CH$_2$), 5.24–5.16 (dt, 1H, P-allyl-trans-CH$_2$), 6.13 (m, 1H, P-allyl-CH) minor isomer: δ 0.22 (s, 18H, NSiCH$_3$), 0.40 (s, 18H, N(SiCH$_3$)$_2$), 1.59 (dd, J = 12.7Hz, 2H, anti-1/3-allyl-CH$_2$), 2.72 (ddt, J = 14.3, 7.0, 1.3Hz, 2H, P-CH$_2$), 2.78 (dd, J = 7.0Hz, 2H, syn-1/3-allyl-CH$_2$), 5.05–4.85 (m, 1H, allyl-CH), 5.24–5.16 (dt, 1H, P-allyl-cis-CH$_2$), 5.34 (dt, 1H, P-allyl-trans-CH$_2$), 6.71 (m, 1H, P-allyl-CH). ^{31}P NMR (121.4MHz, benzene-d6, 298K): major isomer δ 34.26 (s, 1P, P), minor isomer

TABLE 12.1 Ethylene Polymerization using Ni(0) or Ni(II) Complexes and Phosphorane 1[a]

Part 1

Entry	Ni(mmol)[b]	α-olefin (mL)	AlR$_3$[c]	T (°C)	Yield (g)	Activity[d]
1	Ni(0) 2.0	1-Hx (55)	—	20	130	2.17
2	Ni(0) 2.0	1-Bu (50)	—	20	149	2.48
3	Ni(0) 2.0	1-Bu (5)	—	20	105	1.75
4	Ni(0) 1.3	1-Oc (47)	—	20	60	1.54
5	Ni(0) 2.0	4-MP (65)	—	20	120	2.00
6	Ni(0) 2.0	—	—	20	16	0.267
7	Ni(II) 1.0[e]	—	TIBAL	40	61	2.03
8	Ni(II) 2.0[e]	—	TIBAL	30	174	2.90
9	Ni(II) 2.0[e]	—	DEAC	20	100	1.67
10	Ni(II) 2.0[e]	—	TEAL	20	100	1.67
11	Ni(II) 2.0[e]	—	Et$_2$AlOEt	30	24	0.400
12[f]	Ni(II) 2.0[e]	—	TIBAL	20	4	0.0667
13[g]	Ni(II) 2.0[e]	—	TIBAL	20	21	0.350
14[h]	Ni(II) 2.0[e]	—	TIBAL	20	140	2.33
15[i]	Ni(II) 2.0[e]	—	TIBAL	20	84	1.44
16[j]	Ni(II) 2.0[e]	—	—	20	4.7	0.079

Part 2

				NMR Measurements[m]	
Entry	T_m (°C)	[η] (dL/g)[k]	g'[l]	Me	Hx$^+$
1	94.5	1.08	0.70	22	22
2	93.6	0.86	0.69	23	24
3	90.3	1.12	0.67	20	20
4	92.5	1.03	0.73	18	16
5	94.5	1.15	0.68	21	22
6	88.3	1.93	0.70	20	20
7	77.0	1.14	0.86	13	25
8	84.6	1.83	0.71	14	19
9	87.2	1.54	0.72	12	14
10	92.0	1.98	0.66	19	17
11	73.0	1.12	0.75	30	18
12	101.0	0.96	—	12	14
13	93.0	2.88	0.68	17	6
14	91.0	1.32	0.71	22	17
15	88.0	2.15	0.68	22	15
16	96.0	—[n]	—[n]	13	17

33.25 (s, 1P, P). By ^{31}P NMR integration, the ratio of major to minor isomers was 1.5:1.

12.5 REPRESENTATIVE POLYMERIZATION PROCEDURE USING Ni(COD)$_2$[4]

Into a 2-L stainless steel reactor equipped for mechanical stirring which had been thoroughly purged with N_2 there were added 500 mL of toluene, 2.0 mmol of Ni(COD)$_2$, and 2.0 mmol of phosphorane **1**. The temperature was adjusted to 20 °C and 65 mL of 1-hexene was added. The reactor was pressurized to 350 psig with ethylene for a period of 3 h. The reactor was vented and the mixture quenched by the addition of HCl in MeOH. The mixture was poured into MeOH to recover the polymer, which was dried in vacuo for 8 h to provide 130 g of polymer. Characterization data are summarized in Table 12.1, entry 1.

12.6 REPRESENTATIVE POLYMERIZATION PROCEDURE USING Ni(acac)$_2$[4]

Into a 2-L stainless steel reactor equipped for mechanical stirring which had been thoroughly purged with N_2 there were added 500 mL of toluene, 1.0 mmol of Ni(acac)$_2$, and 5.0 mmol of phosphorane **1**. Then 8.0 mmol of triisobutylaluminum (TIBAL) was added and the temperature was adjusted to 40 °C. The reactor was pressurized to 350 psig with ethylene for a period of 3 h. The reactor was vented and the mixture quenched by the addition of HCl in MeOH. The mixture was poured into MeOH to recover the polymer, which was dried in vacuo for 8 h to provide 61 g of polymer. Characterization data are summarized in Table 12.1, entry 7.

TABLE 12.1 *Continued*

[a] All experiments were performed in toluene solution for 3.0 h at 350 psig ethylene using equimolar amounts of phosphorane **1** and Ni, except where noted. For details see ref. 4.

[b] Ni(0) = Ni(COD)$_2$; Ni(II) = Ni(acac)$_2$ unless otherwise noted.

[c] An 8/1 ratio of Al:Ni(II) was used.

[d] Activity is 10^4 g PE/mol Ni × *h*.

[e] A fivefold excess of phosphorane **1** over Ni(II) was used.

[f] Ni(F_6acac)$_2$ was used.

[g] Ni(Ph_2acac)$_2$ was used.

[h] Ni(iPr_2acac)$_2$ was used.

[i] Ni(Phacac)$_2$ was used.

[j] Ni(η^3-C_3H_5)$_2$ was used.

[k] Limiting viscosity measured in dichlorobenzene st 140 °C.

[l] $g' = [\eta]_{brn}/[\eta]_{lin}$.

[m] Methyl branches (Me) and branches of 6 C or greater (Hx^+) per 1000 carbon atoms as measured by ^{13}C NMR spectroscopy.

[n] PE of M_w 105,000, PDI ~2 with ~1 LCB/1000 C atoms by SEC-MALLS. See ref. 9a.

12.7 REPRESENTATIVE POLYMERIZATION PROCEDURE USING $Ni(\eta^3\text{-}C_3H_5)_2$[9]

Into a 0.3-L Parr stainless steel reactor equipped for magnetic stirring which had been thoroughly purged with N_2 there were added 100 mL of toluene, 0.4 mmol of $Ni(C_3H_5)_2$, and 0.4 mmol of phosphorane **1** at 25 °C. The reactor was pressurized to 450 psig with ethylene for a period of 4 h. The reactor was vented and the mixture quenched by the addition of HCl in MeOH. The solvent was removed in vacuo to recover the polymer, which was dried in vacuo to provide 1.26 g of polymer. Characterization data are summarized in Table 12.1, entry 16.

REFERENCES

1. Keim, W., Appel, R., Storeck, A., Krueger, C., and Goddard, R., *Angew. Chem., Int. Ed. Engl.*, **1981**, 20, 116–118.
2. Johnson, L. K., Killian, C. M., and Brookhart, M., *J. Am. Chem. Soc.*, **1995**, 117, 6414–6415.
3. (a) Möhring, V. M., and Fink, G., *Angew. Chem. Int. Ed. Engl.*, 1985, 24, **1001**; (b) Fink, G., and Möhring, V., Process for preparing alpha-olefin polymers and oligomers, European Patent application 194456 A2, **1986**.
4. (a) Yano, A., Naito, Y., Yamada, K., and Ohtsuru, M., European Patent application W0381495, **1990**; (b) Yano, A., Yamada, S., and Yamada, K., European Patent application W0446013, **1991**.
5. Yano, A., Hasegawa, S., and Yamada, S., *Kobunshi Ronbunshu*, **2002**, 59, 377–381. See *Chem. Abstr.*, **137**, 201636.
6. Schubbe, R., Angermund, K., Fink, G., and Goddard, R., *Macromol. Chem. Phys.*, **1995**, 196, 467–478.
7. Ittel, S. D., Johnson, L. K., and Brookhart, M., *Chem. Rev.*, **2000**, 100, 1169–1203.
8. (a) Tomaszewski, R., Vollmerhaus, R., Al-Humydi, A., Wang, Q., Taylor, N. J., and Collins, S., *Can. J. Chem.*, **2006**, 84, 214–224; (b) Vollmerhaus, R., Tomaszewski, R., Shao, P., Taylor, N. J., Wiacek, K. J., Lewis, S. P., Al-Humydi, A., and Collins, S., *Organometallics*, **2005**, 24, 494–507; (c) Collins, S., Vollmerhaus, R., and Wang, Q., U. S. Patent No. 6,268,448, **2001**; (d) Vollmerhaus, R., Shao, P., Taylor, N. J., and Collins, S., *Organometallics*, **1999**, 18, 2731–2733.
9. (a) Stapleton, R. A., Chai, J., Nuanthanom, A., Flisak, Z., Nele, M., Ziegler, T., Rinaldi, P. L., Soares, J. B. P., and Collins, S., *Macromolecules*, **2007**, 40, 2993–3004; (b) Chai, J., Flisak, Z., Nele de Sousa, M., Ziegler, T., Soares, J. B., and Collins, S., *Polym. Prepr.*, **2007**, 48, 183–184; (c) Stapleton, R. L., Chai, J., Taylor, N. J., and Collins, S., *Organometallics*, **2006**, 25, 2514–2524; (d) Stapleton, R. A., Nuamthanom, A., Rinaldi, P. L., Taylor, N. J., and Collins, S., *Polym. Prepr.*, **2004**, 45, 93–94.
10. Stevens, J. C., *Stud. Surf. Sci. Catal.*, **1996**, 101, 11–20.
11. Krysan, D. J., and Mackenzie, P. B., *J. Org. Chem.*, **1990**, 55, 4229–4230.

12. Niecke, E., Oberdorfer, R., and Bajorat, V., *Synthetic Methods Organomet. Inorg. Chem.*, **1996**, 3, 36–37.
13. Niecke, E., Oberdorfer, R., and Bajorat, V., *Synthetic Methods Organomet. Inorg. Chem.*, **1996**, 3, 84–85.
14. (a) Wilke, G., U.S. Patent No. 3,432,530, **1969**; (b) Wilke, G., and Bogdanovic, B., *Angew. Chem.*, **1961**, 73, 756.

13 Late Transition Metal–Catalyzed Co- and Terpolymerization of α-Olefins with Carbon Monoxide–Polyketones: Synthesis and Modification

TIMO M. J. ANSELMENT, MANUELA ZINTL,
MARIA LEUTE, RÜDIGER NOWACK, and
BERNHARD RIEGER
WACKER-Lehrstuhl für Makromolekulare Chemie, Technische
Universität München, 85747 Garching bei München, Germany

13.1 INTRODUCTION AND HISTORICAL OVERVIEW

Polymers, especially polyolefins, have become an important class of common daily-life materials. Functionalized olefin-based polymers are an increasingly interesting field which can compliment nonpolar commodity polymers.

One of the first promising approaches for a functional group containing polymers was the copolymerization of α-olefins with carbon monoxide (OCO) for the introduction of ketone groups in the polymer backbone (Figure 13.1).[1] These so-called polyketones are of significant importance for several reasons. CO as well as simple α-olefins like ethylene or propylene are cheap and readily available basic chemicals. Initial reports concerned the radical copolymerization unfortunately only possible under harsh conditions and requiring a careful reaction control which is problematic for industrial processes.[2] Therefore active catalyst systems for insertion copolymerizations were convenient targets

---

Handbook of Transition Metal Polymerization Catalysts Edited by Ray Hoff and Robert T. Mathers
Copyright © 2010 John Wiley & Sons, Inc.

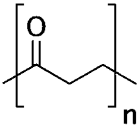

Figure 13.1 Repeating unit of a poly(1,4-ketone) copolymer from ethylene and CO.

in research. The difficulty here is the combination of metal catalysts with monomers containing polar functionalities. Unlike in traditional polyolefin synthesis, early transition metal catalysts are problematic because of their sensitivity to polar functionalities. Therefore late transition metal complexes with nickel or palladium are the most promising candidates in the latter case due to their lower oxophilicity and Lewis acidity.

In the middle of the last century, the first transition metal–catalyzed polymerization reaction for polyketones was discovered by Reppe,[1] who reported on strictly alternating oligomeric material (besides diethylketone and propionic acid) by catalysis with $K_2Ni(CN)_4$ in water in the presence of ethylene and CO. After the introduction of cocatalysts by Shryne et al.[3] ten years passed until the next breakthrough in nickel-catalyzed polyketone synthesis was reached. Klabunde et al.[4a,b] and later Cavell et al.[4c] showed that aryl–nickel(II) compounds bearing (P^O) and (N^O) chelating ligands, similar to those used for ethylene oligomerization in the Shell Higher Olefin Process (SHOP), are able to generate polyketones. The main disadvantage in most of these initial investigations was the instability of nickel complexes toward CO due to their facile reducibility. Therefore, the polymerizations had to be started in the absence of carbon monoxide, which produced blocklike polymer structures. Nickel complexes with increased CO stability, to avoid this problem, were reported by Keim[5] and Kläui,[6] using an in situ formed catalyst based on thiocarboxylic acids and an aryl–nickel(II) species.

Meanwhile, the first example of palladium-catalyzed ethylene–CO (ECO) copolymerization was reported and showed promising results. Here investigations by Gough[7] and Fenton[8] were reported in the 1960s. Unfortunately the polymers still only exhibited low molecular weights and were obtained under harsh reaction conditions. The following initial work of Sen et al.[9] led to the beginning of a new period in polyketone synthesis by the introduction of copolymerization catalysts for reactions under low pressures and ambient temperatures. Here it was shown that cationic Pd(II) complexes such as $[Pd(MeCN)_4](BF_4)_2$ in the presence of 1–3 equivalents of triphenylphosphine (TPP) were capable of copolymerizing olefins with CO. Following those results, Drent et al.[10] reported on improved catalysis by use of chelating bidentate (P^P) phosphine ligands. In particular, 1,3-bis(diphenylphosphino)propane (dppp) led to enhanced copolymerization rates and catalyst lifetimes. The employed combination of bidentate ligands with weakly coordinating anions resulted in highly active catalysts perfectly suitable for industrial application.

The introduction of polar keto groups complements the polymer properties compared to those of classic polyolefins. Besides their photodegradability,[11] it was shown that the polyketones are nontoxic and biocompatible.[12] Additionally, polyketones allow for chemical modification of the keto functionalities and therefore the synthesis of a whole family of new polyketone-based materials with further attractive properties and applications.[2a]

13.2 POLYKETONE SYNTHESIS: GENERAL CONCEPT AND MECHANISM

13.2.1 General Concept

Polyketones can be synthesized by either radical copolymerization processes or catalytic insertion polymerization. Radical polymerization, initiated by free radicals or γ-irradiation, results in nonalternating polyketones with a dependence of the CO incorporation on the employed monomer ratios.[2] The reaction requires an exact, constant, and therefore difficult adjustment of the reaction parameters to produce polymers with uniform properties.

In contrast, metal-catalyzed insertion polymerization is of industrial and academic interest due to several advantages. First this is due to the already mentioned simplified reaction conditions. Second, the polymerization by metal catalysts leads to strictly alternating uniform copolymers with higher molecular weights (an exceptional catalyst system for the nonalternating polyketone synthesis is described in Section 13.3.2). In contrast, the radical copolymerization at elevated pressures can afford α,β-dicarbonyl units by the consecutive incorporation of two CO monomers, leading to thermally unstable products. Thus, research emphasis switched to insertion polymerization reactions with palladium-based systems as the most common case.[13]

13.2.2 General Catalyst Structure

Polyketone formation is performed by a d^8-square planar cationic palladium complex bearing a bidentate chelating ligand (L^L) or two donor ligands L of the general formula (L^L)Pd(φ)R (Figure 13.2), where R represents the growing polymer chain or an alkyl group.

The remaining coordination site (φ) is occupied by (i) an anion, (ii) a solvent molecule, (iii) a carbonyl oxygen of the polymer chain (back-biting, see Section 13.2.3), or (iv) a monomer molecule. Several studies showed that the binding to this "free coordination position" (φ) strongly influences

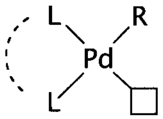

Figure 13.2 General planar catalyst structure for Pd-catalyzed CO/olefin copolymerizations.

the copolymerization. Weakly coordinating anions or solvent molecules ease the competitive coordination of monomer molecules and can accelerate the polymerization rate. This explains the experimentally observed high sensitivity of the catalytic systems, for example, to the choice of solvent and counterion.[14]

13.2.3 Copolymerization Mechanism

Chain Propagation Chain propagation is discussed separately from the other relevant steps of the reaction cycle, namely activation, chain transfer, and deactivation.

Bidentate ligands, like the aforementioned dppp, allow the exclusive copolymerization of α-olefins and CO without side reactions. Unlike these catalyst systems, the use of monodentate phosphines mainly results in the formation of oligomeric materials together with diethylketone and propionic acid. This change in reaction behavior can be explained by a close look at the structure of the catalyst. The bidentate ligand forces the two available coordination sites at the palladium center, besides the chelating ligand, into a cis configuration. The growing polymer chain is now always located cis to the "vacant" coordination site (φ) and consequently also to the coordinated monomer, which is necessary for the migratory insertion. In case of monodentate phosphine ligands, a cis/trans isomerization has to be taken in account that hinders the polymerization reaction (Figure 13.3) and lowers the rate of the polymerization. Furthermore, a trans phosphine resting state enhances the

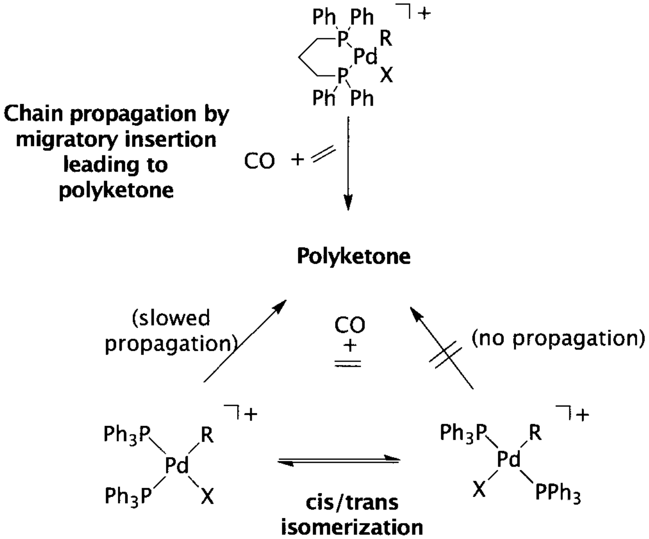

Figure 13.3 Chain propagation for Pd/phosphine catalysts; inhibition for nonchelating phosphine ligands due to cis/trans isomerization at the metal center; X = weakly coordinating anion, R = alkyl group/growing polymer chain.

probability for termination reactions.[13c,15] The importance of the coordination position for catalysts with unsymmetrical bichelating ligands will be further addressed in Section 13.3.3.

The polymerization can be performed by a variety of Pd catalysts which are either readily available or prepared in situ. Despite the huge choice of suitable palladium-based catalyst systems, chain propagation is always subject to the same restrictions. The copolymers are created by successive and alternating propagation with (a) migratory insertion of CO into a Pd–alkyl bond and (b) migratory insertion of olefin into the resulting palladium–acyl bond. In almost all cases no errors are observed and a strictly alternating copolymer is generated (exception, see Section 13.3.2). The reason is based on the characteristic behavior of the polymerization catalysts which does not allow consecutive insertion of two identical monomer units for the reasons discussed below.

1. *Kinetic and Thermodynamic Control* The migratory insertion of coordinated CO into a Pd–acyl bond (double-CO insertion) is disfavored due to thermodynamic reasons.[16] Therefore the continuation of the copolymerization process is dependent on the coordination and exchange behavior of CO and the olefin at the metal center as well as the insertion rate of the olefin into Pd-alkyl bonds.[17]

More surprising is the observation that a double-olefin insertion is typically not observed. This is interesting, as this reaction is exothermic and accordingly thermodynamically favored. For example, it is known that these catalysts dimerize ethylene to butenes in the absence of CO. The reaction rates here are even higher than in OCO copolymerizations.[18] Furthermore, in a batch experiment of a copolymerization with a low CO content only a strictly alternating polyketone is produced as long as the comonomer CO is still available. After complete consumption of CO, butenes are formed as mentioned above. This clearly shows that no thermodynamic barrier for α-olefin insertion into the Pd–alkyl bond exists in this system. One of the reasons for the alternating insertion is the stronger π acidity of CO compared to olefins. Thus, it is expected to bind more readily to the palladium center than the olefin comonomer. Therefore after Pd–alkyl bond formation by migratory insertion, CO coordinates immediately followed (due to its stronger binding ability to the metal) by an insertion into the Pd–alkyl bond. The subsequent monomer coordination is an equilibrium that depends on the concentration and binding strength of CO and the olefin. CO is the stronger ligand, but as it is not able to insert into Pd–acyl bonds, this resting state is maintained until exchange of the CO for an olefin allows the continuation of the polymerization.

2. *Back-Biting; Reversible Coordination of Functional Groups from the Growing Polymer Chain* Another important reason (identified by isolation of intermediates and by theoretic calculations) for the strictly alternating insertion process is the possibility of a strongly reversible coordination of β-carbonyl groups (or weakly with γ-carbonyl groups) from the growing polymer

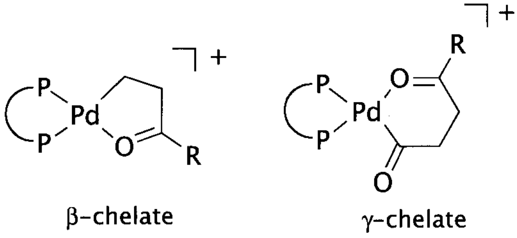

Figure 13.4 Structures of the five- and six-membered intermediate ring structures formed by back-biting of the growing polymer chain.

chain. This process is called "back-biting" and stabilizes the cationic palladium complex to form a possible catalyst resting state (Figure 13.4). For a continued polymerization the chelate has to be opened to allow further monomer addition and incorporation. In case of the five membered β-chelate this step has a high insertion barrier and only the strongly coordinating CO can open it. After the insertion of a CO molecule the chain can undergo a further back-biting process by formation of a six-membered γ-chelate with a lower stability. An olefin monomer is now able to replace the oxygen of this chelate to coordinate to the metal, yielding a new β-chelate after insertion. These chelate intermediates are not only responsible for the strictly alternating structure of the polyketone but also play a crucial role in the prevention of β-H elimination by occupation of the free coordination site. Thus the main chain termination pathway for olefin polymerization in late transition metal catalyzed reactions which often leads to oligomerization (e.g., SHOP process) is inhibited.[19]

Copolymer Chain Initiation and Termination Dicationic Pd catalyst precursors of the general formula (L^L)PdX_nA_2 (where L^L is a chelating ligand and X and A are weak coordinating solvent molecule, e.g., MeCN, and counterion, e.g., CF_3COO^-, respectively; $n = 0,2$) polymerize ethylene and CO in protic, polar solvents such as MeOH (Figure 13.5). Abstraction of a proton from methanol to form a (L^L)Pd(OMe)XA species is often proposed to take place under such conditions. A subsequent exchange of the weakly coordinating X by CO and migratory insertion of the latter into the Pd–alkoxide bond leads to Pd–acyl species (L^L)$PdC(O)OMe^+$, which is able to coordinate ethylene and thus start the chain propagation, as already described above.[13c]

On the other hand, it is reasonable to expect that under the initial conditions of copolymerization, that is, in the presence of a high excess of CO, the dicarbonyl species (L^L)$Pd(CO)_2^{2+}$ will be formed and dominate over others in the equilibrium. A weak coordinating ligand such as methanol (with respect to palladium) will referentially attack one coordinated CO than substitute it at the metal, yielding the copolymerization active (L^L)$Pd(COOMe)(CO)^+$ species. This would also explain why even small amounts of methanol are enough to start the copolymerization in "inert" solvents such as CH_2Cl_2 with an excess of CO present in the reaction[20] (Figure 13.5).

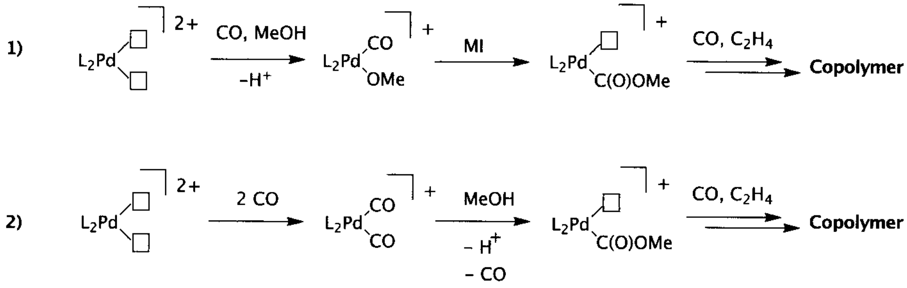

Figure 13.5 Possible initiation process in dicationic Pd(II) systems as proposed by (1) Drent and (2) Rieger.

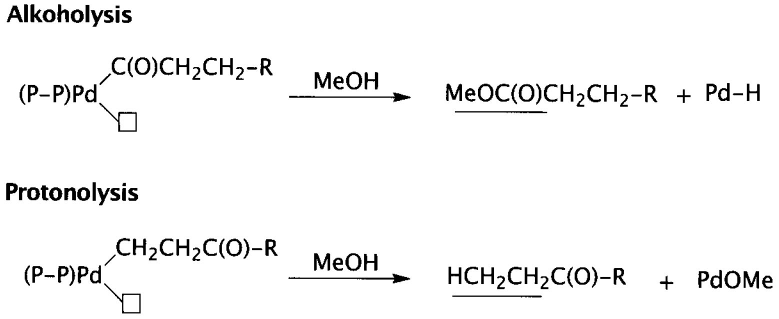
Alkoholysis

Protonolysis

Figure 13.6 Termination reaction by solvolysis, different end-group structures underlined; R = growing polymer chain.

Incorporation of methanol or other alcohols into the copolymer chain under the above conditions is unambiguously determined from end-group analysis by nuclear magnetic resonance (NMR), gas chromatography–mass spectrometry (GC–MS), and matrix–associated laser desorption ionization time-of-flight (MALDI-TOF) MS.[13c,21] One ester and one alkylketo end group are typically present in the copolymer chain, although the diester-, diketo-, and vinylketo-terminated polymers were also observed. To account for these facts, two independently operating methods of chain initiation and termination, respectively, were proposed. Thus, protolysis of the Pd–alkyl bond should result in saturated ketone end group, and the resulting Pd–alkoxide should initiate the copolymer chain with an ester end group. On the other hand, ester end groups are obtained if the termination via alcoholysis occurs on the Pd–acyl species (Figure 13.6). The thus formed Pd–H bond can undergo olefin insertion and lead to a polyketone with an alkylketo end group. β-Hydride elimination should contribute with the formation of a vinylketo end group at the terminated polymer chain and initiate polymer growth with one alkylketo end group. However, termination by β-H elimination is far from playing a significant role upon the copolymerization in MeOH, as the formation of

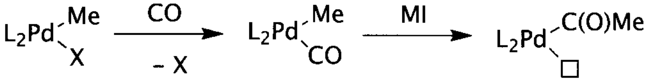

Figure 13.7 Initiation process in monocationic Pd(II) systems.

vinylketo end groups is rarely observed in such systems.[13c,15b] This is expected from the stabilization of reaction intermediates by back-biting of the growing polymer chain (Section 13.3.2).

Catalysts of the general formula (L^L)PdMeXA and their analogues, known as single-component catalysts (SCC), are able to copolymerize CO and olefins in aprotic solvents like CH_2Cl_2 without additional initiation (Figure 13.7). Exchange of the weak ligand X by CO and migratory insertion of the latter into the Pd–methyl bond starts the copolymerization. In these systems the copolymerization is terminated by β-H elimination.

The formation of an unstable Pd–hydride species upon the copolymerization in both methanol-containing and aprotic media has two consequences. On one hand, it plays a role in polymer chain initiation as discussed above. On the other hand, it is considered to be the origin for catalyst deactivation. This process can be described in simple terms as the decomposition of the PdH^+ complex to metallic Pd^0, although its detailed mechanism and possible pathways seem to be rather complex.[13d] A more comprehensive review on the activation of CO/alkene copolymerization catalysts appeared recently, and the interested reader is referred to it.[22]

Demonstrating no strong effect on the copolymerization itself, oxidative additives such as benzoquinone were reported to increase catalyst lifetimes during copolymerization in protic solvents by oxidation of intermediate species to Pd^{2+}. Protic acids with a weakly coordinating conjugated base, for example TsOH, enhance the catalyst performance as well. One of the reasons for this might be the suppression of the disproportionation $PdH^+ \rightleftarrows Pd^0 + H^+$.[15b]

As methanol or other protic cosolvents participate in both polymer chain initiation and termination, it is reasonable to expect that the molecular weight of the resulting copolymers is dependent on the amount of such cosolvent. Indeed, experiments on propylene–CO (PCO) copolymerization explicitly show that a high excess of alcohols or water added to the copolymerization media leads to relatively short copolymers. Optimization of the concentration of such activators results in nearly 10 times increased molecular weights of copolymers with practically no effect on the catalyst activity.[20]

Incorporation of the protic activator into a copolymer chain upon initiation opens a suitable pathway toward new block copolymers. Indeed, if the activator is a polymeric material with at least one OH functionality, for example, polyethylene glycol (PEG), the corresponding PEG-containing polyketone can be obtained. Branched copolymers were reported to form upon initiation of the PCO copolymerization by polyvinyl acetate (PVA).[21]

13.3 INFLUENCE OF CATALYST ON POLYMER STRUCTURE IN α-OLEFIN/CO COPOLYMERIZATION REACTIONS

13.3.1 General Concept

In this section the structural relationship between catalyst, olefin, and the resulting polyketone is discussed. For example, the insertion polymerization is strongly dependent on the steric and electronic environment at the metal center of the catalyst and can be influenced by an appropriate ligand design. Additionally α-olefins show variations in their reactivity depending on their structure (due to steric effects) as well as the strength of the olefin-metal coordination. This leads to case-specific regularities in polymers due to possible 1,2- or 2,1-insertion and stereoselectivity, mostly for steric reasons. As a result the suitable catalyst systems are limited and dependent on the nature of the olefin.

In the following sections these relationships will be explained in detail. For further information the reader is referred to the literature where several good reviews are available.[2a,13c,d,23a,b] First, in the case of ethylene/CO copolymerization, the influence on the polymer structure and polymerization rate by ligand design is discussed. The three principally possible approaches for ligand variation are explained. Second, structural peculiarities of copolymers with higher olefins are reviewed with implications for the polymer microstructure and its dependence on catalysts. In the end terpolymerization reactions as well as copolymerizations with styrene, functionalized monomers, as well as strained cyclic olefins are briefly mentioned.

13.3.2 Ethylene/CO Copolymerization and General Ligand Modification Methods

The dppp-based catalyst system of Drent[24] initiated numerous investigations concerning further improvement of similar catalysts. Three major approaches for catalyst modification and optimization by ligand design have been employed. First, the dppp ligand backbone can be easily derivatized and substituted. Second, exchange of substituents at the phosphine groups can allow the variation of steric and electronic effects in close proximity to the metal center of the complex. Additionally, in the last modification protocol, one or both phosphine functionalities are interchanged with different heteroatom donor functionalities, such as phosphite, sulfonate, or imine groups.

Each possibility or the combination of several can have positive and negative effects on catalyst activity and the structure of the copolymers.

Backbone Modification Drent et al.[15b] found that the use of chelating bidentate phosphines significantly improves the rate and selectivity of polyketone synthesis. Thus several simple α,ω-biphosphane [PPh_2–$(CH_2)_n$–PPh_2] ligands have been used to investigate possible influences of spacer length *n* on

ECO copolymerization. Indeed, it was shown that the polymerization activity and molecular weight can be affected this way. Best results were achieved with the dppp ligand system (n = 3). All other tested spacer lengths (n = 2, 4, 5) appeared to be less active. For spacers larger than five or only with one methylene group, the resulting catalysts showed no or negligible activity. From this observation a steric effect of employed ligands can be derived. The spacer bridge of the ligand controls the PPdP angle and influences the conformation of the aryl groups on the phosphine. Obviously polymerization activity is strongly dependent on the available space on the metal center. If it is (1) too small, the addition and incorporation of monomers could be prevented, or if it is (2) too large, catalyst decomposition or chain termination may be facilitated.[25]

Several methods were reported to optimize catalysts with methylene and ethene spacers.

Dppe [1,2-bis(diphenylphosphino)ethane] itself as ligand leads to catalysts which are less active than dppp. However, Bianchini et al.[26] found that catalysts derived from the ligand cyclo-tetraphos [*cis,trans,cis*-1,2,3,4-tetrakis (diphenylphosphino)–cyclobutane] show comparable activities with respect to standard dppp-based catalysts. This feature is attributed to a fixation of the ligand backbone. The chelate ring in these complexes is preferably pushed in an envelope configuration whereas in dppe-based catalysts the ligand usually assumes a twisted configuration. This affects the alignment of the aryl substituents and thus the available coordination space at the palladium center and is presumably the reason for the enhanced catalytic activity of the complexes. It could be confirmed with other rigid dppe-based ligand systems like *o*-dppbe [*o-bis*(diphenylphosphino)benzene] or *cis*-dppen [*cis-bis*(diphenylphosphino) ethylene], which also show enhanced activity but not as high as for cyclotetraphos, presumably for an electronic reason (Figure 13.8).

Other investigations concerned the optimization of dppp-based ligands. Here several substitution motives were tested and indeed a significantly increased productivity was reported for catalysts based on *meso*-$CH_2(CH_3CHPPh_2)_2$ (*m*-dppp; Figure 13.9). A change in electronic and steric properties of meso compared to racemic $CH_2(CH_3CHPPh_2)_2$ complexes is accountable for different copolymerization results.[24]

This "meso effect" can be found in different ligand systems. In general, it describes the difference of reactivities between the meso and the racemic form of complexes with respective ligands. The change in reactivity originates in an altered steric arrangement of the ligand backbone and the aryl groups on the phosphorus atom. This manipulation of the reaction space occurs at the catalyst metal center.[13d]

Modification of Substituents on Phosphine Groups The second straightforward alteration protocol concerns the variation of the substituents on the phosphine functionalities themselves. This leads to a modification of the steric environment around the metal center as well as to a modified electron donor

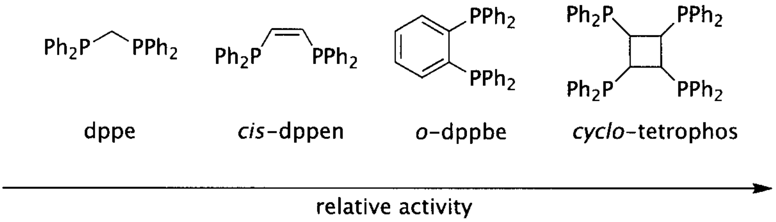

Figure 13.8 Dppe and related rigid chelating ligands in order of increasing copolymerization activity of the derived catalysts.

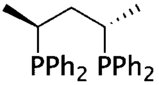

Figure 13.9 Structure of chelating *m*-dppp ligand.

behavior of the phosphines and may result in unsymmetrical catalysts with nonequivalent coordination sites (see more in Section 13.3.3).

This modification method for the dppp ligand was reported by Drent et al. with the introduction of *o*-OMe groups on the aryl ligands. The resulting catalysts show good reactivity and stability.[27]

A similar example for this principle is the exchange of the aryl substituents in bis(diarylphosphino)methane and the derived ligand bis(diarylphosphino)-*N*-methylamine. It was shown that different bulky aryl substituents (functionality present on the ortho position) can significantly increase the activity of catalysts with these ligands to that of dppp-containing catalysts. In this investigation strong dependence of activity on the activation method was observed. Possible substituents at the ortho position on the aryl ligands include, for example, OMe, Me, Et, ^{i}Pr. The enhanced activities in complexes with this nitrogen containing ligand seem to be a combination of an electronic effect by the amino functionality in the backbone and the increase of steric bulk around the coordination positions. The latter reason has the greatest influence on the catalyst activity and overcompensates the negative effect of the small backbone spacer.[28]

The dependence on the substitution position on the aryl groups was demonstrated, for example, in the case of a sulfonated ligand (see the discussion below of water-soluble polymerization catalysts). Here *o*-OMe- and *p*-OMe-substituted meta-sulfonated biphosphines were used in copolymerization reactions.[29] The drastic reduction of activity in a para-substitution pattern shows that the ortho position is crucial due to its proximity to the metal center. Another ligand system (see the discussion below of nonalternating polyketones) shows that not only the steric effect but also the proximity of the electron-rich methoxy group influences the reaction.

Other different examples by Rieger et al.[30] addressed the substitution of one aryl group with a 2-hydroxyethyl group. The resulting ligands are of interest for propylene/CO copolymerization (see below) due to differences in reactivity and selectivity between the rac and meso form. The second publication concerns biphosphines with CF$_3^-$-substituted aryl groups. These ligands are especially interesting for copolymerizations of CO with propylene or higher olefins if substituted asymmetrically.

Exchange of Phosphine Donors As already mentioned, the standard catalysts for α-olefin/CO copolymerizations are based on chelating biphosphines. Coordinating ligands with exchanged donor functionalities are also well known and usually serve specific needs of the polymerization reaction. Thus the discussion of several specific ligand and catalyst properties can be found in the respective chapters.

Besides P^P chelating biphosphines, especially ligand based on P^P(OR)$_3$, P^N, N^N, and P^OSO$_2$R, chelating motifs are among the most common reported cases.

Water-Soluble Polymerization Catalysts Several reports show that the OCO copolymerization is not limited to organic solvents. The performance of reactions in water is of great interest for environment-friendly chemical procedures and is also beneficial because of the low cost. Late transition metal complexes are of special interest in this respect as they show a greatly improved tolerance and stability in the presence of coordinating solvents.

The usual modification concept is the sulfonation of the employed ligands. This is generally carried out by a treatment in oleum neutralization with an inorganic base and isolation as the salt (usually with sodium). Different examples for this type of ligand can be found in the literature (see Figure 13.12 below).[29,31]

It was shown that ligands based on sulfonated dppp are active in OCO co- and terpolymerization in pure water. The results are in principle similar compared to reactions with dppp-based catalysts. Unfortunately lower polymerization rates were observed in aqueous medium, presumably the result of a stronger coordination of water to the Pd center and an electron-withdrawing effect of the sulfonate groups. In addition, the solubility of nonpolar olefins (especially propylene and higher olefins) is significantly decreased in water, which lowers the available monomer concentration.[31a] Some modified water-soluble catalysts can even reach activities close to the dppp system in MeOH, although the molecular weights of the resulting polymers are reduced.[29,31b]

Nonalternating Polyketones Because of the symmetric nature of ethylene no structural differences originate from the regioselectivity (1,2 or 3,4) of the insertion reaction in polyketone synthesis. However, as mentioned above, the lack of double-ethylene incorporation is remarkable since palladium compounds are known in the homopolymerization of ethylene.[32]

Drent et al.[33] reported on the use of new (P^O)-chelating ligands bearing ortho-sulfonate moieties (Figure 13.10) and palladium acetate for the in situ–catalyzed copolymerization of ethylene and carbon monoxide. Detailed

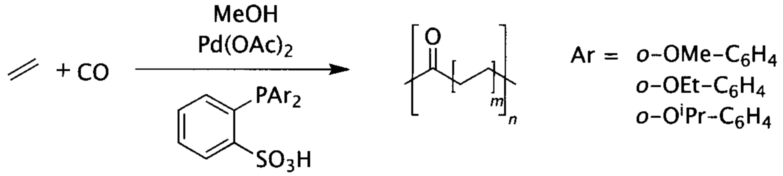

Figure 13.10 Reaction scheme for nonalternating ECO copolymerization with in situ–created catalysts based on phosphine–sulfonic acids.

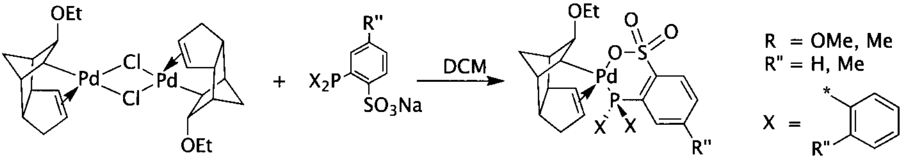

Figure 13.11 Neutral single-component catalyst system for nonalternating ECO copolymerization based on phosphine–sulfonate ligands.

polymer analysis by ^{13}C NMR spectroscopy also shows, beside the normal single ethylene insertion, signals for double-, triple-, and even quadruple-ethylene insertion. This report is therefore the first case of a nonalternating polyketone formed by transition metal catalysis. The in situ polymerizations could be optimized to nearly 20 mol % extra ethylene insertions by modification of the phosphine moiety with substituents leading to greater steric hindrance.[33]

Rieger et al.[34] further improved this system with the synthesis of a readily available single-component catalyst (Figure 13.11). The resulting polymers show an increased amount of extra ethylene insertions compared to in situ–formed catalysts of up to 30 mol %. These nonalternating polyketones show a reduced melting transition (from 260/270 °C to 220 °C) compared to their alternating analogues, which indicates a significant decrease of polymer chain interactions.

The reaction mechanism observed by Drent[35] is supported by density functional theory (DFT) calculations. The neutral (P^O)Pd complexes were compared to the cationic dppp–Pd system. The calculations indicate the main differences in the electron density at the metal center combined with a changed steric hindrance of the ligand. Due to these reasons, back-biting by the oxygen to form intermediate metallacycles is hindered. In addition, the higher electron density at the metal center affords stronger Pd–CO interactions and especially stronger Pd–ethylene bonds. The first effect, respectively, allows a decarbonylation process which is completely hindered in the strictly alternating polyketone formation. The second effect increases the strength of the ethylene binding to the Pd center. This favors additional ethylene insertions into the polymer chain. Control of the monomer concentration is crucial to the copolymerization, as the ratio of ethylene to CO greatly influences the coordination equilibrium at the metal center and hence the ratio of monomer insertions (Figure 13.12).

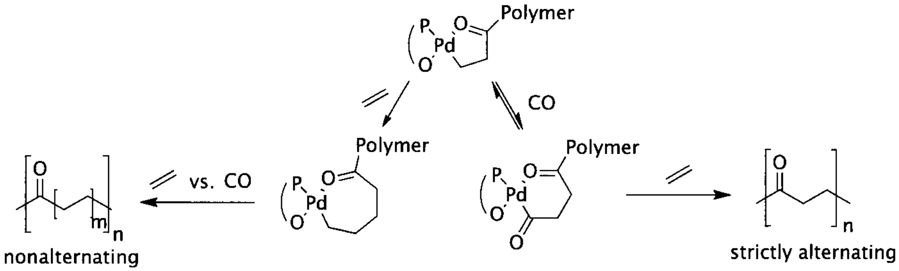

Figure 13.12 Mechanistic suggestions for formation of nonalternating or alternating polyketone segments.

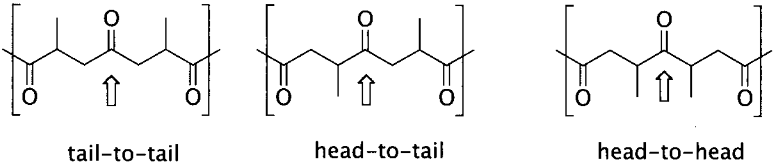

Figure 13.13 Possible EPO copolymer backbone structural motives; reference carbonyl group marked with the arrow.

13.3.3 Propylene/CO Copolymerizations

Copolymer Structure The exchange of ethylene as monomer against higher α-olefins, usually propylene, leads to new copolymer structures. The introduction of side groups on the polymer backbone changes the crystallization behavior and the solubility of the polymers. This can lead to changed mechanical and improved processing properties of the polymer.

The polymer architecture is dependent on the incorporation of the asymmetrically substituted α-olefin. The insertion rates are dependent on the catalyst structure as the orientation of the associated olefin can be disfavored by steric repulsion. Usually this leads to a preferred 1,2-insertion over 2,1-insertion.

These two possibilities can be recognized by several structural motives in the polymer backbone. Considering two consecutive insertions and the orientation of the alkyl groups to the central carbonyl group, head-to-tail, head-to-head, and tail-to-tail structures can be observed (Figure 13.13). The orientation is dependent on the catalyst. Investigations by ^{13}C NMR spectroscopy are possible to determine the degree of regioregularity and regioirregularity, that is, the degree of variation from regular, uniform monomer incorporation. This property is of significant influence for the polymer microstructure. Deviations from a strictly regular incorporation of monomer lead to a changed polymer chain arrangement, as evidenced, for example, by a different melting behavior and crystallinity.

As explained above, the polymer microstructure is dependent on the orientation of the incorporated olefin monomer, which can be influenced by the steric and electronic environment of the metal center, mainly determined by the ligand structure. This implies that a tuning of the reaction and polymer structure (regularity) is possible by ligand design.

Furthermore, in a highly regioregular polymer, an asymmetric chiral configuration of the complex, or induced enantiofacial selectivity through the coordinated polymer chain can control the steric orientation of the coordination of the next olefin monomer to the metal complex. Thus isotactic, syndiotactic, or atactic copolymers, which additionally can be optically active, are obtained depending on the above mentioned parameters (Figure 13.14).

(i) *Control of Regioregularity* Investigations on the regioselectivity in PCO copolymerizations started from the first report with dppp-based catalysts. An exchange of the phosphine substituents can lead to complete regioselectivity with the isopropyl-substituted dipp [1,3-propanediylbis(diisopropylphosphine)] catalyst system.[36] Unfortunately the increase of head-to-tail regioregularity is accompanied by a decrease of obtained molecular weights for the copolymers. Additional investigations showed that substitution with ethyl groups on the phosphines gives almost complete regioregularity at high catalyst activities and polymers with a high molecular weight were obtained. From these investigations it seems that the substitution with alkyl groups instead of aryl groups leads to increased regioregularity, presumably due to increased basicity of the phosphines. Additionally the steric hindrance at the metal center is of great importance to the polymer regularity but can lead to reduced catalyst activities as well as reducing the molecular weight of resulting polymers.[37] Several chiral ligands were also investigated principally regarding

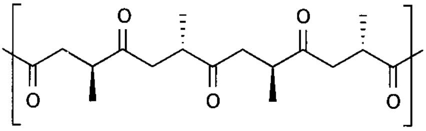

isotactic

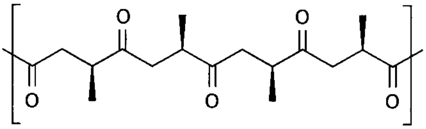

syndiotactic

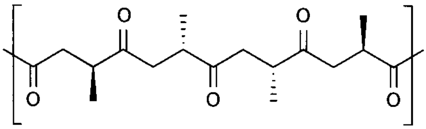

atactic

Figure 13.14 Tacticity of PCO copolymer sections due to stereoregularity.

the stereoregularity (see below) of produced copolymers but also for their degree of regularity.[38] DIOP, *m*-dppp, or BINAP showed a head-to-tail enchainment of 66–78%. Other chiral ligands will be discussed in the next section (Figure 13.15).

(ii) *Control of Stereoregularity* The stereoregularity of copolymers depends on the differentiation of the monomer incorporation as a result of the enantiofacial selectivity of the catalysts. As already mentioned, this can affect the tacticity of the polymers, which can be assessed by a close inspection of the ^{13}C NMR polymer spectra. Signals of different pentades can be recognized and assigned. In isotactic polymers the enantioselectivity is also important as the polymer is chiral and can be either the RRRR- or SSSS-enantiomer. The absolute configuration of the asymmetric backbone carbon atoms could be determined by comparison of polymer circular dichroism (CD) spectra with small chiral ketones or NMR investigation with an optically active NMR shift reagent.[37,39]

Copolymerizations with propane and higher olefins can lead to an additional interesting structural feature of polyketones. Depending on the employed catalyst, the solvent, and the reaction conditions, either the linear or spiroketal structure can be observed (Figure 13.16). The equilibrium of the keto and ketal structure depends on the energetic difference in both forms, which is fairly small in polyketones of higher olefins (the stability of the spiroketal form increases with the length of the α-olefin). Investigation of the dynamic behavior was carried out by NMR spectroscopy in the solution and in solid state.[39] The spiroketal form can also be converted into the linear poly(1,4-ketone) at higher temperatures or by treatment with 1,1,1,3,3,3,-hexafluoro-2-propanol and subsequent precipitation.

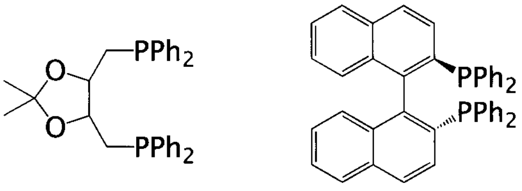

DIOP **BINAP**

Figure 13.15 Structures of chiral chelating DIOP and BINAP ligands.

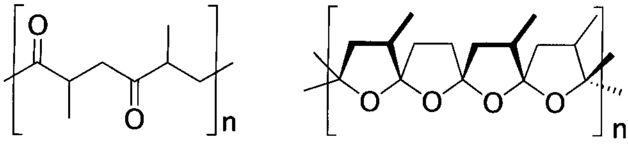

linear poly(1,4-ketone) spiroketal structure

Figure 13.16 Structure of linear and spiroketal forms for poly(1,4-ketone)s.

(R,S)-BINAPHOS and Josiphos-Based Catalysts as Example for Chiral Propylene/CO Copolymerizations A detailed investigation was carried out by Nozaki and Hiyama[40] for the (*R*,*S*)-BINAPHOS ligand system. Following the observations with other chiral ligands to produce isotactic polyketones, the well-known BINAPHOS ligand was tested in the copolymerizations. Pd complexes with this ligand proved to be highly active for CO copolymerization with both propene and higher α-olefins.

Using (*R*,*S*)-BINAPHOS (Figure 13.17), high-molecular-weight copolymers of propylene and CO were prepared with an extremely high molar optical rotation. The simplicity of the ^{13}C NMR spectrum and the molar optical rotation indicate a polymer with a high degree of regio- and stereoselectivity. Only head-to-tail units are present in this isotactic polymer. The mechanism of the polymerization was analyzed in detail to investigate the reasons for this selectivity.[40b]

In this respect, different complexes with ^{13}C-labeled groups were synthesized to study the relevant steps during the copolymerization reaction. First it was shown that in the catalyst precursors as well as in reaction intermediates the alkyl groups are preferably directed into the position trans to that of the coordinated phosphine. Model reactions further point to a cis–trans isomerization process occurring during the polymerization, leading to small amounts of the isomer with a cis arrangement of the phosphine and alkyl group. Subsequent CO coordination and migration of the alkyl group into the trans position respective to the phosphine again leads to the more stable species. The following migration is facilitated and the more stable trans alkyl/acyl complex (with respect to the coordinated phosphine) is obtained. Regarding the stereoselectivity in this system, it was shown that cleavage of the cyclic five-membered model substance, originating by back-biting following a propylene insertion into an acetyl bond, with CO in methanol results in the (*S*)-3-methyl-4-oxo-pentanoate ketoester with a high enantiomeric excess (ee) of 95%. Transferred to the polymerization, this shows that the SSSS-stereoisomer is produced with a high enantioselectivity.[40b]

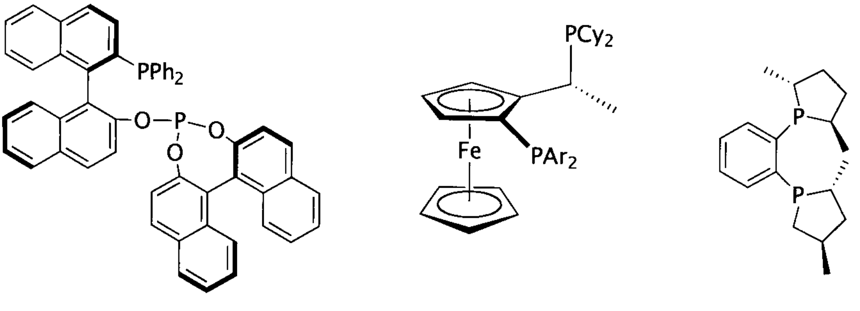

(R,S)-BINAPHOS Josiphos (R,R)-Me-DUPHOS

Figure 13.17 Three chiral examples for OCO copolymerization catalysts: (*R*,*S*)-BINAPHOS, Josiphos, and (*R*,*R*)-Me-DUPHOS.

This study elaborately addresses the interesting points in the copolymerization by catalysts with asymmetric ligands. (i) The asymmetric structure leads to nonequivalent coordination sites which favor or disfavor the stability of coordinated groups. (ii) Additionally enantiofacial selectivity is introduced by the chiral ligand structure, possibly enhanced by the stereochemistry of the conjugated growing polymer chain.[40b] The latter case was shown to be of influence by stereoselective copolymerization with achiral ligands.[41]

In general, the asymmetric copolymerization shows interesting results. First, chain termination by β-hydride elimination seems to be retarded through the weakening of the position trans to the phosphite and leads to high molecular weight polymers. Second, the usage of similar chiral ligands, especially a biphosphine, a biphosphite, as well as the (*R*,*R*)-BINAPHOS diastereomer, surprisingly showed no copolymerization. This is due to the assumption that either the asymmetric structure with two nonequivalent coordination sites is required or in the latter case stable cationic complexes are even not formed due to steric repulsion of the binaphtyl groups.[40b]

Another report on chiral ligands for the synthesis of highly active copolymerization catalysts considers the Josiphos biphosphine ligand system (Figure 13.17). The basic ligand structure here is an asymmetric biphosphine with a substituted ferrocenyl unit in the backbone. A key requirement for highly active copolymerization catalysts of this type is the asymmetric substitution on both phosphines. Two cyclohexyl groups on the phosphine at the 2-position of the ethylene group on the ferrocene and two bis-*m*-CF_3-substituted aryl groups on the second phosphine were reported to achieve the highest activity. This combination seems to induce the optimized steric requirement for regio- and stereoselective propene incorporation. Furthermore the electronic environment by (i) the donating cyclohexyl groups and (ii) the electron-withdrawing CF_3-modified aryl groups compliment the substitution motif on the ferrocene unit to achieve the ideal environment for stereoselective chain propagation (see above). An exchange of the substituents drastically lowers the productivity of the catalysts.[42]

13.3.4 Copolymerizations of CO with Higher α-Olefins

Higher α-olefins such as 1-heptene or 1-hexene can be copolymerized with CO, however they show a significantly lowered reactivity compared to propylene or ethylene. Two main reasons for this effect have been proposed. First, as a side reaction the 1-alkenes can be isomerized to olefins with internal double bonds which are, under these conditions, not polymerizable. Second, due to the steric hindrance of the alkyl chain, the double bond coordinates more slowly to the metal center as well as having a reduced rate of insertion into the Pd–acyl bonds during the copolymerization reaction.[43] To circumvent this problem, the copolymerization reaction can be carried out in liquid monomer to increase the reactivity due to a higher available concentration of the olefin.[30a]

A report by Sen et al.[39] concerns the formation of isotactic poly(1,5-ketone) oligomers in a copolymerization of CO and *cis*-2-butene. This unusual and unexpected observation was explained by a migration of the palladium to the adjacent methyl group by β-H abstraction and isomerization.

13.3.5 Terpolymerization Reaction of Ethylene, Propylene, and CO

The ECO copolymerization affords highly crystalline polymeric materials with high melting points close to decomposition temperature and which are insoluble in common organic solvents. To overcome this problem, a terpolymerization of ethylene and CO with higher α-olefins such as propylene, was studied. Incorporation of the higher olefin comonomer creates side chains in the polymer backbone which hinder the close arrangement of the polyketone chains. This decreases the degree of crystallinity, lowers the melting point and increases the solubility of the polymers. Depending on the catalysts and the polymerization conditions the polymer properties can be controlled in a wide range.*

Terpolymerization in a normal batch experiment with CO and a mixture of propylene and ethylene leads to a range of polymer properties which depend strongly on the ethylene/propylene content. If this ratio is below approximately 50%, thermoplastic elastomers are obtained. A further increase leads to the formation of crystalline thermoplastic terpolymers with a loss of elasticity. A huge difference is observed in the solubility of these polymers. Thermoplastic elastomers are soluble in common organic solvents and crystalline polymers are mainly insoluble. The polymerization can lead to a heterogeneous polymer blend which was shown by a fractionation of a terpolymerization product where three different polymer fractions with different ethylene/propylene content could be obtained. These properties are the result of the different reactivities for ethylene and propylene, which leads to a gradient copolymer in which the amount of propylene/CO units increases with the reaction time and the decrease of ethylene concentration.[44,45]

As an alternative to these batch experiments pulse feed polymerization (PFP) was developed. In this process ethylene is added discontinuously to an ethylene/propylene/CO terpolymerization reactor at defined time intervals. Considering the faster reaction of ethylene compared to propylene, this technique allows control of the ethylene incorporation in the terpolymers with ethylene/CO-rich parts. With this polymerization process terpolymers with up to 70% ethylene/CO content can be obtained which are still highly soluble in organic solvents, in contrast to previous reported terpolymers with equally high ethylene/CO contents. Furthermore the terpolymers are created homogenously and no different polymer fractions could be isolated by fractionation experiments. The resulting terpolymers show a stress–stain behavior similar to cross-linked natural rubber.[46]

---

*In general the terpolymers can exhibit properties of the thermoplastic behavior (similar to vulcanized natural rubber) up to crystalline thermoplastic properties of a pure ECO copolymer with its high melting point.

13.4 OTHER OLEFINS FOR COPOLYMERIZATION WITH CO

13.4.1 Copolymerization of CO with Miscellaneous Olefins

Besides terminal alkenes, molecules containing strained double bonds, for example norbornene and its derivatives, are known to copolymerize with CO in the presence of Pd catalysts, thus enlarging the family of polyketones. These olefins appeared to be especially suitable as substrates to provide insights into the mechanistic details of copolymerization. Their great advantage in late transition metal–catalyzed polymerization is the nonsusceptibility toward β-hydride elimination, which renders the inserted products less labile and allows the isolation of various copolymerization intermediates.[9a,47]

Copolymerization of CO with norbornene and its derivatives, as well as with other strained olefins such as dicyclopentadiene, is in the scope of several other reviews and the interested reader is referred to one of them.[13d] Here we just note some peculiarities. One of those is the increased regio- and stereoregularity of such copolymers induced by the steric effects of the olefin and the growing polymer chain. Another feature concerns the nature of the ligand employed in the catalyst. Thus, besides the mono- and biphosphine ligands, the P^N and N^N chelating molecules such as 2,2′-bipyridyl in the N^N chelating case can give efficient Pd-based catalytic systems. Furthermore, the copolymers of CO and strained olefins are often obtained in polyspiroketal form.

The above is also true for the copolymerization of CO and styrene or its derivatives. The details on this process can again be found in numerous reviews.[13d]

13.4.2 Functional Group Containing α-Olefins for Copolymerization with CO

Introduction of polar functional groups into the polymer side chain by utilizing the appropriately derivatized alkenes for the copolymerization with CO is a major route toward new tailor-made polymeric materials. In this respect, Pd catalysts which are able to tolerate different functional groups and catalyze the CO/olefin copolymerization itself are expected to be the most promising. However, despite this expectation, examples of copolymerizations with functionalized olefins are not that numerous. Competitive coordination of olefins via their functional group instead of the double bond (thus blocking the vacant site on the metal) can still be problematic in such reactions, slowing down or even preventing the copolymerization. Conditions of the polymerization, the nature of the ligands, and applied additives seem to be decisive in overcoming these problems. Olefins bearing hydroxy as well as carboxy functionalities separated from the double bond by an aliphatic spacer, for example, $H_2C{=}CH{-}(CH_2)_xCH_2OH$ ($x = 1, 2, 3, 8$) and $H_2C{=}CH{-}(CH_2)_yCOOH$ ($y = 1, 2, 4, 8$), copolymerize with CO when complexes with bulky ligands such as $[Pd((R,R)\text{-Me-DUPHOS})(MeCN)_2](BF_4)_2$ [ligand structure of (*R*,*R*)-Me-DUPHOS; see

Figure 13.17] are applied.[48] Presumably due to a decrease of the free space around the metal center, coordination of monomers to the metal center with their functional groups instead of the olefin is weakened or prohibited.

Similarly, a Pd system employing the (*R*,*R*)-Me-DUPHOS ligand can additionally catalyze the copolymerization of olefins with carbamate and amide groups.[49] However, additives such as formic acid and 1,4-naphthoquinone are essential for CO copolymerization with olefins bearing epoxide groups. Interestingly, this sensitive functionality remained unaffected during the copolymerization; that is, no side reactions, such as epoxide rearrangement or ring opening, could be detected, indicating very high chemoselectivity of the applied catalytic system. Monomers where the epoxide unit and the double bond are separated by a spacer of one to five methylene units, as well as 4-vinyl-1,2-epoxycyclohexane and allylglycidyl ether, have been copolymerized. However, for the monomer with the double bond vicinal to the epoxy group, as in the case of 1,2-epoxybut-3-ene, no copolymerization was observed.[50]

Controlled introduction of the functional groups into the polymer side chain allows the purpose-directed variation of the physical and chemical properties of polyketones. This was demonstrated in the terpolymerization of carbon monoxide with a benzo-15-crown-5 functionalized 1-alkene [4′-(undec-10-enylcarboxylate)benzo-15-crown-5] and various α-olefins (Figure 13.18).[51] Material properties such as polarity and glass transition temperatures of the formed terpolymers are adjustable by varying the nature of applied α-olefins as well as the reaction conditions, for example, comonomer ratios and amount of catalyst activator. Encapsulation of these terpolymers into a macroporous polyethylene support results in elastic and mechanically stable ion-transporting membranes, the performance of which is controlled by the terpolymer characteristics, as tested, for example, with $NaClO_4$. That is, the glass transition temperature of the material has to be sufficiently low to enable diffusion of the analyte through the membrane and to make the addition of a plasticizer

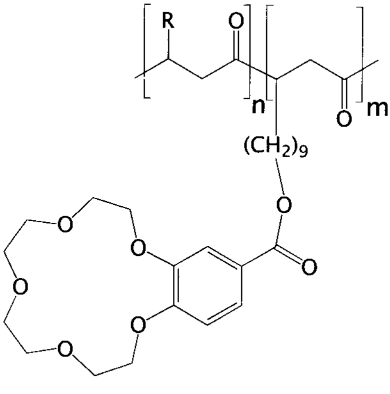

R = CH_3, $(CH_2)_xCH_3$
x = 3, 9, 15

Figure 13.18 Benzo-15-crown-5-functionalized terpolymers for application in ion-selective membranes.

unnecessary. For membrane applications, the α-olefin side chains in the terpolymer should introduce enough hydrophobicity to prevent fouling of the membrane, whereas the CO group offers a significant polarity to assist ions in crossing the water–membrane boundary.[52]

Other functionalized polyketone structures containing monosaccharide fragments in order to enhance the biocompatibility of the polymers have been reported by Rieger et al.[53] The co- and terpolymerization of glycosylated olefins with CO and propylene proceeds smoothly with the common [(dppp) Pd(NCCH$_3$)$_2$](BF$_4$)$_2$ catalyst and the protecting acetyl groups in the resulting polymers can be easily cleaved afterward. The same approach is also suitable for the introduction of vitamins, amino acids, dipeptides, and steroids into the polyketone backbone.[54] The integration of these bioactive molecules is of particular interest from the view of the medical sector. Standard in vitro tests on the glycosylated polymers show no cytotoxicity, and these polymeric materials support the growth of living cells. In vivo tests on tyrosine-functionalized polyketone also show its biocompatibility to urothelial cells.

In general, functionalized polyketones can find application in various fields of materials science. In addition to the above examples, attention to polyketone-based side-chain liquid-crystal polymers (SCLCPs) should be drawn.[55] Thus, 1-alkenes bearing a mesogenic group such as biphenyl or azobenzene (Figure 13.19) can be copolymerized with carbon monoxide resulting in mesomorphic polymers, which can be easily purpose adjusted. This can be fulfilled by changing the structure of the mesogenic 1-alkene monomer, the degree of copolymerization, or by terpolymerization with α-olefins such as 1-hexene. Glass transition in copolymers is observed only if the spacer length is longer than six methylene units. Moreover, a further increase of the spacer results in a decreased isotropization temperature. Typically, the copolymers incorporating methoxybiphenyl exhibit a smectic E mesophase, whereas for cyanobiphenyl- or methoxyazobenzene-based polyketones a nematic mesophase and, as a result, lower glass transition temperature were observed. Upon terpolymerization with 1-hexene, both the isotropization temperatures and the entropy changes associated with isotropization decrease with increasing 1-hexene content, but all these polymers exhibited a smectic E mesophase up to a 1-hexene content of 0.25.

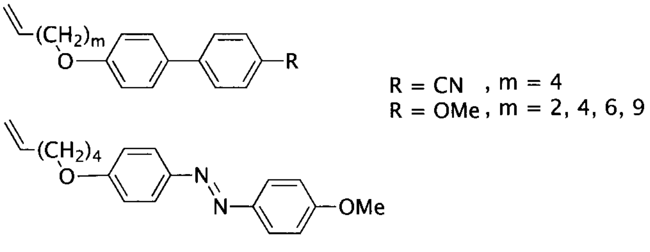

Figure 13.19 Mesogenic monomers for production of SCLCPs by copolymerization with CO.

The use of chiral catalytic palladium complexes leads to SCLCPs with isotactic and syndiotactic backbones. Syndiotactic polymers exhibited liquid-crystalline phases, whereas isotactic polymers were nonmesomorphic. The difference may be attributed either to the different orientation of the mesogenic group or to the changed conformation of the backbone itself.[13d]

Copolymerization of CO with the olefinic monomers suitable for further derivatization is also an attractive route toward functional polymers with tailor-made properties. For example, the use of allenes as comonomers is expected to lead to a high degree of unsaturation in the backbone, which would enable further modifications of the polymer, for example, as in the case of caoutchoucs (Figure 13.20). Indeed, copolymers formed from CO and 3,3-dimethyl allene (DMA) in the presence of the catalyst $[Pd(PPh_3)_2(CH_3CN)_2](BF_4)_2$ are highly unsaturated polyketones. Introduction of steric hindrance at the cumulated double bonds, as in the case of 1,1,3,3-tetramethyl allene (TMA), however, results in much lower copolymerization activity of the allene, as is reflected in the copolymer yields.[56] Interestingly, only cationic palladium complexes with monodentate phosphines lead to fast successive insertions of allene and carbon monoxide at the catalyst center. The use of bidentate phosphines, like dppp or (*R*,*R*)-Me-DUPHOS, results in poor catalytic activity for the allene CO copolymerization. This effect is associated with the chelate η^3-allyl coordination of allene or growing chain of the copolymer to the palladium. Thus, coordination of the subsequent monomer molecule (e.g., CO) would require either a η^3-to-η^1 isomerization of the allylic ligand or the dissociation of one of the coordinated phosphine groups. Due to the chelating effect, the latter would be significantly more difficult in the case of the bidentate phosphines. Pd–N bonds tend to be weaker than Pd–P bonds; therefore the corresponding insertion proceeds more readily in complexes with bidentate nitrogen ligands. For example, the rigid (N^N) chelating ligand bis(*p*-anisylimino)acenaphthene (*p*-An-BIAN) has been used successfully for the copolymerization of CO with DMA, TMA, and propadiene. By stepwise insertion of the corresponding monomer and CO, the copolymerization could be studied in more detail, and the results indeed show the dissociation of one of the N-donors prior to allene insertion, as illustrated in Figure 13.20.[57] As for the postpolymerization modification of these macromolecular materials, only hydrogenation of the DMA copolymers resulting in isopropyl-substituted backbone structures was reported up to date.

Other examples of chemically modifiable polyketones are those prepared from CO and allylphenoles or allylphenol ethers. The monomers with ortho

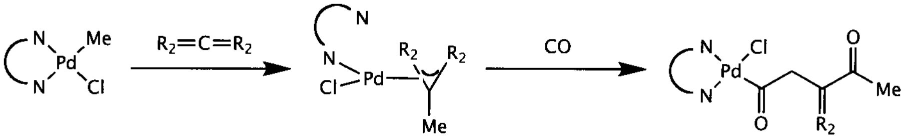

Figure 13.20 Copolymerization of allenes with CO.

substitution pattern are the most active in the copolymerization and are also suitable for the terpolymerization with propene and higher alkenes.[58] The modification of polymers containing free phenolic hydroxyl groups was shown to proceed easily, for example, by reaction with chlorides of carboxylic acids, thus confirming the suitability of such polyketones for the grafting-to or cross-linking processes.

All the above-considered examples of CO copolymerization with substituted olefins explicitly emphasize the importance of separation of the functional group from the polymerization-active double bond. The closer the polar functionality to the double bond, the stronger the negative influence on the copolymerization activity of the olefin. Specifically electron-withdrawing groups such as fluorinated aliphatic chains or aromatic rings hinder the copolymerization, presumably by reducing the ability of the double bond to coordinate to the metal center. The effect of fluorine atoms follows from the experiments on CO copolymerization with different fluoro-substituted allylbenzenes in the presence of $[(R,R\text{-Me-DUPHOS})Pd(Me)(CH_3CN)]BF_4$ catalyst. That is, an increase of fluorine atoms on the benzene ring results in lower polymerization yields.[59]

Another reason for low copolymerization activity of olefins featuring the vicinal arrangement of the double bond and polar functional group is the formation of different chelated structures with the catalyst. Upon 1,2-insertion of the functionalized olefin into, for example, a Pd–acyl bond, a stabilized five-membered ring can be formed due to the binding (back biting) of the olefin substituent to the Pd center. The 2,1-insertion of the olefin into the Pd–acyl species should lead to the less stabilized four-membered ring upon substituent back-biting. However, the electronic effects of the substituent placed at the β′-carbon in this case can lower the nucleophilicity of the α-carbon atom connected to Pd and thus retard the next CO insertion into the Pd–C bond. After the CO insertion a stabilized five-membered chelate via the polar functional group of the olefin unit can again be formed.

In case of fluorinated olefins $CH_2{=}CH{-}(CH_2)_m(C_nF_{2n+1})$, the electron-withdrawing effect of F atoms plays the main role in inhibiting the copolymerization with CO. Decrease of m leads to lower copolymer yields, and no polymer was formed with $m = 0$ in the presence of the Pd-(*R*,*S*)-BINAPHOS complex.[60] The nature of the chelating ligand in the catalytic system and the polymerization conditions, for example CO pressure, were found to strongly affect the copolymerization of allyl-perfluoroalkanes ($m = 1$). The best results in copolymerization of the latter were obtained applying Pd-(*R*,*S*)-BINAPHOS catalyst under 8 MPa of CO in 84 h.[60]

Copolymerization of functionalized olefins with CO seems to have gained attention, as new reports concerning (P^O) chelated phosphine-sulphonate complexes can catalyze interesting reactions such as the vinyl acetate/CO copolymerization (Figure 13.21). These monomers are usually nonpolymerizable with conventional palladium catalysts (e.g., dppp based) but copolymers with molecular weight of around 40.000 $g\,mol^{-1}$ were obtained with these new phosphine-sulphonate catalysts.[61]

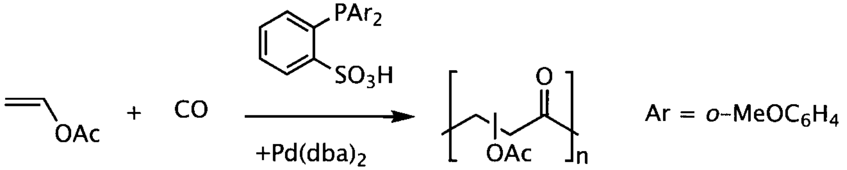

Figure 13.21 (P^O) Chelating phosphine-sulfonate ligands employed in Pd-catalyzed copolymerization of CO and vinyl acetate.

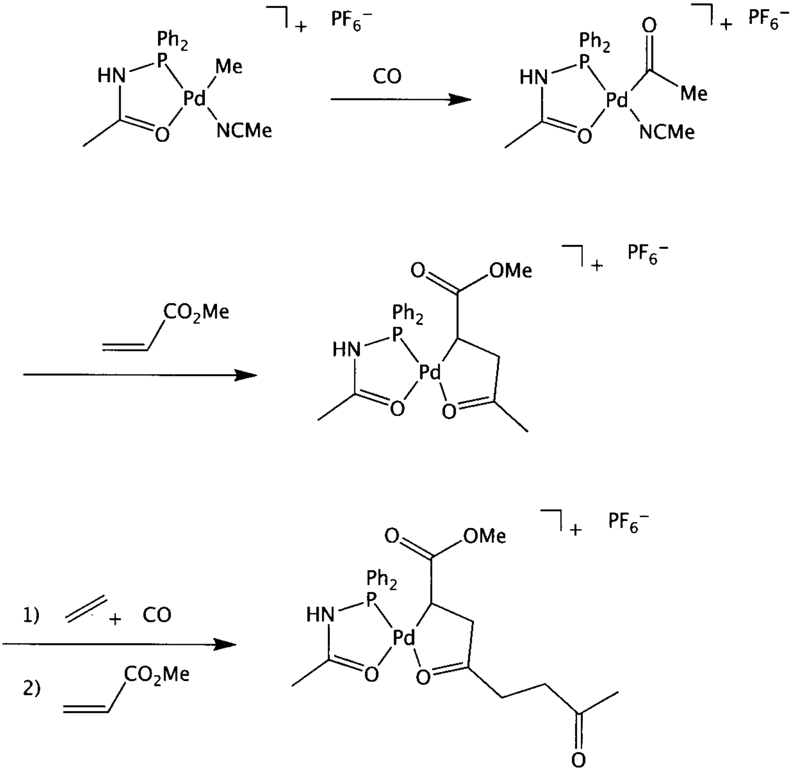

Figure 13.22 Stepwise insertion of ethylene, CO, and methyl acrylate.

This phosphine-sulfonate ligand system was used for the first time by Drent et al.[33] and Rieger et al.[34] for the nonalternating copolymerization of ethylene and CO (Section 13.3.2) and is known to facilitate polar olefin insertions compared to traditional palladium catalysts (e.g., dppp based) with P^P-bichelate ligands. Another methyl-palladium(II) complex stabilized by the (P^O) chelate $Ph_2PNHC(O)Me$ was found to insert ethylene and/or methyl acrylate/CO into the palladium carbon bond (Figure 13.22). Such sequential insertions are facilitated due to the strong unsymmetric nature of the bidentate ligand by orientating the trans-located moieties in a more selective manner, although the relatively low reaction rates for each insertion step should be mentioned. This facilitated the isolation of several individual insertion products, which however made the copolymerization or terpolymerization unfeasible.[62]

13.5 CHEMICAL MODIFICATION OF POLYKETONES

Chemical derivatization of polyketones is of great interest due to the reactivity of keto groups and the huge variety of possible modification protocols in organic chemistry. Thus the chemical properties of polyketones can be further modified and controlled to extend the possible functionalization by the employment of functional comonomers (seen in Section 13.4.2).

Preliminary work, predominantly performed with low-molecular-weight polyketones, is summarized in a review by Sen,[2a] who details numerous possibilities for derivatization or cross-linking.

For high-molecular-weight polyketones the interesting question of the functionalization degree has to be addressed. This ratio should be exploitable to control the properties of the derivatized polymer. Indeed, this concept could be shown in the synthesis of poly-(ketone-*co*-alcohol) thermoplastic elastomers. Here a common modification technique, the reduction of the carbonyl functionalities, was employed. This can be done with, for example, $LiAlH_4$ or in the described case with $NaBH_4$. The properties of the resulting polymers could be controlled by the degree of reduction, especially their glass transition temperature T_g.[63] As already shown in a report concerning the stereoselective copolymerization of CO and propylene, during the reduction of the carbonyl functionalities the configuration of the methyl groups is retained and the reduction occurs by a nonenantioselective attack of the $LiAlH_4$, leading to a random hydroxyl configuration.[39] A polyketone in spiroketal form is not reducible. Despite this observation later contributions showed that a slight preference of the reduction can be achieved leading to an S-configuration at the new chiral center (S/R ratio = 70/30). The increase was achieved with Bu_4NBH_4. For the rationalization of the regioselectivity the polymer structure has to be taken into account. If a zigzag structure for the polymer is assumed (which can be found in molecular structures), the attack on the carbonyl occurs on the opposite side respective to the methyl group adjacent to it.[64]

These results show that asymmetric polymer analogue reactions can be possible, at least to a certain extent. A prediction is, however, difficult as the diastereoselectivity strongly depends on (i) the type of reaction and (ii) the steric environment induced by the polymer structure and conformation.

A further functionalization concerns the reaction of low molecular weight isotactic propylene/CO copolymers with methylating reagents, as opposed to the method of copolymerization of allenes to gain unsaturated polyketones (see Section 13.4.2). Here the carbonyl groups were methylated first with the Tebbe's reagent $Cp_2Ti(\mu\text{-}Cl)(\mu\text{-}CH_2)(AlMe_2)$ (1-dicyclopentadienyl-μmethylene-2-dimethyl-2-aluminum-1-titanium) two consecutive times to afford the modified polymer in low yield and a methylene/keto group content of 93/7. In the optimized reaction the copolymer is converted in good yield and high conversion (94/6 methylene/keto group ratio) with $CH_2(ZnI)_2$ and a low-valent $TiCl_n$ ($n = 2, 3$) species.[65]

In addition to these interesting examples of functionalized asymmetric copolymers, some methods for the functionalization of the polymer backbone are presented. Low to medium molecular weight copolymers (nonalternating) can react with sodium azide in acidic solution and results in a modified polymer with amide groups in the backbone. The molecular weight of the polymers could be retained during this Schmidt reaction and the polymer showed a transition from a brittle compound to an elastomeric product. This polyamide can also be obtained in a two-step process. First the polyketone is reacted with hydroxylamine to the polyoxime. A subsequent Beckman rearrangement with PCl_5 yields the polyamide analogue to the first described method.[66] Paton et al.[67] reported on the oximation of polyethylene/CO copolymers and propylene/ethylene/CO terpolymers. The methyl methyloximes could be further functionalized by deprotonation of the polymer backbone with *n*-BuLi and subsequent reaction with an electrophile.

The alternating structure of 1,4-polyketones was exploited by thioketonization of the carbonyl groups. The thioketone subsequently cyclizises and produces a polymer with a high degree of thiophene units in the polymer backbone (~75%). Additionally ketone, thioketone, and thioenolate functionalities are present in the polymer. Also, polypropylene/CO (not polyethylene/CO) copolymers could be transformed into a polymer containing 3-methylfuranyl units.[68]

REFERENCES

1. Reppe, W., and Magin, A., U.S. Patent No. 2577208, **1951**; *Chem. Abstr.*, **1952**, 46, 6143.
2. (a) Sen, A., *Adv. Polym. Sci.*, **1986**, 73/74, 125; (b) Brubaker, M. M., Coffman, D. D., and Hoehn, H. H., *J. Am. Chem. Soc.*, **1952**, 74, 1509; (c) Steinberg, M., *Polym. Eng. Sci.*, **1977**, 17, 335; (d) Russo, S., and Munari, S., *Polym. Lett.*, **1967**, 5, 827; (e) Colombo, P., Kukacka, L. E., Fontana, J., Chapman, R. N., and Steinberg, M., *J. Polym. Sci. Pt. A1*, **1966**, 4, 29.
3. Shryne, T. M., and Holler, H. V., U.S. Patent No. 3984388, **1976**; *Chem. Abstr.*, **1976**, 85, 178219.
4. (a) Klabunde, U., and Ittel, S. D., *J. Mol. Catal.*, **1987**, 41, 123; (b) Klabunde, U., Tulip, T. H., Roe, D. C., and Ittel, S. D., *J. Organomet. Chem.*, **1987**, 334, 141; (c) Desjardins, S. Y., Cavell, K. J., Hoare, J. L., Skelton, B. W., Sobolev, A. N., White, A. H., and Keim, W., *J. Organomet. Chem.*, **1997**, 544, 163.
5. Driessen, B., Green, M. J., and Keim, W., U.S. Patent No. 5214126, 1993, European Patent No. 470759, 1992; *Chem. Abstr.*, **1992**, 116, 152623.

6. (a) Domhöver, B., Kläui, W., Kremer-Aach, A., Bell, R., and Mootz, D., *Angew. Chem. Int. Ed.*, **1998**, 37, 3050; (b) Kläui, W., Bongards, J., and Reiss, G. J., *Angew. Chem.*, **2000**, 39, 3894.
7. Gough, A. British Patent No. 1081304, **1967**; *Chem. Abstr.*, **1967**, 67, 100569.
8. Fenton, D. M., U.S. Patent No. 3530109, **1970**; *Chem. Abstr.*, **1970**, 73, 110466.
9. (a) Sen, A., and Lai, T. W., *J. Am. Chem. Soc.*, **1982**, 104, 3520; (b) Lai, T. W., and Sen, A., *Organometallics*, **1984**, 3, 866.
10. Drent, E., European Patent application 121965 A2, 1984; *Chem. Abstr.*, **1985**, 102, 46423.
11. (a) Hartley, G. H., and Guillet, J. E., *Macromolecules*, **1968**, 1, 165; (b) Hartley, G. H., and Guillet, J. E., *Macromolecules*, **1968**, 1, 413; (c) Heskins, M., and Guillet, J. E., *Macromolecules*, **1970**, 3, 224.
12. (a) Reuter, P., Fuhrmann, R., Mücke, A., Voegele, J., Rieger, B., and Franke, R.-P., *Macromol. Biosci.*, **2003**, 3, 123; (b) Röhlke, W., Fuhrmann, R., Franke, R-P., Mücke, A., Voegele, J., and Rieger, B., *Macromol. Biosci.*, **2003**, 3, 131.
13. (a) Iwashita, Y., and Sakuraba, M., *Tetrahedron Lett.*, **1971**, 26, 2409; (b) Sen, A., and Brumbaugh, J. S., *J. Organomet. Chem.*, **1985**, 279, C5; (c) Drent, E., and Budzelaar, P. H. M., *Chem. Rev.*, **1996**, 96, 663; (d) Bianchini, C., and Meli, A., *Coord. Chem. Rev.*, **2002**, 225, 35.
14. Dekker, G. P. C. M., Elsevier, C. J., Vrieze, K., and van Leeuwen, P. W. N. M., *Organometallics*, **1992**, 11, 1598.
15. Drent, E., van Broekhoven, J. A. M., and Doyle, M. J., *J. Organomet. Chem.*, **1991**, 417, 235.
16. (a) Chen, J.-T., and Sen, A., *J. Am. Chem. Soc.*, **1993**, 115, 1506; (b) Sen, A., Chen, J.-T., Vetter, W. M., and Whittle, R., *J. Am. Chem. Soc.*, **1987**, 109, 148.
17. (a) Toth, I., and Elsevier, C. J., *J. Am. Chem. Soc.*, **1993**, 115, 10388; (b) Margl, P., and Ziegler, T., *J. Am. Chem. Soc.*, **1996**, 108, 7337; (c) Margl, P., and Ziegler, T., *Organometallics*, **1996**, 15, 5519; (d) Svensson, M., Matsubara, T., and Morokuma, K., *Organometallics*, **1996**, 15, 5568; (e) Shultz, S., Ledford, J., DeSimone, J. M., and Brookhart, M., *J. Am. Chem. Soc.*, **2000**, 122, 6351.
18. Drent, E., *Pure Appl. Chem.*, **1990**, 62, 661.
19. Kuhn, P., Sémeril, D., Matt, D., Chetcuti, M. J., and Lutz, P., *Dalton Trans.*, **2007**, 5, 515.
20. Abu-Surrah, A. S., Wursche, R., Rieger, B., Eckert, G., and Pechhold, W., *Macromolecules*, **1996**, 29, 4806.
21. Mücke, A., and Rieger, B., *Macromolecules*, **2002**, 35, 2865.
22. Anselment, T. M. J., Vagin, S. I., and Rieger, B., *Dalton Trans.*, **2008**, 34, 4537.
23. (a) Durand, J., and Milani, B., *Coord. Chem. Rev.*, **2006**, 250, 542; (b) García Suárez, E. J., Godard, C., Ruiz, A., and Claver, C., *Eur. J. Inorg. Chem.*, **2007**, 18, 2582.
24. Bianchini, C., Lee, H. M., Meli, A., Moneti, S., Vizza, F., Fontani M., and Zanello, P., *Macromolecules*, **1999**, 32, 4183.
25. Koide, Y., Bott, S. G., and Barron, A. R., *Organometallics*, **1996**, 15, 2213.
26. Bianchini, C., Lee, H. M., Meli, A., Oberhauser, W., Vizza, F., Brüggeller, P., Haid, R., and Langes, C., *Chem. Commun.*, **2000**, 9, 777.
27. Drent, E., and Wife, R. L., European Patent application EP0222454, 1987.

28. Dossett, S. J., Gillon, A., Orpen, A. G., Fleming, J. S., Pringle, P. G., Wass, D. F., and Jones, M. D., *Chem. Commun.*, **2001**, 8, 699.
29. Versupui, G., Schanssema, F., and Sheldon, R. A., *Angew. Chem. Int. Ed.*, **2000**, 39, 804.
30. (a) Meier, U. W., Thewalt, U., Debaerdemaeker, T., and Rieger, B., *Eur. J. Inorg. Chem.*, **2004**, 15, 3057; (b) Pérez-Foullerat, D., Meier, U. W., Hild, S., and Rieger, B., *Macromol. Chem. Phys.*, **2004**, 205, 2292.
31. (a) Jiang, Z., and Sen, A., *Macromolecules*, **1994**, 27, 7215; (b) Bianchini, C., Lee, H. M., Meli, A., Moneti, S., Patinec, V., Petrucci, G., and Vizza, F., *Macromolecules*, **1999**, 32, 3859.
32. Especially in α-diimine/Pd catalyst systems: Johnson, L. K., Killian, K. M., and Brookhart, M., *J. Am. Chem. Soc.*, **1995**, 117, 6414 and following literature.
33. Drent, E., van Dijk, R., van Ginkel, R., van Oort, B., and Pugh, R. I., *J. Chem. Soc., Chem. Commun.*, **2002**, 9, 964.
34. Hearley, A. K., Nowack, R. J., and Rieger, B., *Organometallics*, **2005**, 24, 2755.
35. (a) Haras, A., Michalak, A., Rieger, B., and Ziegler, T., *J. Am. Chem. Soc.*, **2005**, 127, 8765; (b) Haras, A., Michalak, A., Rieger, B., and Ziegler, T., *Organometallics*, **2006**, 25, 946–953.
36. Batistini, A., Consiglio, G., and Suter, U. W., *Angew. Chem. Int. Ed. Engl.*, **1992**, 31, 303.
37. Bronco, S., Consiglio, G., Hutter, R., Batistini, A., and Suter, U., *Macromolecules*, **1994**, 27, 4436.
38. Jiang, Z., Adams, S. E., and Sen, A., *Macromolecules*, **1994**, 27, 2694.
39. Jiang, Z., and Sen, A., *J. Am. Chem. Soc.*, **1995**, 117, 4455.
40. Nozaki, K., and Hiyama, T., *J. Organomet. Chem.*, **1999**, 576, 248; (b) Nozaki, K., Sato, N., Tonomura, Y., Yasutomi, M., Takaya, H., Hiyama, T., Matsubara, T., and Koga, N., *J. Am. Chem. Soc.*, **1997**, 119, 12779.
41. Sesto, B., and Consiglio, G., *Chem. Commun.*, **2000**, 12, 1011.
42. (a) Bronco, S., Consiglio, G., di Benedetto, S., Fehr, M., Spindler, F., and Togni, A., *Helv. Chim. Acta*, **1995**, 41, 883; (b) Gambs, C., Chaloupka, S., Consiglio, G., and Togni, A., *Angew. Chem. Int. Ed.*, **2000**, 39, 2486.
43. Jiang, Z., Dahlen, G. M., Houseknecht, K., and Sen, A., *Macromolecules*, **1992**, 25, 2999.
44. Abu-Surrah, A. S., Eckert, G., Pechhold, W., Wilke, W., and Rieger, B., *Macromol. Rapid Commun.*, **1996**, 17, 559.
45. Hollmann, F., Mansour, A. A., and Rieger, B., *Polymer*, **2001**, 42, 93.
46. Huhn, W. E., Hollmann, F., Hild, S., Kriewall, T., and Rieger B., *Macromol. Mater. Eng.*, **2000**, 283, 115.
47. (a) Tsuji, J., and Hosaka, S., *Polym. Lett.*, **1965**, 3, 703; (b) Brumbaugh, J. S., Whittle, R. R., Parvez, M., and Sen, A., *Organometallics*, **1990**, 9, 1735.
48. Kacker, S., Jiang, Z., and Sen, A., *Macromolecules*, **1996**, 29, 5852.
49. Moineau, C., Mele, G., and Alper, H., *Can. J. Chem.*, **2001**, 79, 587.
50. Lee, J. T., and Alper, H., *Chem. Commun.*, **2000**, 22, 2189.
51. Klok, H.-A., Eibeck, P., Schmid, M., Abu-Surrah, A. S., Möller, M., and Rieger, B., *Macromol. Chem. Phys.*, **1997**, 198, 2759.

52. Klok, H.-A., Eibeck, P., Schmid, M., Abu-Surrah, A. S., Möller, M., and Rieger, B., *Macromol. Chem. Phys.*, **1997**, 198, 2759.
53. Malinova, V., and Rieger, B., *Macromol. Rapid Commun.*, **2005**, 26, 945.
54. (a) Malinova, V., and Rieger, B., *Biomarcomolecules*, **2006**, 7, 2931; (b) Bartsch, Jr., G. C., Malinova, V., Volkmer, B. E., Hautmann, R. E., and Rieger, B., *BJU Int.*, **2006**, 1, 17092287.
55. (a) Nieuwhof, R. P., Marcelis, A. T. M., Sudhölter, E. J. R., Wursche, R., and Rieger, B., *Macromol. Chem. Phys.*, **2000**, 201, 2484; (b) Nozaki, K., Kawashima, Y., Oda, T., and Hiyama, T., *Macromolecules*, **2002**, 35, **1140**; (c) Kawashima, Y., Nozaki, K., Hiyama, T., Yoshio, M., Kanie, K., and Kato, T., *J. Polym. Sci. Polym. Chem.*, **2003**, 41, 3556.
56. Kacker, S., and Sen, A., *J. Am. Chem. Soc.*, **1997**, 119, 10028.
57. (a) Groen, J. H., Elsevier, C. J., and Vrieze, K., *Organometallics*, **1996**, 15, 3445; (b) Delis, J. G. P., Groen, J. H., Vrieze, K., and van Leeuwen, P. W. N. M., *Organometallics*, **1997**, 16, 551.
58. Wursche, R., and Rieger, B., *Macromol. Chem. Phys.*, 2000, 201, **2861**; (b) Wursche, R., and Rieger, B., *Macromol. Chem. Phys.*, **2000**, 201, 2869.
59. (a) Murtuza, S., Harkins, S. B., and Sen, A., *Macromolecules*, **1999**, 32, 8697; (b) di Benedetto, S., and Consiglio, G., *Helv. Chim. Acta*, **1997**, 80, 2204.
60. Fujita, T., Nakano, K., Yamashita, M., and Nozaki, K., *J. Am. Chem. Soc.*, **2006**, 128, 1968.
61. Kochi, T., Nakamura, A., Ida, H., and Nozaki, K., *J. Am. Chem. Soc.*, **2007**, 129, 7770.
62. Braunstein, P., Frison, C., and Morise, X., *Angew. Chem. Int. Ed.*, **2000**, 39, 2867.
63. Pérez-Foullerat, D., Hild, S., Mücke, A., and Rieger, B., *Macromol. Chem. Phys.*, **2004**, 205, 374.
64. Nozaki, K., Kosaka, N., Muguruma, S., and Hiyama, T., *Macromolecules*, **2000**, 33, 5340.
65. Nozaki, K., Kosaka, N., Graubner, V. M., and Hiyama, T., *Macromolecules*, **2001**, 34, 6167.
66. Michel, R. H., and Murphey, W. A., *J. Polym. Sci.*, **1961**, 55, 741.
67. Khansawai, P., Paton, R. M., and Reed, D., *Chem. Commun.*, **1999**, 14, 1297.
68. Jiang, Z., Sanganeria, S., and Sen, A., *J. Polym. Sci. Pt. A Polym. Chem.*, **1994**, 32, 841.

14 Copper Catalysts for Olefin Polymerization

ANNA MARIA RASPOLLI GALLETTI
Dipartimento di Chimica e Chimica Industriale, Università di Pisa, 56126 Pisa, Italy

In these last years very intense research in the field of new-generation catalysts for olefin polymerization has been carried out in academic and industrial laboratories. In particular, late transition metal catalysts have been studied for olefin activation because they are less oxophilic and thus less easily poisoned by polar contaminants.[1–3]

To date, olefin polymerization catalyzed by group 11 catalysts, and in particular by copper systems, has been scarcely investigated and a good part of the literature is represented by patents, in particular those developed by Exxon Mobil, published only in the last few years. This statement excludes Cu ATRP (atom transfer radical polymerization) catalysts[4,5]: they are free-radical initiators and will not be considered here.

Copper systems appear particularly intriguing due to the metal low cost, limited toxicity, and limited sensitivity to deactivation by polar species. This last aspect appears particularly important in the perspective of the direct metal-mediated copolymerization of olefins with polar monomers, one of the most pursued goals in the field of polymerization catalysis.[6–8] These copolymers, in fact, represent new high-performance materials with improved characteristics in terms of printability, paintability, and dyeability as well as compatibility with additives and other polar polymers. On the other hand, the currently employed industrial free-radical processes for the copolymerization of α-olefins with polar monomers require extreme conditions and do not enable the control of the resulting polymer architecture in terms of tacticity, molecular weight, and crystallinity.

The catalytic precursors employed for copper-mediated polymerization are generally Cu(II) complexes bearing chelating bulky ligands which

---

Handbook of Transition Metal Polymerization Catalysts Edited by Ray Hoff and Robert T. Mathers
Copyright © 2010 John Wiley & Sons, Inc.

are always employed in the presence of methylaluminoxane (MAO) or triisobutylaluminum (TIBA) as cocatalyst. They have been mainly studied in the activation of ethylene (E), styrene (STY), and acrylic monomers, such as methylacrylate (MA), methylmethacrylate (MMA), *t*-butyl acrylate (*t*BA), and methacrylate (*t*BMA), and for the copolymerization of ethylene or propylene (P) with these (meth)acrylates. Only in this last year also the polymerization of norbornene (NB) and its copolymerization with STY have been reported.

The most significant types of copper systems tested up to now in olefin polymerization are reported in Tables 14.1 and 14.2.

TABLE 14.1 Cu Precatalysts Employed for Olefin Polymerization and Copolymerization

Cu Precatalyst	Cocatalyst	Monomer	References
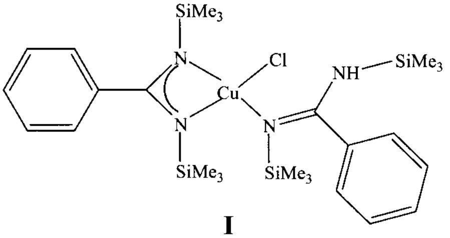 SiMe$_3$ N Cl NH SiMe$_3$ Cu N N SiMe$_3$ SiMe$_3$ **I**	MAO	E MMA *n*BA STY	9–11
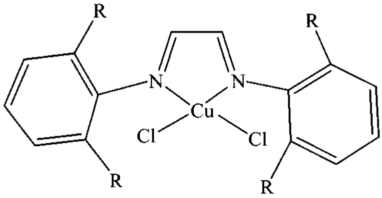 R= Ph (**II a**), *i*-Pr (**II b**) **II**	MAO	E	12
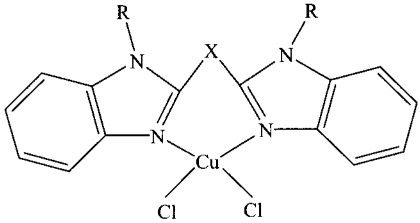 **III a** X= 2,2 biphenyl, R= ethyl **III b** X= $CHOCH_3$, R= methyl **III c** X=C_2F_4, R= *n*-Bu **III**	MAO	E, MA, MMA, *t*BA, *t*BMA, E/*t*BMA, E/MA, E/MMA	14–22

TABLE 14.1 *Continued*

Cu Precatalyst	Cocatalyst	Monomer	References
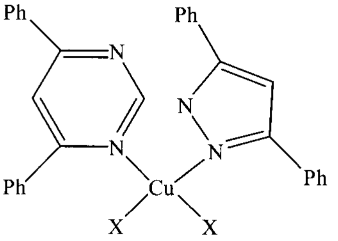 X = Cl (**IV a**), Br (**IV b**) **IV**	MAO or TIBA	E	23
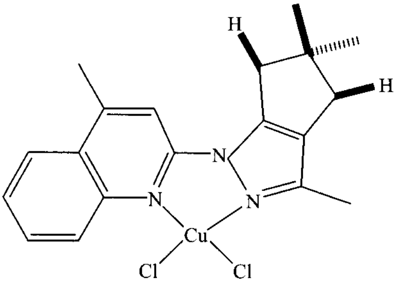 **V**	MAO or TIBA	E	24

TABLE 14.2 Cu Precatalysts Employed for Olefin Polymerization and Copolymerization

Cu Precatalyst	Cocatalyst	Monomer	References
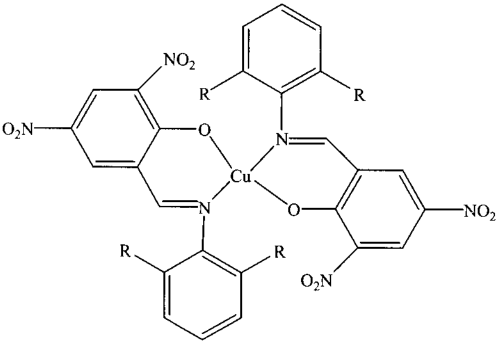 R= H (**VI a**), *i*-Pr (**VI b**), *t*-Bu (**VI c**) **VI**	MAO	E MMA E/MMA NB	25–26

TABLE 14.2 ***Continued***

Cu Precatalyst	Cocatalyst	Monomer	References
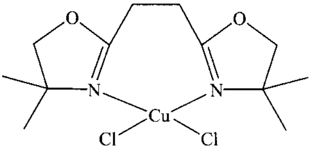 **VII**	MAO	MA MMA E/MA P/MA	27
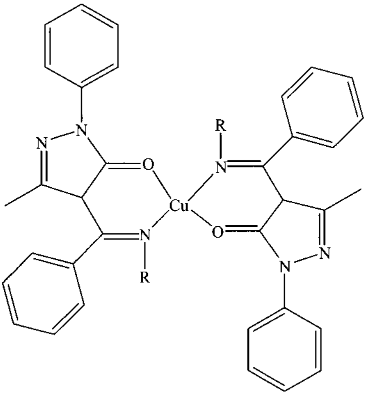 R= o-tolyl (**VIII a**), naphthyl (**VIII b**), p-nitrophenyl (**VIII c**) **VIII**	MAO	NB STY NB/STY	28–30
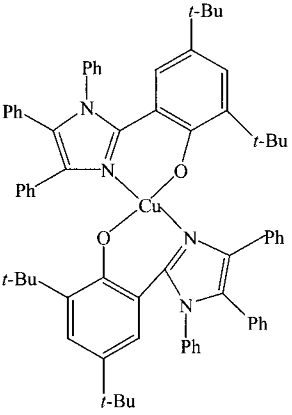 **IX**	MAO	NB	31

The first Cu precursors reported for ethylene, styrene, and acrylic monomer polymerization are Cu(II) benzamidinate complexes (such as **I** in Table 14.1), used in combination with Al cocatalysts. They were studied and patented by Shibayama.[9–11] These precatalysts are characterized by a long and expensive synthesis[11] and have been employed only in the homopolymerization reactions. Their activity in ethylene polymerization is low (entry 1, Table 14.3), whereas quantitative conversions of MMA are claimed, although no activity data are reported. The tacticities of the obtained poly(MMA)s are different from those of the polymers obtained by radical or anionic polymerization, thus indicating that these polymerizations propagate through a copper-mediated process. Electron spin resonance (ESR) studies confirmed that MAO reduces the Cu(II) precursor to the ESR-silent Cu(I) oxidation state responsible for the catalytic process.

The activation of ethylene in the presence of copper catalysts/MAO has been successively described in a very short communication: Only three E homopolymerization runs carried out employing Cu(II) α-diimine complexes **II** (Table 14.1) are reported.[12] These results are summarized in Table 14.3 (entries 2–4): **IIa** showed a good catalytic activity to give high-molecular-weight polymer, while **IIb** was almost inactive. This difference has been ascribed to the effect of the *ortho*-phenyl substituents, due to the stabilization of the active center through weak interactions with them, analogous to that reported for related nickel systems.[13]

On the other hand, a very exhaustive and elegant work on Cu-based catalysts has been carried out by Stibrany and his co-workers at Exxon Mobil: They employed many bis(benzimidazole)Cu(II) complexes (structures **III**, Table 14.1), not only for the homopolymerization of ethylene and of various (meth)acrylates, but also for the coactivation of these two monomer classes without deactivation.[14–22] These Cu-catalyzed copolymers are in-chain copolymers with high levels of polar monomer incorporation. The authors claim that these products are real copolymers by ^{13}C nuclear magnetic resonance (NMR) analysis. In fact, ^{13}C NMR spectra of the copolymers were compared with those of the corresponding homopolymers. The presence of EAE and EAA/AAE triads (A = acrylic unit) supports the formation of true copolymers.

The synthesis of the above bis(benzimidazole)Cu(II) precatalysts is reported in literature[14,21] and follows the synthetic in Figure 14.1 involving three steps.

The first step is represented by the acid-catalyzed condensation of a dicarboxylic acid with two equivalents of phenylenediamine followed by the alkylation of the bis(benzimidazole) using NaH as deprotonating agent. Finally the alkylated bis(benzimidazole) is metalated using $CuCl_2{\cdot}2H_2O$ in a mixture of ethanol and triethylorthoformate (TEOF). TEOF helps the dehydration of the reaction mixture and the crystallization of the metal complex. The activation with MAO of the precatalysts **III** gives polymerization catalysts active in the homopolymerization and copolymerization of ethylene and (meth)acrylates. On the other hand, these systems are inactive in the polymerization of monomers such as styrene, vinyl acetate, and butadiene.

TABLE 14.3 Ethylene Polymerization with Different Cu Precatalysts in Presence of MAO

Entry	Cu Precatalyst (μmol)	MAO/Cu (mol/mol)	P C_2H_4 (psi)	T (°C)	Time (h)	Activity (g PE/mol Cu·h)	PE Characteristics	References
1[a]	**I** (19)	440	16	20	24	3,300	High molecular weight T_m:138	11
2[b]	**IIa** (5.8)	500	440	70	1	300,000	High molecular weight	12
3[b]	**IIa** (20.0)	500	66	25	1	20,000	High molecular weight	12
4[b]	**IIb** (20.0)	500	74	70	1	—	—	12
5[c]	**IIIa** (24.0)	400	270	80	24	28,000	Linear PE, T_m:139	18
6[d]	**IV** (2)	500	150	35	1	350,000	n.d.	23
7[d]	**V** (2)	500	150	35	1	650,000	n.d.	24
8[e]	**VIb** (20.0)	200	735	80	5	1,100	Linear, high molecular weight	26

[a] Solvent: toluene (100 mL).

[b] Solvent: toluene (vol. not indicated).

[c] Solvent: toluene (30 mL).

[d] Solvent: toluene (70 mL).

[e] Solvent: toluene (50 mL).

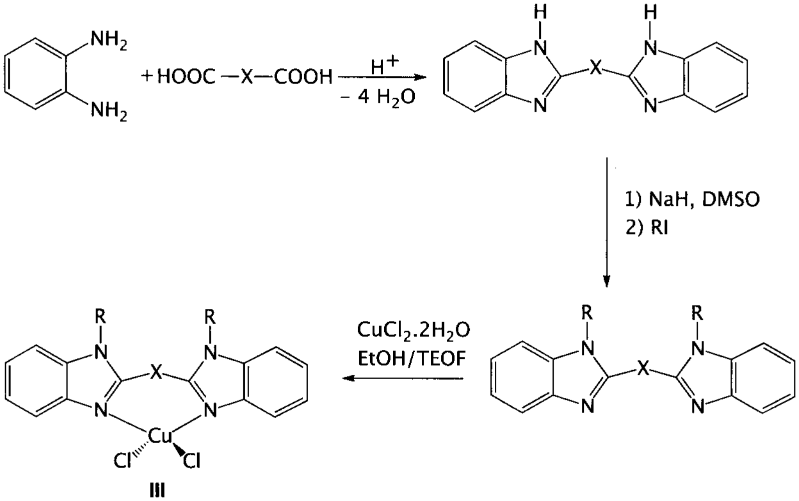

III

Figure 14.1 Synthetic procedure for synthesis of bis(benzimidazole)Cu(II) precatalysts **III**.[14]

Ethylene homopolymers obtained by **III**/MAO systems (typically working at 700–800 psig of ethylene, 80 °C, toluene as solvent, and adopting a MAO/Cu molar ratio >200) are generally high molecular weight, very linear, and with a very high melting point ($T_m > 135\,°C$) (see entry 5 in Table 14.3).

A very high activity in ethylene polymerization has been very recently reported with copper precursors (**IV** and **V**) with new nitrogen-containing heterocyclic ligands.[23,24] These catalytic precursors have been employed only in ethylene activation (entries 6 and 7, Table 14.3) working with a very low catalyst concentration. The obtained polyethylenes up to now have not been characterized.

Finally we have proposed bis(salicylaldiminate)Cu(II) systems (structures **VIa–c**) for olefin activation. These precursors are cheap, stable, and very easy to synthesize if compared with all the other Cu systems up to now reported. In fact, they are prepared in high yields by direct reaction of a light excess of the free salicylaldimine ligand with Cu(II) acetate (L/Cu: 2.1–2.3 mol/mol) in methanol as solvent.[25,26] Their activity in ethylene polymerization is very low, but in MMA homopolymerization these precatalysts in combination with MAO showed the best performance (entries 6–8, Table 14.4) when compared with the other Cu precatalysts.

The molecular weights and, above all, the dispersion indices of all the obtained polymers are much higher that those of the polymers prepared via free-radical initiation. The clear influence of the steric and electronic characteristics of the ligand further supports a metal-mediated mechanism, also confirmed by ESR analysis. In fact, under reaction conditions, the absence of any radical species, organic or Cu(II), was ascertained. This result suggests the formation in the presence of MAO of an ESR-silent Cu(I) species by reduction of the precursor, analogous to what was proposed by Shibayama.

TABLE 14.4 (Meth)acrylates Polymerization with Different Cu Precatalysts in Presence of MAO

Entry	Cu Precatalyst (µmol)	Polar Monomer (mmol)	MAO/Cu (mol/mol)	T (°C)	Time (h)	Activity[a]	Polymer Characteristics	References
1	**I**	MMA	n.d.	25	n.d.	n.d.	*mm, mr, rr*: 26.4, 29.9, 43.6	9
2[b]	**IIIb** (44)	*t*-BA (58)	13	25	18	5300	M_w: 851,000 PDI[c]: 1.8	18
3[b]	**IIIb** (43)	MMA (44)	18	25	16	3300	M_w: 635,000 PDI[c]: 4.6	18
4[d]	**IIIc** (50)	MMA (60)	50	25	16	2600	*mm, mr, rr*: 11, 25, 64	21
5[d]	**IIIc** (50)	*t*-BA (47)	50	25	16	1800	M_w: 386,000 PDI[c]: 1.5	21
6[e]	**VIa** (20)	MMA (47)	100	25	1	3100	M_w: 90,000 PDI[c]: 4.0	26
7[e]	**VIb** (20)	MMA (47)	100	80	5	5600	M_w: 650,000 PDI[c]: 7.4	26
8[e]	**VIc** (20)	MMA (47)	50	70	5	6100	M_w: 1170,000 PDI[c]: 13	26
9[f]	**VII** (22)	MMA (10)	20	60	21	1300	*mm, mr, rr*: 4.6, 29.9, 65.5	27
10[f]	**VII** (22)	MA (10)	20	60	21	910	M_w: 122,000 PDI[c]: 1.8	27

[a] Activity: g polymer/mol Cu·h.

[b] Solvent: toluene (10 mL).

[c] PDI: polydispersity index, determined as M_w/M_n.

[d] Solvent: toluene (30 mL).

[e] Solvent: toluene (20 mL).

[f] Solvent: chlorobenzene (5 mL).

Good activities in acrylic and methacrylic monomer polymerization were also obtained with bis(benzimidazole)Cu(II) complexes studied by Exxon Mobil (entries 2–5, Table 14.4). Also for these precursors the high M_w and the tacticity do not match those for free-radical prepared polymers.

The homopolymerizations of MA and MMA were also studied by Sen in the presence of a N,N chelate Cu(II) precursor (structure **VII**, Table 14.2) activated by MAO (entries 9–10, Table 14.4). The authors demonstrated the unreliability of radical traps as probes for a radical mechanism working in the presence of MAO, thus showing the difficulty of clarifying the reaction mechanism for these type of catalytic systems.[27]

The absence of deactivation by (meth)acrylic monomers prompted the authors to study their copolymerization with ethylene in the presence of these catalytic systems. A few representative examples are reported in Table 14.5.

All the investigated systems are active in the copolymerization reactions, but the activity is still low for application in a commercial setting. All the copolymers contained a high polar monomer incorporation degree (in the 60–95 mol % range) and are in-chain true copolymers and not mixtures of the parent homopolymers. A systematic investigation on these copolymerization reactions was carried out with bis(benzimidazole)Cu(II) complexes and no obvious correlations between the precatalyst structure and copolymer composition were drawn.

Finally, in this last year, copper precatalysts have also been tested for norbornene polymerization.[25,28–32] The most significant examples are reported in Table 14.6.

NB can be polymerized by different routes, affording polymeric products which are very different in structure and properties (Figure 14.2).[33]

Ring-opening polymerization (ROMP) is the most important route, affording a polyalkenamer which still contains double bonds in the polymer backbone. On the contrary, the cationic and radical polymerizations give rise to low-molecular-weight oligomers with a 2,7-connectivity of the monomer units. Finally it is also possible to polymerize NB maintaining the bicyclic structure, that is, only opening the double bond, in a typical vinyl polymerization. This last type of poly(norbornene) (PNB) is a special polymer due to its good mechanical properties, heat resistivity, transparency, high glass transition temperature, and good solubility in organic solvents. Polymer films have excellent optical transparency and heat resistance and good UV resistance. These characteristics explain the great interest in these last few years toward the development of this polymer.

All the investigated systems show appreciable activities and the best performances are observed adopting high MAO/Cu molar ratios (Al/Cu: 2000–2500 mol/mol). The obtained polymers are always characterized by high molecular weights and nonstereoregular vinyl-type structures.

This last characteristic represents an indirect indication that a nonradical reaction mechanism is working in the presence of the experimented Cu(II)/MAO systems, as confirmed for precursors **VI** by ESR study.

TABLE 14.5 Ethylene/(meth)acrylate Copolymerization with Different Cu Precatalysts in Presence of MAO

Entry	Cu Catalyst (μmol)	*E* (psi)	Polar Monomer (mmol)	MAO/Cu (mol/mol)	*T* (°C)	Time (h)	Activity[a]	Polar Monomer Incorporation (mol %)	References
1[b]	**IIIc** (50)	750	*t*BA (47)	220	80	16	2900	67.0	21
2[b]	**IIIc** (50)	750	MA (47)	220	80	16	3300	96.0	21
3[b]	**IIIc** (50)	750	MMA (47)	220	80	16	930	63.0	21
4[c]	**VIa** (20)	735	MMA (47)	200	80	18	350	75.8	26
5[c]	**VIb** (20)	735	MMA (47)	200	80	18	2200	83.7	26
6[c]	**VIc** (20)	735	MMA (47)	100	80	18	550	88.5	26
7[d]	**VII** (22)	500	MA (10)	20	60	21	450	83.6	27

[a] Activity: g copolymer/mol Cu·h.

[b] Solvent: toluene (30 mL).

[c] Solvent: toluene (50 mL).

[d] Solvent: chlorobenzene (5 mL).

TABLE 14.6 Norbornene Polymerization in Presence of Cu Precursors and MAO

Entry	Cu Catalyst (μmol)	MAO/Cu (mol/mol)	T (°C)	Time (h)	Activity[a]	M_w	PDI[b]	References
1[c,d]	**VIa** (1)	2500	80	1	110,000	344,000	2.2	25
2[c,d]	**VIb** (1)	2500	80	1	150,000	432,000	2.6	25
3[c,d]	**VIc** (1)	2500	80	1	70,000	227,000	2.4	25
4[e,f]	**VIIIa** (5)	400	60	4	22,000	846,000	2.6	30
5[e,f]	**VIIIb** (5)	400	60	4	63,000	555,000	2.5	30
6[e,f]	**VIIIc** (5)	400	60	4	45,000	752,000	2.6	30
7[g,h]	**IX** (5)	2000	60	1	316,000	1920,000[i]	n.d.	31

[a] Activity: g polymer/mol Cu·h.
[b] PDI: polidispersity index, determined as M_w/M_n.
[c] Solvent: chlorobenzene: 20 mL.
[d] Norbornene: 10 mmol.
[e] Solvent: toluene: 20 mL.
[f] Norbornene: 53 mmol.
[g] Solvent: chlorobenzene: 15 mL.
[h] Norbornene: 20 mmol.
[i] Average viscometric molecular weight.

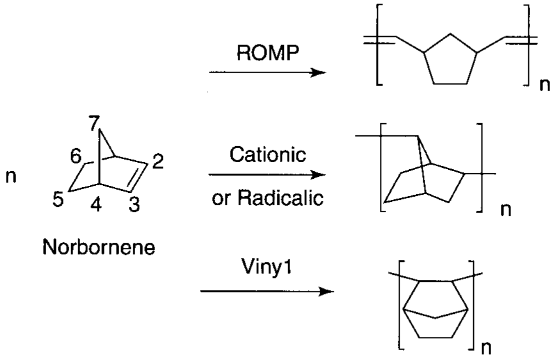

Figure 14.2 Different routes for NB polymerization.

14.1 SYNTHESIS OF VIb

All manipulations were carried out under dry argon atmosphere using Schlenk techniques. Methanol was dried by distillation under dry argon after refluxing for 6 h on magnesium methoxide.

3,5-Dinitro-*N*-(2,6-diisopropylphenyl)salicylaldimine [0.881 g, (2.37 mmol)] was dissolved in 30 mL of methanol and the resulting solution was dropwise added at room temperature to a solution of 0.181 g (1.00 mmol) of Cu(OAc)$_2$ in 20 mL of methanol. The reaction mixture was refluxed for 2 h; then it was allowed to stand overnight at room temperature to precipitate a green solid which was filtered, washed with methanol, and vacuum dried to give 0.76 g (0.797 mmol) of **VIb** (yield 80%).

Elemental analysis found C: 57.43, H: 4.91, N: 10.78%; calculated for $C_{38}H_{38}N_6O_{10}Cu$: C: 56.89, H: 4.77, N: 10.47%.

Fourier transform infrared (FTIR): ν_{CH} (aromatic) 3091; ν_{CH} (aliphatic) 2966, 2869; $\nu_{C=N}$ = 1622, 1511; $\nu_{as\,NO_2}$ = 1530; $\nu_{s\,NO_2}$ = 1311; δ_{CH} (isopropyl) 1387, 1375 cm^{-1}.

14.2 REPRESENTATIVE MMA POLYMERIZATION PROCEDURES WITH PRECURSORS VI

MMA homopolymerization experiments were carried out in a 50-mL Carius vessel under magnetic stirring. MMA was distilled at reduced pressure from CaH_2 and stored under dry argon in the refrigerator. Toluene was refluxed over Na/K alloy and distilled under dry argon. MAO was purchased from Witco [with a trimethyl aluminum (TMA) content equal to 28 mol %] as a 5 wt % solution in toluene. It was stored in the refrigerator and used as received. The selected copper precursor **VI** was dissolved in anhydrous toluene (20 mL) in a Schlenk-type vessel under dry argon. The resulting solution was transferred under argon into the Carius vessel, then MMA (5 mL) and MAO (Al/Cu: 50–200 mol/mol) were added in that order and the polymerization was allowed to proceed in the absence of light. The experiments were carried out at room temperature or in a thermostatted oil bath at 70–80 °C.

At the end of the run the reaction was stopped by fast cooling and a small amount of the liquid inside the Carius tube was collected, weighed, and analyzed by gas cromatography (GC) for the determination of eventual oligomeric products.

The rest of the product was poured into a large excess of acidified methanol to precipitate the PMMA. This was filtered, washed with fresh methanol, dried in vacuo, weighed, and structurally characterized.

14.3 REPRESENTATIVE E POLYMERIZATION PROCEDURES WITH PRECURSORS VI

Ethylene polymerization was carried out in a 250-mL stainless steel reactor under magnetic stirring. In a typical procedure the selected copper precursor was dissolved in anhydrous toluene (50 mL) in a Schlenk-type vessel under argon. The solution was then transferred into the reactor under ethylene atmosphere and MAO (Al/Cu: 100–200 mol/mol) was added at room temperature. The autoclave was then charged with 5 MPa ethylene in a single charge and maintained at the desired temperature by using a thermostatted oil bath.

The reaction was stopped by fast cooling the reactor at 0 °C and venting the unreacted ethylene through a trap cooled at −15 °C to collect lower oligomers for subsequent analysis. The reactor was then opened and the reaction product (solid and liquid) was weighed; then, a small amount of the liquid was collected with a syringe and analyzed by GC to determine whether higher oligomers were formed. Then, the reaction product was poured into a large excess of acidified methanol to precipitate and purify the polymer from metal residues. The polymeric product was filtered, washed with fresh methanol, dried in vacuo, weighed, and structurally characterized.

14.4 REPRESENTATIVE E/MMA POLYMERIZATION PROCEDURES

Ethylene/MMA copolymerization experiments with precursors **VI** were carried out quite analogously to ethylene homopolymerizations with the unique difference of adding into the reactor not only MAO (Al/Cu: 100–200 mol/mol) but also MMA (2.5–5 mL) in that order. The polymerization procedure and product work-up were completely identical to those described above for ethylene homopolymerization.

14.5 REPRESENTATIVE NB POLYMERIZATION PROCEDURES WITH PRECURSORS VI

NB was refluxed for 2 h on Na, distilled, and stored under dry argon. Chorobenzene was reluxed on CaH_2 for 8 h, distilled, and stored under dry argon. NB homopolymerization experiments were carried out in a 50-mL Carius vessel under magnetic stirring and dry argon atmosphere. In a general procedure the copper precursor was dissolved in chlorobenzene and then the proper amount of the solution was transferred into the Carius vessel. Then NB was added as a 20 wt % solution in chlorobenzene. Finally, the chosen amount of MAO was added in order to reach the proper Al/Cu molar ratio. When the polymerization experiment was carried out at a temperature >25 °C, the Carius vessel was immersed in a thermostatted oil bath at the chosen temperature. The polymerization was stopped by adding a large excess of methanol acidified with 5% aqueous. HCl to purify the polymer from catalyst residues. The precipitated polymer was washed by fresh methanol, then filtered, dried under vacuum, weighed, and structurally characterized.

14.6 STRUCTURAL CHARACTERIZATION OF PRODUCTS

The GC analysis of eventual oligomers was carried out on a Hewlett-Packard 5890 equipped with an HP 3396 integrator and a flame ionization detector. A capillary column HP PONA (50 m × 0.2 mm × 0.5 μm), based on polymethylphenylsiloxane as the stationary phase, was adopted and nitrogen as carrier gas was used. The oven temperature program adopted was as follows: 25 °C for 45 min, then the temperature was increased by 8 °C/min heating until 230 °C was reached, and this value was maintained constant for a further 30 min.

The FTIR spectra were carried out on a Perkin-Elmer Spectrum One spectrophotometer equipped with an attenuated total reflectance apparatus. Data elaboration was performed by the Spectrum V 3.2 Perkin-Elmer program.

NMR spectroscopy was carried out on a Gemini 200 spectrometer operating at 200 (^1H) and 50 (^{13}C) MHz. Spectra of poly(MMA) and E/MMA copolymers were obtained in $CDCl_3$ using TMS as internal standard. Spectra of polyethylenes were performed in 1,2,4-trichlorobenzene at 135 °C using 1,1,2,2-d_2-tetrachloroethane as internal standard. Spectra of polynorbornene samples were performed in 1,1,2,2-d_2-tetrachloroethane at room temperature.

For PMMA and E/MMA copolymers the number and weight average molecular weights (M_n and M_w, respectively) as well as polidispersity index (M_w/M_n = DI) were determined by size exclusion chromatography (SEC) on a Waters instrument equipped with a high-performan liquid chromatography (HPLC) pump with a 50-μm Rheodyne loop, a Waters 515 oven programmed at 35 °C, a Waters 2410 RI detector, and a Waters 2487 UV-vis tunable detector operating at 254 nm. An HPLC PLgel 5-μmMixed-C column and chloroform as an eluent (1 mL/min) were used. A calibration curve was obtained with several monodisperse polystyrene samples with different molecular weights.

SEC measurements of polynorbornenes were carried out with the above instrument and column, adopting chorobenzene and 1 mL/min as the eluent and the elution rate, respectively. Also in this case a calibration curve was obtained with several monodisperse polystyrene samples having different molecular weights.

Differential scanning calorimetry (DSC) analysis was performed on a Mettler TA 4000 instrument equipped with a DSC 30 flow calorimeter and assisted by a TA72 GraphWare software. The polymer samples were submitted to a first scan with a 10 °C/min heating rate until the melting temperature was reached; then the samples were cooled with the same rate and finally submitted to a second identical heating scan. The reported melting temperature values were referred to the second heating scan.

REFERENCES

1. Gibson, V. C., and Spitzmesser, S. K., *Chem. Rev.*, **2003**, 103, 283–315.
2. Ittel, S. D., Johnson, L. K., and Brookhart, M., *Chem. Rev.*, **2000**, 100, 1169–1203.
3. Speiser, F., Braunstein, P., and Saussine, L., *Acc. Chem. Res.*, **2005**, 38, 784–793.
4. Matyjaszewski, K., and Xia, J., *Chem. Rev.*, **2001**, 101, 2921–2990.
5. Liu, S., Elyashiv, S., and Sen, A., *J. Am. Chem. Soc.*, **2001**, 123, 12738–12739.
6. Yanjarappa, M. J., and Sivaram, S., *Prog. Polym. Sci.*, **2002**, 27, 1347–1398.
7. Boffa, L. S., and Novak, B. M., *Chem. Rev.*, **2000**, 100, 1479–1493.
8. Younkin, T. R., Connor, E. F., Henderson, J. I., Friedrich, S. K., Grubbs, R. H., and Bansleben, D. A., *Science*, **2000**, 287, 460–462.
9. Shibayama, K., *Polym. J.*, **2003**, 35, 711–713.
10. Shibayama, K., and Ogasa, M., Sekisui Chemical Co., Japan, Patent No. WO 98/35996, Feb. 17, 1998.
11. Shibayama, K., Sekisui Chemical Co., Japan, U.S. Patent Application 20020026031, Feb. 28, 2002.

12. Gibson, V. C., Tomov, A., Wass, D. F., White, A. J. P., and Williams, D. J., *J. Chem. Soc. Dalton Trans.*, **2002**, 2261–2262.
13. Schrekker, H. S., Kotov, V., Preishuber-Pflugl, P., White, P., and Brookhart, M., *Macromolecules*, **2006**, 39, 6341–6354.
14. Stibrany, R. T., Schulz, N. D., Kacker, S., Patil, A. O., Baugh, L. S., Rucker, S. P., Zushma, S., Berluche, E., and Sissano, J. A., *Macromolecules*, **2003**, 36, 8584–8586.
15. Stibrany, R. T., Schulz, D. N., Kacker, S., and Patil, A. O., Exxon, Patent No. WO 99/30822, June 24, 1999.
16. Stibrany, R. T., Schulz, D. N., Kacker, S., and Patil, A. O., Exxon, U.S. Patent No. 6,037,297, Mar. 14, 2000.
17. Stibrany, R. T., Exxon, U. S. Patent No. 6,180,788, Jan. 30, 2001.
18. Stibrany, R. T., Schulz, D. N., Kacker, S., and Patil, A. O., Exxon-Mobil, U.S. Patent No. 6,417,303, July 9, 2002.
19. Stibrany, R. T., in *Beyond Metallocenes: Next-Generation Polymerization Catalysts*, Patil, A. O., and Hlatky, G. G., Eds., ACS Symposium Series 857, American Chemical Society, Washington, DC, 2003, pp. 210–221.
20. Stibrany, R. T., Patil, A. O., and Zushma, S., *Polym. Mat. Sci. Eng.*, **2002**, 86, 323–324.
21. Baugh, L. S., Sissano, J. A., Kacker, S., Berluche, E., Stibrany, R. T., Schulz, D. N., and Rucker, S. P., *J. Polym. Sci. Pt. A Polym. Chem.*, **2006**, 44, 1817–1840.
22. Stibrany, R. T., Schulz, D. N., Kacker, S., Baugh, L. S., Rucker, S. P., Berluche, E., and Sissano, J. A., in *Beyond Metallocenes: Next-Generation Polymerization Catalysts*, Patil, A. O., and Hlatky, G. G., Eds., ACS Symposium Series 857, American Chemical Society, Washington, DC, 2003, pp. 222–230.
23. Beshuev, M. B., Krivopalov, V. P., Semikolenova, N. V., Peresypkina, E. V., Virovets, A. V., Sheludyakova, L. A., Lavrenova, L. G., Zakharov, V. A., and Larionov, S. V., *Russian J. Coord. Chem.*, **2006**, 32(3), 199–207.
24. Larionov, S. V., Savel'eva, Z. A., Semikolenova, N. V., Klevtsova, R. F., Glinskaya, L. A., Boguslavskii, E. G., Ikorskii, V. N., Zakharov, V. A., Popov, S. A., and Tkachev, A. V., *Russian J. Coord. Chem.*, **2007**, 33(6), 436–448.
25. Carlini, C., Giaiacopi, S., Marchetti, F., Pinzino, C., Raspolli Galletti, A. M., and Sbrana, G., *Organometallics*, **2006**, 25, 3659–3664.
26. Raspolli Galletti, A. M., Carlini, C., Giaiacopi, S., Martinelli, M., and Sbrana, G., *J. Polym. Sci. Pt. A Polym. Chem.*, **2007**, 45, 1134–1142.
27. Nagel, M., Paxton, W. F., Sen, A., Zakharov, L., and Rheingold, A. L., *Macromolecules*, **2004**, 37, 9305–9307.
28. Bao, F., Ma, R., and Jiao, Y., *Appl. Organomet. Chem.*, **2006**, 20, 368–374.
29. Bao, F., Ma, R., and Jiao, Y., *J. Coord. Chem.*, **2007**, 60, 557–566.
30. Lu, X.-Q., Bao, F., Kang, B.-S., Wu, Q., Liu, H.-Q., and Zhu, F.-M., *J. Organomet. Chem.*, **2006**, 691, 821–828.
31. Chen, F.-T., Tang, G.-R., and Jin, G.-X., *J. Organomet. Chem.*, **2007**, 692, 3435–3442.
32. Tang, G.-R., Lin, Y.-J., and Jin, G.-X., *J. Organomet. Chem.*, **2007**, 692, 4106–4112.
33. Janiak, C., and Lassahn, P. G., *J. Mol. Catal. A Chem.*, **2001**, 166, 193–209.

15

Ring-Opening Metathesis Polymerizations and Acyclic Diene Metathesis Polymerizations with Homogeneous Ruthenium and Molybdenum Catalysts and Initiators

ROBERT T. MATHERS
Department of Chemistry, Pennsylvania State University,
New Kensington, Pennsylvania 15068

15.1 INTRODUCTION

Well-defined ruthenium and molybdenum complexes that perform ring-opening metathesis polymerization (ROMP) and acyclic diene metathesis (ADMET) polymerizations have become increasingly popular. These well-defined catalysts and initiators embody many desirable characteristics, such as functional group tolerance, high catalyst activity, selectivity, and stability.[1–5] The popularity of well-defined metathesis catalysts underscores the prevalence of alkenes in polymer chemistry, organic synthesis, and asymmetric synthesis. The far-reaching influence of metathesis reactions has also permeated undergraduate laboratory experiments.[6–8] Additionally, the stability of commercially available catalysts makes them easy to acquire and store for reasonably long periods of time. Although a very large number of metathesis catalysts are known for areas such as cross metathesis (CM), ring-closing metathesis (RCM), asymmetric ring-opening metathesis (AROM), and tandem CM/RCM reactions,[9–11] this chapter will focus on the synthesis and application of

Handbook of Transition Metal Polymerization Catalysts Edited by Ray Hoff and Robert T. Mathers
Copyright © 2010 John Wiley & Sons, Inc.

certain homogeneous Grubbs and Schrock alkylidene complexes within the framework of ROMP and ADMET polymerizations. For clarity, the term *initiator* refers to a complex that remains attached to the polymer through initiation and propagation steps. The term *catalyst* is used to describe a complex that polymerizes more than one polymer chain per metal atom.

Many metathesis catalysts and initiators have the ability to polymerize a wide variety of cyclic and acyclic alkenes. During ROMP (Figure 15.1) and ADMET polymerizations (Figure 15.2), the initiation, propagation, and termination steps proceed through the well-known Chauvin mechanism involving a metallocyclobutane intermediate.[12] Regardless of the catalyst, certain requirements, recommendations, and outcomes for ROMP or ADMET

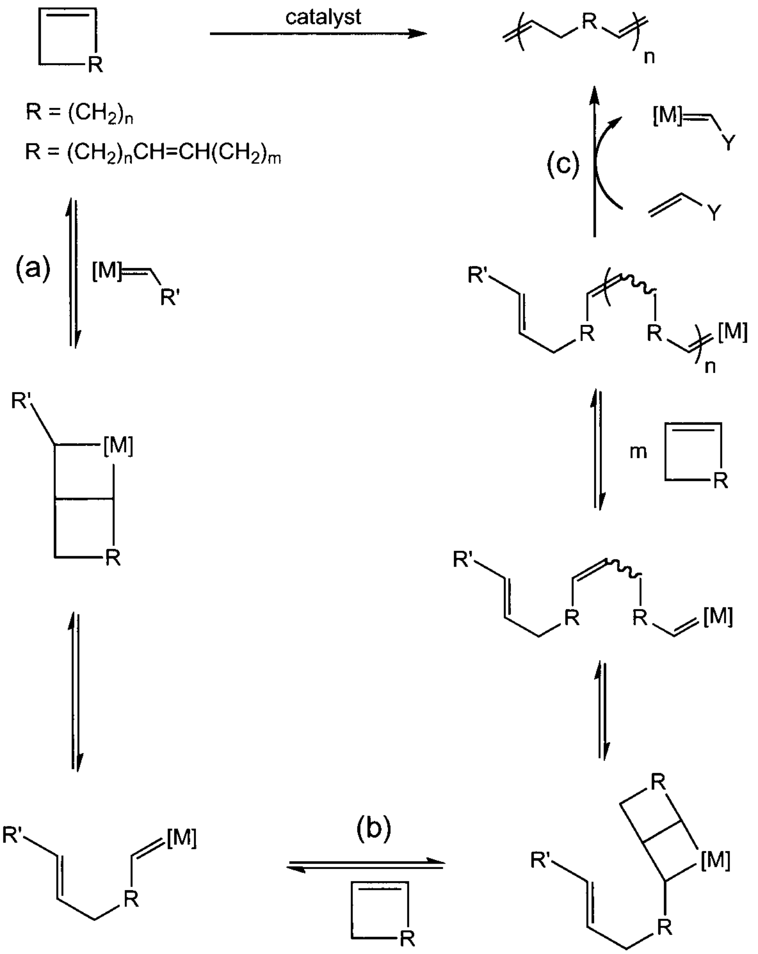

Figure 15.1 ROMP of cyclic alkenes with (*a*) initiation, (*b*) propagation, and (*c*) termination steps. The mechanism omits formation of cyclic oligomers and intermolecular reactions between growing polymer chains.

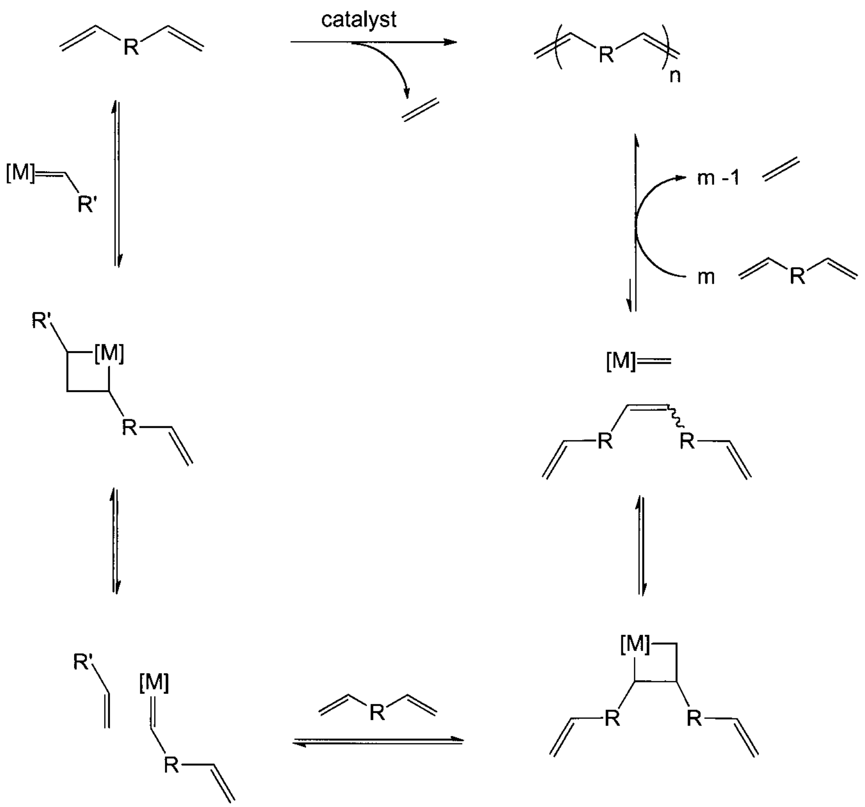

Figure 15.2 ADMET polymerization of α,ω-dienes. The mechanism omits the formation of cyclic oligomers and secondary metathesis reactions.

polymerizations can be summarized. The following recommendations will contribute to a successful ROMP experiment:

1. A sterically accessible alkene with sufficient ring strain will polymerize to give a reasonable yield on the laboratory timescale. If the ring strain of two cyclic alkenes is approximately equal, a disubstituted alkene would ring open faster than a trisubstituted alkene due to steric accessibility. Typically, the ring strain and polymerization yield for cyclic alkenes decreases as follows: cyclopropene > cyclobutene > norbornene > *cis*-cyclooctene > cycloheptene > cyclopentene.[13,14]
2. ROMP has a critical monomer concentration that is often inversely proportional to the ring strain. Conducting a polymerization below the necessary monomer concentration will result in the formation of oligomers.[15,16] For 1,5-cyclooctadiene, the critical monomer concentration is ~0.25 M.[17]

3. The molecular weight scales with the monomer-to-initiator ratio. If the ruthenium or molybdenum complex consumes all the monomer and remains attached to the polymer during the polymerization, then the number average molecular weight (M_n) is equal to grams of monomer divided by moles of initiator.
4. The molecular weight distribution (M_w/M_n) depends on the rate of initiation (k_i) relative to the rate of propagation (k_p).
5. The polymerization will follow chain growth kinetics, but over time some catalyst systems can undergo secondary metathesis reactions. Depending on the reactivity of the catalyst and the accessibility of the alkenes on the polymer backbone, these back-biting reactions can reduce the molecular weight and broaden the M_w/M_n value.

Recommendations for ADMET polymerizations are as follows:

1. ADMET polymerizations work best with terminal alkenes that form ethylene during the polymerization.[18] Although the mechanism in Figure 15.2 is reversible, the loss of volatile components drives the equilibrium toward the formation of polymer. Removal of ethylene is often accomplished by polymerizing neat or highly concentrated monomer solutions under vacuum to favor the formation of polymer. To compensate for increases in solution viscosity, the polymerizations are often heated to 60–70 °C.
2. High monomer purity (>99%) and high conversion ($p > 99\%$) are desirable for the synthesis of high-molecular-weight polymers.[5] Since ADMET polymerizations follow step growth kinetics, the number average degree of polymerization [$X_n = 1/(1 - p)$] and molecular weight distribution ($M_w/M_n = 1 + p$) can be estimated from the conversion (p).
3. Polar functional groups need to be two to three carbon atoms from the terminal alkene. The presence of allylic methyl groups[19] or vinyl ethers[20] results in adverse side reactions or catalyst decomposition.

Other parameters such as appropriate polymerization time, necessary temperature, tolerance for impurities (oxygen and water), and solvent polarity depend on the individual catalyst, although trends are observed for series of catalysts.

15.2 RUTHENIUM CATALYSTS

15.2.1 Synthesis

Figure 15.3 summarizes the development of several well-known ruthenium carbene complexes. Many of these synthetic strategies use $Cl_2Ru(PPh_3)_3$ or $[(COD)RuCl_2]_2$ as starting materials.[21,22] The synthesis of **1** allows the

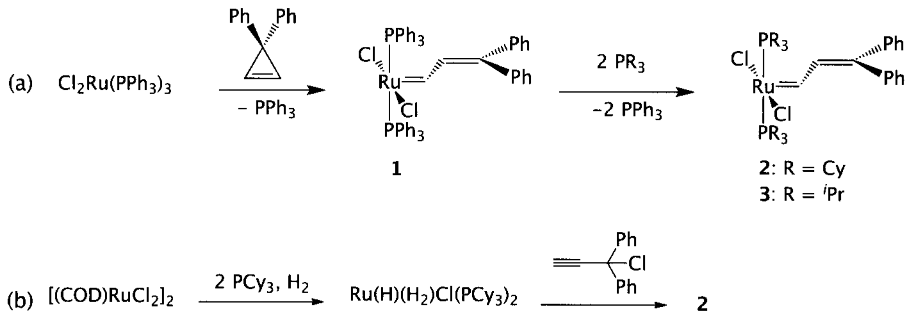

Figure 15.3 Synthesis of ruthenium carbene complexes (Cy = cyclohexyl, ^{i}Pr = isopropyl, Ph = phenyl).

ROMP of strained cyclic alkenes, such as norbornene.[23] Exchanging the PPh_3 ligands with trialkyl phosphines improved the catalyst performance. Compared to **1**, catalyst **2** has better solubility and increased stability in air and will polymerize a wider monomer range of cyclic alkenes, such as 1,5-cyclooctadiene, 7-oxanorbornene, and cyclopentene.[22] Figure 15.3*b* is an alternative one-pot procedure for the synthesis of **2**. This method with propargyl chloride reportedly gives high yields and works well with kilogram quantities.[21]

Figure 15.4 details the synthesis of the first-generation ruthenium carbene complexes using diazoalkanes.[24] This high-yield synthesis procedure represented a major breakthrough in the design of a well-defined ruthenium complex. The 16-electron ruthenium (II) complex has five-coordinate geometry comprised of two neutral trans ligands, two halides, and a carbene ligand. Since catalysts **4**–**7** have faster initiation rates than **1** (k_i/k_p for **6** = 9),[25] the M_w/M_n values are lower. If these catalysts undergo phosphine ligand exchange with trialkyl phosphines, the performance of **8** and **9** is further enhanced for ROMP (Table 15.1) and ADMET polymerizations (Table 15.2).[2] Since catalyst **9** has a much higher initiation rate (~1000 times) than **1**, the resulting

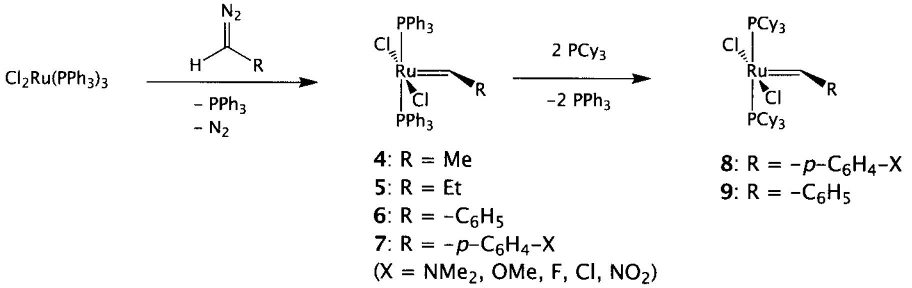

Figure 15.4 Synthesis of ruthenium carbene complexes using diazoalkanes (Cy = cyclohexyl, Ph = phenyl).

TABLE 15.1 ROMP Data for Ruthenium Carbene Complexes

Entry	Catalyst	Monomer	[Mon]/[Cat]	Temperature[a] (°C)	Time (h)	Yield (%)	M_n	M_w/M_n	References
1	**1**	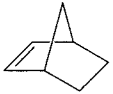	140	rt	—	—	38,640	1.32	23
2	**2**	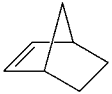	140	rt	24	95	81,500	2.65	23
3	**2**	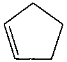	362	rt	24	67	56,820	1.95	22
4	**2**	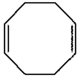	228	rt	24	74	36,670	2.42	22
5	**6–7**	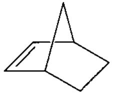	100	rt	1	95–99	31,600–42,300	1.04–1.10	25
6	**8–9**	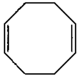	500	rt	2.5	96–99	57,900–63,200	1.56–1.67	25

7	**10**	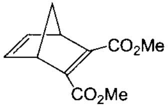	500	25	14	51	206,000	1.8	31
8	**12**	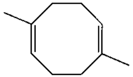	1,000	55	24	90	10,000	2.3	32
9	**12**	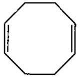	25,000	55	24	89	107,000	2.1	32
10	**12**	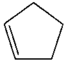	1,000	25	24	50	23,000	2.5	32
11	**13**	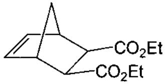	315	80	22	75	68,530	1.1	33
12	**17**	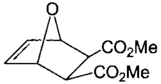	400	23	0.5	85	65,900	1.08	34

---

[a] rt = room temperature.

TABLE 15.2 ADMET Polymerization of α, ω-Diene Monomers

Entry	Catalyst	Monomer	[Mon]/[Cat]	Temperature (°C)	Time (days)	M_n	M_w/M_n	References
1	**9**	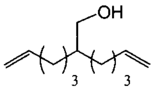	200	rt→70	2–3	38,000	1.6	40
2	**12**	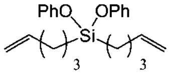	400	60–70	5	18,000	1.8	41
3	**12**	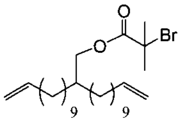	100	rt→65	5	17,000	2.05	42
4	**12**	1,9-decadiene	1000	70	4	43,930	1.8	43
5	**14**	1,9-decadiene	1000	70	4	9,390	1.9	43

polydispersity index (M_w/M_n) is lower. The value of M_w/M_n depends on the rate of initiation (k_i) relative to the rate of propagation (k_p).[26,27] Tables 15.1 and 15.2 compare the polymerization data for various monomers with ruthenium complexes.

Since the proposed mechanism for metathesis reactions involves phosphine dissociation to a 14-electron intermediate, the steric hindrance and Lewis basicity of the phosphine ligand influence the reactivity of the catalyst.[28–30] The activity of metathesis catalysts with phosphine ligands decreases as follows: $PCy_3 > P^iPr_3 > PPh_3$.[1] The trans influence of a trialkyl phosphine stabilizes the metallocyclobutane intermediate more effectively than triphenylphosphine.[28] Although it seems unlikely that the most basic bulky ligand would have the highest activity, less bulky alkyl phosphines have lower activity. For example, the strong coordination of trimethyl phosphine to the ruthenium center reduces the dissociation and catalyst activity.

A number of reports have detailed and elucidated termination, decomposition, and isomerization mechanisms that can occur during ROMP and ADMET polymerizations. Deliberate termination of catalyst activity during ROMP and ADMET polymerizations is usually accomplished by adding ethyl vinyl ether.[20] Other decomposition mechanisms involve the less stable methylidene intermediates that are found during cross-metathesis and ADMET reactions, which lead to the formation of a dinuclear ruthenium complex.[35] In some cases, ruthenium complexes with N-heterocyclic carbene ligands can undergo C–C and C–H bond activation of the mesityl group.[35,36] Olefin isomerization of alkenes on the polymer chain can occur during metathesis reactions.[37,38] The addition of 1,4-benzoquinone or acetic acid will suppress this isomerization.[39] Usually, 10 mol % of the additive will suffice. Some of these side reactions become more significant if high dilution, higher temperatures, or longer reaction times are required. Since ROMP is performed under higher concentrations and shorter times than RCM reactions, these side reactions are less problematic. However, as shown in Table 15.2, ADMET polymerizations do necessitate longer polymerization times to achieve high conversion due to the step growth kinetics.

Although reports of heterocyclic carbene ligands go back to the 1960s and 1970s,[44–47] the synthesis of the first stable heterocyclic carbene by Arduengo et al. occurred in 1991.[48] This crystalline adamantly-substituted N-heterocyclic carbene was followed by a large number of papers in the 1990s describing the use of NHC ligands for organometallic complexes.[31,49–51] The incorporation of NHC ligands with well-defined ruthenium complexes produced tremendous benefits. The resulting second-generation complexes (Figure 15.5) often contain unsaturated (**10**, **11**) or saturated (**12**) NHC ligands. The ortho substituents on the mesityl ligand are necessary for displacement of only one phosphine ligand. The use of isopropyl or cyclohexyl substituents on the NHC ligand results in the displacement of both phosphines (**10**).[31] Catalyst **11** was reported by Herrmann et al. and Nolan et al. and has activities which approach Schrock Mo catalysts.[52] The synthesis of **10**, **11**, and **12** gave a broader range

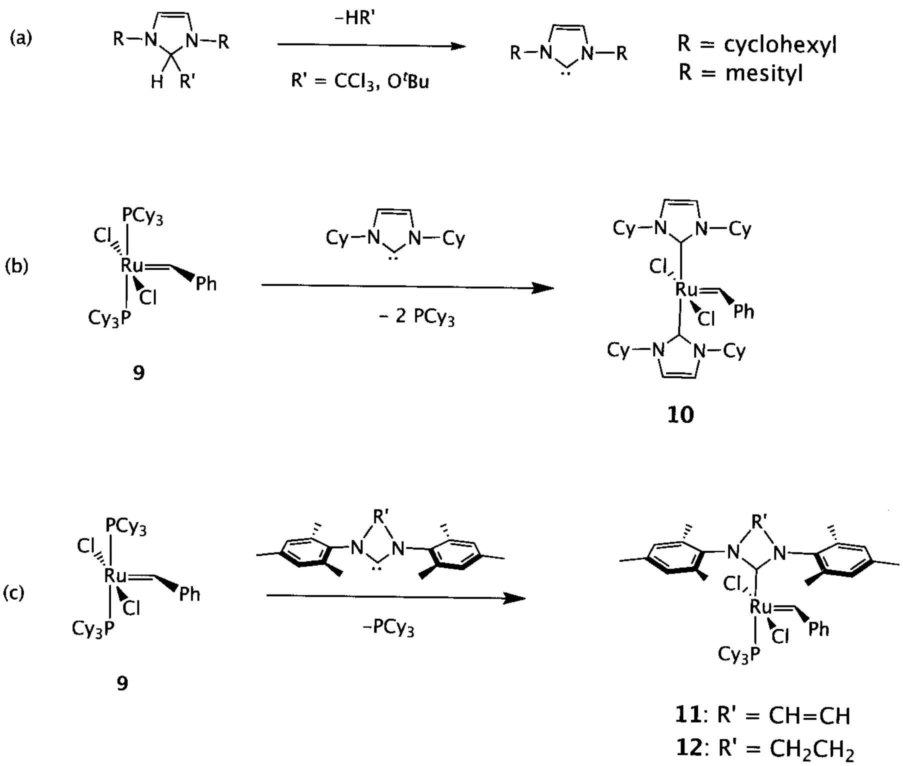

Figure 15.5 Synthesis of second-generation ruthenium carbene complexes.

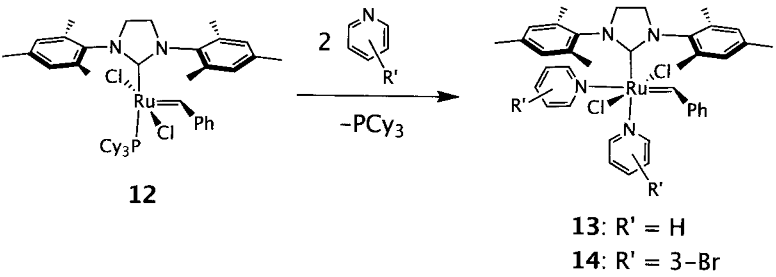

Figure 15.6 Synthesis of third-generation ruthenium catalysts.

of functional group tolerance and a much higher activity than **9**.[51,53–55] Additionally, **12** polymerizes[32] (see Table 15.1) and depolymerizes[56] trisubstituted alkenes.[57] Clever variations in the ligand design of **12** allow the synthesis of cyclic polybutadienes[17,58] or facilitate catalyst recovery.[59]

The synthesis of second-generation ruthenium complexes (**10–12**) led to further improvements. In Figure 15.6, complexes **13** and **14** result from the

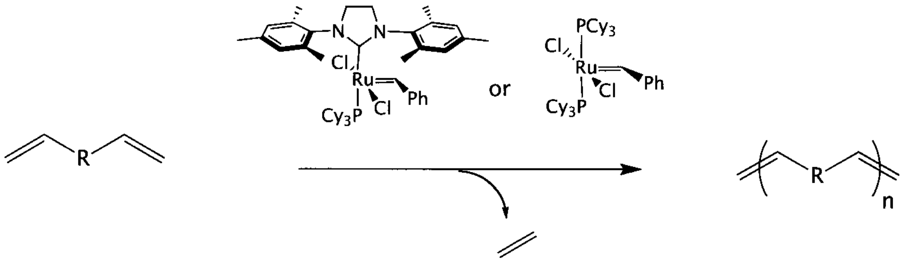

R = $(CH_2)_n$, GeR_2, $Si(OR)_2$, SnR_2,
$C(H)CH_2OH$, $C(CH_3)OH$, $C(H)OAc$,
$C(H)Cl$, $C(H)Ph$, $C(H)CO_2Me$, $C(H)CO_2Et$

Figure 15.7 ADMET polymerizations of α,ω-functionalized dienes.

replacement of a trialkyl phosphine with pyridine ligands.[60,61] As shown in Figure 15.7, ADMET polymerizations commonly employ **9**, **12**, and **14**. For the polymerization of 1,9-decadiene, these catalysts give higher conversions and larger molecular weight values than catalyst **2**. The resulting polymer molecular weight for different Ru catalysts decreased as follows: **12** > **9** > **14** > **2**. In some cases, the solubility of **14** in neat hydrocarbon monomers is limited. Because **14** is less soluble in cyclopentene and cycloheptene than **9** and **12**, low yields are obtained.[13] However, **14** is less prone to back-biting reactions which would otherwise broaden the M_w/M_n values.

15.2.2 Functional Group Tolerance

The ruthenium complexes tolerate a diverse assortment of functional groups, such as carboxylic acids, phenols, alcohols, esters, amides, and anhydrides.[54] Some functionalities, such as pyridine and acetonitrile, poison the catalytic activity of **9** but attenuate the reactivity of **12**. The addition of donor solvents to **12** alters the M_w and M_w/M_n values during the polymerization.[33] Polymerizations with **14** or with **12** in the presence of donor solvents (i.e., pyridine) usually give decreased yields and lower M_w values, but the resulting polymerizations have more narrow M_w/M_n values.[33] The coordination of pyridine reduces the rate of propagation but increases the rate of initiation. For example, complex **14** will undergo a faster initiation rate than first- and second-generation catalysts depicted in Figures 15.4 and 15.5. As a result, the third-generation complexes allow the synthesis of ABC triblock copolymers based on norbornene derivatives.[62]

In some cases, polymers with pendant alkenes can undergo postpolymerization reactions to yield functional polymers. A general functionalization method for alkenes (Figure 15.8) has been reported for amorphous and crystalline homopolymers and block copolymers.[63] The crystalline segments were based on *syndio*-polypropylene while the amorphorous blocks used ethylene/

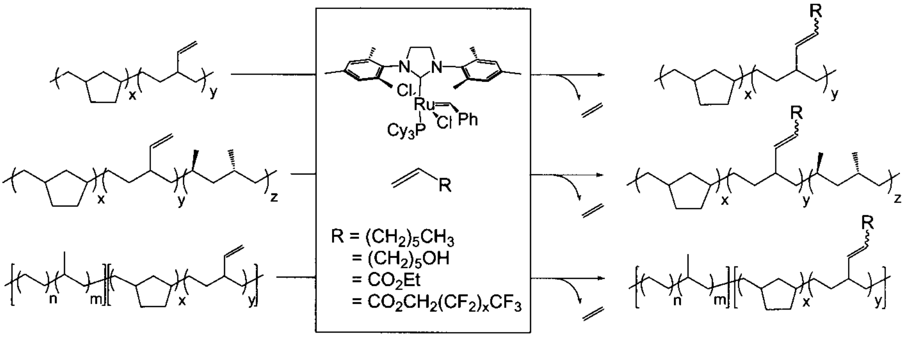

Figure 15.8 Cross-metathesis functionalization of polyolefins containing alkenes.

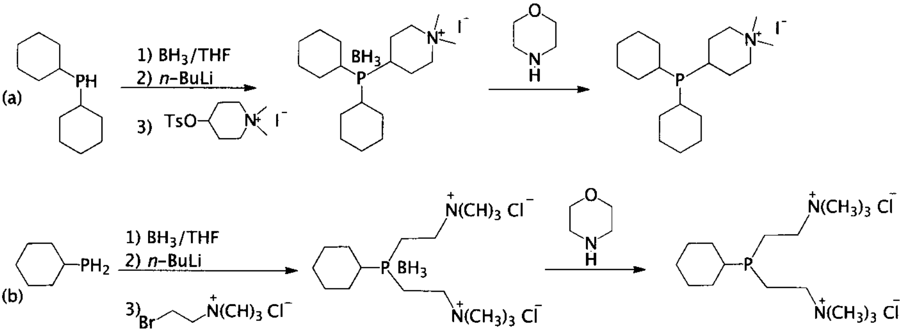

Figure 15.9 Synthesis of water-soluble phosphine ligands.

propylene copolymers. This cross-metathesis (CM) method generates ethylene as a by-product and allows the attachment of alkyl, alcohol, ester, and perfluoroalkyl groups onto the polymer. Since the alkenes are separated by three or more carbon atoms, cyclization is not preferred in the presence of CM partners. In the case of 1,2-polybutadiene, intramolecular reactions result from the proximity of adjacent vinyl groups.[64]

15.2.3 Non-Petroleum-Based Solvents

Water-Soluble Catalysts Water-soluble metathesis complexes are often based on first-, second-, or third-generation ruthenium catalysts. Most strategies involve ligand modification with ionic or neutral hydrophilic moieties that promote water solubility. Since coordination of trialkylphosphines results in robust and versatile catalysts, many water-soluble ligands are designed to give steric and electronic properties similar to tricyclohexyl phosphine. Figure 15.9

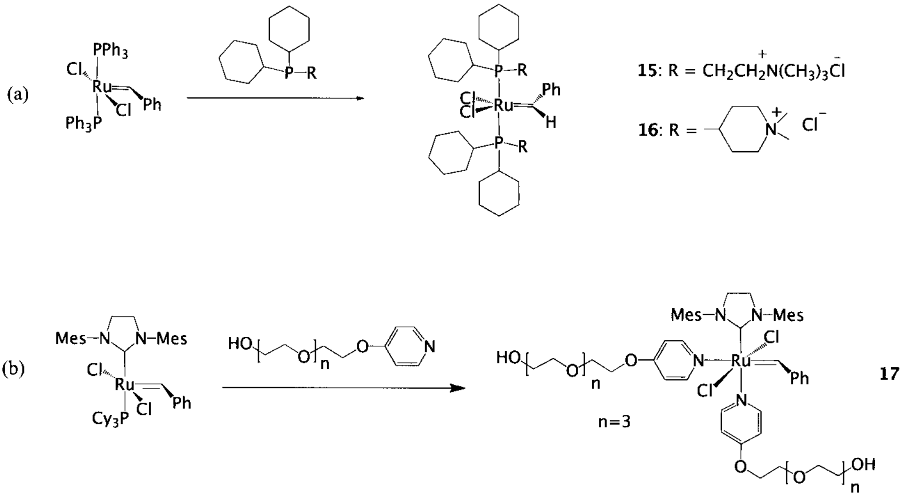

Figure 15.10 Examples of water-soluble metathesis catalysts using (*a*) phosphine ligands with ionic groups and (*b*) polyethylene glycol–substituted pyridines.

depicts the synthesis of ionic ligands. If dicyclohexylphosphine in Figure 15.9*a* is replaced with cyclohexylphosphine, then a difunctionalized ligand is obtained (Figure 15.9*b*). Common types of ionic ligands include ammonium[65–67] or sulfonate[68] groups. An alternative strategy (Figure 15.10) for water-soluble metathesis catalysts replaces the PCy_3 ligand with a poly(ethylene glycol)-substituted pyridine ligand.[34] The resulting amphiphilic catalyst (**17**) is soluble in water and organic solvents and polymerizes substituted 7-oxanorbornene monomers (see Table 15.1). Even though the tetraethylene glycol ligand on **17** is smaller than the polyethylene oxide (5000 g/mol) attached to NHC ligands,[59] the catalyst was soluble and effective despite the use of shorter poly(ethylene glycol) chains. Polymerizations in methylene chloride gave high yields (80–85%), narrow M_w/M_n values (1.04–1.08) and a linear correlation between molecular weight and monomer-to-catalyst ratio.

Monoterpene Polymerization Solvents Monoterpenes, such as *d*-limonene, are a broad class of naturally occurring compounds. *d*-Limonene is produced as a by-product of the citrus industry and can be used as a polymerization solvent.[69,70] During ROMP and ADMET polymerizations with **12**, the vinylidene alkene on *d*-limonene reacts with the growing polymer chain and causes chain transfer. Table 15.3 compares the effect of chain transfer on the molecular weight for the ROMP experiments. ROMP with hydrogenated *d*-limonene and toluene gave similar results. As shown in Figure 15.11, ADMET polymerizations of 1,5-hexadiene in *d*-limonene resulted in oligomers that were characterized by gas chromatography/mass spectrometry (GC/MS).

TABLE 15.3 ROMP in *d*-Limonene with Catalyst 12[69]

Entry	Monomer	Solvent	Yield (%)	M_w	M_w/M_n
1	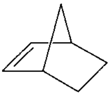	*d*-Limonene	90	26,300	1.3
2	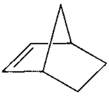	Toluene	88	80,300	1.7
3	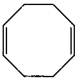	*d*-Limonene	83	11,100	2.4
4	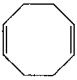	Hydrogenated *d*-Limonene	66	56,100	2.0
5	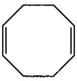	Toluene	68	57,900	2.6
6	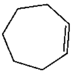	*d*-Limonene	61	6,320	2.0
7	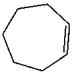	Toluene	50	50,500	2.6

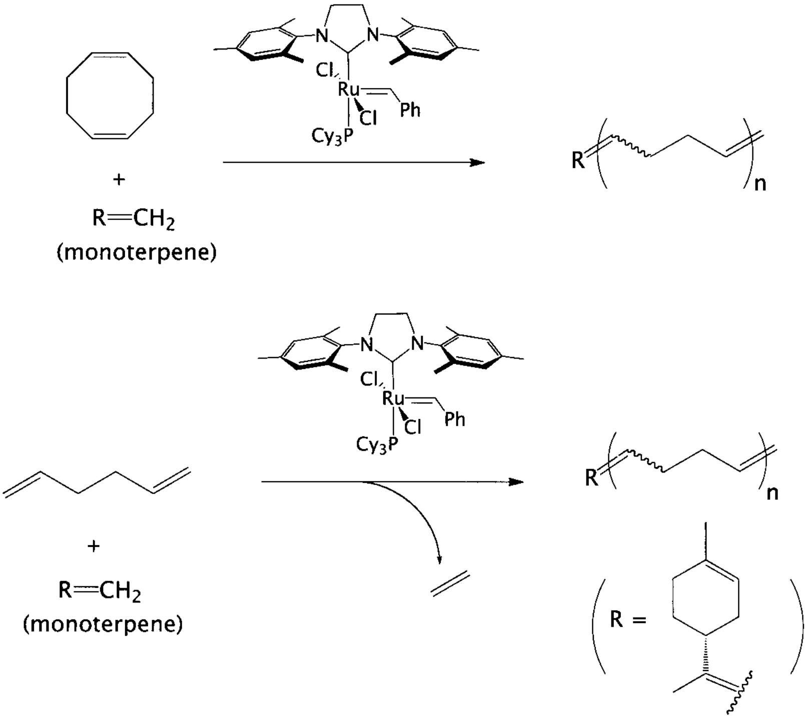

Figure 15.11 ROMP of 1,5-cyclooctadiene and ADMET polymerization of 1,5-hexadiene in *d*-limonene.

15.3 MOLYBDENUM COMPLEXES

15.3.1 Synthesis

Several methods for the formation of Mo alkylidene complexes are discussed in this section.[9,71–73] Although these and other methods have been detailed for various Mo complexes,[74,75] many of the syntheses share common features. For example, the imido ligand stabilizes the high oxidation state of Mo in a similar manner as oxo complexes, but with the additional ability to adjust steric hindrance surrounding the metal and prevent bimolecular decomposition. Adjusting the imido ligand and/or alkoxide ligands influences the electronic nature or the electrophilicity of the metal center and hence its activity in metathesis reactions.[76]

In Figure 15.12, the silylchlorides react with stoichiometric amounts of water formed during the reaction of the anilines with the Mo oxo complexes. Presumably, the generation of HCl in situ would be consumed by the triethylamine or lutidine. The silylchlorides also provide the chloride ligands in **18**. The reaction of alkyl[77] and aromatic[73] isocyanates is an alternative route to complex **18** that also allows high yield (95%). The resulting bisimido complex

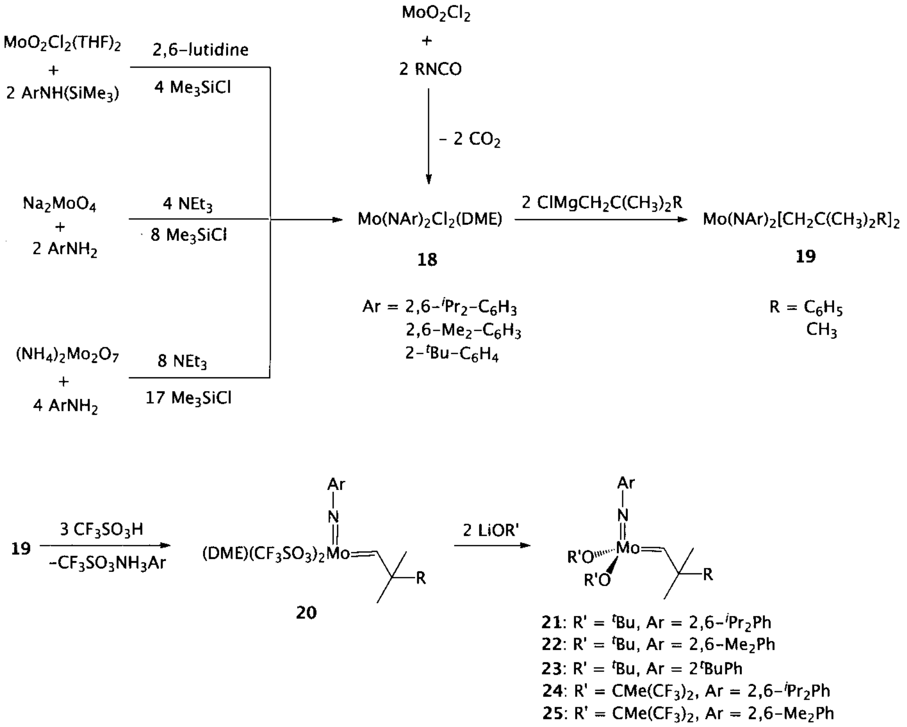

$MoO_2Cl_2(THF)_2$ + 2 $ArNH(SiMe_3)$
2,6-lutidine
4 Me_3SiCl
Na_2MoO_4 + 2 $ArNH_2$
4 NEt_3
8 Me_3SiCl
$(NH_4)_2Mo_2O_7$ + 4 $ArNH_2$
8 NEt_3
17 Me_3SiCl
MoO_2Cl_2 + 2 RNCO
- 2 CO_2
$Mo(NAr)_2Cl_2(DME)$
18
2 $ClMgCH_2C(CH_3)_2R$
$Mo(NAr)_2[CH_2C(CH_3)_2R]_2$
19
Ar = 2,6-^{i}Pr$_2$-C_6H_3
2,6-Me_2-C_6H_3
2-^{t}Bu-C_6H_4
R = C_6H_5
CH_3
19
3 CF_3SO_3H
-$CF_3SO_3NH_3Ar$
Ar
N
$(DME)(CF_3SO_3)_2Mo$
R
20
2 LiOR'
Ar
N
R'O
Mo
R'O
R
21: R' = ^{t}Bu, Ar = 2,6-^{i}Pr$_2$Ph
22: R' = ^{t}Bu, Ar = 2,6-Me_2Ph
23: R' = ^{t}Bu, Ar = 2^{t}BuPh
24: R' = $CMe(CF_3)_2$, Ar = 2,6-^{i}Pr$_2$Ph
25: R' = $CMe(CF_3)_2$, Ar = 2,6-Me_2Ph

Figure 15.12 Synthesis of Mo alkylidene complexes.

will react with Grignard or alkyllithium reagents. Treatment of **19** with triflic acid deprotects the metal center by removing one of the imido ligands to allow the reaction of lithium alkoxides. Using chiral BINAP ligands instead of the two alkoxide ligands affords asymmetric catalysts.[78,79]

Besides ROMP of strained alkenes and ADMET of terminal alkenes, the scope of polymerizable monomers includes 1-alkynes[80,81] and alkenes with electron-withdrawing substituents, such as perfluoroalkyls.[82] Although a number of catalysts are detailed in Figure 15.12, a complete list of catalysts suitable for RCM, AROM, and tandem CM/RCM can be found in comprehensive reviews.[9,10]

Schrock molybdenum catalysts and initiators offer several distinct advantages and possibilities during ROMP or ADMET polymerizations in terms of activity, selectivity, and control of tacticity. The activity and selectivity toward acyclic and cyclic olefins depend on the electron-withdrawing ability of alkoxides attached to the metal center. Changing the electronegativity of the alkoxide substituents influences the electrophilicity of the metal center. As a result, fluorinated alkoxides are more prone to react with internal alkenes than *tert*-butoxy.[83] Although the reactivity of **21** is lower than **24**, the selectivity is higher and less likely to undergo secondary metathesis reactions with alkenes on the polymer backbone. For ADMET polymerizations, the high activity requires less catalyst and shorter polymerization times than Ru metathesis catalysts. For ROMP, the selectivity of **21** results in trans polymers which are highly tactic and have reasonably high melting temperatures.[84] A number of mechanistic details regarding the excellent selectivity and control of tacticity have been thoroughly elucidated.[9] In general, the position of the alkylidene substituent with respect to the imide ligand influences the catalyst reactivity. The orientation of the alkylidene substituent is described as a syn or anti isomer. The syn isomer adopts a configuration with the imide ligand and the alkylidene substituent on the same side of the Mo alkylidene bond. As shown in Figures 15.12 and 15.13, the anti isomer is depicted for **21–26**. The anti isomer is more reactive and leads to trans alkenes in the polymer.

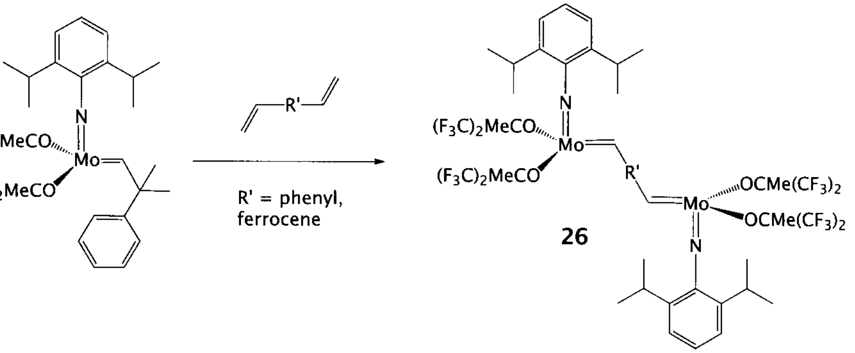

Figure 15.13 Synthesis of bimetallic alkylidene complexes.

The Mo complexes in Figure 15.12 allow interesting polymer architectures and chain-end functionalization. The fast rate of initiation for Mo complexes allows living ROMP for homopolymers and block copolymers with narrow molecular weight distributions.[83–86] Side-chain liquid crystalline polymers[87,88] and star block copolymers[89] are also known. End-group functionalization of the polymer chain results from Wittig-type reactions with aldehydes, such as benzaldehyde. Such chain-end functionalization reactions have been used for the synthesis of macromonomers using a ROMP mechanism.[90] The ADMET polymerization of substituted dienes (entry 4, Table 15.4) with **24** followed by hydrogenation is particularly useful for synthesizing polyethylene with well-defined branches.[91]

15.3.2 Functional Group Tolerance

Although Mo catalysts are less tolerant of certain polar functionalities than Ru catalysts, more chemical functionalities can usually be accommodated than their tungsten analogs. In general, polymerizations with Mo complexes need an inert atmosphere and anhydrous solvents. Mo catalysts have been used for ADMET polymerizations of substituted 1,4-divinylbenzenes[76] and functionalized 7-oxanorbornadienes. Catalyst **25** is the most active metathesis catalyst for disubstituted divinylbenzenes.[97] Initiator **21** will ring open substituted norbornenes with esters,[85] nitriles,[95] carbonates,[94] dithiocarbonates,[94] succinimides,[98] methoxy, and ether[98] functionalities. The polymerization of several functional monomers is detailed in Table 15.5. ADMET polymerizations allow the incorporation of monomers with thioethers,[99] germanium,[100] silicon,[101] and tin.[102] The Mo catalyst will tolerate some functional groups, such as acrylonitrile, which do not work well with Ru catalysts.[103]

15.3.3 Bimetallic Initiators

Bimetallic alkylidene complexes present opportunities for the synthesis of a wide variety of block copolymer architectures. The synthesis of bimetallic alkylidene complexes using divinylbenzene or divinylferrocene is shown in Figure 15.13. Initiator **26** has been reported for the synthesis of triblock copolymers[105,106] or ABA triblock copolymer with liquid crystal side chains.[107,108] The synthesis of ABA block copolymers benefits from the living nature of certain catalyst systems that result from complete and fast initiation relative to propagation. The choice of monomers, the presence of side chains, and any spacer between the monomer and side chain influence the glass transition temperature (T_g) of each polymer block.[87,104] If the T_g for A and B blocks are sufficiently different, then the resulting polymers have many uses as thermoplastic elastomers.

TABLE 15.4 ADMET Polymerization of Acyclic Dienes Using Schrock Catalyst 24

Entry	Monomer	[Mon]/[Cat]	Temperature (°C)	Time (h)	Yield (%)	M_n	M_w/M_n	Polymer	Reference
1	1,9-Decadiene	1,000	45	96	—	15,300	1.8	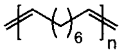	43
2	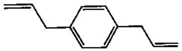	385	55	23	58	2,600	—	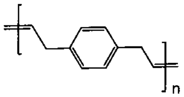	92
3	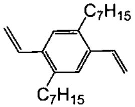	62	rt	24	99.9	3,370	1.8	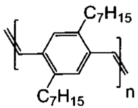	93
4	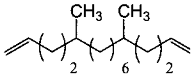	1,500	40	72	—	12,700	1.6	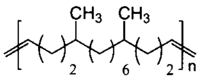	91

TABLE 15.5 Selected ROMP Examples of Functional Monomers Using Mo Catalysts

Entry	Catalyst	Monomer	[Mon]/[Cat]	Temperature (°C)	Time (min)	Yield (%)	M_n	M_w/M_n	References
1	**21**	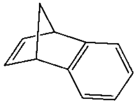	200	22	30	—	28,560	1.05	84
2	**21**	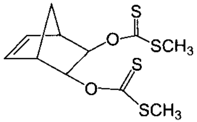	100	rt	90	90	43,000	1.4	94
3	**21**	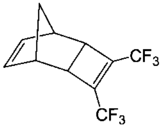	~80	rt	60	—	22,800	1.05	95
4	**24**	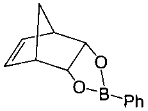	268	rt	10	95	115,000	2.0	96

15.4 SUMMARY

ROMP and ADMET polymerizations have enjoyed a rich and extensive history of catalyst development, polymer synthesis, and polymer characterization. The 2005 Nobel Prize in Chemistry highlights the significance of metathesis reactions. The development of ruthenium and molybdenum catalysts has given researchers many options for polymerizing functional monomers. In this regard, ruthenium and molybdenum metathesis catalysts each have their own merits. Although current metathesis catalysts represent excellent advances from the ill-defined catalysts of the 1970s, the design of new metathesis catalysts will continue to play a central role. Perhaps metathesis catalysts based on more economical metals, such as iron, will emerge. In relation to green chemistry, the efficiency of well-defined metathesis catalysts and the ability to design catalyst systems which are soluble in non-petroleum-based solvents are two important facets of ROMP and ADMET polymerizations.

REFERENCES

1. Trnka, T. M., and Grubbs, R. H., *Acc. Chem. Res.*, **2001**, 34, 18–29.
2. Grubbs, R. H., Ed., *Handbook of Metathesis. Applications in Polymer Synthesis*, Vol. 3, 1st ed., Wiley-VCH, Weinheim, 2003.
3. Grubbs, R. H., and Khosravi, E., *Mater. Sci. Technol.*, **1999**, 20, 65–104.
4. Schrock, R. R., *NATO ASI Ser. C Math. Phys. Sci.*, **1998**, 506, 1–27.
5. Buchmeiser, M. R., *Chem. Rev.*, **2000**, 100, 1565–1604.
6. Taber, D. F., and Frankowski, K. J., *J. Chem. Ed.*, **2006**, 83, 283–284.
7. France, M. B., and Uffelman, E. S., *J. Chem. Ed.*, **1999**, 76, 661–665.
8. Viswanathan, T., and Jethmalani, J., *J. Chem. Ed.*, **1993**, 70, 165–167.
9. Schrock, R. R., and Hoveyda, A. H., *Angew. Chem. Int. Ed.*, **2003**, 42, 4592–4633.
10. Furstner, A., *Angew. Chem. Int. Ed.*, **2000**, 39, 3012–3043.
11. Grubbs, R. H., and Chang, S., *Tetrahedron*, **1998**, 54, 4413–4450.
12. (a) Herisson, J. L., and Chauvin, Y., *Makromol. Chem.*, **1970**, 141, 161–176; (b) Katz, T. J., and McGinnis, J., *J. Am. Chem. Soc.*, **1975**, 97, 1592–1594; (c) Grubbs, R. H., *Tetrahedron*, **2004**, 60, 7117–7140.
13. (a) Hejl, A., Scherman, O. A., and Grubbs, R. H., *Macromolecules*, **2005**, 38, 7214–7218; (b) Singh, R., Czekelius, C., and Schrock, R. R., *Macromolecules*, **2006**, 39, 1316–1317.
14. Schleyer, R. v. R., Williams, J. E., and Blanchard, K. R., *J. Am. Chem. Soc.*, **1970**, 92, 2377–2386.
15. Chen, Z.-R., Claverie, J. P., Grubbs, R. H., and Kornfield, J. A., *Macromolecules*, **1995**, 28, 2147–2154.
16. Reif, L., and Hoecker, H., *Macromolecules*, **1984**, 17, 952–956.
17. Bielawski, C. W., Benitez, D., and Grubbs, R. H., *J. Am. Chem. Soc.*, **2003**, 125, 8424–8425.

18. Brzezinska, K., Wolfe, P. S., Watson, M. D., and Wagener, K. B., *Macromol. Chem. Phys.*, **1996**, 197, 2065–2074.
19. Courchay, F. C., Baughman, T. W., and Wagener, K. B., *J. Organomet. Chem.*, **2006**, 691, 585–594.
20. Wu, Z., Nguyen, S. T., Grubbs, R. H., and Ziller, J. W., *J. Am. Chem. Soc.*, **1995**, 117, 5503–5511.
21. Wilhelm, T. E., Belderrain, T. R., Brown, S. N., and Grubbs, R. H., *Organometallics*, **1997**, 16, 3867–3869.
22. Nguyen, S. T., and Grubbs, R. H., *J. Am. Chem. Soc.*, **1993**, 115, 9858–9859.
23. (a) Nguyen, S. T., Johnson, L. K., and Grubbs, R. H., *J. Am. Chem. Soc.*, **1992**, 114, 3974–3975; (b) Nguyen, S. T., Ph.D. Thesis, California Institute of Technology, 1995.
24. Schwab, P., France, M. B., Ziller, J. W., and Grubbs, R. H., *Angew. Chem. Int. Ed.*, **1995**, 34, 2039–2041.
25. Schwab, P., Grubbs, R. H., and Ziller, J. W., *J. Am. Chem. Soc.*, **1996**, 118, 100–110.
26. Quirk, R. P., and Lee, B., *Polym. Int.*, **1992**, 27, 359.
27. Quirk, R. P., and Hsieh, H. L., *Anionic Polymerization: Principles and Practical Applications*, Marcel Dekker, New York, **1996**.
28. Dias, E. L., Nguyen, S. T., and Grubbs, R. H., *J. Am. Chem. Soc.*, **1997**, 119, 3887–3897.
29. Grubbs, R. H., and Trnka, T. M., in *Ruthenium in Organic Synthesis*, Murahashi, S.-I., Ed., Wiley-VCH, Weinheim, 2004, pp. 153–177.
30. Aagaard, O. M., Meier, R. J., and Buda, F., *J. Am. Chem. Soc.*, **1998**, 120, 7174 -7182.
31. Frenzel, U., Weskamp, T., Kohl, F. J., Schattenmann, W. C., Nuyken, O., and Herrmann, W. A., *J. Organomet. Chem.*, **1999**, 586, 263–265.
32. Bielawski, C. W., and Grubbs, R. H., *Angew. Chem. Int. Ed.*, **2000**, 39, 2903–2906.
33. Slugovc, C., Demel, S., and Stelzer, F., *Chem. Commun.*, **2002**, 2572–2573.
34. Breitenkamp, K., and Emrick, T., *J. Polym. Sci. Pt. A Polym. Chem.*, **2005**, 43, 5715–5721.
35. Hong, S. H., Day, M. W., and Grubbs, R. H., *J. Am. Chem. Soc.*, **2004**, 126, 7414–7415.
36. Jazzar, R. F. R., Macgregor, S. A., Mahon, M. F., Richards, S. P., and Whittlesey, M. K., *J. Am. Chem. Soc.*, **2002**, 124, 4944–4945.
37. Courchay, F. C., Sworen, J. C., Ghiviriga, I., Abboud, K. A., and Wagener, K. B., *Organometallics*, **2006**, 25, 6074–6086.
38. Schmidt, B., *J. Mol. Catal. A Chem.*, **2006**, 254, 53–57.
39. Hong, S. H., Sanders, D. P., Lee, C. W., and Grubbs, R. H., *J. Am. Chem. Soc.*, **2005**, 127, 17160–17161.
40. Valenti, D. J., and Wagener, K. B., *Macromolecules*, **1998**, 31, 2764–2773.
41. Church, A. C., Pawlow, J. H., and Wagener, K. B., *Macromol. Chem. Phys.*, **2003**, 204, 32–39.
42. O'Donnell, P. M., and Wagener, K. B., *J. Polym. Sci. Pt. A Polym. Chem.*, **2003**, 41, 2816–2827.

43. Lehman, S. E., Wagener, K. B., and Akvan, S., *J. Polym. Sci. Pt. A Polym. Chem.*, **2005**, 43, 6134–6145.
44. Metzger, J., Larive, H., Dennilauler, R., Baralle, R., and Gaurat, C., *Bull. Soc. Chim. Fr.*, **1964**, 11, 2857–2867.
45. Cardin, D. J., Cetinkaya, B., and Lappert, M. F., *Chem. Rev.*, **1972**, 5, 545–574.
46. Oefele, K., *J. Organomet. Chem.*, **1968**, 12, P42–P43.
47. Oefele, K., and Kreiter, C. G., *Chem. Ber.*, **1972**, 105, 529–540.
48. Arduengo, A. J., Harlow, R. L., and Kline, M., *J. Am. Chem. Soc.*, **1991**, 113, 361–363.
49. Herrmann, W. A., and Kocher, C., *Angew. Chem. Int. Ed.*, **1997**, 36, 2162–2187.
50. Herrmann, W. A., Elison, M., Fischer, J., Koecher, C., and Artus, G. R. J., *Angew. Chem. Int. Ed.*, **1995**, 34, 2371–2374.
51. Huang, J., Stevens, E. D., Nolan, S. P., and Petersen, J. L., *J. Am. Chem. Soc.*, **1999**, 121, 2674–2678.
52. Bourgeois, D., Pancrazi, A., Nolan, S. P., and Prunet, J., *J. Organomet. Chem.*, **2002**, 643/644, 247–252.
53. Trnka, T. M., Morgan, J. P., Sanford, M. S., Wilhelm, T. E., Scholl, M., Choi, T.-L., Ding, S., Day, M. W., and Grubbs, R. H., *J. Am. Chem. Soc.*, **2003**, 125, 2546–2558.
54. Chatterjee, A. K., Choi, T.-L., Sanders, D. P., and Grubbs, R. H., *J. Am. Chem. Soc.*, **2003**, 125, 11360–11370.
55. Mol, J. C., *Top. Catal.*, **2004**, 27, 97–104.
56. Craig, S. W., Manzer, J. A., and Coughlin, E. B., *Macromolecules*, **2001**, 34, 7929–7931.
57. Chatterjee, A. K., Sanders, D. P., and Grubbs, R. H., *Org. Lett.*, **2002**, 4, 1939–1942.
58. Bielawski, C. W., Benitez, D., and Grubbs, R. H., *Science (Washington, DC, United States)*, **2002**, 297, 2041–2044.
59. Gallivan, J. P., Jordan, J. P., and Grubbs, R. H., *Tet. Lett.*, **2005**, 46, 2577–2580.
60. Love, J. A., Morgan, J. P., Trnka, T. M., and Grubbs, R. H., *Angew. Chem. Int. Ed.*, **2002**, 41, 4035–4037.
61. Sanford, M. S., Love, J. A., and Grubbs, R. H., *Organometallics*, **2001**, 20, 5314–5318.
62. Slugovc, C., Riegler, S., Hayn, G., Saf, R., and Stelzer, F., *Macromol. Rapid Commun.*, **2003**, 24, 435–439.
63. Mathers, R. T., and Coates, G. W., *Chem. Commun.*, **2004**, 422–423.
64. Coates, G. W., and Grubbs, R. H., *J. Am. Chem. Soc.*, **1996**, 118, 229–230.
65. Lynn, D. M., Mohr, B., and Grubbs, R. H., *J. Am. Chem. Soc.*, **1998**, 120, 1627–1628.
66. Mohr, B., Lynn, D. M., and Grubbs, R. H., *Organometallics*, **1996**, 15, 4317–4325.
67. Lynn, D. M., Mohr, B., Grubbs, R. H., Henling, L. M., and Day, M. W., *J. Am. Chem. Soc.*, **2000**, 122, 6601–6609.
68. Saoud, M., Romerosa, A., and Peruzzini, M., *Organometallics*, **2000**, 19, 4005–4007.
69. Mathers, R. T., McMahon, K. C., Damodaran, K., Retarides, C. J., and Kelley, D. J., *Macromolecules*, **2006**, 39, 8982–8986.

70. Mathers, R. T., and Damodaran, K., *J. Polym. Sci. Pt. A Polym. Chem.*, **2007**, 45, 3150–3165.
71. Schrock, R. R., Murdzek, J. S., Bazan, G. C., Robbins, J., DiMare, M., and O'Regan, M., *J. Am. Chem. Soc.*, **1990**, 112, 3875–3886.
72. Fox, H. H., Yap, K. B., Robbins, J., Cai, S., and Schrock, R. R., *Inorg. Chem.*, **1992**, 31, 2287–2289.
73. Bryson, N., Youinou, M.-T., and Osborn, J. A., *Organometallics*, **1991**, 10, 3389–3392.
74. Murdzek, J. S., and Schrock, R. R., *Organometallics*, **1987**, 6, 1373–1374.
75. Hiya, K., Nakayama, Y., and Yasuda, H., *Macromolecules*, **2003**, 36, 7916–7922.
76. Thorn-Csanyi, E., and Zilles, J. U., *J. Mol. Catal. A Chem.*, **2002**, 190, 85–100.
77. Schoettel, G., Kress, J., and Osborn, J. A., *J.Chem. Soc. Chem. Commun.*, **1989**, 1062.
78. La, D. S., Sattely, E. S., Ford, J. G., Schrock, R. R., and Hoveyda, A. H., *J. Am. Chem. Soc.*, **2001**, 123, 7767–7778.
79. Cefalo, D. R., Kiely, A. F., Wuchrer, M., Jamieson, J. Y., Schrock, R. R., and Hoveyda, A. H., *J. Am. Chem. Soc.*, **2001**, 123, 3139–3140.
80. Schrock, R. R., *NATO ASI Ser. C Math. Phys. Sci.*, **1998**, 506, 357–380.
81. Czekelius, C., Hafer, J., Tonzetich, Z. J., Schrock, R. R., Christensen, R. L., and Mueller, P., *J. Am. Chem. Soc.*, **2006**, 128, 16664–16675.
82. Schrock, R. R., Krouse, S. A., Knoll, K., Feldman, J., Murdzek, J. S., and Yang, D. C., *J. Mol. Catal.*, **1988**, 46, 243–253.
83. Schrock, R. R., *Acc. Chem. Res.*, **1990**, 23, 158–165.
84. Bazan, G. C., Khosravi, E., Schrock, R. R., Feast, W. J., Gibson, V. C., O'Reagen, M. B., Thomas, J. K., and Davis, W. M., *J. Am. Chem. Soc.*, **1990**, 112, 8378–8387.
85. Murdzek, J. S., and Schrock, R. R., *Macromolecules*, **1987**, 20, 2640–2642.
86. Wewerka, K., Wewerka, A., Stelzer, F., Gallot, B., Andruzzi, L., and Galli, G., *Macromol. Rapid Commun.*, **2003**, 24, 906–910.
87. Pugh, C., and Kiste, A. L., *Prog. Polym. Sci.*, **1997**, 22, 601–691.
88. Pugh, C., Zhu, P., Kim, G., Zheng, J. X., Rubal, M. J., and Cheng, S. Z. D., *J. Polym. Sci. Pt. A Polym. Chem.*, **2006**, 44, 4076–4087.
89. Saunders, R. S., Cohen, R. E., Wong, S. J., and Schrock, R. R., *Macromolecules*, **1992**, 25, 2055–2057.
90. Nomura, K., Takahashi, S., and Imanishi, Y., *Macromolecules*, **2001**, 34, 4712–4723.
91. Baughman, T. W., Sworen, J. C., and Wagener, K. B., *Macromolecules*, **2006**, 39, 5028–5036.
92. Steiger, D., Weder, C., and Smith, P., *Macromolecules*, **1999**, 32, 5391–5398.
93. Thorn-Csanyi, E., and Kraxner, P., *Macromol. Rapid Commun.*, **1995**, 16, 147–153.
94. Schimetta, M., and Stelzer, F., *Macromolecules*, **1994**, 27, 3769–3772.
95. Saunders, R. S., *Macromolecules*, **1995**, 28, 4347–4349.
96. Wolfe, P. S., and Wagener, K. B., *Macromolecules*, **1999**, 32, 7961–7967.

97. Peetz, R. M., Sinnwell, V., and Thorn-Csanyi, E., *J. Mol. Catal. A Chem.*, **2006**, 254, 165–173.
98. Bazan, G. C., Schrock, R. R., Cho, H.-N., and Gibson, V. C., *Macromolecules*, **1991**, 24, 4495–4502.
99. O'Gara, J. E., Portmess, J. D., and Wagener, K. B., *Macromolecules*, **1993**, 26, 2837–2841.
100. Gomez, F. J., and Wagener, K. B., *J. Organomet. Chem.*, **1999**, 592, 271–277.
101. Smith, D. W., and Wagener, K. B., *Macromolecules*, **1993**, 26, 1633–1642.
102. Wolfe, P. S., Gomez, F. J., and Wagener, K. B., *Macromolecules*, **1997**, 30, 714–717.
103. Crowe, W. E., and Goldberg, D. R., *J. Am. Chem. Soc.*, **1995**, 117, 5162–5163.
104. Komiya, Z., Pugh, C., and Schrock, R. R., *Macromolecules*, **1992**, 25, 3609–3616.
105. Schrock, R. R., Gabert, A. J., Singh, R., and Hock, A. S., *Organometallics*, **2005**, 24, 5058–5066.
106. Mayershofer, M. G., Nuyken, O., and Buchmeiser, M. R., *Macromolecules*, **2006**, 39, 2452–2459.
107. Gabert, A. J., Verploegen, E., Hammond, P. T., and Schrock, R. R., *Macromolecules*, **2006**, 39, 3993–4000.
108. Singh, R., Verploegen, E., Hammond, P. T., and Schrock, R. R., *Macromolecules*, **2006**, 39, 8241–8249.

16 Cobalt Ziegler–Natta Catalysts for Synthesis of Poly-*cis*-1,4-Butadiene

RAY HOFF
Adjunct Faculty, Roosevelt University, Schaumburg, Illinois 60173

16.1 INTRODUCTION

This chapter deals with cobalt catalysts for the polymerization of the conjugated 1,3-butadiene. Cobalt catalyst systems are among the four most important Ziegler–Natta catalysts for butadiene coordination polymerization. The other three compositions contain titanium, nickel, or neodymium. The content of this chapter is based partly on literature and partly on laboratory work done 40 years ago at B. F. Goodrich. It is not a complete survey or an in-depth study of any cobalt catalyst type. Instead, it is a brief reminder that polymerization catalyst chemists in general can learn much from synthetic rubber research.

The poly-monoolefins, mainly high-density polyethylene resins and isotactic polypropylene resins, comprise products of the plastics industry, while the polymers of conjugated dienes, mainly polyisoprene and polybutadiene, are chiefly of interest to the synthetic rubber industry. Polybutadiene, however, also has important uses as an ingredient in high-impact polystyrene and acrylonitrile–butadiene–styrene plastics.

Two of the main factors that are prominent in many published studies of polyolefin catalysis are catalyst productivity and catalyst reactivity. These may be expressed as the yield of polyethylene or polypropylene per unit mass of catalyst and the reactivity as productivity per reaction time unit, frequently grams per gram catalyst per hour. Productivity must be at least about 5000 based on total catalyst weight in order for a catalyst to be of any value in a competitive industry. With catalysts capable of acceptable and comparable productivity, polymer properties become decisive. In many polybutadiene catalyst research papers and patents, however, catalyst productivity is seldom

---

Handbook of Transition Metal Polymerization Catalysts Edited by Ray Hoff and Robert T. Mathers
Copyright © 2010 John Wiley & Sons, Inc.

emphasized despite its obvious importance. In addition, a discussion of long-chain branching and chain-end groups is almost entirely missing.

Like the monoolefin catalysts, transition metal catalysts for dienes have origins in the work of Giulio Natta and Karl Ziegler in the 1950s. Important early advances were achieved by the research groups working with the U.S. government synthetic rubber program during World War II.[1] Although cobalt Ziegler–Natta catalysts have been known for about a half century and currently there is greater research interest in neodymium catalysts for butadiene polymerization,[2] cobalt catalysts remain industrially significant. The Lanxess Corporation and Ube Industries, according to their Internet websites, manufacture synthetic rubber products with cobalt catalysts.[3] In a somewhat rare citation of catalyst productivities for transition metals, cobalt systems (40,000–160,000 g/g Co) were higher than very good neodymium systems (7000–15,000 g/g Nd).[2] However, current research emphasis on neodymium catalysts focuses on aspects that are not accessible by cobalt catalysts.

Polybutadiene microstructure may contain *cis*-1,4-, *trans*-1,4-, or 1,2-polybutadiene, and in the case of 1,2 the structure may be syndiotacitic, isotactic, or atactic. Of course, it is conceptually possible for the microstructure to have an intermingling of these structures. Furthermore, polybutadiene samples may also contain chain branching plus some undesirable cross-linking as well.

Natta, in his Nobel Prize address,[4] reported the preparation of polybutadiene samples with each of the four stereochemically pure structures (>99% pure) and gave their crystalline melting points as follows:

cis-1,4-Polybutadiene	2 °C
trans-1,4-Polybutadiene	146 °C (high-temperature crystalline form)
Isotactic 1,2-polybutadiene	126 °C
Syndiotactic 1,2-polybutadiene	156 °C

Cobalt catalyst variations which yield high cis, high trans, and high 1,2-polybutadiene are known. In this case, high cis or trans means greater than about 95%, and the total of cis, trans, and 1,2 in any sample is 100%. Ube Industries offers an interesting product with a continuous high *cis*-1,4-polybutadiene phase having particles of syndiotactic poly-1,2-butadiene as a dispersed phase. The polymers of both phases are made with cobalt catalysts.[3b] Further discussion of these catalyst variations are provided later in this chapter.

Even 40 years ago it was realized that high *cis*-polybutadiene was an outstanding polymer for making tires, conveyor belts, hoses, and similar products. Accordingly, early research on cobalt catalysts focused on formulations which could lead to higher and higher *cis*-1,4 content while possessing acceptable reactivity and yielding proper molecular weight and molecular weight distribution with low gel content. Sam E. Horne, Jr. of B. F. Goodrich research, working with information from Ziegler and a combination of trialkylaluminum and titanium tetrachloride, was first to synthesize *cis*-1,4-polyisoprene that matched the main polymer structure of natural tree rubber.[1,2] On the other hand, Horne could not make high *cis*-1,4-polybutadiene with these two reagents, although he tried them in various ratios. Before the emergence of neodymium catalysts,[2] cobalt, nickel, and titanium catalysts were the most important types for *cis*-1,4-polybutadiene. The titanium system was an aluminum alkyl compound plus titanium tetraiodide, or at least a reagent that supplied iodide.[5] An early version of the nickel catalyst comprised a nickel compound, an alkyl aluminum compound, and a boron trifluoride–ether complex.[6] One of the first cobalt catalysts was simply R_3Al plus a cobalt chloride, but research workers at Goodrich-Gulf Chemical Company, the Shell Oil Company, and Montecatini soon introduced improvements.

The mechanisms proposed for coordination polymerization of conjugated dienes are related to the Cossee mechanism[7] that has been offered for alkenes. In the Porri model[8] for dienes, an active site has a η^3 allyl bond between the transition metal atom and the growing polymer chain instead of the σ bond in the Cossee mechanism. The allyl group has two carbon atoms at which an incoming monomer can insert: carbon 1 and carbon 3. Insertion at carbon atom 1 results in 1,4 incorporation and insertion at carbon 3 gives 1,2 incorporation. The incoming monomer coordinates η^4 cis (instead of π in Cossee), and cis or trans incorporation depends on whether the monomer is in the anti or syn form, respectively. Taube[9] has also contributed to the understanding of the mechanism of conjugated diene polymerization.

16.2 PROPERTIES

Historically, researchers in industrial synthetic rubber research have relied on intrinsic viscosity (IV) or a single-point solution viscosity measurement, which they call DSV, or dilute solution viscosity, as an indication of the suitability of polymer samples for an intended use. Frequently, a bulk viscosity test, the Mooney viscosity [American Society for Testing and Materials (ASTM) 1646-04], is used in conjunction with DSV or sometimes intrinsic viscosity. ASTM D3616.95 describes a procedure for determining DSV along with swelling index and percent gel. The DSV is measured on the solution after the gel has been removed. However, the term DSV often means just inherent viscosity, or the logarithmic viscosity number recommended by the International Union of Pure and Applied Chemistry (IUAPC): $\eta_{inh} = \ln \eta_{rel}/C$. The solvent, temperature, and concentration should be stated. In the ASTM procedure solution viscosity is measured for the soluble part of 0.39–0.41 g in 100 mL of toluene in the case *cis*-1,4-polybutadiene and the temperature is 25 °C. There is a note in ASTM D 3616.955 that distinguishes between soft gel, which has a large swelling index, and hard gels, which have low swelling indexes. Soft gel breaks up during processing but hard gels do not. An example of the combined use of IV and Mooney viscosity may be found in a patent by Lasis and McCracken,[10] and an illustration of the relationship can be seen in Figure 16.1. The value of IV and Mooney viscosity are often linearly related, and in a family of polybu-

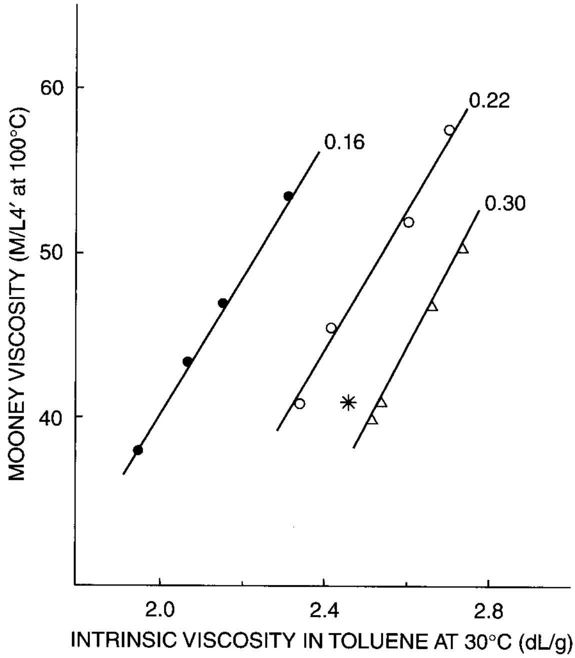

Figure 16.1 Linear relations between Mooney viscosity and intrinsic viscosity for *cis*-1,4-polybutadiene samples having different branching contents.

tadienes having similar molecular weight distributions more linear polymers have higher intrinsic viscosity values than branched polymers of the same Mooney viscosity.

DSV and Mooney viscosity are also often used in conjunction. Linearity in one case[11] is defined by DSV/(Mooney/3.50)$^{0.3623}$, which unfortunately is printed incorrectly in the reference.

Although high *cis*-1,4-polybutadiene is noncrystalline at ambient temperatures (mp = 2 °C), it crystallizes when strained and provides a very useful material for rubber tires. On the other hard, high *trans*-polybutadiene is a hard crystalline material at ambient temperature but, because of its double bonds can be cross-linked or vulcanized and become elastomeric. Syndiotactic 1,2-polybutadiene is also thermoplastic rather than elastomeric, but it also is readily cross-linked.

16.3 BEVERAGE BOTTLES AS POLYMERIZATION REACTORS

In the 1960s at the B. F. Goodrich laboratory catalyst chemists used glass crown cap beverage bottles as vessels for butadiene polymerization. The procedure was a boon because many experiments could be done conveniently and variables scanned rapidly. Similar procedures were also used in other synthetic rubber locations. Because it may be of value to catalyst chemists, a brief description of the Goodrich procedure is given here. Since the polymerization bottles were rotated end-over-end for mixing, there is a complete difference in agitation from common industrial stirred reactors. Also butadiene concentration could not be kept constant.

Before use the bottles were rinsed with distilled water and oven-dried for no less than overnight at about 120 °C. Bottles were cooled to room temperature under flowing nitrogen, then sealed with crown caps and specially designed rubber liners. Solvents, monomer, and all catalyst components and any modifiers were injected by syringe needles through the liner. The metal caps had at least one hole of about $\frac{1}{16}$ in. diameter to allow passage of the needles. The tips of the needles were of the noncoring, closed bevel design. After all reagents were injected, a second cap without a hole was affixed over the first metal cap. Bottles were placed in appropriate metal shields, clamped in place on a rotator in a constant-temperature bath, and rotated end over end for the desired reaction time. The shields and the constant-temperature bath were designed to accommodate the bottle reactors, making the whole setup efficient. As many as 12 reactions could be run at the same time, and part of the convenience was that the bottles were used only once.

Bottles of the same kind were used for laboratory storage of butadiene, which was transferred from a cylinder kept in a pilot plant area using a syringe *needle and special adaptors. If necessary, during butadiene transfer, a second needle was used to vent pressure. Bottles containing monomer were stored in* a refrigerator.

16.4 COBALT CATALYST VARIATIONS FOR HIGH POLY-CIS-1,4-BUTADIENE

The most important Ziegler–Natta cobalt catalyst formulations for butadiene polymerization are listed in Table 16.1. Six of these formulations are listed in a table in the book by Witold Kuran.[12]

16.4.1 $CoCl_2$–$R_{1.1-1.9}AlCl_{1.9-1.1}$

Like all Ziegler–Natta catalysts, the cobalt systems are deactivated by large amounts of water and polar solvents. As a result, the medium of choice is generally a pure hydrocarbon solvent or a mixture of hydrocarbons. Probably the earliest attempts to polymerize butadiene with cobalt compounds were simple combinations of cobalt chloride and aluminum alkyl compounds, and these did control the microstructure so that high *cis*-1,4 polymers were formed. Tucker,[13] however, observed that a soluble reaction product of isoBu$AlCl_2$ and $CoCl_2$, although extremely reactive, produced gelled masses that caused difficulty with agitation and control of temperature, and the products themselves were difficult to process. On the other hand, combinations of isoBu$_2$AlCl and

TABLE 16.1 Main Cobalt Catalysts for Polybutadiene

Number	Formulation	Predominant Microstructure	References
1	$CoCl_2$–isoBu$AlCl_2$	*cis*-1,4	13
2	$CoCl_2$–isoBu$_2$AlCl	*cis*-1,4	13
3	$CoCl_2$–$R_{1.1\text{–}1.9}AlCl_{1.9\text{–}1.1}$	*cis*-1,4	13
4	$CoCl_2$–$AlCl_3$–C_6H_6–$Et_3Al_2Cl_3$–H_2O	*cis*-1,4	18
5	$CoCl_2$–R_3Al soluble product	*cis*-1,4	22
6	$CoCl_2$–pyridine–Et_2AlCl	*cis*-1,4	15
7	$CoCl_2$·2Py–Et_2AlCl–H_2O	*cis*-1,4	12
8	$CoCl_2$·2Py–R_3Al	1,2	12
9	$CoCl_2$·2Py–R_3Al–H_2O	1,2	12
10	$Co(NO)_2Cl$–Et_2AlCl	*cis*-1,4	17
11	Co(Acac)$_2$–CS_2–R_3Al	1,2	12, 29, 31
12	Co(Acac)$_3$–Et_3Al	1,2	12
13	Co(Acac)$_3$–CS_2–R_3Al	1,2	12, 29, 31
14	$CoCl_2$(PisoPrPh$_2$)–MAO	1,2	28
15	Co(Acac)$_2$–Ph_3P–Et_3Al–H_2O	1,2	27
16	$Co(C_7H_{15}COO)_2$–Ph_3P–Et_3Al–H_2O	1,2	27
17	Co(Acac)$_2$–Et_3P–Et_3Al–H_2O	1,2	27
18	$Co(AlCl_4)$–Et_3Al, or Et_2AlCl or $EtAlCl_2$	*cis*-1,4	26, 34
19	Co octoate–Et_3AL–*p*-dodecylphenol–*o*-phenylphenol	75% *trans*-1,4, 22% 1,2	30

$CoCl_2$ did not form completely soluble systems but slurries and polymerization emanated at least in part from the particles in the slurries. The polymer-coated particles tended to agglomerate leading to reactor fouling. To overcome these problems Tucker proposed formulation 3 in Table 16.1. In one example he added diisobutylaluminum chloride and isobutylaluminum chloride separately, but the overall composition amounted to isoBu$_{1.2}$AlCl$_{1.8}$. The procedure started with the preparation of a mixture of anhydrous $CoCl_2$ and neat isoBuAlCl$_2$, which resulted in a deep blue supernatant liquid composed of Co (0.30 mmol/g) and Al (6.22 mmol/g). The diisobutylaluminum chloride was first added to a benzene solution of butadiene; then a quantity of the blue cobalt solution was added. After 3.4 h at 10 °C the conversion was 44% and the polymer microstructure was 94% cis, 4% trans, and 2% 1,2 by infrared spectroscopy. The yield of polybutadiene was 4800 g/g Co and only 65 g/g of isoBu$_{1.2}$AlCl$_{1.8}$. Other productivity values from this Tucker patent are provided in Table 16.2.

Horne[14] published several interrelations of data for the Tucker formulation, and in particular he found for $Et_{1.5}AlCl_{1.5}$ and a soluble cobalt compound (Al/Co = 450) that the polymerization reaction was first order in butadiene. From his kinetic data and experimental conditions the values in Table 16.3 are available or can be calculated. The cobalt productivity increases with the Al/Co ratio, and the rate increases with temperature but the *cis*-1,4 content decreases moderately but significantly with temperature. The optimum temperature

TABLE 16.2 Polymerization with $CoCl_2$–$R_{1.1–1.9}AlCl_{1.9–1.1}$ Catalyst Systems[a]

Part 1

Experiment No.	Co (mmol)	$RAlCl_2$ (mmol)	Ratio[b]	Time (h)	Percent Conversion	DSV	% *cis*-1,4
1	*0.023*	*0.9*	*4.3*	*21*	*13*	*7.86*	*98*
2	0.094	3.6	1.1	4.8	43	4.38	95
3	0.023	0.9	4.3	3	43	3.85	93
4	0.023	0.9	4.3	21	77	4.04	89

Part 2[c]

Experiment No.	Al/Co	g PBD/g Co	g PBD/g Co·h[c]	g PBD/g Al
1	210	9,600	460	100
2	70	7,800	1,600	240
3	210	32,000	11,000	330
4	210	57,000	2,700	590

[a] All polymerization run at 5 °C with 100 g butadiene and 900 g benzene. All polymer products had less than 5% gel.

[b] $isoBu_2AlCl/isoBuAlCl_2$.

[c] Average over total reaction time.

Source: Values calculated from ref. 13.

TABLE 16.3 Rate Data and Catalyst Productivities for $Et_3Al_2Cl_3$ and Cobalt Octoate in Benzene[a]

T (°C)	*k*[b]	Time to 95% conversion[c] (h)	g/g Co·h	g/g Al·h	% *cis*-1,4
5	0.00201	24	2,800	13	97
25	0.00733	6.7	10,100	49	96
50	0.0288	1.7	40,000	190	95
75	0.0513	0.97	70,100	340	91

[a] Derived from ref. 14. Al = 4.5 mmol/L, Co = 0.01 mmol/L, butadiene ($t = 0$) 0.7 M, g PBD/g Co at 95% conversion = 68,000.

[b] Apparent first order in monomer, min^{-1}.

[c] Assumes that temperature control is maintained up to this conversion.

appears to be between 25 and 50 °C. The molecular weight is also temperature dependent evidently because some transfer reaction has a greater activation energy than the propagation rate. At the same Al/Co = 450, ethyl aluminum sesquichloride and initial butadiene concentration of 0.7 M in benzene, M_n is about 5.0×10^5 at 10 °C and about 1.2×10^5 at 75 °C. Molecular weight appears to be linearly dependent on butadiene concentration over accessible ranges in laboratory reactions. Horne maintained that, in commercial-size reactors, both batch and continuous polymerization at constant monomer concentration yielded the same molecular weight distribution. In addition, significant differences from laboratory bottle polymerizations were not reported. It does not appear likely that all of these statements can be true.

Tucker's data do indicate that maintaining the overall Cl/Al ratio less than 2 does tends to prevent the formation of gel. The reason may be that cationic reaction between chains is prevented.

16.4.2 $CoCl_2$–pyridine–Et_2AlCl and $Co(NO)_2Cl$–Et_2AlCl

The use of the solutions of $CoCl_2$ in $RAlCl_2$ compounds is not so convenient because of instability.[14] Inventors have proposed various hydrocarbon-soluble compounds as replacements. Marullo and his co-inventors[15] found that the benzene-soluble complexes of cobalt dichloride with pyridine and other amines made active catalysts with dialkylaluminum chloride for synthesizing poly-*cis*-1,4-butadiene. Most of their work was done with the pyridine complex with which they achieved a productivity of as high as about 26,000 g/g Co and intrinsic viscosity (dL/g) from 1.55 to 7.32 (toluene, 26 °C). Using the Mark–Houwink constants of Johnson and Wolfangel[16] ($a = 0.80$, $K = 1.53 \times 10^{-4}$), the corresponding molecular weights are 1.08×10^5 and 7.20×10^5 g/mol. It is significant that the cobalt chloride–pyridine compounds product has high cis with haloaluminum alkyls but high 1,2 with trialkylaluminum compounds (see formulations 7 and 8 in Table 16.1). Natta, Porri, and Fiore favored the use of $Co(NO)_2Cl$ because of its low solubility in both aromatic and aliphatic hydrocarbons and because its crystals resembled those of β-$TiCl_3$.[17]

16.4.3 Co Octoate–Et_2AlCl–H_2O

Cobalt octoate, $[CH_3(CH_2)_3CH(C_2H_5)COO]_2$ Co, and cobalt naphthenate, the cobalt complex of the acids formed by oxidation of the naphtha fraction of crude oil [Chemical Abstract Services (CAS) number 61739-51-3], are commercially available low-cost materials that are soluble in hydrocarbons. There is no halide in these soluble compounds, and polymerization of 1,3-butadiene with R_2AlCl compounds as cocatalysts does not occur when monomer and solvent are anhydrous. With the addition of small amounts of water, one of the most important cobalt systems for the synthesis of poly-1,4-*cis*-butadiene results. This system is of particular interest because (1) it is the one apparently adapted by Ube Industries for its special products,[18] (2) it has peculiar dependence upon the presence of aromatic solvents and additives,[19] and (3) its component, the reaction products of Et_2AlCl and water, is almost certainly of complex structure similar to the MAO used with metallocene catalysts in alkene polymerization.[20]

Although in one of the earliest disclosures[21] of this formulation the focus was on the total water in the system as the important factor, later work has brought out the significance of the molar ratio H_2O/Et_2AlCl. Horne,[14] in his review of diene polymerization catalysts, showed graphically that molecular weight, reactivity, and the 1,4-*cis* content all vary with this ratio. Since water and aluminum alkyl compounds react rapidly, the functioning catalyst component is without doubt the reaction products of H_2O and Et_2AlCl, and the exact composition of these products will depend on method of mixing and the speed at which an equilibrium composition is attained. Horne found that there was a maximum in the butadiene polymerization rate at the water-to-aluminum ratio of about 0.1, that molecular weight increased to 0.25 and then leveled off, and that the cis content increased from about 80% with little water to 95–96% at the ratio of 0.1. All of these observations were made upon polymerization studies at 25 °C. The dependence on the amount of aromatic solvent is shown by the maximum M_n being 800,000 when the solvent is a mixture of benzene and butane with 50% of the volume benzene but only 400,000 with 30% benzene. Apparently, the aromatic solvent somehow suppresses a transfer rate constant or enhances a propagation rate. If Horne's data are correct, it may be that the Porri mechanism is only an approximation to the actual case.

Gippin,[22] who dried benzene–butadiene mixtures over calcium hydride for 24 h at room temperature, also found optimum reactivity at low ratios, in the range of 0.05–0.15. His data are from reactions run at 5 °C for 19 h with $Al/Co = 500$. With $H_2O/Al = 0.10$ conversion was 92.8% and the *cis*-1,4 content was 97.8% by IR spectroscopy. The yield was about 4×10^4 g of polymer/g cobalt. While the high cis content that results at low polymerization temperatures is an advantage, both the low reaction temperature and the long reaction time are economic detriments.

Lasis and McCracken[10] argue on a theoretical basis that for a given Mooney viscosity more linear *cis*-1,4-polybutadiene samples have larger intrinsic viscosities. The argument involves the Mark–Houwink exponent. Consequently, using Mooney–IV plots like those in Figure 16.1, they found that the linearity of the polybutadiene made with the cobalt octoate–Et_2AlCl–H_2O system varies with the water/Al ratio. The numbers at the ends of the slanted lines in Figure 16.1 are the water/Et_2AlCl ratios of different polymerization experiments, and hence the most linear high *cis*-polybutadiene samples are made in reactions in which the ratio is 0.3.

According to the results of Storr and his colleagues,[20b] the composition of the reaction mixture from water (0.1 mol) and diethylaluminum chloride (1.0 mol) will be dialuminoxane (0.1 mol, EtClAl–O–AlClEt) and of Et_2AlCl (0.8 mol), while larger amounts of water (0.3 mol) and diethylaluminum chloride (1.0 mol) will give more EtClAl–O–AlClEt (0.3 mol) and less Et_2AlCl (0.4 mol). The former mixture gives the fastest butadiene polymerization according to Horne[14] and the latter the most linear polybutadiene by the argument of Lasis and McCracken.[10] One of Horne's graphs shows lower conversion at the ratio of about 0.5. In this case the product mixture might contain almost all EtClAl–O–AlClEt. Complications may arise when diethyl aluminum chloride is added to a dilute solution of water in benzene, butadiene, or some other organic liquid. Local excess of water may result in the formation of polyaluminoxane structures, the occurrence of which depends on the addition rate and the concentration of the aluminum reagent solution, the temperature, and the efficiency of mixing.

With the normal amounts of Et_2AlCl in the catalyst system, a water content of less than 0.036 g water/1000 g (about 2 mmol) of solvent is enough to produce the 0.1 ratio. Poor reproducibility with cobalt catalysts was reported in the works of the 1950s and 1960s, and the presence of adventitious water could easily have been the cause.

In a 1980 patent[16a] Lasis wrote, "The prior art clearly shows that an aromatic compound, especially benzene, must form a major component of the diluents in order to achieve a satisfactory rate of polymerization and in order to produce a linear polymer—in the absence of benzene, the polymerization is slow and the polymer is highly branched." Already when this patent was filed there were health concerns about exposure to low atmospheric concentration of benzene, and the Lasis solution was to substitute cyclohexane together with molecular weight modifiers for all or a major part of the benzene such that the solvent contains no more than 20% benzene. A careful comparison of the DSV and Mooney data in this 1980 patent reveals, however, that polymerizations with cyclohexane as the major solvent component did not yield polybutadiene as free of branching as Lasis and McCracken[10] in their 1972 patent where benzene was the major solvent.

There is an enlightening set of observations in an invention apparently aimed at allowing the use of hexane as solvent.[20] The inventors showed that, if water is present when diethylaluminum chloride is added, the polymerization proceeds fine in benzene. When replacing benzene with increasing volume fractions of hexane, reactivity decreases to commercially insignificant levels. When the water is added after the diethylaluminum chloride, hexane is as good as benzene. The tests upon which these observations were made were done according to a set of mixing procedures. However, when the rate at which the Et_2AlCl solution was added to a combination of hexane, butadiene, and water was increased, the polymerization continued just as well as if benzene were the solvent. It appears that benzene is a more forgiving solvent with respect to orders of addition and mixing. When the combination of Et_2AlCl, water, and a soluble cobalt compound produce a pale yellow but particle-free solution, an active catalyst for butadiene polymerization is formed. However, if the catalyst procedure results in turbidity or even a flocculent precipitate, the system may be completely inactive.

In Lasis's 1980 patent[19a] and in work by Chemische Werke Huls[23] aimed at making hexane a replacement for benzene, molecular weight regulators were used. It is known[24] that alkenes, both with terminal and internal double bonds, are weak transfer agents. A variety of nonconjugated dienes have been tested and three of the most powerful are allene, 1,2-butadiene, and 1,5-cyclooctadiene. The Dow Chemical Company[25] even filed a patent application for a process to make 1,4-*cis*-polybutadiene with bimodal molecular weight distribution by adding 1,5-cyclooctadiene to the second reactor of a two-reactor cascade. In Figure 16.2 the effect of 1,5-cyclooctadiene on Mooney

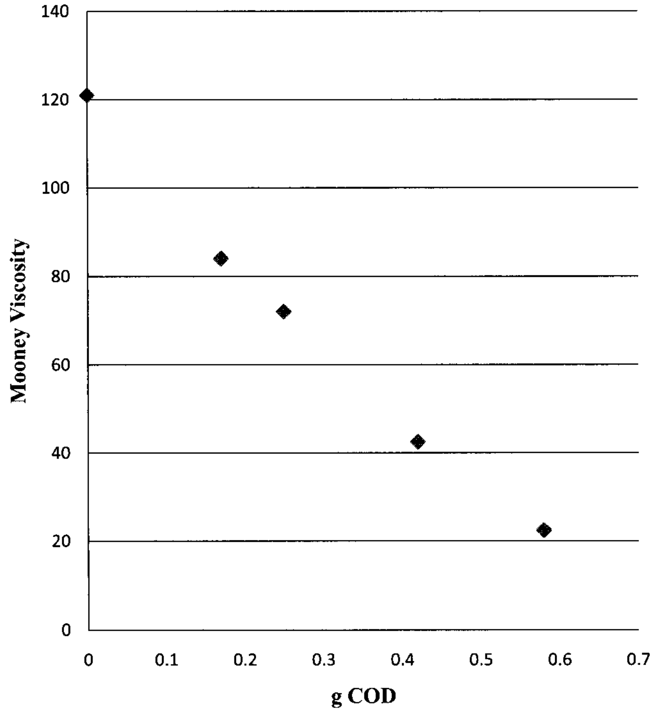

Figure 16.2 Effect of 1,5-cyclooctadiene on Mooney viscosity.

viscosity is shown. The effect of different concentrations of allene on the intrinsic viscosity of *cis*-1,4-polybutadiene made with the catalyst formulation $CoCl_2$–$AlCl_3$–$Et_3Al_2Cl_3$ is shown in Figure 16.3. In general, the relative effectiveness of the known transfer reagents in 1,3-butadiene polymerization is the same for all the formulations of cobalt Ziegler–Natta catalysts and similar also for Ziegler–Natta nickel catalysts.

16.4.4 Poly-*cis*-1,4-Butadiene–Syndiotactic Poly-1,2-Butadiene Composites

Ube Industries researchers[29] showed that syndiotactic poly-1,2- polybutadiene with 95% 1,2 content or higher and high crystalline content could be prepared with the catalyst formulations 11 and 13 in Table 16.1. Actually the cobalt compounds are not restricted to the two acetylacetonates but other hydrocarbon-soluble compounds such as cobalt octoate, cobalt naphenate, and cobalt(II) chloride–amine complexes may be substituted. When the 1,2 content is above 98.5%, the crystalline melting point by DSC is 204–210 °C. Natta's melting point of 126 °C obviously refers to a 1,2-polybutadiene with lower molecular order. As shown by nuclear magnetic resonance (NMR), the fraction of racemic pentads in this polymer increases from 54 to 90%, and the melting point increases from 121 to 198 °C.[32] In a second development[33] it was found

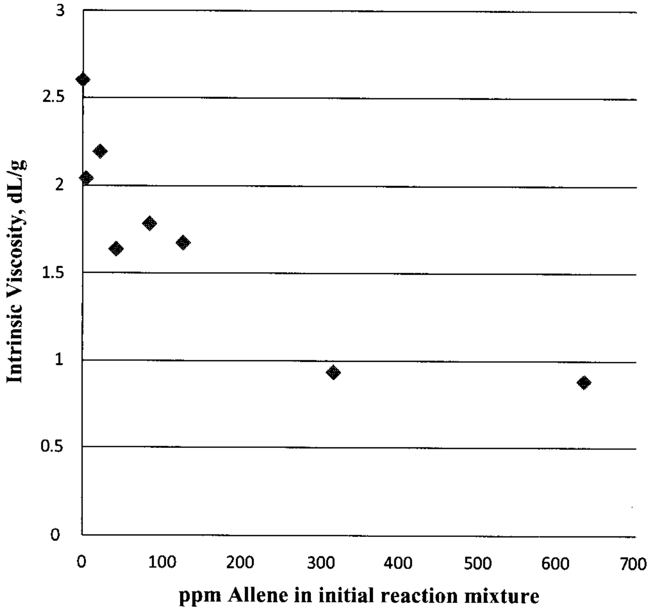

Figure 16.3 Effect of allene on intrinsic viscosity of *cis*-1,4-polybutadiene.

that the syndiotactic polymer and high *cis*-1,4-polybutadiene could be produced at the same time with a mixture of cobalt catalyst formulations. Thus, when a mixture of 85 g butadiene in 860 mL benzene reacted with water 1.5 mmol, Et_2AlCl, ethylaluminoxane 4 mmol as Al, 0.043 mmol cobalt octoate, and 0.13 mmole CS_2, the yield in 30 min at 40 °C was 37 g of total polymer. The insoluble fraction in boiling hexane (4.7 g, 12.7%) was isotactic polybutadiene with a melting point of 205 °C. The hexane-soluble portion was poly-*cis*-1,4-polybutadiene (96.8% cis, $[\eta]$ = 2.60 toluene at 30 °C). Remarkably, a cis-producing formulation and a 1,2-producing formulation act independently, sharing a portion of the cobalt octoate. A further refinement is the solution blending of the *cis*-vinyl polymer composite prepared with the mixed cobalt catalyst with additional cis polymer, which can be made with cobalt octoate–Et_2AlCl–H_2O or a neodymium catalyst. The polymer composite made in this way is claimed to have many advantages in tire applications, including better acceptance of silica reinforcement.[34]

REFERENCES

1. McMillan, F. M., *The Chain Straighteners*, Macmillan, London, 1979, Chapter 10.
2. Friebe, L., Nuyken, O., and Obrecht, W., *Adv. Polym. Sci.*, **2006**, 204, 1.
3. (a) http://techcenter.lanxess.com/pbr/americas/en/products/description/429/index.jsp?pid=429; (b) http://northamerica.ube.com/page.php?pageid=8.

4. Natta, G., *Science*, **1965**, 147, 261.
5. (a) Smith, D. R., and Zelinski, R. P., Phillips Petroleum Company, U.S. Patent No. 3,178,402, 1965; (b) Smith, D. R., and Zelinski, R. P., Phillips Petroleum Company, U.S. Patent No. 3,976,630, 1976.
6. Ueda, K., Ouishi, A., Yoshimoto, T., Hosono, J., and Maeda, Bridgestone Tire Company, U.S. Patent No. 3,170,905, 1965.
7. (a) Cossee, P., *J. Catal.*, **1964**, 3, 80–88; (b) Ivin, K. J., Rooney, J. J., Stewart, C. D., Green, M. L. H., and Mahtab, R., *J. Chem. Soc. Chem. Commun.*, **1978**, 604–606.
8. Porri, L., Guarrusso, A., and Ricci, G., *Prog. Polym. Sci.*, **1991**, 16, 405.
9. Taube, R., in *Metalorganic Catalysts for Synthesis and Polymerization*, Kaminsky, W., Ed., Springer-Verlag, Berlin, 1999.
10. Lasis, E., and McCracken, N. J., Polymer Corp., U.S. Patent No. 3,646,001, 1972.
11. Knauf, T. F., and Osman, A., Polymer Rubber Corporation, U.S. Patent No. 5,397,851, 1995.
12. Kuran, W., 2001, *Principles of Coordination Polymerization*, Wiley, New York, Chapter 5, Table 5.1.
13. Tucker, H., Goodrich-Gulf, U.S. Patent No. 3,094,514, 1963.
14. Horne, Jr., S. E., in *Transition Metal Catalyzed Polymerizations, Alkenes and Dienes*, Quirk, R. P., Ed., Harwood Academic, New York, 1983.
15. Marullo, G., Baroni, A., Maffezzoni, U., Susa, E., and Longiave, C., Montecatini Edison, U.S. Patent No. 3,502,687, 1970.
16. Johnson, B. L., and Wolfangel, R. D., *Ind. Eng. Chem.*, **1952**, 44, 752.
17. Natta, G., Porri, L., and Fiore, L., Motecatini, U.S. Patent No. 3,015,371, 1962.
18. (a) Tsujimoto, N., Suzucki, M., Kawaguchi, N., and Nakazimi, T., Ube Industries, U.S. Patent No. 4,579,920, 1986; (b) Okamoto, N., Anbe, M., Yanashita, J., Nakajima, T., Kitamura, T., Kimura, O., and Wada, T., Ube Industries, European Patent application EP 1,842,875, 2007.
19. (a) Lasis, E., Polysar Limited, U.S. Patent No. 4,242,478, 1980; (b) Odar, J., B. F. Goodrich Co., U.S. Patent No. 4,224,426, 1980; (c) Odar, J., B. F. Goodrich Co., U.S. Patent No. 4,303,796, 1981; (d) Odar, J., B. F. Goodrich Company, U.S. Patent No. 4,314,045, 1982.
20. (a) Lasis, E., and McCracken, N. J., Polymer Corp., U.S. Patent No. 3,646,001, 1972. p. 285; (b) Storr, A., Jones, K., and Laubengayer, A. W., *J. Am. Chem. Soc.*, 1968, 90, 3173.
21. Carlson, G. J., and Dong, W., Shell Oil Company, U.S. Patent No. 3,066,127, 1962.
22. Gippin, M., *I &EC Prod. Res. Dev.*, **1965**, 4(3), 160.
23. Bernemann, P., and Kentschke, D. W., Chemische Werke Huels, U.S. Patent No. 4,182,814, 1980.
24. Donbar, K. W., Saltman, W. M., and Throckmorton, M., Goodyear Tire and Rubber Company, U.S. Patent No. 5,698,643, 1997.
25. Ruehmer, T., Dow Chemical Co., U.S. Patent application 60/385,226, 2003.
26. Carlson, E. J., and Horne, Jr., S. E., Goodrich-Gulf Chemicals, U.S. Patent No. 3,135,725, 1964.
27. Ichikawa, M., Takeuchi, Y., Kogure, A., and Kurita, H., Japan Synthetic Rubber Co., U.S. Patent No. 3,498,963, 1970.

28. Ricci, G., Forni, A., Boglia, A., Motta, T., Zanaoni, G., Canetti, M., and Bertini, F., *Macromolecules*, **2005**, 38, 1064.
29. Sugiura, S., Ueno, H., Kono, M., and Hamada, H., Ube Industries, U.S. Patent No. 3,778,424, 1973.
30. Castner, K. F., Goodyear Tire and Rubber Co., U.S. Patent No. 6,310,152, 2001.
31. Ashitaka, H., Jinda, K., and Ueno, H., *J. Polym. Sci. Polym. Chem. Ed.*, 1983, 21, 1951.
32. Ricci, G., Batistella, M., and Porri, L., *Macromolecules*, **2001**, 34, 5766.
33. Ueno, H., Ashitaka, H., and Nakajima, K., Ube Industries, U.S. Patent No. 4,503,202, 1985.
34. Howell, J. E., Curtis, W. G., and Solomon, J. A., in *Transition Metal Catalyzed Polymerizations, Alkenes and Dienes*, Quirk, R. P., Ed., Harwood Academic, New York, 1983.

Appendix A
Pyrophoricity of Metal Alkyls

DENNIS B. MALPASS
Akzo Nobel Polymer Chemicals (retired), Magnolia Texas 77354

A.1 INTRODUCTION

Metal alkyls used with transition metal polyolefin catalysts are typically highly reactive with air. In fact, many of the commercially available metal alkyls used in the polyolefins industry are pyrophoric; that is, they ignite spontaneously upon exposure to air.[1] Most are also violently reactive with water.

Metal alkyls are often supplied as solutions, usually in aliphatic hydrocarbons, such as isopentane, hexane, and heptane. These solutions, with typical metal alkyl concentrations of 10–25%, exhibit lower reactivity with air relative to the neat (undiluted) metal alkyls and are *perceived* to be less hazardous. Since such solutions contain large amounts of highly flammable, volatile hydrocarbons, hazards of the solvent (toxicity, flash point, lower explosive limit, etc.) should also be recognized and appropriate precautions taken.

Tests have been developed to gauge air reactivity of metal alkyl solutions and results have been used to assign hazard classifications for transport. However, results are frequently misinterpreted or misunderstood. The objectives of this appendix chapter are

- To discuss the intent and meaning of pyrophoricity tests
- To describe procedures for testing pyrophoricity
- To provide results of pyrophoricity testing of metal alkyls and their solutions
- To identify trends in pyrophoricity of metal alkyls.

Excerpted from a technical bulletin published by Akzo Nobel Polymer Chemicals (publication number MA03.322.01/January 2003), with permission.

Handbook of Transition Metal Polymerization Catalysts Edited by Ray Hoff and Robert T. Mathers
Copyright © 2010 John Wiley & Sons, Inc.

Discussions of pryophoricity of metal alkyls in this chapter deal only with compounds of aluminum, boron, magnesium, and zinc. Some metal alkyls (e.g., organolead and many organotin compounds) are not reactive with air, and others (e.g., potassium alkyls) are not soluble in hydrocarbons. Methods discussed here are not applicable to such metal alkyls. Methods are, however, applicable to lithium alkyls, which are used in industrial catalyst systems for the manufacture of synthetic elastomers. Pyrophoricity of the commercially available butyllithium solutions approximates that of triethylalumium and increases in the series:

n-butyl > *sec*-butyl > *tert*-butyl

As indicated above, tests discussed here were developed primarily for the purpose of hazard classification for transport. Results are also useful in comparing relative reactivity of metal alkyl solutions. Results, however, should *not* be interpreted as predictive of whether solutions will self-ignite if spilled. The tests are empirical and results should be regarded as semiquantitative. Finding a solution to be pyrophoric under test conditions should *not* be interpreted as an indication that the particular solution is certain to ignite if spilled. Conversely, if a solution is found to be nonpyrophoric under test conditions, it should *not* be concluded that the solution will not ignite if spilled. So-called self-ignition limits are not easily determined, since variables (wind speed, ambient temperature, humidity, surface onto which the spill occurs, etc.) that may contribute to ignition in a spill are uncontrolled. Under certain conditions, any commercially available solution of a metal alkyl could ignite when spilled.

Though a solution may have been determined to be nonpyrophoric by test, it will remain air reactive and must be handled under an inert atmosphere to maintain product quality. While handling such solutions, workers must continue to wear personal protective equipment to protect against exposure. Even solutions that have been determined to be nonpyrophoric by test may cause burns.

In general, pyrophoricity of a metal alkyl increases as metal content increases. Thus, trimethylaluminum (which contains about 37% Al) ignites spectacularly when exposed to air, while tri-*n*-octylaluminum (which contains about 7% Al) oxidizes slowly but usually does not ignite spontaneously. Nevertheless, tri-*n*-octylaluminum is considered pyrophoric, since it tests positive by the methods described below. Other trends relating degree of pyrophoricity to solution and product characteristics will be developed below.

A.1.1 Sawdust Test

In the 1960s, the Bureau of Explosives (then part of the Association of American Railroads) developed the "sawdust test"[1] to gauge pyrophoricity of air-reactive liquids. The test involved introducing 800 mL of a metal alkyl solution to the "crater" of a volcano-shaped cone of sawdust (~4 L of dry, soft-wood sawdust). If the sawdust ignited or was charred, the solution was deemed to be pyrophoric. As concentration of the metal alkyl was reduced, a solution was achieved which did not cause ignition or charring. This concentration was designated as the nonpyrophoric limit (NPL). Thus, the NPL from this test may be defined as the *maximum* concentration of metal alkyl that does not ignite or char sawdust. The sawdust test is now obsolete and has been replaced by tests based upon the effect of metal alkyls on a specific grade of filter paper and/or silica.

A.1.2 Paper Char Test

A simpler, alternative method for gauging pyrophoricity of metal alkyl solutions was developed in the mid-1970s.[2] The method was developed to provide results *intentionally* comparable to the sawdust test. For this reason, the choice of substrate was a grade of filter paper specifically chosen to simulate the cellulosic composition of sawdust. This method has become known as the "paper char test" and has been in use since the late 1970s in transport classification of metal alkyls.

The paper char test involves syringing a small quantity (~0.5 mL) of the metal alkyl solution onto the surface of dry Whatman No. 3 filter paper (at ambient laboratory temperature, typically 22–25 °C). The test must be performed in a fume hood since profuse smoking or a small fire may occur. Personal protective equipment should be worn during testing, including safety glasses, fire-retardant coveralls, safety shoes, an aluminized suit with face shield and hood, and protective gloves (lined polyvinyl chloride or leather) that are impervious to metal alkyls. The filter paper is suspended on the platform of a tripod to permit airflow above and below the paper. A small indentation (~2.5 cm diameter and ~3 mm deep) should be made in the center of the paper to form a small "cup" for the solution. Care must be taken not to tear the paper when making the indentation. A small metal pan containing a layer (~2.5 cm) of vermiculite should be placed beneath the tripod to catch drippings. The solution should be delivered in a steady stream (not dropwise) within a few seconds to the indentation in the filter paper. The rate of delivery, however, should be slow enough to prevent splattering or overflow of the "cup." The paper is then observed for about 1 min for ignition or charring. Slight charring near the NPL may be more easily detected if the filter paper is held up to sunlight. Tests are usually done in triplicate. If charring is observed in any of the test filter papers, the solution is deemed pyrophoric at that concentration. Other grades of filter paper, common paper towels, and so on, do not provide results comparable to the sawdust test and should not be used. Also, wet paper dulls the sensitivity of the test.

As with the sawdust test, solution concentration may be decreased incrementally until a concentration is achieved at which there is no char or ignition. This concentration is deemed the NPL; that is, it is the *maximum* concentration that does not ignite or char the paper. Though reading char is somewhat subjective near the NPL, test results are usually within ±1% absolute. NPLs for aluminum alkyls are summarized in Table A.1. Data for metal alkyl derivatives of boron, magnesium, and zinc are provided in Table A.2.

TABLE A.1 NPLs of Aluminum Alkyls

Aluminum Alkyl	NPL in Isopentane	NPL in Hexane	NPL in Heptane	NPL in Toluene	NPL by Sawdust Test
Trimethylaluminum	7	11	12	12	10 in hexane
Triethylaluminum	13	12	12	12	15 in hexane
Tri-*n*-propylaluminum			13	19	
Tri-*n*-butylaluminum		30	27		
Triisobutylaluminum	20	22	25	26	17 in isopentane
Triisohexylaluminum[a]		43			
Tri-*n*-hexylaluminum	36	42	42		
Tri-*n*-octylaluminum	49	61	56		
Tri-*n*-decylaluminum	86	79			
Tricitronellylaluminum[b]			91		
Isoprenylaluminum		38			
Diethylaluminum hydride		11	13		
Diisobutylaluminum hydride		18	21	20	26 in benzene
Dimethylaluminum chloride	8	13	14		
Dimethylaluminum bromide			18		
Diethylaluminum fluoride			18		
Diethylaluminum chloride	13	13	13		15 in hexane
Diethylaluminum bromide		16	19		
Diethylaluminum iodide	19	24	27		

Di-*n*-propylaluminum chloride	14	17	18		
Di-*n*-butylaluminum chloride			25		
Diisobutylaluminum chloride	18	20	20		
Di-*n*-hexylaluminum chloride			37		
Diisohexylaluminum chloride			37		
Di-*n*-octylaluminum chloride			49		
Di-*n*-decylaluminum chloride			50		
Methylaluminum sesquichloride		16			
Methylaluminum sesquibromide		21			
Ethylaluminum sesquichloride		15		19	20 in hexane
Ethylaluminum sesquibromide				25	
Isobutylaluminum sesquichloride		22	20		
Ethylaluminum dichloride	20	25	29		
Ethylaluminum dibromide			35		
Isobutylaluminum dichloride	20	25	28		
Diethylaluminum ethoxide	26	26	28		
Diisobutylaluminum ethoxide		51			

[a]Isohexyl = 2-methylpentyl group.

[b]Citronelly = 3,7-dimethyl-6-octenyl group.

Note: wt% by paper char test, unless otherwise noted.

TABLE A.2 NPLs of Other Metal Alkyls

Metal Alkyl	NPL in Isopentane	NPL in Hexane	NPL in Heptane	NPL by Sawdust Test	Other Data
Triethylborane	17	18	18	20 in hexane	16 in THF
Triisobutylborane		34			
Tri-*n*-butylborane			30		
Tri-*n*-octylborane			70		
Diethylboron methoxide					100[a]
Diethylboron isopropoxide					100[a]
sec-Butyllithium					12 in cyclohexane
tert-Butyllithium					9 in *n*-pentane
n-Butylethylmagnesium		14	14		
n-Butylethylmagnesium n-butoxide					100
Dibutylmagnesium[b]		19			
Di-*n*-butylmagnesium[c]		20	20		
Dimethylzinc					13 in toluene; 21 in THF
Diethylzinc	17	23	31	25 in hexane	22 in toluene
Di-n-propylzinc			31		
Di-*n*-butylzinc			29		

[a] Though the neat product is nonpyrophoric by the paper char test, it has been shown to be pyrophoric by the silica test. Accordingly, UN mandates that the product be classified as pyrophoric and assigned hazard class 4.2.

[b] Product contains both n-butyl and sec-butyl groups.

[c] Contains about 12 molar % triethylaluminum.

Note: wt% by paper char test, unless otherwise noted.

In rare cases, an oxide film forms on the surface of the test solution and prevents sufficient contact with air. This sometimes occurs with metal alkyls with high molecular weights or solvents with relatively high viscosity, such as mineral oil. For these solutions, the standard paper char test procedure is modified slightly. When a crust forms, it may be necessary to agitate the solution in the indentation gently (using the tip of the syringe needle). It may also be necessary to extend the observation time beyond the 1-min standard. NPL values thus obtained are usually lower than values obtained if the crust is not disturbed.

Advantages of the paper char test relative to the sawdust test are as follows:

- It can be run in a standard laboratory fume hood.
- It is simple to run with commonly available laboratory equipment.
- Small quantities are used (safer, reduced risk of exposure).
- Results are comparable (by design) to those from the sawdust test.
- Replicate tests can easily be run, improving accuracy and reproducibility.

Both the paper char and sawdust tests rely upon the reactivity of a metal alkyl solution with a cellulosic material in air as a measure of pyrophoricity. Ignition need not occur for a solution to be adjudged pyrophoric. Hence, the strict definition of the term "pyrophoric" may not be applicable to solutions of metal alkyls using these tests, especially near the NPL.

A.1.3 Silica Test

In recent years, a supplemental test has been used in conjunction with the paper char test to determine shipping classification (see Section A.2). We shall refer to this test as the "silica test" because it involves introducing a small quantity of the metal alkyl solution to silica or diatomaceous earth in a porcelain cup in air and observing whether the mixture ignites within 5 min. This test is prescribed by United Nations (UN) regulations.[3,4] The silica test is repeated 6 times. If a solution in any of the silica test ignites, it is classified as pyrophoric and assigned hazard classification 4.2. In this situation, additional testing by the paper char test would not be required. However, if none of the tests results in ignition, the solution is deemed nonpyrophoric by the silica test. In this case, UN regulations require additional testing by the paper char test to confirm a nonpyrophoric rating. If the solution is also nonpyrophoric by the paper char test, the solution is then classified as nonpyrophoric and assigned hazard classification 4.3. Only if *all* tests (silica and paper char) are negative is the solution classified as nonpyrophoric.

A.2 HAZARD CLASSIFICATIONS

The UN Economic and Social Council's Committee of Experts on Transport of Dangerous Goods has adopted the paper char test in conjunction with the silica test (as described above) for classifying solutions of metal alkyls for international transport.[3,4] Transport hazard class assignments are Division 4.2 (spontaneously combustible) and Division 4.3 (dangerous when wet). All metal alkyls and their solutions are assigned to Packing Group I. Commonly used UN identification numbers are UN 2845 (pyrophoric liquids, organic), UN 3051 (aluminum alkyls), UN 3052 ("aluminum alkyl halides"), and UN 3207 (organometallic compound, solution, water reactive).

Other transport regulatory agencies have accepted the UN recommendations. These include the U.S. Department of Transportation (DOT), International Maritime Organization (IMO), International Civil Aviation Organization (ICAO), the European agency governing the international carriage of dangerous goods by road and rail (abbreviated from the French as ADR/RID), and International Air Transport Association (IATA).

Note that UN regulations do not require that the NPL be determined by any test. For this reason, the silica test has not been widely used to determine the maxium concentration of a specific metal alkyl solution that does not ignite under test conditions. Rather, it has been used simply to determine whether a specific solution is pyrophoric or nonpyrophoric for transport classification. If adjudged to be nonpyrophoric, it does not necessarily mean that the specific solution is at the NPL. Additional tests would be required to determine the NPL.

A.3 TRENDS FROM PYROPHORICITY DATA

Using data from pyrophoricity testing, certain tendencies have been recognized. Discussions below identify several trends. These interpretations are based upon data from the paper char test. In some cases, trends may be used to predict or estimate pyrophoricity of metal alkyls that have not been tested.

A.3.1 Effect of Metal Content

In general, NPLs tend to decrease with increasing metal content of the metal alkyl. This trend is illustrated in Figure A.1 for a variety of R_3Al and R_2AlCl ($R = C_1$ to C_{10} alkyl) compounds in hexane or heptane.

A.3.2 Effect of Solvent

NPLs increase as the boiling point (bp) of the solvent increases. Stated differently, pyrophoricity of hydrocarbon solutions of metal alkyls tends to increase as the vapor pressure (or volatility) of the solvent increases. A plot of NPLs

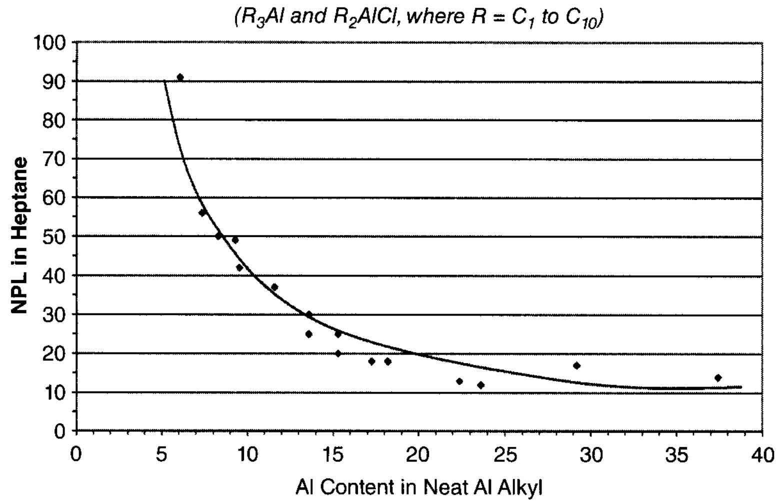

Figure A.1 NPL as function of Al content.

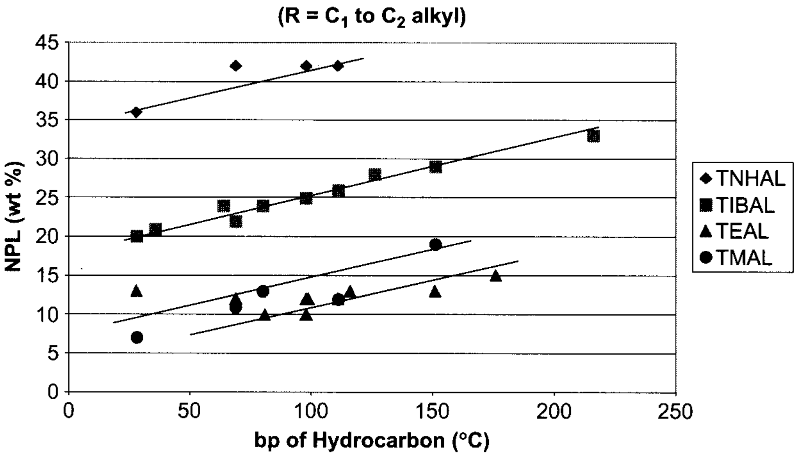

Figure A.2 NPLs of R_3Al in various hydrocarbons (R = C_1 to C_6).

for a range of R_3Al (R = C_1 to C_6 alkyl) compounds versus bp of the solvent is shown in Figure A.2. Though data are limited for some of the R_3Als, the trend of increasing NPLs as the atmospheric bp of the solvent increases is clear. Results suggest that trimethylaluminum (TMAL) solutions are slightly less pyrophoric than triethylaluminum (TEAL) solutions by the paper char test. This result is anomalous since TMAL contains about 58% more aluminum than TEAL.

A.3.3 Effect of Ligand

Incorporation of oxygen-containing ligands into an aluminum alkyl tends to increase the NPL (lower pyrophoricity). For example, if an ethoxide ligand replaces one of the ethyl groups in TEAL, the NPL increases from 12% for TEAL to 28% for diethylaluminum ethoxide (both in heptane). Similarly, triisobutylaluminum has an NPL of 22%, while diisobutylaluminum ethoxide has an NPL of 51% (both in hexane). The same trend is also observed in other series of metal alkyls. Note from Table A.2 that triethylborane (TEB) and *n*-butyl(ethyl)magnesium (BEM) have NPLs of 18 and 14%, respectively, in heptane. However, alkoxide derivatives of TEB and BEM [diethylboron methoxide (DEB-M), diethylboron isopropoxide (DEB-IP), and *n*-butyl(ethyl)magnesium *n*-butoxide (BEM-B)] are nonpyrophoric by the paper char test as neat products.

Methylaluminoxanes (methylaluminum compounds containing Al–O–Al linkages) have grown in importance in recent years because of their use as cocatalysts for single-site catalysts.[5] Methylaluminoxanes are most commonly produced by controlled reaction of trimethylaluminum with water. Since methylaluminoxanes contain oxygen, they also show diminished pyrophoricity. (See Chapter 1 for additional information on properties and compositions of alkylaluminoxanes.) Limited data on pyrophoricity testing of solutions of methylaluminoxanes have shown them to be nonpyrophoric by the paper char test at the concentrations (28–35%) commonly supplied in the merchant market.

A.3.4 Effect of Temperature

A few NPLs were conducted at elevated temperatures (35–55 °C).[2] Results indicate that NPLs decrease slightly as temperature increases. This is consistent with the finding that pyrophoricity increases (or NPLs decrease) as the vapor pressure of the solvent increases (see Figure A.2).

A.4 SUMMARY OF TRENDS

In general, pyrophoricity of metal alkyls is inversely proportional to NPLs; that is, pyrophoricity increases as NPLs decrease. The following may be helpful in understanding trends for pyrophoricity of metal alkyls:

Metal content ↑	NPL ↓	Pyrophoricity ↑
Oxygen content ↑	NPL ↑	Pyrophoricity ↓
Solvent vapor pressure ↑ (or bp↓)	NPL ↓	Pyrophoricity ↑
Temperature ↑	NPL ↓	Pyrophoricity ↑

As suggested above, using trends allows one to estimate an NPL for an unknown system. For example, knowing that the NPL for TIBAL in heptane (bp = 98 °C) is 26%, one may conclude that the NPL for TIBAL in dodecane (bp = 216 °C) will be greater than 26%. Further, from Figure A.2, it may be estimated that the NPL for TIBAL in dodecane is about 35%. The experimentally determined value is 33%. Since some systems behave anomalously (see Section A.3.2), it is recommended that estimated NPLs be verified with actual tests.

REFERENCES

1. Anonymous, *Pyrophoric Apparatus Description and Procedure for Use*, Technical Bulletin 16-1991, Bureau of Explosives, Mar. 1968.
2. Mudry, W., Burleson, D., Malpass, D., and Watson, S., *J. Fire Flammability*, **1975**, 6, 478.
3. Anonymous, *Recommendations on the Transport of Dangerous Goods—Model Regulations*, 11th rev. ed., United Nations, New York, 1999, p. 73.
4. Anonymous, *Recommendations on the Transport of Dangerous Goods-Manual of Tests and Criteria*, 3rd rev. ed., United Nations, New York, 1999, p. 329.
5. Montagna, A., Burkhart, R., and Dekmezian, A., *Chemtech*, Dec. 1997, p. 26.

Appendix B
Rheological Terms for Polymerization Catalyst Chemists

GREGORY W. KAMYKOWSKI
TA Instruments—Waters LLC, Schaumburg, Illinois 60173

Dynamic Rheometry

Frequency The frequency at which oscillation occurs when testing a sample in a dynamic, sinusoidal mode. For rheologists, this is most often expressed in units of radians per second. Symbol: ω (omega). When frequency is expressed in terms of cycles per sec, that is, hertz, as it sometimes is, the symbol is ν (nu).

Strain The amount of deformation of the sample, normalized to take into account the type of geometry (e.g., parallel plate, cone and plate, tensile) and the specimen dimensions. Symbols: shear strain: γ (gamma). Tensile/flexural strain: ε (epsilon). Strain is often given in terms of percent.

Stress The amount of force (linear) or torque (rotational), normalized to take into account the type of geometry (e.g., parallel plate, cone and plate, tensile) and the specimen dimensions. Symbols: Shear stress: σ (sigma). Tensile/flexural stress: τ (tau). Units: pascals. *Note*: σ and τ appear to be used most frequently to denote shear stress and tensile stress, respectively. There are numerous instances, though, in the literature where the symbols have been used in the opposite fashion. One must verify from the author's description which type of strain is appropriate—shear or tensile.

Delta The angle that indicates the phase shift between the strain wave and the stress wave. Symbol: δ (delta). Units: radians.

Handbook of Transition Metal Polymerization Catalysts Edited by Ray Hoff and Robert T. Mathers
Copyright © 2010 John Wiley & Sons, Inc.

Storage Modulus The stress in phase with the deformation divided by the strain. This is a measure of the elasticity of the sample. Symbols: G' (shear), E' (elongational and flexural). Units: pascals.

Loss Modulus The Stress 90° out of phase with the deformation divided by the strain. This is a measure of the viscous nature of the sample. Symbol: G'' (shear), E'' (elongational and flexural). Units: pascals.

Complex Modulus This is a combination of both the storage modulus and the loss modulus: $[(G')^2 + (G'')^2]^{1/2}$ for shear and $[(E')^2 + (E'')^2]^{1/2}$ for elongational and flexural deformations. Symbol: G^* for shear and E^* for elongation and flexural deformations. Units: pascals.

Tan Delta The tangent of the angle, delta, which was described above. This is the ratio of the loss modulus to the storage modulus. Symbol: $\tan\delta$.

Storage Compliance The strain in phase with the deformation divided by the stress. This is usually obtained in controlled dynamic stress tests. Symbols: J' (shear), D' (elongation and flexural). Units: reciprocal pascals.

Loss Compliance The strain out of phase with the deformation divided by the stress. This is usually obtained in controlled dynamic stress tests. Symbols: J'' (shear), D'' (elongation and flexural). Units: reciprocal pascals.

Complex Compliance This is a combination of both the storage compliance and the loss compliance: $[(J')^2 + (J'')^2]^{1/2}$ for shear and $[(D')^2 + (D'')^2]^{1/2}$ for elongational and flexural deformations. Symbol: J^* for shear and D^* for elongation and flexural deformations. Units: pascals.

Complex Viscosity The complex modulus divided by the frequency, ω. Symbol: η^* (eta asterisk). This is used primarily in shear testing. Units: pascal-seconds.

Crossover Modulus The point in a frequency sweep, a time sweep, or a temperature ramp where the storage modulus is equal to the loss modulus. Units: pascals.

Crossover Frequency The frequency in a frequency sweep at which the storage modulus is equal to the loss modulus. Units: radians per second.

Dynamic Mechanical Analysis Dynamic rheometry. However, this term is usually associated with solids testing.

Two examples of rheometry are shown in Figures B.1 and B.2.

Steady Rheometry

Shear Rate The change in the velocity versus change in distance in shear testing. This normalizes velocity to take into account the type of geometry and the dimensions. Symbol: $\dot{\gamma}$ (gamma dot) Units: reciprocal seconds.

Shear Stress See above. Usual symbol: σ (sigma). Units: pascals.

Viscosity The ratio of shear stress to shear rate. Symbol: η (eta). Units: pascal seconds, although, in some industries, one often sees poise, centipoise, and millipascals seconds.

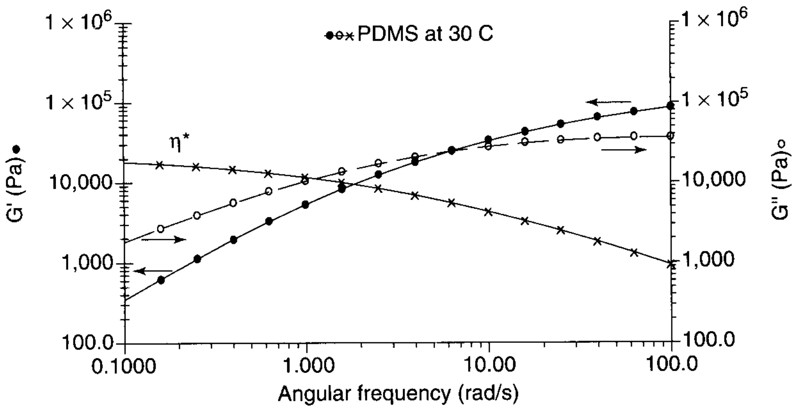

Figure B.1 Example of an isothermal dynamic frequency sweep for PDMS, a typical thermoplastic material.

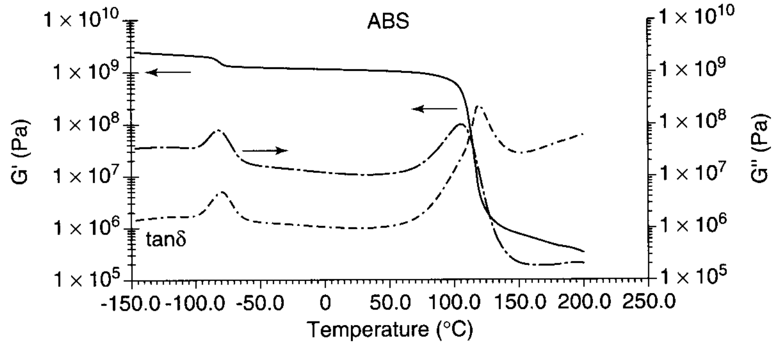

Figure B.2 Example of an isochromal temperature ramp on ABS, a typical thermoplastic material.

Elongational Rate The velocity normalized to take into account the length of the specimen. Symbol: $\dot{\varepsilon}$ (epsilon dot). Units: reciprocal seconds.

Elongational Stress See above. Usual symbol: τ (tau). Units: pascals.

Elongational Viscosity The ratio of the elongational stress to the elongation rate. Symbol: η_e. Units: pascal seconds.

Length-to-Diameter Ratio In capillary rheometry, the ratio of the die length to the die diameter.

Die Swell In capillary rheometry, the ratio of the melt extrudate diameter to the die diameter.

Normal Force In rotational rheometry, the forces exerted by the fluid perpendicular to the rotational motion. Symbol: F. Units: newtons.

Normal Stress The normal force divided by the area of the rotating geometry, usually a cone. Symbol: N_1. Units: pascals.

Normal Stress Coefficient The normal stress divided by the shear rate squared, that is, $N_1/\dot{\gamma}^2$. Symbol: Ψ (psi). Units: pascal seconds squared.

Transient Rheometry

Stress Relaxation Modulus The stress divided by the strain in a stress relaxation (constant strain) test. Symbols: G (shear), E (elongation and flexural). Units: pascals.

Creep Compliance The strain divided by the stress in a creep test (constant-stress) test. Symbols: J (shear), D (elongation and flexural). Units: reciprocal pascals.

Recoverable Compliance In a creep/creep recovery test, the compliance obtained during the creep recovery step (stress = 0), using the last data point from the creep test as the reference point. Symbol: J_r. Units: reciprocal pascals.

BIBLIOGRAPHY

1. American Society for Testing and Materials (ASTM), ASTM D 3835-02, Determination of properties of polymeric materials by means of a capillary rheometer, *Annual Book of ASTM Standards*, Vol. 08.02, ASTM, West Conshohocken, PA, 2008.
2. American Society for Testing and Materials (ASTM), ASTM D 4065-01, Plastics: Dynamic mechanical properties: Determination and report of procedures, *Annual Book of ASTM Standards*, Vol. 08.02, ASTM, West Conshohocken, PA, 2008.
3. American Society for Testing and Materials (ASTM), ASTM D 4440-01, Plastics: Dynamic mechanical properties melt rheology, *Annual Book of ASTM Standards*, Vol. 08.02, ASTM, West Conshohocken, PA, 2008.
4. Barnes, H. A., Hutton, J. F., and Walters, K., *An Introduction to Rheology*, Elsevier, New York, 2001.
5. Bird, R. B., Armstrong, R. C., and Hassager, O., *Dynamics of Polymeric Liquids—Fluid Mechanics*, Volume 1, Wiley, New York, 1977.
6. Ferry, J. D., *Viscoelastic Properties of Polymers*, 2nd ed., Wiley, New York, 1970.
7. Macosko, C. W., *Rheology Principles, Measurements, and Applications*, Wiley-VCH, New York, 1994.

INDEX

- Acetonitrile, solvent for chromium oxide, 345, 347
- Acetylene, reaction with chromium catalyst, 316, 370, 388
- Acrylates
  - methyl acrylate, 91, 92
  - methyl acrylate with Pd catalyst, 491
  - polymerization with ethylene/CO, 491
  - *t*-butyl acrylate monomer with Cu catalyst, 498
- Acrylonitrile
  - ABS plastics, 537
  - tolerance by Mo catalyst, 529
- Activation
  - energy, 54, 543
  - C–H bond, 521
- Activation of catalysts
  - activation by cocatalysts, 61, 64, 68, 122, 124
    - boron containing, 210
    - by cocatalysts in prepolymerization, 238
    - with internal/external donors, 173
    - fourth-generation catalysts, 174
    - fifth-generation catalysts, 182
    - solid ionic, 212
  - activation by hydrogen, 145
  - activation by light energy, 202
  - activation temperature effect on polymerization rate and molecular weight, 313
  - activation of titanium catalysts by magnesium chloride, 174
  - thermal activation of chromium-silica catalysts, 39
    - activation temperature, 313–314
    - effect on surface hydroxyl groups, 39, 295
    - effect on hexavalent chromium surface concentration, 301–302
    - fluidized bed depth, 300
    - carbon monoxide reduction, 308, 315–316, 335, 349, 380
- Active
  - centers, 41, 90, 140, 142, 144, 150, 168, 185, 315
  - sites, 36–37, 62, 137, 140, 160, 163, 173, 177, 183, 185, 188–191, 200, 204
  - species, 33, 165, 171, 173, 183, 206, 210, 213
- Acyclic diene metathesis (ADMET) polymerizations, 513–516
- Adsorption
  - nitrogen, 35
  - titanium tetrachloride on magnesium chloride, 173
- Agostic complex/interaction, 55, 69, 71–75, 77, 150
- Alcohols, 6, 109, 133
  - BHT, 18
  - *t*-butanol, 346
  - *n*-butyl alcohol, 19
  - ethanol, 138
  - methanol, 472
- Aldehydes, 6
- Alkaline aging, 407–408
- Alkoxides
  - aluminum, 319
  - ligands, 527, 528
  - magnesium, 131, 133
  - molybdenum, 528
  - palladium, 473
  - titanium, 72, 134
- Alkyl lithiums, *sec*-butyllithium, 17

Handbook of Transition Metal Polymerization Catalysts Edited by Ray Hoff and Robert T. Mathers

Copyright © 2010 John Wiley & Sons, Inc.

Allene
  3,3-dimethyl allene, 489
  effect on intrinsic viscosity, 548
Aluminum alkyls (R_3Al), 3–9
  cost evaluation, 9
  hazards of TMAL, 7
  β-hydride elimination, 7
  selection criteria, 8
  thermal decomposition, 8
  TIBAL, 463
  triethylaluminum (TEAL), 4, 131, 231, 236, 239, 449
  tri-*n*-butylaluminum, 8
  use of Cp_2TiMe_2, 190
Alumina in Phillips chromium catalysts, 302, 325
  surface modification of silica by alumina, 49
Alumina in fluoride-modified catalysts, 324–327
  surface modification of alumina by silica, 326
Alumina modified with phosphate and borate, 326
Alumina-Cr catalysts
  carbon monoxide reduction, 358
  chain branching across molecular weight distribution, 410
  chain transfer, 356
  ethylene-hexene copolymerization, 381
  hydrogen response, 332, 357
  long chain branching in high density polyethylene, 410, 418
  methyl groups and double bonds in high density polyethylene, 369
  molecular weight distribution, 357
  porosity, 419
  reduction and reoxidation activation, 359–360
  sulfate modification, 357, 419–420
Alumina-homoleptic zirconium alkyl catalyst, 163
Aluminoxanes
  analysis, 10–11
  cages, 67
  commercial availability, 12
  cost, 14–15
  t-butylaluminoxane (TBAO), 14
  differential scanning calorimetry, 10
  ethylaluminoxane (EAO), 13
  isobutylaluminoxane (IBAO), 12
  methylaluminoxanes (MAO), 10–11, 64, 163, 193–194
  modified methylaluminoxanes (MMAO), 11
  nonhydrolytic method, 13
  polymethylaluminoxane (PMAO), 13
  polymethylaluminoxane improved performance (PMAO-IP), 13
Aluminum hydride (AlH_3), 4
Aluminum oxy-fluoride support for Phillips catalysts, 324
Aluminum phosphate ($AlPO_4$), 302–303, 315, 366
Ammonia, 325
Ammonium fluoride, 323–324
Amphiphilic metathesis catalysts, 525
Aromatic isocyanates, 527
Atactic, 158–159, 201–202, 216, 232

Back-biting reactions, 472
Back-bonding, 63
Back-donation, 70, 72
Ball-milling, see catalyst preparation
Ballard catalysts [e.g., supported tetra-(π-allyl)zirconium], 308, 329, 332
Basis sets, 58
BEM, *see* Magnesium alkyls
BET surface area, 244, 245, 255, 283
B.F. Goodrich, 537–538
Bidentate ligands, 482–483
Bimetallic alkylidene complexes, 529
BINAPHOS ligands, 483
Blocking, 374
Blow molding, 29, 35, 44, 46, 117, 126–127, 425
Bond angle, 315, 476
Born–Oppenheimer approximation, 54, 56
Boron
  alkyl exchange, 364
  $B(C_6F_5)_3$, 64, 80, 163
  BCl_3, 297
  reducing agents, 318
  triethylboron cocatalyst, 320–321, 364, 389, 420, 423
Branch dispersion index (BDI), 375
Bronsted acidity, 322–323, 326, 342
Bronsted-enhancing oxides, 326
Bulk density, 207–208, 240–242
Butadiene, 501. *See also* Polybutadiene
Butylated hydroxytoluene (BHT), 18, 19, 24

^{13}C NMR, 152–153, 193
Calcination, 140, 209
Calcium hydroxide, 111
Carbon-metal bond, 68, 82

Carbon monoxide, 41, 185
  ^{14}CO-labeling experiment, 334
  copolymerization with α-olefins, 467
  copolymer structure, 480
Carboxylic acids, 6
Catalyst performance
  activity, 3, 4, 9, 36, 50, 90, 117, 124, 141, 151–152, 231–232, 237
  activators, *see* Cocatalysts
  activation, 42–43, 62, 107
  fragmentation, 177
  impurities/poisons, 41–42, 90, 198, 308, 311, 319, 335, 338, 373, 402
  porosity, 165, 174, 249
  surface area, 132–133, 137, 139, 141
Catalyst preparation
  ball-milling, 135, 141, 171, 234
  emulsion-quenching method, 234–236
  filter and wash, 109
  make-or-buy, 114–122
  pilot plants, 128
  process scale-up, 104, 115, 120
  reactive precipitation method, 235, 237, 240
  recovery and recycle process, 110
  spray drying, 135
  support formation, 108
  waste treatment, 111
Chain
  migration, 86, 160, 162
  propagation, 55–56, 61, 92
  termination, 61–62
Chelate, 472
Chemical hardness/softness, 62–63
Chemisorption, 315–316, 338, 447
Chirality, 160–161, 171, 193–194, 201
Chlorinated aluminum alkyls, 8
Chromocene, *see* Chromium
Chlorosilane, 297
Chrome-silica catalysts
  effect of activation temperature, 39
  effect of impurities, 41–44
  modification by aluminum, 46
  modification by titanium, 44–45
  pore size, 35
  reduced supported catalyst, 448
  sodium content, 42
  surface area, 36
Chromates
  bis-adamantyl, 304
  bis-triphenyltin, 304
  triphenylsilyl, 303, 319, 366, 448, 450
Chromium
  chromocene, 330, 332, 351, 370, 386
  CrO_3, 294–303
  Cr_2O_3, 294–295, 353–354
  Cr(II), 33, 317, 450
  Cr(III), 33, 294, 308, 359, 388
  Cr(IV), 44, 308
  Cr(VI), 302, 308, 450
  dichromate, 294, 404, 419
  loading, 38
CO reduction, 308, 315, 327, 335
Cobalt, 537–538
  butadiene productivity, 542–543
  catalysts for polybutadiene, 542
  cobalt chloride and R_3Al, 539
  cobalt octoate, 543–544
Cocatalysts, 61, 64, 68
  with chromate catalysts, 304
  with chromium-silica catalysts, 35, 313, 318–320
  with copper catalysts, 498–500
  with metallocenes, 30
  with single-site catalysts, 206–210
  with Ziegler–Natta catalysts, 49, 131, 173, 182
Commercialization, 113, 115–116, 118, 119
Contact ion pair, 64–67
Coordination site, 61, 68, 73, 85
Copolymers, 153, 159, 165–166, 175, 180, 182, 184, 192, 197, 212, 216, 232
Copolymerization,
  comonomer distribution, 371
  comonomer incorporation, 451
  ethylene/1-butene, 238, 293
  ethylene/1-hexene, 139, 145, 240, 250, 271
  ethylene/propylene, 165, 175
  gas-phase, 278
  kinetics, 142
  reactivity ratios, 143
  with hydrogen, 145
  with styrene, 212
Copper
  bis(benzimidazole)Cu(II), 501
  Cu(II)benzamidinate, 501
  ethylene polymerization, 502
  ethylene/MMA copolymerization, 509
  methacrylate polymerization, 504
  with MAO, 502
Cossee–Arlman mechanism, 61, 90, 159, 327, 539
Counteranion effects, 64, 66, 80
Cross metathesis, 524
Crown ethers, 487
Crystalline polymers, 141, 158, 169, 171, 184–185, 281, 293
Curtin–Hammett regime, 160

Cyclic alkenes
  cycloheptene, 526
  1,5-cyclooctadiene, 546
  cyclopentene, 526
Cyclopentadienyl, 62, 64–65

Degree of cross-linking, 283
Dehydroxylation, 349
  effect on melt index, 351
Density, 367
  relation to flow index, 451
Density functional theory (DFT), 53, 57, 62, 64, 68
Deuterium (D_2), 152–153
Dewar–Chatt–Duncanson model, 63
Disastereoisomeric, 161
Dichromate, *see* Chromium
Dienes, 415–417
Differential scanning calorimetry (DSC), 10
Dioctylphthalate, 184

Early transition metal catalysts, 64
EDX, 269, 273
Elastomeric, 163, 202, 216, 392
Electron spin resonance (ESR), 501
Enantiomeric excess (ee), 483
Enantiomorphic site control, 160, 162
Environmental stress crack resistance, 343, 371, 376, 454
Epoxides, 487
  epichlorohydrin, 175
Ethers, 15–16, 22, 136, 462
  alkyl glycidyl, 487
  allylphenol ethers, 489
  diisoamyl, 170
  dibutyl, 236
  ethyl vinyl, 521
Esters, ethyl acetate, 137. *See also* External donors; Internal donors
Ethylene, 139. *See also* Copolymerization
  partial pressure, 451
Exchange correlation (XC), 57
External donors
  alkoxysilane, 174, 179, 180, 182
  alkyl benzoates, 182
  ethyl *p*-ethoxybenzoate (PEEB), 173
  $MeSi(OEt)_3$, 179
  $PhSi(OEt)_3$, 179, 188

First generation chromium catalysts, *see* Chromium catalysts
Flory
  components, 144–147, 152
  MWD theory, 144

Flow index (FI), 448, 452
Fluorine
  CO copolymerization, 490
  fluoride, 323, 325, 362
    effect on density, 382
  fluorinated alkoxides, 528
  fluorinated olefins, 490
Fourth generation catalysts, *see* Ziegler–Natta catalysts
FTIR, 315, 509
Functional group tolerance, 523, 529

Gas chromatography/mass spectrometry, 152, 473
Gas-phase polymerization, 239, 278–280, 282, 284–285
Gel-permeation chromatography (GPC), 148, 152, 333, 398
  activation condition, 336
  Cr/$AlPO_4$, 360
  Cr/silica, 371
  effect of titania, 343
  ethylene homopolymers, 144–145
  experimental conditions, 243–244
  Schultz–Flory components, 372, 378
Geometry optimization, 59
Geometry distortion, 69
Glass transition temperature, 159, 184, 492
Green–Rooney mechanism, 327–328
Grignard reagents, 15, 22–23, 133, 138

Hafnium
  ancillary ligands, 76–77
  Cp_2HfMe_2, 211
  $(CpMe_4)_2HfMe_2$, 265
  Dow/Symyx, 204
  Hf(IV), 68
  olefin binding energy, 70–71
  rac-$Me_2Si(Ind)_2HfMe_2$, 211
  reaction energies, 82–84
  structural developments, 197
Hartree–Fock method, 56
Heptane insoluble fraction, 184–185
N-heterocyclic carbine, 521–522
Heterogeneous catalysts, 133, 162–168, 204–216. *See also* Alumina; Catalyst preparation
Heterophasic alloy, 232
1,5-Hexadiene, *see* Olefins
Hexamethyldisilazane, 49
1-Hexene, *see* α-Olefins
High density polyethylene (HDPE), *see* Polyethylene
HOMO, 62

Hydrocarbon solvents
  cyclohexane, 17
  heptane, 138
  iso-octane, 138
  toluene, 64, 65
Hydrogel precursor, 31
Hydrogen, 145, 149, 450
  hydrogen-to-ethylene ratio, 451
β-Hydride elimination, 80–84, 152, 473
β-Hydrogen transfer, 69, 81–85
Hydrothermal treatment, 32
Hydrofluoric acid (HF), 323–324
Hydrosilanes, 390–391

Imido ligand, *see* Ligands
Impact copolymers, 159
Induction time, 319, 322
Initiation, 68, 142, 327–328
Insertion
  1,2- and 2,1-, 78–80, 87–90
  ethylene, 91
  vinylamine, 91
Internal donors
  diisobutyl phthalate, 174, 186–187
  dioctyl phthalate, 176
  ethyl benzoate, 173
Intrinsic viscosity, *see* Viscosity
Ion pair separation energy, 64, 66–67
Ion pair dissociation, 67
Isocyanates, 527
Isoelectronic, 303
Isomerization
  chain, 62, 84–86, 89
  cis/trans, 470
  ROMP and ADMET, 521
  suppression, 522
Isospecific, 173
Isotactic, 158–159, 481, 484

Kinetics
  control, 218
  copolymerization, 147–150
  ethylene polymerization, 317
  first order, 329
  hydrogen effect, 146
  mechanism, 142–143
  polymerization, 44
  product, 160
  profile, 145, 164

Ligands
  amido, 76
  ancillary, 70–71, 77
  chelating, 497
  chlorine, 527
  diimine, 73, 79
  donor, 62–63, 66
  imido, 527
  ionic, 525
  metal-ligand bonding, 72
d-Limonene, 526–527
Linear low density polyethylene (LLDPE), *see* Polyethylene
Liquid crystal polymers, 488
  mesophase, 488
  nonmesomorphic, 489
Local density approximation (LDA), 57
Long chain branching (LCB), 36–37
  activation temperature, 397
  Arnett plot, 412
  definition, 394
  Janzen–Colby grid, 398, 405
  mechanism, 403
  minimizing LCB, 418–419
  polymer-molding characteristics, 393
  polymer yield, 410
  porosity, 404
  reactor temperature, 402
LUMO, 62–63

Macromonomers, 393–394, 398, 402, 411, 422
Magnesium
  Grignard compounds, 462, 528
  magnesium alkyls, 15–20
    n-butyl(ethyl)magnesium (BEM), 16–20
    complex with TEAL, 16
    dibutylmagnesium (DBM), 16, 140, 236
    ethylmagnesium chloride, 138
    modified with BHT, 18
    storage, 17
    thermal stability, 17
  magnesium alkoxides, $Mg(OC_2H_5)_2$, 137
  magnesium chloride ($MgCl_2$), 48, 135–138
    $MgCl_2$-ethanol, 135, 138
    $MgCl_2$-ethyl acetate, 137
    $MgCl_2$-heptane, 138
    $MgCl_2 \cdot 6H_2O$, 141
    $MgCl_2$-supported Ti, 232, 234, 245, 249
  magnesium oxide, 357
MALDI-TOF MS, 473
Mark–Houwink exponent, 545
Melt flow ratio (MFR), 452
Melt index (MI), 35–36, 38, 40, 47, 50
  effect of reaction temperature, 330
  ethylene concentration, 331
  high-load, 298, 330
  relation to molecular weight, 330, 340

Melting point, 177
Meso, 193–194, 200, 265
Mesopore, 244, 268–269, 282–283
Metal alkyls
  aluminum alkyls, *see* Aluminum
  magnesium alkyls, *see* Magnesium
Metal-hydride, 82, 86
Metallocene catalysts, 192–203
Metallocyclobutane, 514
Methylaluminoxane (MAO), 3, 6, 9–15, 64, 163
Methylacrylate (MA), *see* Acrylates
Methylmethacrylate (MMA), 501
Metathesis reactions, *see* Acyclic diene metathesis; Ring opening metathesis polymerizations
Migratory insertion, 73, 159–161
Modulus, 127, 158
Modified methylaluminoxanes (MMAO), *see* Aluminoxanes
Molecular weight
  Ansa indenes, 195–196
  chromium-silica, 44
  dialkylmagnesium, 16
  effect of activation temperature, 40
  effect of chain termination, 80
  effect of deuterium, 152
  effect of hydrogen, 145
  effect of pore size, 35, 210, 341
  ethylene/1-hexene copolymerization, 145–146
  IPRA as cocatlyst, 9
  multicenter sites, 144
  polypropylene, 185
  rac-Et(Ind)$_2$ZrCl$_2$, 194
  single-site catalysts, 62
  syndiotactic catalysts, 200
  supported systems, 208
  zinc alkyls, 3
Molecular weight distribution, 44–50, 158, 163, 179–181, 183–185, 191, 209, 213, 216
  chromium-silica, 35
  comparison with metallocene catalysts, 294
  diffusional restrictions, 341
  effect of hydrogen, 145
  effect of sodium, 44
  HDPE, 30, 47, 132, 452–453
  modification by titanium, 45
  modification by aluminum, 46
  multicenter sites, 143
  nickel catalysts, 461
  Phillips catalyst, 293
  ROMP, 521
  titania, 343
  Ziegler–Natta catalysts, 48, 136
Molybdenum catalysts, 292
Monoterpenes, 525
Morphology, 30, 33, 44, 48, 133, 138, 231–232, 245, 249, 253, 256
  environmental stress crack resistance, 423

Nanoribbons, 177
Nanoporosity, 174–175
Natural orbitals for chemical valence (NOCV), 63
Natural rubber, 485, 538
Neodymium catalyst, 548
Nickel
  K$_2$Ni(CN)$_4$, 468
  nickel catalysts, 329
  nickel-diimine, 55, 56, 72, 77, 84, 87
  Ni(acac)$_2$, 460
  NiCl$_2$, 462
  Ni(COD)$_2$, 459, 462
  Ni(0), 461
  Ni(η^3-C$_3$H$_5$)$_2$, 459, 462
  salicylaldimidato-based nickel(II), 68
Nitrogen
  ammonium ligands, 525
  2,2′-bipyridyl, 486
  Bu$_4$NBH$_4$, 492
  sorption, 306, 405
Norbornene (NB), 505, 507
Number average molecular mass, 185

Off-gas treatment, 111
Olefins
  ADMET, 520
  1-butene, 132, 137, 143, 163, 240, 293, 3 76
  1,9-decadiene, 416
  1,5-hexadiene, 525
  1-hexene, 132, 139, 140, 143, 145–150, 154, 384
  incorporation efficiency, 370
  4-methyl-1-pentene, 367
  1-octene, 132, 376
  1-pentene, 370
Oligomers, 386
Organoboron compounds
  anionic counterions, 23
  arylboranes, 22–23
  commercial availability, 21
  decomposition, 22
  Lewis acidity, 23
  triethylborane (TEB), 20
  tris(pentafluorophenyl)borane, 22

Organozinc compounds
  chain shuttling, 24
  chain transfer agent, 24
  diethyl zinc (DEZ), 23
  purity, 23
  synthesis of DEZ, 23
  thermal stability, 23
Oxophilic, 497
Oxygen poisoning, 339

π-complex, 68–94
Palladium
  acetate, 478
  diimine, 72–73, 78–79, 85, 87, 88, 89, 91
  ethylene/CO copolymerization, 468
  $(L^\wedge L)PdX_nA_2$, 472
  methyl-palladium(II), 491
  Pd^0, 474
  Pd(II), 72
  $[Pd(MeCN)_4](BF_4)_2$, 468
  $[Pd(PPh_3)_2(CH_3CN)_2](BF_4)_2$, 489
Particles
  ASTM methods, 232, 252
  cauliflower-like, 271, 272–274, 278, 280, 281, 283, 284
  concentric-shell, 249, 271, 274, 278, 279, 281, 284
  growth, 232, 245–246
  fragmentation, 168, 212, 214, 249
  hollow shell, 255, 274, 276, 278
  morphology-controlled, 234
  nascent polymer particles, 232–234, 241, 243
  particle form technology, 132
  porosity, 256
  prepolymer particles, 243
  preferred size range, 133
  reactor granule technology, 232
  uniformly porosity, 271, 278–279, 283–284
Patents
  chemopetrol, 455
  Chevron, 456
  Dow Chemical Company, 546
  Fina Oil and Chemical Company, 196
  heterocene complex, 199
  Himont, 180
  litigation, 115
  metallocene catalysts, 262
  Mobil, 451
  Montedison, 137
  Phillips, 293
  royalty fees, 115
  SABIC, 456
  Showa Denko, 455
  single-site catalysts, 193
  strength, 115
  Shell, 171, 175
  Union Carbide, 451
Pennsylvania Notched Test (PENT), 452, 454
Phenols, BHT, 18
Phillips catalysts, 2, 20, 22, 29–30, 48, 113, 132
Phosphorane, 459–462
Phosphines
  BINAP, 482
  (R,S)-BINAPHOS, 483
  1,2-*bis*(diphenylphosphino)ethane (dppe), 476–477
  1,3-*bis*(diphenylphosphino)propane (dppp), 468, 470, 475
  DIOP, 482
  Josiphos, 483
  (*R,R*)-Me-DUPHOS, 483, 487, 489
  1,3-propanediylbis(diisopropylphosphine) (dipp), 481
  trialkyl phosphines, 524
  triphenylphosphine, 468
Physical properties, 293, 373, 375
Polarization functions, 58
Polybutadiene, 537–548
  crystalline melting points, 538
  poly-1,2-butadiene, 547
  syndiotactic, 547
Polyethylene
  blow molding, 454
  catalyst history, 30
  chrome-silica catalysts, 35
  consumption, 30–31
  film applications, 454
  fluidized-bed process conditions, 452
  gas-phase polymerization, 447
  high density (HDPE), 29, 46, 50, 293
  linear low-density (LLDPE), 9, 18, 19, 31, 234, 237, 293
  low-density (LDPE), 30, 231
  silica-titania, 38
  ultrahigh molecular weight, 9
Polyethylene glycol (PEG), 474, 525
Polyketones, 468, 470
Polyvinyl acetate (PVA), 474
Polymethylaluminoxane, *see* Aluminoxanes
Polypropylene, 4, 9, 261, 263
  syndio-polypropylene, 523–524
Polydispersity, 44, 45, 159, 211
Polymerizations
  copolymerization, 139, 231–232, 238, 240, 250, 251

Polymerizations (*Continued*)
  gas-phase, 249–257
  homopolymerization, 370, 375
  initiation, 61, 62, 68, 73, 142, 153
  propagation, 55, 56, 61, 73–75, 92, 142, 144
  rate, 143, 238, 249–252
  slurry, 30, 34, 47–48, 132–134, 232–234, 267–268
  temperature, 164–165, 170, 184–185, 250, 251
  termination, 80, 81, 83, 84, 86, 90
Pore size, 32, 35–36, 48, 210, 245, 268–269
Pore volume, 31–36, 38
Porosity, 132–133, 137, 165–166, 174
Porri mechanism, 545
Potential energy surface (PES), 54–55
Precatalysts
  boron activated, 210
  MAO activated, 206
  metallocene, 207
  polymer bound, 211–214
Primary insertion, 160, 161, 163
Propene, 73, 79–80
Pulse feed polymerization, 485
Pyridine, 523, 542
Pyrophoric, 4, 10, 17, 23, 111

Rate of initiation, 311
Reaction rates, 280
Reactors
  beverage bottles, 540
  Büchi, 107
  poisons, 311
Reactivity ratio, 139, 143, 375
Reduction, 380–381, 388
  reducing agents, 321
  temperature programmed reduction experiment (TPR), 323
Regioregularity, 481
Regiospecificity, 158, 163
Relaxation time, 398, 425
Reynolds number, 104–105
Ring opening metathesis polymerizations (ROMP), 514–516
Ruthenium
  carbene complexes, 516–517
  Grubbs and Nolan catalysts, 522

Scale-up, 111
Scanning electron microscopy, 236, 237, 241, 243
Schultz–Flory components, 372, 378, 386, 389, 390
Secondary insertion, 160–161, 163
Shear
  response, 365
  thinning, 365
Silanols
  surface, 39
  triphenylsilanol, 304
Silica
  activation, 33, 39
  catalyst support, 29, 32, 140
  fragmentation, 132–133
  gel, 31–32
  particles, 33
  surface groups, 39, 315
Silylchlorides, 527
Single site catalysts (SSC), 10, 14
Sintering, 351–352, 355, 398–399, 405
Size exclusion chromatography, 243. *See also* GPC
  experimental conditions, 510
  HDPE, 454
  SEC-MALS, 394
Slurry processes, 167, 239, 280, 285, 319, 333
Solvent polarity, 67
Solution process, 237
Spheripol process, 165, 238
Stereospecific polymerization, 158, 162, 192
Styrene, 501
Sulfur compounds
  carbon disulfide, 353–354
  hydrogen sulfide, 350
  sulfate loading, 323, 326, 357, 359, 419–420
  sulfonate ligands, 478
Surface area, 176, 244, 323–326
  silica, 406, 409
Syndiotactic, 158–159, 161, 190, 199–201, 204, 210, 212, 215, 481
Synthetic rubber, 537–538

Tacticity, 157, 185, 200–201, 214
Terpolymerization, 485, 488
Termination, *see* Polymerizations
Tetrahydrofuran (THF), 136, 138
Thermoplastic
  elastomers, 163, 202, 216
  polyethylene, 30
Thermodynamic
  barrier, 81
  control, 83
  functions, 61, 192
Thermoforming, 35
Titanium
  Cp_2TiCl_2, 194
  Cp_2TiMe_2, 190

  Cp_2TiPh_2, 193
  rac-/meso- $Et(Ind)_2TiCl_2$, 194
  supported on $MgCl_2$, 171
  titanium tetrachloride ($TiCl_4$), 135, 169, 274, 278
  $TiCl_4(THF)_2$, 136
  Ti(II), 138, 173
  Ti(III), 76, 82, 138
  Ti(IV), 68, 72, 80, 86, 173
  $TiCl_3$, 131, 169, 170
Toluene, 64, 65, 344
Toughness, 158, 367, 371, 383
Transition state, 54, 60, 73–76, 78–83
Transition state optimization, 60
Transmission electron microscopy (TEM), 171
Trialkyl phosphines, 522
Trialkyl aluminium, *see* Aluminium alkyls
Triethyl borane (BEt_3), 20, 22
Triethylorthoformate (TEOF), 501
Triflic acid, 527
Triblock copolymers, 529
Triphenylphosphine, 447

Union Carbide, 447
Unsaturation, 453

Valence orbitals, 59
Vaseline, 138
Vinyl acetate, 491, 501
Vinylidene end groups, 368–369
Viscosity
  branching ratio, 460
  intrinsic, 39, 185–186, 463, 539
  long chain branching, 402, 405
  melt, 39, 402–403, 405, 416
  Mooney, 539
  reduction, 17–19
  zero-shear, 398, 421–422

Water soluble catalysts
  metathesis complexes, 524
  sulfonate-palladium, 478
Waste treatment, 111

X-ray diffraction, 141, 177, 303, 353
XANES, 295, 315
Xylene, 185, 187–188
XPS, 59, 315, 322, 449
  binding energy, 450

Zeigler, Karl, 4, 30, 231, 292
Ziegler–Natta catalysts
  comparison with Phillips catalysts, 426
  fifth generation, 184
  first generation, 231
  fourth generation, 184
  second generation, 132, 170
  third generation, 171, 173
Zinc compounds, $CH_2(ZnI)_2$, 493
  diethyl zinc, 23–24, 365–366
  metal, 23
  zinc oxide, 357
Zirconium catalysts
  (n-BuCp)$_2$ZrCl$_2$, 265, 268–271, 277–280, 283, 285
  Cp_2ZrMe_2, 65
  Cp_2ZrCl_2, 216, 264–265, 268, 282
  C_s-symmetric metallocenes, 200
  $Et[Flu]_2ZrCl_2$, 270
  heterocene ligands, 198–199, 203
  $Me_2Si(2\text{-}MeBenzInd)_2ZrCl_2$, 264
  oscillating metallocenes, 202
  rac-$Et(Ind)_2ZrCl_2$, 195, 264
  rac-$Et(H_4\text{-}Ind)_2ZrCl_2$, 195
  rac-$Me_2Si(Ind)_2ZrCl_2$, 196, 264
  $Zr(CH_2Ph)_4$, 163

A one-stop resource for understanding and applying polymerization catalysts

An edited volume featuring contributions from leading researchers, the *Handbook of Transition Metal Polymerization Catalysts* covers the design and synthesis of catalysts, and their applications in synthesis of polymers. Dealing with those polymerization catalysts that afford commercially acceptable yields of polymer with respect to catalyst mass and promising newer catalysts, this practical reference provides polymer and organic chemists with a comprehensive overview of the known methods for developing and applying these important catalysts.

With both recent advances and historically important catalysts, the subjects covered in this text include:

- Metal alkyls and other compounds that function as co-catalysts with a large number of catalysts
- The varieties of porous silica either necessary or valuable in certain catalyst formulations
- Catalyst scale-up and commercialization
- Copper catalysts for olefin polymerization
- Morphology control

Along with the above topics, the *Handbook of Transition Metal Polymerization Catalysts* provides tables of valuable data to assist in reproducing a synthesis or applying the knowledge to a new problem. Polymerization reactivities, polymer properties, monomer and solvent purity requirements, molecular weights, distribution, and reactivity ratios are also covered. The *Handbook of Transition Metal Polymerization Catalysts* offers an excellent one-stop resource for understanding and applying polymerization catalysts.

RAY HOFF is a member of the adjunct faculty at Roosevelt University in Schaumburg, Illinois. He is a former research scientist in polymerization catalysts for B.F. Goodrich, Chemplex Company, and Quantum Chemical Corporation. He holds twenty-seven U.S. patents in the field of polymerization catalysts, and his silica-based catalyst inventions scaled up to manufacturing more than 100 million pounds of production in the U.S. and the Netherlands.

ROBERT T. MATHERS is an Assistant Professor of Chemistry at Penn State University. He has coauthored over twenty scientific papers in the areas of anionic, metallocene, and ring-opening polymerizations, and holds one U.S. patent. After receiving a BS (1996) in chemistry from North Carolina State University and a PhD (2002) in polymer science from the University of Akron, he spent two years as a postdoctoral researcher at Cornell University in the Department of Chemistry and Chemical Biology. Currently, Dr. Mathers research investigates new methods to integrate renewable resources and catalysis.

Subscribe to our free Chemistry eNewsletter at
wiley.com/enewsletters

Visit wiley.com/chemistry

WILEY
wiley.com

ISBN 978-0-470-13798-7
90000
9 780470 137987